# Mono- and Dichromophoric Platinum Complexes with Multiple Emissions

## Dissertation

**for the academic degree of doctor in the natural sciences**

**(Dr. rer. nat.)**

by

Peter Irmler

at the

Universität Konstanz

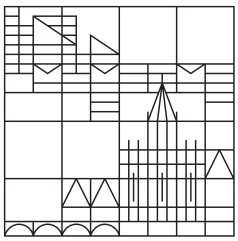

Section of Mathematics and Natural Sciences

Department of Chemistry

Konstanz, 2019

Tag der mündlichen Prüfung: 6. März 2020
1. Referent: Prof. Dr. Rainer F. Winter
2. Referent: Jun. Prof. Dr. Andreas Lorbach
3. Referentin: Prof. Dr. Karin Hauser

Diese Arbeit wurde im Zeitraum von Juli 2015 bis Juli 2019 in der Arbeitsgruppe von Herrn Prof. Dr. Rainer F. Winter an der Universität Konstanz angefertigt. Diese Arbeit wurde aus Mitteln der Deutschen Forschungsgemeinschaft (DFG) finanziert.

Für Tanja, Moritz und Paula

# Contents

# 1 Danksagung

An erster Stelle und aufs Allerherzlichste möchte ich mich bei Herrn Prof. Dr. Rainer F. Winter bedanken. Seine angenehme Art die Arbeitsgruppe zu leiten, hat es mir leicht gemacht, mich für eine Promotion in seiner Arbeitsgruppe zu entscheiden. Ebenfalls danken möchte ich ihm für die hervorragende Betreuung und die interessante Themenstellung. Des Weiteren danke ich Herrn Juniorprofessor Dr. Andreas Lorbach für die Übernahme des Zweitgutachtens und Frau Prof. Dr. Christine Peter für die Übernahme des Prüfungsvorsitzes.

Ebenfalls sehr herzlich danke ich

- meinen HiWis und Praktikanten und meiner Bachelor-Studentin für ihren Beitrag zu dieser Dissertation: Maite Mißun, Ronja Schneck, Jan Herberger, André Mang und Franciska Gogesch
- allen meinen Kollegen aus der Arbeitsgruppe Winter für eine unvergessliche Zeit
- allen Mitstreitern auf dem Gebiet der 'lumineszenten Platinkomplexe': Dr. Matthias Rank, Dr. Fabian Geist, Dr. Andrej Jackel und Jan Herberger für den anregenden Austausch
- Jan Herberger insbesondere für das Korrekturlesen der Einleitung dieser Arbeit und den angenehmen Laboralltag
- Gernot Haug danke ich für die Synthese einiger Ausgangsverbindungen und seine Hilfestellung bei synthetischen Fragestellungen
- Dr. Michael Linseis für seine Hilfestellungen im Bereich der Computerchemie und seinen Support bezüglich der Messinstrumente
- Nils Rotthowe und Dr. Steffen Oßwald für die Einführung und Hilfestellungen bezüglich der EPR-Spektroskopie
- Udo Dölling für den technischen Support im Labor
- Bernhard Weibert für die durchgeführten kristallographischen Messungen
- Anke Friemel und Ulrich Haunz für ihre freundliche Unterstützung bei aufwendigen NMR-spektroskopischen Messungen

- Prof. Dr. Oliver S. Wenger und Christopher B. Larsen für die Möglichkeit, in Basel Messungen mittels transienter Absorptionsspektroskopie durchzuführen
- meiner Frau Tanja, die mit bewundernswerter Hingabe unsere Kinder Moritz und Paula umsorgt hat, während ich an der Universität war, und die mir eine große emotionale Stütze war
- meinen Eltern Wolfgang Irmler und Barbara Reck-Irmler für ihre großzügige finanzielle Unterstützung und ihren Rückhalt
- meinen Geschwistern Lukas und Annalotte für den wunderbaren Zusammenhalt

# 2 Abbrevations

**Abb.** Abbildung

**Ant** anthracene

**BDP** Bodipy as a short form of 4,4-difluoro-4-bora-3a,4a-diaza-*s*-indacen-8-yl

**bpy** bipyridine

***ca.*** circa

**CT** charge transfer

**DFT** density functional theory

**Eq.** equation

***et al.*** et alii

**ET** energy transfer

**EtB** 8-ethynyl-bodipy

**EtNI** 4-ethynyl-1,8-naphthalimide

**Fig.** Figure

**IC** internal conversion

**ILCT** intraligand charge-transfer

**ISC** intersystem crossing

**LC** ligand-centered

**LL'CT** ligand-to-ligand' charge-transfer

**MLCT** metal-to-ligand charge-transfer

**MLL'CT** metal/ligand-to-ligand' charge-transfer

**NIR** near-infrared

**OLED** organic light-emitting diode

$\Phi_{\mathbf{f}}$ fluorescence quantum yield

$\Phi_{\mathbf{p}}$ phosphorescence quantum yield

**r.t.** room temperature

**SOC** spin-orbit coupling

**SOCT-ISC** spin-orbit charge transfer intersystem crossing

**TA** transient absorption

$\tau_{\mathbf{f}}$ fluorescence lifetime

$\tau_{\mathbf{p}}$ phosphorescence lifetime

**TD-DFT** time-dependent density functional theory

**Tx** thioxanthon-2-yl

# 3 Introduction

Color impressions are evoked by the interaction of electromagnetic radiation (e.g. visible light between 400 and 750 nm) with dyes or pigments. Mankind always aspired to mimic nature's beauty for adorning themselves with colorful fabrics - prestigious goods since time immemorial reserved to the rich and royal. The roots of Chemisty can be found in the development of dyes and pigments. The first chemist to commercially produce a colorant was William Henry Perkin in 1856, working at the Royal College of Chemistry in London. Perkin, whose dye colors silk in a rich purple color, named his synthetic dye 'mauveine' based on the color of the mauve.[1] Besides the original intention of inventing bright and photostable dyes, it became evident to scientists in the 1950s that the excited states of many chromophores render them also interesting for applications in luminescence and photocatalysis.[2] The concept of photosensitizing, which has been perfected by nature in the context of photosynthesis, uses the energy of a dye molecule excited by light and transfers this energy to a substrate, which subsequently undergoes a chemical transformation. We shall see that for photosensitizing purposes a high population of long-lived triplet states is essential.

## 3.1 Photophysics of Singlet and Triplet States

In his 1999 publication 'From Jabłoński to Femtoseconds',[4] M. Kasha outlines in an admirable manner the evolution of the modern understanding of photophysics. G. G. Stokes[5, 6] was one of the early scientists to reveal the relationship between molecular fluorescence and absorption. Prior to the 1940s, the concept of phosphorescence was

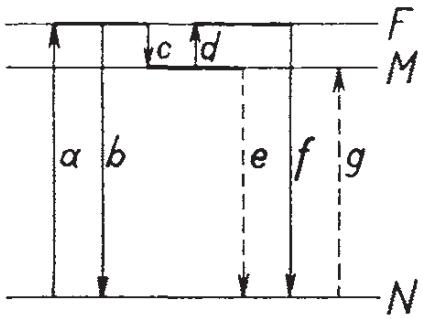


FIG. 1.—Energy levels in a phosphorescent molecule. *a*–absorption, *b*–fluorescence, *c*–transition to metastable level, *d*–thermal excitation, *e* and *f*–phosphorescence, *g*–absorption of very small transition probability.

Figure 1: The famous Jabłoński Diagram formulated by Jabłoński in 1933. Reprinted by permission from Springer Nature [3].

strictly regarded as a solid state phenomenon, predominantly observed in mineral crystals doped with an impurity.[4] The first huge step ahead was taken by A. Jabłoński in the 1930s with his famous Jabłoński Diagram, shown in Fig. 1, where he identified the lowest three critical states *N*, *F*, and *M* as quantized molecular electronic states.[3, 7] *N* refers to the *normal* state, where the molecule is in its electronic ground state (nowadays refered to as the $S_0$). From the *fluorescent* state *F*, which designates the first electronic excited singlet state $S_1$, molecules can relax either by the *F*-*N* transion to the *normal* state, emitting a photon by fluorescence, or pass to the *metastable* state *M*. This *metastable* state *M*, nowadays termed the $T_1$ state, was identified as the source for phosphorescence. Jabłoński howewer did not consider his state *M* to be a triplet state. Among others,[8, 9] Kasha and Lewis have characterized the *M* state to be of triplet state multiplicity.[10] In the following we will see how triplet states are populated. Since the $S_0 \rightarrow T_1$ absorption is not of interest for this thesis it is not further discussed here although there are several cases where this transition is weakly allowed and can be directly observed in the absorption spectra with low oscillator strength.[11, 12]

By the interaction of a chromophore with light, an electron is excited from the singlet ground state $S_0$ to a singlet excited state $S_n$ (see Fig. 2). Since absorption is a fast process, the initially populated state is, in accordance with the Franck-Condon principle, a vibronically excited state of $S_n$. From here non-radiative equilibration takes place via internal conversion (IC) to the vibronic ground state of $S_n$, or along a crossing point with an energetically high vibronic excited state of an energetically lower $S_n$ state, respectively.

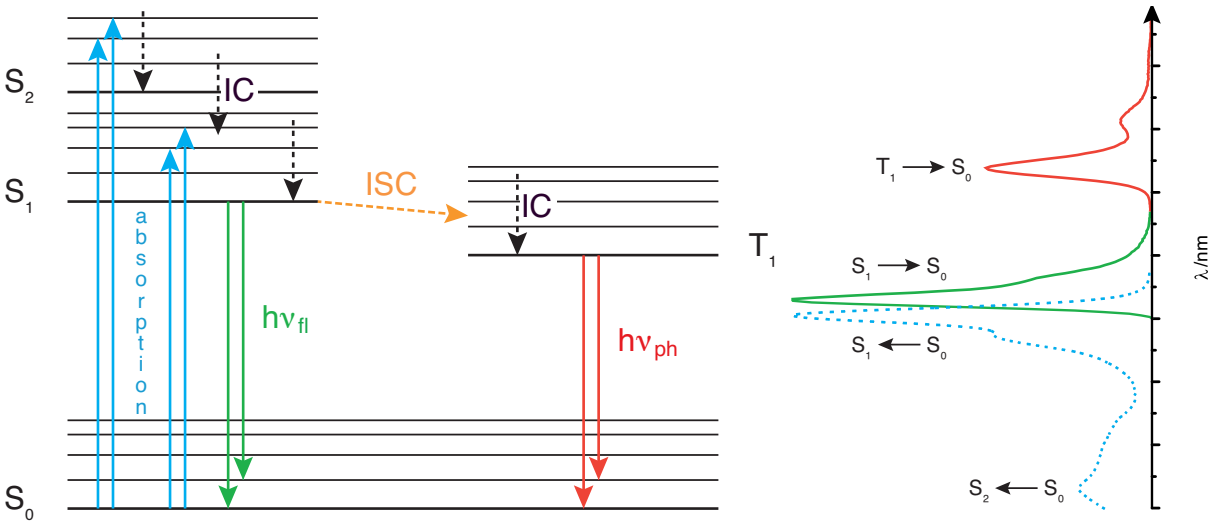


Figure 2: A modern version of the Jabłoński Diagram and examples of spectra resulting from the shown transitions.

Eventually the vibronic ground state of $S_1$ is populated. In rigid, purely organic systems the energy stored in the electronic $S_1$ state can be emitted in the form of light, namely fluorescence. Non-radiative processes such as IC, where the excited energy is dispensed via vibrational modes, are always competing with radiative processes. In spectroscopy the term intersystem crossing (ISC) refers to a radiative or non-radiative transition between states with different spin multiplicities. The most important examples are singlet-triplet transitions, which are under the consideration of spectroscopic selection rules rigorously forbidden. This is true for small, purely organic molecules, but is not strictly obeyed for larger polyaromatic hydrocarbons or compounds having heteroatoms with occupied non-bonding electron pairs (lone pairs). An increasing similarity of the energies and structures of excited singlet and triplet states when increasing the size of the aromatic system was found to promote triplet state population.[13] This can be rationalized under the consideration of spin-orbit perturbation theory.[4] Two 'pure' states are admixed to form a hybridized state. McGlynn and coworkers[14] have distilled the essence of first-order perturbation theory in Eq. (1).

$$T_1' = T_1^0 + \sum_m \left[ \frac{\langle S_m^0 | \hat{H}_{\mathrm{SO}} | T_1^0 \rangle}{E_m(S_m^0) - E_1(T_1^0)} \right] \cdot S_m^0 \tag{1}$$

The latter equation contains the interaction of the first excited triplet state $T_1^0$ with an energetically close-lying excited singlet state $S_m^0$ via the spin-orbit Hamiltonian $\hat{H}_{\mathrm{SO}}$ in the numerator. The denominator equals the energy difference between the respective singlet and triplet states. Two principal mechanisms are relevant in terms of ISC: the 'internal' and the 'external' effect of spin-orbit coupling. The rule of El-Sayed refers to the 'internal' effect, predicting a large rate of ISC if the singlet and triplet states differ in exactly one orbital component with respect to the transition under consideration.[15, 16] A change in orbital angular momentum is required to promote ISC, as it is the case for ${}^1n\pi^* \longrightarrow {}^3\pi\pi^*$, or ${}^1\pi\pi^* \longrightarrow {}^3n\pi^*$ transitions, respectively. This leads to a non-vanishing, sufficiently large value of the matrix element $\hat{H}_{\mathrm{SO}}$ in Eq. 1. The matrix element containing the spin-orbit Hamiltonian becomes zero for ${}^1\pi\pi^* \longrightarrow {}^3\pi\pi^*$, or ${}^1n\pi^* \longrightarrow {}^3n\pi^*$ transitions. It is thus evident that chomophores, that exhibit an orbital angular momentum change in the form of charge transfer (CT) transitions, also should exhibit higher rates of ISC. Wasielewski and coworkers have, for example, studied several donor-bridge-acceptor systems which have a 3,5-dimethyl-4-(9-anthracenyl)-julolidine donor entity and a pyromellitimide, or naphthalene-1,8:4,5-bis(dicarboximide) acceptor entity (see Fig. 3). The excited triplet states of anthracene were populated via spin-orbit charge transfer intersystem crossing

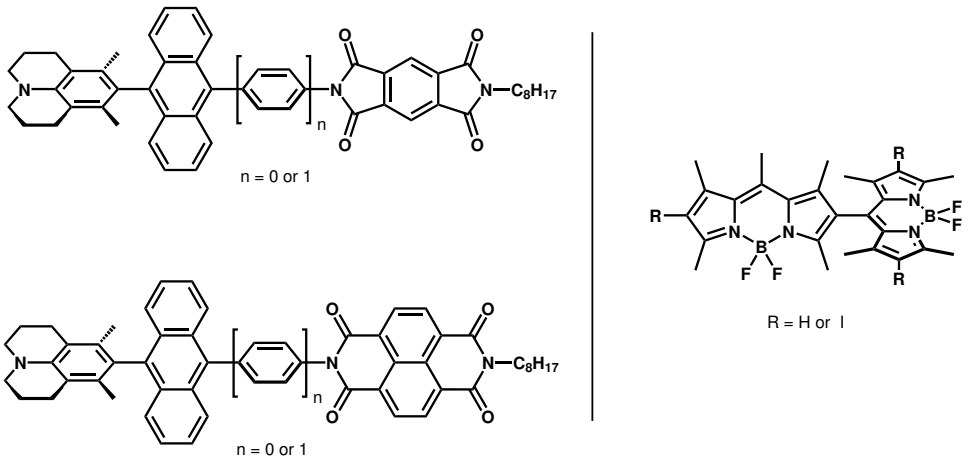


Figure 3: Donor-bridge-acceptor based dyads by Wasielewski and coworkers[17] (left) and orthogonally linked BDP dimers by Ortiz and coworkers[18] (right).

(SOCT-ISC).[17] Other beautiful examples by Ortiz and coworkes (depicted in Fig. 3) are orthogonally linked 4,4-difluoro-4-bora-3a,4a-diaza-*s*-indacen-8-yl (BDP) dimers that exhibit high ISC rates by a SOCT-ISC mechanism.[18]

The concept of El-Sayed can be expanded to transition metal complexes when d-orbitals are admixed to the relevant excited states. In transition metal complexes, $^1d\pi^* \longrightarrow {}^3\pi\pi^*$, or $^1\pi\pi^* \longrightarrow {}^3d\pi^*$ transitions greatly enhance the spin-orbit coupling matrix term $\langle S_m^0|\hat{H}_{\mathrm{SO}}|T_1^0\rangle$ of Eq. 1 and therefore the rate of ISC is drastically accelerated.[19, 20] In the context of this expansion of El-Sayed's rule to transition metal complexes it has to be noted that the position of the attachment of the transition metal to the chromophore plays a crucial role in terms of perturbation of the 'pure' states. Dyes that have large orbital coefficients at the point of metal attachment can profit from admixture of $d\pi$-metal orbital contributions to the ligand $\pi$ MOs and are particularly prone to the 'internal' heavy-atom effect. When there is no favorable orbital overlap, the 'external' heavy-atom effect comes into play and may also trigger ISC. A transition metal complex with a chromophore ligand may have different absorption features compared with the free chromophore with varying contributions of a charge-transfer between a metal entity and the ligand such as metal-to-ligand or ligand-to-metal CT. In a concept proposed by Chou *et al.*[19] the efficiency of the ISC from a higher-lying $S_n$ state with a larger contribution of d-orbitals ($S_n \longrightarrow T_m \longrightarrow T_1$) and from the $S_1$ state with negligible metal contribution ($S_n \longrightarrow S_1 \longrightarrow T_1$) may differ drastically and lead to an excitation energy-dependent ratio between fluorescence and phosphorescence emissions. Experimental verification of this concept was reported in the literature.[20–22]

In cases where no 'internal' effect is operative, ISC can still be promoted by the so-called 'external' heavy-atom effect. Regarding the 'external' heavy-atom effect, the Hamilton-operator for spin-orbit coupling is of crucial importance. For a single heavy-atom with a Coulombic field it can be expressed as:[4]

$$\hat{H}_{\mathrm{SO}} = \xi \left( \frac{Z^4}{n^3} \right) \sum_i \hat{l}_i \cdot \hat{s}_i \tag{2}$$

Here $\xi$ is the spin-orbit coupling constant of the heavy-atom (note Pt has a rather large value of $\xi = 4481\ cm^{-1}$[23]), $Z$ is the atomic number and $n$ is the principal quantum number of the valence electron. $\hat{l}_i$ and $\hat{s}_i$ are the orbital angular momentum operator and the spin operator, respectively. When calculating the transition dipole moment from Eq. 2, a simplified term can be derived.[19]

$$k_{\mathrm{isc}} \propto \left( \frac{Z^8}{d^6} \right) \tag{3}$$

Eq. 3 highlights the high dependency of the ISC rate from the atomic number $Z$, due to the power of 8, and the inverse proportional dependency from the distance $d$ between the chromophore and the heavy-atom to the power of 6. The correlation between the rate of ISC and the distance of the center of the $\pi$-system of the chromophore to the heavy-atom was studied by Chou and coworkers on oligo(phenylene)-bridged bimetallic gold(I) complexes of the type (PhC≡C)AuPPh$_2$-(C$_6$H$_4$)$_n$PPh$_2$Au(C≡CPh) (see Fig. 4).[20] Upon plotting $(k_{\mathrm{isc}})^{1/2} \times \Delta E_{\mathrm{S_1\text{-}T_1}}$ against the effective distance $r^{-3}$ they found a linear dependency for their binuclear Au(I) complexes. Consequently, the proportion of phosphorescence with respect to the fluorescence increases, when the heavy-atom is in closer proximity to the dye. As mentioned before, all radiative processes always compete with non-radiative deactivation pathways. The first excited triplet state is subject to non-radiative deactivation by overlap of $T_1$ with vibrational excited states of the electronic ground state. The non-radiative decay rate is related to the energy gap between the states

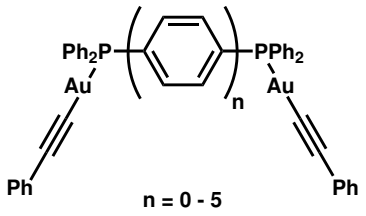


Figure 4: Structures of Au(I) complexes studied by Chou and coworkers.[20]

involved as it is expressed by the energy gap law:[24]

$$k_{\mathrm{nr}} \propto \exp\left(\frac{-\gamma \Delta E}{\hbar \omega_{\mathrm{M}}}\right) \tag{4}$$

In Eq. 4 $\Delta E$ is the energy difference between the states involved, $\gamma$ is a parameter accounting for various molecular parameters, and $\omega_{\mathrm{M}}$ is the dominant vibrational fequency of the system. In aromatic hydrocarbons this is usually the C-H stretching frequency at 3000 $\mathrm{cm}^{-1}$. Especially its fourth harmonic at 12,000 $\mathrm{cm}^{-1}$ (ca. 833 nm) has a favourable overlap to vibronic wavefunctions with energies in the near-infrared (NIR). The exponential dependency of $k_{\mathrm{nr}}$ on the energy gap between the $T_1$ and the $S_0$ states is a crucial factor affecting NIR emitters. Experimental evidence is, for example, given in a publication by Schanze and coworkers.[25] They prepared two series of Pt(bpy)($-$C$\equiv$C$-$Ar)$_2$ complexes (bpy = 2,2'-bipyridine) (Fig. 5). Absorption profiles of these complexes are dominated by a Pt $\rightarrow$ bpy metal-to-ligand charge-transfer (MLCT) absorption. For complexes of the series 1, the excited state energy is varied by the substituents on the 4,4'- and/or 5,5'-positions, respectively, of the bpy ligand. For complexes of series 2 the excited state energies are altered by changing the *para*-substituent X on the aryl ring. Photophysical studies revealed that for complexes of series 1 the lowest lying excited state of the complexes, mainly the Pt $\rightarrow$ bpy $^3$MLCT state, suffers from increasing non-radiative decay rates that quantitatively correlate with the energy gap law in a linear fashion (Fig. 5). Complexes of series 2 also exhibit a strong tendency for larger values of ln $k_{\mathrm{nr}}$ with a smaller $T_1 \rightarrow S_0$ energy gap.

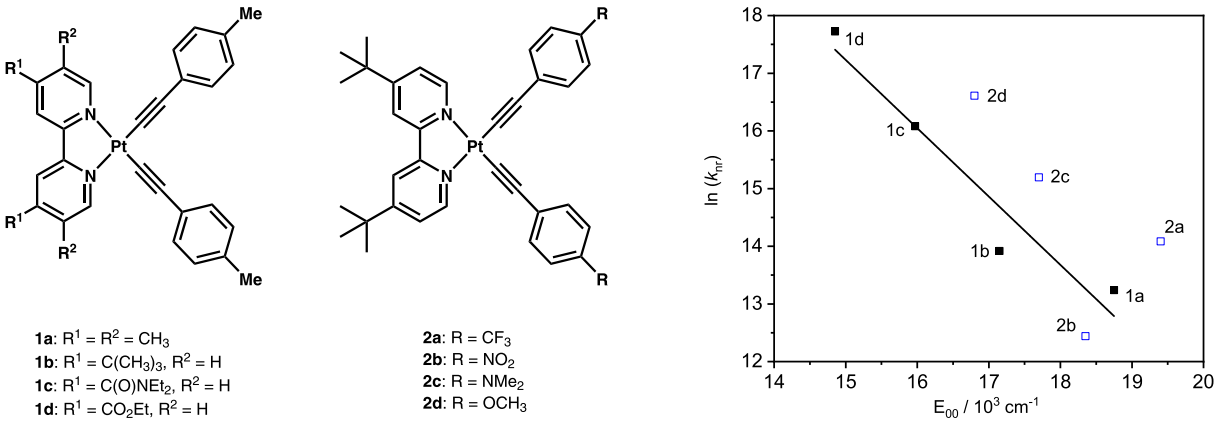


Figure 5: Pt(bpy)(acetylide)$_2$ complexes by Schanze and coworkers with quantitative energy gap law analysis by plotting the *ln* $\Sigma k_{\mathrm{nr}}$ vs. the 0-0 energy. Adapted with permission from reference [25]. © (2001) American Chemical Society.

## 3.2 The Photochemistry of Platinum

For effective photocatalytic processes the lifetime of the excited state has to be sufficiently long to enable energy transfer from the sensitzer to the substrate. Metal organic complexes have proven to possess long-lived excited triplet states, which are accessible via ISC (*vide infra*) with high efficiencies. Triplet states also play an important role in organic light-emitting diode (OLED) technology where their superior spin statistics allows for a theoretical maximum of 100% quantum efficiency, while singlet state emitters reach only a maximum of 25%.[26] Since long-lived excited triplet states of molecules can interact with triplet molecules by the means of triplet-triplet annihilation, they can be utilized in sensing these molecules due to the concomitant phosphorescence quenching.[27, 28] Among this large family of photo-active metal organic complexes, coordination compounds of platinum have particularly notable characteristics. As can be seen from Fig. 6, metal ions in the oxidation state +2 with a $d^8$ electronic configuration have, in the presence of strong-field ligands, a strong thermodynamic preference to form square-planar complexes. This destabilizes the single unoccupied $d_{x^2-y^2}$ orbital. Compared to other metal ions that are often utilized in photochemistry, like Cr(III), Ru(II), Os(II), Rh(III), or Ir(III), which form 6-coordinate, octahedral complexes, as well as Ni(II), or Cu(I), which mostly form 4-coordinate tetrahedral complexes, the square-planar coordination of Pt(II) makes it unique in terms of its absorption and luminescence properties.[29]

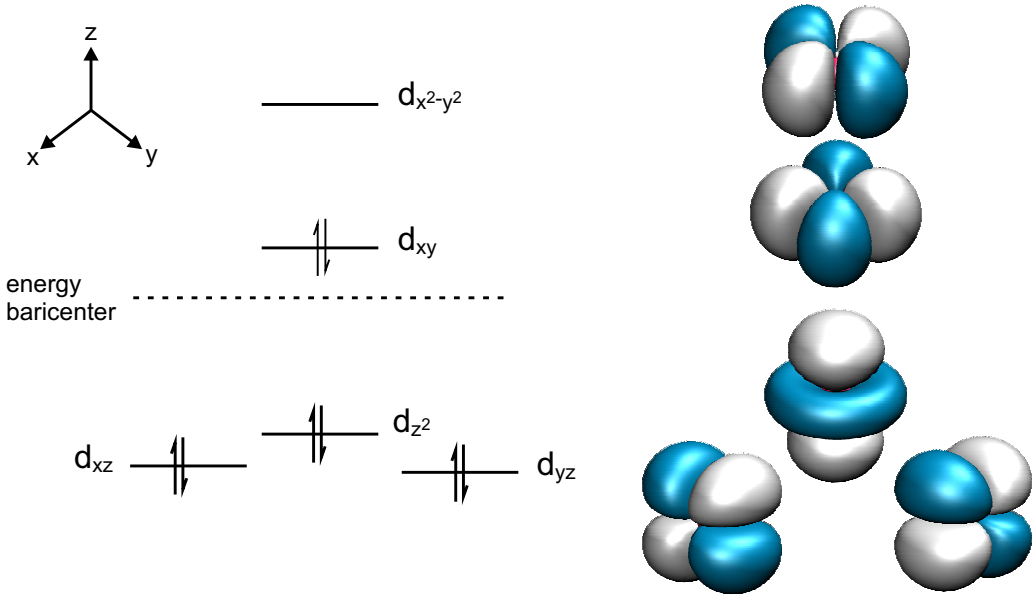


Figure 6: Ligand field splitting diagram of metal d orbitals in the square-planar coordination geometry.

The square-planar coordination geometry with sterically undemanding ligands makes platinophilic or $\pi$-$\pi$ interactions between individual molecules feasible. The $d_{z^2}$ orbital has a perpendicular orientation towards the coordination plane at the Pt ion. An intermolecular separation of *ca.* 3 - 3.5 Å is sufficent for the interaction of two $d_{z^2}$ orbitals of neighboring molecules to form a pair of molecular orbitals: the weakly bonding $d\sigma$ and its antibonding pendant $d\sigma^*$.[29] Along with the possibility of non-radiative deactivation, the emission profile can be substantially altered by such platinophilic interactions towards bathochromic emission or low-energy metal-metal transitions.[30] A similar effect is observed upon $\pi$-$\pi$ stacking of planar organic coligands, where aggregation leads to a red-shift of the absorption and the emission.[31] With an increase of concentration of a fluorescent species (for example pyrene) the quantum yield is often decreased. This is due to the formation of an excimer (*exci*ted di*mer*), which is the combination of a molecule in its ground state with a molecule in the excited state. The fluorescence of the excimer is observed at lower energy than the fluorescence from the $\pi\pi^*$ transition on the monomer.[32, 33] As depicted in Fig. 6, the $d_{x^2-y^2}$ orbital is strongly antibonding and the population of this orbital leads to non-radiative deactivation by structural distortion. By introducing aromatic hydrocarbons with extended $\pi$-conjugation as ligands into the ligand field of the Pt(II) ion, both ligand-centered (LC) ($\pi\pi^*$ or $n\pi^*$) and CT (MLCT or ligand-to-ligand' charge-transfer (LL'CT)) states emerge. Though many platinum complexes have LC and CT states with large radiative rate constants $k_r$, excited dd* states are still detrimental to luminescence, i.e. population of the $d_{x^2-y^2}$ orbital by thermal energy affords effective luminescence quenching. The introduction of aromatic hydrocarbon ligands offers two major advantages: Firstly, $\sigma$-aryl ligands are strong $\sigma$-donors, further destabilizing the strongly antibonding $d_{x^2-y^2}$ orbital and, secondly, extended $\pi$-chromophores introduce energetically low-lying $\pi\pi^*$-states that further decrease the energy gap between emissive and non-emissive excited states. In summary this renders emission more effective than deactivation through population of dd*-states.[29]

## 3.3 Luminescent Dye-Modified Complexes of Platinum

One important subset among the large family of luminescent platinum complexes are those complexes where chromophores are directly coordinated to the heavy-metal ion. The coordinated chromophores have usually high molar extinction coefficents $\varepsilon$ and are luminescent by themselves. Cyclometalating ligands have the favorable characteristic of introducing a strong ligand-field. As an example, the benzothiazole-functionalized coumarin 6 has been used as a cyclometalating ligand and was found to endow the resulting complexes

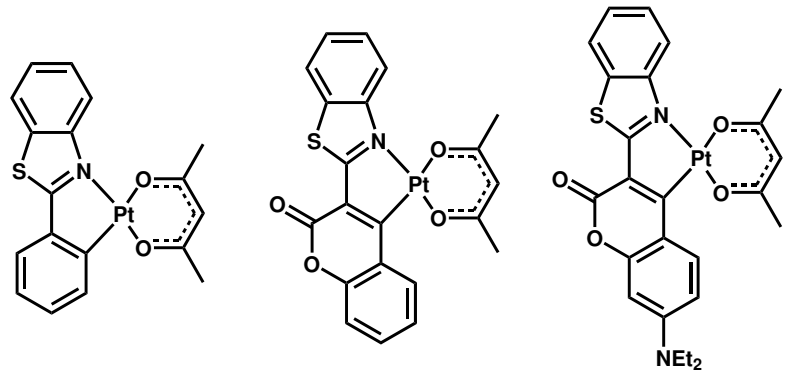


Figure 7: Luminescent Pt complexes with cyclometalating C^N ligands by Thompson and Zhao.[34, 35]

with favorable luminescent properties.[34, 35] Comparing the properties of the complexes depicted in Fig. 7, **CN-2** has a higher molar absorption coefficent in the visible region between 400 - 500 nm while **CN-1** only modestly absorbs above 400 nm. **CN-3** is intensly absorbing at around 500 nm due to an additional intraligand charge-transfer from the $NEt_2$ donor to the lactonic acceptor. **CN-1** and **CN-3** have comparable phosphorescence quantum yields of 0.36 and 0.37; **CN-2** with a quantum yield of 0.03, is only modestly luminescent. Andrej Jackel from our research group has shown[36] that cyclometalated pyridyl-substituted coumarins (Fig. 8) show a ligand based phosphorescence with a phosphorescence quantum yield $\Phi_p$ of *ca.* 0.21. The site of attachment of the pyridyl unit to the coumarine dye has a large impact on the absorption and emission properties. The absorption spectrum of **CN-4** is dominated by the $\pi\pi^*$ transition on the coumarin and the complex dually emits from the $^1\pi\pi^*$ and $^3\pi\pi^*$ excited states of the coumarin ligand.

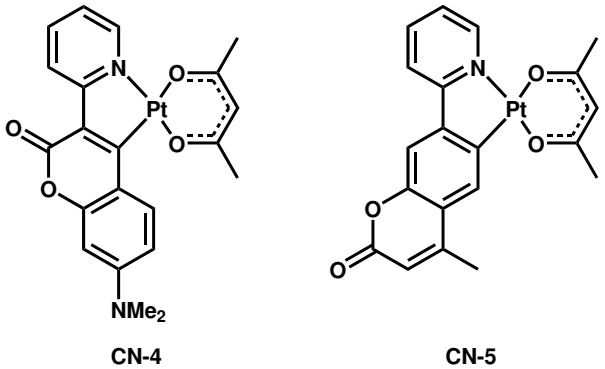


Figure 8: Cyclometalating platinum complexes with pyridyl-coumarin ligands.[36]

**CN-5** exhibits very different electronic transitions. The lowest energy absorption features are intra-ligand CT in character. **CN-5** displays phosphorescence from an intra-ligand charge-transfer based triplet excited state. Electron donation of the $NMe_2$ group shifts the main absorption in the visible region and concomitantly the emission is red-shifted with respect to the compound lacking this donor functionality.

Numerous Pt(II) complexes were studied where one or two dyes are attached to the platinum ion via acetylide linkers. A particularly beautiful example is **Pt(bpy)AP** (Fig. 9), which displays structured pyrene-acetylide-based $\pi\pi^*$ absorption bands at higher energy compared to the Pt $\rightarrow$ bpy MLCT absorption. Regarding the triplet excited states, an alkynyl-pyrene based $^3\pi\pi^*$ phosphorescence with a lifetime $\tau_p$ of 48.5 $\mu$s is observed, which is by 2800 $cm^{-1}$ lower in energy than the observed $^3$MLCT emission of the reference compound **Pt(bpy)APh**.[37, 38] Like **Pt(bpy)AP**, **Pt(PBu$_3$)AP** also shows ligand centered phosphorescence. However, the presence of a MLCT in **Pt(bpy)AP** dramatically accelerates the formation of the pyrenylacetylide-based triplet state.[38] This proves the above-mentioned concept of expanding El-Sayed's rule to metal-organic complexes.

In 2008 the research group of Ziessel reported on a platinum terpyridine complex with a $\sigma$-alkynyl-BDP ligand (**Pt-8-BDP** in Fig. 10).[39] Due to the enhanced spin-orbit coupling by the platinum ion, dual fluorescence and phosphorescence from the BDP's singlet and triplet $\pi\pi^*$ states is observed in a glassy matrix at 77 K. The presence of singlet and triplet

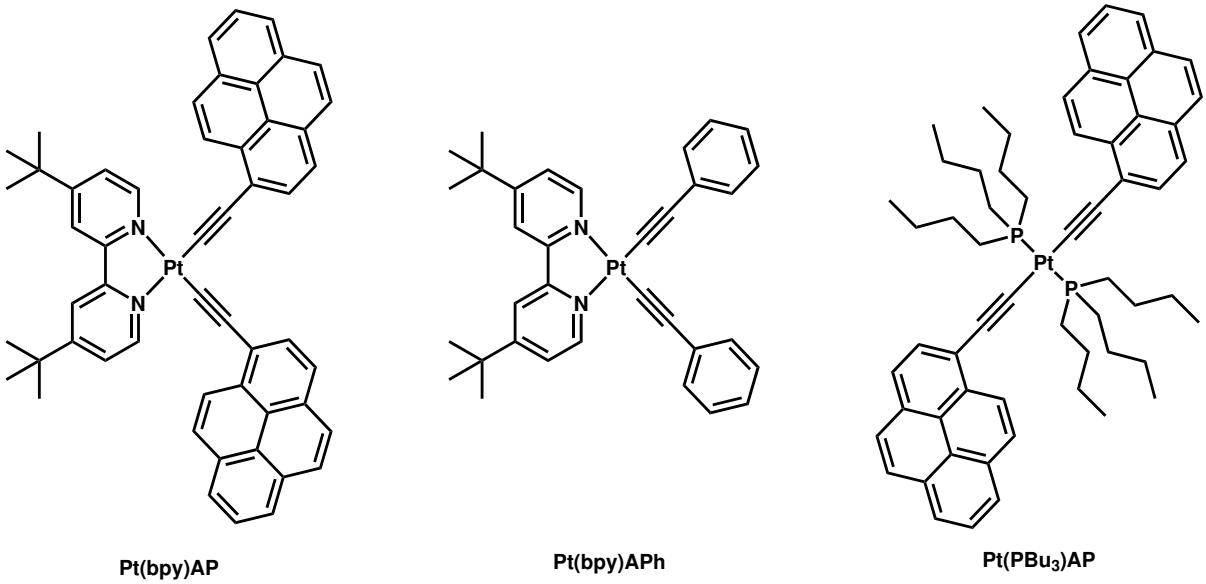


Figure 9: Pt bis-acetylide complexes **Pt(bpy)AP**, **Pt(bpy)APh** and **Pt(PBu$_3$)AP** reported by Ziessel and coworkers.[37, 38]

MLCT states promotes an ultrafast intersystem crossing between the excited $^{1/3}$MLCT states. From here the BDP-centered $^3\pi\pi^*$ excited state is directly populated without passing through the BDP-centered $^1\pi\pi^*$ state.

Zhao and coworkers have reported on platinum bipyridine complexes with two $\sigma$-alkynyl-BDP ligands.[41] The two complexes differ in the position of the alkyne at the BDP (see Fig. 10). **Pt-2,2-BDP$_2$** emitts from the BDP centered singlet and triplet states with a phosphorescence quantum yield $\Phi_p$ of 0.06% ($\tau_p = 36$ $\mu$s) in toluene solution at r.t. The complex **Pt-8,8-BDP$_2$** emitts solely by fluorescence from the BDP, but a triplet state was also detected by transient absorption (TA) spectroscopy with a lifetime of 162 $\mu$s. Most likely ISC is promoted for **Pt-2,2-BDP$_2$** because of the closer proximity of the dye to the heavy-metal center. The coordination of the BDP dye via an acetylide

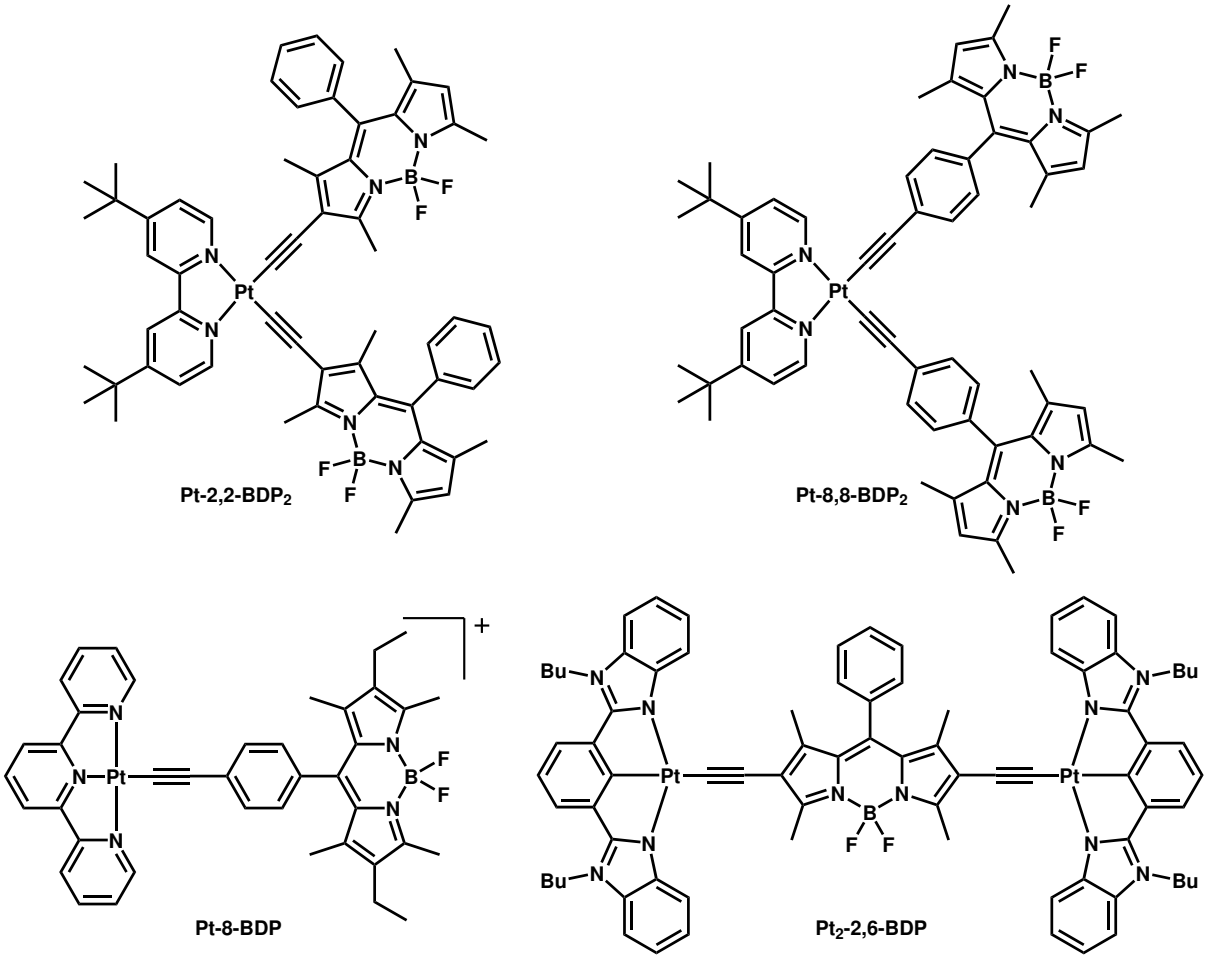


Figure 10: $\sigma$-Alkynyl-BDP complexes **Pt-8-BDP** reported by Ziessel and coworkers[39] as well as **P-2,2-BDP$_2$**, **P-8,8-BDP$_2$** and **Pt$_2$-2,6-BDP** studied by Zhao and coworkers.[40, 41]

linker in C2 position of the dye for **Pt-2,2-BDP$_2$** has the consequence of delocalizing the spin density of the triplet state over the platinum ion, acetylide bridge and the BDP, as has been revealed by means of computational chemistry. This promotes the ISC. The phenyl group in **Pt-8,8-BDP$_2$** isolates the dye from the platinum ion and the spin density of the triplet state is localized on the BDP. The group of Zhao has also reported on a dinuclear platinum complex containing a bridging bisalkynyl-BDP ligand (**Pt$_2$-2,6-BDP** in Fig. 10).[40] The complex is dually emissive from the $^3$MLCT excited state at 660 nm and the $^3\pi\pi^*$ state of BDP at 770 nm. The emission has a phosphorescence quantum yield of 3.5% in solution at r.t. Since the two triplet states are in an equilibrium, only one phosphorescence lifetime $\tau_p$ of 128 $\mu$s is observed.

## 3.4 Luminescent $\sigma$-aryl Complexes of Platinum

Eq. 3 describes the $d^{-6}$ dependency of the intersystem crossing rate constant $k_{isc}$, with $d$ as the distance between the center of the $\pi$-system of the chromophore and the heavy-atom. Due to this sensitive dependency it is, in terms of relying on the 'external' heavy-atom effect for promoting ISC, crucial to have the chromophore in close proximity to the platinum ion. This can be best realized by the formation of a direct Pt-C $\sigma$-bond to the dye-ligand. The family of complexes constructed according to these guiedelines is still rather small. In the following an overview over these compounds will be provided, focusing on instructive examples that illustrate the effect of the Pt-dye distance, the number and attachment site of platinum ions, and the effect of metal d-orbital perturbation on the $\pi$-system of the dye, respectively. As a welcome side effect, $\sigma$-aryl ligands are strong-field ligands, which destabilize the antibonding metal-centered d$\sigma^*$ orbital. An example for the depencence of the efficiency of ISC on the distance between Pt ion and dye ligand is given in a study by Nguyen and Yip published in 2010.[42] The relevant two complexes are displayed in Fig. 11. They are both $\sigma$-metalated tetracenes, with **5,12-Pt$_2$AT** being a dinuclear bis-acetylide complex and **5-PtT** being a mononuclear $\sigma$-aryl Pt complex. In their electronic absorption spectra the complexes are characterized by the prominent $\pi\pi^*$ absorption band of the tetracene. The latter is red-shifted with respect to the unsubstituted tetracene by perturbation of the frontier orbitals by the Pt moiety. Emission spectroscopy revealed that the two complexes show only fluorescence from excited tetracene-centered $\pi\pi^*$ states. The conclusions that can be drawn from the difference in fluorescence quantum yield $\Phi_f$ or the fluorescence lifetime $\tau_f$ between the two complexes are remarkable: **5,12-Pt$_2$AT** has a $\tau_f$ of 8.6 ns and a $\Phi_f$ of 0.60, while $\tau_f$ of **5-PtT** is only half as long ($\tau_f$ = 3.9 ns) and $\Phi_f$ has decreased by a factor of ten to 0.06. This clearly indicates that $k_{isc}$ has increased for

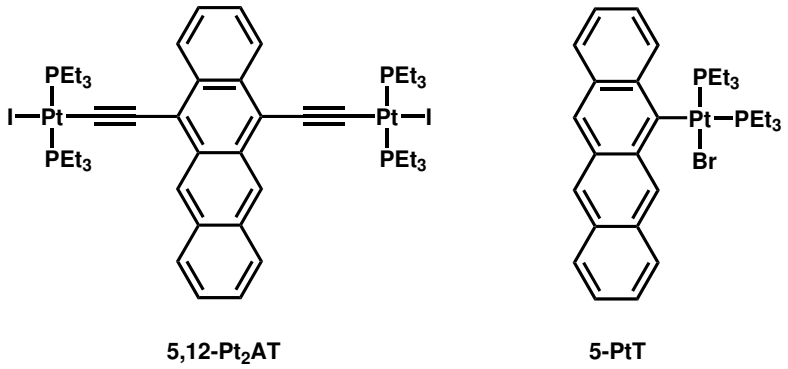


Figure 11: $\sigma$-tetracene platinum complexes.[42]

the complex where the Pt ion is in closer proximity to the dye, and in consequence, the fluorescence quantum yield is decreased in favour of a larger triplet-state quantum yield. However, phosphorescence emission was not observed.

In 2007, Yip and coworkers[43] studied a series of pyrenyl complexes containing one or two *trans*-$PtBr(PEt_3)_2$ units (see Fig. 12). The $\pi\pi^*$ transitions of the pyrenyl ligand are

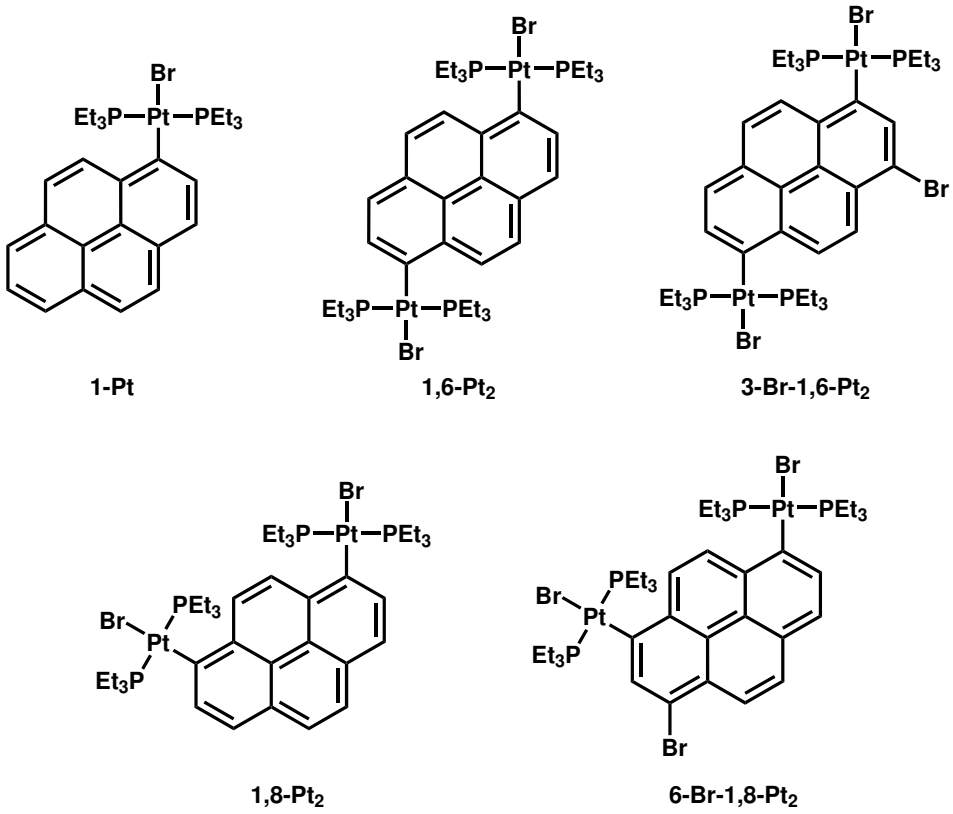


Figure 12: $\sigma$-Pyrenyl platinum complexes by Yip and coworkers.[43]

perturbed by the metal centers. The PT ion introduces a red-shift which further increases on introduction of a second Pt center. All five complexes show dual fluorescence and phosphorescence emissions, indicating that the rate of ISC is comparable with the fluorescence time scale. Introduction of a second Pt ion in the 6-position makes triplet state population more efficient, however an additional bromo-substituent in 3-position (**3-Br-1,6-Pt$_2$**) is mildly detrimental to the phosphorescence quantum yield ($\Phi_p = 2.31 \times 10^{-3}$) in comparison to **1,6-Pt$_2$** ($\Phi_p = 2.88 \times 10^{-3}$). Comparing the diplatinum complexes with a 1,6-platinum attachment to their 1,8-congeners provides evidence for the positional dependence of the heavy-atom effect in terms of ISC efficiency and phosphorescence quantum yield. For **1,8-Pt$_2$** quantum yields of $\Phi_f = 2.72 \times 10^{-3}$ and $\Phi_p = 0.80 \times 10^{-3}$ were reported, and for **6-Br-1,8-Pt$_2$** values of $\Phi_f = 1.17 \times 10^{-3}$ and $\Phi_p = 0.62 \times 10^{-3}$ were found. The 1,8-isomers also exhibit larger $\Phi_f$ values than their 1,6-congeners ($\Phi_f$ of $0.50 \times 10^{-3}$ or $0.42 \times 10^{-3}$).

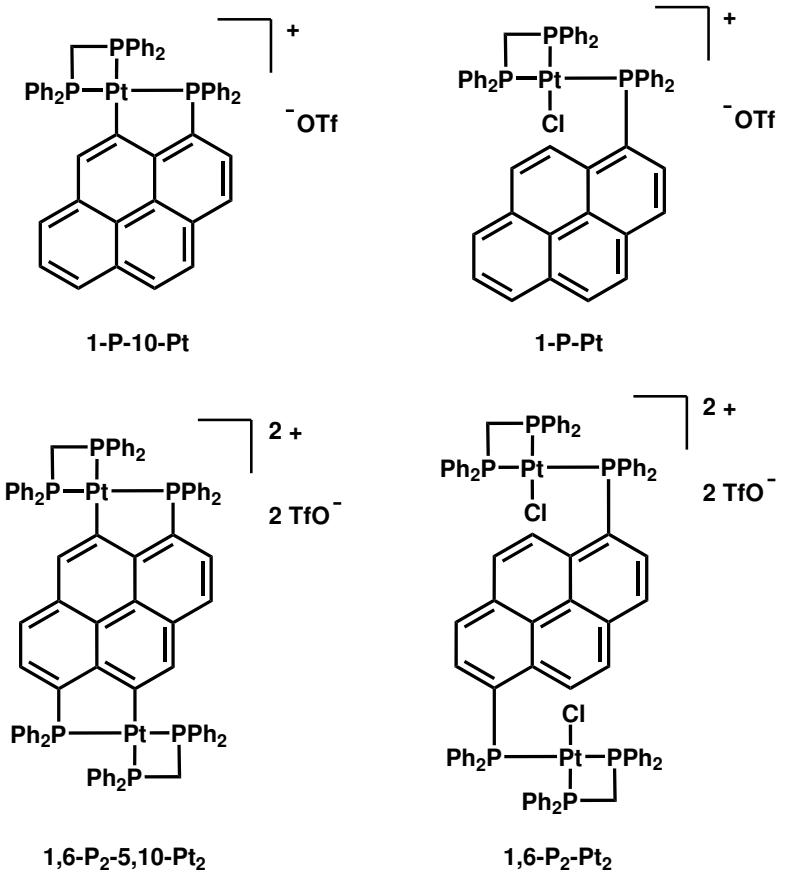


Figure 13: Cyclometalating $\sigma$-pyrenyl platinum complexes published by Yip and coworkers.[44]

In the latter system, the Pt coordination plane is aligned perpendicular to the pyrene plane. The two planes can be forced into a coplanar arrangement by a P^C chelating coordination mode (see Fig. 13). In addition to the close proximity of the heavy-atom and the dye ligand, the Pt-pertubation of the $\pi\pi^*$ transitions is larger and the whole system is more rigid, which prevents vibronic deactivation. These effects combined increase the phosphorescence quantum yield to up to $1.5 \times 10^{-2}$ for the dually emissive chelating systems with respect to the systems presented in Fig. 12. Again the effect of introducing a second heavy-atom on $k_{\mathrm{isc}}$ is additive, because the $\Phi_{\mathrm{f}}$ decreases from $3.2 \times 10^{-4}$ for **1-P-10-Pt** to $7.9 \times 10^{-5}$ for **1,6-P$_2$-5,10-Pt$_2$** while the phosphorescence intensifies. Upon "opening" of the chelate ring, the resulting complexes **1-P-Pt** and **1,6-P$_2$-Pt$_2$** are rendered weakly fluorescent at 410 nm. Solely the symmetric compound **1,6-P$_2$-Pt$_2$** shows a very weak emission feature at 650 nm, which is most likely due to phosphorescence.[44]

In 2010, Zhao and coworkers[45] reported on a series of C^N cycloplatinated complexes, where the distance of the pyrene moiety from the platinum ion was varied by absence of a spacer group (**CN-6**), a phenyl spacer (**CN-7**) and a phenyl-ethynyl spacer (**CN-8**), as illustrated in Fig. 14. Since the UV/Vis spectra of the three complexes as well as those of the free ligands differ from that of free pyrene, a ground state coupling of the pyrene and the pyridine or phenylpyridine, as well as the Pt(acac) increments is indicated. The absorption bands at lowest energy are, based on density functional theory (DFT) assignments, $^1$MLCT (Pt→pyrene/pyridine), $^1$LC (pyrene-localized) and $^1$LL'CT (pyrene→pyridine) transitions. All three complexes are phosphorescent between 650 and 800 nm at r.t. and

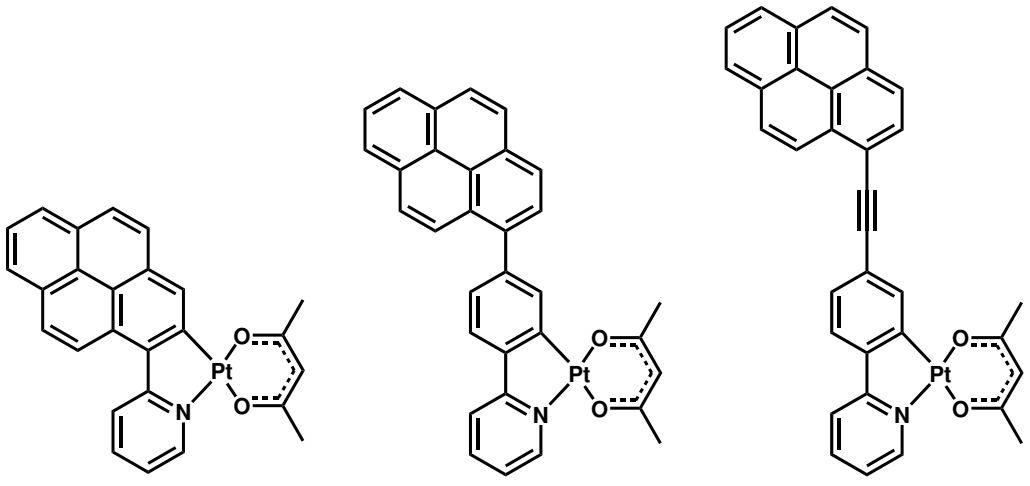


**CN-6** **CN-7** **CN-8**

Figure 14: Cyclometalating pyrenyl platinum complexes by Zhao and coworkers.[45]

emit from a pyrene-localized triplet state. In addition, a weaker [(ppy)Pt(acac)]-based phosphorescence at *ca.* 580 nm and a weak pyrene-based fluorescence are observed at *ca.* 470 nm. Surprisingly, complex **CN-7** shows the highest $\Phi_p$ of this series ($\Phi_p = 0.0065$) for the pyrene based luminescence, although the pyrene is not directly cyclometalated. This becomes even more puzzling when regarding the phosphorescence lifetimes for this series of complexes. With an increasing pyrene-Pt distance, $\tau_p$ increases from 856 ns for **CN-6** to 6.22 $\mu$s for **CN-7** to 15.8 $\mu$s for **CN-8**, indicating that the 'external' heavy-atom effect becomes less effective. On the other hand the ISC for populating the emissive triplet state ($S_n \longrightarrow T_m$) seems to be brought about by a different mechanism, since **CN-7** has the highest $\Phi_p$. Most likely the rate of triplet-state population is primarily affected by the different admixture of CT-states to the involved singlet and triplet states.

The platinum complexes depicted in Fig. 15 share the same C^N cyclometalating coordination motive as the above-discussed systems by Thompson, Jackel and Zhao, but incorporate different chromophores. **CN-9** exhibits a r.t. phosphorescence between 600 and 800 nm in solution with a $\Phi_p$ of 0.05 and a phosphorescence lifetime $\tau_p$ of 5.1 $\mu$s. In a 2-MeTHF matrix at 77 K the distinct vibronic structuring of the $\pi$-conjugated ligand is resolved which, in combination with the absence of a rigidochromic shift, proves a coranulene based $^3\pi\pi^*$ transition triggered by the heavy-atom effect of the platinum.[46] The benzophenanthroline complexes **CN-10/11** both display ligand-based phosphorescence in dilute PMMA polymers that shows a vibronic structure, again indicating a $^3\pi\pi^*$-character of the emissive state. Restriction of torsional motion by changing the phenyl-substituent to a 2,6-dimethyl-phenyl substituent makes it possible to observe the phosphorescence in fluid solution at r.t.[47] The dinitrophenylphenanthridine system **CN-12** by Sicilia and

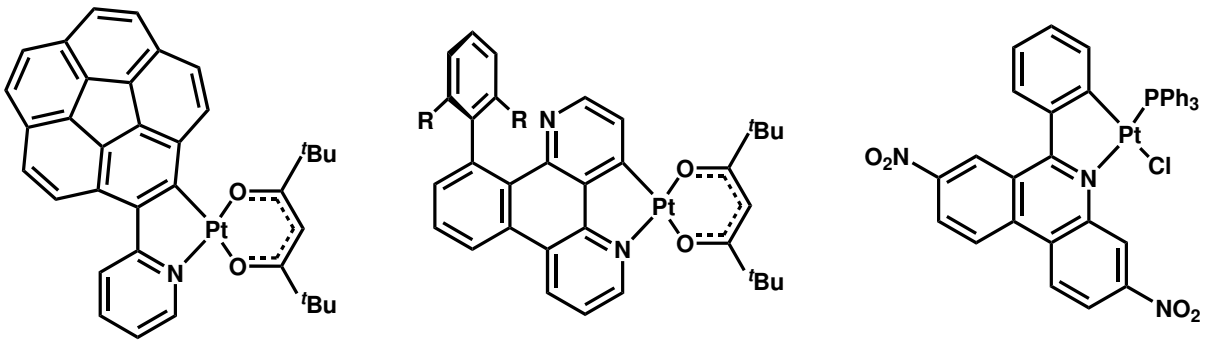


**CN-9**

**CN-10**: R = H
**CN-11**: R = $CH_3$

**CN-12**

Figure 15: Cyclometalating platinum complexes by Thompson[46, 47] and Sicilia.[48]

coworkers[48] also displays phosphorescence at 77 K. The authors also mention r.t. phosphorescence but did not pay further attention to it. Although the 77 K spectrum shows a very similar vibronic pattern as present for the free ligand, the authors assign the phosphorescence as a mixed $^3$MLCT/$^3$LC/$^3$LL'CT, while $^3$LC is for sure the predominant character of the emissive state.

Espinet and coworkers have published two complexes with a direct Pt-C $\sigma$-bond (see Fig. 16). Both compounds, the perylene (**Pt-1**) and the perylene monoimide (**Pt-2**), only show fluorescence at r.t. in solution or in a glassy matrix at 77 K. Quantum yields rank between 0.70 and 0.30.[49] The larger distance between the center of the dye and the platinum ion as well as a small orbital overlap between the chromophore and heavy-atom may be the reason for a small rate of intersystem crossing. The $\sigma$-Pt anthracenyl complex **Pt-3** reported by Sharp[50] has a much closer proximity between chromophoric center and the Pt ion, affording a high rate of intersystem crossing $k_{\mathrm{isc}}$. Owing to the intrinsically unfavourable Franck-Condon factor of anthracene, *P*-type delayed fluorescence in the blue region with $\tau_{\mathrm{em}}$ of 3.24 $\mu$s and a $\Phi_{\mathrm{em}}$ of 0.50 was observed. The Pt ion increases spin-orbit coupling and therefore the quantum-yield of the triplet state is increased, which subsequently leads to an increased quantum yield for the delayed florescence.

In the following, platinum complexes will be discussed that bear chromophores coordinated by a single Pt-C $\sigma$-bond, but were only studied in terms of their synthesis while their emissive properties remained unexplored. When reacting $Pt(PEt_3)_4$ with 1,2-dibromoacenaphthylene in hexane, the $\pi$-intermediate $Pt(PEt_3)_2(\eta^2$-1,2-dibromoacenaphthylene) (**Pt-4a**) precipitates from the solution (see Fig. 17). We have observed a similar $\pi$-intermediate during the oxidative addition reaction of a 3-Cl-BDP with *cis*-$Pt(\eta^2{-}C_2H_4)(PEt_3)_2$ (*vide infra*, Chapter 5.3). When a solution of **Pt-4a** in toluene is heated to 120 °C, the thermodynamically favored product *trans*-$Pt(PEt_3)_2$(1,2-dibromo-

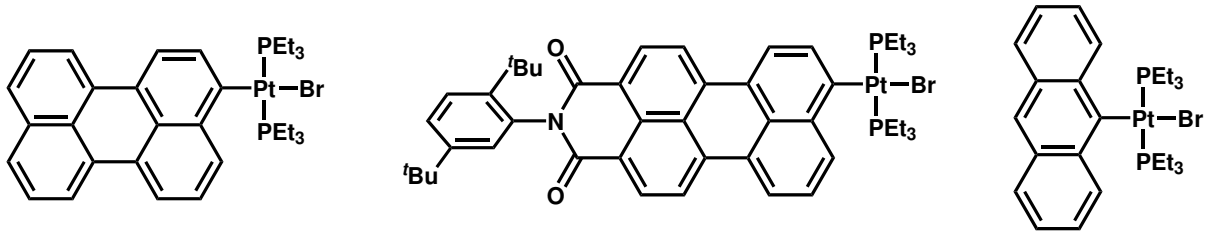


**Pt-1** **Pt-2** **Pt-3**

Figure 16: $\sigma$-bonded Pt comlexes with polycyclic aromatic ligands by Espinet[49] and Sharp.[50]

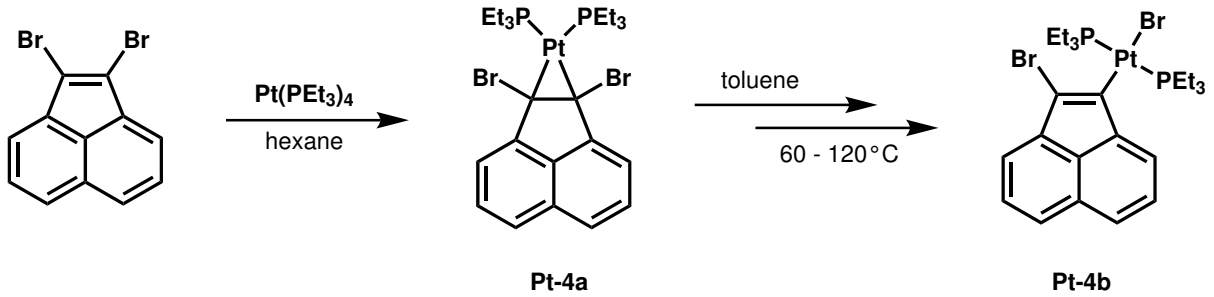


Figure 17: Formation of the $\pi$-intermediate $Pt(PEt_3)_2(\eta^2-1,2$-dibromoacenaphthylene) which, upon heating, subsequently forms oxidative addition product *trans*-$Pt(PEt_3)_2(1,2$-dibromoacenaphthylene).[51]

acenaphthylene) (**Pt-4b**) is formed. The absorption and emission properties of the products and intermediates were, however not reported.[51]

Sharp and coworkers have published several other $\sigma$-bonded platinum complexes with polycyclic aromatic hydrocarbons.[51–53] The complexes displayed in Fig. 18 were only studied from a synthetic point of view. Owing to the chromophoric nature of the corannulene (and the findings for **CN-9**, *vide supra*) and of the dibenz[*a*,*c*]anthracene, interesting photophysical properties can be expected, including considerable rates of intersystem crossing. The large $\pi$-systems of these chromophores introduce ligand-centered $|S\rangle$ and $|T\rangle$ components that may lead to moderate values for $k_{\mathrm{isc}}$, having the consequence of dual fluorescence and phosphorescence emission. Upon heating a solution of the dibenz[*a*,*c*]anthracene platinum complex **Pt-6a** in toluene to 160 °C, the platinum ion undergoes a 1,4-migration resulting in a different regioisomer of the compound (**Pt-6b**).

Prior to this PhD thesis, Fabian Geist from our research group has published three sets of platinum complexes, which are characterized by a single covalent Pt-C $\sigma$-bond to a thioxanthon-2-yl (Tx),[54] or a 4,4-difluoro-4-bora-3a,4a-diaza-*s*-incacen-8-yl (bodipy, in

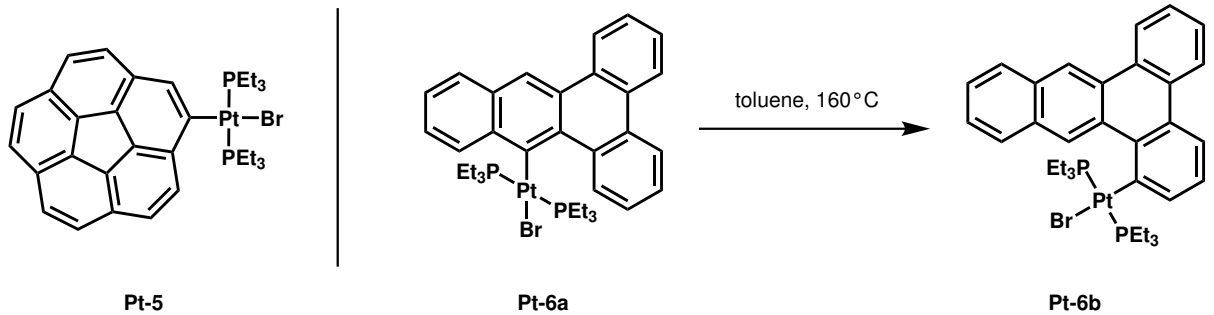


Figure 18: $\sigma$-Aryl Pt complexes by Sharp based on corannulene[52] or on dibenz[*a*,*c*]anthracene.[53] For the latter, the 1,4-Pt migration is displayed.

the following BDP) ligand.[55, 56] The photophysical properties of these compounds will be briefly reviewed. Thioxanthones undergo efficient intersystem crossing because of n$\pi^*$ admixture to the $\pi\pi^*$ transition. This provides sufficient spin-orbit coupling consistent with the rule of El-Sayed. ISC occurs between the $S_1(^1\pi\pi^*)$ and the almost isoenergetic $T_2(^3n\pi^*)$ state.[57] By internal conversion the $T_1(^3\pi\pi^*)$ state is populated, which has a lifetime of *ca.* 100-140 ms. Owing to the long lifetime of the excited triplet state, non-radiative deactivation is highly efficient, rendering the thioxanthone triplet state $T_1$ non-emissive.[57–59] As displayed in Fig. 19, oxdidative addition of Pt into the Br-C bond of **Br-Tx** yields **Pt-7**. Subsequent halogen abstraction with an appropriate silver salt and treatment with the desired anion yielded the series of complexes **Pt-8** to **Pt-10**. All complexes feature the typical thioxanthon-2-yl (Tx) based $\pi\pi^*$ transition at *ca.* 400 nm and 390 nm in their absorption spectra. Absorption bands at higher energies are sensitive to the solvent polarity and have CT character, with overlapping intraligand charge-transfer (ILCT) and metal/ligand-to-ligand' charge-transfer (MLL'CT) components. Excitation of the four complexes at 400 nm results in dual emission at *ca.* 450 and 510 nm. The former emission was insensitive towards molecular oxygen, whereas the latter was. This led to the conlusion that the emissions are fluorescence and phosphorescence from the Tx ligand. The attached platinum ion increases the spin-orbit coupling and, as a consequence, the phosphorescence lifetime is reduced to 2.2 $\mu$s. With increasing $\sigma$-basicity of the ligand X, the phosporescence quantum yield increases for the three halogenido complexes in the order I < CN < Br < Cl from 0.02 for **Pt-10** to 0.19 for **Pt-9**. It was proposed that with an increasing $\sigma$-basicity of the ligand X, the ligand-field splitting also increases. This destabilizes the energy of the non-emissive Pt 5d states with the consequence of making a thermal population from the emissive Tx-centered $^3\pi\pi^*$-states to the Pt 5d states less likely. Closing this radiationless decay channel improves the phosphorescence quantum yield. According to the ordering of the ligands within the spectrochemical

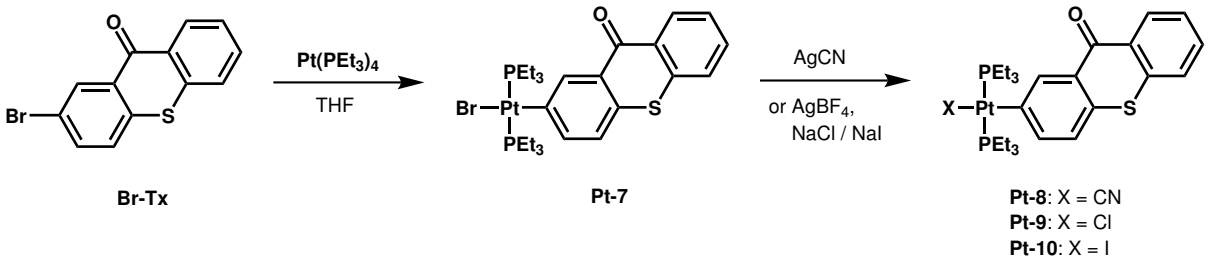


Figure 19: Square-planar platinum(II) complexes of the type *trans*-[$Pt(PEt_3)_2(Tx)(X)$] (X = Br, Cl, I or CN).[54]

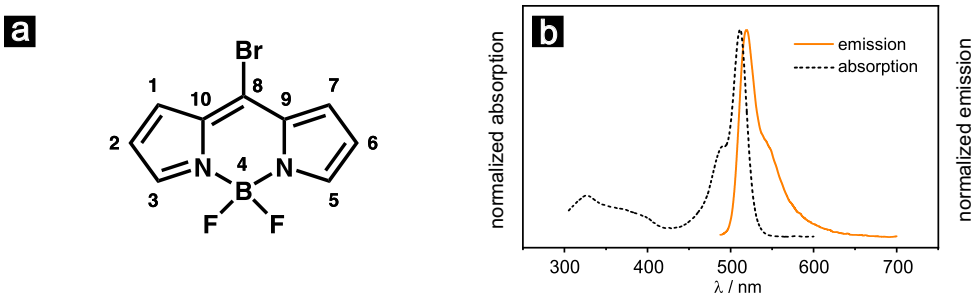


Figure 20: a) Chemical structure of 8-Br-BDP which was first synthesized and published by Leen *et al.*[60] with numbering of the atoms and b) absorption and emission spectra of 8-Br-BDP in $CH_2Cl_2$ solution at r.t.

series, complex **Pt-8** with the strong-field $CN^-$ ligand should exhibit the largest value of $\Phi_p$, which was, however, not observed. Geist *et al.* argue that most probably the high energy of the C≡N-stretching vibration might be a major deactivation channel for the excited triplet state of this compound.[54]

The family of BDP dyes has become very popular among photochemists thanks to their inherently favorable properties such as intense, sharp absorption and emission profiles (Fig. 20b), robustness against photochemical fatigue, chemical stability, rewarding variety and synthetic accessibility.[61–63] The main absorption and emission feature at 508 and 510 nm arise from the singlet $\pi\pi^*$ transition of the chromophore. BDPs have a negliglible rate of ISC, which is dramatically increased upon halogenation of the dye, rendering them efficient photosensitizers.[64–66] Until the work of Fabian Geist from our research group, phosphorescence emission of BDP was only observed with rather moderate phosphorescence quantum yields of up to 3.5% in solution at r.t.(**$Pt_2$-2,6-BDP** in Fig. 10, *vide supra*).[40]

Oxidative addition of 8-Br-BDP to either $Pt(\eta^2{-}C_2H_4)(PEt_3)_2$ or $Pt(\eta^2{-}C_2H_4)(PPh_3)_2$ led to complexes **Pt-11** and **Pt-12**, respectively (see Fig. 21). Spin-orbit coupling implemented by the *cis-*/*trans*-$[PtBr(PR_3)_2]$ fragment linked to the *meso*-position of BDP triggers dual fluorescence and phosphorescence from the BDP based $^1\pi\pi^*$ and $^3\pi\pi^*$ states with a $\Phi_p$ of up to 32%. When comparing the ratio of fluorescence and phosphorescence for the pairs of *cis-* and *trans*-isomers, the proportion of phosphorescence is for both sets larger for the *trans*-complex. Molecular structures from X-ray structure determination showed that the Pt-C8 distance is significantly shorter for the the *trans*-isomer. Since $k_{isc}$ scales with $d^{-6}$ (*vide supra*), the increased phosphorescence quantum yield for **Pt-11b** and **Pt-12b** can be explained by the closer proximity between dye and platinum ion but it is not wholly clear, whether this is the (only) responsible factor. The differences between

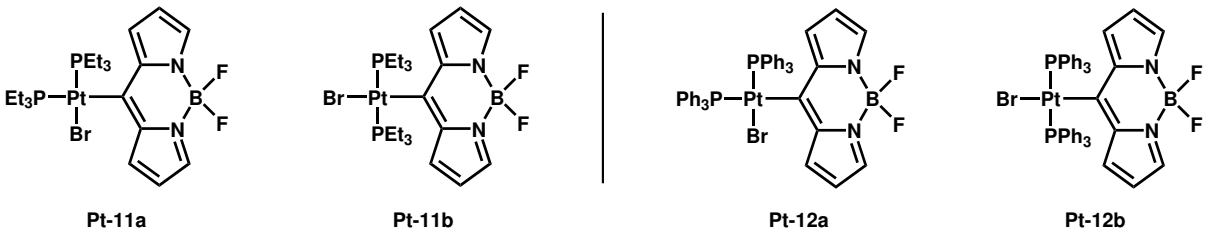


Figure 21: C8/*meso*-platinated BDP complexes *cis*-/*trans*-[Pt(BDP)Br($PEt_3$)$_2$] and *cis*-/*trans*-[Pt(BDP)Br($PPh_3$)$_2$].[55]

$\Phi_p$ of **Pt-11b** and **Pt-12b** might be explicable by the larger ligand-field splitting induced by the stronger donor-ligand $PEt_3$, destabilizing the metal-centered excited states that provide non-radiative deactivation channels.[55]

When the bromido ligand of **Pt-11b** is substituted by 4-ethynyl-1,8-naphthalimide (EtNI) or 8-ethynyl-bodipy (EtB), complexes **EtNPtB** and **KBPtB** are obtained, respectively (see Fig. 22). The dyad **EtNPtB** exhibits, in addition to the prominent BDP $\pi\pi^*$ absorption feature at 470 nm, a broad absorption at $\lambda_{max}$ = 424 nm. Based on time-dependent density functional theory (TD-DFT) assignments, the latter is due to a mixture of EtNI $\pi\pi^*$ and EtNI-to-BDP CT contributions. **KBPtB** has absorption bands at $\lambda_{max}$ = 550, 470 and 390 nm, which were assigned as the KB (alkylated BDP) $\pi\pi^*$, the BDP $\pi\pi^*$ and a BDP-to-KB CT features. Both dyads display dual fluorescence and phosphorescence emission from the dye ligand with the lowest energy absorption band. When the panchromatic absorbers are excited into one of the higher energy transitions, the excitation energy is funneled by efficient energy transfer (ET) to the BDP with the lowest absorption energy rendering the second dye an antenna. The phosphorescence quantum yield of **EtNPtB** of 41% exceeds that of **Pt-11b**.[56]

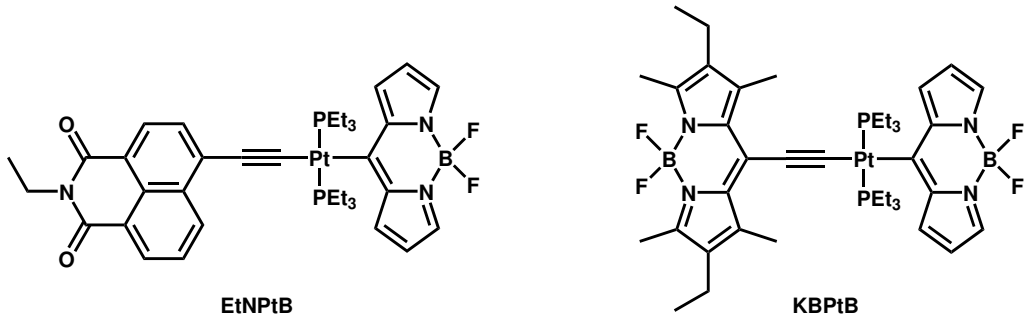


Figure 22: $\sigma$-Aryl-BDP complexes with acetylide linked dyes.[56]

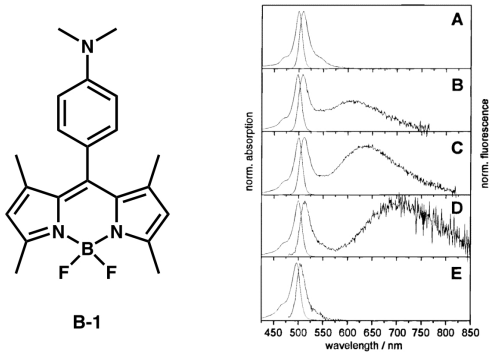


Figure 23: Dimethylaniline-BDP and its solvent polarity-dependent emission spectra in a) $Et_2O$, b) 1,4-dioxane, c) THF, and e) MeCN. Emission spectra are reprinted with permission from reference [67]. © (1998) American Chemical Society.

Besides the above discussed heavy-atom-based spin-orbit coupling, heavy-atom free donor-acceptor based BDP-dyads were recently proven to possess accessible excited triplet states. Prominent examples are discussed in the following. In 1998 Daub and coworkers[67] have published a dimethylaniline-subsituted BDP that shows in unpolar solvents only $\pi\pi^*$-based fluorescence (Fig. 23a). When the solvent polarity is increased, a second emission is observed. The latter is solvatochromic and hence is CT in character (Fig. 23b-d). In highly polar solvents such as MeCN the CT emission vanishes (Fig. 23e). Most interestingly, the overall quantum yield decreases when solvents with higher polarity are used. The authors reasoned cautiously for an increase of $k_{\mathrm{isc}}$ and the population of a triplet state.[67] In 2018, Zhang and coworkers have looked into this issue with greater detail and found that in solvents of medium polarity charge-recombination of the charge transfer state promotes intersystem crossing and forms the BDP-centered $^3\pi\pi^*$ excited state. This excited triplet state could be used for the formation of singlet-oxygen.[68]

Efficient intersystem crossing has also been observed for a large variety of donor-acceptor-based BDP dyads where a second dye was attached to the *meso*-position C8 of the BDP dye. Many of these are orthogonally linked BDP dimers.[18, 69–79] In the following, two examples will be discussed that illustrate the mechanism of the ISC in such dyads.

In 2017, Filatov *et al.*[78] as well as Zhang *et al.*[77] have independently published studies on BDP-anthracene dyads (Fig. 24). In these systems the polycyclic aromatic hydrocarbon is attached to the *meso*-position of the BDP chromophore and acts as an electron-donor that transfers an electron to the electron-accepting BDP. Exceptionally high quantum yields for the generation of singlet oxygen were found for the systems of Zhang. For the dyads by Filatov, the methyl-substituted anthracene reacts with singlet oxygen forming

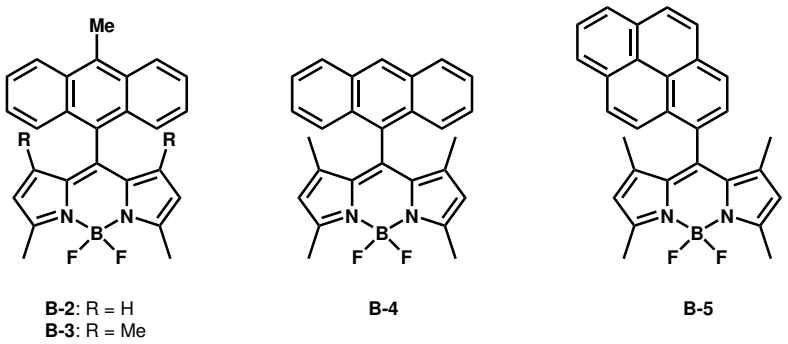


Figure 24: BDP-dyads reported by Senge[78] and Zhang.[77]

highly fluorescent endoperoxides. The mechanism of charge transfer-promoted intersystem crossing in these dyad systems was studied by both research groups in great detail, including TA spectroscopy. The deduced sequence of events following primary excitation of the anthracene $\pi\pi^*$ band (Eq. 5) is provided by Eq. 6-8b.

Formation of the anthracene singlet excited state

$$S_0(\text{Ant}) + h\nu \longrightarrow S_1(\text{Ant}^*) \tag{5}$$

Energy transfer

$$S_1(\text{Ant}^*) \longrightarrow S_1(\text{BDP}^*) \tag{6}$$

Electron transfer

$$S_1(\text{BDP}^*) \longrightarrow \text{CT}(\text{BDP}^- + \text{Ant}^+) \tag{7}$$

Charge recombination

$$\text{CT}(\text{BDP}^- + \text{Ant}^+) \longrightarrow T_1(\text{BDP}^*) \tag{8a}$$

Charge recombination

$$\text{CT}(\text{BDP}^- + \text{Ant}^+) \longrightarrow T_1(\text{Ant}^*) \tag{8b}$$

Upon exciting the anthracene (Ant), which has the highest-energy absorption, fast energy transfer to the BDP occurs. Subsequent photoinduced electron transfer generates a charge transfer state with a radical ion pair, consisting of an anthracene radical cation ($\text{Ant}^{\bullet+}$) and a BDP radical anion ($\text{BDP}^{\bullet-}$). The CT state undergoes recombination and populates the triplet state of either Ant or BDP. In a detailed follow-up study Filatov *et al.* have reported on a variety of BDP-anthracene dyads, as depicted in Fig. 25. Here the BDP

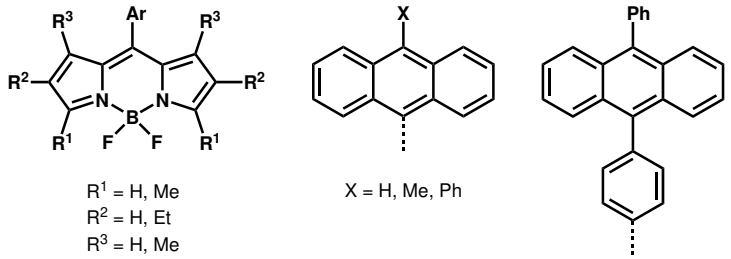


Figure 25: BDP-anthracene dyads studied by Senge and coworkers.[79]

moiety is modified by the introduction of alkyl substituents at different positions of the BDP dye. The anthracene is attached either directly or via a phenylene spacer to the *meso*-position of the BDP. The essence of this study is that the intersystem crossing takes place from the CT state. Efficient ISC accompanying the $S^{CT} \longrightarrow T^{CT}$ transition relies on an orthogonal orientation of the donor and the BDP acceptor subunits. Separation by a phenyl ring has the same consequence as the lack of methyl-substituents in the 1- and 7-positions of the BDP ($R^3$ in Fig. 25), namely allowing for rotation of the Ant donor around the Ant-C8 bond. This increases the singlet-triplet energy gap and hence results in negligible ISC for such dyads. For the compounds with a non-alkylated BDP-core high triplet-state and singlet oxygen quantum yields were observed in unpolar solvents. Alkylation of the BDP destabilized the CT state and, in consequence, the triplet state is populated with higher yields in polar solvents. Interestingly, no phosphorescence emission of any donor-acceptor based BDP-dyad has been observed.[18, 69–79]

In summary, phosphorescence and population of the underlying triplet state are not phenomena that can only be observed in solids, as Jabłoński and his contemporaries thought. Modern photophysics shows that the efficient population of the triplet state depends on a complex interplay of electronic and structural factors as well as the solvent environment. The following statements apply here and summarize the experimental findings discussed above:

i. The 'internal' heavy-atom effect constitutes the most efficient mechanism for promoting spin-orbit coupling (SOC). The larger the MLCT character of either singlet or triplet state, the larger is the SOC integral. It is crucial that the singlet ($^1$d$\pi^*$) and triplet ($^3$d'$\pi^*$) states involved in the ISC do not have exactly the same orbital character or have different d-orbital contributions (d $\neq$ d'). Otherwise, there exists an only negligible one-center SOC. This is analogous to the rule of El-Sayed.[15]

ii. In the absence of any significant 'internal' heavy-atom effect, SOC can also be promoted by the 'external' heavy-atom effect. Heavy transition metal elements have large one-electron SOC constants for their d electrons and are therefore able to promote intersystem crossing by the remote heavy-atom effect.

iii. A myriad of transition metal complexes have very similar orbital character for the $S_1$ and $T_1$ states and therefore have negligible SOC and, hence, a low $k_{isc}$. In consequence the intersystem crossing rate constant can be substanitially increased when the molecule is excited in a higher singlet state $S_n$ (n > 1) with a different orbital character. More efficient ISC channels for populating a higher lying triplet state $T_m$ (m > 1) may then exist. This leads to an excitation energy-dependent emission spectrum; in dually emissive systems an excitation wavelength-dependent ratio of fluorescence and phosphorescence is observed.[15]

iv. When regarding transition metals of the same group, the one-electron SOC increases for the elements with higher atomic numbers and a larger 'external heavy-atom effect' can be obtained. In parallel, the d-orbital contraction leads to a smaller contribution of the metal centered orbitals to electronic transitions and, in consequence, the influence of the 'internal heavy-atom effect' decreases.[15]

v. When the 'external heavy-atom effect' is to be employed for promoting ISC, the distance between the heavy-atom and the center of the chromophore has to be small, since $k_{isc}$ scales with $d^{-6}$.

vi. Heavy-atom-free BDP-systems can undergo fairly efficient intersystem crossing when they have a donor-acceptor type architecture. Then the charge transfer is pivotal in promoting the triplet state population. In such systems the donor and acceptor unit have to be in an orthogonal orientation in order to induce a small singlet-triplet gap, which favors ISC. In addition, the polarity of the solvent plays a crucial role since polar solvents stabilize the charge-separated state.

# 4 Objectives

Because the *meso*-platinated BDP complex *trans*-Pt(BDP)Br($PEt_3$)$_2$ showed exceptionally high phosphorescence quantum yields of up to 31 % in solution at r.t., the aim of the fist research project was to elucidate how the identity and the $\sigma$-*trans*-influence of the anionic ligand X coordinated to the platinum ion (see Fig. 26) affects the photophysical properties and, if possible, to enhance the phosphorescence efficiency. TD-DFT calculations have shown that absorption bands at higher energies have substantial MLCT contributions. When exciting into these high energy absorption bands, the rate of ISC should be increased due to a more pronounced 'internal heavy-atom effect' in addition to the 'external' one that applies also for the $S_1$ transition. The ratio of fluorescence and phosphorescence emissions should therefore change in favour of the phosphorescence when exciting into $S_n$ (n > 1). The performance of these new Pt-BDP complexes as one-component oxygen sensors and their photocatalytic activities in terms of singlet oxygen generation should also be tested.

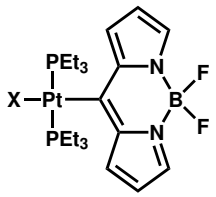


X = Cl, I, $NO_2$, NCS, $CH_3$

Figure 26: *Meso*-coordinated *trans*-Pt(BDP)($PEt_3$)$_2$X complexes.

The orbital overlap between the $\pi$-orbitals of the BDP-ligand and the platinum-centered d-orbitals is weak when the BDP ligand is coordinated via C8, at its *meso*-position. The working hypothesis for the second research project was that the coordination of the platinum ion to C2 or C3 of the BDP dye should change the coupling of the metal-centered orbitals with the ligand-centered orbitals. The same applies to the absorption and emission wavelengths, as these positions contribute differently to the ground and excited states of the complexes. As a consequence, the absorption and emission properties as well as the photocatalytic activities should significantly differ from the C8-coordinated complexes. The presence of alkyl substituents at the BDPs should also change the photophysical properties of the complexes under consideration. Changing from a phenyl- to a mesityl-substituent was expected to increase the phosphorescence quantum yield because of lesser freedom for aryl rotation around the aryl-C8 bond. Spectroscopic and computational

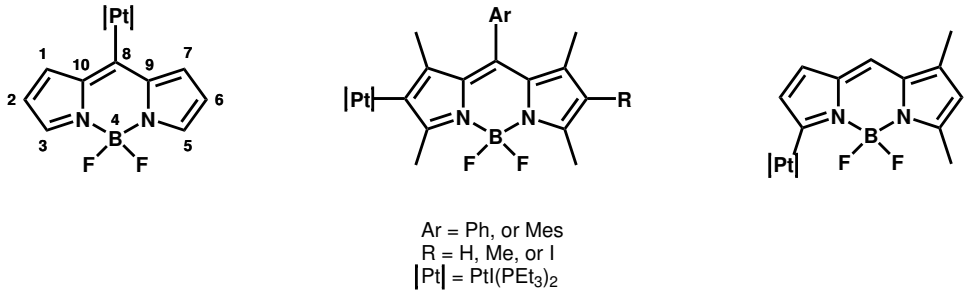


Figure 27: Target complexes of the second project with platination and different degrees of alkylation at positions C2, C3 and C8 of the BDP dye.

data should be correlated to electrochemical data in order to get deeper insights into the electronic structures of the respective compounds.

The third research project dealt with panchromatic absorbers. Heavy-atom free BDP-dyads having a pronounced donor-acceptor character have been shown to allow for an

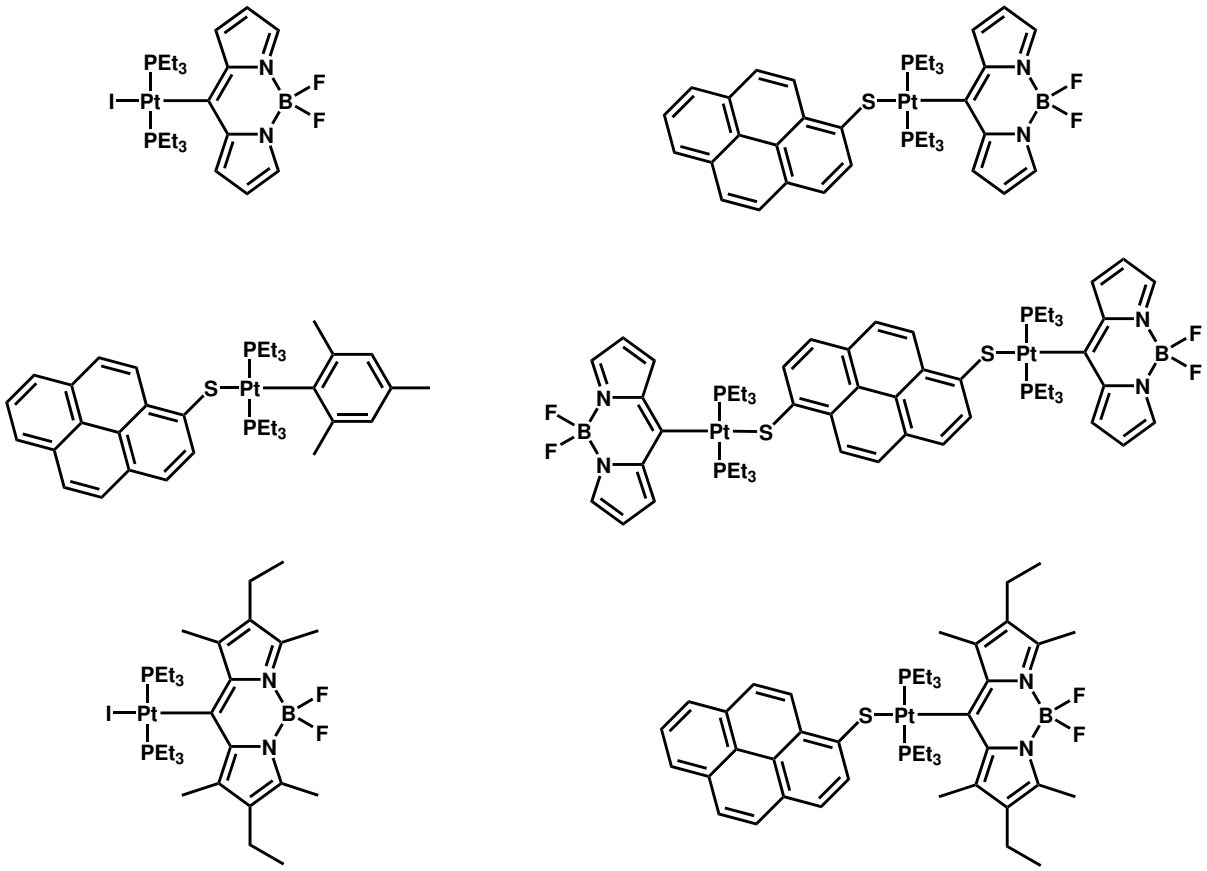

Figure 28: Pt(BDP)(mercaptopyrene) dyads and reference compounds of the third research project.

efficient triplet-state population. However, no phosphorescence was observed from either BDP-centered or CT states.[18, 69–79] In the work of Fabian Geist, $\sigma$-BDP Pt complexes with alkynyl-linked chromophores have proven to act as dyads with broadband light absorption that efficiently transferred the absorbed energy to the dye ligand with the lowest triplet energy. These systems have, however, be proven to be photolabile due to the placement of two $\sigma$-carbyl ligands with a strong $\sigma$-*trans* influence *trans* to each other, thus weakening the Pt-C(BDP) $\sigma$-bond. The hope was that *S*-bonded mercaptopyrenes would form more stable complexes. The complex excited-state interplay of the two chromophores in the coordination sphere of the platinum ion should be decoded with the help of reference complexes that bear either the marcaptopyrene- or the BDP-ligand as well as by changing the excited state energies of either dye ligand by alkylation of the bodipy or coordinating two Pt(BDP)-moieties to a dimercapto-substituted pyrene. Detailed insight into the energy cascade of the dyad system should be obtained with the help of transient absorption spectroscopy. Another goal was to assay the new dyads for their efficiency for the photocatalytic generation of singlet oxygen.

# 5 Publications

## 5.1 Record of Contributions

The first publication included as Chapter 5.2 has been published in *Dalton Transactions* **2016**, *45*, 10420-10434 (DOI: 10.1039/c6dt01623e). All syntheses and spectroscopic characterizations of the presented Pt-BDP complexes as well as the DFT-, TD-DFT calculations and the photocatalytic experiments have been performed by myself. The acquisitions and refinement of the crystallographic data was performed by Berhard Weibert and Dr. Fabian Geist. The manuscript for publication was written by Prof. Dr. Rainer Winter and myself.

Chapter 5.3 is the second publication of this dissertation. It was published in *Organometallics* **2018**, *37*, 235-253 (DOI: 10.1021/acs.organomet.7b00806). My contribution to this work included, beyond the synthesis and spectroscopic characterization of the complexes, their electrochemical characterization and the photocatalytic studies as well as the computational analysis of the reported complexes. X-ray crystallographic determination of molecular structures and the refinement of the data was conducted by Bernhard Weibert and Dr. Michael Linseis. Prof. Dr. Rainer Winter and myself have written the manuscript for publication together.

Publication number three can be found in Chapter 5.4 and was published in *Dalton Transactions* **2019**, *48*, 1171-1174 (DOI: 10.1039/c8dt04823a). The synthesis and parts of the spectroscopic characterization of the reported Pt(Bodipy)$(PEt_3)_2$(S-Pyrene) dyad were a substantial part of the Bachelor Thesis of Franciska S. Gogesch under my supervision. I synthesized the reference compounds and performed the electrochemical characterization as well as the quantum chemical calculations. Transient absorption spectroscopy was kindly performed by Christopher B. Larsen in the laboratories of Oliver S. Wenger at the University of Basel. The manuscript for publication was written by Prof. Dr. Rainer Winter and myself and reviewed by Christopher B. Larsen and Prof. Oliver S. Wenger prior to submission.

Chapter 5.5 includes the fourth publication within the frame of this dissertation. The paper was published in *Dalton Transactions* and can be found under the DOI 10.1039/c9dt01737b. Synthetic work leading to this publication was performed in parts during an internship by André Mang under my supervision and by myself. I performed the spectroscopic and electrochemical characterizations as well as the DFT and TD-DFT calculations. Transient absorption spectroscopy was performed by Christopher B. Larsen in the laboratories of Prof. Oliver S. Wenger at the University of Basel. X-ray

diffraction analysis for this work was carried out by Bernhard Weibert and the refinement of the data was kindly performed by Dr. Michael Bodensteiner at the Universität Regensburg. Prof. Dr. Rainer Winter and myself have written the manuscript for this paper and Christopher B. Larsen and Prof. Oliver S. Wenger have reviewed the manuscript prior to submission.

## 5.2 Complexes *trans*-Pt(Bodipy)X($PEt_3$)$_2$: Excitation Energy-Dependent Fluorescence and Phosphorescence Emissions, Oxygen Sensing and Photocatalysis

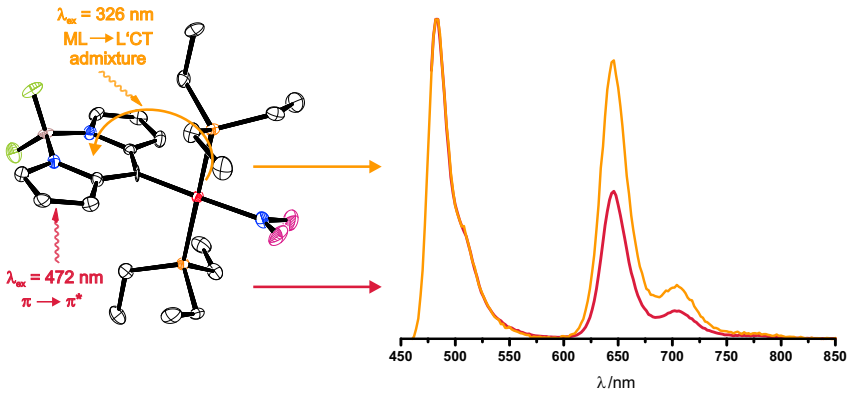


*Dalton Transactions* **2016**, *45*, 10420-10434 (DOI: 10.1039/c6dt01623e).
Published by The Royal Society of Chemistry.

Dalton Transactions

PAPER

View Article Online
View Journal | View Issue



Cite this: *Dalton Trans.*, 2016, **45**, 10420

# Complexes *trans*-Pt(BODIPY)X($PEt_3$)$_2$: excitation energy-dependent fluorescence and phosphorescence emissions, oxygen sensing and photocatalysis†

Peter Irmler and Rainer F. Winter*

Received 26th April 2016,
Accepted 24th May 2016

DOI: 10.1039/c6dt01623e

www.rsc.org/dalton

We report on five new complexes with the general formula *trans*-Pt(BODIPY)X($PEt_3$)$_2$ (**Pt–X**), where the platinum(II) ion is σ-bonded to a 4,4-difluoro-4-bora-3a,4a-diaza-*s*-indacen-8-yl (BODIPY) and an anionic ligand $X^-$ ($X^-$ = $Cl^-$, $I^-$, $NO_2^-$, $NCS^-$, $CH_3^-$). All five complexes were characterized by multinuclear NMR, electronic absorption and luminescence spectroscopy and by X-ray diffraction analysis. Four of these complexes show efficient intersystem crossing (ISC) from an excited singlet state to a BODIPY-centred $T_1$ state and exhibit dual fluorescence and phosphorescence emission from the BODIPY ligand. In **Pt–I**, the fluorescence is almost completely quenched, whereas the phosphorescence quantum yield reaches a value of 40%. The rate of ISC and the ratio of phosphorescence to fluorescence emissions depend on the excitation wavelength (*i.e.* on which specific transition is excited). The performance of these complexes as one-component oxygen sensors and their photocatalytic activities were tested by Stern–Volmer quenching experiments and by monitoring the oxidation of 1,5-dihydroxynaphthalene with $^1O_2$ generated from the long-lived triplet state of the sensitizer by triplet–triplet annihilation with $^3O_2$. Exceptionally high $^1O_2$ generation quantum yields of up to near unity were obtained.



## Introduction

4,4-Difluoro-4-bora-3a,4a-diaza-*s*-indacene (BODIPY) dyes have been known for three decades for their excellent performances as fluorophores, their versatility and their chemical and photochemical robustness.[1–10] A particularly favourable asset of the BODIPY family of dyes is their modular construction from readily available building blocks, thus allowing for easy implementation of desirable properties or functionalities, *e.g.* for substrate binding, with important implications in the analytical sciences, or fine-tuning of the absorption and emission wavelengths.[3,11,12] Phosphorescence from BODIPY dyes has, however, only rarely been observed and usually relies on the heavy atom effect of bromine or iodine substituents.[13–16] In particular, there are only a handful of phosphorescent metal–organic BODIPY derivatives, and until very recently, the phosphorescence quantum yields of such compounds did not exceed the rather modest value of 3.5%.[17] In these complexes, the BODIPY dye(s) are either appended to a 2,2′-bipyridine ligand as in **Ru–BDP** or **Ir–BDP** or bonded to Pt(N^C^N) entities with cyclometalating bis(benzimidazol-2-yl)phenyl-derived ligands as in **$Pt_2$–BDP**, Fig. 1.[3,14,17–19] Much higher quantum yields of up to 31% for the $PEt_3$ derivative **Pt–Br** (Fig. 1) were achieved in complexes *trans*-Pt(BODIPY)Br($PR_3$)$_2$ (R = Ph, Et) featuring a σ-bonded 4,4-difluoro-4-bora-3a,4a-diaza-*s*-indacenyl dye, which connects to the platinum(II) ion *via* its *meso* position.[20] In the latter complexes, the Pt coordination centre acts as a remote heavy metal ion, as the HOMO and the LUMO are heavily biased to the BODIPY ligand and receive only very minor contributions from the coordination centre. As a consequence, the relevant excitation is adequately described as a BODIPY-based π → π* transition with essentially no charge-transfer contributions from the {PtBr($PR_3$)$_2$} fragment. Long-lived excited triplet states of BODIPY dyes are of great interest for applications such as chemical sensing,[16,21,22] triplet–triplet

*Fachbereich Chemie der Universität Konstanz, Universitätsstraße 10, D-78464 Konstanz, Germany. E-mail: rainer.winter@uni-konstanz.de*

†Electronic supplementary information (ESI) available: Multinuclear NMR spectra of the complexes, packing diagrams with short interatomic contacts, absorption, emission and excitation spectra recorded at different excitation wavelengths, figures displaying oxygen quenching of the phosphorescence emission, changes of the absorption spectra of DHN in the presence of catalytic amounts of MB or **Pt-I** and plots showing the absence of the reaction in the dark; table with the cell parameters and structure refinement data for the complexes; atomic positions for the geometry-optimized structures in the $S_0$ and the $T_1$ states and comparison with the experimental structure parameters. CCDC 1474955–1474959. For ESI and crystallographic data in CIF or other electronic format see DOI: 10.1039/c6dt01623e

 

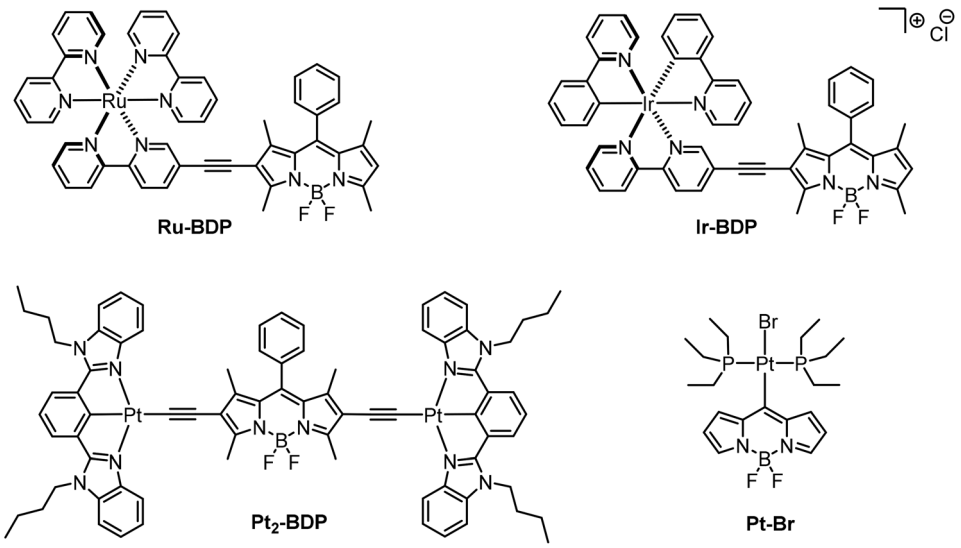


Fig. 1 Molecular structures of room-temperature phosphorescent BODIPY complexes **Ru–BDP**, **Ir–BDP**, **$Pt_2$–BDP** and **Pt–Br**.

annhilation-based upconversion[17–19,23] and photodynamic therapy.[13,15,24,25] For photodynamic therapy the ability of triplet emitters to transform triplet oxygen ($^3O_2$) to singlet oxygen ($^1O_2$) in a triplet–triplet annihilation process is of pivotal relevance. Its cell toxicity makes the highly reactive $^1O_2$ molecule a powerful weapon against cancer cells.[26–29]

The different structural and electronic influences of a transition metal coligand entity on the photophysical properties of complexes, particularly the phosphorescence quantum yield $\Phi_{Ph}$, are not trivial, though. Decisive factors are the rate constant of the intersystem crossing ($k_{ISC}$), the ratio of the radiative and non-radiative decay rates, and the thermal accessibility of excited d-states, which typically provide non-radiative deactivation pathways.[30] In the case of square-planar Pt(II) complexes, the relative positioning of the $d_z^2$ orbital with respect to the emissive $T_1$ state is often of crucial relevance.[31] This energy separation largely depends on the ligand-field splitting. Thus, by introducing strong-field ligands, the $d_z^2$ orbital can be pushed to higher energy, increasing the energy barrier for non-radiative decay *via* excited d-states.[30–33] In complexes of the type *trans*-Pt(Dye)X($PR_3$)$_2$ ($X^-$ = $Br^-$, $Cl^-$, $I^-$ or $CN^-$), where Dye represents a σ-bonded thioxanthonyl or a BODIPY attached *via* its *meso* position, the ligand-field splitting can be modulated by the $PR_3$ ligand and the anionic ligand $X^-$.[34] Our previous study has already shown that $PEt_3$ ligands endow the BODIPY complexes with superior photophysical properties when compared to their $PPh_3$ counterparts.[20] Here we report our results on five new BODIPY complexes *trans*-Pt(BODIPY)X($PEt_3$)$_2$ with anionic ligands $X^-$ that cover a wider range of the spectrochemical series and differ with respect to their *trans*-influence[35] and the results of our investigations into the performance of some representatives as one-component triplet sensors and sensitizers for the photocatalytic oxidation of 1,5-dihydroxynaphthalene (DHN) with molecular oxygen.

# Results and discussion

### Synthesis and NMR spectroscopy

All complexes were synthesized starting from *cis*-Pt($\eta^2$-$C_2H_4$)($PEt_3$)$_2$, which is obtained by heating *cis*-Pt(Et)$_2$($PEt_3$)$_2$ in $C_6D_6$ for 45 min to 114 °C.[36] Oxidative addition of 8-bromo-4,4-difluoro-4-bora-3a,4a-diaza-*s*-indacene (**Br–BODIPY**, see Fig. 2) to the reactive $Pt^0$-species is fast at room temperature (r.t.). The resulting complex *cis*-Pt(BODIPY)Br($PEt_3$)$_2$ is then transformed by AgOTf to *trans*-Pt(BODIPY)(OTf)($PEt_3$)$_2$. Subsequent treatment with NaX ($X^-$ = $Cl^-$, $NO_2^-$, $NCS^-$) resulted in the replacement of the weakly coordinated $OTf^-$ by the respective counter ion and provided complexes **Pt–Cl**, **Pt–$NO_2$** and **Pt–NCS** (see Fig. 2) in moderate to good yields. Our attempts to introduce a methyl ligand by transmetalation using the Grignard reagent MeMgI failed and the complex *trans*-Pt(BODIPY)I($PEt_3$)$_2$ (**Pt–I**) was formed instead. The use of $MgMe_2$ as a transmetalating agent was likewise unsuccessful. Reaction of **Pt–OTf** with MeLi finally afforded **Pt–$CH_3$** (Fig. 2).

$^{195}$Pt NMR spectra of the *trans*-complexes show a triplet with a coupling constant $J_{PtP}$ in the range of 2692 Hz to 2450 Hz. Correspondingly, the $^{31}$P NMR spectra give a singlet for the two *trans*-disposed P donors, which is flanked by the $^{195}$Pt satellite doublet with the same $J_{PtP}$ coupling constant. The formation of a direct Pt–C σ-bond is confirmed by the observation of platinum satellites in the $^{13}$C NMR spectra, which range from 492 Hz to 409 Hz for $J_{PtC}$ and from 25 Hz to 17 Hz for $^2J_{PtC}$ and $^3J_{PtC}$ couplings, respectively. Some couplings could, however, not be detected due to a low signal-to-noise ratio. The NMR spectra can be found in the ESI, Fig. S1–S23.†

### Single crystal X-ray diffraction

Single crystals suitable for X-ray diffraction analysis were obtained for all five Pt complexes. Fig. 3 displays the ORTEP representations of their molecular structures. Relevant bond

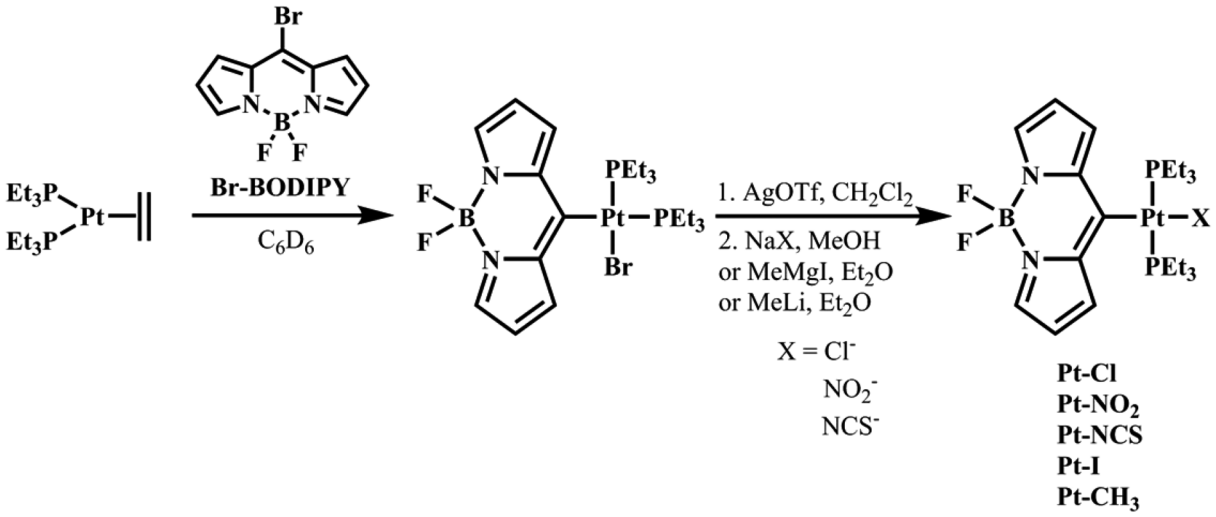


**Fig. 2** Synthesis of the complexes **Pt–X**.

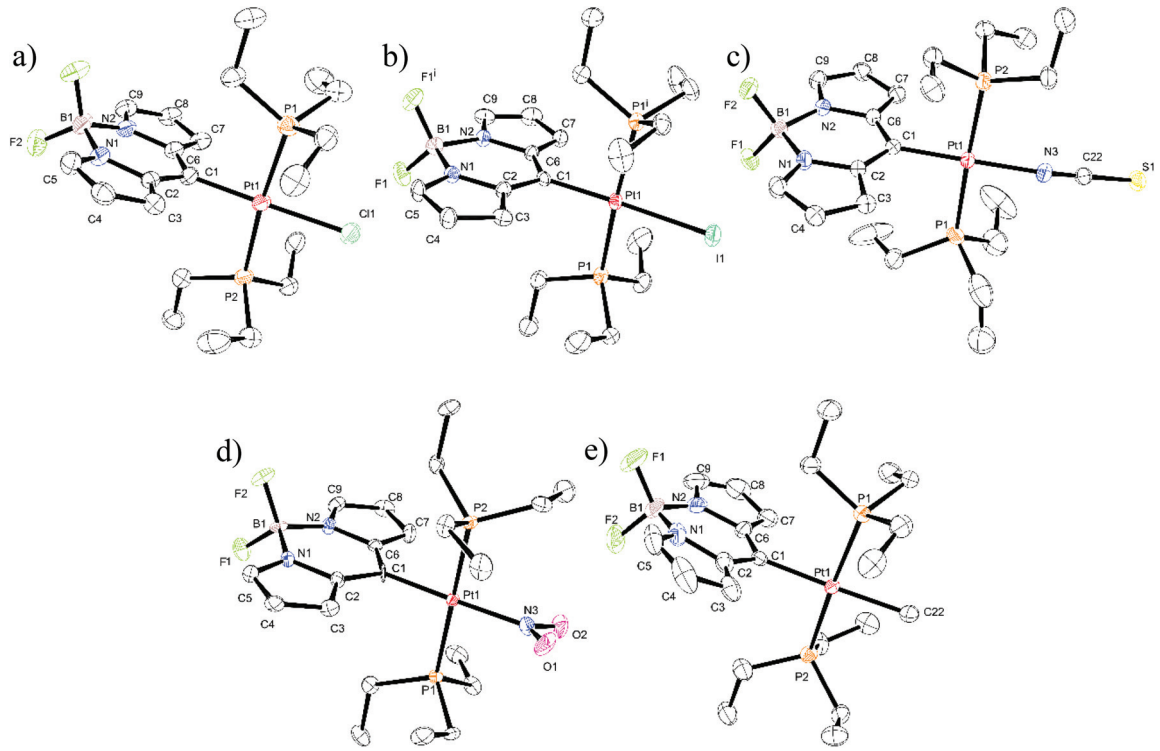


**Fig. 3** ORTEP representations of the molecular structures of (a) **Pt–Cl**, (b) **Pt–I**, (c) **Pt–NCS**, (d) **$Pt–NO_2$**, and (e) **$Pt–CH_3$**. For **Pt–Cl** and **$Pt–CH_3$** only one of the independent molecules per unit cell are shown. The ellipsoids are drawn at a 40% probability level. Hydrogen atoms are omitted for reasons of clarity. Atom C1 of **$Pt–NO_2$** remained isotropic and could not be refined further.

lengths and angles can be taken from Table 1, and Table S1 of the ESI† summarizes the crystal and refinement data. **Pt–Cl**, **Pt–NCS**, **$Pt–NO_2$** and **$Pt–CH_3$** crystallize in the monoclinic space groups $P2_1/c$, $P2_1/n$, $P2_1/c$, or $P2_1$, respectively. The single crystal of **Pt–I** complies with the symmetry operations of the $Cmc2_1$ space group in the orthorhombic crystal system. The unit cells of **Pt–Cl** and **$Pt–CH_3$** contain two independent molecules with different sets of bond lengths and angles as given in Table 1.

In the present series of complexes the length of the C1–Pt σ-bond provides a measure for the *trans*-influence and consequently for the σ-donor strength of the anionic ligand $X^-$,[35] which increases in the order **$Pt–NO_2$** < **Pt–Cl** ≈ **Pt–Br** < **Pt–I** ≈ **Pt–NCS** < **$Pt–CH_3$**. This ordering complies with that of a

 

Table 1 Selected bond lengths [Å] and bond angles [°] of the complexes *trans*-Pt(BODIPY)X($PEt_3$)$_2$ (**Pt–X**) and of **Pt–Br**[20]

| | **Pt–Br** | | **Pt–Cl** | | **Pt–I** | **Pt–NCS** | **Pt–$NO_2$** | **Pt–$CH_3$** | |
|---|---|---|---|---|---|---|---|---|---|
| | Molecule 1 | Molecule 2 | Molecule 1 | Molecule 2 | | | | Molecule 1 | Molecule 2 |
| Bond lengths/Å | | | | | | | | | |
| C1—Pt1 | 1.984(10) | 1.964(11) | 1.976(7) | 1.971(8) | 1.994(10) | 1.984(4) | 1.956(9)[c] | 2.039(11) | 2.053(12) |
| X—Pt1[a] | 2.4973(12) | 2.5118(12) | 2.3750(19) | 2.385(2) | 2.6689(8) | 2.048(4) | 2.019(8) | 2.127(12) | 2.137(11) |
| P1—Pt1 | 2.315(3) | 2.320(3) | 2.319(2) | 2.316(2) | 2.3206(15) | 2.3135(13) | 2.329(2) | 2.299(3) | 2.304(3) |
| P2—Pt1 | 2.327(3) | 2.324(3) | 2.309(2) | 2.310(2) | 2.3206(15)[b] | 2.3249(11) | 2.334(2) | 2.290(3) | 2.285(3) |
| Bond angles/° | | | | | | | | | |
| C1–Pt1–P1 | 93.7(3) | 92.9(3) | 91.2(2) | 91.6(2) | 91.37(7) | 91.44(12) | 92.3(3) [c] | 91.3(3) | 90.7(3) |
| C1–Pt1–P2 | 91.3(3) | 90.5(3) | 94.0(2) | 93.0(2) | 91.37(7)[b] | 90.79(12) | 89.3(3) [c] | 91.9(3) | 92.7(3) |
| P1–Pt1–X[a] | 87.73(8) | 88.41(8) | 87.13(7) | 87.68(8) | 88.71(7) | 87.28(12) | 88.6(2) | 86.3(3) | 86.7(3) |
| P2–Pt1–X[a] | 87.28(8) | 88.16(8) | 87.61(7) | 87.76(8) | 88.71(7)[b] | 90.62(11) | 90.0(2) | 90.5(3) | 89.9(3) |
| P1–Pt1–P2 | 175.01(11) | 176.02(11) | 174.74(8) | 175.00(7) | 176.8(3) | 177.17(5) | 173.83(8) | 176.05(12) | 176.57(12) |
| C1–Pt1–X[a] | 178.6(3) | 178.6(3) | 178.3(2) | 179.0(2) | 176.03(8) | 175.77(17) | 178.2(4)[c] | 177.6(4) | 177.2(5) |

[a] X represents the donor atom of the anionic ligand in *trans*-position to the dye at the Pt ion. [b] The molecule has a mirror plane which is defined by the plane of the dye's inner heterocycle. [c] Atom C1 could not be refined anisotropically.

related series of platinum complexes with a σ-bonded perylene or perylene monoimide dye.[37] For **Pt–$CH_3$** the difference between the Pt–C bond lengths to the methyl (2.127(12) or 2.137(11) Å) and the BODIPY ligands (2.039(11) or 2.053(12) Å for the two independent molecules of the unit cell) reflects the difference of the covalent radii of a $sp^3$ and a $sp^2$ carbon atom. Similar differences have *e.g.* been observed for *trans*-Pt($CH_3$)(Ph)($PPh_3$)$_2$ $d$(Pt–$CH_3$) = 2.226(4) Å, $d$(Pt–Ph = 2.058(4) Å).[38] The Pt–Me bond of **Pt–$CH_3$** is expectedly longer than in complexes *trans*-Pt($CH_3$)Cl($PR_3$)$_2$ owing to the opposite placement of two σ-carbyl ligands, which both exert a strong σ-*trans*-influence (*cf.* 2.08(1) Å for R = Ph or 2.069(8) Å for R = $C_6H_4$F-4).[39,40]

With deviations of 2.8° to 6.2° for the angle P1–Pt–P2 and 1.0° to 4.2° for bond angle C1–Pt–X (X = donor atom of the anionic ligand) and a maximum deviation of 4.0° for *cis*-angles X–Pt–P and C1–Pt–P from the ideal values and a coplanarity of all donor atoms with the Pt(II) ion the coordination centre exhibits a close to ideal square planar coordination geometry. This is also indicated by the summations of bond angles at the Pt(II) ion, which range from 359.94° to 360.20°. The P1–Pt–P2 angle opens to the side of the sterically demanding BODIPY ligand.

The various steric and electronic influences of a $PtL_3$ fragment for tipping the scale towards either κ*N* or κ*S* coordination of a thiocyanate ligand are textbook examples for the phenomenon of coordination isomerism.[41,42] *N* coordination in spite of the soft character of the {Pt(BODIPY)($PEt_3$)$_2$} fragment is here favoured by the strong *trans*-influence of the opposite carbyl ligand, the light donor atom, and by steric effects. Thus, *N* coordination maintains a near coincidence of the $NCS^-$ axis with the C1–Pt–N vector Pt–N3–C22 = 162.2(4)°, S1–C22–N3 = 179.7(4)°, thus avoiding unfavourable steric interactions with the *cis*-disposed $PEt_3$ ligands (Fig. 3c). *N* coordination of the $NCS^-$ ligand has likewise been observed in the related perylene complex of Espinet and coworkers.[37]

Packing diagrams of individual molecules in the crystal lattice are shown in Fig. S24–S28 of the ESI.† All structures exhibit several short intermolecular contacts. Most prevalent are hydrogen bonding interactions H···F–B between pyrrolic or methyl protons and the $BF_2^-$ fluorine atoms. These latter contacts are in the range of 2.330 to 2.539 Å, which is by 0.330 to 0.131 Å shorter than the sum of the van der Waals radii. Most notably, H···F contacts to methyl hydrogens of the $PEt_3$ ligands are frequently shorter than those to the hydrogen atoms attached to the heterocycles. These hydrogen bonds are sometimes augmented by C–H···π interactions between methyl protons and a pyrrolic carbon atom ranging from 2.634 to 2.757 Å. In several cases, additional contacts exist between pyrrolic or methyl protons and heteroatoms of the anionic ligand $X^-$, most importantly to the oxygen atoms of the nitrite ligand of **Pt–$NO_2$** (2.378 to 2.487 Å with the shorter contacts again to $PEt_3$ methyl protons), the S atom of the κ*N*-thiocyanate ligand in **Pt–NCS** (2.842 and 2.921 Å) or, very weakly, to the $I^-$ ligand in **Pt–I** (3.127 Å). The latter complex exhibits an interesting brick-wall packing in the *ac* plane, where individual molecules associate weakly along the *c* axis *via* C–H···I interactions and, more strongly so, along the *a* axis by CH···π interactions between the pyrrolic carbon atom C9 and a $PEt_3$ methyl proton of neighbouring molecules positioned above and below (C–H···C = 2.684 Å, see Fig. S25b of the ESI†). The structural relevance of CH···π interactions has recently been highlighted.[43]

## UV-vis spectroscopy, TD-DFT calculations and luminescence properties

The UV-Vis absorption spectra of complexes **Pt–Cl** to **Pt–$CH_3$** are shown in Fig. 4. They are dominated by the sharp, vibrationally structured band of the attached BODIPY dye with extinction coefficients $\varepsilon$ of 52 600 to 57 400 $M^{-1}$ $cm^{-1}$. Peaking at a narrow range of 461 to 472 nm (Table 2), the position is almost invariant to the identity of the ligand $X^-$. At higher energies in the near UV another weaker, asymmetric absorption is observed at $\lambda$ = 370 to 300 nm with a maximum extinction coefficient of *ca.* 11 000 $M^{-1}$ $cm^{-1}$. In some cases that feature is resolved into two distinct bands which are separated

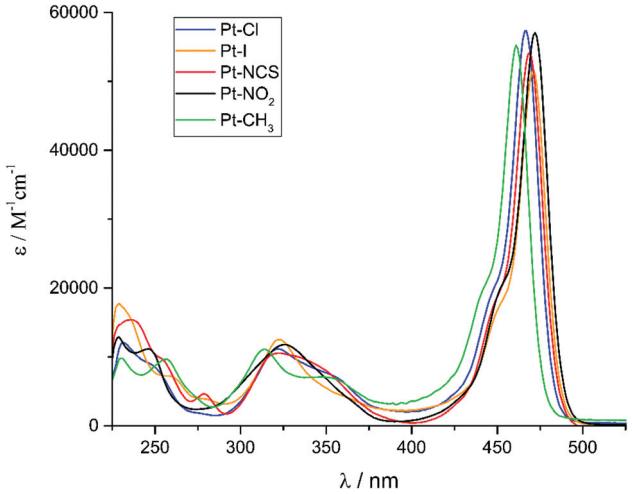


**Fig. 4** Electronic absorption spectra of **Pt–Cl**, **Pt–I**, **Pt–NCS**, **Pt–$NO_2$** and **Pt–$CH_3$** in a *ca.* $10^{-5}$ M $CH_2Cl_2$ solution at 298 K.

by 20 to 30 nm. Time-dependent DFT (TD-DFT) calculations carried out on geometry optimized structures accordingly predict two separate absorptions in this energy range. The comparison of experimental and calculated TD-DFT data in Table 2 shows that our calculations reproduce the general absorption features well but overestimate the energy of the prominent BODIPY-based $\pi \rightarrow \pi^*$ transition by *ca.* 4200 $cm^{-1}$. The TD-DFT data reveal that the intense band at the lowest energy arises from the HOMO → LUMO transition. As it is evident from the graphical depictions of the relevant orbitals of **Pt–$NO_2$** and **Pt–I** in Fig. 5 and the compilation in Tables 2 and 3, the latter is adequately described as a $\pi \rightarrow \pi^*$ transition of the BODIPY ligand with only very small contributions of the $\{PtX(PEt_3)_2\}$ fragment. This also explains the negligible influence of the $X^-$ ligand on the transition energies. The absorption near 320 nm originates from two energetically close-lying transitions (HOMO−5 → LUMO, HOMO−6 → LUMO for **Pt–I**, HOMO−6 → LUMO, HOMO−7 → LUMO/HOMO−8 → LUMO for **Pt–$NO_2$**, Table 2). One has distinct $Pt(PEt_3)_2$ → BODIPY charge-transfer (CT) character, while the second one involves another $\pi \rightarrow \pi^*$ transition within the dye ligand. As we will see later, the more significant metal contribution to the higher energy transition has important implications on the intersystem crossing rate constants $k_{ISC}$ from the different excited states.

Table S15 of the ESI† compares the calculated structure parameters of complexes **Pt–Cl**, **Pt–I**, **Pt–NCS**, and **Pt–$NO_2$** to the experimental data from X-ray crystal diffraction and to those calculated for the $T_1$ state. Calculated bond parameters for the $S_0$ state retrace experimentally observed bond lengths and angles well. The only structural difference between the $T_1$ and the $S_0$ states is a slight elongation of the Pt–C1 bond by 2–3 pm while all other bond lengths and bond angles remain essentially unaffected.

Like the previously reported complex **Pt–Br**[20] all complexes exhibit dual fluorescence at $\lambda \approx 480$ nm and phosphorescence at $\lambda \approx 640$ nm when excited into their lowest energy absorption band. Emission spectra of the complexes and of **Br–BODIPY** are compared in Fig. 6 while relevant photophysical data are collected in Table 4. The small Stokes shifts of <500 $cm^{-1}$ and luminescence decay rates in the subnanosecond range are typical assets of BODIPY-based fluorescence emissions. The congruence of electronic absorption and excitation spectra as documented in Fig. S29–S33 of the ESI† and the blue shift of the fluorescence peaks compared to that of the **Br–BODIPY** precursor ($\lambda_{Fl}$ = 517 nm) demonstrate, that both emissions originate from the complexes and not from impurities or unreacted **Br–BODIPY**. That blue shift has been traced to a preferential lifting of the BODIPY LUMO owing to a slightly larger contribution of the strongly electron-donating $\{Pt(PEt_3)_2X\}$ moiety[44] to the receptor orbital.[20] The long lifetimes of 162 to 439 μs at r.t. and the large Stokes shifts of *ca.* 5600 $cm^{-1}$ characterize the low-energy emission band as phosphorescence

**Table 2** Absorption data of complexes **Pt–Cl**, **Pt–I**, **Pt–NCS**, **Pt–$NO_2$** and **Pt–$CH_3$** in *ca.* $10^{-5}$ M $CH_2Cl_2$ solutions at 298 K and TD-DFT calculations in $CH_2Cl_2$

| | Absorption data | TD-DFT data | | | |
|---|---|---|---|---|---|
| | $\lambda_{max}$ [nm] ($\varepsilon \times 10^{-3}$ [$M^{-1}$ $cm^{-1}$]) | $\lambda$ [nm] | Major contributions [%] | $f^a$ | Assignment |
| **Pt–Cl** | 321 (11.1), 340 (7.4), 467 (57.4) | 293 | H−6 → LUMO (93) | 0.16 | $\pi \rightarrow \pi^*$ (BODIPY) |
| | | 310 | H−5 → LUMO (81) | 0.10 | $Pt(PEt_3)_2$ → BODIPY CT |
| | | 390 | HOMO → LUMO (97) | 0.39 | $\pi \rightarrow \pi^*$ (BODIPY) |
| **Pt–I** | 322 (12.5), 352 (4.3) 471 (52.6) | 295 | H−6 → LUMO (90) | 0.17 | $\pi \rightarrow \pi^*$ (BODIPY) |
| | | 309 | H−5 → LUMO (81) | 0.07 | $Pt(PEt_3)_2$ → BODIPY CT |
| | | 392 | HOMO → LUMO (97) | 0.39 | $\pi \rightarrow \pi^*$ (BODIPY) |
| **Pt–NCS** | 320 (10.5), 337 (9.2), 469 (54.2) | 294 | H−6 → LUMO (93) | 0.18 | $\pi \rightarrow \pi^*$ (BODIPY) |
| | | 310 | H−5 → LUMO (88) | 0.07 | $Pt(PEt_3)_2$ → BODIPY CT |
| | | 393 | HOMO → LUMO (95) | 0.37 | $\pi \rightarrow \pi^*$ (BODIPY) |
| **Pt–$NO_2$** | 325 (11.7), 472 (57.0) | 265 | H−8 → LUMO (39) | 0.08 | $Pt(NO_2)(PEt_3)_2$ → BODIPY CT |
| | | | H−7 → LUMO (56) | | $Pt(NO_2)(PEt_3)_2$ → BODIPY CT |
| | | 294 | H−6 → LUMO (90) | 0.17 | $\pi \rightarrow \pi^*$ (BODIPY) |
| | | 392 | HOMO → LUMO (97) | 0.40 | $\pi \rightarrow \pi^*$ (BODIPY) |
| **Pt–$CH_3$** [b] | 314 (11.1), 346 (7.1) 461 (55.2) | n.c. | | | |

[a] Oscillator strength. [b] n.c. = not calculated.

 

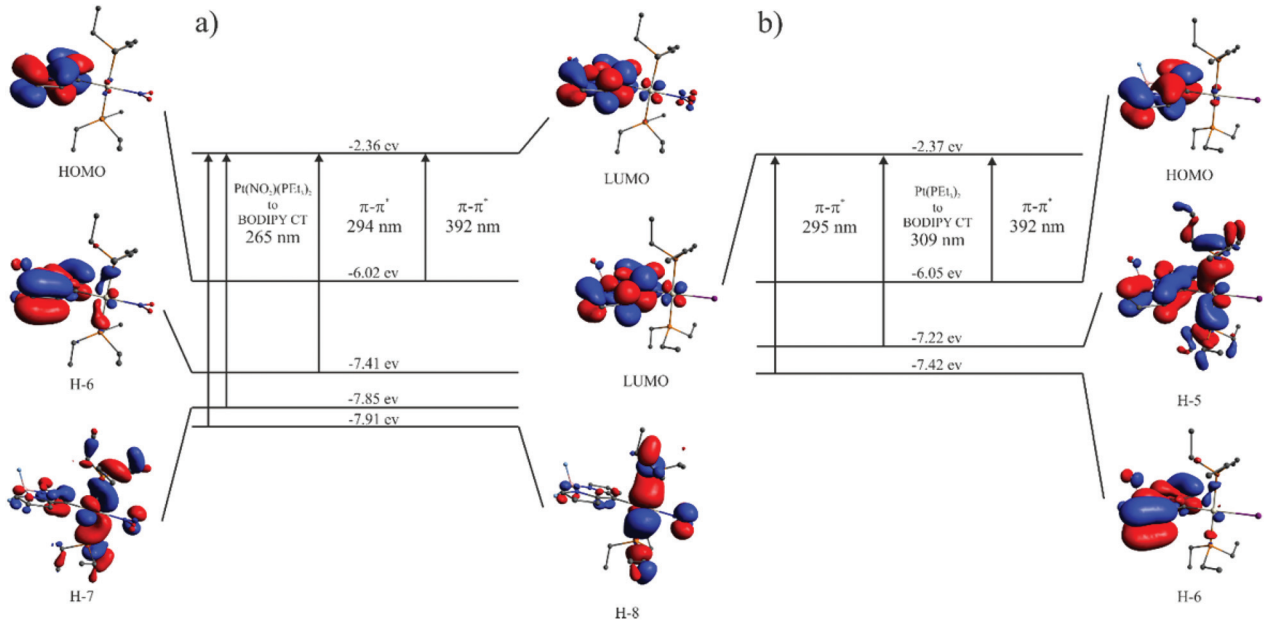


Fig. 5 Energies and graphical representations of the relevant molecular orbitals along with calculated electronic transitions of (a) **Pt–NO$_2$** and (b) **Pt–I**.

Table 3 Calculated Mulliken parameters of **Pt–Cl**, **Pt–I**, **Pt–NCS** and **Pt–NO$_2$** [a]

| | | Pt | BODIPY | $PEt_3$ | $X^-$ [b] |
|---|---|---|---|---|---|
| **Pt–Cl** | LUMO | 4 | 94 | 2 | 0 |
| | HOMO | 1 | 98 | 1 | 0 |
| | H−5 | 16 | 43 | 40 | 1 |
| | H−6 | 2 | 95 | 3 | 0 |
| | Spin density[c] | 0.012 | 1.975 | 0.017 | −0.004 |
| **Pt–I** | LUMO | 3 | 94 | 2 | 0 |
| | HOMO | 1 | 98 | 1 | 0 |
| | H−5 | 14 | 47 | 39 | 0 |
| | H−6 | 3 | 92 | 5 | 1 |
| | Spin density[c] | 0.009 | 1.978 | 0.019 | −0.006 |
| **Pt–NCS** | LUMO | 3 | 94 | 2 | 1 |
| | HOMO | 1 | 98 | 1 | 0 |
| | H−5 | 18 | 41 | 41 | 0 |
| | H−6 | 2 | 93 | 5 | 0 |
| | Spin density[c] | 0.003 | 1.978 | 0.020 | 0.000 |
| **Pt–NO$_2$** | LUMO | 3 | 93 | 2 | 2 |
| | HOMO | 1 | 98 | 1 | 0 |
| | H−6 | 3 | 90 | 7 | 0 |
| | H−7 | 40 | 16 | 37 | 7 |
| | H−8 | 50 | 6 | 31 | 13 |
| | Spin density[c] | −0.003 | 1.982 | 0.020 | 0.001 |

[a] Percent contributions of the given fragments. [b] $X^-$ represents the anionic ligand in *trans*-position to the dye at the Pt ion. [c] Spin density contribution of the respective fragment to the spin density surface.

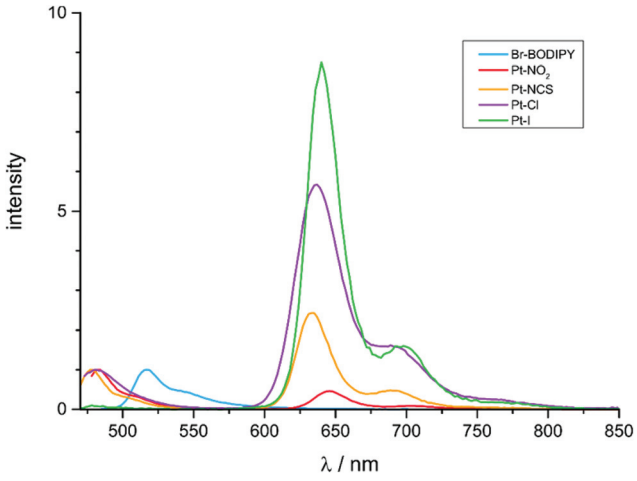


Fig. 6 Emission spectra of **Pt–Cl**, **Pt–I**, **Pt–NO$_2$** **Pt–NCS** and **Br–BODIPY** in degassed $CH_2Cl_2$ solutions at concentrations of *ca.* $10^{-6}$ M upon irradiation into the lowest energy absorption band of the complexes.

(Table 4). From the comparison of emission spectra in Fig. 6 and the data in Table 4 it becomes immediately apparent that larger phosphorescence quantum yields $\Phi_{Ph}$ go along with a decrease of those of the fluorescence emission $\Phi_{Fl}$ and *vice versa*. No luminescence data could be obtained for **Pt–CH$_3$**, as this complex decomposed when irradiated in the fluorescence spectrometer. Fig. S34 of the ESI† illustrates that the decomposition product still constitutes a BODIPY dye. The distinct red-shift of the fluorescence peak and its similar position to that of the **Br–BODIPY** precursor suggest that the BODIPY-ligand is detached from the Pt atom during photochemical degradation. Facile Pt-BODIPY bond breaking in this complex is likely caused by the strong σ-*trans*-influence of the methyl ligand and the concomitant weakening of the Pt-C(BODIPY) σ-bond, which is even amplified in the excited $T_1$ state (Tables 1 and S15 of the ESI†).

The ratio of phosphorescence to fluorescence intensities increases in the order **Pt–NO$_2$** < **Pt–NCS** < **Pt–Cl** < **Pt–I**; **Pt–Br**

Table 4 Luminescence data of **Pt–Br**,[20] **Pt–Cl**, **Pt–I**, **Pt–NO$_2$** and **Pt–NCS** in $N_2$ saturated $CH_2Cl_2$ and toluene solutions, respectively, at concentrations of *ca*. $10^{-6}$ M. If not stated otherwise the samples were excited into the lowest energy absorption band

| | $\lambda_{max,Fl}$ [nm] (Stokes shift [cm$^{-1}$]) | $\lambda_{max,Ph}$ [nm] (Stokes shift [cm$^{-1}$]) | $\Phi_{Fl,exc467}$ ($\Phi_{Fl,exc322}$)[a] | $\Phi_{Ph,exc467}$ ($\Phi_{Ph,exc322}$)[a] | $\tau_{Fl}$ [ns] | $\tau_{Ph}$ [μs] |
|---|---|---|---|---|---|---|
| **Pt–Br**[20] | 479 (491) | 637(5669) | 0.011 | 0.312 | n.d.[b] | 162 |
| **Pt–Cl** | 478 (493) | 633 (5615) | 0.016 (0.005) | 0.349 (0.356) | 0.174 | 277 |
| | 479 (491)[c] | 631 (5520)[c] | | | | 243[c] |
| | 478[d] | 626[d] | | | | 450[d] |
| **Pt–I** | 481 (441) | 641 (5631) | 0.002 (0.000) | 0.364 (0.397) | 0.484 | 297 |
| **Pt–NO$_2$** | 483 (483) | 645 (5683) | 0.115 (0.052) | 0.166 (0.209) | 0.470 | 439 |
| **Pt–NCS** | 480 (489) | 637 (5623) | 0.048 (0.024) | 0.244 (0.323) | 1.027 | 313 |

[a] Fluorescence and phosphorescence quantum yields measured at an excitation wavelength of 467 nm or 322 nm, respectively. [b] Not determined. [c] Measured in toluene solution at r.t. [d] Measured in a toluene glass at 77 K.

occupies a position intermediate between **Pt–NCS** and **Pt–Cl**. This ordering parallels an increasing *trans*-influence of the ligand X$^-$,[35] but shows no clear correlation to its positioning within the spectroelectrochemical series. This indicates that thermal population of excited d-states is most probably not the dominant pathway for radiationless decay of the excited states, although the documented complexities of such processes still warrant caution.[30]

As the already very weak fluorescence of **Pt–I** was found to vanish altogether on excitation into the high-energy absorption band at 322 nm, the intensities of the phosphorescence and fluorescence emissions were monitored at different excitation wavelengths. Fig. 7a and b illustrate that, on irradiation into the higher energy absorption band(s), the phosphorescence quantum yield $\Phi_{Ph}$ of **Pt–NO$_2$** further increases at the expense of that of the fluorescence emission ($\Phi_{Fl}$). The notion that the ratio of phosphorescence and fluorescence emission intensities may depend on the excitation wavelength has been perspectively proposed by Chou *et al.*[33] and was experimentally demonstrated soon after.[45–47] This phenomenon relies on the different involvement of a heavy atom in the different excited states. In particular, a larger degree of charge-transfer between a metal/coligand entity and the emissive ligand (metal-to-ligand or ligand-to-metal charge-transfer) provides a more direct pathway for ISC, and hence a larger rate constant $k_{ISC}$, than the remote heavy-metal effect alone.[45,46,48] The efficiencies of the ISC from a higher-lying $S_n$ state ($S_n \rightarrow T_m \rightarrow T_1$) and from the $S_1$ state ($S_n \rightarrow S_1 \rightarrow T_1$) may thus drastically differ if the initially populated states differ in character.

For the BODIPY-centred excited $S_1$ state, which is initially populated by irradiation into the prominent HOMO → LUMO $\pi \rightarrow \pi^*$ absorption band, the coordination centre merely acts as a remote heavy metal atom, and the efficiency of ISC relies on the close proximity of the Pt ion to the dye (note that $k_{ISC}$ in that case relates to $r^{-6}$ where $r$ is the distance of the heavy metal atom to the midpoint of the dye).[47] This is readily inferred from the spin density surfaces for the excited triplet states of **Pt–Cl**, **Pt–I**, **Pt–NCS**, and **Pt–NO$_2$** in Fig. 8. Complying with the compositions of the HOMO and the LUMO, almost the entire spin density resides at the BODIPY ligand with only very modest contributions of 0.3% to 1.2% from the Pt ion. As it was already discussed, the higher energy absorption band,

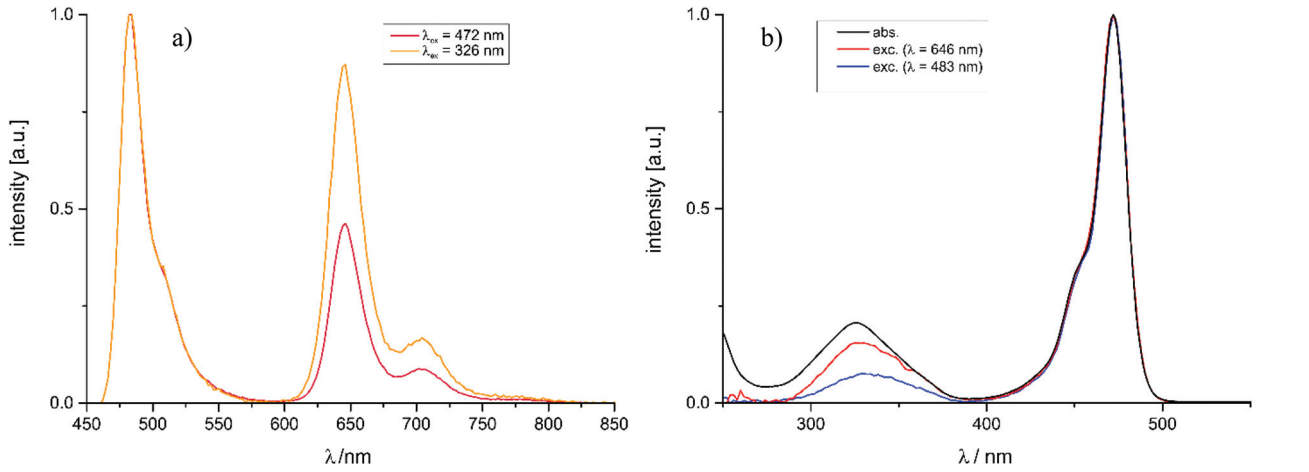


Fig. 7 (a) Emission spectra of **Pt–NO$_2$** on excitation at $\lambda$ = 326 nm and $\lambda$ = 472 nm, respectively. (b) Absorption and excitation spectra of **Pt–NO$_2$**. The excitation spectra were recorded for the fluorescence band at 483 nm and the phosphorescence band at 646 nm. Measurements were performed on degassed $CH_2Cl_2$ solutions at concentrations of *ca*. $10^{-6}$ M.

 

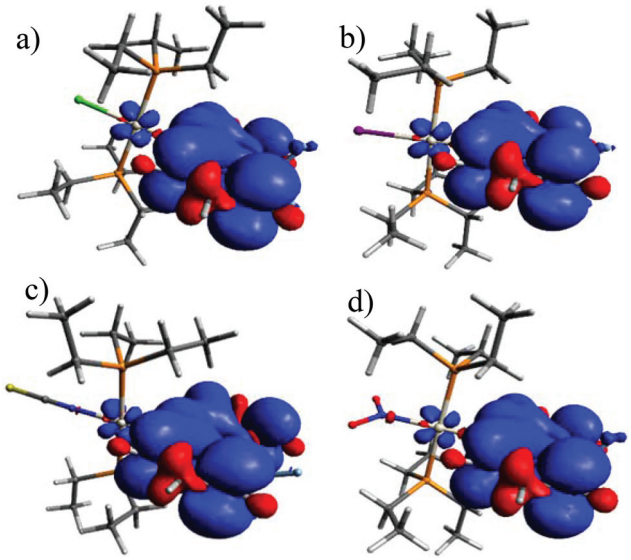


Fig. 8 Spin density surfaces of the $T_1$ state of (a) **Pt–Cl**, (b) **Pt–I**, (c) **Pt–NCS**, and (d) **Pt–NO$_2$**.

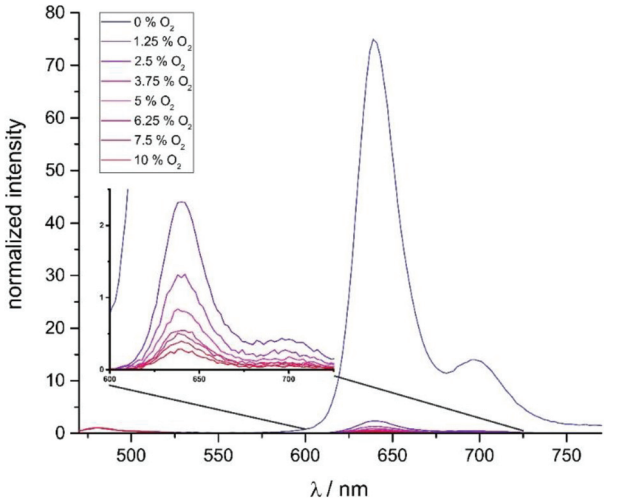


Fig. 9 Stacked luminescence spectra of **Pt–I** in $CH_2Cl_2$ solution at different oxygen concentration levels.

populating (a) higher $S_n$ state(s), has more significant contributions from $Pt(PEt_3)_2$ → BODIPY charge-transfer (ML → L′CT, Fig. 5 and Tables 2 and 3). As is illustrated in Scheme 1, the faster $k_{ISC,n}$ from the higher-lying ML → L′CT excited state provides an even more competitive pathway for population of the phosphorescent $T_1$ state than ISC from $S_1$. Excitation into (a) higher $S_n$ state(s) thus decreases the fluorescence quantum yield $\Phi_{Fl}$ while further boosting $\Phi_{Ph}$. The highest phosphorescence quantum yields are found for the simple halogenido complexes. The values of $\Phi_{Ph}$ of 36.4% or 39.7% for **Pt–I** on excitation at 467 or at 322 nm, respectively, are, to the best of our knowledge, the highest phosphorescence quantum yields of any BODIPY derivative, even surpassing those of **Pt–Br**.[20]

### Emission quenching by $^3O_2$ and $^1O_2$ generation

The very long lifetimes of the excited triplet states of up to 439 μs make these compounds interesting candidates for applications such as triplet molecule sensing and photocatalysis. Their capabilities to act as one-component sensors for triplet molecules were tested by Stern–Volmer quenching experiments using $^3O_2$ as the quencher. Fig. 9 and as Fig. S35 and S37 of the ESI† illustrate the results of such experiments for **Pt–I**, **Pt–Cl** and **Pt–NO$_2$**. The Stern–Volmer equation is given as $I_0/I = 1 + K_{SV}[O_2]$, where $I_0$ is the luminescence intensity under exclusion of oxygen, $I$ is the luminescence intensity at a specific oxygen concentration, and $K_{SV}$ is the Stern–Volmer quenching constant, which is a measure for the sensitivity of the sensor. Fig. 10 displays plots of $(I_0/I) - 1$ and $(\tau_0/\tau) - 1$ as a function of the partial oxygen pressure $(p(O_2))$. The quenching constants of $K_{SV} = 2380 \pm 170$ bar$^{-1}$ for **Pt–Cl** and $K_{SV} = 2580 \pm 70$ bar$^{-1}$ for **Pt–I** are identical within the experimental error limits. As expected from the longer triplet state lifetime, **Pt–NO$_2$** has an even larger $K_{SV}$ of 2810 ± 110 bar$^{-1}$. Quenching constants evaluated by the ratios of lifetimes are somewhat smaller but still reach values of close to 2000 to 2200 bar$^{-1}$. All complexes show high sensitivities for small partial oxygen pressures. Above $p(O_2) = 0.1$ bar the plots start to deviate from linearity which relates to the low intensity of the residual signal. Our results render complexes **Pt–Cl**, **Pt–I** and **Pt–NO$_2$** particularly efficient oxygen sensors when compared to other

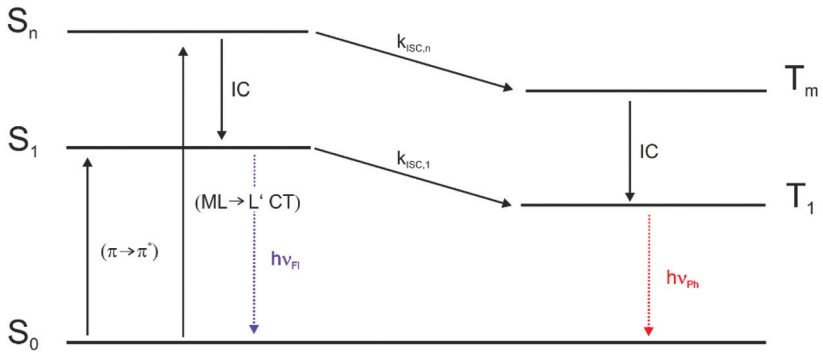


Scheme 1 Jablonski diagram for the relevant optical processes in the complexes *trans*-Pt(BODIPY)X$(PEt_3)_2$.

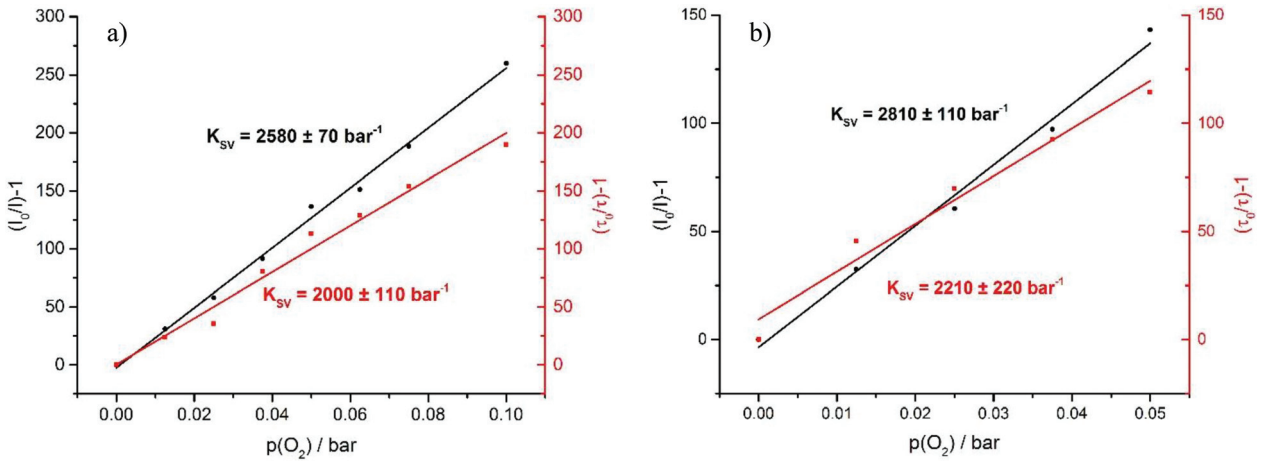


**Fig. 10** Stern–Volmer plot (a) of **Pt–I** and (b) of **Pt–$NO_2$**.

successful platinum-based systems.[49–54] We note here that a lower lifetime of the phosphorescence emission and hence lesser sensitivity towards $O_2$ quenching as it was observed for **Pt–Br** allows for $O_2$ detection in solution up to atmospheric concentration levels of the surrounding gas phase.

The feasibility of using these complexes as sensitizers for $^1O_2$ generation from $^3O_2$ by triplet–triplet annihilation in productive chemical reactions[55,56] such as the oxidation of 1,5-dihydroxynaphthalene (DHN) was investigated using the complexes **Pt–Cl** and **Pt–I** as catalysts. The catalytic cycle of the photocatalytic system consisting of the sensitizer, aereal $O_2$ and DHN is shown in Scheme 2. On the basis of this mechanism, the rate-law of DHN consumption can be written as $\nu_i = k_r\,[O_2][DHN]$. At the initial stage of the reaction oxygen concentration can be treated as constant. The previous equation can therefore be simplified to $\nu_i = k_{obs}\cdot[DHN]$ using a pseudo first-order rate constant $k_{obs}$. Rewriting this formula as $\ln(C_t/C_0) = -k_{obs}\cdot t$, where $C_t$ denotes the concentration of DHN at a certain reaction time $t$ while $C_0$ is the initial concentration of DHN, allows for determining $k_{obs}$ from the slope of a plot of $\ln(C_t/C_0)$ *vs.* reaction time $t$. The associated values of $\nu_i$ and the number of photons absorbed by the sensitizer provide the $^1O_2$ generation quantum yield ($\Phi_\Delta$) by using the relative method with methylene blue (MB) as a reference sensitizer.[57] Details of these experiments are provided in the Experimental section. Fig. 11a depicts the changes of the absorption spectra of the reaction mixture with irradiation time $t$ using **Pt–Cl** as a sensitizer, while Fig. 11b compares plots of $\ln(C_t/C_0)$ as a function of $t$ for **Pt–Cl**, **Pt–I** and the MB standard. The rate constants $k_{obs}$, the rates $\nu_i$ of DHN consumption, and quantum yields for the generation of $^1O_2$ ($\Phi_\Delta$) in the photooxidation of DHN are summarized in Table 5. Both platinum complexes obey a linear relation between $\ln(C_t/C_0)$ and the irradiation time $t$ from which $\nu_i$ was determined. This precludes side reactions and proves that the sensitizers are stable under these conditions. Control experiments in the absence of light showed that none of the sensitizers promotes oxidation of DHN to Juglone under dark conditions (see Fig. S38 and S39 in the ESI†). Both complexes show a significantly higher rate $\nu_i$ of DHN consumption than MB. Most remarkably, **Pt–I** and **Pt–Cl** have exceptionally high quantum efficiencies $\Phi_\Delta$ of 0.95 (**Pt–I**) or even near unity (**Pt–Cl**) and clearly outperform the MB standard ($\Phi_\Delta$ of 0.57).[58–60] Contributing factors are the high ISC efficiencies and the long lifetimes of the triplet state ($\tau_{Ph}$ = 277 μs for **Pt–Cl**, $\tau_{Ph}$ = 297 μs for **Pt–I**).

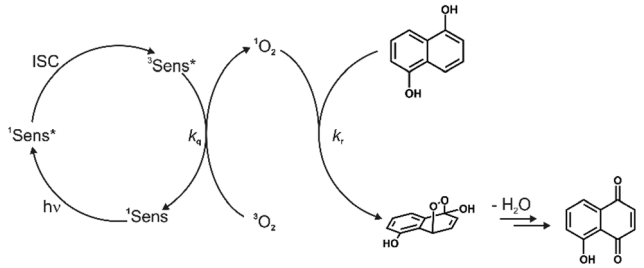


**Scheme 2** Mechanism for the photooxidation of 1,5-dihydroxynaphthalene (DHN) by $^1O_2$ catalyzed by a sensitizer, producing Juglone after the elimination of a water molecule.

## Summary and conclusions

We report on the synthesis and the spectroscopic and photophysical properties of five new complexes *trans*-Pt(BODIPY)X$(PEt_3)_2$ (**Pt–X**, $X^-$ = $Cl^-$, $I^-$, $NO_2^-$, $NCS^-$, $CH_3^-$). All contain a σ-bonded BODIPY ligand that binds to the platinum ion *via* its *meso* position. With the exception of **Pt–$CH_3$**, all complexes show dual fluorescence and phosphorescence emissions from the attached BODIPY dye at wavelengths that are largely invariant to the nature of the ligand $X^-$. Phosphorescence quantum yields and Pt–C(BODIPY) bond lengths increase in the order **Pt–$NO_2$** < **Pt–NCS** < **Pt–Cl** < **Pt–I** in parallel with the σ-*trans*-influence of the ligand $X^-$.

 

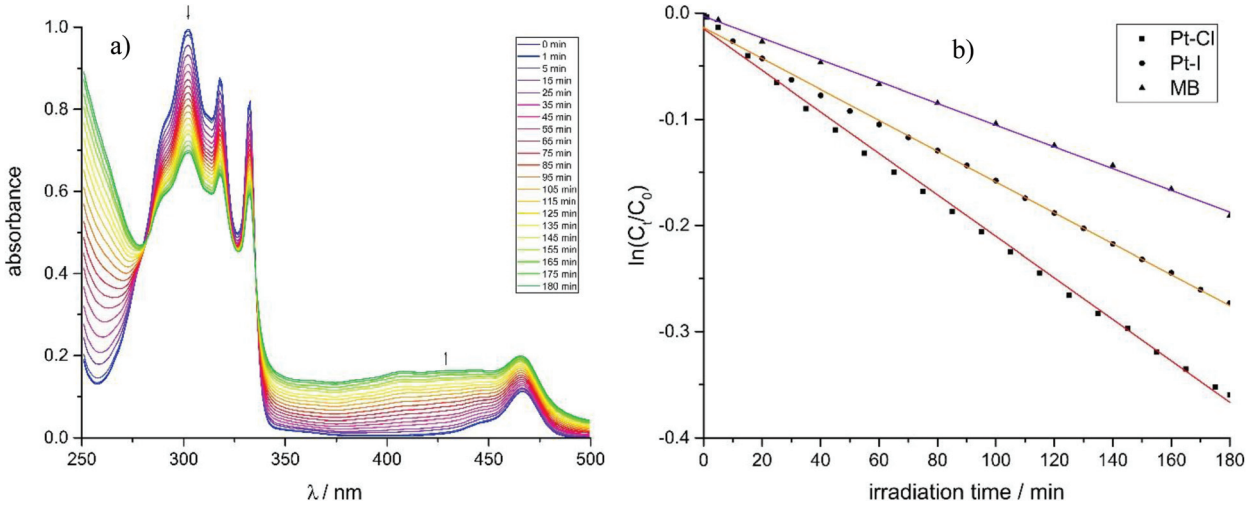


**Fig. 11** (a) Spectral change in the UV-Vis region for the photooxidation of DHN using **Pt–Cl** as the sensitizer. (b) Plots of $\ln(C_t/C_0)$ *vs.* irradiation time for the photooxidation using complexes **Pt–Cl**, **Pt–I** and MB.

**Table 5** Parameters of the pseudo first-order kinetics, $^1O_2$ generation quantum yields of the photooxidation of DHN using the complexes **Pt–Cl**, **Pt–I** ($\lambda_{exc}$ = 460 nm) and MB ($\lambda_{exc}$ = 655 nm) as sensitizers, and turnover frequency, as well as Stern–Volmer constants $K_{SV}$ for the phosphorescence quenching of **Pt–Cl** and **Pt–I** by $^3O_2$

| | $k_{obs}$ [a] [$min^{-1}$] | $\nu_i$ [b] [$\times 10^{-6}$ M $min^{-1}$] | $I$ [c] | $\Phi_\Delta$ [d] | Yield [e] [%] | TOF [f] [$s^{-1}$] | $K_{SV}$ [g] [$bar^{-1}$] |
|---|---|---|---|---|---|---|---|
| **Pt–Cl** | 0.00195 | 0.236 | 1.033 | 1.00 | 35 | 0.0019 | 2380 ± 170 |
| **Pt–I** | 0.00145 | 0.176 | 0.810 | 0.95 | 25 | 0.0014 | 2580 ± 70 |
| MB | 0.00102 | 0.130 | 1.000 | 0.57 | 14 | 0.0008 | |

[a] Pseudo first-order rate constant for DHN consumption. [b] Rate of DHN consumption. [c] Relative value of the number of photons absorbed by the sensitizer ($I$ = 1 for the standard sensitizer MB). [d] Corrected $^1O_2$ generation quantum yield using the value of MB ($\Phi_\Delta$ = 0.57)[58–60] as a reference. [e] Yield of Juglone after a reaction time of 180 min. [f] Turnover frequency. [g] In $CH_2Cl_2$ solution.

Most importantly, the ratio of phosphorescence to fluorescence intensities of each complex depends on the excitation wavelength. This is a direct consequence of the different natures of the initially populated excited states (BODIPY-based $\pi \rightarrow \pi^*$ or a higher excited state with appreciable $Pt(PEt_3)_2 \rightarrow$ BODIPY $\pi^*$ ML $\rightarrow$ L′ charge-transfer character), which results in different rate constants $k_{ISC}$. Thus, the higher-energy MLCT absorption offers a more direct pathway for Pt-triggered ISC than just the heavy atom effect. Our present results provide experimental manifestation of the concept of excitation energy-dependent emission properties as recently discussed and observed by Chou and his coworkers.[33,45–47]

Additional studies into phosphorescence quenching by $^3O_2$ have yielded exceptionally large Stern–Volmer quenching constants of *ca.* 2000 $bar^{-1}$ and demonstrated that these complexes are excellent one-component sensors for triplet molecules. Moreover, they constitute highly efficient sensitizers for photocatalytic reactions involving $^1O_2$ as the reactant, combining exceptionally high quantum efficiencies near unity for $^1O_2$ generation with good photostabilities. These treats will be further explored in our future work.

# Experimental section

## Materials and general methods

DHN was bought form Acros Organics and purified by sublimation ($p = 4 \times 10^{-3}$ mbar, 160° C oil bath). *cis*-Pt(BODIPY)Br-$(PEt_3)_2$ was prepared as described elsewhere.[20] All manipulations where conducted under air except for reactions involving MeMgI, $MgMe_2$ and MeLi, which were performed under $N_2$ atmosphere by standard Schlenk techniques. Solvents for the reactions under inert gas atmosphere were distilled over adequate drying agents and stored under $N_2$ atmosphere. All other solvents were used as received from the suppliers.

NMR experiments were carried out on a Bruker Avance III DRX 400 or a Bruker Avance DRX 600 spectrometer. $^1H$ and $^{13}C$ NMR spectra were referenced to the solvent signal, while $^{31}P$ and $^{195}Pt$ NMR spectra were referenced using the Absolute Reference tool in the MestReNova software. NMR data are given as follows: chemical shift ($\delta$ in ppm), multiplicity (br, broad; d, doublet; dd, doublet of doublets; m, multiplet; s, singlet; t, triplet), integration, coupling constant (Hz). Unequivocal signal assignments were achieved by 2D NMR experiments. The numbering of the nuclei follows that of the crystal structures in

Fig. 3. Combustion analysis was conducted with an Elementar vario MICRO cube CHN-analyzer from Heraeus.

X-ray diffraction analysis of single crystals was performed at 100 K on a STOE IPDS-II diffractometer equipped with a graphite-monochromated radiation source ($\lambda$ = 0.71073 Å) and an image plate detection system. A crystal mounted on a fine glass fiber with silicon grease was employed. If not indicated otherwise, the selection, integration, and averaging procedure of the measured reflex intensities, the determination of the unit cell dimensions and a least-squares fit of the $2\theta$ values as well as data reduction, LP-correction, and space group determination were performed using the X-Area software package delivered with the diffractometer. A semiempirical absorption correction was performed.[61] All structures were solved by the heavy-atom methods (SHELXS-97, SHELXS-2013, or SHELXS-2014).[62,63] Structure solutions were completed with difference Fourier syntheses and full-matrix last-squares refinements using SHELXL-97, SHELXS-2013, or SHELXS-2014,[63] minimizing $\omega(F_o^2 - F_c^2)^2$. The weighted $R$ factor ($wR^2$) and the goodness of the fit GOF are based on $F^2$. All non-hydrogen atoms were refined with anisotropic displacement parameters, while hydrogen atoms were treated in a riding model. Molecular structures in this work are plotted with ORTEP 32[64,65] or Mercury.[66] CIF files of **Pt–Cl**, **Pt–I**, **Pt–NCS**, **Pt–NO$_2$**, and **Pt–CH$_3$** have been deposited at the Cambridge Structure Data Base as CCDC 1474955 (**Pt–Cl**), 1474956 (**Pt–NCS**), 1474957 (**Pt–I**), 1474958 (**Pt–NO$_2$**), and 1474959 (**Pt–CH$_3$**).

UV-Vis absorption spectra were recorded on a TIDAS fiber-optic diode array spectrometer MCS from j&m in HELLMA quartz cuvettes with 1 cm optical path length at room temperature.

### Computational details

The ground sate electronic structures were calculated by density functional theory (DFT) methods using the Gaussian 09[67] program packages. Quantum chemical studies were performed without any symmetry constraints. Open shell systems were calculated by the unrestricted Kohn-Sham approach (UKS).[68] Geometry optimization followed by vibrational analysis was made either in vacuum or in solvent media. The quasirelativistic Wood-Boring small-core pseudopotentials (MWB)[69,70] and the corresponding optimized set of basis functions[71] for Pt and the 6-31G(d) polarized double-$\zeta$ basis set[72] for the remaining atoms were employed together with the Perdew, Burke and Ernzerhof exchange and correlation functional (PBE1PBE).[73–75] Solvent effects were accounted for by the Polarizable Conductor Continuum Model (PCM)[76–78] with standard parameters for dichloromethane. Absorption spectra and orbital energies were calculated using time-dependent DFT (TD-DFT)[79] with the same functional/basis set combination as mentioned above. For easier comparison with the experiment, the obtained absorption and emission energies were converted into wavelengths and broadened by a Gaussian distribution (full width at half-maximum = 3000 cm$^{-1}$) using the programm GaussSum.[80] Molecular orbitals were visualized with the GaussView programm[81] or with Avogadro.[82]

### Luminescence spectroscopy and quenching experiments

All luminescence spectra and excited state lifetimes were recorded for *ca.* $10^{-6}$ M solutions in $CH_2Cl_2$ or toluene with a PicoQuant FluoTime 300 spectrometer at room temperature, if not stated otherwise. Luminescence experiments under inert gas atmosphere and defined $O_2$ concentrations were conducted in a quartz cuvette modified with an angle valve from Normag. Defined $O_2$ concentrations were adjusted by completely degassing the sample and subsequent injection of adequate volumes of air and nitrogen by syringe. Quantum yields were measured using a Hamamatsu Absolute PL Quantum Yield Measurement System C9920-02 equipped with an integrating sphere.

### $^1O_2$ generation from Pt–X sensitizers

For the photoreactions involving $^1O_2$ generation, a $CH_2Cl_2$/MeOH (9/1) solution containing DHN ($1.2 \times 10^{-4}$ M) and a sensitizer (1.7 mol% with respect to DHN) was irradiated in a quartz cell of 1 cm path length using the Xenon lamp of a PicoQuant FluoTime 300 spectrometer ($\lambda_{ex}$(**Pt–Cl**, **Pt–I**) = 460 ± 5 nm, $I_f$(460 ± 5 nm) = 1.3 mW; $\lambda_{ex}$(MB) = 655 ± 5 nm, $I_f$(655 ± 5 nm) = 580 μW). UV-Vis absorption spectra were recorded at intervals of 5–20 min on a Varian Cary 50 spectrometer. The consumption of DHN was monitored by the decrease of the absorption at 301 nm ($\varepsilon$ = 7664 M$^{-1}$ cm$^{-1}$),[57] while Juglone production was monitored by an increase of the absorption at 427 nm ($\varepsilon$ = 3811 M$^{-1}$ cm$^{-1}$).[57] The yield of Juglone was calculated from the concentration of Juglone and the initial concentration of DHN. The singlet oxygen quantum yield ($\Phi_\Delta$) was determined using eqn (1),[57,83]

$$\Phi_\Delta = \Phi_{\Delta,std}(\nu_i \cdot I_{std}/\nu_{i,std} \cdot I) \quad (1)$$

where $\Phi_{\Delta,std}$ is the singlet oxygen quantum yield of the standard sensitizer MB ($\Phi_\Delta$ = 0.57),[58–60] $\nu_i$ is the rate of DHN consumption and $I$ and $I_{std}$ are the number of photons absorbed by the sensitizer and the standard, respectively. $I$ was estimated from eqn (2) using the $\lambda$ interval 455 to 465 nm for **Pt–Cl** and **Pt–I**, and 650 to 660 nm for MB,

$$I = \int I_f(\lambda)\ (1 - 10^{-\varepsilon(\lambda)C_s^l})d\lambda \quad (2)$$

where $I_f(\lambda)$ is the wavelength dependence of the intensity of the incident light evaluated with a photometer (for values *vide supra*), $\varepsilon(\lambda)$ is the extinction coefficient of the respective sensitizer recorded in $CH_2Cl_2$/MeOH (9/1), $C_s$ is the concentration of the sensitizer, and $l$ is the length of the optical cell.

### *trans*-Chloro-(4,4-difluoro-4-bora-3a,4a-diaza-*s*-indacen-8-yl)-bis(triethylphosphine)-platinum(II) (Pt–Cl)

40 mg (57 μmol, 1 eq.) of *cis*-Pt(BODIPY)Br(PEt$_3$)$_2$ and 19.5 mg (76 μmol, 1.4 eq.) of AgOTf were dissolved in 0.8 ml of $CD_2Cl_2$. The solution was heated to reflux for 5 min which led to the

 

formation of *trans*-Pt(BODIPY)(OTf)($PEt_3$)$_2$. The heterogeneous mixture was filtered and the filtrate was added to a solution of 66.6 mg (114 μmol, 2 eq.) of NaCl in 2.6 ml of MeOH. The orange suspension was stirred for 45 min. The solvents were then removed *in vacuo* and the solid was extracted with $CH_2Cl_2$. The product was purified by column chromatography (silica, $CH_2Cl_2$, $R_f$ = 0.72). After washing with *n*-pentane (2 × 0.6 ml) the analytically pure product was obtained. Yield: 32%. Single crystals were obtained by slow evaporation of a $CH_2Cl_2$ solution. $^1$H NMR (400 MHz, $CD_2Cl_2$): $\delta$ 7.65 (br s, 2H, H5, H9), 7.46 (d, 2H, $^3J_{HH}$ = 3.68 Hz, H3, H7), 6.46 (dd, 2H, $^3J_{HH}$ = 3.68 Hz, $^3J_{HH}$ = 2.04 Hz, H4, H8), 1.74 (m, 12H, P–C$H_2$–), 1.06 (dt, 18H, $^3J_{HH}$ = 7.66 Hz, $^3J_{PH}$ = 15.58 Hz, P–$CH_2$–C$H_3$). $^{31}$P NMR (161.9 MHz, $CD_2Cl_2$): $\delta$ 11.70 (s, with satellites $J_{PtP}$ = 2502 Hz). $^{13}$C NMR (150.9 MHz, $CD_2Cl_2$): $\delta$ 178.5 (t, $^2J_{PC}$ = 7.8 Hz, with satellites $J_{PtC}$ = 492 Hz, C1), 143.5 (s, with satellites $^2J_{PtC}$ = 22.4 Hz, C2, C6), 137.1 (s, C5, C9), 133.8 (s, with satellites $^3J_{PtC}$ = 25.2 Hz, C3, C7), 116.6 (s, C4, C8), 14.28 (t, $J_{PC}$ = 33.0 Hz, with satellites $^2J_{PtC}$ = 17.0 Hz, P–*C*$H_2$–), 8.2 (t, $^2J_{PC}$ = 10.0 Hz, P–$CH_2$–*C*$H_3$). $^{195}$Pt NMR (86.0 MHz, $CD_2Cl_2$): $\delta$ −4134 (t, $J_{PtP}$ = 2502 Hz). C, H, N analysis calculated for $C_{21}H_{36}ClBF_2N_2P_2Pt{\cdot}0.3\ C_5H_{12}$: C, 39.77; H, 5.87; N, 4.12. Found: C, 39.44; H, 6.09; N, 4.06.

### *trans*-Iodo-(4,4-difluoro-4-bora-3a,4a-diaza-*s*-indacen-8-yl)-bis(triethylphosphine)-platinum(II) (Pt–I)

*trans*-Pt(BODIPY)(OTf)($PEt_3$)$_2$ prepared as described above was dissolved in 5 ml of dry THF under $N_2$ atmosphere. To this solution 0.08 ml of a freshly prepared 1 M MeMgI solution (1.4 eq.) in diethyl ether were added. The solution was stirred for 20 min, the precipitate was filtered off and the solution was evaporated to dryness.

The crude product was purified by column chromatography (silica deprotonated with 5% $NEt_3$, $CH_2Cl_2$ : PE = 5 : 1, $R_f$ = 0.46). After washing twice with 0.3 ml of *n*-pentane the yellow product was obtained in 58% yield. Single crystals suitable for X-ray diffraction analysis were obtained by slow evaporation of a $C_6D_6$ solution. $^1$H NMR (400 MHz, $C_6D_6$): $\delta$ 7.81 (br s, 2H, H5, H9), 7.43 (d, 2H, $^3J_{HH}$ = 3.51 Hz, H3, H7), 6.19 (dd, 2H, $^3J_{HH}$ = 3.51 Hz, $^3J_{HH}$ = 1.89 Hz, H4, H8), 1.68 (m, 12H, P–C$H_2$–), 0.72 (dt, 18H, $^3J_{HH}$ = 7.68 Hz, $^3J_{PH}$ = 15.89 Hz, P–$CH_2$–C$H_3$). $^{31}$P NMR (161.9 MHz, $C_6D_6$): $\delta$ 4.02 (s with satellites, $J_{PtP}$ = 2450 Hz). $^{13}$C NMR (100.6 MHz, $C_6D_6$): $\delta$ 181.1 (s, C1), 143.3 (s, C2, C6), 138.5 (s, C5, C9), 133.3 (s with satellites, $^3J_{PtC}$ = 25.0 Hz, C3, C7), 116.7 (s, C4, C8), 16.2 (t, $J_{PC}$ = 34.2 Hz, with satellites $^2J_{PtC}$ = 17.6 Hz, P–*C*$H_2$–), 8.36 (t, $^2J_{PC}$ = 11.5 Hz, P–$CH_2$–*C*$H_3$). $^{195}$Pt NMR (86.0 MHz, $C_6D_6$): $\delta$ −4503.4 (t, $J_{PtP}$ = 2450 Hz). C, H, N analysis calculated for $C_{21}H_{36}BF_2IN_3P_2Pt$: C, 33.66; H, 4.84; N, 3.74. Found: C, 33.85; H, 5.06; N, 3.86.

### *trans*-κ*N*-(4,4-difluoro-4-bora-3a,4a-diaza-*s*-indacen-8-yl)-(thiocyanato)-bis(triethylphosphine)-platinum(II) (Pt–NCS)

A solution of 30 mg (57 μmol, 1 eq.) of *cis*-Pt(BODIPY)Br($PEt_3$)$_2$ and 19.5 mg (76 μmol, 1.4 eq.) of AgOTf in 0.8 ml of $CH_2Cl_2$ was refluxed for 5 min. The solution was filtered and 2.6 ml of a methanolic solution of NaSCN (9.2 mg, 114 μmol, 2 eq.) was added. After stirring the reaction mixture for 1.5 h all volatiles were removed and the crude product was extracted with $CH_2Cl_2$. The product was further purified by column chromatography (silica deprotonated with 5% $NEt_3$, PE : EE = 3 : 1, $R_f$ = 0.32). The product was washed with small amounts of *n*-pentane. Yield: 36%. Single crystals for X-ray diffraction analysis were obtained by slow evaporation of a $CH_2Cl_2$ solution. $^1$H NMR (400 MHz, $C_6D_6$): $\delta$ 7.80 (br s, 2H, H5, H9), 7.28 (d, 2H, $^3J_{HH}$ = 3.67 Hz, H3, H7), 6.18 (dd, 2H, $^3J_{HH}$ = 3.67 Hz, $^3J_{HH}$ = 2.00 Hz, H4, H8), 1.27 (m, 12H, P–C$H_2$–), 0.68 (m, 18H, P–$CH_2$–C$H_3$). $^{31}$P NMR (161.9 MHz, $C_6D_6$): $\delta$ 12.50 ppm (s, with satellites $J_{PtP}$ = 2450 Hz). $^{13}$C NMR (150.9 MHz, $C_6D_6$): $\delta$ 174.3 (s, C1), 143.4 (s, C2, C6), 138.3 (s, C5, C9), 132.5 (s, with satellites $^3J_{PtC}$ = 22.5 Hz, C3, C7), 116.7 (s, C4, C8), 14.6 (t, $J_{PC}$ = 17.0 Hz, P–*C*$H_2$–), 7.6 (br s, P–$CH_2$–*C*$H_3$), signal for C10 not detected. $^{195}$Pt NMR (129.0 MHz, $C_6D_6$): $\delta$ −4181.5 (t, $J_{PtP}$ = 2450 Hz). C, H, N analysis calculated for $C_{22}H_{36}BF_2N_3P_2PtS$: C, 38.83; H, 5.33; N, 6.18. Found: C, 38.81; H, 5.59; N, 6.20.

### *trans*-(4,4-Difluoro-4-bora-3a,4a-diaza-*s*-indacen-8-yl)-(nitrito)-bis(triethylphosphine)-platinum(II) (Pt–$NO_2$)

To *trans*-Pt(BODIPY)(OTf)($PEt_3$)$_2$ prepared as described above from 40 mg (57 μmol, 1 eq.) of *cis*-Pt(BODIPY)Br($PEt_3$)$_2$ in $CH_2Cl_2$, a solution of 7.9 mg (114 μmol, 2 eq.) of $NaNO_2$ in 2.6 ml of MeOH was added. The orange solution was stirred for 1.5 h at r.t., the solvents were removed and the crude solid was extracted with $CH_2Cl_2$. The product was purified by column chromatography (silica deprotonated with 5% $NEt_3$, PE : EE = 1 : 1, $R_f$ = 0.41). After removing the solvent at low temperature the yellow product was washed two times with *n*-pentane and dried *in vacuo*. Yield: 26%. Single crystals for X-ray diffraction analysis were obtained by slow evaporation of a $CH_2Cl_2$ solution. $^1$H NMR (400 MHz, $C_6D_6$): $\delta$ 7.81 (br s, 2H, H5, H9), 7.58 (d, 2H, $^3J_{HH}$ = 3.65 Hz, H3, H7), 6.22 (dd, 2H, $^3J_{HH}$ = 3.65 Hz, $^3J_{HH}$ = 1.89 Hz, H4, H8), 1.29 (m, 12H, P–C$H_2$–), 0.73 (m, 18H, P–$CH_2$–C$H_3$). $^{31}$P NMR (161.9 MHz, $C_6D_6$): $\delta$ 9.69 (s, with satellites $J_{PtP}$ = 2600 Hz). $^{13}$C NMR (150.9 MHz, $C_6D_6$): $\delta$ 174.9 (t, $^2J_{PC}$ = 8.8 Hz, with satellites $J_{PtC}$ = 409 Hz, C1), 143.5 (s, with satellites $^3J_{PtC}$ = 15.8 Hz, C2, C6), 138.6 (s, C5, C9), 133.2 (s, with satellites $^3J_{PtC}$ = 22.0 Hz, C3, C7), 116.7 (s, C4, C8), 14.7 (t, $J_{PC}$ = 32.5 Hz, with satellites $^2J_{PtC}$ = 17.0 Hz, P–*C*$H_2$–), 7.6 (br s, P–$CH_2$–*C*$H_3$). $^{195}$Pt NMR (129.0 MHz, $C_6D_6$): $\delta$ −4081.6 (t, $J_{PtP}$ = 2600 Hz). C, H, N analysis calculated for $C_{21}H_{36}BF_2N_3O_2P_2Pt$: C, 37.74; H, 5.43; N, 6.29. Found: C, 37.78; H, 5.73; N, 6.40.

### *trans*-(4,4-Difluoro-4-bora-3a,4a-diaza-*s*-indacen-8-yl)-(methyl)-bis(triethylphosphine)-platinum(II) (Pt–$CH_3$)

A $CH_2Cl_2$ solution containing 40 mg (57 μmol, 1 eq.) of *cis*-Pt(BODIPY)Br($PEt_3$)$_2$ and 19.5 mg (76 μmol, 1.4 eq.) of AgOTf was refluxed for 5 min, then filtered and evaporated to dryness. The crude solid was placed under nitrogen atmosphere, 10 ml of diethyl ether were added and the solution was cooled to −78° C. To this bright orange solution 0.5 ml of a 0.18 M solution of methyl lithium in diethyl ether was added dropwise. The reaction mixture turned green while it was

allowed to warm to room temperature over 4 h. The mixture was filtered, the solvent was removed and the crude solid was purified by column chromatography (silica deprotonated with 5% $NEt_3$, petroleum ether : ethyl acetate = 8 : 3, $R_f$ = 0.73). The product was washed two times with *n*-pentane and dried *in vacuo*. Yield: 49%. Single crystals were obtained by slow diffusion of *n*-pentane in a saturated $C_6D_6$ solution. $^1$H NMR (600 MHz, $C_6D_6$): $\delta$ 7.92 (br s, 2H, H5, H9), 7.47 (d, 2H, $^3J_{HH}$ = 3.48 Hz, C3, C7), 6.31 (dd, 2H, $^3J_{HH}$ = 3.48 Hz, $^3J_{HH}$ = 2.05 Hz, H4, H8), 1.35 (m, 12H, P–C$H_2$–), 0.70 (dt, 18H, $^3J_{HH}$ = 7.67 Hz, $^3J_{PH}$ = 15.68 Hz, P–$CH_2$–C$H_3$), −0.24 (t with satellites, 3H, $^3J_{PH}$ = 6.82 Hz, $^2J_{PtH}$ = 24.9 Hz, C$H_3$). $^{31}$P NMR (161.9 MHz, $C_6D_6$): $\delta$ 9.18 (s, with satellites $J_{PtP}$ = 2692 Hz). $^{13}$C NMR (150.9 MHz, $C_6D_6$): $\delta$ 210.6 (t, $^2J_{PC}$ = 9.41 Hz, C1), 146.4 (s with satellites, $^2J_{PtC}$ = 22.0 Hz, C2, C6), 136.4 (s, C5, C9), 132.2 (s with satellites, $^3J_{PtC}$ = 37.0 Hz, C3, C7), 115.6 (s, C4, C8), 14.3 (t with satellites, $J_{PC}$ = 17.0 Hz, $^2J_{PtC}$ = 67.1 Hz, P–C$H_2$–), 8.0 (s with satellites, $^3J_{PtC}$ = 25.5 Hz, P–$CH_2$–C$H_3$), −14.0 (t, $^2J_{PC}$ = 8.80 Hz, with satellites $J_{PtC}$ = 412.7 Hz, C10). $^{195}$Pt NMR (86.0 MHz, $C_6D_6$): $\delta$ −4396 (t, $J_{PtP}$ = 2692 Hz). C, H, N analysis calculated for $C_{22}H_{39}BF_2N_2P_2Pt$: C, 41.46; H, 6.17; N, 4.39. Found: C, 41.34; H, 6.47; N, 4.51.

## Notes

The authors declare no competing financial interest.

## Acknowledgements

We thank the state of Baden-Württemberg and the Deutsche Forschungsgemeinschaft for providing us with access to the computational facilities of the bwFor computer cluster JUSTUS.

## References

1 A. Treibs and F.-H. Kreuzer, *Liebigs Ann. Chem.*, 1968, **718**, 208–223.
2 A. Loudet and K. Burgess, *Chem. Rev.*, 2007, **107**, 4891–4932.
3 G. Ulrich, R. Ziessel and A. Harriman, *Angew. Chem., Int. Ed.*, 2008, **47**, 1184–1201.
4 N. Boens, B. Verbelen and W. Dehaen, *Eur. J. Org. Chem.*, 2015, 6577–6595.
5 F. Li, S. I. Yang, Y. Ciringh, J. Seth, C. H. Martin, D. L. Singh, D. Kim, R. R. Birge, D. F. Bocian, D. Holten and J. S. Lindsey, *J. Am. Chem. Soc.*, 1998, **120**, 10001–10017.
6 J. Chen, A. Burghart, A. Derecskei-Kovacs and K. Burgess, *J. Org. Chem.*, 2000, **65**, 2900–2906.
7 F. E. Alemdaroglu, S. C. Alexander, D. Ji, D. K. Prusty, M. Börsch and A. Herrmann, *Macromolecules*, 2009, **42**, 6529–6536.
8 M. T. Whited, P. I. Djurovich, S. T. Roberts, A. C. Durrell, C. W. Schlenker, S. E. Bradforth and M. E. Thompson, *J. Am. Chem. Soc.*, 2011, **133**, 88–96.
9 R. Ziessel, G. Ulrich, A. Haefele and A. Harriman, *J. Am. Chem. Soc.*, 2013, **135**, 11330–11344.
10 T. Lazarides, T. M. McCornick, K. C. Wilson, S. Lee, D. W. McCamant and R. Eisenberg, *J. Am. Chem. Soc.*, 2011, **133**, 350–364.
11 M. Cordaro, P. Mineo, F. Nastasi and G. Magazzu, *RSC Adv.*, 2014, **4**, 43931–43933.
12 N. Boens, V. Leen and W. Dehaen, *Chem. Soc. Rev.*, 2012, **41**, 1130–1172.
13 T. Yogo, Y. Urano, Y. Ishitsuka, F. Maniwa and T. Nagano, *J. Am. Chem. Soc.*, 2005, **127**, 12162–12163.
14 J. Zhao, K. Xu, W. Yang, Z. Wang and F. Zhong, *Chem. Soc. Rev.*, 2015, **44**, 8904–8939.
15 A. Gorman, J. Killoran, C. O'Shea, T. Kenna, W. M. Gallagher and D. F. O'Shea, *J. Am. Chem. Soc.*, 2004, **126**, 10619–10631.
16 X.-F. Zhang and X. Yang, *J. Phys. Chem. B*, 2013, **117**, 5533–5539.
17 W. Wu, J. Zhao, J. Sun, L. Huang and X. Yi, *J. Mater. Chem. C*, 2013, **1**, 705–716.
18 W. Wu, J. Zhao, H. Guo, J. Sun, S. Ji and Z. Wang, *Chem. – Eur. J.*, 2012, **18**, 1961–1968.
19 J. Sun, F. Zhong, X. Yi and J. Zhao, *Inorg. Chem.*, 2013, **52**, 6299–6310.
20 F. Geist, A. Jackel and R. F. Winter, *Inorg. Chem.*, 2015, **54**, 10946–10957.
21 P. Batat, M. Cantuel, G. Jonusauskas, L. Scarpantonio, A. Palma, D. F. O'Shea and N. D. McClenaghan, *J. Phys. Chem. A*, 2011, **115**, 14034–14039.
22 X.-D. Wang and O. S. Wolfbeis, *Chem. Soc. Rev.*, 2014, **43**, 3666–3761.
23 W. Wu, J. Sun, X. Cui and J. Zhao, *J. Mater. Chem. C*, 2013, **1**, 4577–4589.
24 S. G. Awuah and Y. You, *RSC Adv.*, 2012, **2**, 11169–11183.
25 A. Kamkaew, S. H. Lim, H. B. Lee, L. V. Kiew, L. Y. Chung and K. Burgess, *Chem. Soc. Rev.*, 2013, **42**, 77–88.
26 R. Bonnett, *Chem. Soc. Rev.*, 1995, **24**, 19–33.
27 T. J. Dougherty, C. J. Gomer, B. W. Henderson, G. Jori, D. Kessel, M. Korbelik, J. Moan and Q. Peng, *J. Natl. Cancer Inst.*, 1998, **90**, 889–905.
28 D. E. J. G. J. Dolmans, D. Fukumura and R. K. Jain, *Nat. Rev. Cancer*, 2003, **3**, 380–387.
29 P. Agostinis, K. Berg, K. A. Cengel, T. H. Foster, A. W. Girotti, S. O. Gollnick, S. M. Hahn, M. R. Hamblin, A. Juzeniene, D. Kessel, M. Korbelik, J. Moan, P. Mroz, D. Nowis, J. Piette, B. C. Wilson and J. Golab, *CA – Cancer J. Clin.*, 2011, **61**, 250–281.
30 W. H. Lam, E. S.-H. Lam and V. W.-W. Yam, *J. Am. Chem. Soc.*, 2013, **135**, 15135–15143.
31 J. A. G. Williams, *Top. Curr. Chem.*, 2007, **281**, 205–268.
32 V. W.-W. Yam and K. M.-C. Wong, *Chem. Commun.*, 2011, **47**, 11579–11592.

 

33 P.-T. Chou, Y. Chi, M.-W. Chung and C.-C. Lin, *Coord. Chem. Rev.*, 2011, **255**, 2653–2665.
34 F. Geist, A. Jackel and R. F. Winter, *Dalton Trans.*, 2015, **44**, 3974–3987.
35 T. G. Appleton, H. C. Clark and L. E. Manzer, *Coord. Chem. Rev.*, 1973, **10**, 335–422.
36 T. J. McCarthy, R. G. Nuzzo and G. M. Whitesides, *J. Am. Chem. Soc.*, 1981, **103**, 3396–3403.
37 S. Lentijo, J. A. Miguel and P. Espinet, *Inorg. Chem.*, 2010, **49**, 9169–9177.
38 P. Nilsson, F. Plamper and O. F. Wendt, *Organometallics*, 2003, **22**, 5235–5242.
39 R. Bardi and A. M. Piazzesi, *Inorg. Chim. Acta*, 1981, **47**, 249–254.
40 C. Albrecht, C. Wagner, K. Merzweiler, T. Lis and D. Steinborn, *Appl. Organomet. Chem.*, 2005, **19**, 1155–1163.
41 S. J. Anderson and R. J. Goodfellow, *J. Chem. Soc., Dalton Trans.*, 1977, 1683–1686.
42 J. L. Burmeister and F. Basolo, *Inorg. Chem.*, 1964, **3**, 1587–1593.
43 E. Hartmann and R. M. Gschwind, *Angew. Chem., Int. Ed.*, 2013, **52**, 2350–2354.
44 C. Hansch, A. Leo and R. W. Taft, *Chem. Rev.*, 1991, **91**, 165–195.
45 C.-W. Hsu, C.-C. Lin, M.-W. Chung, Y. Chi, G.-H. Lee, P.-T. Chou, C.-H. Chang and P.-Y. Chen, *J. Am. Chem. Soc.*, 2011, **133**, 12085–12099.
46 C.-C. Hsu, C.-C. Lin, P.-T. Chou, C.-H. Lai, C.-W. Hsu, C.-H. Lin and Y. Chi, *J. Am. Chem. Soc.*, 2012, **134**, 7715–7724.
47 Y.-C. Chang, K.-C. Tang, H.-A. Pan, S.-H. Liu, I. O. Koshevoy, A. J. Karttunen, W.-Y. Hung, M.-H. Cheng and P.-T. Chou, *J. Phys. Chem. C*, 2013, **117**, 9623–9632.
48 E. Yu-Tzu Li, T.-Y. Jiang, Y. Chi and P.-T. Chou, *Phys. Chem. Chem. Phys.*, 2014, **16**, 26184–26192.
49 W. Wu, C. Cheng, W. Wu, H. Guo, S. Ji, P. Song, K. Han, J. Zhao, X. Zhang, Y. Wu and G. Du, *Eur. J. Inorg. Chem.*, 2010, **2010**, 4683–4696.
50 W. Wu, W. Wu, S. Ji, H. Guo, P. Song, K. Han, L. Chi, J. Shao and J. Zhao, *J. Mater. Chem.*, 2010, **20**, 9775–9786.
51 Y. Liu, H. Guo and J. Zhao, *Chem. Commun.*, 2011, **47**, 11471–11473.
52 W. Wu, W. Wu, S. Ji, H. Guo and J. Zhao, *Dalton Trans.*, 2011, **40**, 5953–5963.
53 H. Sun, H. Guo, W. Wu, X. Liu and J. Zhao, *Dalton Trans.*, 2011, **40**, 7834–7841.
54 H. Xiang, L. Zhou, Y. Feng, J. Cheng, D. Wu and X. Zhou, *Inorg. Chem.*, 2012, **51**, 5208–5212.
55 H. Wasserman and R. W. Murray, *Singlet Oxygen*, Academic Press, New York, 1979.
56 H. H. Wasserman and J. L. Ives, *Tetrahedron*, 1981, **37**, 1825–1852.
57 S.-Y. Takizawa, R. Aboshi and S. Murata, *Photochem. Photobiol. Sci.*, 2011, **10**, 895–903.
58 Y. Usui, *Chem. Lett.*, 1973, **2**, 743–744.
59 F. Wilkinson, W. P. Helman and A. B. Ross, *J. Phys. Chem. Ref. Data*, 1993, **22**, 113–262.
60 J. N. Chaon, G. R. Jamieson and R. S. Sinclair, *Chem. Phys. Lipids*, 1987, **43**, 81–99.
61 W. Herrendorf and W. Bärnighausen, *X-Area, Version 1.06*, Stoe, Darmstadt, Karslruhe, Gießen, 1999.
62 G. M. Sheldrick, *SHELXL-97, Program for Crystal Structure Solution and Refinement*, Universität Göttingen, 1997.
63 G. M. Sheldrick, *Acta Crystallogr., Sect. A: Fundam. Crystallogr.*, 2008, **64**, 112–122.
64 L. J. Farrugia, *J. Appl. Crystallogr.*, 1997, **30**, 565.
65 L. J. Farrugia, *J. Appl. Crystallogr.*, 2012, **45**, 849–854.
66 P. R. Edgington, P. McCabe, C. F. Macrae, E. Pidcock, G. P. Shields, R. Taylor, M. Towler and J. Van De Streek, *J. Appl. Crystallogr.*, 2006, **39**, 453–457.
67 M. J. Frisch, G. Trucks, H. B. Schlegel, G. E. Scuseria, M. A. Robb, J. R. Cheeseman, G. Scalmani, V. Barone, B. Mennucci, G. A. Petersson, H. Nakatsuji, M. Caricato, X. Li, H. P. Hratchian, A. F. Izmaylov, J. Blonio, G. Zheng, J. L. Sonnenberg, M. Hada, M. Ehara, K. Toyota, R. Fukuda, J. Hasegawa, M. Ishida, T. Nakajima, Y. Honda, O. Kitao, H. Nakai, T. Vreven, J. A. M. Jr., J. E. Peralta, F. Ogliaro, M. Bearpark, J. J. Heyd, E. Brothers, K. N. Kudin, V. N. Staroverov, R. Kobayashi, J. Normand, K. Raghavachari, A. Rendell, J. C. Burant, S. S. Iyengar, J. Tomasi, M. Cossi, N. Rega, J. M. Millam, M. Klene, J. E. Knox, J. B. Cross, V. Bakken, C. Adamo, J. Jaramillo, R. Gomperts, R. E. Stratmann, O. Yazyev, A. J. Austin, R. Cammi, C. Pomelli, J. W. Ochterski, R. L. Martin, K. Morokuma, V. G. Zakrzewski, G. A. Voth, P. Salvador, J. J. Dannenberg, S. Dapprich, A. D. Daniels, Ö. Farkas, J. B. Foresman, J. V. Ortiz, J. Cioslowski and D. J. Fox, *Gaussian 09, Revision C.01*, Gaussian, Inc., Wallingford, CT, USA, 2009.
68 O. Gunnarsson and B. I. Lundqvist, *Phys. Rev. B: Solid State*, 1976, **13**, 4274.
69 W. Küchle, M. Dolg, H. Stoll and H. Preuss, *J. Chem. Phys.*, 1994, **100**, 7535–7532.
70 M. Dolg, H. Stoll and H. Preuss, *J. Chem. Phys.*, 1989, **90**, 1730–1734.
71 D. Andrae, U. Haeussermann, M. Dolg, H. Stoll and H. Preuss, *Theor. Chim. Acta*, 1990, **77**, 123.
72 P. H. Hariharan and J. A. Pople, *Theor. Chim. Acta*, 1973, **28**, 213–222.
73 J. P. Perdew, K. Burke and M. Enzerhof, *Phys. Rev. Lett.*, 1996, **77**, 3865–3868.
74 J. P. Perdew, K. Burke and M. Ernzerhof, *Phys. Rev. Lett.*, 1997, **78**, 1396–1396.
75 C. Adamo and V. Barone, *J. Chem. Phys.*, 1999, **110**, 6158–6170.
76 E. Cancés, B. Menucci and J. Tomasi, *J. Chem. Phys.*, 1997, **107**, 3032–3041.
77 B. Mennucci and J. Tomasi, *J. Chem. Phys.*, 1997, **106**, 5151–5158.

78 M. Cossi, N. Rega, G. Scalmani and V. Barone, *J. Comput. Chem.*, 2003, **24**, 669–681.
79 E. Runge and K. U. G. E, *Phys. Rev. Lett.*, 1984, **52**, 997–1000.
80 N. M. O'Boyle, A. L. Tenderholt and K. M. Langner, *J. Comput. Chem.*, 2008, **29**, 839–845.
81 T. Keith and J. Millam, *GaussView, Version 3*, Shawnee Mission, KS, USA, 2009.
82 M. D. Hanwell, D. E. Curtis, D. C. Lonie, T. Vandermeersch, E. Zurek and G. R. Hutchinson, *J. Cheminf.*, 2012, **4**, 17.
83 N. Adarsh, M. Shanmugasundaram, R. R. Avirah and D. Ramaiah, *Chem. – Eur. J.*, 2012, **18**, 12655–12662.



 

# Complexes *trans*-Pt(BODIPY)X($PEt_3$)$_2$: Excitation Energy-Dependent Modulation of Fluorescence and Phosphorescence Emissions and Application to Oxygen Sensing and Photocatalysis

Peter Irmler and Rainer F. Winter*

Fachbereich Chemie der Universität Konstanz, Universitätsstraße 10, D-78464 Konstanz, Germany

## Supporting Information

### Table of Contents



### List of Figures

## List of Tables

## NMR Spectra

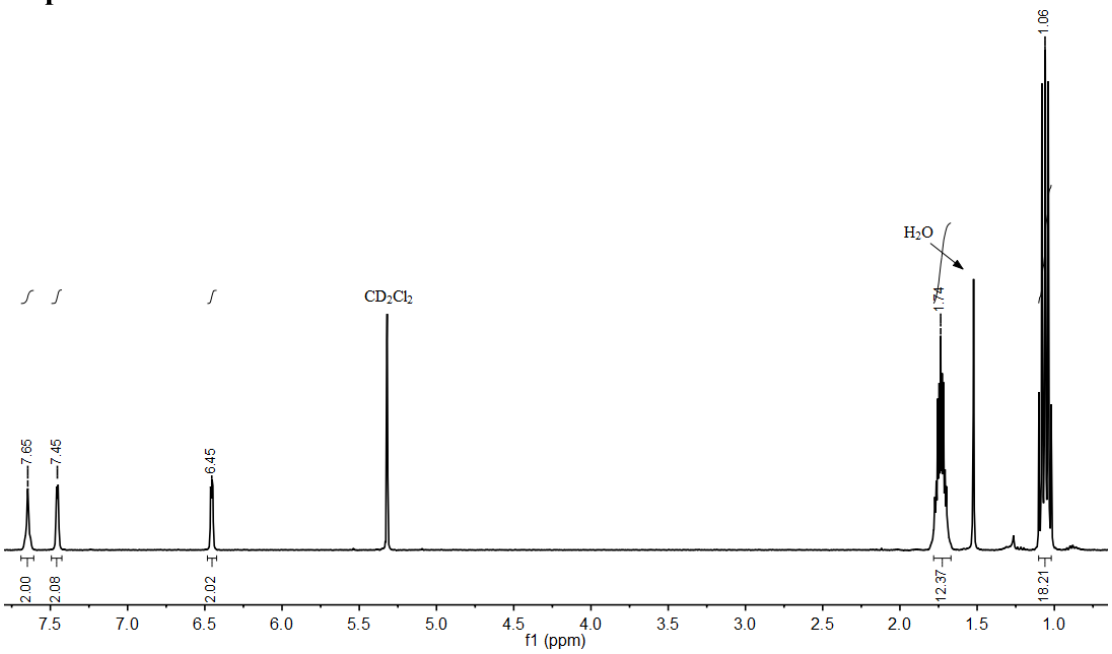


**Figure S1:** $^{1}H$ NMR spectrum of **Pt-Cl** in $CD_2Cl_2$.

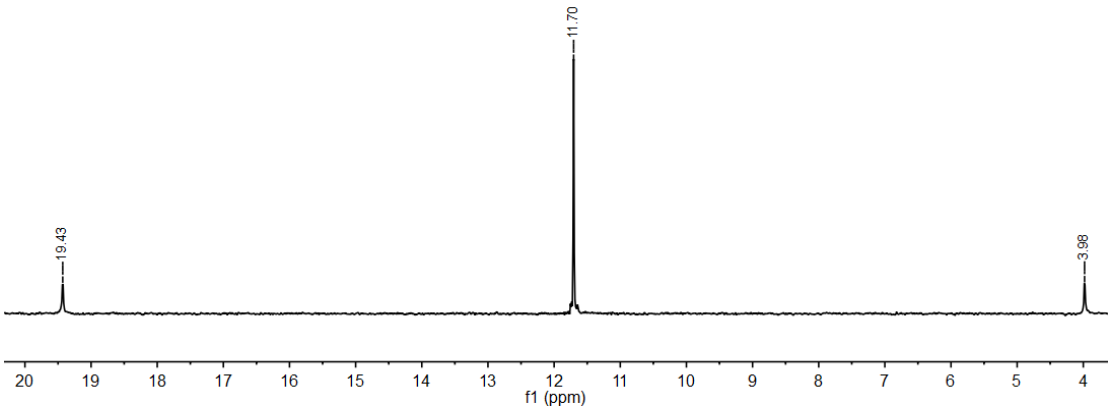


**Figure S2:** $^{31}P\{^{1}H\}$ NMR spectrum of **Pt-Cl** in $CD_2Cl_2$.

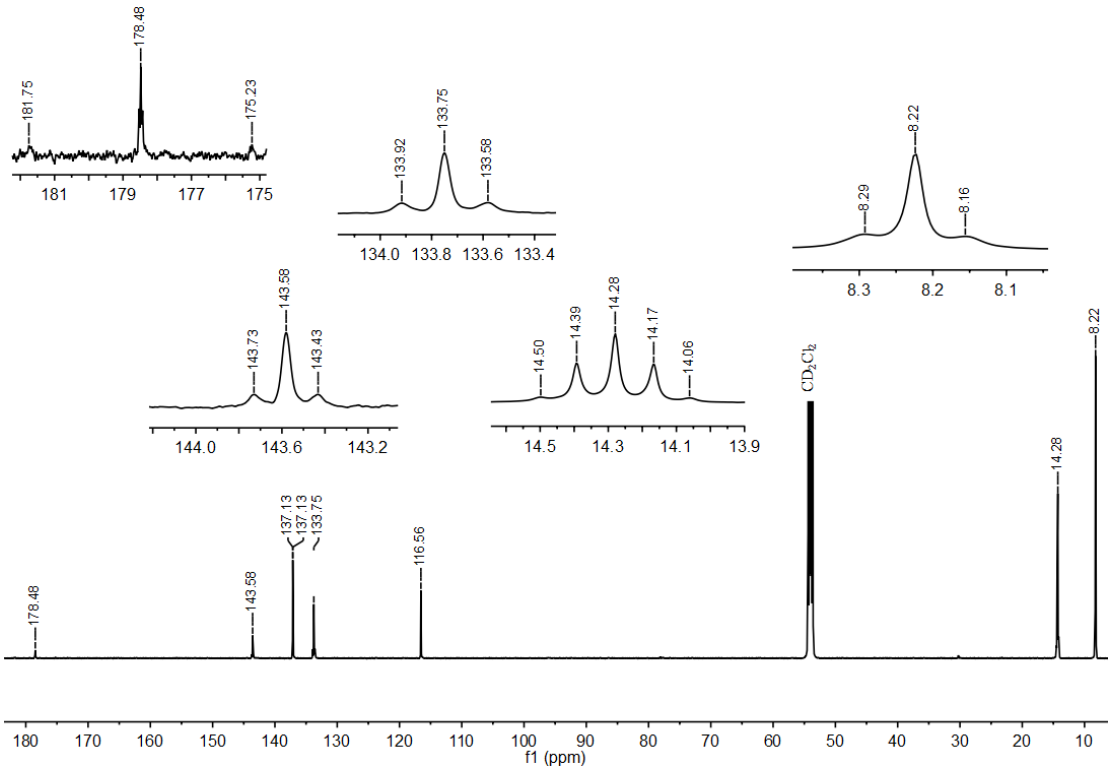


**Figure S3:** $^{13}C\{^{1}H\}$ NMR spectrum of **Pt-Cl** in $CD_2Cl_2$.

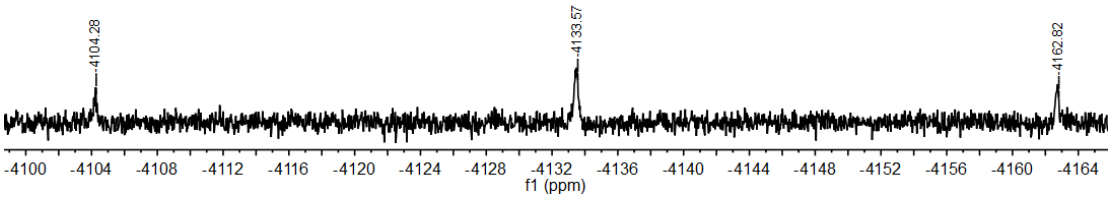


**Figure S4:** $^{195}Pt\{^{1}H\}$ NMR spectrum of **Pt-Cl** in $CD_2Cl_2$.

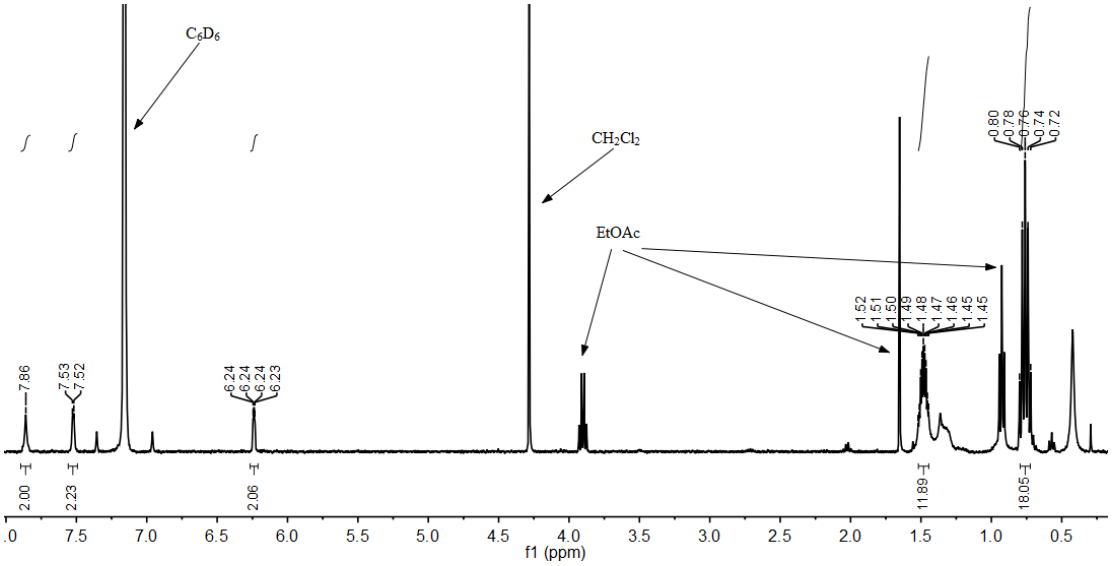


**Figure S5:** $^{1}$H NMR spectrum of **Pt-Cl** in $C_6D_6$.

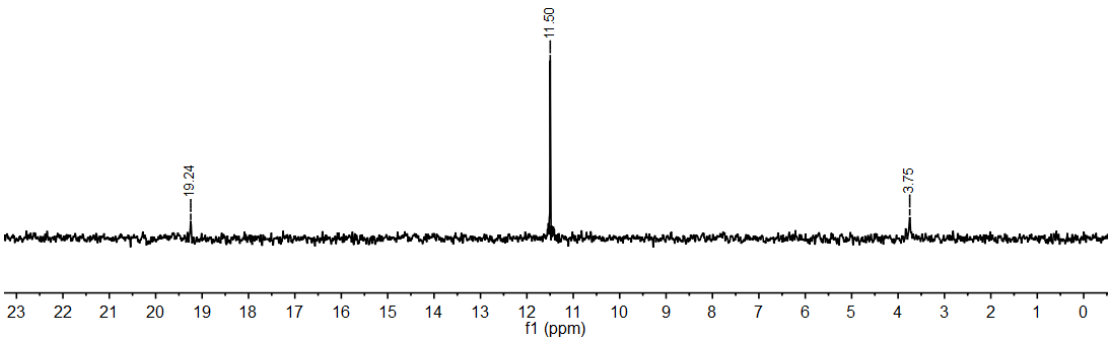


**Figure S6:** $^{31}$P{$^{1}$H} NMR spectrum of **Pt-Cl** in $C_6D_6$.

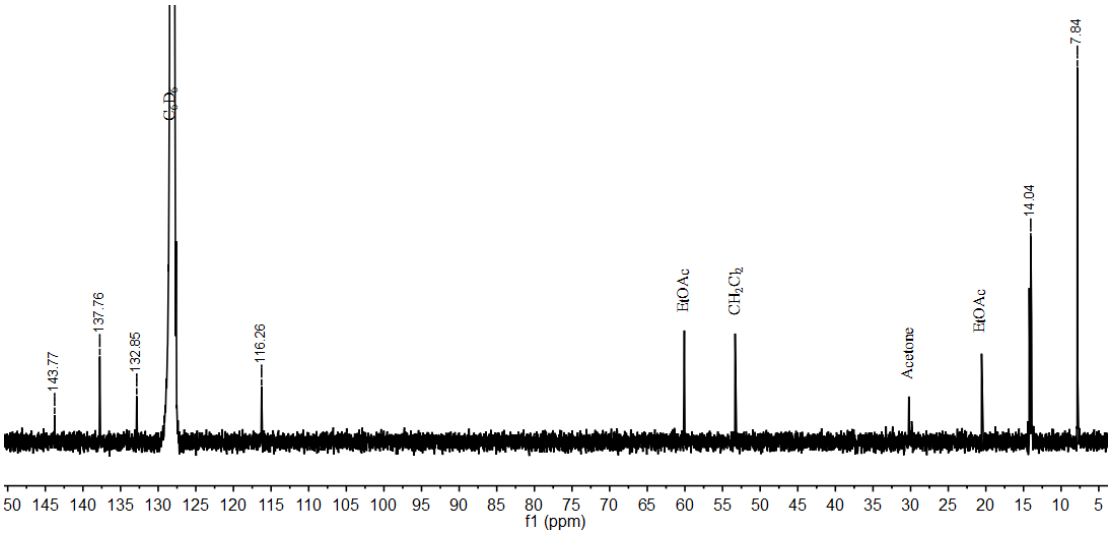


**Figure S7:** $^{13}$C{$^{1}$H} NMR spectrum of **Pt-Cl** in $C_6D_6$.

**Pt-Cl**: $^{1}$H NMR (600 MHz, $C_6D_6$): δ 7.86 (br s, 2H, H5, H9), 7.52 (d, 2H, $^{3}J_{HH}$ = 3.56 Hz, H3, H7), 6.24 (dd, 2H, $^{3}J_{HH}$ = 3.56 Hz, $^{3}J_{HH}$ = 1.56 Hz, H3, H8), 1.48 (m, 12H, P-C$H_2$-), 0.76 (m, 18H, P-$CH_2$-C$H_3$). $^{31}$P NMR (161.9 MHz, $C_6D_6$): δ 11.50 ppm (s, with satellites $J_{PtP}$ = 2508 Hz). $^{13}$C NMR (150.9 MHz, $C_6D_6$): δ 143.77 (s, C2, C6), 137.76 (s, C5, C9), 132.85 (s, C3, C7), 116.26 (s, C3, C7), 14.04 (t, $J_{PC}$ = 17.1 Hz, P-$CH_2$-), 7.84 (br s, P-$CH_2$-$CH_3$), C1 was not detected due to a low signal to noise ratio.

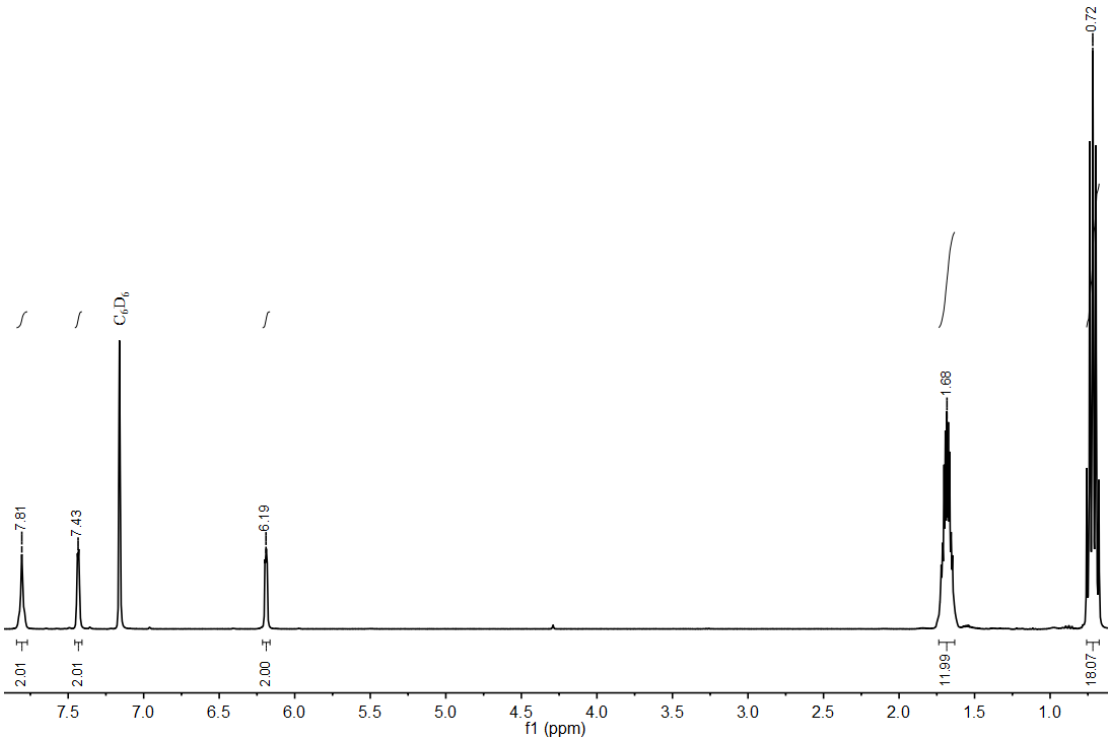


**Figure S8:** $^{1}$H NMR spectrum of **Pt-I** in $C_6D_6$.

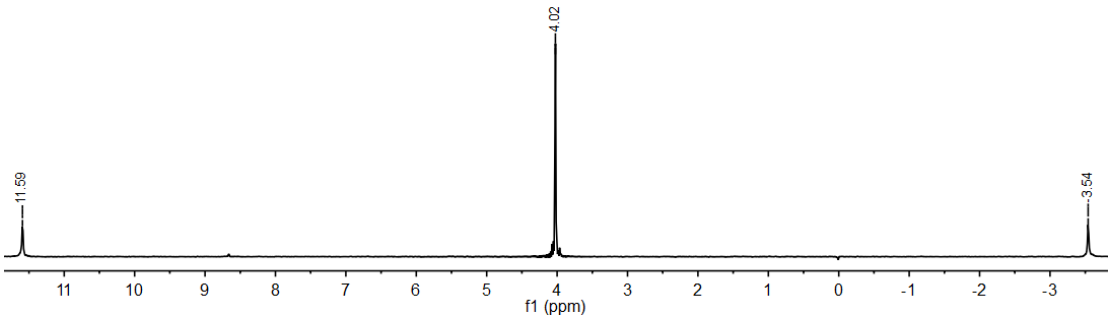


**Figure S9:** $^{31}$P{$^{1}$H} NMR spectrum of **Pt-I** in $C_6D_6$.

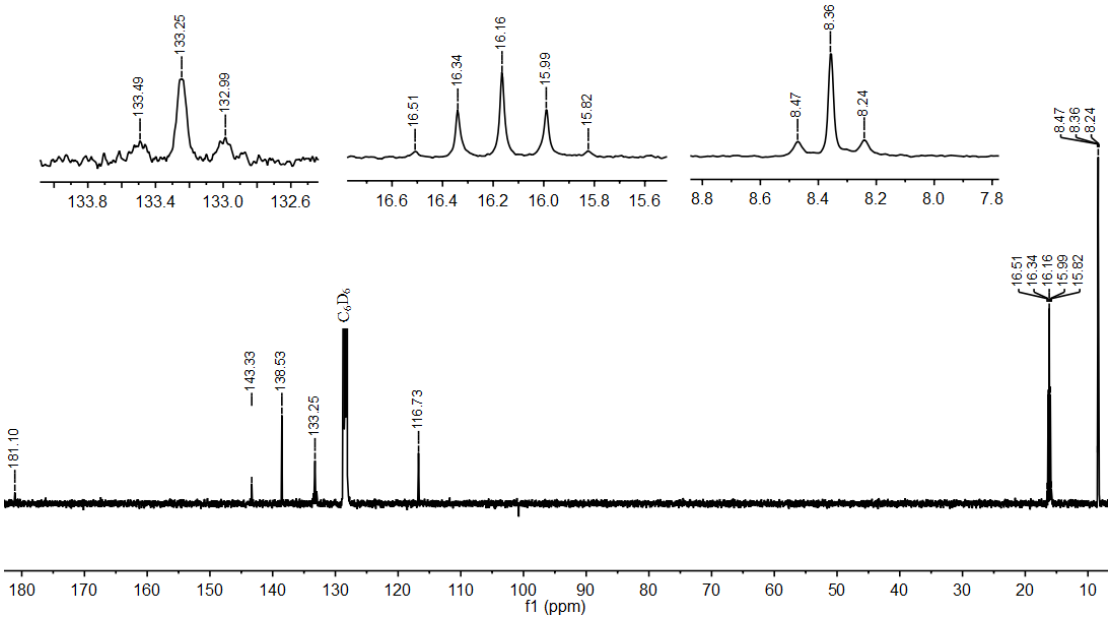


**Figure S10:** $^{13}C\{^{1}H\}$ NMR spectrum of **Pt-I** in $C_6D_6$.

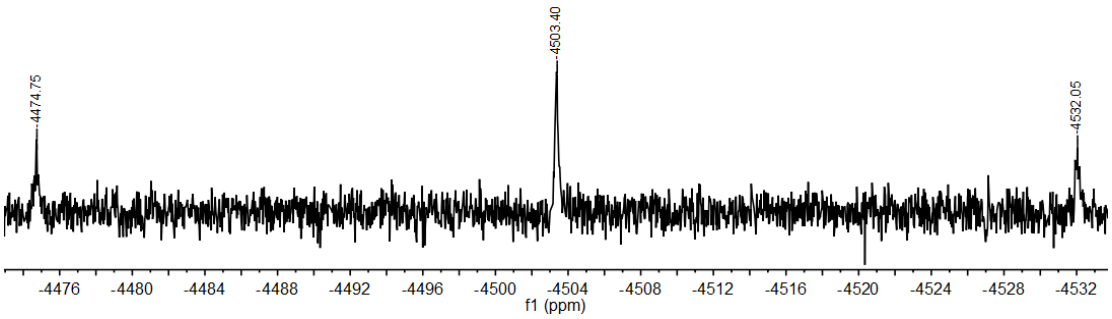


**Figure S11:** $^{195}Pt\{^{1}H\}$ NMR spectrum of **Pt-I** in $C_6D_6$.

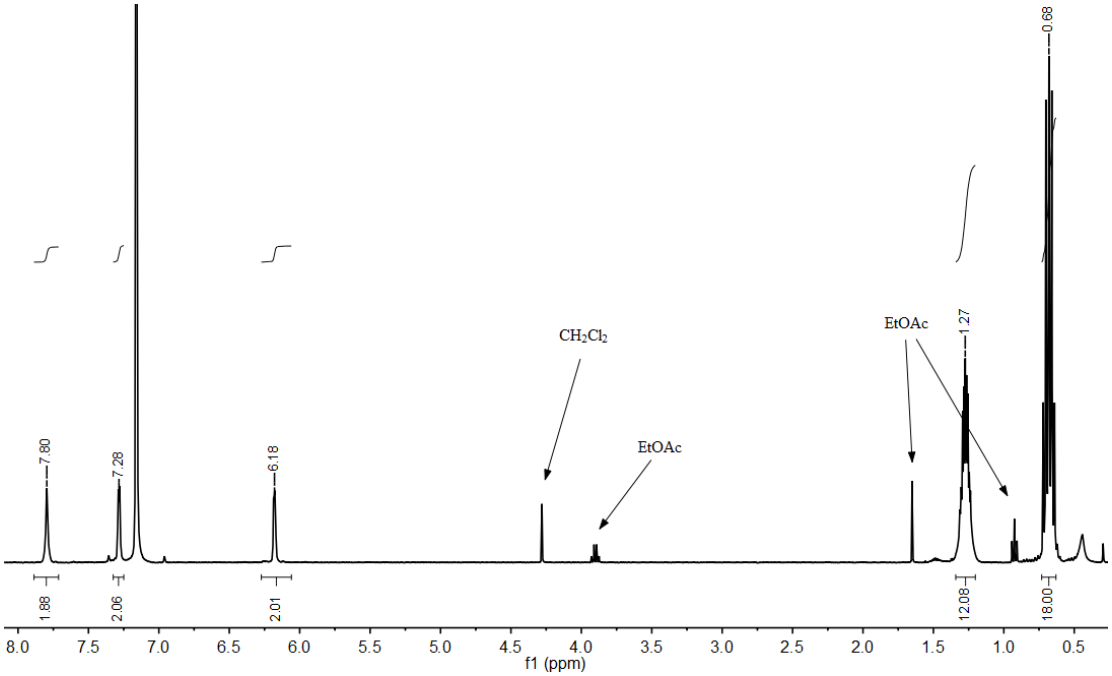


**Figure S12:** $^{1}H$ NMR spectrum of **Pt-NCS** in $C_6D_6$.

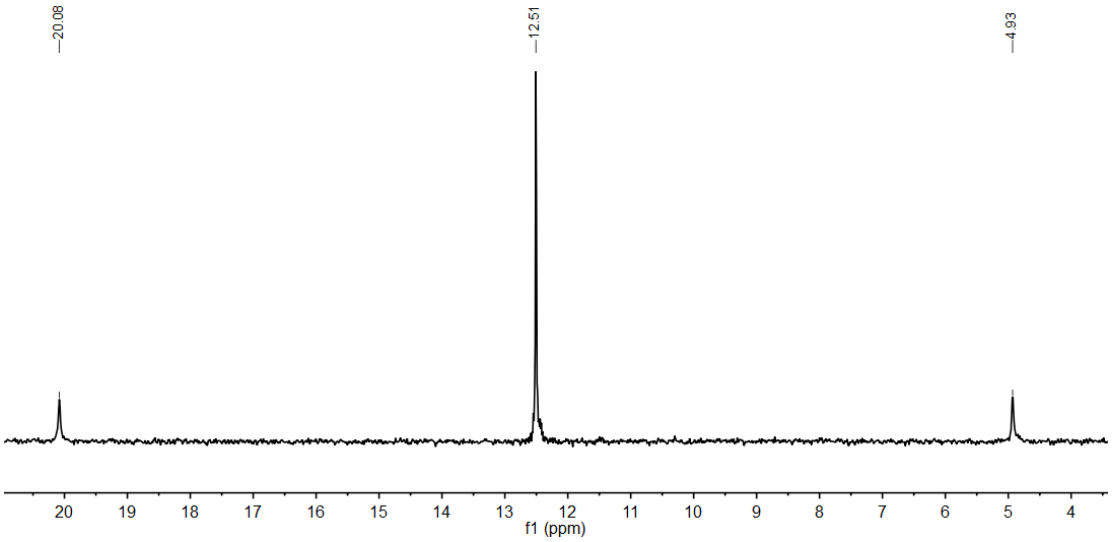


**Figure S13:** $^{31}P\{^{1}H\}$ NMR spectrum of **Pt-NCS** in $C_6D_6$.

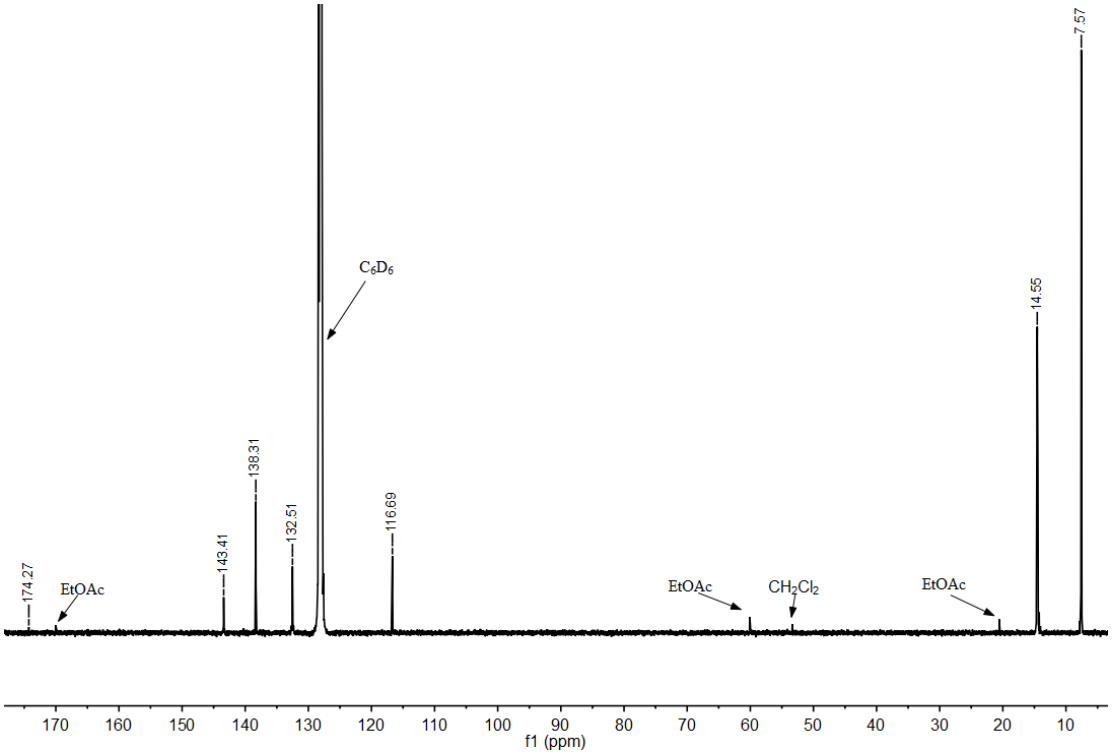


**Figure S14:** $^{13}C\{^{1}H\}$ NMR spectrum of **Pt-NCS** in $C_6D_6$.

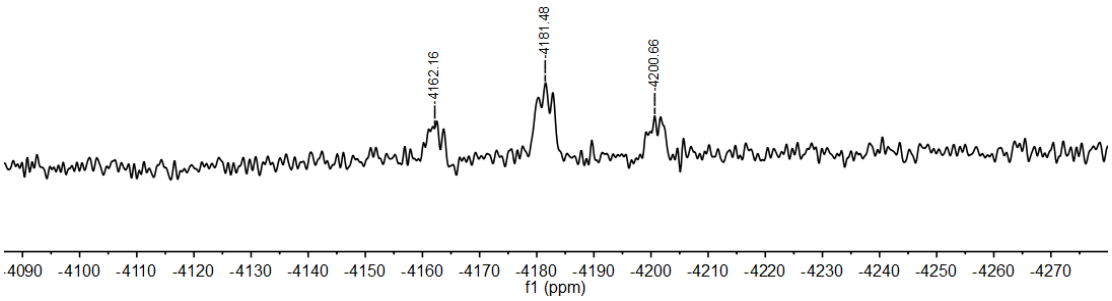


**Figure S15:** $^{195}Pt\{^{1}H\}$ NMR spectrum of **Pt-NCS** in $C_6D_6$.

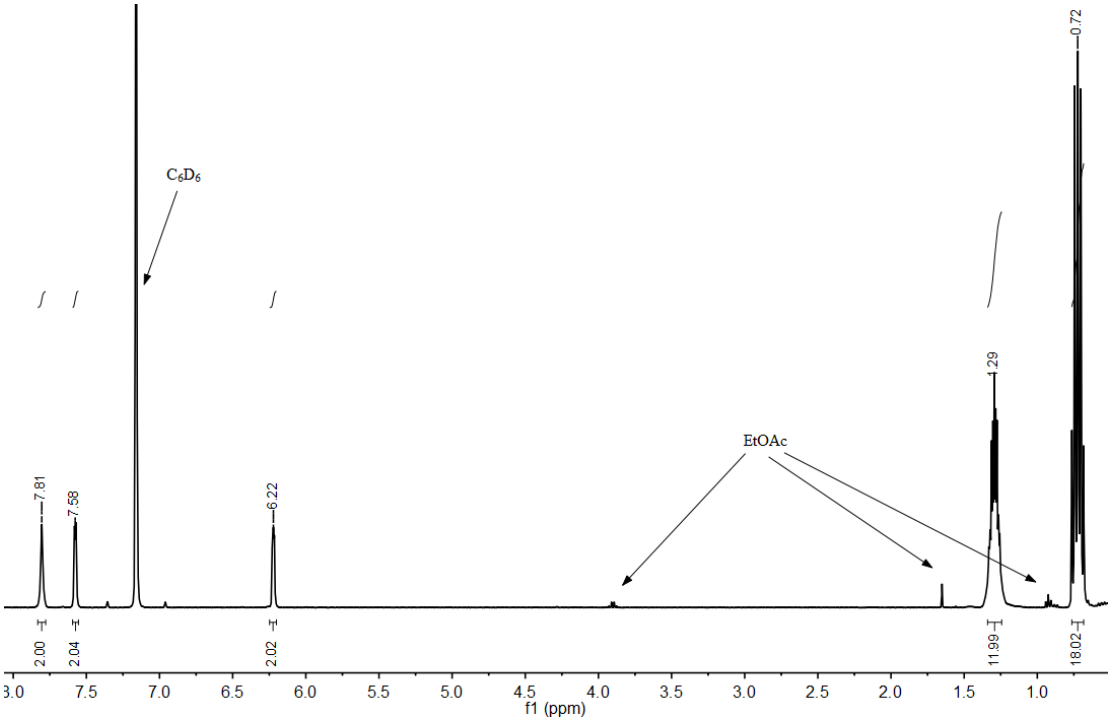


**Figure S16:** $^{1}$H NMR spectrum of **Pt-NO$_2$** in $C_6D_6$.

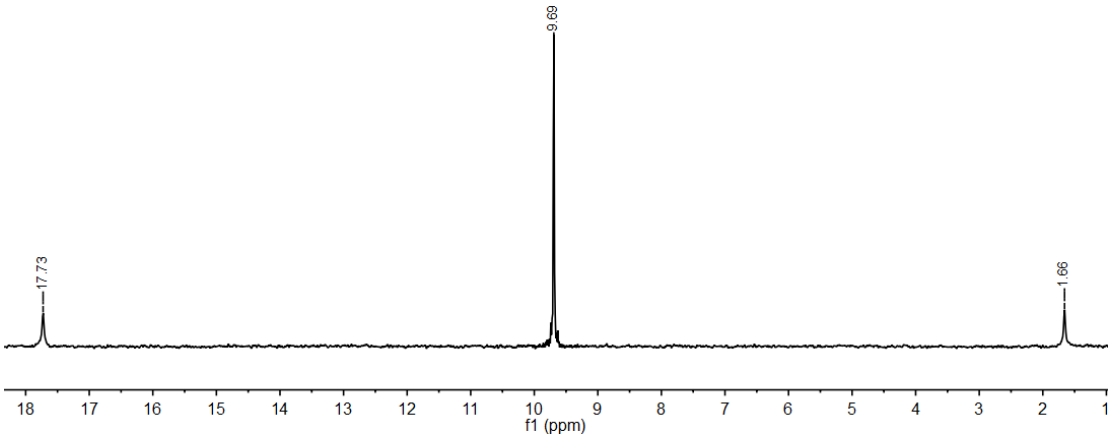


**Figure S17:** $^{31}$P{$^{1}$H} NMR spectrum of **Pt-NO$_2$** in $C_6D_6$.

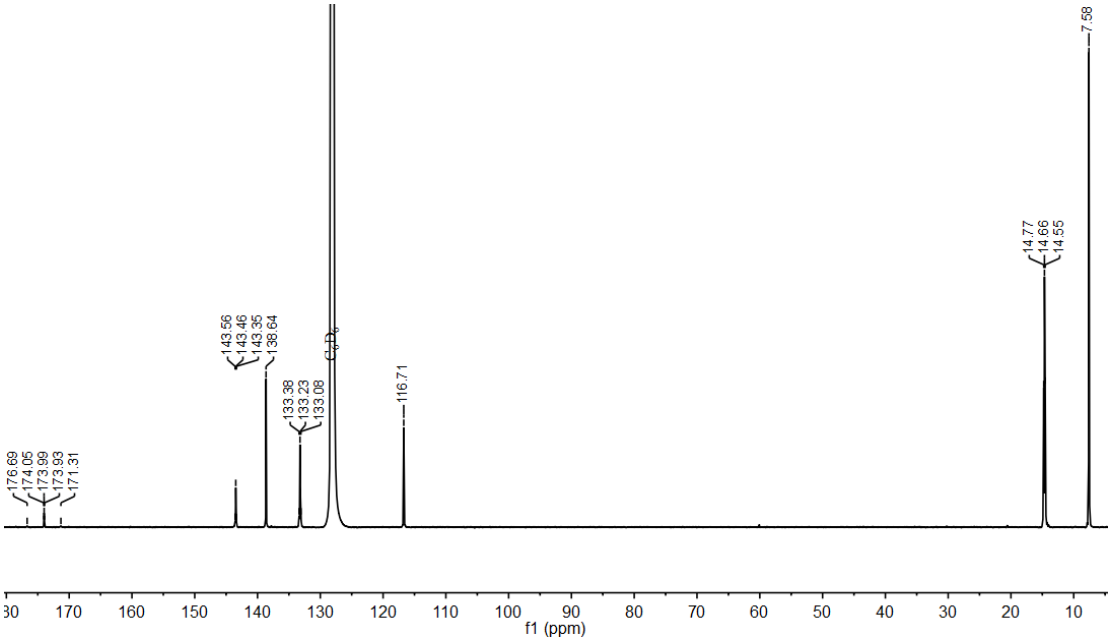


**Figure S18:** $^{13}C\{^{1}H\}$ NMR spectrum of **Pt-NO₂** in $C_6D_6$.

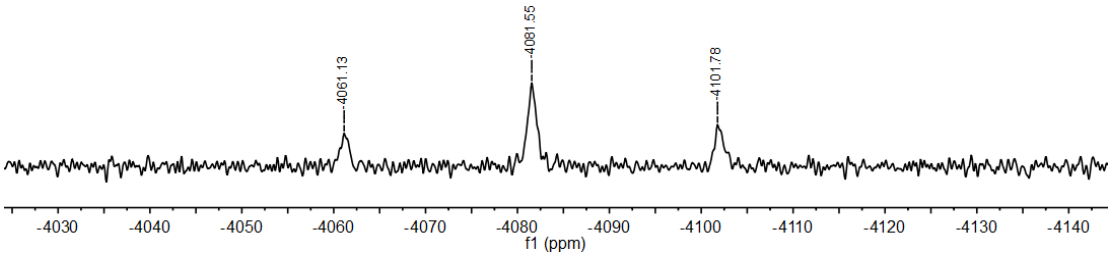


**Figure S19:** $^{195}Pt\{^{1}H\}$ NMR spectrum of **Pt-NO₂** in $C_6D_6$.

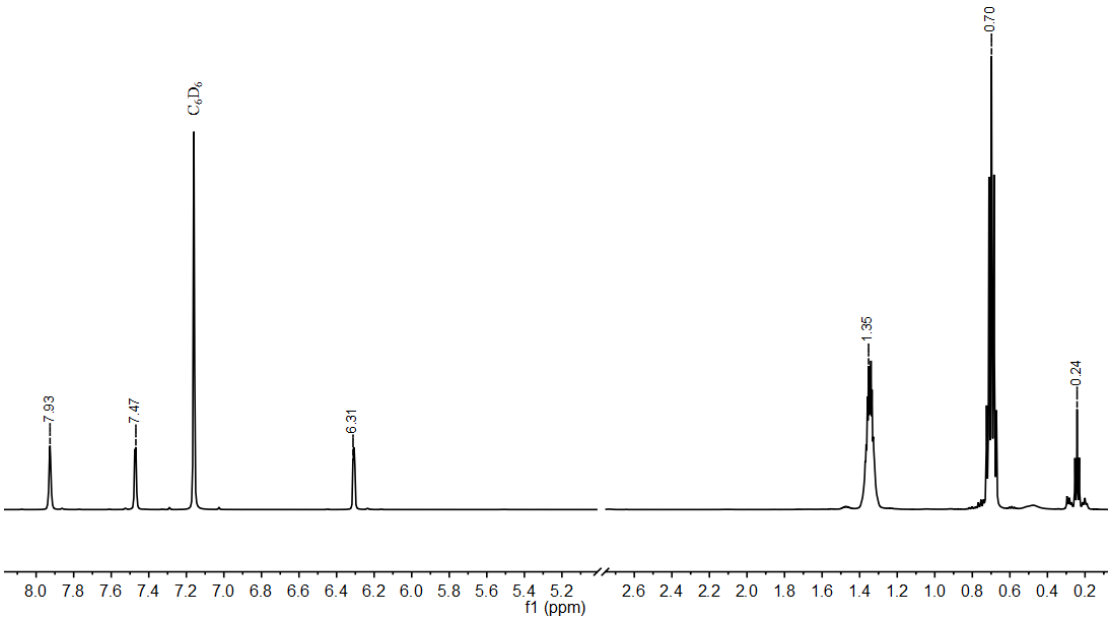


**Figure S20:** $^{1}H$ NMR spectrum of **Pt-CH₃** in $C_6D_6$.

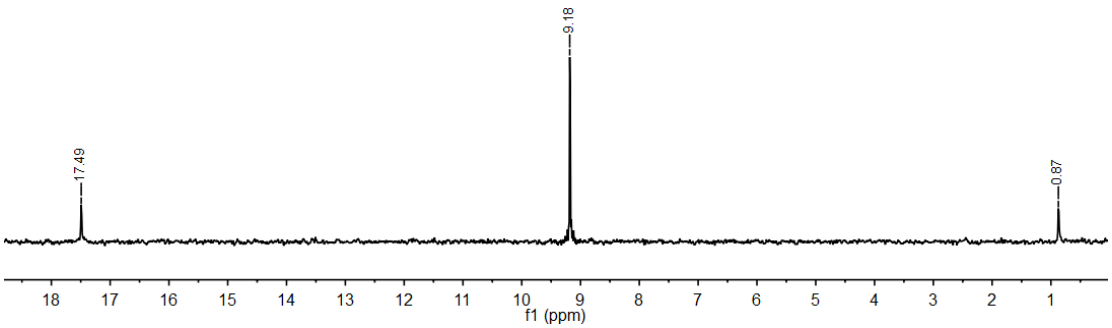


**Figure S21:** $^{31}P\{^{1}H\}$ NMR spectrum of **Pt-CH$_3$** in $C_6D_6$.

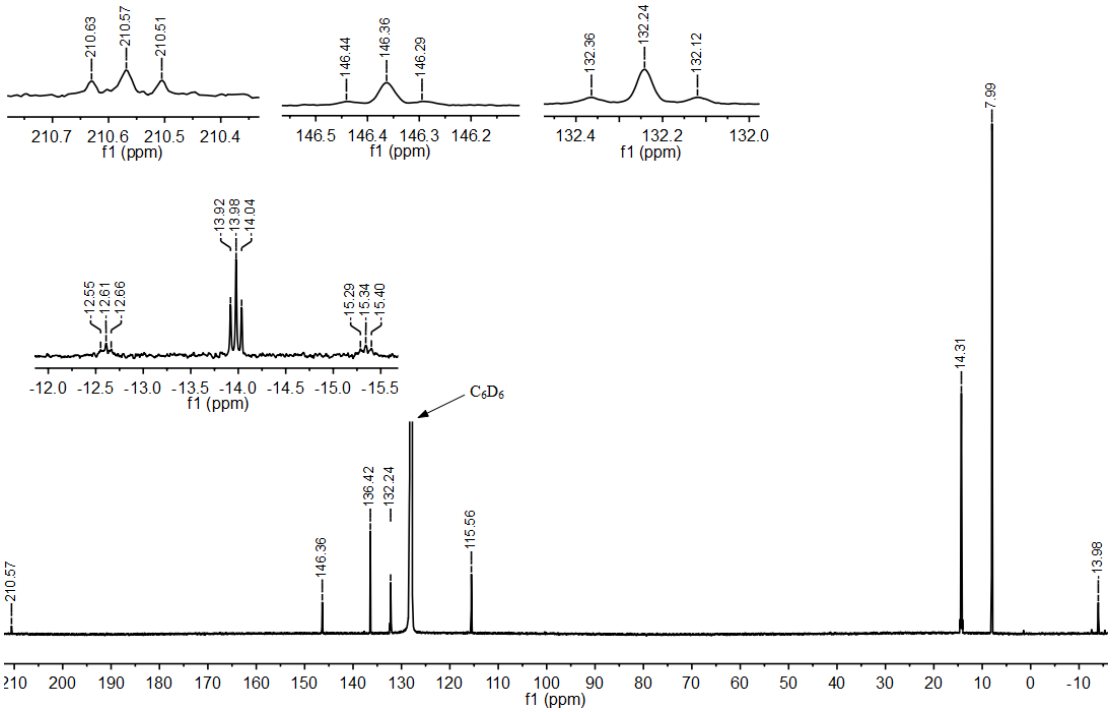


**Figure S22:** $^{13}C\{^{1}H\}$ NMR spectrum of **Pt-CH$_3$** in $C_6D_6$.

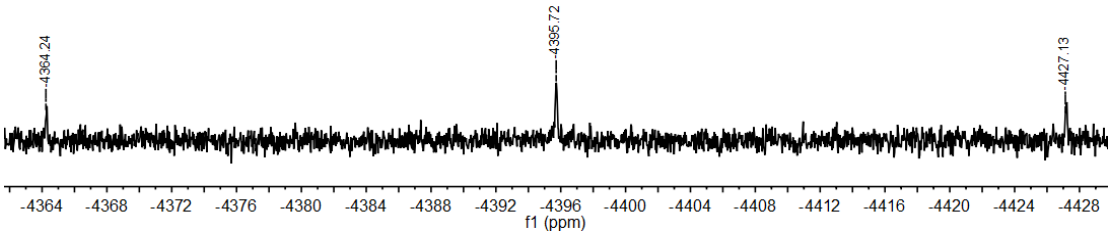


**Figure S23:** $^{195}Pt\{^{1}H\}$ NMR spectrum of **Pt-CH$_3$** in $C_6D_6$.

## Single Crystal X-ray Diffraction

**Table S1:** Crystal and refinement data for **Pt-Cl**, **Pt-I**, **Pt-NCS**, **Pt-$NO_2$** and **Pt-$CH_3$**.

| | **Pt-Cl** | **Pt-I** | **Pt-NCS** |
|---|---|---|---|
| Emp. formula / f. wt. / g $mol^{-1}$ | $C_{21}H_{36}BClF_2N_2P_2Pt$ / 657.81 | $C_{21}H_{36}F_2IN_2P_2Pt$ / 749.26 | $C_{22}H_{36}BF_2N_3P_2PtS$ / 680.44 |
| Temperature / K | 100(2) | 100(2) | 100(2) |
| Crystal system | monoclinic | orthorhombic | monoclinic |
| Space group | P $2_1/c$ | C *m c* $2_1$ | P $2_1/n$ |
| *a*, *b*, *c* / Å | 17.4058(6), 17.0196(5), 17.2625(6) | 13.4838(7), 14.5951(10), 13.7759(7) | 9.3599(4), 18.0669(7), 16.1360(7) |
| α, β, γ / deg | 90, 94.973(3), 90 | 90, 90, 90 | 90, 104.104(3), 90 |
| V / $Å^3$ | 5094.6(3) | 2711.1(3) | 2646.41(19) |
| Z | 8 | 4 | 4 |
| $D_{calcd}$ / g $cm^{-3}$ | 1.715 | 1.836 | 1.708 |
| Absorption coefficient / $mm^{-1}$ | 5.765 | 6.457 | 5.531 |
| θ range for data collection / deg | 1.677 to 28.061 | 2.056 to 26.795 | 1.722 to 27.343 |
| Limiting Indices | -22≤h≤22, -22≤k≤22, -22≤l≤22 | -17≤h≤17, -18≤k≤18, -17≤l≤17 | -12≤h≤12, -23≤k≤23, -20≤l≤20 |
| Reflections collected / unique (> 2σ(I)) | 83167 / 12219 [R(int) = 0.0818] | 18705 / 2982 [R(int) = 0.0936] | 41294 / 5964 [R(int) = 0.0666] |
| Data / Restraints / Parameter | 12219 / 0 / 553 | 2982 / 1 / 160 | 5964 / 0 / 319 |
| R (I> 2σ(I)) | $R_1$ = 0.0484, $wR_2$ = 0.0747 | $R_1$ = 0.0255, $wR_2$ = 0.0632 | $R_1$ = 0.0311, $wR_2$ = 0.0757 |
| $R_w$ (all data) | $R_1$ = 0.0620, $wR_2$ = 0.0755 | $R_1$ = 0.0282, $wR_2$ = 0.0640 | $R_1$ = 0.0346, $wR_2$ = 0.0773 |
| GooF (all Data) | 2.128 | 1.120 | 1.040 |
| Max. and min. res. dens. / $eÅ^{-3}$ | 2.559 and -2.016 | 1.607 and -1.633 | 2.892 and -1.740 |
| | **Pt-$NO_2$** | **Pt-$CH_3$** | |
| Emp. formula / f. wt. / g $mol^{-1}$ | $C_{21}H_{36}BF_2N_3O_2P_2Pt$ / 668.37 | $C_{22}H_{39}BF_2N_2P_2Pt$ / 637.39 | |
| Temperature / K | 100(2) | 100(2) | |
| Crystal system | monoclinic | monoclinic | |
| Space group | P $2_1/c$ | P $2_1$ | |
| *a*, *b*, *c* / Å | 9.6174(6), 16.8233(8), 16.3882(10) | 11.0980(4), 13.1409(6), 18.4244(6) | |
| α, β, γ / deg | 90, 103.184(5), 90 | 90, 106.287(3), 90 | |
| V / $Å^3$ | 2581.7(3) | 2579.14(18) | |
| Z | 4 | 4 | |
| $D_{calcd}$ / g $cm^{-3}$ | 1.720 | 1.641 | |
| Absorption coefficient / $mm^{-1}$ | 5.596 | 5.590 | |
| θ range for data collection / deg | 1.759 to 26.067 | 1.912 to 25.981 | |
| Limiting Indices | -11≤h≤11, -20≤k≤20, -20≤l≤19 | -13≤h≤13, -16≤k≤16, -22≤l≤22 | |
| Reflections collected / unique (> 2σ(I)) | 33380 / 5044 [R(int) = 0.1517] | 33984 / 10000 [R(int) = 0.0379] | |
| Data / Restraints / Parameter | 5044 / 0 / 295 | 10000 / 1 / 555 | |
| R (I> 2σ(I)) | $R_1$ = 0.0544, $wR_2$ = 0.0560 | $R_1$ = 0.0344, $wR_2$ = 0.0747 | |
| $R_w$ (all data) | $R_1$ = 0.0985, $wR_2$ = 0.0620 | $R_1$ = 0.0370, $wR_2$ = 0.0756 | |
| GooF (all Data) | 0.995 | 1.049 | |
| Max. and min. res. dens. / $eA^{-3}$ | 1.887 and -3.164 | 1.338 and -1.047 | |

**Table S2:** Bond lengths [Å] and angles [°] for **Pt-Cl**.

| | | | | | |
|---|---|---|---|---|---|
| C(1)-C(2) | 1.411(9) | B(2)-N(4) | 1.549(9) | F(4)-B(2)-N(3) | 110.4(6) |
| C(1)-C(6) | 1.427(8) | Cl(1)-Pt(1) | 2.3742(16) | F(3)-B(2)-N(4) | 109.7(6) |
| C(1)-Pt(1) | 1.980(6) | Cl(2)-Pt(2) | 2.3842(16) | F(4)-B(2)-N(4) | 109.6(6) |
| C(2)-C(3) | 1.386(8) | P(1)-Pt(1) | 2.3173(17) | N(3)-B(2)-N(4) | 106.6(5) |
| C(2)-N(1) | 1.393(8) | P(2)-Pt(1) | 2.3097(16) | C(5)-N(1)-C(2) | 108.4(5) |
| C(3)-C(4) | 1.388(9) | P(3)-Pt(2) | 2.3158(18) | C(5)-N(1)-B(1) | 126.0(6) |
| C(4)-C(5) | 1.403(9) | P(4)-Pt(2) | 2.3120(18) | C(2)-N(1)-B(1) | 125.3(6) |
| C(5)-N(1) | 1.339(8) | C(2)-C(1)-C(6) | 117.5(6) | C(9)-N(2)-C(6) | 107.3(6) |
| C(6)-N(2) | 1.394(8) | C(2)-C(1)-Pt(1) | 120.6(4) | C(9)-N(2)-B(1) | 125.2(5) |
| C(6)-C(7) | 1.402(9) | C(6)-C(1)-Pt(1) | 121.8(5) | C(6)-N(2)-B(1) | 127.2(5) |
| C(7)-C(8) | 1.378(9) | C(3)-C(2)-N(1) | 107.3(6) | C(26)-N(3)-C(23) | 107.4(5) |
| C(8)-C(9) | 1.383(10) | C(3)-C(2)-C(1) | 129.6(6) | C(26)-N(3)-B(2) | 127.0(6) |
| C(9)-N(2) | 1.360(8) | N(1)-C(2)-C(1) | 122.7(6) | C(23)-N(3)-B(2) | 125.5(5) |
| C(10)-C(11) | 1.535(9) | C(4)-C(3)-C(2) | 108.5(6) | C(30)-N(4)-C(27) | 108.4(6) |
| C(10)-P(1) | 1.820(7) | C(3)-C(4)-C(5) | 106.1(6) | C(30)-N(4)-B(2) | 126.8(6) |
| C(12)-C(13) | 1.526(10) | N(1)-C(5)-C(4) | 109.7(6) | C(27)-N(4)-B(2) | 124.5(5) |
| C(12)-P(1) | 1.799(8) | N(2)-C(6)-C(7) | 107.8(5) | C(12)-P(1)-C(10) | 107.4(3) |
| C(14)-C(15) | 1.526(11) | N(2)-C(6)-C(1) | 121.2(6) | C(12)-P(1)-C(14) | 101.5(4) |
| C(14)-P(1) | 1.838(7) | C(7)-C(6)-C(1) | 131.0(6) | C(10)-P(1)-C(14) | 106.9(3) |
| C(16)-C(17) | 1.544(9) | C(8)-C(7)-C(6) | 107.5(6) | C(12)-P(1)-Pt(1) | 111.9(2) |
| C(16)-P(2) | 1.823(7) | C(7)-C(8)-C(9) | 107.6(6) | C(10)-P(1)-Pt(1) | 114.6(2) |
| C(18)-C(19) | 1.514(9) | N(2)-C(9)-C(8) | 109.8(6) | C(14)-P(1)-Pt(1) | 113.6(2) |
| C(18)-P(2) | 1.823(7) | C(11)-C(10)-P(1) | 116.3(6) | C(20)-P(2)-C(18) | 102.3(3) |
| C(20)-C(21) | 1.533(10) | C(13)-C(12)-P(1) | 112.8(6) | C(20)-P(2)-C(16) | 106.3(3) |
| C(20)-P(2) | 1.817(6) | C(15)-C(14)-P(1) | 114.0(5) | C(18)-P(2)-C(16) | 107.3(3) |
| C(22)-C(23) | 1.406(8) | C(17)-C(16)-P(2) | 117.3(5) | C(20)-P(2)-Pt(1) | 112.8(2) |
| C(22)-C(27) | 1.414(8) | C(19)-C(18)-P(2) | 114.8(4) | C(18)-P(2)-Pt(1) | 112.5(2) |
| C(22)-Pt(2) | 1.969(6) | C(21)-C(20)-P(2) | 114.3(5) | C(16)-P(2)-Pt(1) | 114.7(2) |
| C(23)-N(3) | 1.391(8) | C(23)-C(22)-C(27) | 117.1(6) | C(37)-P(3)-C(39) | 106.4(4) |
| C(23)-C(24) | 1.413(8) | C(23)-C(22)-Pt(2) | 121.7(5) | C(37)-P(3)-C(41) | 106.5(4) |
| C(24)-C(25) | 1.409(9) | C(27)-C(22)-Pt(2) | 121.2(5) | C(39)-P(3)-C(41) | 102.7(3) |
| C(25)-C(26) | 1.363(10) | C(22)-C(23)-N(3) | 122.8(6) | C(37)-P(3)-Pt(2) | 115.0(2) |
| C(26)-N(3) | 1.370(9) | C(22)-C(23)-C(24) | 129.3(6) | C(39)-P(3)-Pt(2) | 111.8(2) |
| C(27)-C(28) | 1.396(9) | N(3)-C(23)-C(24) | 107.9(5) | C(41)-P(3)-Pt(2) | 113.4(3) |
| C(27)-N(4) | 1.397(8) | C(25)-C(24)-C(23) | 106.7(6) | C(33)-P(4)-C(35) | 105.5(3) |
| C(28)-C(29) | 1.385(9) | C(26)-C(25)-C(24) | 107.5(6) | C(33)-P(4)-C(31) | 106.2(3) |
| C(29)-C(30) | 1.397(10) | N(3)-C(26)-C(25) | 110.5(6) | C(35)-P(4)-C(31) | 103.4(3) |
| C(30)-N(4) | 1.336(8) | C(28)-C(27)-N(4) | 107.0(6) | C(33)-P(4)-Pt(2) | 110.8(2) |
| C(31)-C(32) | 1.526(9) | C(28)-C(27)-C(22) | 130.4(6) | C(35)-P(4)-Pt(2) | 109.7(2) |
| C(31)-P(4) | 1.844(6) | N(4)-C(27)-C(22) | 122.5(6) | C(31)-P(4)-Pt(2) | 120.1(3) |
| C(33)-C(34) | 1.537(9) | C(29)-C(28)-C(27) | 108.3(6) | C(1)-Pt(1)-P(2) | 93.91(17) |
| C(33)-P(4) | 1.824(7) | C(28)-C(29)-C(30) | 106.4(6) | C(1)-Pt(1)-P(1) | 91.33(17) |

| | | | | | |
|---|---|---|---|---|---|
| C(35)-C(36) | 1.556(10) | N(4)-C(30)-C(29) | 109.9(6) | P(2)-Pt(1)-P(1) | 174.76(6) |
| C(35)-P(4) | 1.839(7) | C(32)-C(31)-P(4) | 114.6(5) | C(1)-Pt(1)-Cl(1) | 178.39(18) |
| C(37)-C(38) | 1.533(10) | C(34)-C(33)-P(4) | 114.5(5) | P(2)-Pt(1)-Cl(1) | 87.59(6) |
| C(37)-P(3) | 1.822(8) | C(36)-C(35)-P(4) | 115.9(5) | P(1)-Pt(1)-Cl(1) | 87.17(6) |
| C(39)-C(40) | 1.525(9) | C(38)-C(37)-P(3) | 116.7(5) | C(22)-Pt(2)-P(4) | 92.85(18) |
| C(39)-P(3) | 1.825(7) | C(40)-C(39)-P(3) | 114.1(4) | C(22)-Pt(2)-P(3) | 91.69(18) |
| C(41)-C(42) | 1.508(9) | C(42)-C(41)-P(3) | 114.3(5) | P(4)-Pt(2)-P(3) | 175.07(6) |
| C(41)-P(3) | 1.825(7) | F(1)-B(1)-F(2) | 109.0(6) | C(22)-Pt(2)-Cl(2) | 179.19(19) |
| B(1)-F(1) | 1.388(8) | F(1)-B(1)-N(2) | 110.1(6) | P(4)-Pt(2)-Cl(2) | 87.82(6) |
| B(1)-F(2) | 1.379(9) | F(2)-B(1)-N(2) | 112.5(6) | P(3)-Pt(2)-Cl(2) | 87.66(6) |
| B(1)-N(2) | 1.528(10) | F(1)-B(1)-N(1) | 108.9(5) | | |
| B(1)-N(1) | 1.561(9) | F(2)-B(1)-N(1) | 110.5(6) | | |
| B(2)-F(3) | 1.389(9) | N(2)-B(1)-N(1) | 105.6(5) | | |
| B(2)-F(4) | 1.404(8) | F(3)-B(2)-F(4) | 108.9(6) | | |
| B(2)-N(3) | 1.527(10) | F(3)-B(2)-N(3) | 111.6(6) | | |

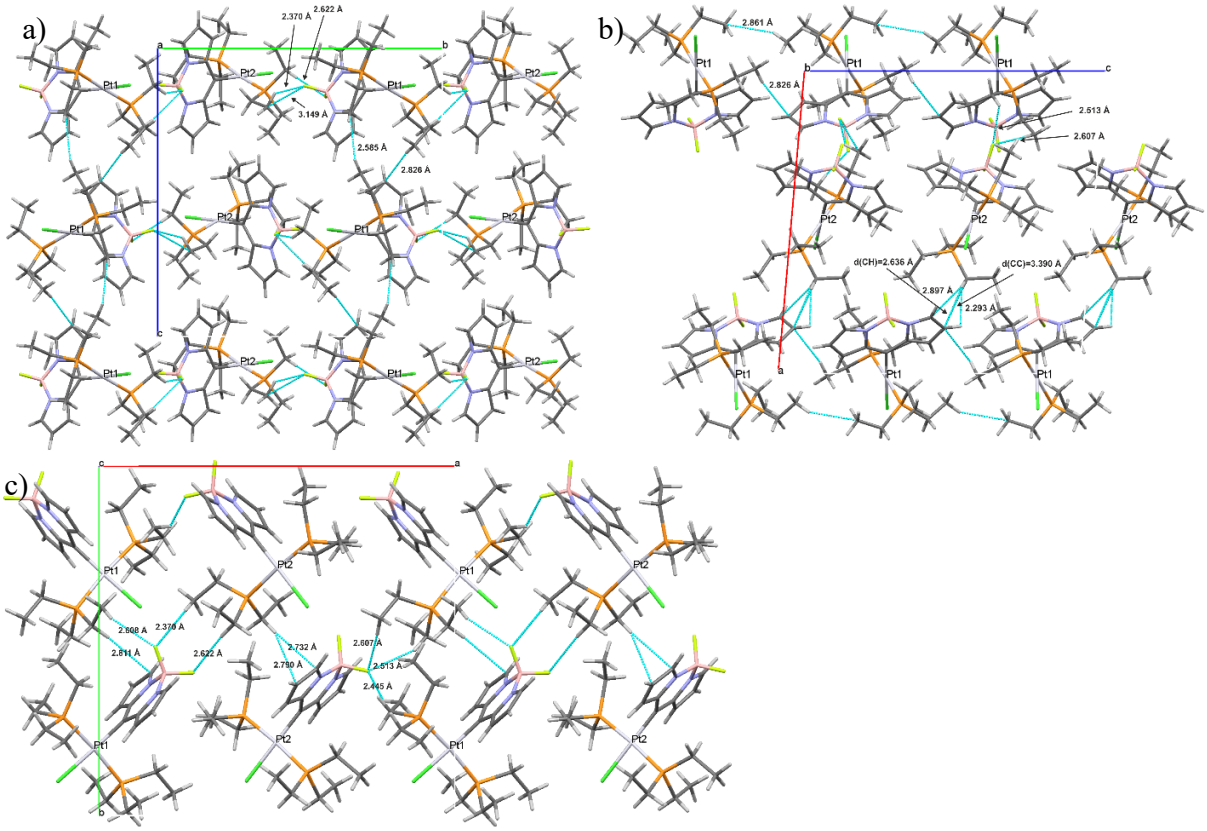


**Figure S24:** Packing of molecules of **Pt-Cl** along the crystallographic *a* (a), *b* (b), and *c* axis (c).

**Table S3:** Bond lengths [Å] and angles [°] for **Pt-I**.

| | | | | | |
|---|---|---|---|---|---|
| Pt(1)-C(1) | 1.994(10) | C(1)-Pt(1)-P(1) | 91.37(7) | N(1)-C(5)-C(4) | 108.9(9) |
| Pt(1)-P(1) | 2.3206(15) | C(1)-Pt(1)-P(1)#1 | 91.37(7) | C(1)-C(6)-N(2) | 121.1(9) |
| Pt(1)-P(1)#1 | 2.3207(15) | P(1)-Pt(1)-P(1)#1 | 176.03(8) | C(1)-C(6)-C(7) | 132.0(9) |
| Pt(1)-I(1) | 2.6689(8) | C(1)-Pt(1)-I(1) | 176.8(3) | N(2)-C(6)-C(7) | 106.9(8) |
| N(1)-C(5) | 1.361(12) | P(1)-Pt(1)-I(1) | 88.71(7) | C(8)-C(7)-C(6) | 109.0(10) |
| N(1)-C(2) | 1.402(13) | P(1)#1-Pt(1)-I(1) | 88.71(7) | C(7)-C(8)-C(9) | 106.3(10) |
| N(1)-B(1) | 1.538(15) | C(5)-N(1)-C(2) | 108.6(9) | N(2)-C(9)-C(8) | 110.0(10) |
| N(2)-C(9) | 1.351(14) | C(5)-N(1)-B(1) | 124.1(10) | C(12)-P(1)-C(14) | 102.3(4) |
| N(2)-C(6) | 1.408(13) | C(2)-N(1)-B(1) | 127.3(9) | C(12)-P(1)-C(10) | 105.5(4) |
| N(2)-B(1) | 1.556(13) | C(9)-N(2)-C(6) | 107.8(9) | C(14)-P(1)-C(10) | 105.7(4) |
| B(1)-F(1) | 1.382(8) | C(9)-N(2)-B(1) | 125.1(10) | C(12)-P(1)-Pt(1) | 115.0(3) |
| B(1)-F(1)#1 | 1.382(8) | C(6)-N(2)-B(1) | 127.0(9) | C(14)-P(1)-Pt(1) | 113.1(2) |
| C(1)-C(6) | 1.403(13) | F(1)-B(1)-F(1)#1 | 109.7(9) | C(10)-P(1)-Pt(1) | 114.1(3) |
| C(1)-C(2) | 1.412(13) | F(1)-B(1)-N(1) | 111.6(6) | C(11)-C(10)-P(1) | 116.2(6) |
| C(2)-C(3) | 1.407(14) | F(1)#1-B(1)-N(1) | 111.6(6) | C(13)-C(12)-P(1) | 113.8(6) |
| C(3)-C(4) | 1.393(14) | F(1)-B(1)-N(2) | 109.7(6) | C(15)-C(14)-P(1) | 113.9(6) |
| C(4)-C(5) | 1.392(17) | F(1)#1-B(1)-N(2) | 109.7(6) | | |
| C(6)-C(7) | 1.410(15) | N(1)-B(1)-N(2) | 104.6(9) | | |
| C(7)-C(8) | 1.374(17) | C(6)-C(1)-C(2) | 118.6(9) | | |
| C(8)-C(9) | 1.416(18) | C(6)-C(1)-Pt(1) | 122.3(7) | | |
| P(1)-C(12) | 1.818(10) | C(2)-C(1)-Pt(1) | 119.1(7) | | |
| P(1)-C(14) | 1.827(6) | N(1)-C(2)-C(3) | 107.0(9) | | |
| P(1)-C(10) | 1.832(9) | N(1)-C(2)-C(1) | 121.4(9) | | |
| C(10)-C(11) | 1.539(11) | C(3)-C(2)-C(1) | 131.5(10) | | |
| C(12)-C(13) | 1.540(13) | C(4)-C(3)-C(2) | 107.6(10) | | |
| C(15)-C(14) | 1.536(14) | C(5)-C(4)-C(3) | 107.8(9) | | |

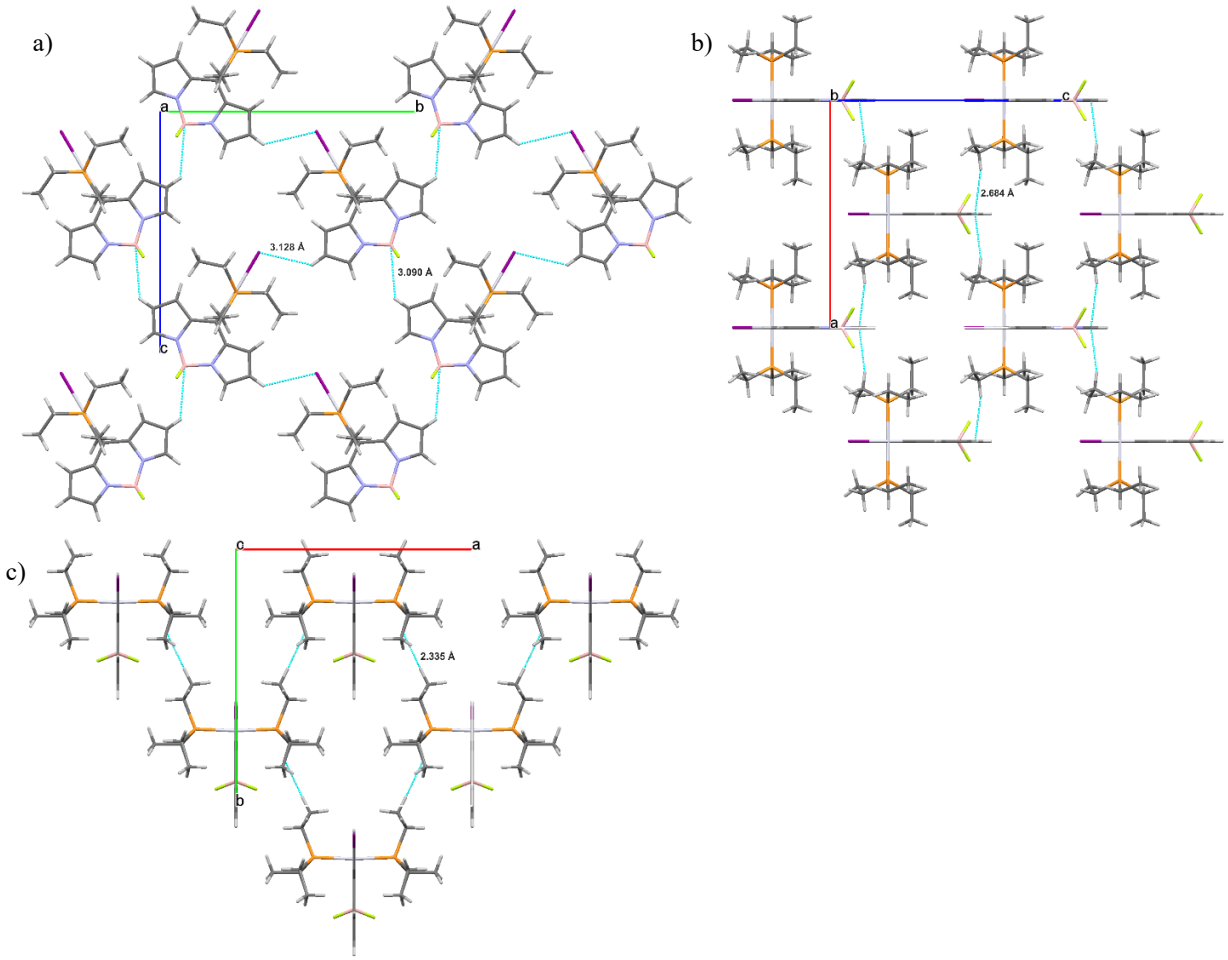


**Figure S25:** Packing of molecules of **Pt-I** along the crystallographic *a* (a), *b* (b), and *c* axis (c).

**Table S4:** Bond lengths [Å] and angles [°] for **Pt-NCS**.

| | | | | | |
|---|---|---|---|---|---|
| C(1)-C(2) | 1.404(6) | B(1)-N(1) | 1.546(6) | F(2)-B(1)-N(1) | 110.6(4) |
| C(1)-C(6) | 1.413(6) | N(3)-Pt(1) | 2.048(4) | N(2)-B(1)-N(1) | 106.4(3) |
| C(1)-Pt(1) | 1.984(4) | P(1)-Pt(1) | 2.3135(13) | C(5)-N(1)-C(2) | 108.4(4) |
| C(2)-N(1) | 1.395(5) | P(2)-Pt(1) | 2.3249(11) | C(5)-N(1)-B(1) | 125.9(4) |
| C(2)-C(3) | 1.412(6) | C(2)-C(1)-C(6) | 117.9(4) | C(2)-N(1)-B(1) | 125.6(3) |
| C(3)-C(4) | 1.374(6) | C(2)-C(1)-Pt(1) | 122.1(3) | C(9)-N(2)-C(6) | 108.0(4) |
| C(4)-C(5) | 1.395(6) | C(6)-C(1)-Pt(1) | 119.9(3) | C(9)-N(2)-B(1) | 126.3(4) |
| C(5)-N(1) | 1.340(6) | N(1)-C(2)-C(1) | 122.2(4) | C(6)-N(2)-B(1) | 125.6(4) |
| C(6)-N(2) | 1.396(5) | N(1)-C(2)-C(3) | 106.8(3) | C(22)-N(3)-Pt(1) | 162.2(4) |
| C(6)-C(7) | 1.410(6) | C(1)-C(2)-C(3) | 131.1(4) | C(14)-P(1)-C(10) | 113.4(3) |
| C(7)-C(8) | 1.391(6) | C(4)-C(3)-C(2) | 108.0(4) | C(14)-P(1)-C(12) | 103.2(3) |
| C(8)-C(9) | 1.392(6) | C(3)-C(4)-C(5) | 107.0(4) | C(10)-P(1)-C(12) | 100.0(2) |
| C(9)-N(2) | 1.348(6) | N(1)-C(5)-C(4) | 109.8(4) | C(14)-P(1)-Pt(1) | 113.0(2) |
| C(10)-C(11) | 1.504(8) | N(2)-C(6)-C(7) | 107.4(4) | C(10)-P(1)-Pt(1) | 120.87(16) |
| C(10)-P(1) | 1.815(5) | N(2)-C(6)-C(1) | 122.2(4) | C(12)-P(1)-Pt(1) | 103.07(19) |
| C(12)-C(13) | 1.435(9) | C(7)-C(6)-C(1) | 130.4(4) | C(18)-P(2)-C(16) | 103.2(2) |
| C(12)-P(1) | 2.038(8) | C(8)-C(7)-C(6) | 107.6(4) | C(18)-P(2)-C(20) | 105.5(2) |
| C(14)-C(15) | 1.477(9) | C(7)-C(8)-C(9) | 106.8(4) | C(16)-P(2)-C(20) | 105.5(2) |
| C(14)-P(1) | 1.765(6) | N(2)-C(9)-C(8) | 110.3(4) | C(18)-P(2)-Pt(1) | 111.63(16) |
| C(16)-C(17) | 1.525(7) | C(11)-C(10)-P(1) | 114.7(5) | C(16)-P(2)-Pt(1) | 115.92(16) |
| C(16)-P(2) | 1.823(4) | C(13)-C(12)-P(1) | 112.4(5) | C(20)-P(2)-Pt(1) | 113.93(16) |
| C(18)-C(19) | 1.520(7) | C(15)-C(14)-P(1) | 117.4(6) | C(1)-Pt(1)-N(3) | 175.77(17) |
| C(18)-P(2) | 1.822(4) | C(17)-C(16)-P(2) | 113.9(3) | C(1)-Pt(1)-P(1) | 91.44(12) |
| C(20)-C(21) | 1.528(7) | C(19)-C(18)-P(2) | 113.2(3) | N(3)-Pt(1)-P(1) | 87.28(12) |
| C(20)-P(2) | 1.826(4) | C(21)-C(20)-P(2) | 115.1(3) | C(1)-Pt(1)-P(2) | 90.79(12) |
| C(22)-N(3) | 1.162(6) | N(3)-C(22)-S(1) | 179.7(4) | N(3)-Pt(1)-P(2) | 90.62(11) |
| C(22)-S(1) | 1.625(4) | F(1)-B(1)-F(2) | 108.7(3) | P(1)-Pt(1)-P(2) | 177.17(5) |
| B(1)-F(1) | 1.389(5) | F(1)-B(1)-N(2) | 110.8(4) | | |
| B(1)-F(2) | 1.394(5) | F(2)-B(1)-N(2) | 110.1(4) | | |
| B(1)-N(2) | 1.540(6) | F(1)-B(1)-N(1) | 110.3(4) | | |

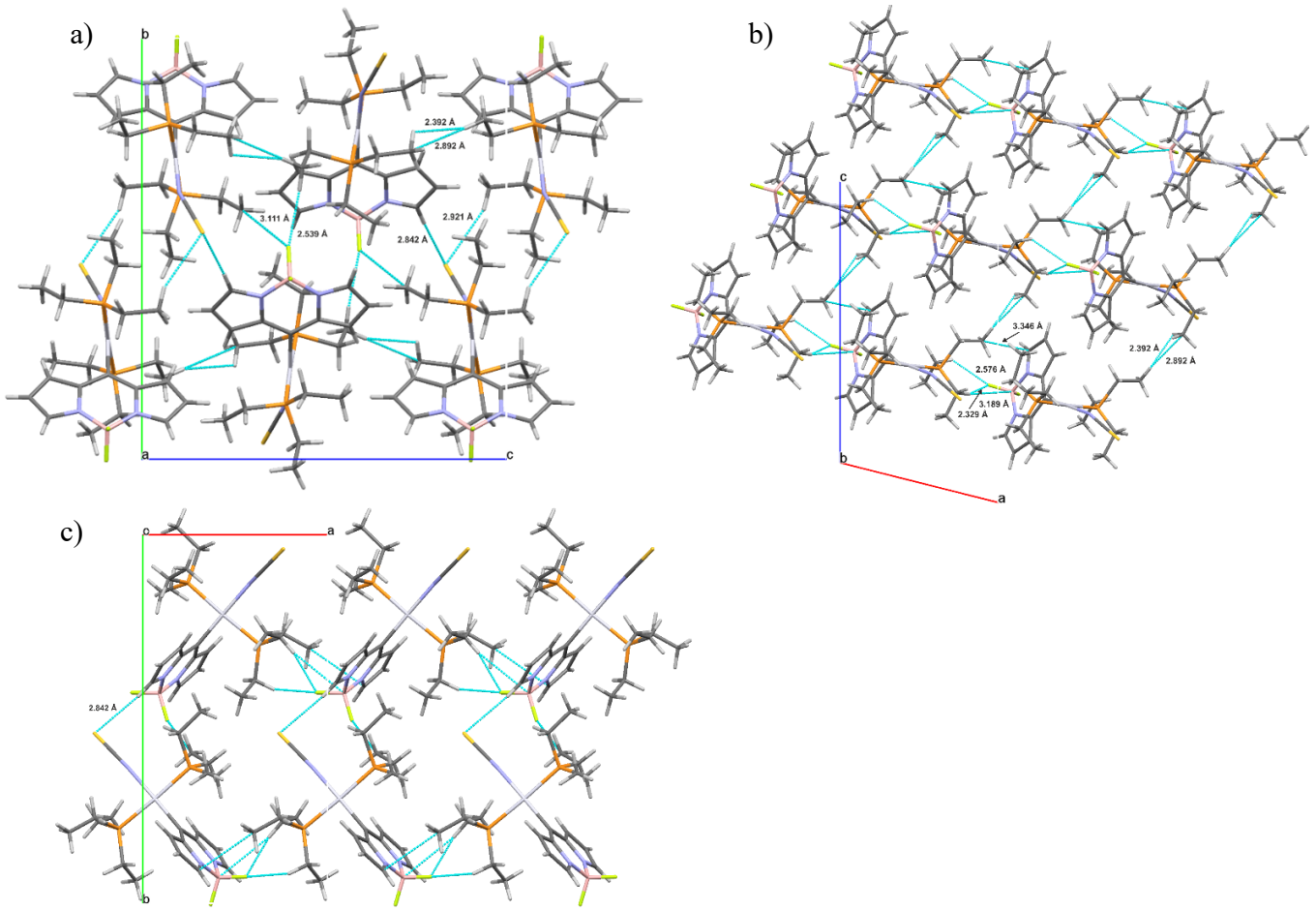


**Figure S26:** Packing of molecules of **Pt-NCS** along the crystallographic *a* (a), *b* (b), and *c* axis (c).

**Table S5:** Bond lengths [Å] and angles [°] for **Pt-NO2**.

| | | | | | |
|---|---|---|---|---|---|
| Pt(1)-C(1) | 1.956(9) | C(14)-C(15) | 1.515(12) | C(10)-P(1)-Pt(1) | 115.0(3) |
| Pt(1)-N(3) | 2.019(8) | C(16)-C(17) | 1.546(11) | C(18)-P(2)-C(16) | 105.9(4) |
| Pt(1)-P(1) | 2.329(2) | C(18)-C(19) | 1.527(11) | C(18)-P(2)-C(20) | 104.2(4) |
| Pt(1)-P(2) | 2.334(2) | C(20)-C(21) | 1.521(11) | C(16)-P(2)-C(20) | 105.4(4) |
| B(1)-F(2) | 1.389(9) | C(1)-Pt(1)-N(3) | 178.2(4) | C(18)-P(2)-Pt(1) | 114.7(3) |
| B(1)-F(1) | 1.398(10) | C(1)-Pt(1)-P(1) | 92.3(3) | C(16)-P(2)-Pt(1) | 113.1(3) |
| B(1)-N(1) | 1.534(10) | N(3)-Pt(1)-P(1) | 88.6(2) | C(20)-P(2)-Pt(1) | 112.8(3) |
| B(1)-N(2) | 1.548(11) | C(1)-Pt(1)-P(2) | 89.3(3) | C(6)-C(1)-C(2) | 115.5(8) |
| N(1)-C(5) | 1.342(10) | N(3)-Pt(1)-P(2) | 90.0(2) | C(6)-C(1)-Pt(1) | 122.1(6) |
| N(1)-C(2) | 1.419(9) | P(1)-Pt(1)-P(2) | 173.83(8) | C(2)-C(1)-Pt(1) | 122.4(6) |
| N(2)-C(9) | 1.352(10) | F(2)-B(1)-F(1) | 108.4(6) | C(3)-C(2)-N(1) | 106.6(7) |
| N(2)-C(6) | 1.409(9) | F(2)-B(1)-N(1) | 111.1(6) | C(3)-C(2)-C(1) | 130.9(7) |
| N(3)-O(1) | 1.232(10) | F(1)-B(1)-N(1) | 110.3(7) | N(1)-C(2)-C(1) | 122.5(7) |
| N(3)-O(2) | 1.293(10) | F(2)-B(1)-N(2) | 110.0(7) | C(4)-C(3)-C(2) | 108.4(7) |
| P(1)-C(14) | 1.823(8) | F(1)-B(1)-N(2) | 110.1(6) | C(3)-C(4)-C(5) | 107.3(7) |
| P(1)-C(12) | 1.826(8) | N(1)-B(1)-N(2) | 107.0(6) | N(1)-C(5)-C(4) | 110.5(7) |
| P(1)-C(10) | 1.830(9) | C(5)-N(1)-C(2) | 107.2(6) | C(1)-C(6)-N(2) | 124.9(7) |
| P(2)-C(18) | 1.814(9) | C(5)-N(1)-B(1) | 127.1(7) | C(1)-C(6)-C(7) | 128.9(7) |
| P(2)-C(16) | 1.816(8) | C(2)-N(1)-B(1) | 125.7(7) | N(2)-C(6)-C(7) | 106.2(7) |
| P(2)-C(20) | 1.830(8) | C(9)-N(2)-C(6) | 108.2(7) | C(8)-C(7)-C(6) | 108.3(8) |
| C(1)-C(6) | 1.406(11) | C(9)-N(2)-B(1) | 127.4(6) | C(9)-C(8)-C(7) | 106.6(7) |
| C(1)-C(2) | 1.440(11) | C(6)-N(2)-B(1) | 124.2(6) | N(2)-C(9)-C(8) | 110.7(7) |
| C(2)-C(3) | 1.401(11) | O(1)-N(3)-O(2) | 115.7(8) | C(11)-C(10)-P(1) | 114.1(6) |
| C(3)-C(4) | 1.368(11) | O(1)-N(3)-Pt(1) | 124.0(6) | C(13)-C(12)-P(1) | 113.0(5) |
| C(4)-C(5) | 1.384(11) | O(2)-N(3)-Pt(1) | 120.2(6) | C(15)-C(14)-P(1) | 115.6(6) |
| C(6)-C(7) | 1.423(11) | C(14)-P(1)-C(12) | 104.3(4) | C(17)-C(16)-P(2) | 115.6(5) |
| C(7)-C(8) | 1.392(11) | C(14)-P(1)-C(10) | 105.6(4) | C(19)-C(18)-P(2) | 113.8(6) |
| C(8)-C(9) | 1.389(12) | C(12)-P(1)-C(10) | 105.9(4) | C(21)-C(20)-P(2) | 114.9(6) |
| C(10)-C(11) | 1.554(11) | C(14)-P(1)-Pt(1) | 115.6(3) | | |
| C(12)-C(13) | 1.511(11) | C(12)-P(1)-Pt(1) | 109.6(3) | | |

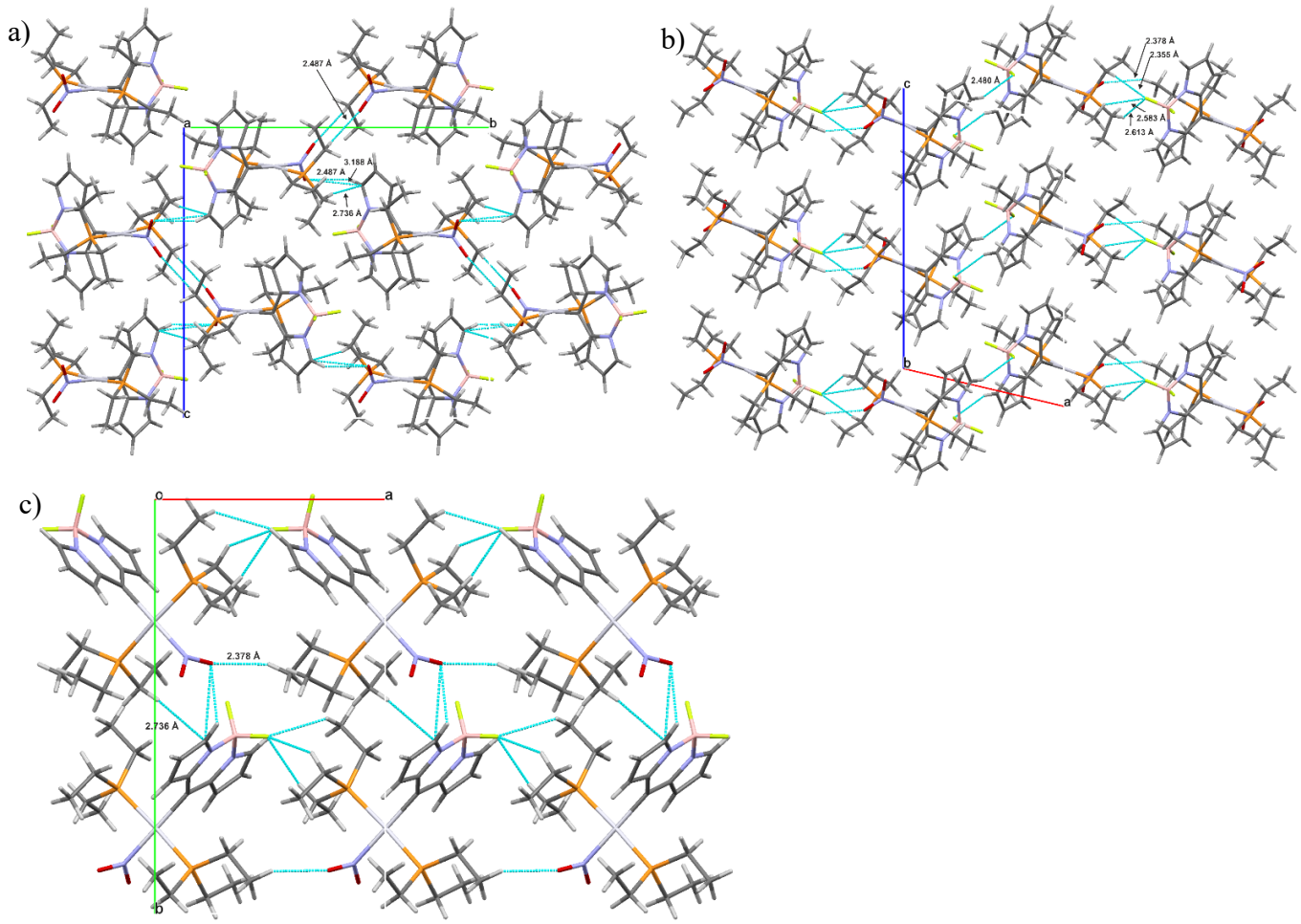


**Figure S27:** Packing of molecules of **Pt-NO$_2$** along the crystallographic *a* (a), *b* (b), and *c* axis (c).

**Table S6:** Bond lengths [Å] and angles [°] for **Pt-CH3**.

| | | | | | |
|---|---|---|---|---|---|
| Pt(1)-C(1) | 2.039(11) | C(28)-C(29) | 1.39(2) | C(16)-P(2)-Pt(1) | 114.4(4) |
| Pt(1)-C(22) | 2.127(12) | C(29)-C(30) | 1.40(2) | C(20)-P(2)-Pt(1) | 116.2(5) |
| Pt(1)-P(2) | 2.290(3) | C(30)-C(31) | 1.38(2) | C(36)-P(3)-C(34) | 102.8(6) |
| Pt(1)-P(1) | 2.299(3) | C(32)-C(33) | 1.529(16) | C(36)-P(3)-C(32) | 105.2(6) |
| Pt(2)-C(23) | 2.053(12) | C(34)-C(35) | 1.510(17) | C(34)-P(3)-C(32) | 104.4(7) |
| Pt(2)-C(44) | 2.137(11) | C(36)-C(37) | 1.52(2) | C(36)-P(3)-Pt(2) | 114.4(4) |
| Pt(2)-P(4) | 2.285(3) | C(38)-C(39) | 1.56(2) | C(34)-P(3)-Pt(2) | 113.9(4) |
| Pt(2)-P(3) | 2.304(3) | C(40)-C(41) | 1.40(3) | C(32)-P(3)-Pt(2) | 114.8(4) |
| B(1)-F(1) | 1.382(15) | C(42)-C(43) | 1.55(3) | C(38)-P(4)-C(42) | 108.8(10) |
| B(1)-F(2) | 1.411(17) | C(1)-Pt(1)-C(22) | 177.6(4) | C(38)-P(4)-C(40) | 100.0(13) |
| B(1)-N(2) | 1.53(2) | C(1)-Pt(1)-P(2) | 91.9(3) | C(42)-P(4)-C(40) | 104.0(11) |
| B(1)-N(1) | 1.55(2) | C(22)-Pt(1)-P(2) | 90.5(3) | C(38)-P(4)-Pt(2) | 115.2(5) |
| B(2)-F(3) | 1.395(16) | C(1)-Pt(1)-P(1) | 91.3(3) | C(42)-P(4)-Pt(2) | 116.9(6) |
| B(2)-F(4) | 1.403(15) | C(22)-Pt(1)-P(1) | 86.3(3) | C(40)-P(4)-Pt(2) | 110.1(7) |
| B(2)-N(3) | 1.525(19) | P(2)-Pt(1)-P(1) | 176.05(12) | C(6)-C(1)-C(2) | 117.5(11) |
| B(2)-N(4) | 1.54(2) | C(23)-Pt(2)-C(44) | 177.2(5) | C(6)-C(1)-Pt(1) | 121.8(8) |
| N(1)-C(5) | 1.329(19) | C(23)-Pt(2)-P(4) | 92.7(3) | C(2)-C(1)-Pt(1) | 120.2(9) |
| N(1)-C(2) | 1.398(15) | C(44)-Pt(2)-P(4) | 89.9(3) | C(3)-C(2)-N(1) | 107.5(12) |
| N(2)-C(9) | 1.33(2) | C(23)-Pt(2)-P(3) | 90.7(3) | C(3)-C(2)-C(1) | 129.9(12) |
| N(2)-C(6) | 1.419(16) | C(44)-Pt(2)-P(3) | 86.7(3) | N(1)-C(2)-C(1) | 122.2(12) |
| N(3)-C(27) | 1.347(18) | P(4)-Pt(2)-P(3) | 176.57(12) | C(2)-C(3)-C(4) | 107.9(15) |
| N(3)-C(24) | 1.402(14) | F(1)-B(1)-F(2) | 108.3(11) | C(5)-C(4)-C(3) | 105.8(15) |
| N(4)-C(31) | 1.342(18) | F(1)-B(1)-N(2) | 111.4(13) | N(1)-C(5)-C(4) | 110.8(13) |
| N(4)-C(28) | 1.405(16) | F(2)-B(1)-N(2) | 109.5(12) | C(7)-C(6)-C(1) | 130.8(11) |
| P(1)-C(10) | 1.830(12) | F(1)-B(1)-N(1) | 111.6(13) | C(7)-C(6)-N(2) | 107.0(12) |
| P(1)-C(14) | 1.832(13) | F(2)-B(1)-N(1) | 108.9(12) | C(1)-C(6)-N(2) | 122.0(12) |
| P(1)-C(12) | 1.842(13) | N(2)-B(1)-N(1) | 107.1(11) | C(8)-C(7)-C(6) | 108.1(13) |
| P(2)-C(18) | 1.830(14) | F(3)-B(2)-F(4) | 108.5(10) | C(9)-C(8)-C(7) | 106.3(14) |
| P(2)-C(16) | 1.831(13) | F(3)-B(2)-N(3) | 109.6(13) | N(2)-C(9)-C(8) | 111.5(13) |
| P(2)-C(20) | 1.831(15) | F(4)-B(2)-N(3) | 109.9(10) | C(11)-C(10)-P(1) | 116.4(9) |
| P(3)-C(36) | 1.816(14) | F(3)-B(2)-N(4) | 111.2(10) | C(13)-C(12)-P(1) | 115.2(9) |
| P(3)-C(34) | 1.818(12) | F(4)-B(2)-N(4) | 110.9(13) | C(15)-C(14)-P(1) | 112.5(10) |
| P(3)-C(32) | 1.833(11) | N(3)-B(2)-N(4) | 106.6(10) | C(17)-C(16)-P(2) | 116.8(9) |
| P(4)-C(38) | 1.744(17) | C(5)-N(1)-C(2) | 108.0(13) | C(19)-C(18)-P(2) | 114.6(9) |
| P(4)-C(42) | 1.824(16) | C(5)-N(1)-B(1) | 127.5(12) | C(21)-C(20)-P(2) | 113.6(9) |
| P(4)-C(40) | 1.88(2) | C(2)-N(1)-B(1) | 124.3(11) | C(24)-C(23)-C(28) | 116.8(11) |
| C(1)-C(6) | 1.412(18) | C(9)-N(2)-C(6) | 107.1(13) | C(24)-C(23)-Pt(2) | 122.4(9) |
| C(1)-C(2) | 1.425(16) | C(9)-N(2)-B(1) | 128.0(13) | C(28)-C(23)-Pt(2) | 120.5(9) |
| C(2)-C(3) | 1.385(19) | C(6)-N(2)-B(1) | 124.9(12) | N(3)-C(24)-C(23) | 123.3(12) |
| C(3)-C(4) | 1.40(2) | C(27)-N(3)-C(24) | 107.9(11) | N(3)-C(24)-C(25) | 106.8(11) |
| C(4)-C(5) | 1.39(3) | C(27)-N(3)-B(2) | 127.5(10) | C(23)-C(24)-C(25) | 129.9(11) |

| | | | | | |
|---|---|---|---|---|---|
| C(6)-C(7) | 1.398(19) | C(24)-N(3)-B(2) | 124.0(11) | C(26)-C(25)-C(24) | 108.4(11) |
| C(7)-C(8) | 1.391(18) | C(31)-N(4)-C(28) | 107.9(12) | C(25)-C(26)-C(27) | 106.5(12) |
| C(8)-C(9) | 1.38(2) | C(31)-N(4)-B(2) | 127.0(11) | N(3)-C(27)-C(26) | 110.4(11) |
| C(10)-C(11) | 1.536(15) | C(28)-N(4)-B(2) | 124.3(11) | C(29)-C(28)-N(4) | 107.0(12) |
| C(12)-C(13) | 1.508(19) | C(10)-P(1)-C(14) | 105.7(6) | C(29)-C(28)-C(23) | 130.5(12) |
| C(14)-C(15) | 1.53(2) | C(10)-P(1)-C(12) | 105.9(7) | N(4)-C(28)-C(23) | 122.4(12) |
| C(16)-C(17) | 1.520(16) | C(14)-P(1)-C(12) | 102.4(7) | C(28)-C(29)-C(30) | 108.1(14) |
| C(18)-C(19) | 1.517(17) | C(10)-P(1)-Pt(1) | 114.3(4) | C(31)-C(30)-C(29) | 106.4(15) |
| C(20)-C(21) | 1.51(2) | C(14)-P(1)-Pt(1) | 112.3(4) | N(4)-C(31)-C(30) | 110.6(13) |
| C(23)-C(24) | 1.404(17) | C(12)-P(1)-Pt(1) | 115.1(4) | C(33)-C(32)-P(3) | 116.7(9) |
| C(23)-C(28) | 1.409(17) | C(18)-P(2)-C(16) | 103.4(7) | C(35)-C(34)-P(3) | 114.8(9) |
| C(24)-C(25) | 1.405(17) | C(18)-P(2)-C(20) | 104.2(6) | C(37)-C(36)-P(3) | 114.1(12) |
| C(25)-C(26) | 1.384(17) | C(16)-P(2)-C(20) | 104.2(7) | C(39)-C(38)-P(4) | 117.6(12) |
| C(26)-C(27) | 1.39(2) | C(18)-P(2)-Pt(1) | 113.0(4) | C(41)-C(40)-P(4) | 115.3(17) |
| | | | | C(43)-C(42)-P(4) | 110.9(13) |

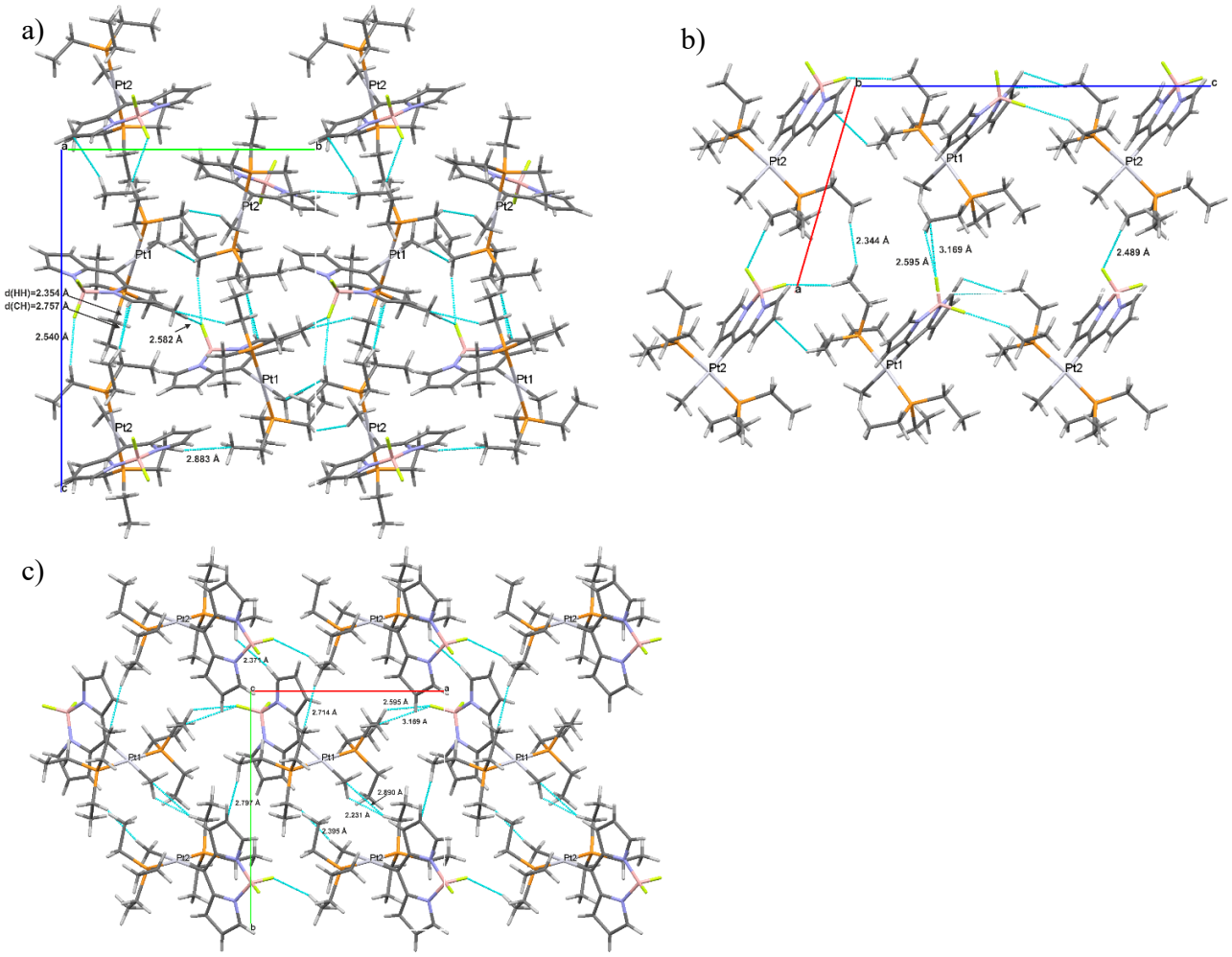


**Figure S28:** Packing of molecules of **Pt-CH$_3$** along the crystallographic *a* (a), *b* (b), and *c* axis (c).

## DFT and TD-DFT calculations

**Table S7:** Atomic coordinates of **Pt-Cl** in the optimized ground state geometry.

| Atom | X | Y | Z |
|---|---|---|---|
| Pt | 5.92902 | 9.33451 | 3.12565 |
| B | 10.63911 | 10.54426 | 1.72252 |
| F | 11.5403 | 10.26961 | 2.75179 |
| F | 11.35508 | 11.04624 | 0.62428 |
| N | 9.91030 | 9.26302 | 1.32638 |
| N | 9.55581 | 11.54428 | 2.17879 |
| P | 6.92251 | 8.88588 | 5.15589 |
| P | 4.82302 | 9.77157 | 1.17428 |
| C | 7.74125 | 9.88064 | 2.33088 |
| C | 8.59559 | 8.95947 | 1.70483 |
| C | 8.35976 | 7.62961 | 1.3193 |
| H | 7.55369 | 7.14602 | 1.45724 |
| C | 9.49963 | 7.14208 | 0.7074 |
| H | 9.61975 | 6.27609 | 0.33425 |
| C | 10.43536 | 8.16838 | 0.741 |
| H | 11.3203 | 8.10793 | 0.40145 |
| C | 8.23908 | 11.18685 | 2.51481 |
| C | 7.63372 | 12.31828 | 3.05597 |
| H | 6.73691 | 12.38004 | 3.36015 |
| C | 8.58068 | 13.35115 | 3.07012 |
| H | 8.44994 | 14.23685 | 3.38845 |
| C | 9.73828 | 12.82552 | 2.53426 |
| H | 10.55229 | 13.30385 | 2.42992 |
| C | 8.69677 | 9.33661 | 5.25952 |
| H | 9.17897 | 8.85697 | 4.53974 |
| H | 8.77988 | 10.30509 | 5.07383 |
| C | 9.40342 | 9.04357 | 6.58236 |
| H | 10.3453 | 9.30901 | 6.51516 |
| H | 9.34769 | 8.08428 | 6.7769 |
| H | 8.97116 | 9.54818 | 7.30214 |
| C | 6.87140 | 7.13157 | 5.63091 |
| H | 7.33958 | 7.02644 | 6.49747 |
| H | 5.92661 | 6.87006 | 5.76885 |
| C | 7.49184 | 6.18542 | 4.6317 |
| H | 7.47855 | 5.27476 | 4.99248 |
| H | 8.41752 | 6.45481 | 4.45662 |
| H | 6.98047 | 6.21302 | 3.7952 |
| C | 6.13927 | 9.70981 | 6.57175 |
| H | 5.24628 | 9.30770 | 6.71853 |
| H | 6.68332 | 9.53635 | 7.37995 |
| C | 5.97698 | 11.2105 | 6.40551 |
| H | 5.61360 | 11.59422 | 7.2314 |
| H | 5.36276 | 11.39185 | 5.66274 |
| H | 6.84900 | 11.61393 | 6.21274 |
| C | 5.82206 | 9.80311 | -0.25466 |
| H | 6.53146 | 10.47855 | -0.11495 |
| H | 6.26874 | 8.92136 | -0.33248 |
| C | 5.12685 | 10.10535 | -1.61287 |
| H | 5.73467 | 9.88327 | -2.34857 |
| H | 4.90005 | 11.0607 | -1.65709 |
| H | 4.30895 | 9.57446 | -1.68892 |
| C | 4.19702 | 11.54691 | 1.17075 |
| H | 4.97333 | 12.15533 | 1.11946 |
| H | 3.65170 | 11.6862 | 0.35547 |
| C | 3.42306 | 11.9096 | 2.28137 |
| H | 3.04933 | 12.80449 | 2.13989 |

| | | | |
|---|---|---|---|
| H | 3.98693 | 11.91354 | 3.0825 |
| H | 2.69422 | 11.26569 | 2.39809 |
| C | 3.33292 | 8.77681 | 0.8312 |
| H | 2.68522 | 8.88588 | 1.57043 |
| H | 2.90597 | 9.10139 | -0.00177 |
| C | 3.69357 | 7.27612 | 0.67557 |
| H | 4.04707 | 6.93708 | 1.52445 |
| H | 4.36986 | 7.17362 | -0.02476 |
| H | 2.89036 | 6.77151 | 0.43151 |
| Cl | 4.07992 | 8.78863 | 4.0481 |

**Table S8:** Atomic coordinates of **Pt-Cl** in the optimized geometry of the first excited triplet state.

| Atom | X | Y | Z |
|---|---|---|---|
| Pt | 0.95950 | 0.24470 | 0.02348 |
| B | -3.93644 | -0.82976 | 0.01013 |
| F | -4.69757 | 0.33577 | 0.07523 |
| F | -4.76201 | -1.94281 | -0.03828 |
| N | -3.0084 | -0.78449 | -1.22772 |
| N | -2.98719 | -0.90666 | 1.23087 |
| P | 0.39809 | 2.52047 | -0.02308 |
| P | 1.62197 | -2.00746 | 0.06879 |
| C | -0.94813 | -0.30095 | 0.01021 |
| C | -1.66007 | -0.44774 | -1.20037 |
| C | -1.21264 | -0.37971 | -2.53764 |
| H | -0.19617 | -0.15600 | -2.83458 |
| C | -2.2959 | -0.67873 | -3.35823 |
| H | -2.3119 | -0.73154 | -4.43854 |
| C | -3.38391 | -0.91743 | -2.50724 |
| H | -4.40556 | -1.17288 | -2.758 |
| C | -1.6387 | -0.56881 | 1.21424 |
| C | -1.17168 | -0.62553 | 2.54555 |
| H | -0.15238 | -0.42481 | 2.84987 |
| C | -2.24329 | -0.99895 | 3.35125 |
| H | -2.24357 | -1.14963 | 4.42238 |
| C | -3.34372 | -1.15752 | 2.49833 |
| H | -4.36197 | -1.43483 | 2.73957 |
| C | -1.39745 | 2.90296 | -0.15218 |
| H | -1.75164 | 2.42733 | -1.07383 |
| H | -1.89056 | 2.36456 | 0.66604 |
| C | -1.77069 | 4.38169 | -0.12808 |
| H | -2.85745 | 4.48890 | -0.21065 |
| H | -1.32277 | 4.93169 | -0.96203 |
| H | -1.46238 | 4.86750 | 0.80352 |
| C | 1.20545 | 3.42729 | -1.40459 |
| H | 0.92789 | 4.48522 | -1.31988 |
| H | 2.28133 | 3.35528 | -1.21078 |
| C | 0.88000 | 2.88413 | -2.79073 |
| H | 1.37285 | 3.49083 | -3.55781 |
| H | -0.1956 | 2.89626 | -2.9976 |
| H | 1.23478 | 1.85395 | -2.89714 |
| C | 0.99674 | 3.42985 | 1.45931 |
| H | 2.07727 | 3.25088 | 1.49353 |
| H | 0.84931 | 4.50255 | 1.28162 |
| C | 0.33956 | 2.99753 | 2.76486 |
| H | 0.76592 | 3.55640 | 3.6045 |
| H | 0.49991 | 1.93121 | 2.95233 |
| H | -0.74064 | 3.17876 | 2.75982 |
| C | 0.38250 | -3.1894 | -0.61114 |
| H | -0.51488 | -3.08011 | 0.00988 |
| H | 0.10341 | -2.81818 | -1.60377 |

| | | | |
|---|---|---|---|
| C | 0.81391 | -4.65102 | -0.68303 |
| H | -0.00557 | -5.25657 | -1.08458 |
| H | 1.06757 | -5.05539 | 0.30205 |
| H | 1.67786 | -4.79108 | -1.3409 |
| C | 1.95312 | -2.63971 | 1.76614 |
| H | 0.98502 | -2.65366 | 2.28197 |
| H | 2.28378 | -3.6818 | 1.67764 |
| C | 2.96868 | -1.82083 | 2.5559 |
| H | 3.07115 | -2.2275 | 3.56764 |
| H | 2.66102 | -0.77325 | 2.63194 |
| H | 3.95708 | -1.83993 | 2.08605 |
| C | 3.16557 | -2.33512 | -0.87171 |
| H | 3.93885 | -1.70298 | -0.42469 |
| H | 3.45187 | -3.38056 | -0.70335 |
| C | 3.03345 | -2.02831 | -2.35975 |
| H | 2.74042 | -0.98438 | -2.51505 |
| H | 2.28954 | -2.6687 | -2.84636 |
| H | 3.99123 | -2.18934 | -2.86556 |
| Cl | 3.28199 | 0.97402 | 0.07211 |

**Table S9:** Atomic coordinates of **Pt-I** in the optimized ground state geometry.

| Atom | X | Y | Z |
|---|---|---|---|
| Pt | 1.06754 | 0.27428 | 0.0463 |
| B | -3.92647 | -0.84735 | -0.02201 |
| F | -4.76401 | 0.26602 | 0.0524 |
| F | -4.68793 | -2.00788 | -0.09856 |
| N | -2.99214 | -0.72936 | -1.2476 |
| N | -2.99147 | -0.89104 | 1.20866 |
| P | 0.59145 | 2.54162 | 0.01073 |
| P | 1.70935 | -1.96283 | 0.05867 |
| C | -0.9255 | -0.26361 | 0.01567 |
| C | -1.64331 | -0.3908 | -1.19661 |
| C | -1.18745 | -0.2869 | -2.52817 |
| H | -0.16839 | -0.05073 | -2.80748 |
| C | -2.26311 | -0.56543 | -3.36853 |
| H | -2.27058 | -0.58717 | -4.45025 |
| C | -3.35677 | -0.82975 | -2.53441 |
| H | -4.37493 | -1.08318 | -2.80172 |
| C | -1.6423 | -0.54857 | 1.20228 |
| C | -1.18911 | -0.61125 | 2.53767 |
| H | -0.17241 | -0.40585 | 2.84849 |
| C | -2.26633 | -0.99175 | 3.33502 |
| H | -2.27623 | -1.14601 | 4.40585 |
| C | -3.35814 | -1.15029 | 2.47252 |
| H | -4.37678 | -1.43469 | 2.70461 |
| C | -1.18965 | 2.98266 | -0.16228 |
| H | -1.54618 | 2.47591 | -1.06629 |
| H | -1.70511 | 2.48756 | 0.66942 |
| C | -1.52821 | 4.46878 | -0.20315 |
| H | -2.61138 | 4.60018 | -0.30006 |
| H | -1.06001 | 4.97218 | -1.05553 |
| H | -1.21581 | 4.98747 | 0.70939 |
| C | 1.44011 | 3.45200 | -1.34833 |
| H | 1.21693 | 4.52014 | -1.23735 |
| H | 2.51546 | 3.33133 | -1.17588 |
| C | 1.07489 | 2.96128 | -2.74472 |
| H | 1.61665 | 3.53646 | -3.50328 |
| H | 0.00403 | 3.06751 | -2.94938 |
| H | 1.33834 | 1.90565 | -2.86713 |
| C | 1.15217 | 3.46067 | 1.508 |
| H | 2.23285 | 3.29650 | 1.58595 |

| | | | |
|---|---|---|---|
| H | 1.00651 | 4.53292 | 1.32696 |
| C | 0.45921 | 3.02758 | 2.79513 |
| H | 0.86535 | 3.57987 | 3.6493 |
| H | 0.60647 | 1.95874 | 2.98049 |
| H | -0.61923 | 3.21591 | 2.76154 |
| C | 0.47902 | -3.12528 | -0.67555 |
| H | -0.43274 | -3.0113 | -0.07666 |
| H | 0.22894 | -2.73184 | -1.66751 |
| C | 0.88845 | -4.59206 | -0.7627 |
| H | 0.07304 | -5.17843 | -1.2001 |
| H | 1.10596 | -5.01859 | 0.22183 |
| H | 1.77038 | -4.73514 | -1.39593 |
| C | 1.98051 | -2.65265 | 1.74831 |
| H | 0.99041 | -2.69248 | 2.21945 |
| H | 2.32776 | -3.68783 | 1.64403 |
| C | 2.94331 | -1.85051 | 2.61661 |
| H | 3.01349 | -2.29799 | 3.61396 |
| H | 2.60357 | -0.81552 | 2.72584 |
| H | 3.95291 | -1.82889 | 2.19242 |
| C | 3.27063 | -2.32873 | -0.84685 |
| H | 4.05350 | -1.70797 | -0.3999 |
| H | 3.54396 | -3.37462 | -0.66177 |
| C | 3.16613 | -2.04679 | -2.34258 |
| H | 2.84413 | -1.01559 | -2.52395 |
| H | 2.44932 | -2.71453 | -2.83272 |
| H | 4.13751 | -2.18981 | -2.82785 |
| I | 3.12137 | 0.82342 | 0.06675 |

**Table S10:** Atomic coordinates of **Pt-I** in the optimized geometry of the first excited triplet state.

| Atom | X | Y | Z |
|---|---|---|---|
| Pt | 0.63375 | 0.02754 | -0.00791 |
| B | -4.39671 | -0.09788 | 0.01699 |
| F | -4.99919 | 1.15626 | 0.07064 |
| F | -5.36201 | -1.09322 | -0.01834 |
| N | -3.47515 | -0.18918 | -1.22405 |
| N | -3.46381 | -0.28785 | 1.23867 |
| P | 0.51701 | 2.37608 | -0.04291 |
| P | 0.73844 | -2.32765 | 0.08287 |
| C | -1.35595 | -0.10193 | 0.00213 |
| C | -2.08733 | -0.10831 | -1.20348 |
| C | -1.64162 | -0.10742 | -2.54321 |
| H | -0.60269 | -0.06273 | -2.84322 |
| C | -2.76511 | -0.19103 | -3.35891 |
| H | -2.79687 | -0.22311 | -4.43962 |
| C | -3.87422 | -0.23704 | -2.50218 |
| H | -4.9264 | -0.29912 | -2.74922 |
| C | -2.07547 | -0.20878 | 1.21214 |
| C | -1.61994 | -0.30847 | 2.54493 |
| H | -0.5799 | -0.28378 | 2.84266 |
| C | -2.73721 | -0.45017 | 3.3616 |
| H | -2.75978 | -0.5612 | 4.43729 |
| C | -3.8527 | -0.42996 | 2.51321 |
| H | -4.90301 | -0.5083 | 2.76344 |
| C | -1.19062 | 3.06892 | -0.10576 |
| H | -1.63098 | 2.71537 | -1.04548 |
| H | -1.76274 | 2.57917 | 0.69058 |
| C | -1.31016 | 4.58561 | 0.00571 |
| H | -2.36263 | 4.87608 | -0.08037 |
| H | -0.76249 | 5.10454 | -0.78763 |
| H | -0.94634 | 4.95626 | 0.96932 |
| C | 1.39815 | 3.15596 | -1.45949 |

| | | | |
|---|---|---|---|
| H | 1.25759 | 4.24089 | -1.3794 |
| H | 2.46244 | 2.95428 | -1.2958 |
| C | 0.97142 | 2.64736 | -2.83087 |
| H | 1.51199 | 3.18688 | -3.6158 |
| H | -0.10014 | 2.78668 | -3.00976 |
| H | 1.19904 | 1.58163 | -2.93743 |
| C | 1.31357 | 3.17907 | 1.40883 |
| H | 2.37367 | 2.90699 | 1.35673 |
| H | 1.25018 | 4.26452 | 1.26334 |
| C | 0.72577 | 2.76902 | 2.7534 |
| H | 1.23340 | 3.30175 | 3.56444 |
| H | 0.85484 | 1.69528 | 2.92279 |
| H | -0.3436 | 2.99611 | 2.82369 |
| C | -0.73881 | -3.17736 | -0.62474 |
| H | -1.59662 | -2.84192 | -0.03047 |
| H | -0.89303 | -2.76639 | -1.62862 |
| C | -0.68673 | -4.70172 | -0.67007 |
| H | -1.63327 | -5.08702 | -1.06408 |
| H | -0.54306 | -5.14123 | 0.3221 |
| H | 0.11203 | -5.06704 | -1.32331 |
| C | 0.80964 | -2.96544 | 1.81069 |
| H | -0.1631 | -2.73314 | 2.26127 |
| H | 0.88511 | -4.05836 | 1.75743 |
| C | 1.93994 | -2.39532 | 2.66045 |
| H | 1.90293 | -2.82691 | 3.66646 |
| H | 1.86199 | -1.30707 | 2.74947 |
| H | 2.92354 | -2.61979 | 2.23541 |
| C | 2.16174 | -3.12295 | -0.76771 |
| H | 3.07148 | -2.73963 | -0.29612 |
| H | 2.11075 | -4.19799 | -0.55591 |
| C | 2.19338 | -2.85732 | -2.26863 |
| H | 2.25547 | -1.78291 | -2.47132 |
| H | 1.30475 | -3.25168 | -2.77367 |
| H | 3.06996 | -3.33592 | -2.71776 |
| I | 3.39136 | 0.25810 | 0.00283 |

**Table S11:** Atomic coordinates of **Pt-NCS** in the optimized ground state geometry.

| Atom | X | Y | Z |
|---|---|---|---|
| C | 4.26823 | 12.6649 | 9.25673 |
| C | 4.70155 | 12.0705 | 8.0611 |
| C | 4.37516 | 12.34873 | 6.71523 |
| H | 3.77940 | 13.02262 | 6.41163 |
| C | 5.07285 | 11.47067 | 5.92024 |
| H | 5.05374 | 11.43093 | 4.97187 |
| C | 5.81218 | 10.64863 | 6.77001 |
| H | 6.38504 | 9.94402 | 6.48675 |
| C | 4.76673 | 12.14638 | 10.4727 |
| C | 4.48827 | 12.51494 | 11.80448 |
| H | 3.90028 | 13.2051 | 12.08461 |
| C | 5.23138 | 11.68025 | 12.63547 |
| H | 5.24542 | 11.6929 | 13.5854 |
| C | 5.94935 | 10.82388 | 11.80448 |
| H | 6.54737 | 10.14998 | 12.10651 |
| C | 1.47628 | 10.93047 | 8.74968 |
| H | 0.63337 | 10.49687 | 8.35688 |
| H | 2.21596 | 10.93047 | 7.98129 |
| C | 1.81045 | 10.1554 | 9.99382 |
| H | 2.12717 | 9.26109 | 9.74656 |
| H | 1.01020 | 10.07591 | 10.55251 |
| H | 2.51189 | 10.62334 | 10.49148 |
| C | 0.43959 | 13.21594 | 7.19098 |

| | | | |
|---|---|---|---|
| H | 0.27302 | 14.19155 | 7.1722 |
| H | 1.11104 | 13.00997 | 6.49301 |
| C | -0.78086 | 12.52578 | 6.88895 |
| H | -0.59546 | 11.57004 | 6.77314 |
| H | -1.16519 | 12.88712 | 6.06421 |
| H | -1.41628 | 12.64683 | 7.62604 |
| C | -0.14703 | 13.04069 | 10.11432 |
| H | -0.6026 | 13.86092 | 9.79664 |
| H | -0.79591 | 12.29633 | 10.04077 |
| C | 0.17818 | 13.22316 | 11.54313 |
| H | 0.69099 | 12.45171 | 11.86395 |
| H | -0.6517 | 13.30085 | 12.05957 |
| H | 0.70866 | 14.03979 | 11.65581 |
| C | 6.24660 | 15.27737 | 8.61353 |
| H | 6.40971 | 14.25478 | 8.87331 |
| H | 6.82847 | 15.8266 | 8.92026 |
| C | 6.17366 | 15.42552 | 7.09708 |
| H | 7.00868 | 15.10573 | 6.69802 |
| H | 6.04333 | 16.36861 | 6.86704 |
| H | 5.42339 | 14.89797 | 6.75279 |
| C | 5.22253 | 15.90791 | 11.20666 |
| H | 5.51363 | 15.04973 | 11.47114 |
| H | 6.02432 | 16.51315 | 11.18945 |
| C | 4.10917 | 16.39752 | 12.11747 |
| H | 4.43823 | 16.4463 | 13.03923 |
| H | 3.35307 | 15.77602 | 12.07209 |
| H | 3.81782 | 17.28822 | 11.82795 |
| C | 4.26266 | 17.38216 | 8.89522 |
| H | 4.06239 | 17.3370 | 7.92651 |
| H | 3.43625 | 17.66943 | 9.35688 |
| C | 5.33804 | 18.4445 | 9.11901 |
| H | 5.47382 | 18.57458 | 10.0799 |
| H | 5.05317 | 19.28822 | 8.71056 |
| H | 6.17808 | 18.15001 | 8.70743 |
| C | 0.76172 | 16.37222 | 9.85767 |
| B | 6.18960 | 10.30355 | 9.29116 |
| F | 5.77480 | 8.97907 | 9.34765 |
| F | 7.58340 | 10.33607 | 9.25344 |
| S | -0.38317 | 17.36789 | 10.43577 |
| N | 5.59468 | 10.99895 | 8.04545 |
| N | 5.67604 | 11.08874 | 10.51182 |
| N | 1.58219 | 15.6640 | 9.43826 |
| P | 1.19226 | 12.70302 | 9.01431 |

**Table S12:** Atomic coordinates of **Pt-NCS** in the optimized geometry of the first excited triplet state.

| Atom | X | Y | Z |
|---|---|---|---|
| C | 1.27376 | -0.17925 | -0.00132 |
| C | 2.01624 | -0.43795 | -1.17591 |
| C | 1.58514 | -0.75642 | -2.48293 |
| H | 0.55022 | -0.80128 | -2.79793 |
| C | 2.7189 | -1.00632 | -3.24985 |
| H | 2.76111 | -1.293 | -4.29194 |
| C | 3.81994 | -0.82241 | -2.40162 |
| H | 4.8763 | -0.90709 | -2.62222 |
| C | 1.989 | -0.06788 | 1.21229 |
| C | 1.52718 | 0.00243 | 2.54583 |
| H | 0.48455 | 0.01753 | 2.83781 |
| C | 2.64327 | -0.00575 | 3.37679 |
| H | 2.66163 | 0.01817 | 4.45799 |
| C | 3.76399 | -0.06936 | 2.53621 |
| H | 4.81486 | -0.08061 | 2.79566 |

| | | | |
|---|---|---|---|
| C | 0.29372 | -3.45231 | 0.0926 |
| H | -0.04377 | -4.42133 | -0.29415 |
| H | 1.0766 | -3.09363 | -0.58542 |
| C | 0.84153 | -3.6208 | 1.50623 |
| H | 1.71313 | -4.28334 | 1.48449 |
| H | 0.10162 | -4.07445 | 2.17345 |
| H | 1.15757 | -2.66694 | 1.93802 |
| C | -1.86831 | -2.73684 | -1.70859 |
| H | -2.63117 | -1.9763 | -1.91004 |
| H | -1.08371 | -2.59842 | -2.46233 |
| C | -2.46793 | -4.13697 | -1.80918 |
| H | -1.72528 | -4.9215 | -1.63269 |
| H | -2.87178 | -4.28998 | -2.81555 |
| H | -3.28943 | -4.27885 | -1.10021 |
| C | -2.37449 | -2.77487 | 1.16575 |
| H | -3.34904 | -2.51817 | 0.73395 |
| H | -2.34412 | -3.86747 | 1.26133 |
| C | -2.22202 | -2.09766 | 2.52512 |
| H | -1.25627 | -2.31536 | 2.99057 |
| H | -3.00804 | -2.44483 | 3.20437 |
| H | -2.31373 | -1.01141 | 2.42565 |
| C | 1.0394 | 3.02079 | -0.97483 |
| H | 1.92294 | 2.48569 | -0.60704 |
| H | 1.16554 | 4.07204 | -0.68742 |
| C | 0.9243 | 2.88527 | -2.48958 |
| H | 1.83913 | 3.25182 | -2.96644 |
| H | 0.08666 | 3.46722 | -2.88802 |
| H | 0.78958 | 1.84072 | -2.78674 |
| C | -0.16095 | 3.02653 | 1.64635 |
| H | 0.75583 | 2.5554 | 2.01971 |
| H | 0.04269 | 4.10165 | 1.56664 |
| C | -1.32559 | 2.76092 | 2.59448 |
| H | -1.08464 | 3.12824 | 3.59736 |
| H | -1.54441 | 1.69022 | 2.66937 |
| H | -2.24013 | 3.26661 | 2.26737 |
| C | -1.86911 | 3.26805 | -0.72824 |
| H | -2.02462 | 2.89037 | -1.74561 |
| H | -2.73686 | 2.93001 | -0.15241 |
| C | -1.76574 | 4.78992 | -0.71817 |
| H | -1.6543 | 5.18477 | 0.29684 |
| H | -2.67856 | 5.22351 | -1.1401 |
| H | -0.92291 | 5.1508 | -1.31662 |
| C | -3.92425 | 0.31156 | -0.17255 |
| B | 4.27787 | 0.01136 | 0.00266 |
| F | 5.42218 | -0.75445 | 0.13538 |
| F | 4.59866 | 1.35444 | -0.20356 |
| S | -5.54863 | 0.40471 | -0.21345 |
| N | 3.40476 | -0.49207 | -1.17154 |
| N | 3.37724 | -0.11295 | 1.25479 |
| N | -2.74828 | 0.24965 | -0.14301 |
| P | -1.11607 | -2.28152 | -0.08741 |

**Table S13:** Atomic coordinates of **Pt-$NO_2$** in the optimized ground state geometry.

| Atom | X | Y | Z |
|---|---|---|---|
| Pt | -2.41755 | 3.46964 | 10.11004 |
| B | -5.7657 | 7.23402 | 10.30933 |
| F | -7.1456 | 7.19532 | 10.53432 |
| F | -5.39204 | 8.55633 | 10.1019 |
| N | -5.01526 | 6.63006 | 11.50286 |
| N | -5.40506 | 6.37939 | 9.06953 |
| N | -1.02448 | 2.01711 | 9.94872 |

| | | | |
|---|---|---|---|
| O | -0.19774 | 1.75467 | 10.82472 |
| O | -0.97804 | 1.27352 | 8.89242 |
| P | -4.00439 | 1.81978 | 10.54182 |
| P | -0.74985 | 5.08938 | 9.91362 |
| C | -3.75578 | 4.8939 | 10.20721 |
| C | -4.06897 | 5.57524 | 11.43744 |
| C | -3.60533 | 5.37168 | 12.74266 |
| H | -2.96894 | 4.71893 | 13.01073 |
| C | -4.22463 | 6.27004 | 13.5676 |
| H | -4.0836 | 6.36762 | 14.50104 |
| C | -5.09458 | 7.01027 | 12.78574 |
| H | -5.6688 | 7.69329 | 13.11444 |
| C | -4.43851 | 5.35486 | 9.06953 |
| C | -4.34366 | 4.89894 | 7.72442 |
| H | -3.77798 | 4.20414 | 7.41168 |
| C | -5.22301 | 5.64758 | 6.94576 |
| H | -5.36522 | 5.56346 | 6.00912 |
| C | -5.85304 | 6.53922 | 7.8042 |
| H | -6.50845 | 7.17345 | 7.53933 |
| C | -5.65029 | 2.44274 | 11.04013 |
| H | -5.53888 | 3.06184 | 11.80443 |
| H | -6.03493 | 2.95922 | 10.28859 |
| C | -6.65466 | 1.32736 | 11.44382 |
| H | -7.54992 | 1.71429 | 11.54594 |
| H | -6.3736 | 0.92696 | 12.2927 |
| H | -6.67539 | 0.6376 | 10.74813 |
| C | -3.43132 | 0.76546 | 11.91772 |
| H | -4.13331 | 0.09926 | 12.12675 |
| H | -2.62254 | 0.27254 | 11.63051 |
| C | -3.10981 | 1.54942 | 13.16869 |
| H | -2.79939 | 0.93706 | 13.86758 |
| H | -3.91421 | 2.01711 | 13.47824 |
| H | -2.40793 | 2.20553 | 12.97243 |
| C | -4.31331 | 0.64938 | 9.17963 |
| H | -3.43903 | 0.34824 | 8.82221 |
| H | -4.77377 | -0.14468 | 9.54822 |
| C | -5.1379 | 1.18772 | 8.02759 |
| H | -5.27708 | 0.47946 | 7.36541 |
| H | -4.66489 | 1.93804 | 7.60954 |
| H | -6.00502 | 1.49559 | 8.36267 |
| C | -1.29443 | 6.56613 | 9.0073 |
| H | -1.65703 | 6.27845 | 8.1329 |
| H | -2.03613 | 6.98503 | 9.51312 |
| C | -0.20802 | 7.6361 | 8.75839 |
| H | -0.607 | 8.4066 | 8.30204 |
| H | 0.50214 | 7.25757 | 8.19832 |
| H | 0.17022 | 7.92377 | 9.61524 |
| C | 0.75996 | 4.52547 | 9.0807 |
| H | 1.44243 | 5.24046 | 9.13974 |
| H | 1.11176 | 3.73309 | 9.55779 |
| C | 0.55313 | 4.16377 | 7.61113 |
| H | 1.41346 | 3.91646 | 7.21063 |
| H | 0.18018 | 4.93427 | 7.13404 |
| H | -0.06629 | 3.40672 | 7.54571 |
| C | -0.16403 | 5.7031 | 11.53477 |
| H | 0.3843 | 6.51398 | 11.38638 |
| H | -0.95071 | 5.96891 | 12.0725 |
| C | 0.65587 | 4.70548 | 12.33737 |
| H | 0.85272 | 5.08064 | 13.22135 |

**Table S14:** Atomic coordinates of **Pt-NO$_2$** in the optimized geometry of the first excited triplet state.

| Atom | X | Y | Z |
|---|---|---|---|
| Pt | -0.93063 | 0.04278 | -0.01087 |
| B | 4.12903 | -0.24379 | -0.00969 |
| F | 5.07467 | 0.77316 | 0.00665 |
| F | 4.76069 | -1.48359 | -0.03238 |
| N | 3.20431 | -0.14217 | 1.22899 |
| N | 3.19833 | -0.10007 | -1.23896 |
| N | -3.02118 | 0.13693 | -0.05396 |
| O | -3.66739 | 0.09495 | 0.99615 |
| O | -3.6016 | 0.24417 | -1.13809 |
| P | -0.9472 | 2.39103 | -0.03878 |
| P | -1.00741 | -2.30186 | 0.11043 |
| C | 1.08094 | -0.03997 | 0.002 |
| C | 1.81471 | -0.08919 | 1.20579 |
| C | 1.36986 | -0.0686 | 2.54629 |
| H | 0.33156 | -0.02283 | 2.84755 |
| C | 2.49423 | -0.10672 | 3.36401 |
| H | 2.52694 | -0.09993 | 4.44513 |
| C | 3.60352 | -0.15203 | 2.50819 |
| H | 4.65624 | -0.19159 | 2.75769 |
| C | 1.80928 | -0.04398 | -1.20569 |
| C | 1.35514 | 0.00906 | -2.54179 |
| H | 0.31422 | 0.05828 | -2.83345 |
| C | 2.47388 | -0.01168 | -3.36774 |
| H | 2.49936 | 0.02017 | -4.44864 |
| C | 3.58899 | -0.07992 | -2.52086 |
| H | 4.63992 | -0.11547 | -2.77849 |
| C | 0.70285 | 3.20299 | -0.03392 |
| H | 1.24013 | 2.80919 | 0.83679 |
| H | 1.24063 | 2.82239 | -0.91004 |
| C | 0.69052 | 4.72787 | -0.02211 |
| H | 1.71899 | 5.10371 | -0.01606 |
| H | 0.18984 | 5.1271 | 0.86586 |
| H | 0.19553 | 5.14086 | -0.90684 |
| C | -1.86765 | 3.08996 | 1.39401 |
| H | -1.9505 | 4.17339 | 1.24286 |
| H | -2.88117 | 2.67746 | 1.32873 |
| C | -1.26043 | 2.7731 | 2.75522 |
| H | -1.86262 | 3.22813 | 3.54842 |
| H | -0.23927 | 3.15716 | 2.85162 |
| H | -1.23571 | 1.69335 | 2.93051 |
| C | -1.86573 | 3.09956 | -1.46721 |
| H | -2.88994 | 2.71946 | -1.38179 |
| H | -1.91037 | 4.18653 | -1.32604 |
| C | -1.29191 | 2.74724 | -2.83396 |
| H | -1.87518 | 3.23656 | -3.62094 |
| H | -1.33597 | 1.66804 | -3.00689 |
| H | -0.25073 | 3.06919 | -2.94312 |
| C | 0.37015 | -3.15755 | -0.76194 |
| H | 0.40671 | -2.74984 | -1.77858 |
| H | 1.29212 | -2.821 | -0.27353 |
| C | 0.30142 | -4.68156 | -0.78803 |
| H | 1.18113 | -5.07828 | -1.3056 |
| H | -0.584 | -5.04425 | -1.3199 |
| H | 0.29273 | -5.11053 | 0.21891 |
| C | -2.54717 | -3.05321 | -0.56078 |
| H | -2.54329 | -4.11559 | -0.28612 |
| H | -3.38827 | -2.59151 | -0.03222 |
| C | -2.70389 | -2.87676 | -2.06856 |
| H | -3.64438 | -3.32881 | -2.4004 |
| H | -1.89143 | -3.3598 | -2.62184 |

| | | | |
|---|---|---|---|
| H | -2.72732 | -1.81676 | -2.33745 |
| C | -0.89819 | -2.9136 | 1.8421 |
| H | -0.91024 | -4.00999 | 1.81151 |
| H | 0.08986 | -2.61253 | 2.21065 |
| C | -1.99451 | -2.38924 | 2.76372 |
| H | -1.82816 | -2.75285 | 3.78319 |

**Table S15:** Selected bond lengths and bond angles of the calculated structures of **Pt-Cl**, **Pt-I**, **Pt-NCS**, and **Pt-NO₂** in comparison with the structure data from X-ray crystal structure analysis.

| | | **Pt-Cl** | | **Pt-I** | **Pt-NCS** | **Pt-NO₂** |
|---|---|---|---|---|---|---|
| | | molecule 1 | molecule 2 | | | |
| | | bond lengths / Å | | | | |
| **C1-Pt1** | X-ray | 1.976(7) | 1.971(8) | 1.994(10) | 1.984(4) | 1.956(9)[c] |
| | $S_0$ | 1.984 | - | 1.994 | 1.989 | 2.013 |
| | $T_1$ | 2.013 | - | 2.021 | 2.017 | 2.038 |
| **X1-Pt1**[a] | X-ray | 2.3750(19) | 2.385(2) | 2.6689(8) | 2.048(4) | 2.019(8) |
| | $S_0$ | 2.435 | - | 2.767 | 2.058 | 2.093 |
| | $T_1$ | 2.443 | - | 2.773 | 2.060 | 2.087 |
| **P1-Pt1** | X-ray | 2.319(2) | 2.316(2) | 2.3206(15) | 2.3135(13) | 2.329(2) |
| | $S_0$ | 2.348 | - | 2.352 | 2.349 | 2.348 |
| | $T_1$ | 2.339 | - | 2.350 | 2.342 | 2.342 |
| **P2-Pt1** | X-ray | 2.309(2) | 2.310(2) | -[b] | 2.3249(11) | 2.334(2) |
| | $S_0$ | 2.344 | - | 2.359 | 2.356 | 2.349 |
| | $T_1$ | 2.336 | - | 2.345 | 2.347 | 2.345 |
| | | bond angles / deg | | | | |
| **C1-Pt1-P1** | X-ray | 91.2(2) | 91.6(2) | 91.37(7) | 91.44(12) | 92.3(3)[c] |
| | $S_0$ | 90.4 | - | 88.8 | 94.1 | 92.8 |
| | $T_1$ | 89.7 | - | 88.2 | 93.8 | 91.9 |
| **C1-Pt1-P2** | X-ray | 94.0(2) | 93.0(2) | -[b] | 90.79(12) | 89.3(3)[c] |
| | $S_0$ | 92.1 | - | 90.9 | 89.0 | 89.5 |
| | $T_1$ | 91.4 | - | 90.1 | 88.1 | 88.1 |
| **P1-Pt1-X**[a] | X-ray | 87.13(7) | 87.68(8) | 88.71(7) | 87.28(12) | 88.6(2) |
| | $S_0$ | 91.0 | - | 92.2 | 86.0 | 87.0 |
| | $T_1$ | 91.8 | - | 92.9 | 86.5 | 87.8 |
| **P2-Pt1-X**[a] | X-ray | 87.61(7) | 87.76(8) | -[b] | 90.62(11) | 90.0(2) |
| | $S_0$ | 86.4 | - | 88.1 | 91.0 | 90.8 |
| | $T_1$ | 87.1 | - | 88.7 | 91.7 | 92.4 |
| **P1-Pt1-P2** | X-ray | 174.74(8) | 175.00(7) | 176.8(3) | 177.17(5) | 173.83(8) |
| | $S_0$ | 177.5 | - | 178.6 | 176.9 | 176.8 |
| | $T_1$ | 178.6 | - | 178.4 | 178.0 | 175.0 |
| **C1-Pt1-X**[a] | X-ray | 178.3(2) | 179.0(2) | 176.03(8) | 175.77(17) | 178.2(4)[c] |
| | $S_0$ | 178.3 | - | 178.8 | 179.7 | 179.2 |
| | $T_1$ | 178.1 | - | 178.2 | 179.7 | 178.1 |

[a]X represents here the atom of the anionic ligand in *trans*-position to the dye bond to the Pt ion. [b]The molecule has a mirror plane which is defined by the plane of the dye's inner heterocycle. [c]C1 remained isotropic and could not further be refined.

## Photophysical properties

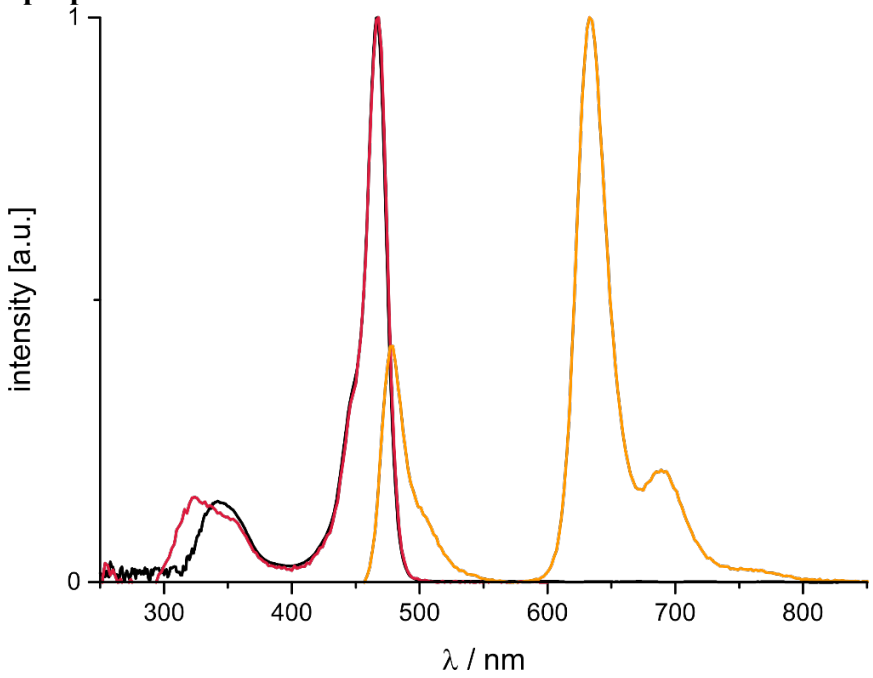


**Figure S29:** UV-Vis absorption (black), excitation (detection at 635 nm, red) and emission spectra (orange, excited at 450 nm) of **Pt-Cl** in a ca. $10^{-6}$ M $CH_2Cl_2$ solution at r.t.

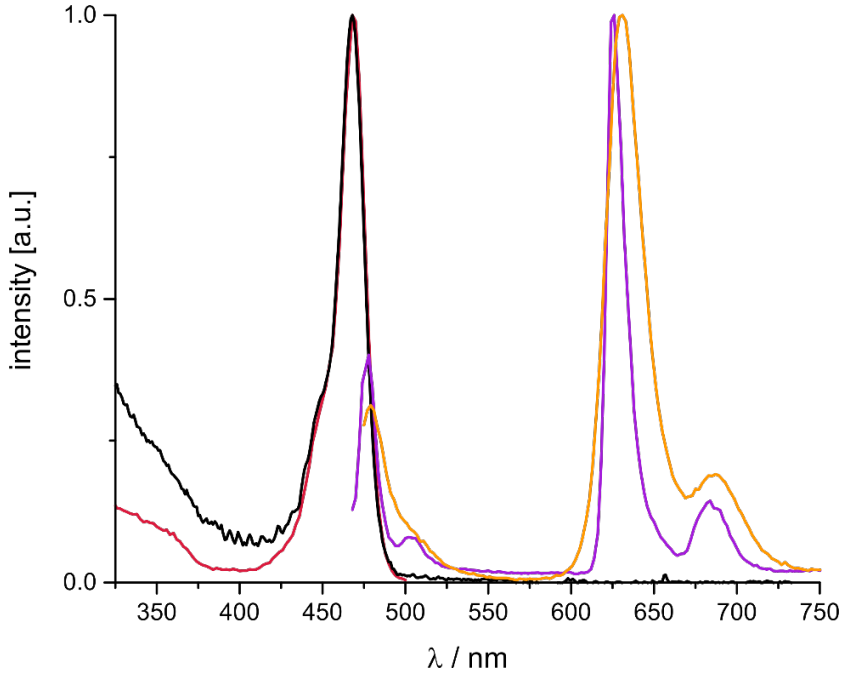


**Figure S30:** UV-Vis absorption (black), excitation (detection at 635 nm, r.t., red) and emission spectra (orange, r.t., excited at 468 nm; violet, 77 K, excited at 450 nm) of **Pt-Cl** in a ca. $10^{-6}$ M toluene solution.

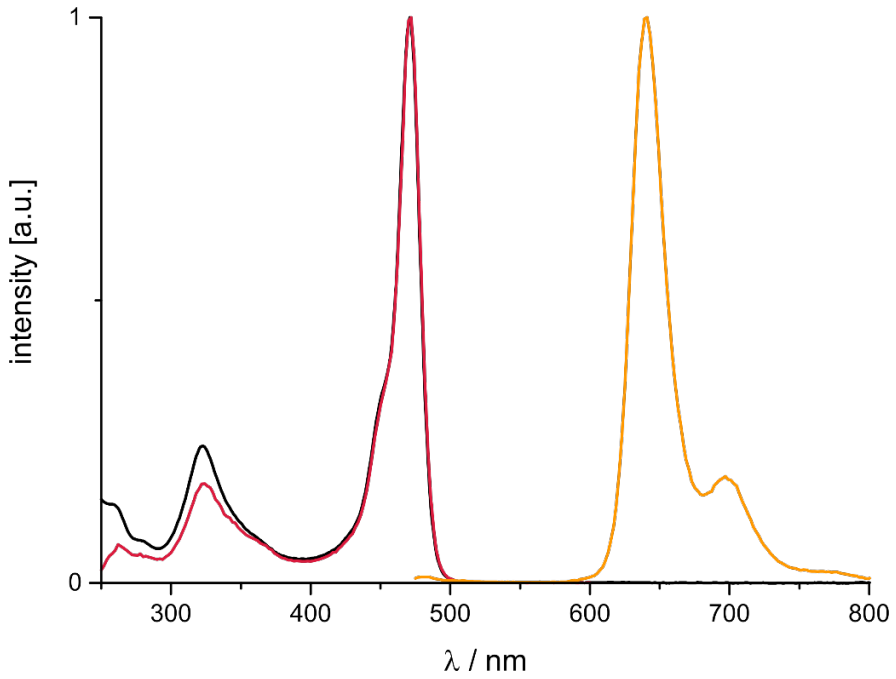


**Figure S31:** UV-Vis absorption (black), excitation (detection at 640 nm, red) and emission spectra (orange, excited at 471 nm) of **Pt-I** in a ca. $10^{-6}$ M $CH_2Cl_2$ solution at r.t.

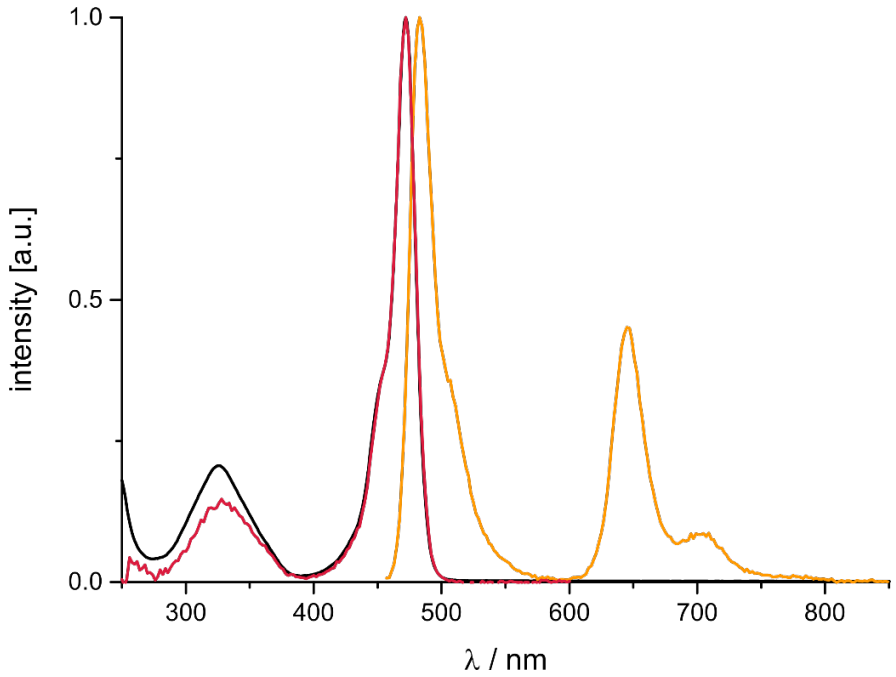


**Figure S32:** UV-Vis absorption (black), excitation (detection at 646 nm, red) and emission spectra (orange, excited at 450 nm) of **Pt-$NO_2$** in a ca. $10^{-6}$ M $CH_2Cl_2$ solution at r.t.

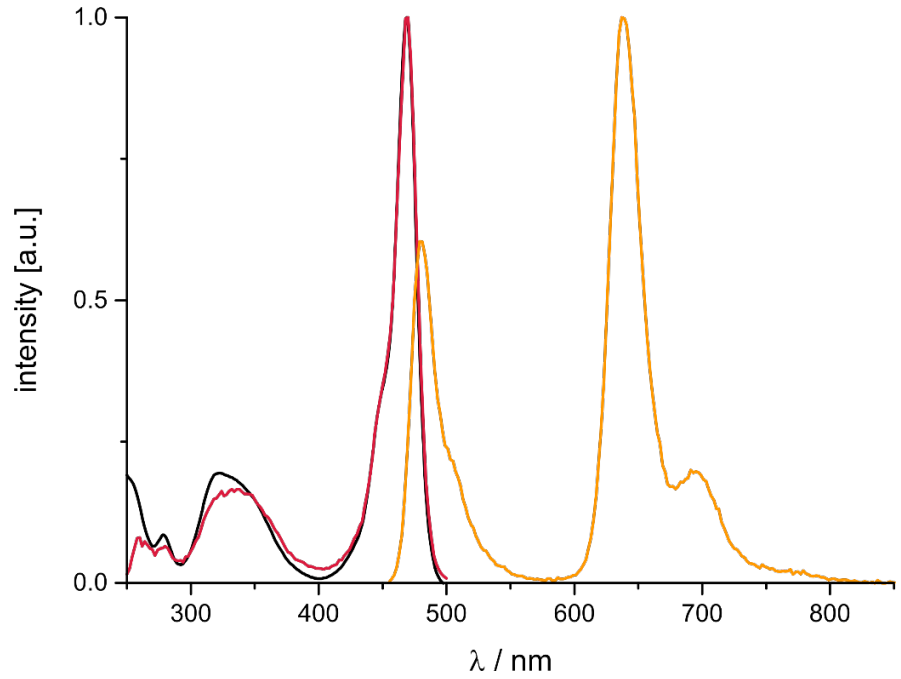


**Figure S33:** UV-Vis absorption (black), excitation (detection at 638 nm, red) and emission spectra (orange, excited at 450 nm) of **Pt-NCS** in a ca. $10^{-6}$ M $CH_2Cl_2$ solution at r.t.

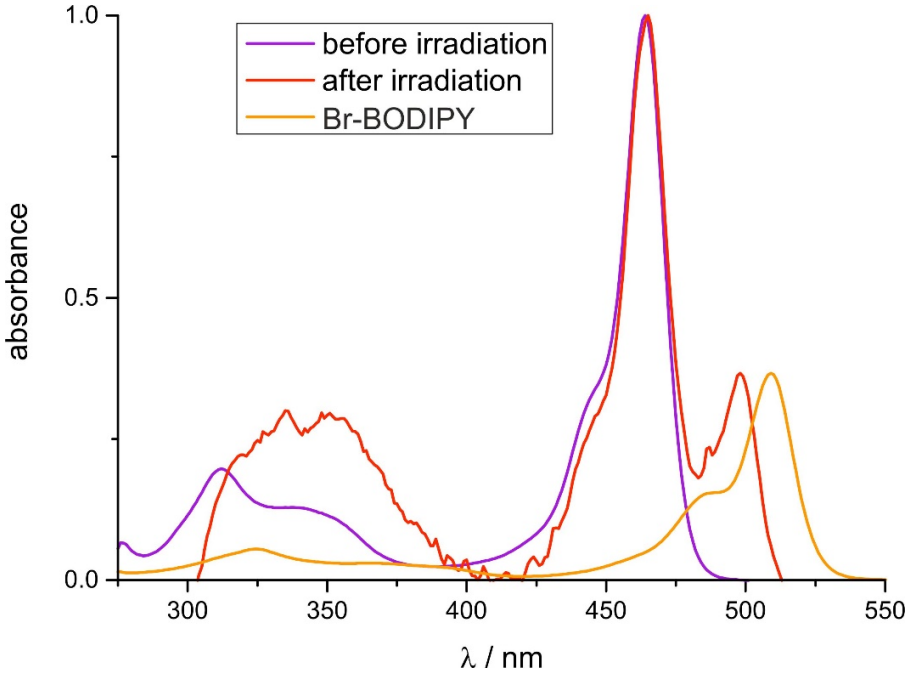


**Figure S34:** Electronical absorption spectra of **Pt-CH₃** in a ca. $10^{-6}$ M benzene solution before and after irradiating the sample into its lowest energy absorption band, and of **Br-BODIPY** in benzene solution, respectively.

## Stern-Volmer quenching experiments

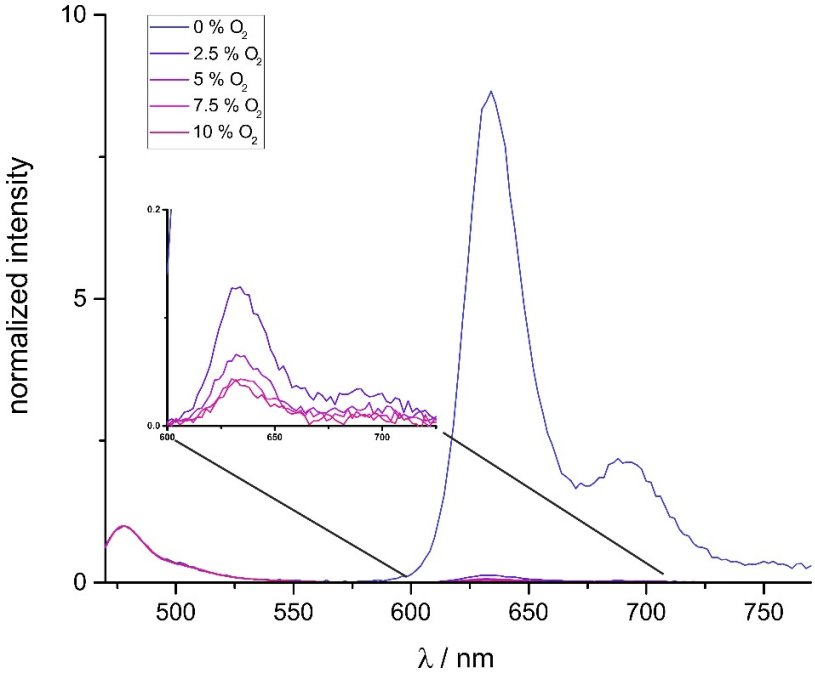


**Figure S35:** Stacked luminescence spectra of **Pt-Cl** at different oxygen concentrations.

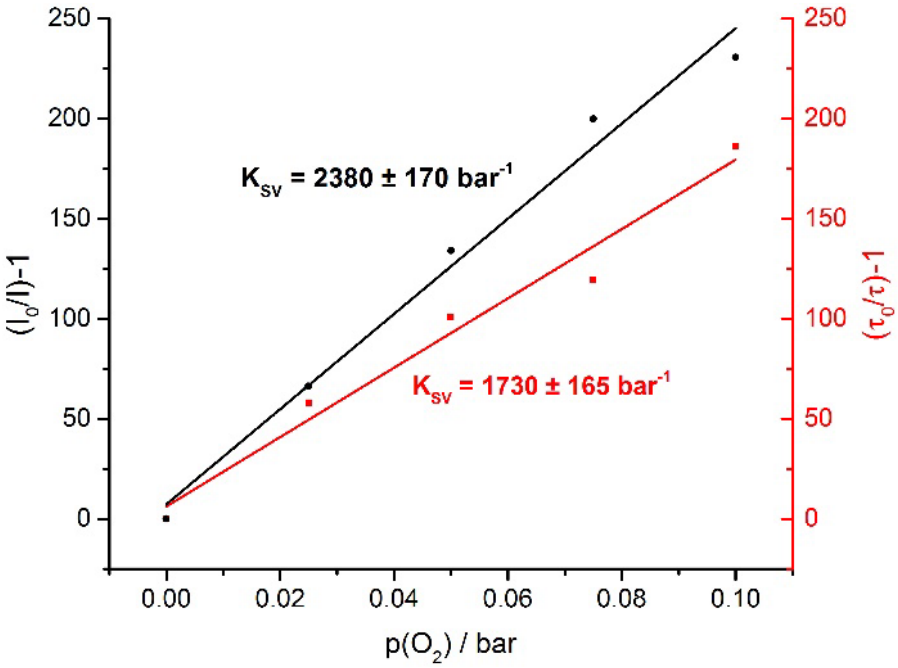


**Figure S36:** Stern-Volmer plot of **Pt-Cl**.

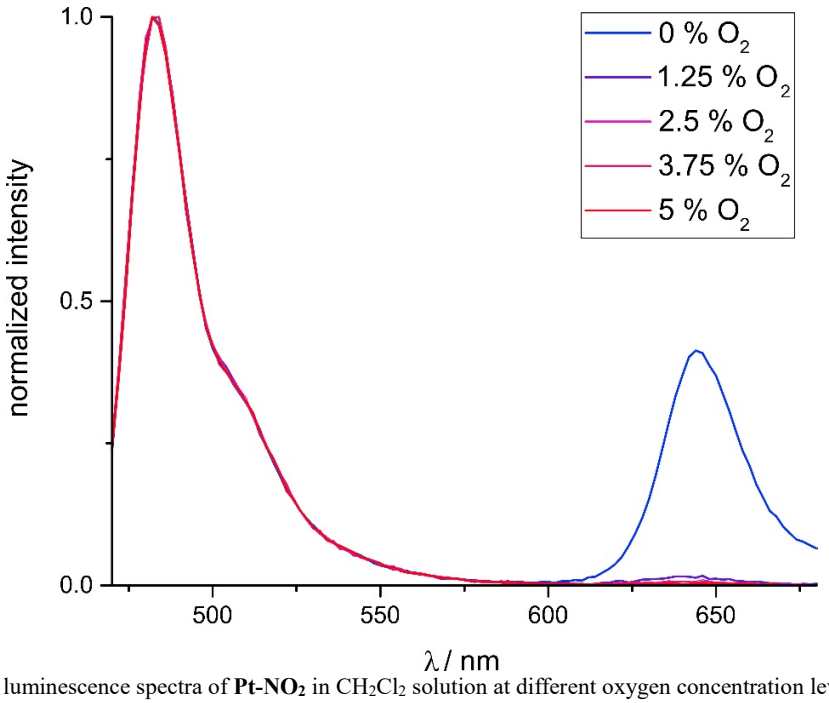


**Figure S37:** Stacked luminescence spectra of **Pt-NO₂** in $CH_2Cl_2$ solution at different oxygen concentration levels.

## Photoreaction

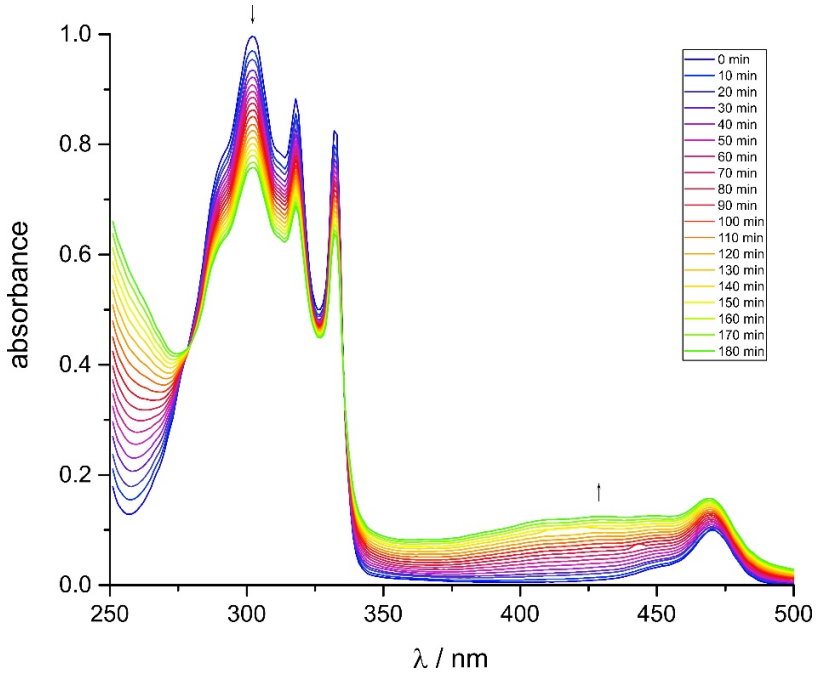


**Figure S38:** Spectral change in the absorption spectra of the reaction mixture containing **DHN** and **Pt-I**.

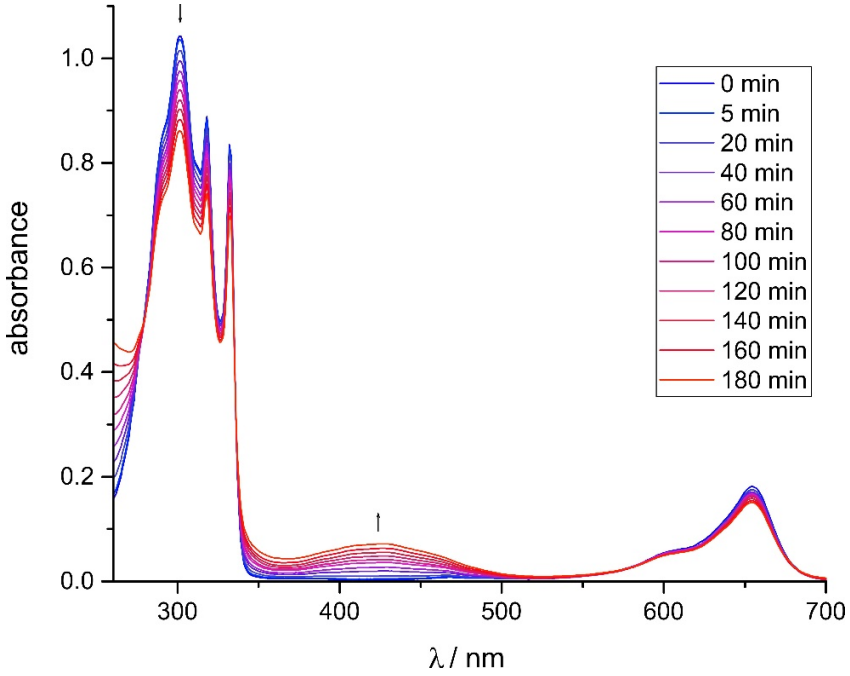


**Figure S39:** Spectral change in the absorption spectra of the reaction mixture containing **DHN** and the reference sensitizer **MB**.

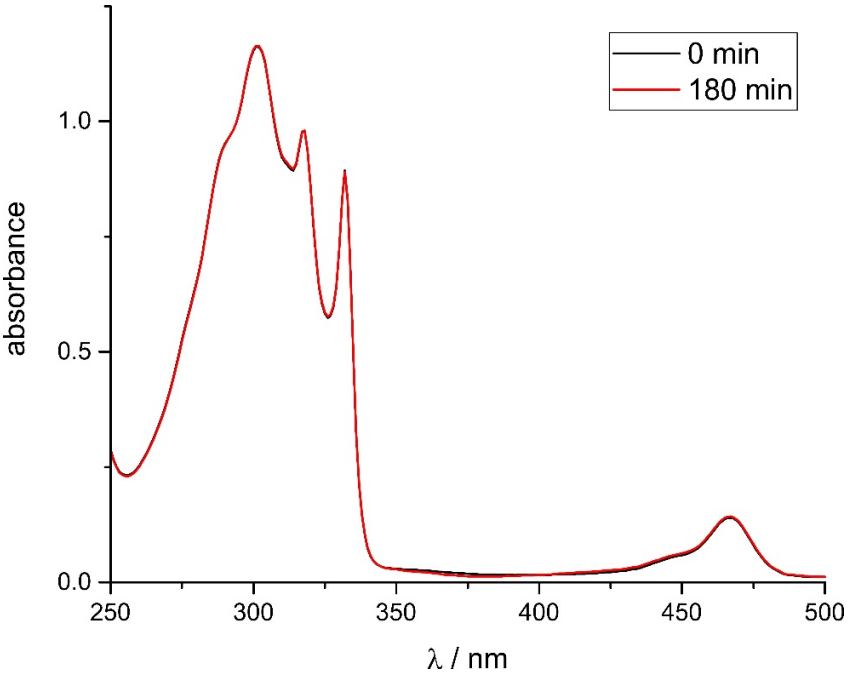


**Figure S40:** Sample of the reaction mixture of **DHN** and **Pt-Cl** kept in the dark for 180 min; UV-Vis spectra were taken before and after that time period.

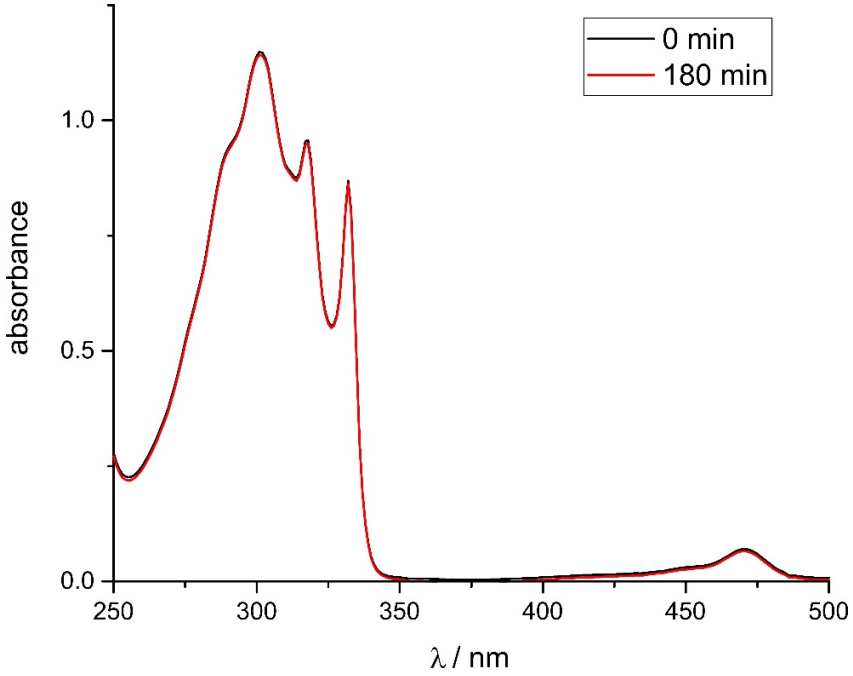


**Figure S41:** Sample of the reaction mixture of **DHN** and **Pt-I** kept in the dark for 180 min; UV-Vis spectra were taken before and after that time period.

## 5.3 $\sigma$-Pt-Bodipy Complexes with Platinum Attachment to Carbon Atoms C2 or C3: Spectroscopic, Structural, and (Spectro)Electrochemical Studies and Photocatalysis

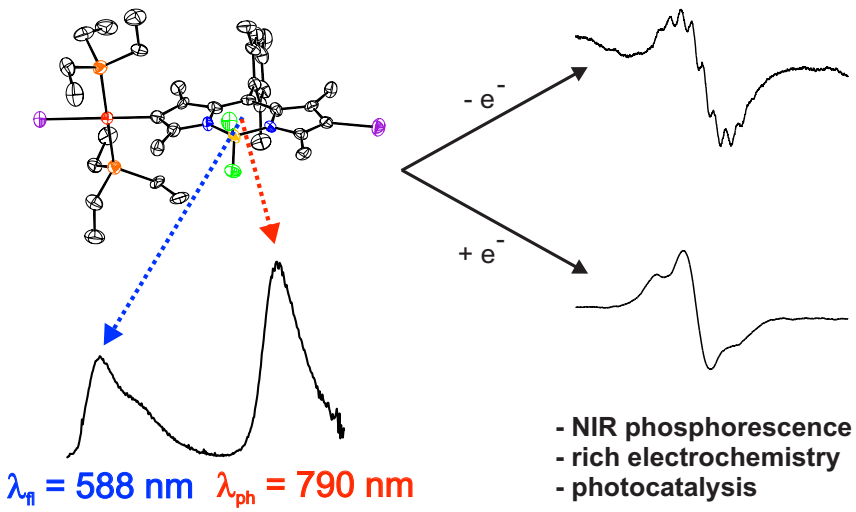


Reprinted with permission from *Organometallics* **2018**, *37*, 235-253
(DOI: 10.1021/acs.organomet.7b00806). 

ORGANOMETALLICS

Article

Cite This: *Organometallics* 2018, 37, 235−253

# σ-Pt-BODIPY Complexes with Platinum Attachment to Carbon Atoms C2 or C3: Spectroscopic, Structural, and (Spectro)Electrochemical Studies and Photocatalysis

Peter Irmler and Rainer F. Winter*

Fachbereich Chemie, Universität Konstanz, Universitätsstraße 10, D-78457 Konstanz, Germany

Supporting Information

**ABSTRACT:** In this work we discuss five new complexes with the general formula *trans*-Pt(bodipy)I($PEt_3$)$_2$, where differently substituted bodipy dyes attach to the coordination center via a direct Pt−C σ-bond to the pyrrolic carbon atom C2 or C3. We also report an isolable intermediate of the oxidative addition step where the bodipy is $\eta^2$-bonded to the *cis*-Pt(0)($PEt_3$)$_2$ moiety. Comparison between the new complexes, *meso*-platinated analogue **8-Pt**, and the parent dyes reveals that the site of platinum attachment influences the spectroscopic, photophysical, electrochemical, and electronic properties. In contrast to **8-Pt**, absorption and emission bands are red-shifted with respect to the parent dyes. 2-Platinated bodipy dyes **2-Pt-6H**, **2-Pt-6I**, **2-Pt-Mes-6I**, and **2-Pt-6Et** exhibit dual fluorescence and NIR phosphorescence emissions, with low quantum yields, whereas **3-Pt** emits solely by fluorescence ($\Phi_{Fl}$ = 52.7%). The complexes are modestly efficient sensitizers for photochemical $^1O_2$ production but outperform methylene blue. They also undergo one reversible one-electron reduction and oxidation as indicated by cyclic voltammetry. Half-wave potentials are cathodically shifted by 340−510 mV with respect to the parent dyes. The one-electron reduced and some of the one-electron oxidized forms were generated and investigated by UV/vis/NIR and EPR spectroscopy as well as TD-DFT calculations. The similarity of their spectra to those of the one-electron reduced or oxidized forms of other bodipy dyes as well as the richly structured EPR spectra and *g*-values close to $g_e$ attest to a dominant bodipy character of the relevant frontier MOs.

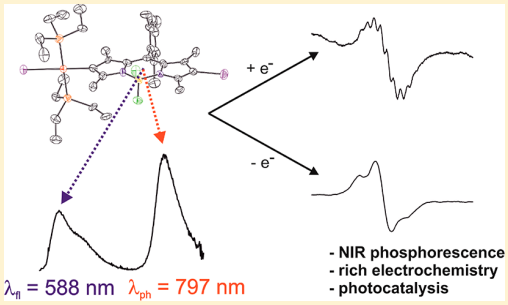


## INTRODUCTION

Color has always fascinated mankind. The fabrication of dyes has been key to the development of synthetic organic chemistry and the shaping of modern chemical industry. Nowadays, myriads of dyes allow for generating any desired hue of color. More recently, dyes have gained importance as sensitizers in organic or organometallic light-emitting diodes (OLEDs)[1,2] or for bioimaging purposes.[3,4] Further applications of modern dyes rely on their capability to undergo efficient intersystem crossing (ISC) to their excited triplet states $T_1$ and to radiatively relax to the electronic ground $S_0$ state by phosphorescence emission. The significantly longer phosphorescence lifetime (usually by three or more orders of magnitude) compared to fluorescence from the excited singlet state $S_1$ opens further avenues for such photosensitizers like their utilization in dye-sensitized solar cells (DSSCs),[5] photocatalysis,[6−8] photodynamic therapy,[9−12] or triplet−triplet annihilation (TTA) upconversion.[13,14]

The family of 4,4-difluoro-4-bora-3*a*,4*a*-diaza-*s*-indacen-8-yl (bodipy) fluorophores holds a particularly prominent place in these respects. Their chemical robustness and easy derivatization allow for precise adjustment of the energy levels of the excited singlet and triplet states of bodipy dyes, to decorate bodipys with a huge variety of substituents, and to incorporate them into a vast number of functional arrays.[15−18] This endows them with the capabilities of energy or charge transfer between their individual constituents on photoexcitation[2,19−21] or makes them amenable to bioconjugate chemistry for medical purposes.[22−24] Effective ISC to the excited triplet state of bodipys has been known since 2005,[25] when it was observed that the fluorescence quantum yield (QY) of 2,6-diiodo-bodipy is strongly reduced with respect to the nonhalogenated dye due to the competitiveness of ISC with fluorescence emission. Further progress was made by linking two bodipys to rigid orthogonal arrays[26−30] or bringing bodipy dyes into the coordination sphere of a heavy metal ion such as ruthenium, rhodium, iridium, or platinum, usually by covalently attaching them to a polypyridine ligand motif or by introducing them as acetylide ligands.[31−40] Representative examples of the latter kind of compounds are mono- and dinuclear Pt(II) bipyridine or diphosphane bis(acetylide) complexes with two identical or nonidentical bodipy-acetylide ligands.[32−35,40] Most of these complexes exhibit dual fluorescence and phosphorescence emissions with, however, usually rather modest phosphorescence QYs at room temperature (r.t.). Upon lowering the temperature or embedding the compounds into solid films, the phosphorescence QY may be significantly increased.[32,34,41]

**Received:** November 6, 2017
**Published:** January 4, 2018






DOI: 10.1021/acs.organomet.7b00806
*Organometallics* 2018, 37, 235−253

**Scheme 1. Overview of the Complexes and Their Syntheses**

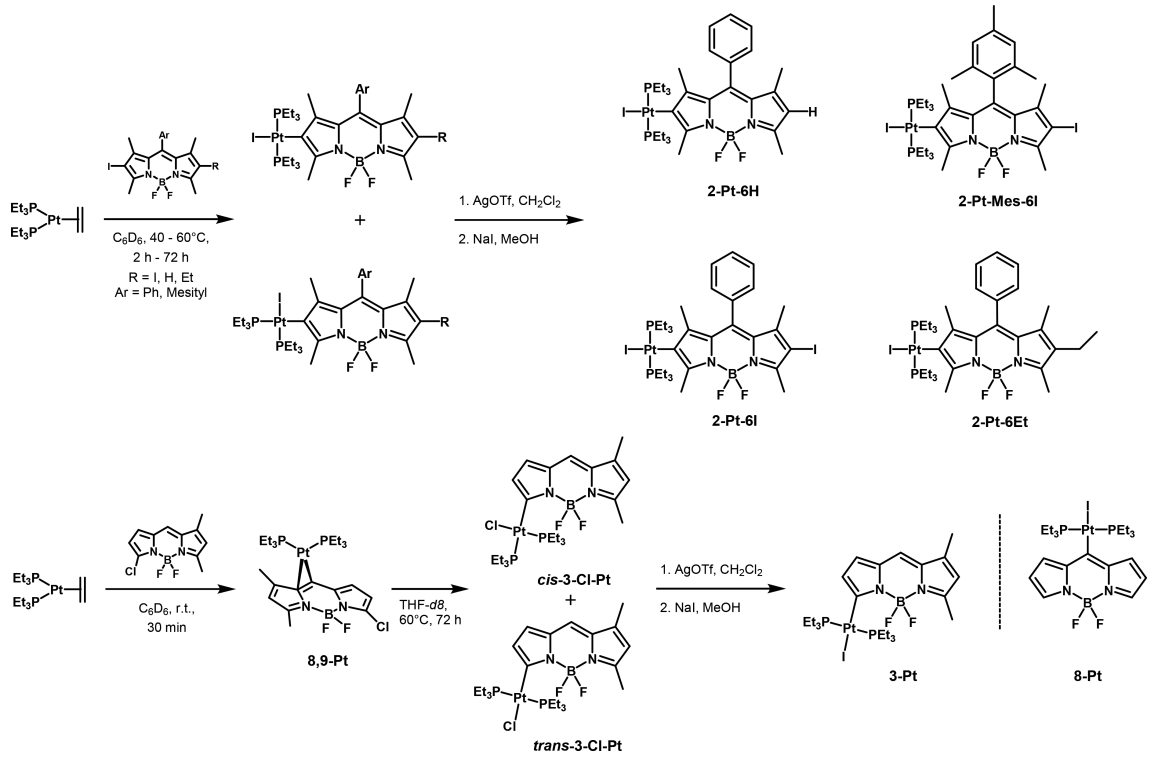


Experimental and quantum chemical studies show that the frontier molecular orbitals (FMOs) of the latter platinum complexes are dominated by the acetylide ligands with only modest contributions from the platinum ion(s). The platinum ion then acts as a remote heavy atom. In this scenario, the efficacy of ISC scales with $d^{-6}$ and therefore rapidly decreases with increasing spatial separation $d$ of the center of the $\pi$ chromophore from the heavy metal ion.[42−44] It is therefore advantageous to bring the platinum ion as close to the chromophore as possible, in particular by attaching the dye to the heavy metal ion via a direct metal−carbon $\sigma$-bond. That approach was first applied to anthracenes,[45] perylenes,[46] corannulenes,[47,48] or dibenz[*a*,*c*]anthracenes.[49] The latter chromophores were introduced into the coordination sphere of a platinum ion via oxidative addition of the corresponding haloarene to a bis(phosphane) platinum(0) source such as $Pt(PR_3)_4$ or $Pt(PR_3)_2(\eta^2$-olefin). The resulting $\sigma$-aryl Pt(II) complexes, however, were mostly only fluorescent, again as a result of the large distance between the heavy metal ion and the center of the extended $\pi$-chromophore.

We have recently observed that platinum complexes *cis*/*trans*-$Pt(PR_3)_2X$ (R = Ph, Et; X = monoanionic ligand) with a $\sigma$-bonded thioxanthonyl or bodipy ligand show dual fluorescence and phosphorescence emissions with phosphorescence QYs of up to 41% in fluid solution at r.t., even though the free ligands are not or only very weakly phosphorescent under these conditions. So far these studies only involved complexes where the platinum ion attaches to the bodipy dye via its *meso* position C8. As an expansion of our previous work, we here report on five new complexes where the metal ion binds to the pyrrolic carbon atoms C2 or C3 of a bodipy dye (see Scheme 1). Monoplatination of diiodo-derivatives of the bodipys also allows us to compare analogous complexes with or without additional iodo atoms at the bodipy dye and to probe for the additional heavy atom effect of the remaining iodo substituent.

In this context one should note that the HOMO of bodipys has a nodal plane along the B−C8 vector.[50,51] This severely limits platinum contribution to the HOMO, thus reducing the impact of the $Pt(PR_3)_2X$ fragment to that of a potent electron donor with a remote heavy atom. In contrast, positions C2 and C3 have large contributions to the FMOs. Platinum attachment to any of these positions is therefore expected to cause major perturbations of the bodipy $\pi$-system which should become manifest in their optical, photophysical, and electrochemical properties.[8,33,41,52−56] Quantum chemical calculations have also been performed and are augmented by UV/vis/NIR and EPR spectroelectrochemical studies to directly probe for the identity of the respective redox sites and the platinum contribution to the SOMO of the reduced and oxidized forms of these complexes.

## RESULTS AND DISCUSSION

**Synthesis and Characterization.** All new complexes of this study and their syntheses are summarized in Scheme 1. The platinum fragment was introduced by oxidative addition of the corresponding 2- or 3-halogenated bodipy dye to $Pt(\eta^2$-$C_2H_4)(PEt_3)_2$, which itself is conveniently prepared from the diethyl complex by thermally induced reductive elimination of ethane.[57] Those reactions inevitably afforded mixtures of the *cis* and *trans* isomers, which were conveniently converted to the pure *trans* complexes by successive treatment with AgOTf and NaI. Quite interestingly, further reaction of complexes **2-Pt-Mes-6I** and **2-Pt-6I** with an additional equivalent of $Pt(\eta^2$-$C_2H_4)(PEt_3)_2$ or direct treatment of the 2,6-diiodinated dye with 2 equiv of the platinum precursor failed in our hands to


DOI: 10.1021/acs.organomet.7b00806
*Organometallics* 2018, 37, 235−253

Table 1. Selected Bond Lengths [Å] and Angles [deg] for the Complexes

| bond parameter | 2-Pt-6H[a] | 2-Pt-6I | 2-Pt-Mes-6I | 2-Pt-6Et[a] | 3-Pt |
|---|---|---|---|---|---|
| Pt−$C_{bodipy}$ | 2.027(4) | 2.018(4) | 1.991(11) | 2.016(7) | 1.977(7) |
| | 2.023(4) | | | 2.020(7) | |
| Pt1−I | 2.6943(4) | 2.6852(3) | 2.6812(9) | 2.6766(6) | 2.6849(5) |
| | 2.6872(4) | | | 2.6841(7) | |
| Pt1−P1 | 2.3119(14) | 2.2992(11) | 2.299(3) | 2.305(2) | 2.326(2) |
| | 2.3022(14) | | | 2.301(2) | |
| Pt1−P2 | 2.3142(14) | 2.3181(10) | 2.304(4) | 2.306(2) | 2.325(2) |
| | 2.3064(15) | | | 2.303(2) | |
| C8−C9 | 1.404(7) | 1.427(5) | 1.425(17) | 1.421(11) | 1.392(11) |
| | 1.393(7) | | | 1.400(11) | |
| C−Pt1−P1 | 89.73(14) | 92.82(11) | 90.3(4) | 90.6(3) | 89.7(3) |
| | 90.56(15) | | | 90.1(2) | |
| C−Pt1−P2 | 91.46(14) | 88.16(11) | 90.2(4) | 91.4(3) | 90.6(3) |
| | 91.10(15) | | | 89.6(2) | |
| I1−Pt1−P1 | 89.37(3) | 88.77(3) | 90.56(9) | 89.28(5) | 91.24(7) |
| | 89.20(3) | | | 90.08(6) | |
| I1−Pt1−P2 | 89.48(3) | 90.27(3) | 88.95(8) | 89.45(6) | 89.29(7) |
| | 89.22(4) | | | 90.24(5) | |
| P1−Pt1−P2 | 178.48(5) | 177.31(3) | 177.15(16) | 172.68(8) | 175.18(9) |
| | 176.02(5) | | | 178.56(9) | |
| C−Pt1−I1 | 177.11(15) | 178.38(10) | 177.30(11) | 174.4(2) | 170.0(2) |
| | 178.63(14) | | | 179.2(3) | |
| [B]−[Pt][b] | 85.7 | 85.4 | 88.28 | 88.8 | 89.6 |
| | 85.5 | | | 88.5 | |
| [B]−[Ar][c] | 76.9 | 80.3 | 86.86 | 79.8 | |
| | 83.7 | | | 88.9 | |
| [Pyr]−[Pyr][d] | 5.2 | 3.4 | 7.0 | 2.0 | 6.5 |
| | 3.2 | | | 6.4 | |

[a]Data for the two independent molecules of the unit cell. [b]Interplanar angle between the best plane through the inner six-membered ring of the bodipy ligand and the coordination plane at the platinum ion. [c]Interplanar angle between the best plane through the inner six-membered ring of the bodipy ligand and the *meso*-aryl substituent. [d]Interplanar angle between the two pyrrolic subunits of the bodipy ligand.

provide the dinuclear complexes, even under forcing conditions. This is possibly due to electronic deactivation on the introduction of the first platinum fragment. The stronger C−Cl bond of the 3-chloro-5,7-dimethylbodipy increases the energy barrier for oxidative addition such that the intermediate substitution product **8,9-Pt**, where the ethylene ligand of the precursor is replaced by the $\eta^2$-coordinated bodipy, can be isolated. Owing to the poor solubility of that complex in benzene, crystals suitable for X-ray molecular structure determination were directly deposited from the reaction solution. Above 40 °C in THF-$d_8$, **8,9-Pt** slowly converts to the products of oxidative addition. Full conversion required 72 h at 60 °C as depicted in Figure S1 and afforded a mixture of ***trans***- and ***cis*-3-Cl-Pt** with the *cis* isomer as the kinetic and the *trans* isomer as the thermodynamically preferred product. Van der Boom and co-workers have reported on a similar intermediate with $\eta^2$-coordination of a $d^{10}$ Pt(0) center to the C=C double bond of a brominated stilbazole. After primary coordination to a remote double bond, the low valent platinum center migrates along the conjugated $\pi$-system until it reaches the halogenated double bond.[58]

All complexes were readily identified by multinuclear ($^1$H, $^{13}$C, $^{31}$P, and $^{195}$Pt) NMR spectroscopy and their purities confirmed (see Figures S2−S30). The $^{31}$P NMR spectra of the *trans*-Pt(bodipy)I($PEt_3$)$_2$ complexes feature just one sharp singlet which is located at 7.69 ppm for **3-Pt** or in between 9.03 and 9.75 ppm for the 2-platinated bodipy complexes and is symmetrically flanked by $^{195}$Pt satellites ($J_{PtP}$ = 2540−2560 Hz). The $^{195}$Pt NMR resonance signal of every complex is consequently split into a triplet with a chemical shift of −4784 to −4802 ppm for the complexes where platinum(II) ion is bound to C2 and of −4599 ppm for complex **3-Pt**. The presence of a direct Pt−C $\sigma$-bond was also confirmed by platinum satellites of the corresponding adjacent nuclei in the $^1$H and $^{13}$C NMR spectra of the complexes. Owing to the orthogonal arrangement of the platinum coordination plane to the bodipy ligand (*vide infra*) and a hindered rotation around the Pt−C axis the methylene protons of the $PEt_3$ ligands are diastereotopic. For complexes with the platinum ion attached to carbon atom C2, shift differences are rather minor such that only slight broadening of the respective resonance signals is observed. **3-Pt**, however, shows two separate resonances for the methylene protons in its $^1$H NMR spectrum (Figure S27).

Platinum coordination to the C8=C9 double bond of 3-chloro-5,7-dimethylbodipy in the complex **8,9-Pt** splits the resonance signal for H8 into a doublet of doublets with $^3J_{PH}$ couplings of 9.1 and 4.3 Hz to the two inequivalent phosphane ligands and additional platinum satellites with a $^2J_{PtH}$ coupling constant of 49.2 Hz. As the result of $\eta^2$-coordination, all corresponding resonance signals appear at higher field as compared to the parent dye. This is most dramatically seen for H8 and C8, whose resonances are shifted from 6.15 to 3.83 ppm (compare Figures S21 and S23) or from 123.5 to 42.1 ppm (compare Figures S22 and S26, $J_{PtC}$ = 43.6 Hz). The $^{195}$Pt NMR spectrum of **8,9-Pt** shows the expected doublet of doublets at $\delta$ = −4950 ppm; the coupling constants $J_{PtP}$ of 4800


DOI: 10.1021/acs.organomet.7b00806
*Organometallics* 2018, 37, 235−253

and 3320 Hz match with the $^{195}$Pt satellites in the $^{31}$P NMR spectrum.

**Single-Crystal X-ray Diffraction Analysis.** Single crystals of complexes **2-Pt-6H**, **2-Pt-6I**, **2-Pt-Mes-6I**, and **2-Pt-6Et** as well as of complexes **3-Pt** and **8,9-Pt** were grown by the procedures given in the Experimental Section and were successfully subjected to X-ray diffraction analyses. Details of the data collection and structure refinement are collected in Table S1. The most important metric parameters derived from the structure solutions are provided in Tables 1 and 2. The unit cell of **8,9-Pt** contains both different enantiomers that result from platinum coordination to either the Re or Si face of the prochiral olefin. The crystal of **2-Pt-6I** contained highly disordered molecules of *n*-pentane. All attempts to refine the solvent molecules were unsuccessful and the corresponding reflexes were removed using the solvent mask tool in OLEX2.

**Table 2. Selected Bond Lengths [Å] and Angles [deg] for 8,9-Pt**

| bond parameters | 8,9-Pt |
|---|---|
| C8−Pt1 | 2.127(9) |
| C9−Pt1 | 2.226(9) |
| Pt1−P1 | 2.301(2) |
| Pt1−P2 | 2.229(3) |
| C8−C9 | 1.431(13) |
| | |
| C8−Pt1−C9 | 38.3(4) |
| C8−Pt1−P2 | 97.5(3) |
| C9−Pt1−P1 | 120.0(3) |
| C8−Pt1−P1 | 157.9(3) |
| | |
| C9−Pt1−P2 | 135.8(3) |
| P1−Pt−P2 | 103.92(9) |
| [B]−[Pt][a] | 81.6 |
| [Pyr]−[Pyr][b] | 17.0 |

[a]Interplanar angle between the best plane through the inner six-membered ring of the bodipy ligand and the coordination plane at the platinum ion. [b]Interplanar angle between the planes of the pyrrolic subunits.

The molecular structures are displayed in Figure 1. Every σ-bodipy platinum complex exhibits an almost ideal square-planar coordination geometry at the coordination center with the *cis* bond angles at the platinum ion close to 90°. The P−Pt−P angle is slightly bent at 172.68−178.56°. The coordination plane at the platinum atom as defined by the atoms Pt, P1, P2, I, and C2 or C3 is in a close to orthogonal orientation (interplanar angles 85.4−89.6°) with respect to the plane through the inner six-membered ring of the attached bodipy ligand. The lengths of the Pt−C2 σ-bonds fall within a narrow range of 1.991(11)−2.027(4) Å and are nearly identical within the limits of the standard deviations, while the bond length Pt−C3 of 1.977(7) Å is slightly shorter. Previously reported **8-Pt**, where the Pt ion attaches to the *meso* position of the bodipy, has a similar Pt−C bond length of 1.994(10) Å.[59] With interplanar angles of 76.9−88.9°, the *meso* aryl substituents are also in a close to orthogonal orientation with the bodipy plane. The C8−Pt−C9 bond angle of 38.3(4)° and the angle P1−Pt−P2 of 103.92(9)° (Table 2) closely resemble those of other diphosphane platinum olefin complexes in the literature.[58,60,61] The Pt−C bond lengths are longer than those of 2.031(3)−2.114(4) Å found for related compounds, while the C−C bond length of 1.431(13) Å is still in the usual range of 1.275(3)−1.454(6) Å.[58,60,61]

Not unexpectedly, the Pt−C bond to the sterically less hindered carbon atom C8 of 2.127(9) Å is significantly shorter than that of 2.226(9) Å to the pyrrolic carbon atom C9. The coordination plane at the platinum atom as defined by the atoms Pt, P1, P2, C8, and C9 forms an interplanar angle of 81.5° with the plane of the bodipy ligand. $\eta^2$-Coordination to the C8═C9 bond and concomitant rehybridization of the *meso* carbon atom causes a larger deviation of the pyrrole rings from coplanarity of 17.0° (Table 2) as compared to that of 2.0−7.0° for the other complexes (Table 1). The distortion nevertheless remains small and is thus not expected to severely impact on π-conjugation within the bodipy ligand.

Packing diagrams of the various crystal structures are provided as Figures S31−S36. Short intermolecular H···I contacts between pyrrolic (**3-Pt**, **2-Pt-6H**) or the *meso* H atom (**3-Pt**, $d$(H···I = 3.005 Å) and the iodide ligand as well as short intermolecular H···F contacts between the $BF_2$ group and methyl (**8,9-Pt**, $d$(H···F) = 2.612 Å) and/or methylene protons of the $PEt_3$ ligands (**8,9-Pt**, $d$(H···F) = 2.579 Å; **2-Pt-6I**, $d$(H···F) = 2.561 Å, **2-Pt-6H**, and $d$(H···F) = 2.490 Å) or to cocrystallized benzene (**2-Pt-6I**, $d$(H···F) = 2.537, 2.571, and 2.658 Å) or $CH_2Cl_2$ molecules (**2-Pt-6Et**, $d$(H···F) = 2.480 Å) are found.

**Electronic Absorption Spectroscopy.** Figures 2 and S37 display the electronic absorption spectra of the parent dyes and their platinum complexes, while Table 3 lists all relevant data including band assignments and calculated transition energies derived from time-dependent density functional theory (TD-DFT; for comparisons of experimental and calculated spectra see Figures S38−S40). Remarkably, $\eta^2$-coordination of the 3-chloro-5,7-dimethylbodipy dye to the $Pt(PEt_3)_2$ moiety does not affect the position and intensity of the characteristic bodipy $\pi \rightarrow \pi^*$ band. Complex **8,9-Pt** and the parent dye have their absorption maximum at 508 nm, and, on platinum coordination, the extinction coefficient is reduced by about the same factor as the molecular mass increases. Geometry optimization of the molecular structure on the pbe1pbe/6-31g(d) level with the $CH_2Cl_2$ solvent accounted for by the PCM formalism overestimates the structural perturbation due to $\eta^2$-coordination somewhat. Thus, the two pyrrole rings are more bent with a calculated interplanar angle of 24.5° as opposed to the experimental value of 17.0° (*vide supra*). The calculated stronger structural distortion might also cause some differences between the TD-DFT calculated and experimental spectra in terms of the energetic ordering of the individual transitions as indicated by Figure S40.

According to our calculations all relevant MOs of **8,9-Pt** receive strong contributions from the $Pt(PEt_3)_2$ fragment (40 and 37%, respectively as inferred from Mulliken decomposition analysis, see Table S2). An intense absorption arising from the typical $\pi \rightarrow \pi^*$ excitation of the π-coordinated bodipy dye is calculated as the HOMO−1 → LUMO transition and hence at higher energy than the weaker, but still rather strong, HOMO → LUMO band (see Figure S41). The latter transition is predicted to have appreciable intraligand charge-transfer (CT) character with a shifting of electron density from the chloro-substituted to the dimethyl-substituted pyrrole ring. Both, the relative intensities and the solvatochromism of these bands rather point to an opposite ordering of the HOMO and HOMO−1 levels. Thus, the prominent band at ca. 500 nm is only slightly solvatochromic with a blue shift of 280 cm$^{-1}$


DOI: 10.1021/acs.organomet.7b00806
Organometallics 2018, 37, 235−253

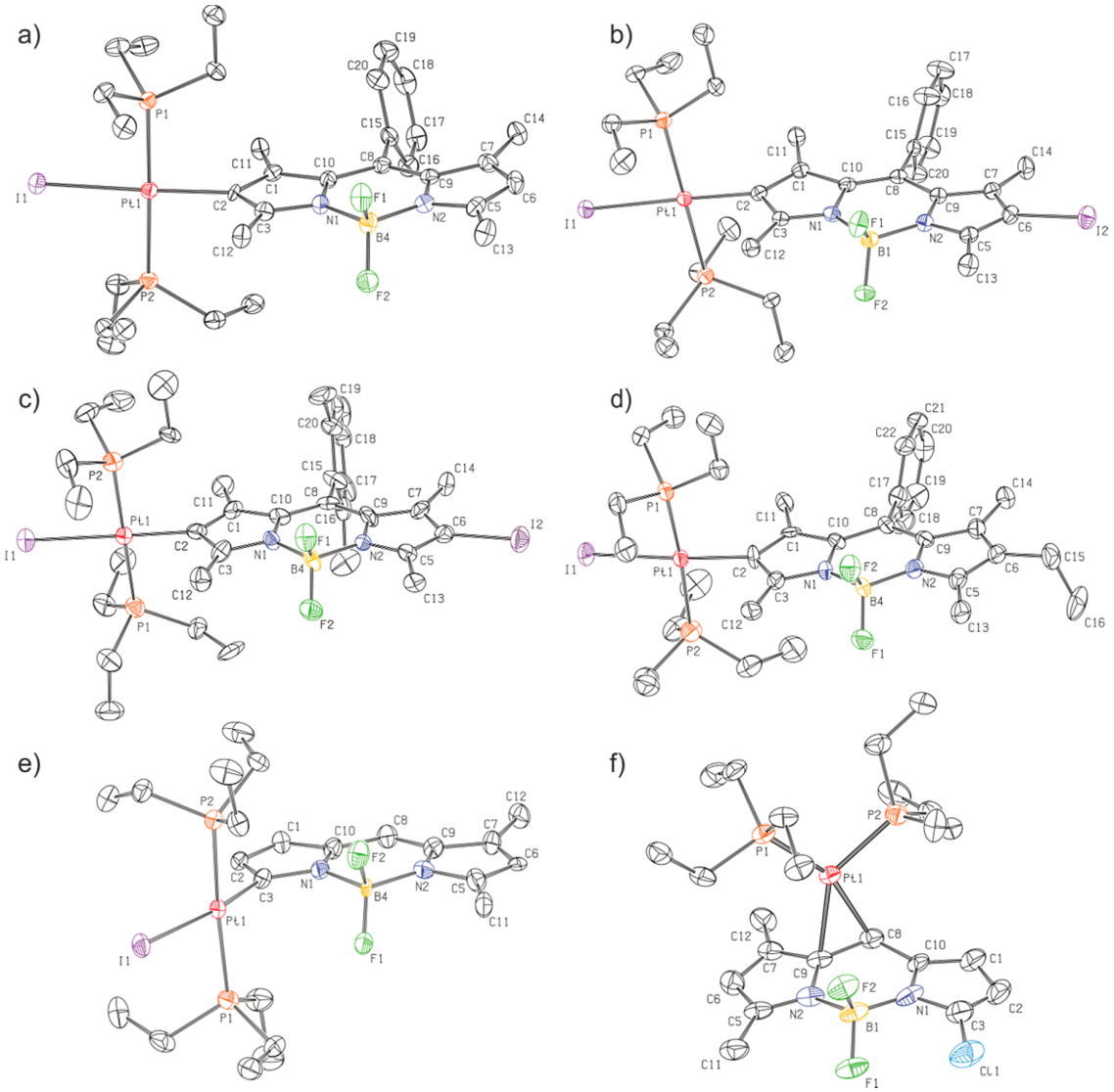


**Figure 1.** ORTEP[62] diagrams of (a) **2-Pt-6H**, (b) **2-Pt-6I**, (c) **2-Pt-Mes-6I**, (d) **2-Pt-6Et**, (e) **3-Pt**, and (f) **8,9-Pt**. The ellipsoids are drawn at a 50% probability level. Solvent molecules and hydrogen atoms are omitted for reasons of clarity. For **2-Pt-6H**, **2-Pt-6Et**, and **8,9-Pt** only one of the two independent molecules of the unit cell are shown.

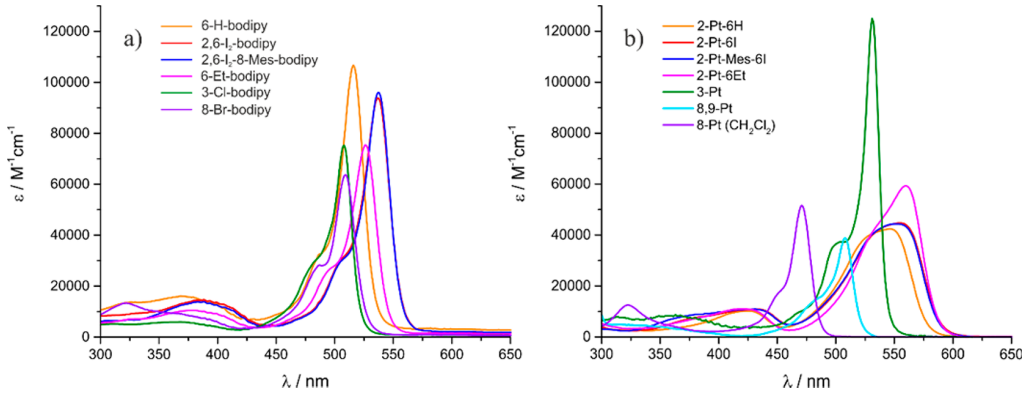


**Figure 2.** (a) Electronic absorption spectra of the halogenated dye precursors in ca. $1 \times 10^{-5}$ M toluene solutions. (b) UV−vis spectra of the bodipy platinum complexes in ca. $1 \times 10^{-5}$ M toluene solutions.



DOI: 10.1021/acs.organomet.7b00806
*Organometallics* 2018, 37, 235−253

Table 3. Absorption Data of the Complexes in ca. $1 \times 10^{-5}$ M Solutions in THF, Toluene, or $CH_2Cl_2$ and TD-DFT-Calculated (PBE1PBE/6-31G(d) PCM ($CH_2Cl_2$)) Energies and Band Assignments[a]

| | absorption data | | TD-DFT calculations | | | |
|---|---|---|---|---|---|---|
| compound | solvent | $\lambda_{max}$/nm ($\varepsilon$/L mol$^{-1}$ cm$^{-1}$) | $\lambda$ (nm) | $f$[a] | major contributions | Assigment |
| **2-Pt-6H** | toluene | 324 (3100), 399 (7500), 425 (10300), 532 (40700), 546 (42400) | | | n.c.[b] | |
| | $CH_2Cl_2$ | 321 (4200), 400 (8000), 425 (10700), 531 (36100) | | | | |
| | THF | 321 (4500), 400 (8200), 424 (10700), 537 (39300) | | | | |
| **2-Pt-6I** | toluene | 393 (7600), 433 (11000), 534 (41200), 554 (44700) | | | n.c.[b] | |
| | $CH_2Cl_2$ | 393 (7600), 433 (11000), 535 (36000), 552 (35900) | | | | |
| | THF | 393 (7600), 431 (11100), 535 (36000), 555 (34200) | | | | |
| **2-Pt-Mes-6I** | toluene | 362 (7300), 384 (8900), 430 (10900), 530 (38300), 553 (44400) | 465 | 0.66 | HOMO → LUMO (94%) | $\pi \rightarrow \pi^*$ |
| | | | 392 | 0.26 | HOMO−3 → LUMO (23%), HOMO−1 → LUMO (70%) | ML→L′CT[a] |
| | $CH_2Cl_2$ | 381 (7400), 418 (10700), 430 (11300), 528 (38800), 553 (40900) | 352 | 0.032 | HOMO−5 → LUMO (76%), HOMO−3 → LUMO (11%) | ML→L′CT,[a] ILCT[a] |
| | THF | 378 (6200), 415 (8600), 430 (9110), 529 (39300), 554 (40800) | 335 | 0.083 | HOMO−7 → LUMO (97%) | ILCT[a] |
| | | | 261 | 0.082 | HOMO−13 → LUMO (91%) | ML→L′CT[a] |
| **2-Pt-6Et** | toluene | 377 (6900), 420 (11000), 541 (47400), 560 (59300) | | | n.c.[b] | |
| | $CH_2Cl_2$ | 378 (8000), 420 (11600), 535 (40700), 556 (49000) | | | | |
| | THF | 384 (7700), 421 (10700), 539 (44000), 556 (51500) | | | | |
| **8,9-Pt** | toluene | 320 (4800), 508 (38900) | 409 | 0.19 | HOMO → LUMO (96%) | ILCT[a] with mc[c] |
| | THF | 349 (4800), 501 (37900) | 334 | 0.36 | HOMO−1 → LUMO (86%) | $\pi \rightarrow \pi^*$ with mc[c] |
| **3-Pt** | toluene | 314 (7900), 359 (8300), 531 (125000) | 439 | 0.77 | HOMO → LUMO (99%) | $\pi \rightarrow \pi^*$ |
| | $CH_2Cl_2$ | 312 (4400), 355 (4400), 528 (101100) | 334 | 0.070 | HOMO−4 → LUMO (97%) | ILCT[a] |
| | THF | 312 (4400), 355 (4400), 527 (109300) | 248 | 0.064 | HOMO−10 → LUMO (91%) | ML→L′CT[a] |
| **8-Pt** | $CH_2Cl_2$ | 323 (12500), 344 (6500), 471 (51600) | 392 | 0.39 | HOMO → LUMO (97%) | $\pi \rightarrow \pi^*$ |
| | | | 309 | 0.07 | HOMO−5 → LUMO (81%) | ML→L′CT[a] |
| | | | 295 | 0.17 | HOMO−6 → LUMO (90%) | $\pi \rightarrow \pi^*$ |

[a]$f$ = Oscillator strength, ML → L′CT = metal/ligand to ligand′ charge transfer, ILCT = intraligand charge transfer. [b]Not calculated. [c]mc = Metal contribution.

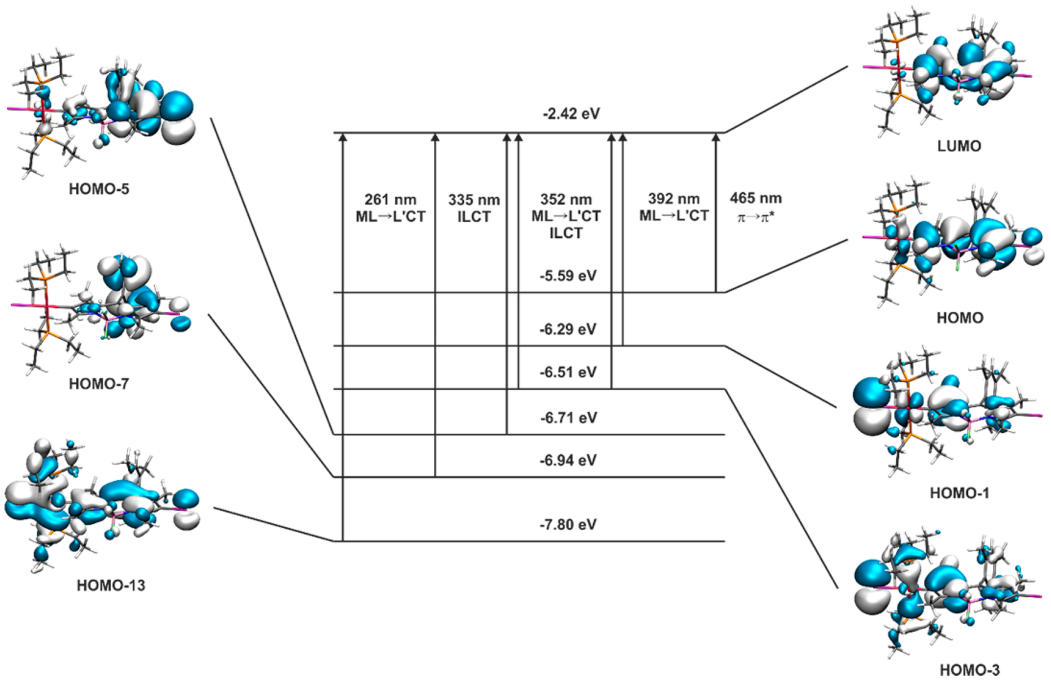


Figure 3. Graphical representation of the relevant MOs, transitions, and TD-DFT energies of **2-Pt-Mes-6I**. Solid arrows symbolize the main contributor(s) to the respective transition.



DOI: 10.1021/acs.organomet.7b00806
Organometallics 2018, 37, 235−253

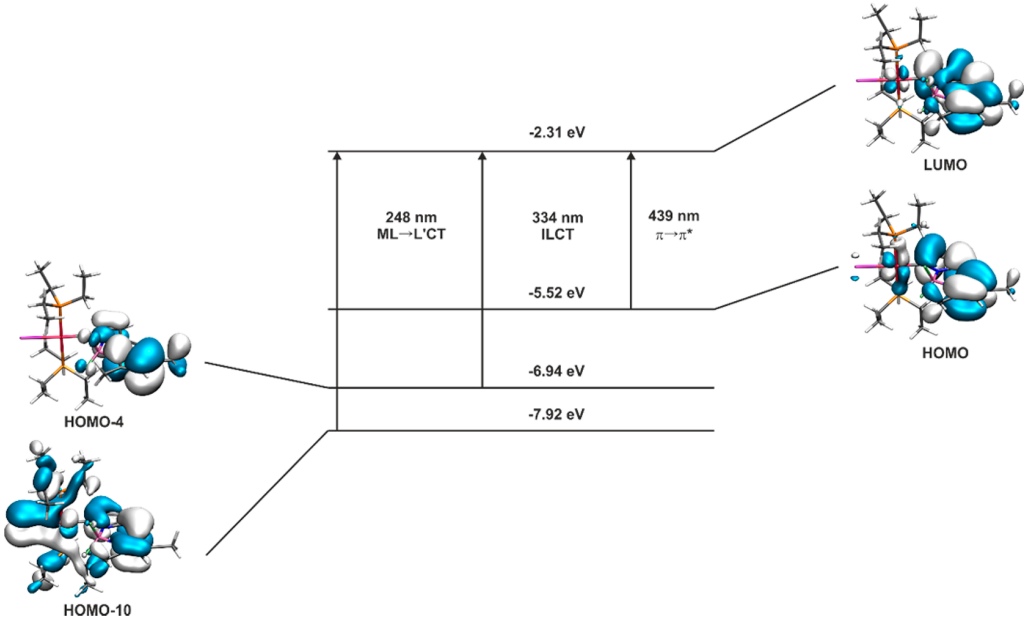


**Figure 4.** Graphical representation of the relevant MOs, transitions, and TD-DFT energies of **3-Pt**. Solid arrows symbolize the main contributor to the respective transition.

**Table 4. Photophysical Data of the σ-Bodipy Platinum Complexes in Degassed $CH_2Cl_2$, Toluene, or 2-Me-THF Solutions at Concentrations of ca. $10^{-6}$ M at r. t.**

| | $\lambda_{max,Fl}$/nm (Stokes shift/ $cm^{-1}$) | $\lambda_{max,Ph}$/nm (Stokes shift/ $cm^{-1}$) | $\Phi_{Fl}$ | $\Phi_{Ph}$ | $\Phi_{\Delta}$[c] | $\tau_{Fl}$ (ns) | $\tau_{Ph}$ ($\mu$s) | $k_{ISC,S1\rightarrow T1}$ ($s^{-1}$)[f] | $k_{ISC,T1\rightarrow S0}$ ($s^{-1}$)[f] |
|---|---|---|---|---|---|---|---|---|---|
| **8-Pt** | 481 (441) | 637 (5669)[a] | 0.002 | 0.364[a] | 0.95 | 0.484 | 297 ± 2[a] | $2.1 \times 10^9$ | $2.0 \times 10^3$ |
| **2-Pt-6H** | 580 (1074) | 804 (5877) | 0.0008[b] | 0.0009[b] | 0.51 | 4.5 ± 0.2 | 80 ± 4, 765 ± 8,[d] 475 ± 9[d] | $2.2 \times 10^8$ | $1.3 \times 10^4$ |
| **2-Pt-6I** | 590 (1036) | 804 (5548) | 0.0003[b] | 0.0004[b] | 0.53 | 3.7 ± 0.2,[d] 30 ± 1[d] | 67 ± 3, 433 ± 11,[d] 247 ± 5[d] | | $1.5 \times 10^4$ |
| **2-Pt-Mes-6I** | 588 (1109) | 797 (5569) | 0.0009[b] | 0.0014[b] | 0.48 | n.d.[e] | 150 ± 10, 843 ± 64,[d] 269 ± 9[d] | | $6.7 \times 10^3$ |
| **2-Pt-6Et** | 587 (853) | 815 (5619) | 0.0006[b] | 0.0003[b] | 0.34 | 4.12 ± 0.0.09, 0.0459 ± 0.008,[d] 4.23 ± 0.09[d] | 243 ± 4, 683 ± 18[d] | $2.4 \times 10^8$ | $4.1 \times 10^3$ |
| **8,9-Pt** | 516 (305) | | 0.486 | | n.d.[e] | 5.33 ± 0.02, 6.28 ± 0.04[g] | | $0.96 \times 10^8$ | |
| **3-Pt** | 535 (141) | | 0.527 | | 0.19 | 2.30 ± 0.01, 2.52 ± 0.01[d] | | $2.06 \times 10^8$ | |
| **3-Cl-5,7-$Me_2$-bodipy**[h] | 501 (532) | | 0.73 | | | 5.60 ± 0.01 | | | |

[a]Measured in $CH_2Cl_2$ solution at r.t. [b]Determined using 2,6-$I_2$-8-Ph-Bodipy ($\Phi$ = 3.13%) as a standard. [c]$^1O_2$ generation quantum yield corrected using the value of methylene blue (MB, $\Phi_{\Delta}$ = 0.57) as a reference. [d]Measured in 2-Me-THF glass at 77 K. [e]Not determined. [f]$k_{ISC}$ is the rate constant for intersystem crossing and was estimated from eq 2. [g]Measured in toluene glass at 77 K. [h]According to ref 64.

between toluene and THF, while the second, less intense band exhibits a sizable red shift of 2600 $cm^{-1}$, indicating a more polar excited state (see Figure S37f).

All complexes exhibit the characteristic sharp and intense $\pi \rightarrow \pi^*$ absorption band of a bodipy dye. Platinum coordination to the 2- or 3-position shifts the main absorption band bathochromic, e.g., from 508 nm for 3-chloro-5,7-dimethylbodipy to 531 nm ($\Delta\tilde{\nu}$ = 850 $cm^{-1}$) for **3-Pt** or from 516 nm for 2-iodo-8-phenylbodipy to 546 nm ($\Delta\tilde{\nu}$ = 1070 $cm^{-1}$) in **2-Pt-6H**. This is in striking contrast to the hypsochromic shift of 1600 $cm^{-1}$ observed for the previously reported complex **8-Pt**, where the platinum ion attaches to the *meso* position C8.[63] (TD)-DFT calculations explain this disparate behavior. Thus, the HOMO of a bodipy dye has a nodal plane along the C8−B vector, whereas the LUMO has not. Hence, the electron-donating $Pt(PR_3)_2I$ fragment destabilizes the LUMO more than the HOMO, thereby increasing the HOMO−LUMO gap. In contrast, when bound to carbon atoms C2 or C3, the $Pt(PR_3)_2I$ moiety contributes more to the HOMO than to the LUMO, which decreases the HOMO−LUMO gap by 500 or 1100 $cm^{-1}$ with respect to the free halogenated dye (Figures 3 and 4).

Similar to **8-Pt**, the $\pi \rightarrow \pi^*$ band of **3-Pt** is sharp, whereas it is broadened significantly in all of the 2-platinated bodipy complexes. Such broadening suggests a stronger perturbation of the bodipy $\pi$-system by the attached $Pt(PEt_3)_2I$ fragment and additional underlying transitions resulting in richer absorption


DOI: 10.1021/acs.organomet.7b00806
Organometallics 2018, 37, 235−253

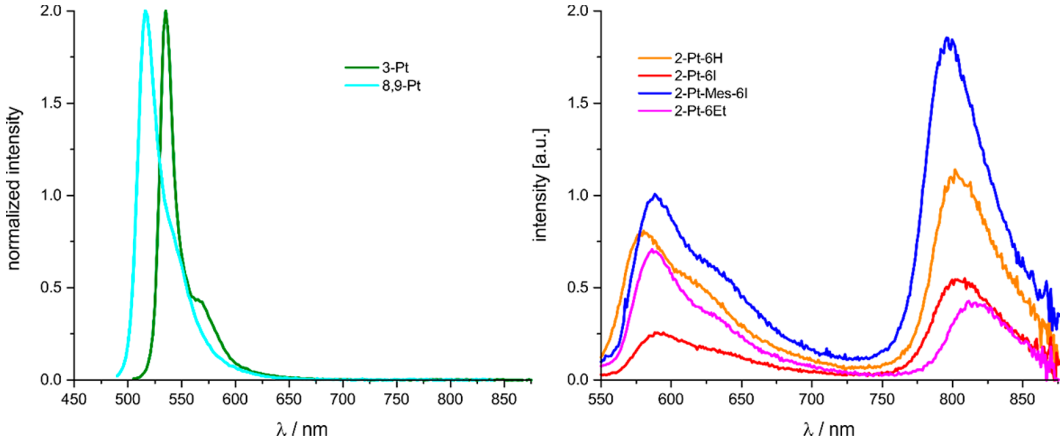


**Figure 5.** Left: Luminescence spectra of **3-Pt** (green) and **8,9-Pt** (cyan) in ca. $10^{-6}$ M toluene solution; right: luminescence spectra of **2-Pt-6H** (orange), **2-Pt-6I** (red), **2-Pt-Mes-6I** (blue), and **2-Pt-6Et** (magenta).

features. This is also borne out by our TD-DFT calculations on model complexes **3-Pt** and **2-Pt-Mes-6I**. Calculated and experimental spectra are compared in Figures S38 and S39, while Figures 3 and 4 display the crucial MOs and the computed transitions. Electron density difference maps (EDDMs) of the calculated transitions are also included as Figures S43 and S44; fragment contributions to the corresponding MOs according to Mulliken decomposition analysis are provided as Tables S3 and S4. Our calculations provide only a qualitative level of agreement with the experimental data (see Table 3) because the energies of the electronic transitions are overestimated by DFT methods. This is a known problem for bodipys and related cyanine dyes.[33,34] Nevertheless, TD-DFT calculations agree with our experimental observations in predicting additional, rather intense HOMO−1/HOMO−3 → LUMO transitions with PtI → bodipy CT character for **2-Pt-Mes-6I** at rather close energies to the dominant $\pi \rightarrow \pi^*$ transition (see Table 3 and Figure 3). The latter have no equivalent in **3-Pt** (Figure 4) or **8-Pt**.[59] The predicted ML → L′CT admixture to the high-energy part of this band still fails to cause any notable solvatochromism (see Figure S37a−d). A similar broadening of the HOMO → LUMO absorption band of a Pt(bipy)(2-ethynylbodipy)$_2$ complex was recently observed by Zhong et al. and likewise attributed to MLCT and intraligand charge-transfer (ILCT) admixtures to the main $\pi \rightarrow \pi^*$ excitation.[41] The results of our TD-DFT calculations for **3-Pt** provide an excellent match with the experimental spectrum in predicting a single, intense bodipy-based $\pi \rightarrow \pi^*$ band and additional ML → L′CT and ILCT bands of only minor intensity in the UV (see Figures 4 and S39).

**Luminescence Spectroscopy.** As just discussed, changing the site of platinum attachment to the bodipy chromophore from *meso*/C8 to C2 or C3 gauges platinum contribution to the relevant frontier MOs and, in case of the 2-complexes, also mixes some PtI → bodipy CT character into the main $\pi \rightarrow \pi^*$ absorption. One therefore expects that the positioning of the Pt(PEt$_3$)$_2$I entity influences the ISC rates and emission energies as well as the relative intensities of the fluorescence and phosphorescence emissions. This is indeed the case.

Table 4 and Figure 5 summarize the luminescence properties of the new complexes as measured in gastight cuvettes under rigorous exclusion of air, along with those of the previously reported **8-Pt** as a point of comparison. The latter complex is very weakly fluorescent but phosphoresces at 641 nm with a quantum yield of up to 41%.[59] Complexes **3-Pt** and **8,9-Pt** are strongly fluorescent in solution at r.t. ($\Phi_{Fl}$ ca. 50%) with an emission peak at 535 or 516 nm, respectively, but do not phosphoresce, even in a 2-MeTHF glass matrix at 77 K (Figures S45 and S46). Like in the absorption spectrum, platinum binding to the C═C double bond does not cause any appreciable shift of the emission wavelength with respect to 3-chloro-5,7-dimethyl-bodipy but decreases the quantum yield from 76 to 53%.[64]

In contrast, the C2-plantinated complexes exhibit dual luminescence with a fluorescence peak at 580−590 nm and phosphorescence in the near-infrared (NIR), at 797−815 nm. NIR phosphorescence of a bodipy dye at r.t. in fluid solution is a rather rare asset.[26,30,41,65−67] Comparison of the excitation spectra recorded for the fluorescence and the phosphorescence emissions with the absorption spectra in Figure S47 proves that both emissions emanate from the same complex and that none of them is due to an impurity. As an unfortunate consequence of the small energy gap between the $^3\pi\pi^*$ and the $S_0$ states of the **2-Pt-bodipy** complexes and the concomitantly higher probability of radiationless decay to the ground state as expressed by the energy gap law,[68,69] phosphorescence quantum yields are significantly smaller than those for **8-Pt**.

$$k_{ISC} = (1 - \Phi_{F1})/\tau_{F1} - k_{IC} \quad (1)$$

$$k_{ISC} \leq (1 - \Phi)/\tau \quad (2)$$

ISC rate constants $k_{ISC}$ were estimated from eq 2.[70] By assuming $k_{IC} \approx 0$ in eq 1 for all complexes, an upper limit for $k_{ISC}$ is obtained.[70] Overall, the rate of ISC from the $S_1$ to the $T_1$ state follows the trend **8-Pt** > **2-Pt-6H,Et,I** > **3-Pt** (Table 4).

Comparison of the luminescence properties of the complexes **2-Pt-6H**, **2-Pt-6Et**, **2-Pt-6I**, and **2-Pt-Mes-6I** reveals that the substituent in 6-position at the second pyrrole ring, and, in particular, the presence of the iodine heavy atom or blocking the rotation of the *meso* aryl substituent, have only minor effects on the ISC rates, emission lifetimes, and, consequently, the relative intensities of the fluorescence and phosphorescence emissions. It was observed on other occasions that replacing the *meso* phenyl by a mesityl substiuent serves to close channels for radiationless decay by rotation of the aryl substituent around the C8-aryl bond.[71,72] In the case of complexes **2-Pt-6I** and **2-Pt-Mes-6I**, this modification also increases the QY of the NIR


DOI: 10.1021/acs.organomet.7b00806
*Organometallics* 2018, 37, 235−253

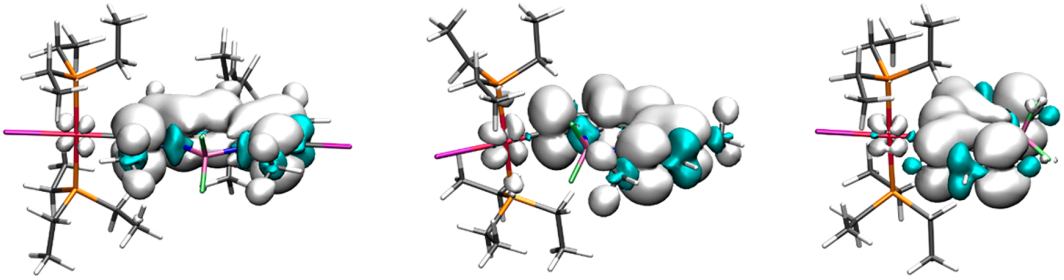

**Figure 6.** Spin density surfaces of the $T_1$ state of **2-Pt-Mes-6I** (left), **3-Pt** (middle), and **8-Pt** (right).[73]

phosphorescence emission, but it still remains very modest at 0.14%. Phosphorescence lifetimes of the 2-Pt-bodipy complexes range from 67 and 243 $\mu$s at r.t. and increase significantly upon cooling to 77 K in a rigid 2-MeTHF matrix (Table 4). DFT calculations indicate that the fluorescence and phosphorescence emissions emanate from the $^1\pi\pi^*$ and $^3\pi\pi^*$ excited states of the bodipy ligand. Figure 6 shows that the spin density of the triplet state $T_1$ of complexes **8-Pt**, **2-Pt-Mes-6I**, and **3-Pt** concentrates on the bodipy ligand with only minor contributions from the $Pt(PEt_3)_2I$ fragment (see also Table S5 for fragment contributions according to Mulliken).

An important asset of bodipy dyes is their potency to form $^1O_2$ from $^3O_2$ via TTA. This makes bodipys highly interesting sensitizers for applications in photocatalysis[31,74−77] and photodynamic therapy (PDT).[10,25,26,78,79] **8-Pt** and its closely related *trans*-Pt(bodipy)Cl$(PEt_3)_2$ analogue have shown up to almost unitarian quantum yields for photochemical $^1O_2$ generation with no signs of decomposition over 3 h. The model photooxidation of 1,5-dihydroxynaphthalene (DHN) to Juglone pursuant to Scheme 2 was monitored by recording UV/vis spectra at regular intervals during photoirradiation and calculating the pseudo first-order kinetics for DHN consumption (for details see the Experimental Section and Figures S48−S52). Slight deviations of the slopes when plotting $\ln(C_t/C_0)$ as a function of time $t$ after 60 min mark the onset of photodecomposition.

**Scheme 2. Photooxidation of DHN to Juglone with $^1O_2$ in the Presence of a Photosensitizer**

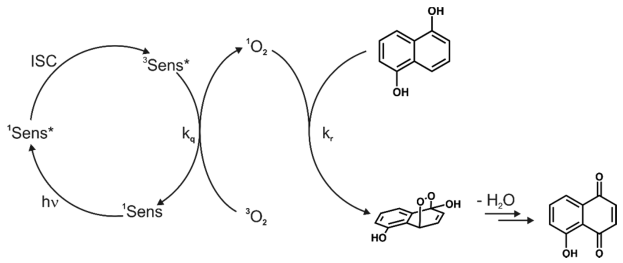


Table 5 summarizes the results of these experiments. Complexes of the **2-Pt** series reach only modest quantum yields of 53 and 34%. Still, DHN oxidation to Juglone occurs with higher turnover frequencies (TOFs) than for **8-Pt** as a result of a better overlap of their absorption envelopes with the radiation of the light source as expressed by the higher value of $I$ (Table 5). Although **3-Pt** is nonphosphorescent, its excited triplet state is still populated to an appreciable extent. This follows from the reduction of the fluorescence lifetime $\tau_{Fl}$ compared to 3-chloro-5,7-dimethyl-bodipy (5.46 ± 0.01 ns)[64] and from the $^1O_2$ quantum yield of 19% using **3-Pt** as the sensitizer. We suspect that the substantially lower quantum yields of the present complexes for $^1O_2$ generation when compared to **8-Pt** are also rooted in the comparatively low energies of their $T_1$ states, which renders energy transfer to $^3O_2$ less exergonic while making decay by other pathways more efficient. In summary, we note that the QYs for $^1O_2$ generation mirror the trend for the ISC rates and decrease from **8-Pt** to the 2-platinated complexes and to **3-Pt**, paralleling the trends obtained from luminescence spectroscopy (vide supra).

In order to probe whether DHN oxidation occurs preferably via the direct reductive quenching of the excited state of the complexes with DHN as the electron donor or by energy transfer to $^3O_2$ and the subsequent reaction of DHN with photogenerated $^1O_2$ we exemplarily monitored the phosphorescence quenching of **2-Pt-Mes-6I** with oxygen or DHN as the quencher. Stern−Volmer plots and stack plots showing the emission intensities and decays without or with the respective quencher at various concentration levels are provided as Figures

**Table 5. Pseudo First-Order Kinetics, $^1O_2$ Generation Quantum Yields, and Turnover Frequencies for the DHN Photooxidation Using the Complexes 8-Pt,[59] 2-Pt-6H, 2-Pt-6I, 2-Pt-Mes-6I, 2-Pt-6Et, 3-Pt, and Methylene Blue (MB) as Sensitizers**

| | $\lambda_{ex}$ (nm) | $k_{obs}$ (min$^{-1}$)[a] | $\nu_i$ (× 10$^{-6}$ M min$^{-1}$)[b] | $I$[c] | $\Phi_\Delta$[d] | yield (%)[e] | TOF (s$^{-1}$)[f] |
|---|---|---|---|---|---|---|---|
| **8-Pt** | 460 ± 5 | 0.00145 | 0.1757 | 0.810 | 0.95 | 25 | 0.0014 |
| **2-Pt-6H** | 550 ± 5 | 0.00377 | 0.4649 | 3.988 | 0.51 | 35 | 0.0037 |
| **2-Pt-6I** | 550 ± 5 | 0.00413 | 0.5093 | 4.221 | 0.53 | 24 | 0.0025 |
| **2-Pt-Mes-6I** | 550 ± 5 | 0.00449 | 0.5130 | 4.665 | 0.48 | 26 | 0.0029 |
| **2-Pt-6Et** | 550 ± 5 | 0.00344 | 0.4242 | 5.462 | 0.34 | 23 | 0.0024 |
| **3-Pt** | 530 ± 5 | 0.00337 | 0.4155 | 9.557 | 0.19 | 26 | 0.0027 |
| **MB** | 655 ± 5 | 0.00102 | 0.1296 | 1 | 0.57 | 5 | 0.0003 |

[a]Pseudo-first-order rate constant for DHN consumption. [b]Initial rate of DHN consumption. [c]Relative number of photons absorbed by the sensitizer ($I$ = 1 for the standard sensitizer MB). [d]Corrected $^1O_2$ generation quantum yields using the value of MB ($\Phi_\Delta$ = 0.57)[81−83] as a reference. [e]Yield of Juglone after a reaction time of 60 min. [f]Turnover frequency.



DOI: 10.1021/acs.organomet.7b00806
*Organometallics* 2018, 37, 235−253

S53–S58. With a Stern–Volmer quenching constant $K_{SV}$ of 2150 ± 200 $bar^{-1}$ or 670 ± 61 $\mu M^{-1}$, the phosphorescence emission of **2-Pt-Mes-6I** was found to be almost as sensitive to oxygen as that of **8-Pt** ($K_{SV}$ = 2580 ± 71 $bar^{-1}$).[59] The quenching constant for DHN as the quencher is smaller by a factor of 22 ($K_{SV}$ = 31 ± 2 $\mu M^{-1}$), which identifies energy transfer as the dominant pathway. In agreement with that, quenching by electron transfer is calculated to be endergonic by 1.01 eV (97.5 kJ/mol) based on the Rehm–Weller equation (see also Figure S59 for the peak potential of electrochemical DHN oxidation).[80] Similar values were derived for the other complexes so that this statement should apply for these as well.

**Electrochemistry and UV/Vis/NIR and EPR Spectroelectrochemistry.** Bodipys are generally electroactive and can be oxidized and reduced by one electron each.[41,53,54,56] Their associated radical cations or anions are sometimes sufficiently persistent to allow for their spectroscopic characterization by UV/vis/NIR[84−90] or EPR spectroscopy.[91] Such investigations are particularly relevant for the spectroscopic identification of bodipy radical species in the photoexcited, charge-separated states. Examples are dyads or triads, where a bodipy is linked to a peripheral 2,4,5-trimethoxybenzene,[85] phenylanthracene,[86] triarylamine[87] or *N*-(2-ethylhexyl)dithieno[3,2-*b*:2′,3′-*d*]pyrrole (DTP)[92] electron donor or a fullerene[89] or carborane acceptor.[90] The latter are of great interest with respect to light-to-energy conversion schemes or mimicking natural enzymes.[85,87,90,92,93]

The results of our voltammetric studies on the $\sigma$-platinum bodipy complexes are summarized in Table 6. In their cyclic voltammograms, all complexes except for **8-Pt** show a fully or nearly reversible one-electron oxidation and a reversible to partially reversible reduction within the electrochemical window of the $CH_2Cl_2/NBu_4PF_6$ supporting electrolyte (see Figures 7 and 8). Figure S60 illustrates the voltammetric traces of the 8-mesityl-2,6-diiodobodipy, 3-chloro-5,7-dimethyl-bodipy, and 8-bromo-bodipy precursors under the same conditions as points of comparison. For the latter two compounds, higher sweep rates were required in order to outrun chemical follow processes following oxidation or reduction. Similar to related bis(phosphane) platinum alkynyl complexes containing 2- or 8-ethynylated bodipy ligands,[33,35] attachment of the electron-rich platinum entity causes sizable cathodic shifts of both redox waves. The cathodic shift of 450–540 mV for the 0/+ redox couple on platinum attachment to the bodipy carbon atom C2 or C3 slightly surpasses that of 340–510 mV for the 0/− process (Table 6). This is consistent with the higher contribution of the $Pt(PEt_3)_2I$ fragment to the HOMO (c. f. Figures 3 and 4 and Tables S3 and S4).

**Table 6. Electrochemical Data for all Complexes and Representative Halogenated Bodipys**[a]

| complex | $E_{1/2}$ 0/+ | $E_{1/2}$ 0/− |
|---|---|---|
| **8-Br-bodipy** | | −1530 |
| **8-Mes-2,6-$I_2$-bodipy** | 890 | −1520 |
| **3-Cl-bodipy** | 950 | −1420 |
| **2-Pt-6H** | 450 | −1920 |
| **2-Pt-6I** | 540 | −1810 |
| **2-Pt-Mes-6I** | 540 | −1860 |
| **2-Pt-6Et** | 370 | −1960 |
| **3-Pt** | 410 | −1930 |
| **8-Pt** | | −1770 |

[a]All potentials are given in mV relative to the $Cp_2Fe^{0/+}$ couple ($E_{1/2}$ = 0.000 V) and were measured in $CH_2Cl_2$ at 293 K with $NBu_4PF_6$ as the supporting electrolyte.

The oxidation (0/+) or reduction (0/−) half-wave potentials also trace the degree of the electronic interaction of the $Pt(PR_3)_2I$-fragment with the bodipy chromophore. Attachment to the *meso*-position C8 causes a smaller potential difference $\Delta E_{1/2}$ of 240 mV with respect to the parent dye than platinum attachment to carbon atom C2 ($\Delta E_{1/2}$ = 340 mV) or C3 ($\Delta E_{1/2}$ = 510 mV; note, however, that the presence of a chloro substituent in **3-Cl-bodipy** instead of the iodo substituent in the other dyes likely contributes to the increased potential shift of **3-Pt**). Exchanging the substituent in 6-position of the 2-platinated dyes has a similar effect on both half-wave potentials and causes a cathodic shift with increasing electron donating capability in the ordering Et > H > I.

All our previous data indicate that the HOMO and LUMO of the platinum $\sigma$-bodipy complexes are dominated by the bodipy ligand. Monitoring the changes in the UV/vis/NIR spectra on one-electron reduction or oxidation provides a direct means to experimentally probe for the identity of the corresponding redox site. Some accounts of spectroelectrochemical investigations on bodipy dyes have already appeared in the literature. The results of these studies can serve as reference points for our present results.[84,85,87,89,91,92,94,95] Like for the other studies, the radical cations or anions were generated inside a transparent UV/vis/NIR cell[96] or inside an EPR tube under the in situ conditions of spectroelectrochemistry. The results of these studies are displayed in Figures 9 and S61–S63, while Table 7 summarizes the relevant data and the TD-DFT calculated band energies and assignments. Plots of the pertinent MOs and transitions along with the corresponding electron density difference maps (EDDMs) of the oxidized and reduced forms of representative complexes as well as fragment contributions according to Mulliken analysis can be retrieved from Figures S64–S71 and Tables S7–S10.

As it was previously observed for other bodipy dyes, the prominent $\pi \rightarrow \pi^*$ band partially bleaches on reduction while a new, weaker absorption band grows in. The latter is by ca. 40–50 nm to the red from the former HOMO → LUMO band (see Figures 9a–c, S61a, and S62a). According to our TD-DFT results, the new low-energy band of the radical anions is assigned as a bodipy → $Pt(PEt_3)_2$ CT transition (see Table 7, Figures S64, S65, and S68–S71). As shown in Figure S62a, the reduction of 8-mesityl-2,6-diiodo-bodipy produces nearly identical spectroscopic changes. All reduction processes are highly reversible as shown by the multiple isosbestic points and the nearly complete recovery of the original spectra after a full reduction/reoxidation cycle (c.f. Figures S62b and S63).

On the time scale of spectroelectrochemical experiments, only **2-Pt-Mes-6I** (Figures 9d and S63e) and **2-Pt-6Et** (Figure S61b and S63f) can be reversibly oxidized. Concomitant with the bleaching of the characteristic $\pi \rightarrow \pi^*$ transition, a weak, broad NIR band enveloping the entire regime between 750 and 1750 nm is observed. This again agrees with previous studies on other bodipys.[87,88,94,95] TD-DFT calculations suggest that the NIR absorption of the **2-Pt-Mes-6I** radical cation originates from a mixed ILCT (Mes → bodipy) and PtI → bodipy ML → L′CT transition at 1162 nm and at 805 nm with CT from the iodo and mesityl substituents to the bodipy $\pi$ system (see Figures S66 and S67 and Table 7).


DOI: 10.1021/acs.organomet.7b00806
*Organometallics* 2018, 37, 235–253

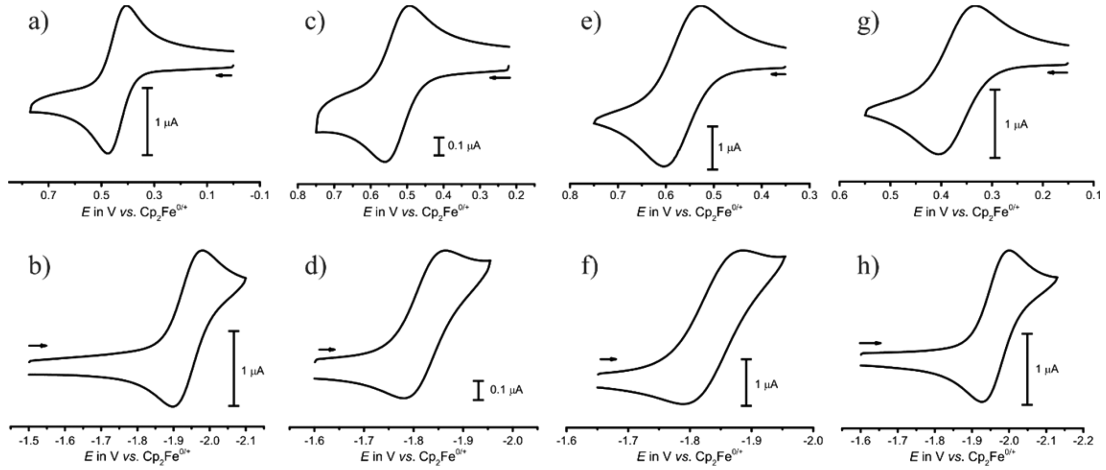


**Figure 7.** Cyclic voltammograms ($v$ = 100 mV/s) recorded for anodic (top) and cathodic (bottom) sweeps of (a, b) **2-Pt-6H**, (c, d) **2-Pt-6I**, (e, f) **2-Pt-Mes-6I**, and (g, h) **2-Pt-6Et** in $CH_2Cl_2$ at $T$ = 293 K with $NBu_4PF_6$ (0.1 M) as the supporting electrolyte.

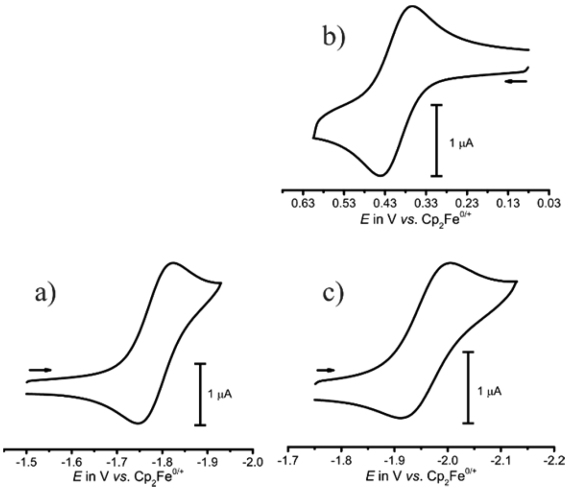


**Figure 8.** Cyclic voltammograms recorded for anodic (top) and cathodic (bottom) sweeps of (a) **8-Pt** ($v$ = 100 mV/s) and (b, c) **3-Pt** ($v$ = 200 mV/s) in $CH_2Cl_2$ solution at $T$ = 293 K with $NBu_4PF_6$ (0.1 M) as the supporting electrolyte.

Owing to the presence of multiple nuclei with a nuclear spin $I \neq 0$, and the fundamental differences between ligand- and metal-centered spin, EPR spectroscopy provides another potent tool to probe for the identity of the respective redox site. In particular, the hyperfine splittings (hfs) to the abundant (33.8%) $^{195}$Pt $I$ = 1/2 nucleus provides a means for probing the platinum contribution to the relevant SOMO. We note that EPR spectroscopic investigations on bodipy-derived radical cations or anions are extremely rare.[91] The radical forms of all compounds were prepared by electrochemical oxidation or reduction inside an EPR tube using a three-electrode configuration. EPR spectra of the one-electron reduced forms of the complexes **2-Pt-Mes-6I**, **3-Pt**, and **8-Pt** as well as those of oxidized **2-Pt-Mes-6I** and **3-Pt** are displayed in Figures 10−12. Comparison with the EPR spectra of the oxidized and reduced forms of the 8-mesityl-2,6-diiodo-bodipy precursor (see Figure S72) aids in the identification of the $^{195}$Pt and $^{31}$P hfs.

The radical cation of 8-mesityl-2,6-diiodo-bodipy gives a partially resolved EPR spectrum at a $g$-value of 2.0042. The EPR spectra of the radical cations of the Pt complexes are broader but exhibit clearly resolved hfs to the platinum nucleus of the $^{195}$Pt-containing isotopomer. At 100.9 G, the value of the 2-platinated complex **2-Pt-Mes-6I** is larger than that of 81.7 G for **3-Pt**. As a result of the minor metal contribution to the SOMO (for calculated spin densities, see Figures 13 and 14, and for fragment analysis, see Tables S7−S10), the $g$-values are only moderately increased with respect to the Landé factor $g_e$ of 2.002319 of the free electron and that of the 8-mesityl-2,6-diiodo-bodipy radical cation.

Quite remarkably, the EPR spectrum of the **8-Pt** radical anion is entirely dominated by hyperfine interactions with $^{31}$P and the $^{195}$Pt nuclei of the $Pt(PEt_3)_2$ fragment (see Figure 10, Table 8). Calculated spin densities are displayed in Figure S73, while a fragment analysis is provided in Table S11. The EPR spectra of the radical anions of free dyes and associated platinum complexes **2-Pt-Mes-6I** and **3-Pt** offer an even richer structuring due to resolved hfs to the $^{14}$N, $^{10/11}$B, and $^{19}$F nuclei (see Figures 13 and 14 for calculated spin density distributions). Comparison of the spectra of the 8-mesityl-2,6-diiodo-bodipy radical anion (see Figure S72 and Table S11 for calculated spin density distributions) with those of reduced **2-Pt-Mes-6I** and **3-Pt** evidence the presence of hfs interactions with the $^{195}$Pt nucleus in the latter. Spectra simulated with the hfs constants compiled in Table 8 are also displayed in Figures 10−12 and S72. Despite the overall good agreement between experimental and simulated spectra, the multitude of possible hfs interactions render our simulations and assignments of hfs constants only tentative. Again, the $g$-values of the reduced complexes (1.9917−1.9993) are close to that of 1.9935 for the 8-mesityl-2,6-diiodo-bodipy radical anion. This again confirms the organic parentage of these paramagnetic species.

In summary, the close resemblance of the UV/vis/NIR and EPR spectra of the oxidized and reduced forms of 8-mesityl-2,6-diiodo-bodipy and related bodipy dyes to those of the electrogenerated radical cations and anions of the $\sigma$-bodipy platinum complexes fully agrees with our conclusions derived from their optical and photophysical properties and reconfirms that their HOMOs and LUMOs are largely based on the bodipy ligands.


DOI: 10.1021/acs.organomet.7b00806
Organometallics 2018, 37, 235−253

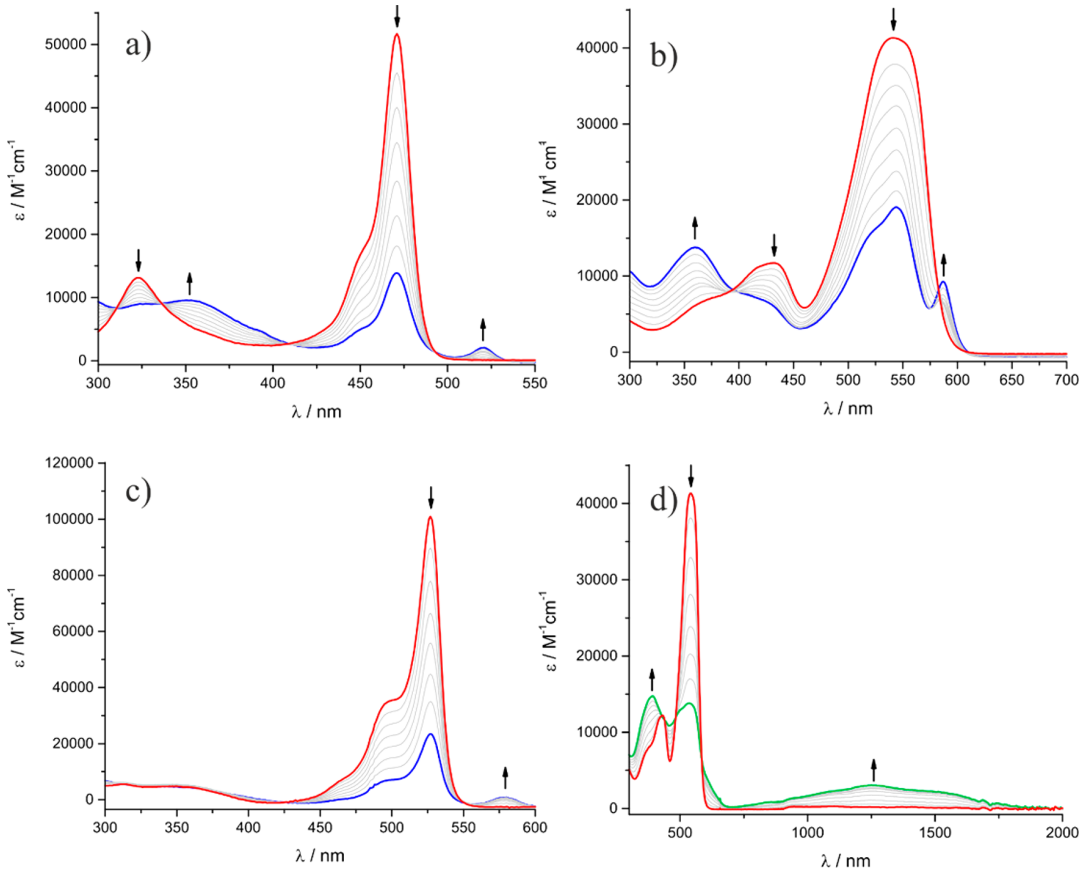


**Figure 9.** Changes of the UV/vis/NIR spectra (1,2-$C_2H_4Cl_2$, $NBu_4PF_6$, $T$ = 293 K) on (a) reduction of **8-Pt**, (b) reduction of **2-Pt-Mes-6I**, (c) reduction of **3-Pt**, and (d) oxidation of **2-Pt-Mes-6I**.

## SUMMARY AND CONCLUSIONS

Five new platinum bodipy complexes, where a *trans*-$Pt(PEt_3)_2I$ moiety attaches to the pyrrolic carbon atom C2 or C3 of a bodipy dye via a direct Pt−bodipy $\sigma$-bond have been prepared. They complement previous series of complexes where a *trans*-$Pt(PR_3)_2X$ (R = Ph, X = Br; R = Et, X = Cl, Br, I, NCS, $NO_2$, and $CH_3$) entity binds to the *meso* bodipy position C8.[59,63] The higher activation barrier for oxidative addition of the $Pt(PEt_3)_2$ fragment to a $C_{aryl}$−Cl bond as compared to a $C_{aryl}$−I bond has also allowed us to isolate complex **8,9-Pt** as a direct precursor to complexes *cis*/*trans* **3-Cl-Pt**, Pt−Cl analog of the iodo complex **3-Pt**. Thermal conversion of **8,9-Pt** to **3-Cl-Pt** and the gradual (yet incomplete) *cis* → *trans* isomerization of **3-Cl-Pt** were followed by $^{31}P$ NMR spectroscopy. The spectroscopic, structural, photophysical, and electrochemical properties of all complexes were studied and compared to those of the *meso*-substituted complex **8-Pt** and the corresponding bodipy precursors. Contrary to **8-Pt**, platinum attachment to either position C2 or C3 puts the $Pt(PEt_3)_2I$ entity within the conjugated $\pi$-system and thus induces a sizable red shift of the characteristic bodipy absorption band along with a broadening for the 2-isomers. Its dominant bodipy $\pi \rightarrow \pi^*$ character is retained as inferred from the DFT-calculated frontier MOs and the TD-DFT based band assignments.

All complexes can be oxidized or reduced by one electron each as probed by cyclic voltammetry. Introduction of the electron-donating $Pt(PEt_3)_2I$ entity causes strong cathodic shifts of 340−510 mV for both oxidation and reduction. UV/vis/NIR and EPR spectroelectrochemistry allowed for spectroscopic characterization of the persistent radical anions and of some sufficiently stable radical cations of the complexes and provides direct experimental evidence for ligand-centered frontier MOs. Thus, their UV/vis/NIR spectroscopic patterns are very similar to those of the one-electron oxidized or reduced forms of their bodipy precursors. Moreover, richly structured EPR spectra with resolved hfs to heteronuclei ($^{195}Pt$, $^{31}P$, $^{14}N$, and $^{19}F$) with $g$ values close to $g_e$ have been recorded and attest to a dominantly organic spin, again in full agreement with DFT calculated spin density distributions.

Like **8-Pt**, all complexes where the Pt ion is bonded to carbon atom C2 dually emit through fluorescence and phosphorescence with phosphorescence emission well in the NIR, at 797−815 nm. However, quantum yields are severely reduced from 41% in **8-Pt** to meager values of 0.14% or less. Nevertheless, all complexes are active sensitizers for photochemical $^1O_2$ generation and outperform methylene blue as a catalyst for the photooxidation of 1,5-dihydroxynaphthalene to Juglone. Our present results show that attachment to either the 2- or 3-positions is no viable route to Pt−bodipy dyes with intense NIR phosphorescence emission. It remains to be investigated whether such compounds are accessible from appropriately substituted 8-bromo (*meso*) bodipys with extended $\pi$-conjugation at the pyrrole rings. Work along these lines is presently being pursued in our laboratories.


DOI: 10.1021/acs.organomet.7b00806
*Organometallics* 2018, 37, 235−253

Table 7. UV/Vis/NIR Data[a] of the Oxidized and/or Reduced Forms of Complexes 8-Pt, 2-Pt-Mes-6I, 2-Pt-6Et, and 3-Pt and TD-DFT Calculated Data (PBE1PBE/6-31G(d), PCM ($CH_2Cl_2$))

| | absorption data | | TD-DFT data | | | | |
|---|---|---|---|---|---|---|---|
| compound | ox. state | $\lambda_{max}$/nm ($\varepsilon$/L mol$^{-1}$ cm$^{-1}$) | ox. state | $\lambda$ (nm) | $f$ | major contributions | assignment |
| **8-Pt** | – | 520 (2100), 471 (13900), 352 (9500) | – | 677 | 0.002 | HOMO($\alpha$) → LUMO($\alpha$) (91%) | LMCT[c] |
| | | | | 433 | 0.069 | HOMO($\beta$) → LUMO($\beta$) (81%) | $\pi \rightarrow \pi^*$ |
| **8-Mes-2,6-$I_2$-bodipy** | – | 562 (15800), 534 (22500), 356 (17700), 306 (16200) | n.c.[b] | | | | |
| **2-Pt-Mes-6I** | + | 1260 (3000), 538 (13800), 391 (14700) | + | 1162 | 0.09 | H-2($\beta$) → LUMO($\beta$) (33%), HOMO($\beta$) → LUMO($\beta$) (43%) | ML → L′CT[d], ILCT[e] |
| | | | | 805 | 0.05 | H-6($\beta$) → LUMO($\beta$) (27%), H-5($\beta$) → LUMO($\beta$) (59%) | ILCT[e] |
| | – | 587 (9300), 544 (19000), 360 (13800) | – | 507 | 0.14 | (31%), HOMO($\beta$) → LUMO($\beta$) (55%), HOMO($\alpha$) → L+2($\alpha$) | $\pi \rightarrow \pi^*$ with metal contribution |
| | | | | 501 | 0.08 | HOMO($\alpha$) → L+2($\alpha$) (27%), HOMO($\alpha$) → L+3($\alpha$) (24%), HOMO($\alpha$) → L+4($\alpha$) (15%) | ILCT[e] with metal contribution |
| **2-Pt-6Et** | + | 1211 (2500), 555 (12100), 381 (18700) | n.c.[b] | | | | |
| | – | 603 (6900), 556 (25100), 361 (12400) | | | | | |
| **3-Pt** | – | 580 (900), 527 (23500), 350 (4700 | – | 584 | 0.002 | HOMO($\alpha$) → LUMO($\alpha$) (91%) | LMCT[c] |
| | | | | 494 | 0.203 | HOMO($\beta$) → LUMO($\beta$) (90%) | $\pi \rightarrow \pi^*$ |

[a]All band positions are given in nm, and extinction coefficients are given in L mol$^{-1}$ cm$^{-1}$. Measured in 1,2-$C_2H_4Cl_2$. [b]n.c. = Not calculated. [c]LMCT = ligand to metal charge transfer. [d]ML → L′CT = metal/ligand to ligand′ charge transfer. [e]ILCT = intra ligand charge transfer.



DOI: 10.1021/acs.organomet.7b00806
Organometallics 2018, 37, 235−253

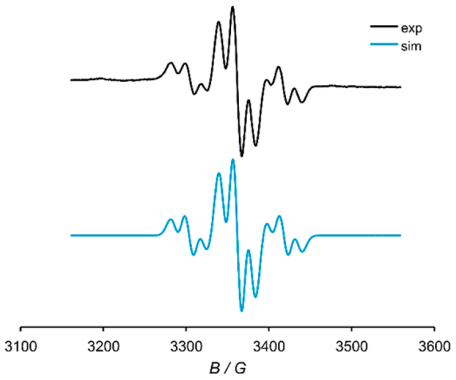


**Figure 10.** Experimental (top curve) and simulated (bottom curve) EPR spectra of the radical anion of **8-Pt** in $CH_2Cl_2/NBu_4^+ PF_6^-$ at 248 K.

## EXPERIMENTAL SECTION

**Materials and Methods.** The oxidative addition reactions were performed under a $N_2$ atmosphere using standard Schlenk techniques or inside a glovebox. The *cis*/*trans* isomerization reactions and workup were conducted in air. $C_6D_6$, $CD_2Cl_2$, $CDCl_3$ and THF-$d_8$ were supplied from Eurisotop. Compounds 6-H-bodipy,[97] 6-I-bodipy,[97] 2,6-$I_2$-bodipy,[97] 2,6-$I_2$-8-Mes-bodipy,[53,98] 6-Et-bodipy,[99] 3-Cl-bodipy,[100,101] and $Pt(Et)_2(PEt_3)_2$[57] were synthesized according to literature protocols. NMR experiments were carried out on a Varian Unity Inova 400, a Bruker Avance III DRX 400, or a Bruker Avance DRX 600 spectrometer. $^1H$ and $^{13}C$ spectra were referenced to the solvent signal, while $^{31}P$ and $^{195}Pt$ spectra were referenced to external standards (85% $H_3PO_4$ or saturated $K_2[PtCl_6]$ in $D_2O$, respectively). NMR data are given as follows: chemical shift ($\delta$ in ppm), multiplicity (br, broad; d, doublet; dd, doublet of doublets; m, multiplet; s, singlet; t, triplet, vt virtual triplet), integration, and coupling constant (Hz). Unequivocal signal assignments were achieved by 2D NMR experiments. The numbering of the nuclei follows that of the chemical structures in Figure 1. Combustion analysis was conducted with an Elementar vario MICRO cube CHN-analyzer from Heraeus.

X-ray diffraction analysis of single crystals was performed at 100 K on a STOE IPDS-II diffractometer equipped with a graphite-monochromated radiation source ($\lambda$ = 0.71073 Å) and an image plate detection system. A crystal mounted on a fine glass fiber with silicon grease was employed. If not indicated otherwise, then the selection, integration, and averaging procedure of the measured reflection intensities, the determination of the unit cell dimensions and a least-squares fit of the $2\theta$ values as well as data reduction, LP-correction and space group determination were performed using the X-Area software package delivered with the diffractometer. A semiempirical absorption correction was performed.[102] All structures were solved by the heavy-atom methods (SHELXS-97,[103] SHELXS-2013,[104] SHELXS-2014,[105] or OLEX2[106]). Structure solutions were completed with difference Fourier syntheses and full-matrix least-squares refinements using SHELXL-97,[103] SHELXS-2013,[104] SHELXS-2014,[105] or OLEX2[106] minimizing $\omega(F_0^2 - F_c^2)^2$. The weighted $R$ factor ($wR^2$) and the goodness of the fit GOF are based on $F^2$. All non-hydrogen atoms were refined with anisotropic displacement parameters, while hydrogen atoms were treated in a riding model. Molecular structures in this work are plotted with PLATON[107] or Mercury.[108] CIF files of the complexes have been deposited at the Cambridge Structure Data Base as CCDC 1583642 (**2-Pt-6H**), CCDC 1583615 (**2-Pt-6I**), CCDC 1583616 (**2-Pt-Mes-6I**), CCDC 1583637 (**2-Pt-6Et**), CCDC 1583640 (**8,9-Pt**), and CCDC 1583638 (**3-Pt**) and can be obtained free of charge via www.ccdc.cam.ac.uk/conts/retrieving.html or from the Cambridge Crystallographic Data Center, 12 Union Road, Cambridge CB2 1EZ, U.K.; fax (+44)1223−336−033, or at deposit@ccdc.cam.ac.uk. Luminescence spectra and lifetimes as well as quantum yields were measured on thoroughly deaerated solutions (three freeze−pump−thaw cycles in a quartz cuvette equipped with an angle valve from Normag) of the complexes in $CH_2Cl_2$, 2-MeTHF, or toluene solutions on a PicoQuant FluoTime 300 spectrometer. Unless stated otherwise absolute quantum yields were determined with an integrating sphere. UV/vis/NIR spectra were recorded on a TIDAS fiber optic diode array spectrometer (combined MCS UV/NIR and PGS NIR instrumentation) from J&M in HELLMA quartz cuvettes with 0.1 cm optical path lengths. Electron paramagnetic resonance (EPR) experiments were performed on a MiniScope MS400 table-top X-band spectrometer from Magnettech. Simulation of the experimental EPR spectra was performed with the MATLAB EasySpin program.[109] All electrochemical experiments were executed in a home-built cylindrical vacuum-tight one-compartment cell. A spiral shaped Pt wire and an Ag wire as the counter and pseudoreference electrodes are sealed into glass capillaries and fixed by quickfit screws via standard joints. A platinum electrode is introduced as the working electrode through the top port via a Teflon screw cap with a suitable fitting. It is polished first with 1 $\mu$m diamond paste and then 0.25 $\mu$m diamond paste before measurements. The cell may be attached to a conventional Schlenk line via a side arm equipped with a Teflon screw valve, allowing experiments to be performed under an argon atmosphere with approximately 5−7 mL of analyte solution. $NBu_4PF_6$ (0.1 mM) was used as the supporting electrolyte. Referencing was done with addition of an appropriate amount of decamethylferrocene ($Cp^*_2Fe$) as an internal standard to the analyte solution after all data of interest had been acquired. Representative sets of scans were repeated with the added standard. Electrochemical data were acquired with a computer-controlled BASi CV50 potentiostat. The optically transparent thin-layer electrochemical (OTTLE) cell was lab-built and followed the design of Hartl and co-workers.[96] It

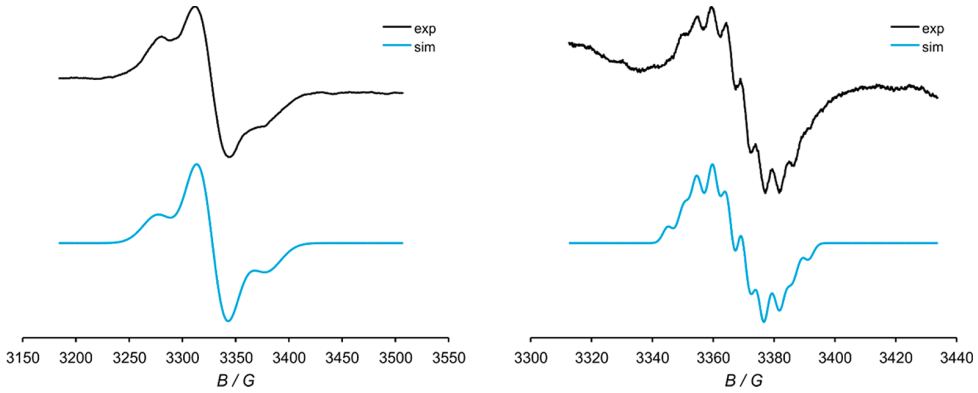


**Figure 11.** Experimental (top curve) and simulated (bottom curve) EPR spectra of the radical cation (left) and the radical anion (right) of **2-Pt-Mes-6I** in $CH_2Cl_2$/ $NBu_4PF_6$ at 248 K.


DOI: 10.1021/acs.organomet.7b00806
*Organometallics* 2018, 37, 235−253

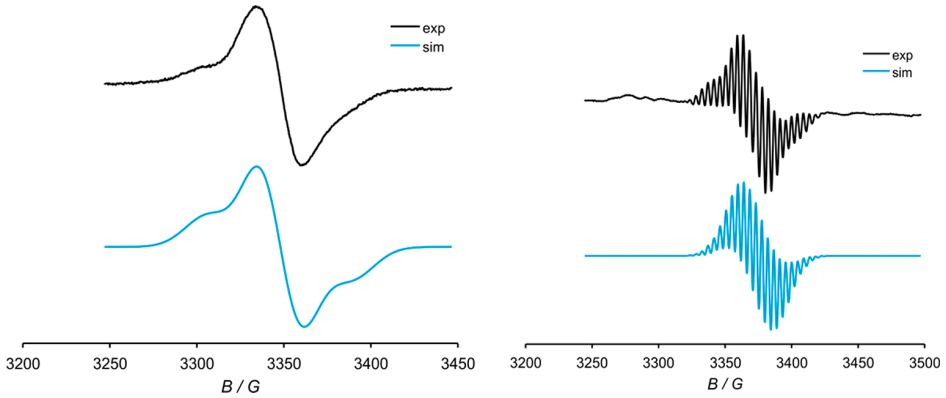


**Figure 12.** Experimental (top curve) and simulated (bottom curve) EPR spectra of the radical cation (left) and the radical anion (right) of complex **3-Pt** in $CH_2Cl_2/NBu_4PF_6$ at 233 K.

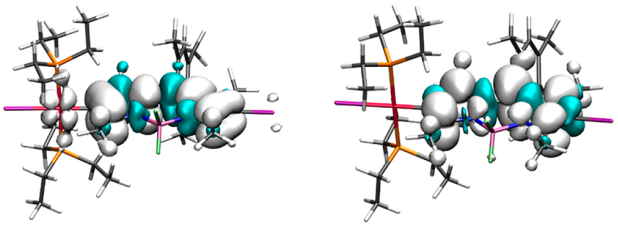

**Figure 13.** Calculated spin densities of the radical cation (left) and the radical anion (right) of **2-Pt-Mes-6I** (PBE1PBE/6-31G(d) PCM ($CH_2Cl_2$)).

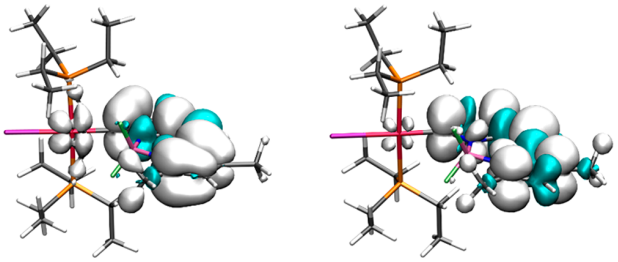

**Figure 14.** Calculated spin densities of the mono-cationic (left) and mono-anionic (right) form of **3-Pt** (PBE1PBE/6-31G(d) PCM ($CH_2Cl_2$)).

comprised a Pt working and counter electrode and a thin silver wire as a pseudoreference electrode sandwiched in between two $CaF_2$ windows of a conventional liquid IR cell with the working electrode positioned in the center of the spectrometer beam.

**Computational Details.** The ground-state electronic structures were calculated by density functional theory (DFT) methods using the Gaussian 09[110] program package. Quantum-chemical studies were performed without any symmetry constraints. Open-shell systems were calculated by the unrestricted Kohn–Sham approach.[111] Geometry optimizations followed by vibrational analysis were performed either in a vacuum or in solvent media. The quasi-relativistic Wood–Boring small-core pseudopotentials (MWB),[112,113] the corresponding optimized set of basis functions[114] for platinum and the halogen atoms, and the 6-31G(d)-polarized double-$\zeta$ basis set[115] for the remaining atoms were employed together with the Perdew–Burke–Ernzerhof exchange and correlation functional (PBE0).[116,117] Solvent effects were accounted for by the polarizable conductor continuum model (PCM)[118−121] with standard parameters for dichloromethane. Absorption spectra and orbital energies were calculated using time-dependent DFT (TD-DFT)[122] with the same functional/basis set combinations as those mentioned above. For an easier comparison with the experiment, the obtained absorption and emission energies were converted into wavelengths and broadened by a Gaussian distribution (full width at half-maximum = 3000 $cm^{-1}$) using the program GaussSum.[123] Atomic coordinates of the calculated structures are provided as a separate file in the Supporting Information.

**$^1O_2$ Generation from Sensitizers.** For the photoreactions involving $^1O_2$ generation, a $CH_2Cl_2$/MeOH (9/1) solution containing **DHN** ($1.2 \times 10^{-4}$ M) and a sensitizer (1.7 mol % vs **DHN**) was irradiated in a quartz cell of 1 cm path length using the xenon lamp of a PicoQuant FluoTime 300 spectrometer ($\lambda_{exc}$(**3-Pt**) = 530 ± 5 nm, $I_f$(530 ± 5 nm) = 2.40 mW; ($\lambda_{exc}$(**2-Pt-6H**, **2-Pt-6I**, **2-Pt-Mes-6I**, **2-Pt-6Et**) = 550 ± 5 nm, $I_f$(550 ± 5 nm) = 2.37 mW; $\lambda_{exc}$(**MB**) = 655 ± 5 nm, $I_f$ (655 ± 5 nm) = 580 $\mu$W). UV–vis absorption spectra were recorded at intervals of 5–20 min on a Varian Cary 50 spectrometer. The consumption of **DHN** was monitored by the decrease in absorption at 301 nm ($\varepsilon$ = 7664 $M^{-1}$ $cm^{-1}$),[124] while Juglone production was monitored by an increase of the absorption at 427 nm ($\varepsilon$ = 3811 $M^{-1}$ $cm^{-1}$).[124] The yield of Juglone was calculated from the

**Table 8. EPR Data of 8-Pt, 8-Mes-2,6-$I_2$-bodipy, 2-Pt-Mes-6I, and 3-Pt[a]**

| | $q$ | $g$-value | $A(^{195}Pt)^b$ | $A(^{31}P)^b$ | $A(^{14}N)^{b,c}$ | $A(^{10/11}B)^b$ | $A(^{19}F)^b$ | $A(^{127}I)^b$ |
|---|---|---|---|---|---|---|---|---|
| **8-Pt** | – | 1.9993 | 153.8 (1) | 21.6 (2) | | | | |
| **8-Mes-2,6-$I_2$-bodipy** | + | 2.0042 | | | 9.6 (2) | 11.1 (1) | 9.6 (2) | |
| | – | 1.9935 | | | 12.4 (2) | | 6.2 (2) | |
| **2-Pt-Mes-6I**[c] | + | 2.0194 | 100.9 (1) | | | | | |
| | – | 1.9955 | | 12.0 (2) | 5.8 (1), 3.4 (1) | | 8.2 (2) | |
| **3-Pt**[c] | + | 2.0075 | 81.7 (1) | | | | | |
| | – | 1.9917 | 37.5 (1) | | 7.2 (1), 5.3 (1) | 5.8 (1) | 11.1 (2) | 5.8 (1) |

[a]In $CH_2Cl_2$ solution; all hyperfine coupling constants are given in G. [b]The number of interacting nuclei is given in parentheses. [c]Unsymmetrically substituted complexes give two different hyperfine couplings for the two $^{14}N$ nuclei.



DOI: 10.1021/acs.organomet.7b00806
Organometallics 2018, 37, 235–253

concentration of Juglone and the initial concentration of **DHN**. The singlet oxygen quantum yield ($\Phi_\Delta$) was determined using eq 3:[124,125]

$$\Phi_\Delta = \Phi_{\Delta,\mathrm{std}}(v_i I_{\mathrm{std}}/v_{i,\mathrm{std}} I) \quad (3)$$

where $\Phi_{\Delta,\mathrm{std}}$ is the singlet oxygen quantum yield of a standard sensitizer ($\Phi_\Delta$ = 0.57 for methylene blue, **MB**),[81−83] $v_i$ is the initial rate of DHN consumption, and $I$ and $I_{\mathrm{std}}$ are the number of photons absorbed by the sensitizer and the standard, respectively.

$$I = \int I_f(\lambda)(1 - 10^{-\varepsilon(\lambda)c_s l})\, \mathrm{d}\lambda \quad (4)$$

$I$ was estimated from eq 4 using the $\lambda$ interval 525−535 nm for **3-Pt**, 545−555 nm for the 2-Pt-bodipy sensitizers, and 650−660 nm for **MB**, where $I_f(\lambda)$ is the wavelength dependence of the intensity of the incident light evaluated with a photometer (for values vide supra), $\varepsilon(\lambda)$ is the extinction coefficient of the respective sensitizer recorded in $CH_2Cl_2$/MeOH (9/1), $c_s$ is the concentration of the sensitizer, and $l$ is the length of the cell. Stern−Volmer plots for emission quenching by oxygen or DHN were obtained by admitting appropriate amounts of air or of a DHN stock solution into the cuvette with enough time for equilibration between solvent and gas phase. As for the oxygen quenching experiment, partial pressures were also transformed into concentrations with the literature-known oxygen solubilities in toluene.[126]

**Synthesis and Characterization.** Except for **8,9-Pt** and **3-Pt**, all other synthesis followed the representative synthesis protocol provided below. Individual parameters, such as reaction time and temperature, eluent mixtures for chromatography, and crystallization parameters, are given for each compound separately.

Typically, a Young tube was filled with 150 $\mu$mol (1 equiv) of $Pt(Et)_2(PEt_3)_2$ and 0.7 mL of $C_6D_6$. The solution was frozen, evacuated, and heated to 110 °C for 90 min. Inside a glovebox, 1.09 equiv of the respective bodipy dye was added. The mixture was allowed to react for the given time at the stated temperature. Prior to the next step all volatiles were removed, and 1.4 equiv of AgOTf was added. The mixture was refluxed in $CH_2Cl_2$ for 15 min. The precipitate was filtered off and the resulting solution was added to a methanolic solution of 2 equiv of NaI. After stirring for 20 min the solvents were removed and the crude product was purified as detailed for every compound separately.

*trans-Iodo-(1,3,5,7-tetramethyl-8-phenyl-4,4-difluoro-4-bora-3a,4a-diaza-s-indacene-2-yl)-bis(triethylphosphane)platinum(II)* ***(2-Pt-6H)***. The oxidative addition was performed at 45 °C for 8 h. The final product was purified by column chromatography (silica, $CH_2Cl_2$/petrol ether 1:2), washed with 4 × 2 mL of *n*-pentane, and dried in vacuo. Yield: 32%. Single crystals for X-ray structure analysis were obtained cooling a saturated $C_6H_6$/*n*-pentane solution of the complex to −25 °C. $^1$H NMR (399.79 MHz, $C_6D_6$, 304 K): $\delta$ 7.07 (m, 3H, H17/H18/H19), 7.00 (m, 2H, H16/H20), 5.75 (s, 1H, H6), 3.02 (s, 3H, H12), 2.70 (s, 3H, H13), 1.72 (m, 12H, P−C$H_2$CH$_3$), 1.57 (s with shoulders, 3H, H11), 1.32 (s, 3H, H14), 0.81 (dt, $^3J_{HH}$ = 7.7 Hz, $^3J_{PH}$ = 16.4 Hz, 18H, P−CH$_2$C$H_3$). $^{31}$P NMR (161.84 MHz, $C_6D_6$, 304 K): $\delta$ 9.56 (s with satellites, $J_{PtP}$ = 2556 Hz). $^{195}$Pt NMR (85.56 MHz, $C_6D_6$, 304 K): $\delta$ −4784 (t, $J_{PtP}$ = 2556 Hz). $^{13}$C NMR (100.53 MHz, $CDCl_3$, 300 K): $\delta$ 162.3 (s with satellites, $^2J_{PtC}$ = 82.8 Hz, C3), 150.0 (s, C5), 143.6 (s with satellites, $^3J_{PtC}$ = 45.8 Hz, C10), 139.2 (s, C9), 137.3 (s with shoulders, C8), 136.2 (s, C7), 134.5 (s with satellites, $^2J_{PtC}$ = 71.1 Hz, C1), 133.6 (t, $^2J_{PC}$ = 9.4 Hz, C2), 129.6 (s, C15), 129.1 (s, C16/C20), 128.6 (s, C18), 128.4 (s, C17/C19), 119.3 (s, C6), 18.2 (t, $^4J_{CF}$ = 2.6 Hz, with satellites $^3J_{PtC}$ = 37.2 Hz, C12), 18.1 (s with satellites, $^3J_{PtC}$ = 60.2 Hz, C11), 16.0 (vquint, $J_{PC}$ = $^3J_{PC}$ = 17.9 Hz, with satellites $^2J_{PtC}$ = 36.1 Hz, P−CH$_2$CH$_3$), 14.3 (m, C13), 14.1 (s, C14), 8.4 (s with satellites, $^3J_{PtC}$ = 24.4 Hz, P−CH$_2$CH$_3$). Anal. Calcd for $C_{31}H_{48}BF_2IN_2P_2Pt$: C, 42.24; H, 5.49; N, 3.18. Found: C, 42.82; H, 5.67; N, 3.39.

*trans-Iodo-(6-idodo-1,3,5,7-tetramethyl-8-phenyl-4,4-difluoro-4-bora-3a,4a-diaza-s-indacene-2-yl)-bis(triethylphosphane)-platinum(II)* ***(2-Pt-6I)***. The oxidative addition was conducted at 45 °C for 4h. The final product was purified by column chromatography (silica, $CH_2Cl_2$/petrol ether 60:40 → 50:50), the vacuum-dried residue was washed with 2 mL of *n*-pentane once and dried in vacuo. Yield: 58%. Single crystals were obtained by cooling a saturated $C_6H_6$/*n*-pentane solution to −25 °C. $^1$H NMR (399.79 MHz, $C_6D_6$, 304 K): $\delta$ 7.03 (m, 3H, H17/H18/H19), 6.88 (m, 2H, H16/H20), 3.00 (s, 3H, H12), 2.84 (s, 3H, H13), 1.70 (m, 12 H, P−C$H_2$CH$_3$), 1.53 (s with shoulders, 3H, H11), 1.35 (s, 3H, H14), 0.80 (dt, $^3J_{HH}$ = 7.7 Hz, $^3J_{PH}$ = 16.3 Hz, 18H, P−CH$_2$C$H_3$). $^{31}$P NMR (161.84 MHz, $C_6D_6$, 305 K): $\delta$ 9.42 (s with satellites, $J_{PtP}$ = 2540 Hz). $^{195}$Pt NMR (85.55 MHz, $C_6D_6$, 300 K): $\delta$ −4779 (t, $J_{PtP}$ = 2540 Hz). $^{13}$C NMR (100.53 MHz, $CDCl_3$, 300 K): $\delta$ 164.8 (s with satellites $^2J_{PtC}$ = 85.3 Hz, C3), 149.4 (s, C5), 144.7 (s with satellites $^3J_{PtC}$ = 45.8 Hz, C10), 139.1 (s, C8), 136.6 (s, C9), 135.9 (s, C7), 135.4 (t, $^2J_{PC}$ = 9.4 Hz, with satellites $J_{PtC}$ = 1090 Hz, C2), 134.9 (s with satellites $^2J_{PtC}$ = 37.2 Hz, C1), 129.5 (s, C15), 129.3 (s, C17/C19), 128.9 (s, C18), 128.3 (s, C16/C20), 81.7 (s, C6), 18.4 (t, $^4J_{CF}$ = 2.4 Hz, C12), 18.3 (s with satellites $^3J_{PtC}$ = 60.9 Hz, C11), 16.2 (s, C14), 16.0 (vquint, $J_{PC}$ = $^3J_{PC}$ = 17.6 Hz, with satellites $^2J_{PtC}$ = 35.8 Hz, P−CH$_2$CH$_3$), 15.5 (t, $^4J_{CF}$ = 2.5 Hz, C13), 8.4 (s, with satellites $^3J_{PtC}$ = 24.2 Hz, P−CH$_2$CH$_3$). Anal. Calcd for $C_{31}H_{47}BF_2I_2N_2P_2Pt$: C, 36.96; H, 4.70; N, 2.78. Found: C, 36.21, H, 4.34, N, 2.73.

*trans-Iodo-(6-idodo-1,3,5,7-tetramethyl-8-mesityl-4,4-difluoro-4-bora-3a,4a-diaza-s-indacene-2-yl)-bis(triethylphosphane)-platinum(II)* ***(2-Pt-Mes-6I)***. Oxidative addition was conducted at 60 °C for 7 h. The final crude product was purified by column chromatography ($Al_2O_3$, petrol ether/$CH_2Cl_2$ 6:1). The product fraction was recrystallized form a saturated *n*-pentane/$CH_2Cl_2$ mixture forming single crystals at −25 °C. Yield: 42%. $^1$H NMR (399.78 MHz, $CDCl_3$, 300 K): $\delta$ 6.95 (s, 2H, H17/H19), 2.68 (s, 3H, H12), 2.58 (s, 3H, H13), 2.34 (s, 3H, H22), 2.06 (s, 6H, H21/H23), 1.85 (m, 12H, P−C$H_2$CH$_3$), 1.34 (s, 3H, H11), 1.33 (s, 3H, H14), 1.01 (dt, $^3J_{HH}$ = 7.7 Hz, $^3J_{PH}$ = 16.3 Hz, 18H, P−CH$_2$C$H_3$). $^{31}$P NMR (161.83 MHz, $CDCl_3$, 300 K): $\delta$ 5.14 (s with satellites, $J_{PtP}$ = 2539 Hz). $^{195}$Pt NMR (85.55 MHz, $CDCl_3$, 300 K): $\delta$ −4802 (t, $J_{PtP}$ = 2539 Hz). $^{13}$C NMR (100.53 MHz, $CDCl_3$, 300 K): $\delta$ 164.1 (s with satellites, $^2J_{PtC}$ = 82.1 Hz, C3), 149.4 (s, C5), 144.0 (s with satellites, $^3J_{PtC}$ = 43.2 Hz, C10), 138.6 (s, C16/C20), 138.3 (s, C7), 136.2 (s, C9), 134.9 (s, C8), 134.7 (t, $^2J_{PC}$ = 9.7 Hz, C2), 134.2 (s with satellites, $^2J_{PtC}$ = 72.1 Hz, C1), 132.0 (s, C15), 129.2 (s, C17/C19), 128.4 (s, C18), 81.3 (s, C6), 21.4 (s, C22), 19.5 (s, C21/C23), 18.4 (t, $^4J_{CF}$ = 2.5 Hz, with satellites, $^3J_{PtC}$ = 39.5 Hz, C12), 17.3 (s with satellites, $^3J_{PtC}$ = 60.5 Hz, C11), 16.2 (vquint, $J_{PC}$ = $^3J_{PC}$ = 17.5 Hz, with satellites $^2J_{PtC}$ = 35.9 Hz, P−CH$_2$CH$_3$), 15.6 (t, $^4J_{CF}$ = 2.5 Hz, C13), 15.1 (s, C14), 8.4 (s with satellites, $^3J_{PtC}$ = 24.3 Hz, P−CH$_2$CH$_3$). Anal. Calcd for $C_{34}H_{53}BF_2I_2N_2P_2Pt$: C, 38.91; H, 5.09; N, 2.61. Found: C, 39.44; H, 5.22; N, 2.91.

*trans-Iodo-(6-ethyl-1,3,5,7-tetramethyl-8-phenyl-4,4-difluoro-4-bora-3a,4a-diaza-s-indacene-2-yl)-bis(triethylphosphane)-platinum(II)* ***(2-Pt-6Et)***. For the oxidative addition step, the reaction mixture was heated to 50 °C for 72 h. The final product was purified on a short silica column (petrol ether/ethyl acetate 40:1). Crystals suitable for X-ray structure analysis were obtained from diffusion of *n*-pentane into a concentrated $CH_2Cl_2$ solution of the product. Yield 26%. $^1$H NMR (399.78 MHz, $C_6D_6$, 300 K): $\delta$ 7.09 (m, 3H, H19/H20/H21), 7.02 (m, 2H, H18/H22), 3.04 (s, 3H, H12), 2.66 (s, 3H, H13), 2.11 (q, $^3J_{HH}$ = 7.5 Hz, 2H, H15), 1.73 (m, 12H, P−C$H_2$CH$_3$), 1.59 (s with shoulders, 3H, H11), 1.27 (s, 3H, H14), 0.82 (m, 21 H, H16/P−CH$_2$C$H_3$). $^{31}$P NMR (161.83 MHz, $C_6D_6$, 300 K): $\delta$ 9.75 (s with satellites, $J_{PtP}$ = 2561 Hz). $^{195}$Pt NMR (85.55 MHz, $C_6D_6$, 300 K): $\delta$ −4788 (t, $J_{PtP}$ = 2561 Hz). $^{13}$C NMR (100.53 MHz, $CDCl_3$, 300 K): $\delta$ 160.8 (s with satellites, $^2J_{PtC}$ = 83 Hz, C3), 149.1 (s, C5), 143.0 (s with satellites, $^3J_{PtC}$ = 46 Hz, C10), 137.0 (s, C8), 136.5 (s, C9), 136.3 (s, C7), 134.1 (s with satellites, $^2J_{PtC}$ = 71 Hz, C1), 132.7 (t, $^2J_{PC}$ = 9.3 Hz, C2), 131.4 (s, C6), 129.3 (s, C17), 129.1 (s, C19/C21), 128.6 (s, C20), 128.5 (s, C18/C22), 18.16 (m with satellites, $^3J_{PtC}$ = 38 Hz, C12), 18.15 (s with satellites, $^3J_{PtC}$ = 60 Hz, C11), 17.2 (s, C15), 16.0 (vquint, $J_{PC}$ = $^3J_{PC}$ = 17.5 Hz, with satellites $^2J_{PtC}$ = 36.1 Hz, P−CH$_2$CH$_3$), 15.0 (s, C16), 12.3 (t, $^4J_{CF}$ = 2.5 Hz, C13), 11.5 (s, C14), 8.4 (s with satellites, $^3J_{PtC}$ = 24.6 Hz, P−CH$_2$CH$_3$). Anal. Calcd for $C_{33}H_{52}BF_2IN_2P_2Pt$: C, 43.58; H, 5.76; N, 3.08. Found: C, 43.50; H, 5.73; N, 3.28.


DOI: 10.1021/acs.organomet.7b00806
*Organometallics* 2018, 37, 235−253

*cis-(8,9-η²-3-Chloro-5,7-dimethyl-4,4-difluoro-4-bora-3a,4a-diaza-s-indacene)-bis(triethylphosphane)platinum(II) (**8,9-Pt**).* A Young tube was filled with 216 μmol (1 equiv) of $Pt(Et)_2(PEt_3)_2$ and 0.7 mL of $C_6D_6$. The solution was frozen, evacuated, and heated to 110 °C for 90 min. Inside a glovebox, 1.09 equiv of 3-Cl-bodipy was added. The complex crystallized directly from the reaction mixture forming single crystals. After removing the solvent the compound was dried under reduced pressure. Yield: 94%. The following signal assignment follows the atom numbering in Figure 1. $^1$H NMR (399.78 MHz, THF-$d_8$, 300 K): δ 5.85 (s, 1H, H6), 5.80 (br s, 1H, H1), 5.75 (d, $^3J_{HH}$ = 2.54 Hz, 1H, H2), 3.83 (dd, $^3J_{PH}$ = 9.10 Hz, 4.34 Hz, with satellites $^2J_{PtH}$ = 49.2 Hz, 1H, H8), 2.40 (d with shoulders, $^6J_{PH}$ = 5.90 Hz, 3H, H11), 1.82 (m, 3H, H12), 1.80−1.48 (m, 12H, P−$CH_2CH_3$), 0.96 (m, 18H, P−$CH_2CH_3$). $^{31}$P NMR (161.83 MHz, THF-$d_8$, 300 K): δ 19.10 (d, $^2J_{PP}$ = 9.70 Hz, with satellites $J_{PtP}$ = 4801 Hz, P2), 6.89 (d, $^2J_{PP}$ = 9.70 Hz, with satellites $J_{PtP}$ = 3321 Hz, P1). $^{195}$Pt (85.51 MHz, THF-$d_8$, 300 K): δ −4950 (dd, $J_{PtP}$ = 4801 Hz, $J_{PtP}$ = 3321 Hz). $^{13}$C NMR (150.97 MHz, THF-$d_8$, 290 K): δ 152.5 (s, C5), 132.8 (s, C10), 127.5 (s, C9), 119.1 (s, C3), 112.8 (s, C6), 106.9 (s, C2), 106.2 (s, C1), 103.3 (s, C7), 42.1 (d, $^2J_{PC}$ = 43.6 Hz, C8), 17.7 (d, $J_{PC}$ = 30.7 Hz, with satellites $^2J_{PtC}$ = 80.5 Hz, P2-$CH_2CH_3$), 15.6 (d with shoulders, $J_{PC}$ = 25.7 Hz, P1-$CH_2CH_3$), 14.8 (s, C11), 14.3 (s, C12), 8.6 (s with satellites, $^3J_{PtC}$ = 35.6 Hz, P2-$CH_2CH_3$), 8.5 (s with shoulders, P1-$CH_2CH_3$). Anal. Calcd for $C_{23}H_{40}BF_2ClN_2P_2Pt$: C, 40.28; H, 5.88; N, 4.08. Found: C, 40.47; H, 6.14; N, 4.51.

*trans-Iodo-(5,7-dimethyl-4,4-difluoro-4-bora-3a,4a-diaza-s-indacene-3-yl)-bis(triethylphosphane)platinum(II) (**3-Pt**).* First, 100 μmol of **8,9-Pt** was loaded into a Young tube and heated in THF-$d_8$ to 60 °C for 72 h. The resulting isomeric mixture was treated as explained in the general protocol (vide supra). Purification by column chromatography (silica, ethyl acetate/pentane 10:1) and recrystallization from $CH_2Cl_2$ yielded orange needles. Yield: 54%. $^1$H NMR (399.78 MHz, $C_6D_6$, 300 K): δ 6.60 (d with shoulders, $^3J_{HH}$ = 4.1 Hz, 1H, H1), 6.49 (s with satellites, $^5J_{PtH}$ = 13.3 Hz, 1H, H8), 6.40 (d, $^3J_{HH}$ = 4.1 Hz, with satellites $^3J_{PtH}$ = 20.2 Hz, 1H, H2), 5.72 (s, 1H, H6), 2.57 (s, 3H, H11), 2.11 (m, 6H, P−$CH_2CH_3$), 1.84 (s, 3H, H12), 1.80 (m, 6H, P−$CH_2CH_3$), 0.98 (dt, $^3J_{HH}$ = 7.9 Hz, $^3J_{PH}$ = 16.3 Hz, 18H, P−$CH_2CH_3$). $^{31}$P NMR (161.83 MHz, $C_6D_6$, 300 K): δ 7.69 (s with satellites, $J_{PtP}$ = 2547 Hz). $^{195}$Pt (85.55 MHz, $C_6D_6$, 300 K): δ −4599 (t, $J_{PtP}$ = 2547 Hz). $^{13}$C NMR (100.53 MHz, $CDCl_3$, 300 K): δ 174.3 (t, $^2J_{PC}$ = 10.1 Hz, with satellites $J_{PtC}$ = 1150 Hz, C3), 151.4 (s, C5), 137.7 (s with satellites $^3J_{PtC}$ = 81.6 Hz, C10), 136.2 (s, C7), 131.7 (s, C9), 128.7 (s with satellites $^3J_{PtC}$ = 59.4 Hz, C1), 128.6 (s with satellites $^2J_{PC}$ = 101 Hz, C2), 117.8 (s, C8), 117.1 (s, C6), 15.7 (vt, $J_{PC}$ = $^3J_{PC}$ = 17.7 Hz, with satellites $^2J_{PtC}$ = 34.8 Hz, P−$CH_2CH_3$), 14.7 (s, C11), 11.3 (s, C12), 8.1 (s with satellites, $^3J_{PtC}$ = 25.5 Hz, P−$CH_2CH_3$). Anal. Calcd for $C_{23}H_{40}BF_2IN_2P_2Pt$: C, 35.54; H, 5.19; N, 3.60. Found: C, 35.06; H, 5.26; N, 3.77.

## ■ ASSOCIATED CONTENT

### Supporting Information

The Supporting Information is available free of charge on the ACS Publications website at DOI: 10.1021/acs.organomet.7b00806.

$^1$H, $^{31}$P, $^{195}$Pt, and $^{13}$C NMR spectra; NMR spectroscopic monitoring of the conversion of **8,9-Pt** to **3-Pt**; tabulated data for the X-ray structure determination as well as packing diagrams with intermolecular interactions; electronic absorption spectra; comparison of TD-DFT calculated and experimental spectra; TD-DFT calculations and electron density difference maps; luminescence spectra of **3-Pt** and **8,9-Pt**; comparison of excitation and absorption spectra; spectroscopic monitoring of DHN oxidation to Juglone; cyclic voltammograms; UV/vis/NIR spetctroelectrochemistry of **2-Pt-6Et** and 8-mesityl-2,6-diiodo-bodipy; EPR spectrum (PDF)

Spin density distributions and atomic coordinates of the DFT-optimized structures (XYZ)

### Accession Codes

CCDC 1583615−1583616, 1583637−1583638, 1583640, and 1583642 contain the supplementary crystallographic data for this paper. These data can be obtained free of charge via www.ccdc.cam.ac.uk/data_request/cif, or by emailing data_request@ccdc.cam.ac.uk, or by contacting The Cambridge Crystallographic Data Centre, 12 Union Road, Cambridge CB2 1EZ, UK; fax: +44 1223 336033.

## ■ AUTHOR INFORMATION


### Corresponding Author

*E-mail: rainer.winter@uni-konstanz.de.

### ORCID

Rainer F. Winter: 0000-0001-8381-0647


### Notes

The authors declare no competing financial interest.

## ■ ACKNOWLEDGMENTS

Financial support of this work by Deutsche Forschungsgemeinschaft through grant Wi1262/10-2 and the Fachbereich Chemie of the University of Konstanz are gratefully acknowledged. We also thank Bernhard Weibert for data collection and structure refinement in X-ray crystallography as well as Nils Rotthowe and Steffen Oßwald for their help with the EPR spectroscopy.

## ■ REFERENCES


(1) Thejo Kalyani, N.; Dhoble, S. J. *Renewable Sustainable Energy Rev.* **2012**, *16*, 2696−2723.
(2) Ulrich, G.; Ziessel, R.; Harriman, A. *Angew. Chem., Int. Ed.* **2008**, *47*, 1184−1201.
(3) Kobayashi, H.; Ogawa, M.; Alford, R.; Choyke, P. L.; Urano, Y. *Chem. Rev.* **2010**, *110*, 2620−40.
(4) Sauer, M.; Heilemann, M. *Chem. Rev.* **2017**, *117*, 7478−7509.
(5) Pashaei, B.; Shahroosvand, H.; Graetzel, M.; Nazeeruddin, M. K. *Chem. Rev.* **2016**, *116*, 9485−564.
(6) Ghogare, A. A.; Greer, A. *Chem. Rev.* **2016**, *116*, 9994.
(7) Skubi, K. L.; Blum, T. R.; Yoon, T. P. *Chem. Rev.* **2016**, *116*, 10035−74.
(8) Zheng, B.; Sabatini, R. P.; Fu, W. F.; Eum, M. S.; Brennessel, W. W.; Wang, L.; McCamant, D. W.; Eisenberg, R. *Proc. Natl. Acad. Sci. U. S. A.* **2015**, *112*, E3987−96.
(9) Celli, J. P.; Spring, B. Q.; Rizvi, I.; Evans, C. L.; Samkoe, K. S.; Verma, S.; Pogue, B. W.; Hasan, T. *Chem. Rev.* **2010**, *110*, 2795−838.
(10) Kamkaew, A.; Lim, S. H.; Lee, H. B.; Kiew, L. V.; Chung, L. Y.; Burgess, K. *Chem. Soc. Rev.* **2013**, *42*, 77−88.
(11) Dougherty, T. J.; Gomer, C. J.; Henderson, B. W.; Jori, G.; Kessel, D.; Korbelik, M.; Moan, J.; Peng, Q. *J. Natl. Cancer Inst.* **1998**, *90*, 889−905.
(12) Wilson, B. C.; Patterson, M. S. *Phys. Med. Biol.* **2008**, *53*, R61−109.
(13) Zhao, J.; Ji, S.; Guo, H. *RSC Adv.* **2011**, *1*, 937.
(14) Singh-Rachford, T. N.; Castellano, F. N. *Coord. Chem. Rev.* **2010**, *254*, 2560−2573.
(15) Boens, N.; Verbelen, B.; Dehaen, W. *Eur. J. Org. Chem.* **2015**, *2015*, 6577−6595.
(16) Ulrich, G.; Ziessel, R.; Harriman, A. *Angew. Chem., Int. Ed.* **2008**, *47*, 1184−1201.
(17) Loudet, A.; Burgess, K. *Chem. Rev.* **2007**, *107*, 4891−4932.
(18) Zhao, J.; Xu, K.; Yang, W.; Wang, Z.; Zhong, F. *Chem. Soc. Rev.* **2015**, *44*, 8904−8939.
(19) Harriman, A.; Izzet, G.; Ziessel, R. *J. Am. Chem. Soc.* **2006**, *128*, 10868−10875.




DOI: 10.1021/acs.organomet.7b00806
*Organometallics* 2018, 37, 235−253

(20) Zhang, C.; Zhao, J.; Wu, S.; Wang, Z.; Wu, W.; Ma, J.; Guo, S.; Huang, L. *J. Am. Chem. Soc.* **2013**, *135*, 10566−10578.
(21) Loudet, A.; Burgess, K. *Chem. Rev.* **2007**, *107*, 4891−4932.
(22) Luo, Y.; Prestwich, G. D. *Bioconjugate Chem.* **1999**, *10*, 755−763.
(23) Hermanson, G. T. *Bioconjugate techniques*, 3.rd ed.; Academic Press: Amsterdam, 2013.
(24) Niu, S. L.; Massif, C.; Ulrich, G.; Renard, P. Y.; Romieu, A.; Ziessel, R. *Chem. - Eur. J.* **2012**, *18*, 7229−42.
(25) Yogo, T.; Urano, Y.; Ishitsuka, Y.; Maniwa, F.; Nagano, T. *J. Am. Chem. Soc.* **2005**, *127*, 12162−12163.
(26) Epelde-Elezcano, N.; Palao, E.; Manzano, H.; Prieto-Castaneda, A.; Agarrabeitia, A. R.; Tabero, A.; Villanueva, A.; de la Moya, S.; Lopez-Arbeloa, I.; Martinez-Martinez, V.; Ortiz, M. J. *Chem. - Eur. J.* **2017**, *23*, 4837−4848.
(27) Ventura, B.; Marconi, G.; Bröring, M.; Krüger, R.; Flamigni, L. *New J. Chem.* **2009**, *33*, 428−438.
(28) Cakmak, Y.; Kolemen, S.; Duman, S.; Dede, Y.; Dolen, Y.; Kilic, B.; Kostereli, Z.; Yildirim, L. T.; Dogan, A. L.; Guc, D.; Akkaya, E. U. *Angew. Chem., Int. Ed.* **2011**, *50*, 11937−41.
(29) Duman, S.; Cakmak, Y.; Kolemen, S.; Akkaya, E. U.; Dede, Y. *J. Org. Chem.* **2012**, *77*, 4516−27.
(30) Wu, W.; Cui, X.; Zhao, J. *Chem. Commun. (Cambridge, U. K.)* **2013**, *49*, 9009−11.
(31) Zhao, J.; Xu, K.; Yang, W.; Wang, Z.; Zhong, F. *Chem. Soc. Rev.* **2015**, *44*, 8904−8939.
(32) Wu, W.; Zhao, J.; Sun, J.; Huang, L.; Yi, X. *J. Mater. Chem. C* **2013**, *1*, 705−716.
(33) Jia, H.; Küçüköz, B.; Xing, Y.; Majumdar, P.; Zhang, C.; Karatay, A.; Yaglioglu, G.; Elmali, A.; Zhao, J.; Hayvali, M. *J. Mater. Chem. C* **2014**, *2*, 9720−9736.
(34) Yang, W.; Karatay, A.; Zhao, J.; Song, J.; Zhao, L.; Xing, Y.; Zhang, C.; He, C.; Yaglioglu, H. G.; Hayvali, M.; Elmali, A.; Kucukoz, B. *Inorg. Chem.* **2015**, *54*, 7492−505.
(35) Majumdar, P.; Cui, X.; Xu, K.; Zhao, J. *Dalton Trans.* **2015**, *44*, 4032−45.
(36) Galletta, M.; Campagna, S.; Quesada, M.; Ulrich, G.; Ziessel, R. *Chem. Commun. (Cambridge, U. K.)* **2005**, 4222−4.
(37) Rachford, A. A.; Ziessel, R.; Bura, T.; Retailleau, P.; Castellano, F. N. *Inorg. Chem.* **2010**, *49*, 3730−6.
(38) Wu, W.; Sun, J.; Cui, X.; Zhao, J. *J. Mater. Chem. C* **2013**, *1*, 4577.
(39) Yi, X.; Zhao, J.; Sun, J.; Guo, S.; Zhang, H. *Dalton Trans.* **2013**, *42*, 2062−74.
(40) Wang, P.; Koo, Y. H.; Kim, W.; Yang, W.; Cui, X.; Ji, W.; Zhao, J.; Kim, D. *J. Phys. Chem. C* **2017**, *121*, 11117−11128.
(41) Zhong, F.; Karatay, A.; Zhao, L.; Zhao, J.; He, C.; Zhang, C.; Yaglioglu, H. G.; Elmali, A.; Kucukoz, B.; Hayvali, M. *Inorg. Chem.* **2015**, *54*, 7803−17.
(42) Hsu, C.-W.; Lin, C.-C.; Chung, M.-W.; Chi, Y.; Lee, G.-H.; Chou, P.-T.; Chang, C.-H.; Chen, P.-Y. *J. Am. Chem. Soc.* **2011**, *133*, 12085−12099.
(43) Yu-Tzu Li, E.; Jiang, T. Y.; Chi, Y.; Chou, P. T. *Phys. Chem. Chem. Phys.* **2014**, *16*, 26184−92.
(44) Chang, Y.-C.; Tang, K.-C.; Pan, H.-A.; Liu, S.-H.; Koshevoy, I. O.; Karttunen, A. J.; Hung, W.-Y.; Cheng, M.-H.; Chou, P.-T. *J. Phys. Chem. C* **2013**, *117*, 9623−9632.
(45) Wang, B.-Y.; Karikachery, A. R.; Li, Y.; Singh, A.; Lee, H. B.; Sun, W.; Sharp, P. R. *J. Am. Chem. Soc.* **2009**, *131*, 3150−3151.
(46) Lentijo, S.; Miguel, J. A.; Espinet, P. *Inorg. Chem.* **2010**, *49*, 9169−77.
(47) Lee, H. B.; Sharp, P. R. *Organometallics* **2005**, *24*, 4875−4877.
(48) Choi, H.; Kim, C.; Park, K.-M.; Kim, J.; Kang, Y.; Ko, J. *J. Organomet. Chem.* **2009**, *694*, 3529−3532.
(49) Singh, A.; Sharp, P. R. *J. Am. Chem. Soc.* **2006**, *128*, 5998−5999.
(50) Vu, T. T.; Badré, S.; Dumas-Verdes, C. c.; Vachon, J.-J.; Julien, C.; Audebert, P.; Senotrusova, E. Y.; Schmidt, E. Y.; Trofimov, B. A.; Pansu, R. B.; Clavier, G.; Méallet-Renault, R. *J. Phys. Chem. C* **2009**, *113*, 11844−11855.
(51) Wu, W.; Guo, H.; Wu, W.; Ji, S.; Zhao, J. *J. Org. Chem.* **2011**, *76*, 7056−64.
(52) Lim, H.; Seo, S.; Pascal, S.; Bellier, Q.; Rigaut, S.; Park, C.; Shin, H.; Maury, O.; Andraud, C.; Kim, E. *Sci. Rep.* **2016**, *6*, 18867.
(53) Nepomnyashchii, A. B.; Bröring, M.; Ahrens, J.; Bard, A. J. *J. Am. Chem. Soc.* **2011**, *133*, 8633−8645.
(54) Huang, L.; Yang, W.; Zhao, J. *J. Org. Chem.* **2014**, *79*, 10240−10255.
(55) Lazarides, T.; McCormick, T. M.; Wilson, K. C.; Lee, S.; McCamant, D. W.; Eisenberg, R. *J. Am. Chem. Soc.* **2011**, *133*, 350−64.
(56) Goze, C.; Ulrich, G.; Mallon, L. J.; Allen, B. D.; Harriman, A.; Ziessel, R. *J. Am. Chem. Soc.* **2006**, *128*, 10231−10239.
(57) McCarthy, T. J.; Nuzzo, R. G.; Whitesides, G. M. *J. Am. Chem. Soc.* **1981**, *103*, 3396−3403.
(58) Strawser, D.; Karton, A.; Zenkina, O. V.; Iron, M. A.; Shimon, L. J.; Martin, J. M.; van der Boom, M. E. *J. Am. Chem. Soc.* **2005**, *127*, 9322−3.
(59) Irmler, P.; Winter, R. F. *Dalton Trans.* **2016**, *45*, 10420−10434.
(60) Bauer, F.; Braunschweig, H.; Gruss, K.; Kupfer, T. *Organometallics* **2011**, *30*, 2869−2884.
(61) Braunschweig, H.; Bertermann, R.; Brenner, P.; Burzler, M.; Dewhurst, R. D.; Radacki, K.; Seeler, F. *Chem. - Eur. J.* **2011**, *17*, 11828−37.
(62) Farrugia, L. J. *J. Appl. Crystallogr.* **2012**, *45*, 849−854.
(63) Geist, F.; Jackel, A.; Winter, R. F. *Inorg. Chem.* **2015**, *54*, 10946−10957.
(64) Al Anshori, J.; Slanina, T.; Palao, E.; Klán, P. *Photochem. Photobiol. Sci.* **2016**, *15*, 250−9.
(65) Geist, F.; Jackel, A.; Irmler, P.; Linseis, M.; Malzkuhn, S.; Kuss-Petermann, M.; Wenger, O. S.; Winter, R. F. *Inorg. Chem.* **2017**, *56*, 914.
(66) Whited, M. T.; Djurovich, P. I.; Roberts, S. T.; Durrell, A. C.; Schlenker, C. W.; Bradforth, S. E.; Thompson, M. E. *J. Am. Chem. Soc.* **2011**, *133*, 88−96.
(67) Wu, W.; Zhao, J.; Guo, H.; Sun, J.; Ji, S.; Wang, Z. *Chem. - Eur. J.* **2012**, *18*, 1961−1968.
(68) Siebrand, W.; Williams, D. F. *J. Chem. Phys.* **1968**, *49*, 1860−1871.
(69) Englman, R.; Jortner, J. *Mol. Phys.* **1970**, *18*, 145−164.
(70) Scott, D. R.; Maltenieks, O. *J. Phys. Chem.* **1968**, *72*, 3354−3356.
(71) Zaitsev, A. B.; Méallet-Renault, R.; Schmidt, E. Y.; Mikhaleva, A. b. I.; Badré, S.; Dumas, C.; Vasil'tsov, A. M.; Zorina, N. V.; Pansu, R. B. *Tetrahedron* **2005**, *61*, 2683−2688.
(72) Badré, S.; Monnier, V.; Méallet-Renault, R.; Dumas-Verdes, C.; Schmidt, E. Y.; Mikhaleva, A. b. I.; Laurent, G.; Levi, G.; Ibanez, A.; Trofimov, B. A.; Pansu, R. B. *J. Photochem. Photobiol., A* **2006**, *183*, 238−246.
(73) Irmler, P.; Winter, R. F. *Dalton Trans.* **2016**, *45*, 10420−34.
(74) Yang, P.; Zhao, J.; Wu, W.; Yu, X.; Liu, Y. *J. Org. Chem.* **2012**, *77*, 6166−78.
(75) Huang, L.; Zhao, J. *RSC Adv.* **2013**, *3*, 23377−23388.
(76) Huang, L.; Zhao, J.; Guo, S.; Zhang, C.; Ma, J. *J. Org. Chem.* **2013**, *78*, 5627−5637.
(77) Wu, W.; Geng, Y.; Fan, W.; Li, Z.; Zhan, L.; Wu, X.; Zheng, J.; Zhao, J.; Wu, M. *RSC Adv.* **2014**, *4*, 51349−51352.
(78) Gorman, A.; Killoran, J.; O'Shea, C.; Kenna, T.; Gallagher, W. M.; O'Shea, D. F. *J. Am. Chem. Soc.* **2004**, *126*, 10619−31.
(79) Awuah, S. G.; You, Y. *RSC Adv.* **2012**, *2*, 11169−11183.
(80) Rehm, D.; Weller, A. *Isr. J. Chem.* **1970**, *8*, 259−271.
(81) Usui, Y. *Chem. Lett.* **1973**, *2*, 743−744.
(82) Wilkinson, F.; Helman, W. P.; Ross, A. B. *J. Phys. Chem. Ref. Data* **1993**, *22*, 113−262.
(83) Chaon, J. N.; Jamieson, G. R.; Sinclair, R. S. *Chem. Phys. Lipids* **1987**, *43*, 81−99.
(84) Rurack, K.; Kollmannsberger, M.; Daub, J. *Angew. Chem., Int. Ed.* **2001**, *40*, 385−387.
(85) Hattori, S.; Ohkubo, K.; Urano, Y.; Sunahara, H.; Nagano, T.; Wada, Y.; Tkachenko, N. V.; Lemmetyinen, H.; Fukuzumi, S. *J. Phys. Chem. B* **2005**, *109*, 15368−75.



DOI: 10.1021/acs.organomet.7b00806
*Organometallics* 2018, 37, 235−253

(86) Teki, Y.; Tamekuni, H.; Haruta, K.; Takeuchi, J.; Miura, Y. *J. Mater. Chem.* **2008**, *18*, 381−391.
(87) Summers, G. H.; Lefebvre, J. F.; Black, F. A.; Davies, E. S.; Gibson, E. A.; Pullerits, T.; Wood, C. J.; Zidek, K. *Phys. Chem. Chem. Phys.* **2016**, *18*, 1059−70.
(88) Hendel, S. J.; Poe, A. M.; Khomein, P.; Bae, Y.; Thayumanavan, S.; Young, E. R. *J. Phys. Chem. A* **2016**, *120*, 8794−8803.
(89) Iagatti, A.; Cupellini, L.; Biagiotti, G.; Caprasecca, S.; Fedeli, S.; Lapini, A.; Ussano, E.; Cicchi, S.; Foggi, P.; Marcaccio, M.; Mennucci, B.; Di Donato, M. *J. Phys. Chem. C* **2016**, *120*, 16526−16536.
(90) Jin, G. F.; Cho, Y. J.; Wee, K. R.; Hong, S. A.; Suh, I. H.; Son, H. J.; Lee, J. D.; Han, W. S.; Cho, D. W.; Kang, S. O. *Dalton Trans.* **2015**, *44*, 2780−7.
(91) Richards, V. J.; Gower, A. L.; Smith, J. E.; Davies, E. S.; Lahaye, D.; Slater, A. G.; Lewis, W.; Blake, A. J.; Champness, N. R.; Kays, D. L. *Chem. Commun. (Cambridge, U. K.)* **2012**, *48*, 1751−3.
(92) Hendel, S. J.; Poe, A. M.; Khomein, P.; Bae, Y.; Thayumanavan, S.; Young, E. R. *J. Phys. Chem. A* **2016**, *120*, 8794−8803.
(93) Belzile, M.-N.; Godin, R.; Durantini, A. M.; Cosa, G. *J. Am. Chem. Soc.* **2016**, *138*, 16388−16397.
(94) Ruff, A.; Heyer, E.; Roland, T.; Haacke, S.; Ziessel, R.; Ludwigs, S. *Electrochim. Acta* **2015**, *173*, 847−859.
(95) Benniston, A. C.; Copley, G.; Harriman, A.; Howgego, D.; Harrington, R. W.; Clegg, W. *J. Org. Chem.* **2010**, *75*, 2018−27.
(96) Krejčik, M.; Daněk, M.; Hartl, F. *J. Electroanal. Chem. Interfacial Electrochem.* **1991**, *317*, 179−187.
(97) Chen, Y.; Zhao, J.; Guo, H.; Xie, L. *J. Org. Chem.* **2012**, *77*, 2192−206.
(98) Fu, L.; Jiang, F. L.; Fortin, D.; Harvey, P. D.; Liu, Y. *Chem. Commun. (Cambridge, U. K.)* **2011**, *47*, 5503−5.
(99) Lerrick, R. I.; Winstanley, T. P.; Haggerty, K.; Wills, C.; Clegg, W.; Harrington, R. W.; Bultinck, P.; Herrebout, W.; Benniston, A. C.; Hall, M. J. *Chem. Commun. (Cambridge, U. K.)* **2014**, *50*, 4714−6.
(100) Ghelfi, M.; Ulatowski, L.; Manor, D.; Atkinson, J. *Bioorg. Med. Chem.* **2016**, *24*, 2754−61.
(101) Zhou, X.; Yu, C.; Feng, Z.; Yu, Y.; Wang, J.; Hao, E.; Wei, Y.; Mu, X.; Jiao, L. *Org. Lett.* **2015**, *17*, 4632−5.
(102) Herrendorf, W.; Bärnighausen, W. *HABITUS, program for the optimization of the crystal shape for numerical absorption correction in X-SHAPE*, version 1.06; Fa. Stoe: Darmstadt, Germany, 1999.
(103) Sheldrick, G. M. *SHELXL-97, Program for Crystal Structure Solution and Refinement*; Universität Göttingen: Göttingen, Germany, 1997.
(104) Sheldrick, G. M. *Acta Crystallogr., Sect. A: Crystallogr.* **2008**, *64*, 112−122.
(105) Sheldrick, G. M. *Acta Crystallogr., Sect. A: Crystallogr.* **2008**, *64*, 112−22.
(106) Dolomanov, O. V.; Bourhis, L. J.; Gildea, R. J.; Howard, J. A. K.; Puschmann, H. *J. Appl. Crystallogr.* **2009**, *42*, 339−341.
(107) Spek, A. L. *Acta Crystallogr., Sect. D: Biol. Crystallogr.* **2009**, *65*, 148−155.
(108) Macrae, C. F.; Bruno, I. J.; Chisholm, J. A.; Edgington, P. R.; McCabe, P.; Pidcock, E.; Rodriguez-Monge, L.; Taylor, R.; Van De Streek, J.; Wood, P. A. *J. Appl. Crystallogr.* **2008**, *41*, 466−470.
(109) Stoll, S.; Schweiger, A. *J. Magn. Reson.* **2006**, *178*, 42−55.
(110) Frisch, M. J.; Trucks, G. W.; Schlegel, H. B.; Scuseria, G. E.; Robb, M. A.; Cheeseman, J. R.; Scalmani, G.; Barone, V.; Mennucci, B.; Petersson, G. A.; Nakatsuji, H.; Caricato, M.; Li, X.; Hratchian, H. P.; Izmaylov, A. F.; Bloino, J.; Zheng, G.; Sonnenberg, J. L.; Hada, M.; Ehara, M.; Toyota, K.; Fukuda, R.; Hasegawa, J.; Ishida, M.; Nakajima, T.; Honda, Y.; Kitao, O.; Nakai, H.; Vreven, T.; Montgomery, J. A., Jr.; Peralta, J. E.; Ogliaro, F.; Bearpark, M.; Heyd, J. J.; Brothers, E.; Kudin, K. N.; Staroverov, V. N.; Kobayashi, R.; Normand, J.; Raghavachari, K.; Rendell, A.; Burant, J. C.; Iyengar, S. S.; Tomasi, J.; Cossi, M.; Rega, N.; Millam, J. M.; Klene, M.; Knox, J. E.; Cross, J. B.; Bakken, V.; Adamo, C.; Jaramillo, J.; Gomperts, R.; Stratmann, R. E.; Yazyev, O.; Austin, A. J.; Cammi, R.; Pomelli, C.; Ochterski, J. W.; Martin, R. L.; Morokuma, K.; Zakrzewski, V. G.; Voth, G. A.; Salvador, P.; Dannenberg, J. J.; Dapprich, S.; Daniels, A. D.; Farkas, O.; Foresman, J. B.; Ortiz, J. V.; Cioslowski, J.; Fox, D. J. *Gaussian 09*, revision E.01; Gaussian, Inc.: Wallingford, CT, 2009.
(111) Gunnarsson, O.; Lundqvist, B. I. *Phys. Rev. B* **1976**, *13*, 4274−4298.
(112) Küchle, W.; Dolg, M.; Stoll, H.; Preuss, H. *J. Chem. Phys.* **1994**, *100*, 7535−7542.
(113) Dolg, M.; Stoll, H.; Preuss, H. *J. Chem. Phys.* **1989**, *90*, 1730.
(114) Andrae, D.; Häußermann, U.; Dolg, M.; Stoll, H.; Preuß, H. *Theor. Chim. Acta* **1990**, *77*, 123−141.
(115) Hariharan, P. C.; Pople, J. A. *Theor. Chim. Acta* **1973**, *28*, 213−222.
(116) Perdew, J. P.; Burke, K.; Ernzerhof, M. *Phys. Rev. Lett.* **1996**, *77*, 3865−3868.
(117) Adamo, C.; Barone, V. *J. Chem. Phys.* **1999**, *110*, 6158−6170.
(118) Cancés, E.; Mennucci, B.; Tomasi, J. *J. Chem. Phys.* **1997**, *107*, 3032−3041.
(119) Mennucci, B.; Tomasi, J. *J. Chem. Phys.* **1997**, *106*, 5151−5158.
(120) Cossi, M.; Rega, N.; Scalmani, G.; Barone, V. *J. Comput. Chem.* **2003**, *24*, 669−681.
(121) Scalmani, G.; Frisch, M. J. *J. Chem. Phys.* **2010**, *132*, 114110.
(122) Runge, E.; Gross, E. K. U. *Phys. Rev. Lett.* **1984**, *52*, 997−1000.
(123) O'Boyle, N. M.; Tenderholt, A. L.; Langner, K. M. *J. Comput. Chem.* **2008**, *29*, 839−845.
(124) Takizawa, S.-y.; Aboshi, R.; Murata, S. *Photochem. Photobiol. Sci.* **2011**, *10*, 895−903.
(125) Adarsh, N.; Shanmugasundaram, M.; Avirah, R. R.; Ramaiah, D. *Chem. - Eur. J.* **2012**, *18*, 12655−12662.
(126) Field, L. R.; Wilhelm, E.; Battino, R. *J. Chem. Thermodyn.* **1974**, *6*, 237−243.


DOI: 10.1021/acs.organomet.7b00806
*Organometallics* 2018, 37, 235−253

# σ-Pt-BODIPY Complexes With Platinum Attachment to Carbon Atoms C2 or C3: Spectroscopic, Structural and (Spectro)Electrochemical Studies and Photocatalysis

*Peter Irmler and Rainer F. Winter**

Fachbereich Chemie der Universität Konstanz, Universitätsstraße 10, D-78464 Konstanz, Germany

# Supporting Information

## Table of Contents



## List of Figures

**List of Tables**

## NMR Spectra

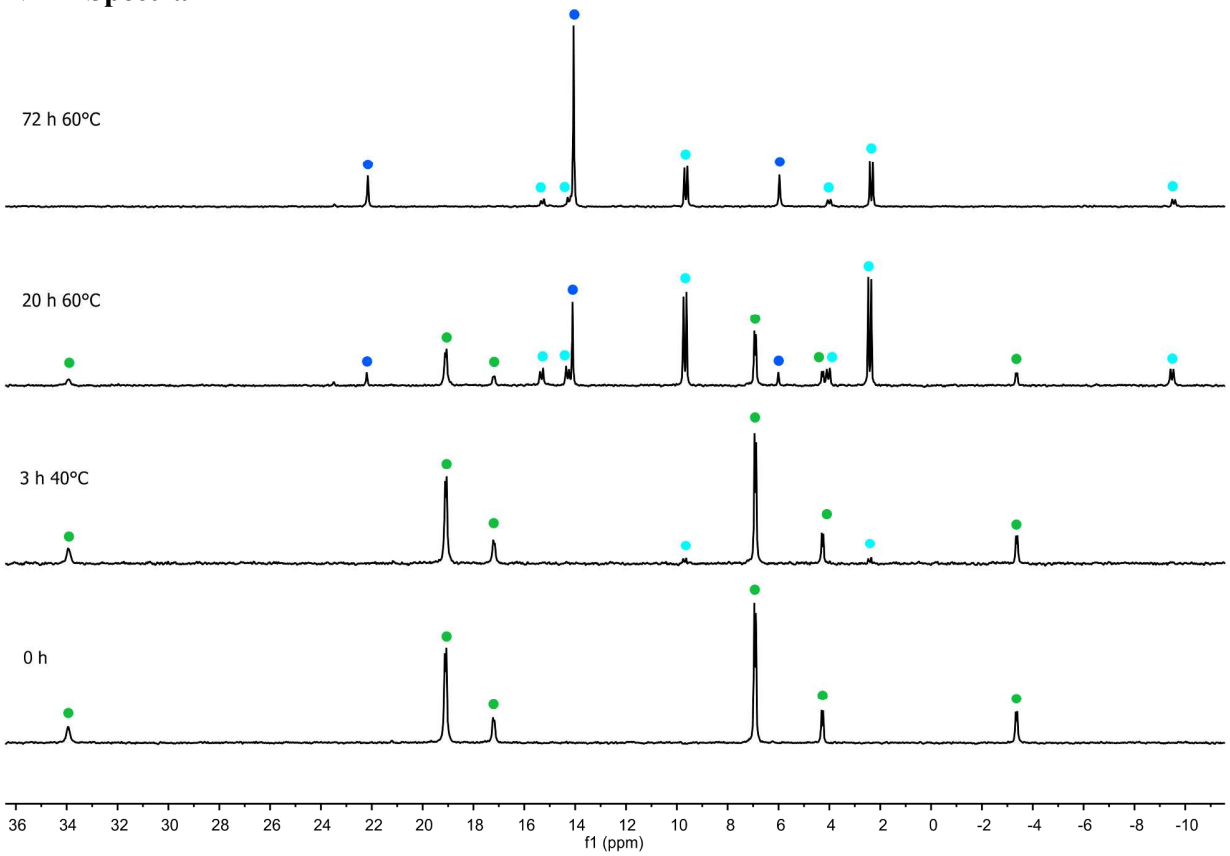


**Figure S1.** Conversion of **8,9-Pt** (green) to ***cis*-3-Cl-Pt** (cyan) and ***trans*-3-Cl-Pt** (blue) monitored by $^{31}P\{^{1}H\}$ NMR spectroscopy in a THF-*d8*.

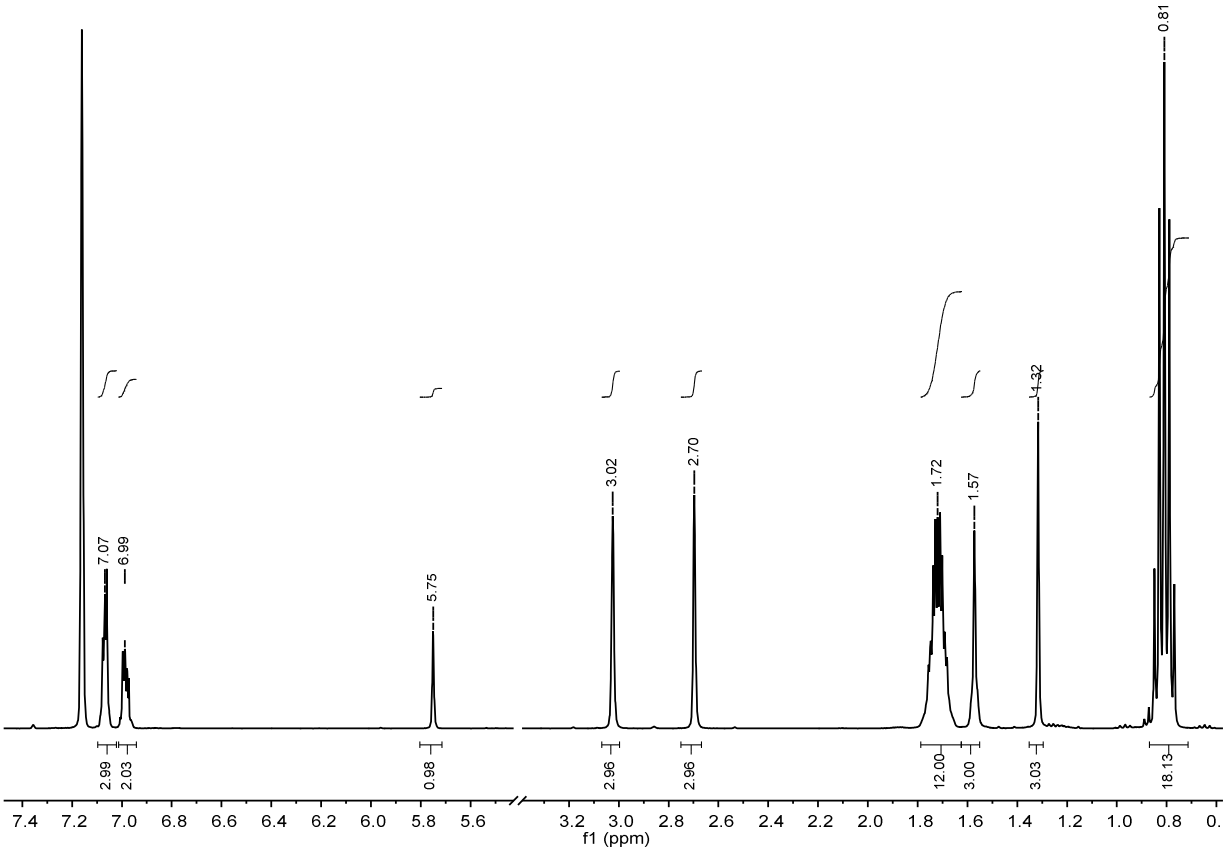


**Figure S2.** $^{1}H$ NMR spectrum of **2-Pt-6H** in $C_6D_6$.

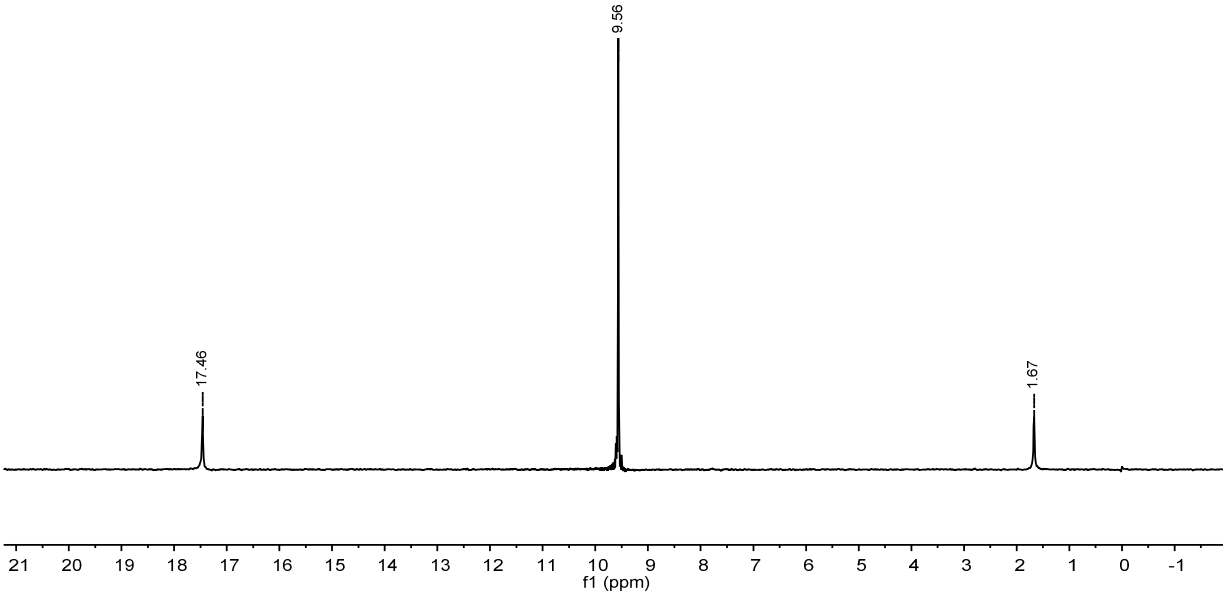


**Figure S3.** $^{31}P\{^{1}H\}$ NMR spectrum of **2-Pt-6H** in $C_6D_6$.

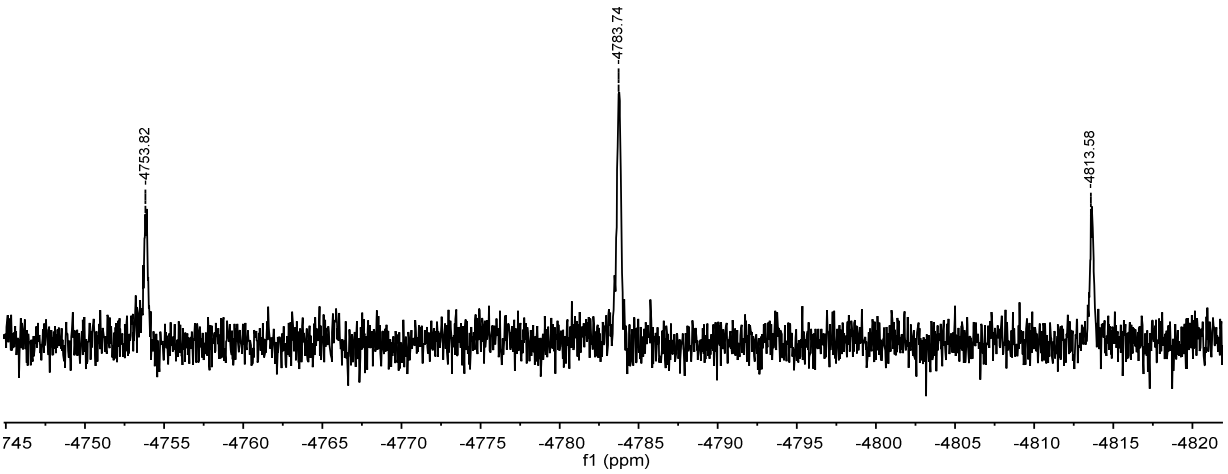


**Figure S4.** $^{195}Pt\{^{1}H\}$ NMR spectrum of **2-Pt-6H** in $C_6D_6$.

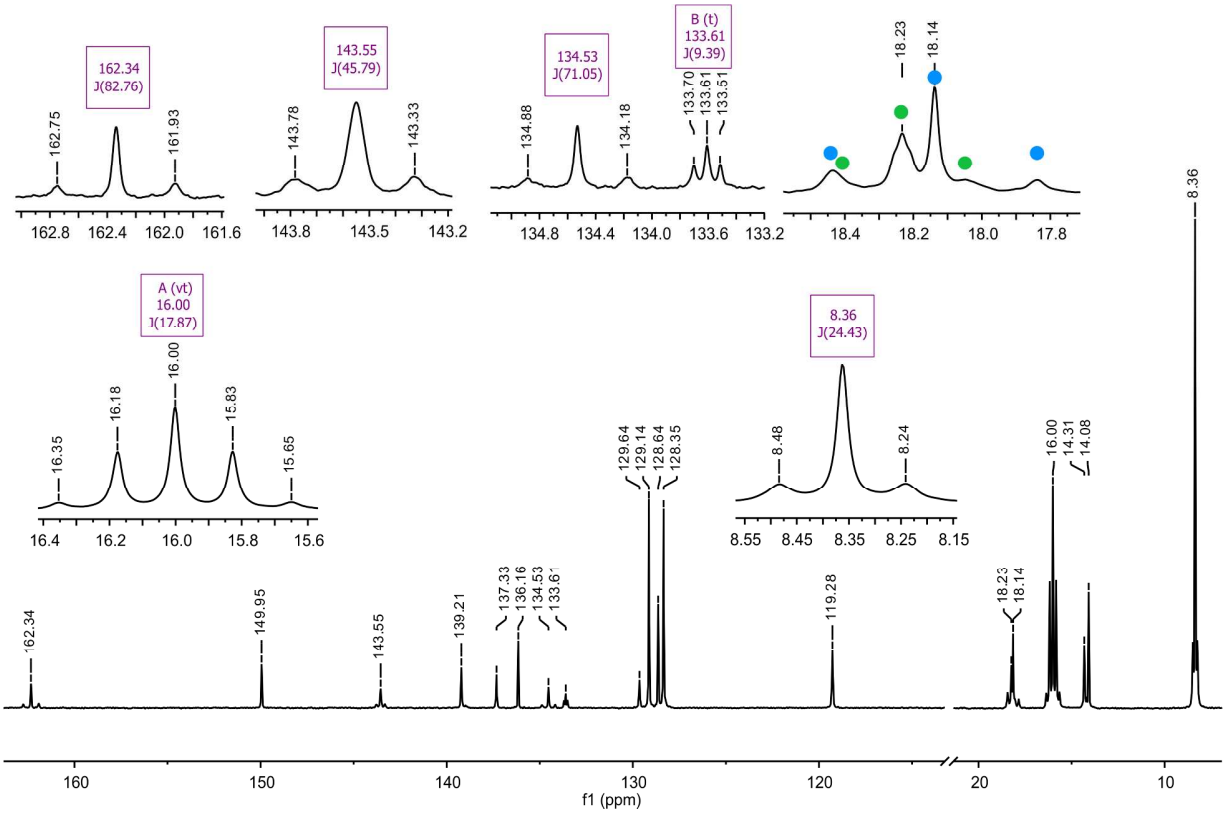


**Figure S5.** $^{13}C\{^{1}H\}$ NMR spectrum of **2-Pt-6H** in $CDCl_3$.

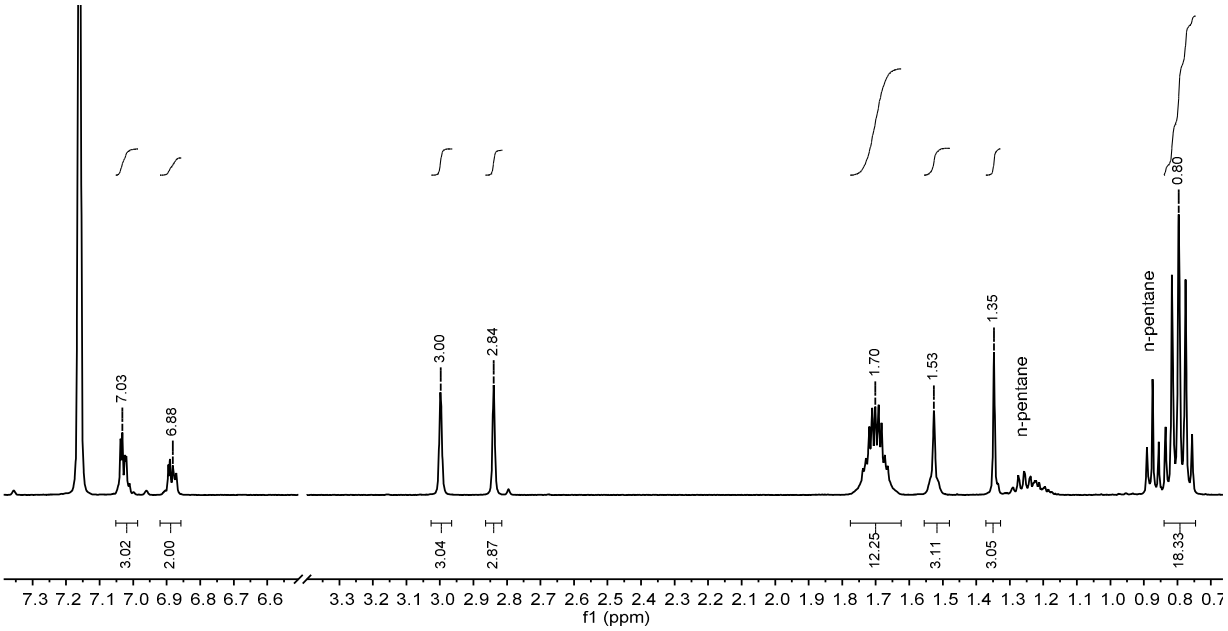


**Figure S6.** $^{1}$H NMR spectrum of **2-Pt-6I** in $C_6D_6$.

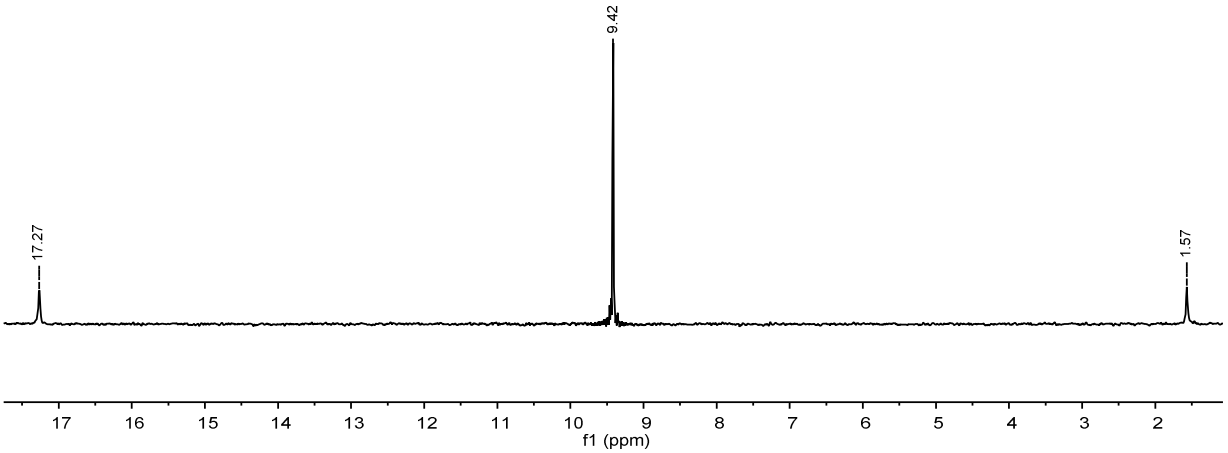


**Figure S7.** $^{31}$P{$^{1}$H} NMR spectrum of **2-Pt-6I** in $C_6D_6$.

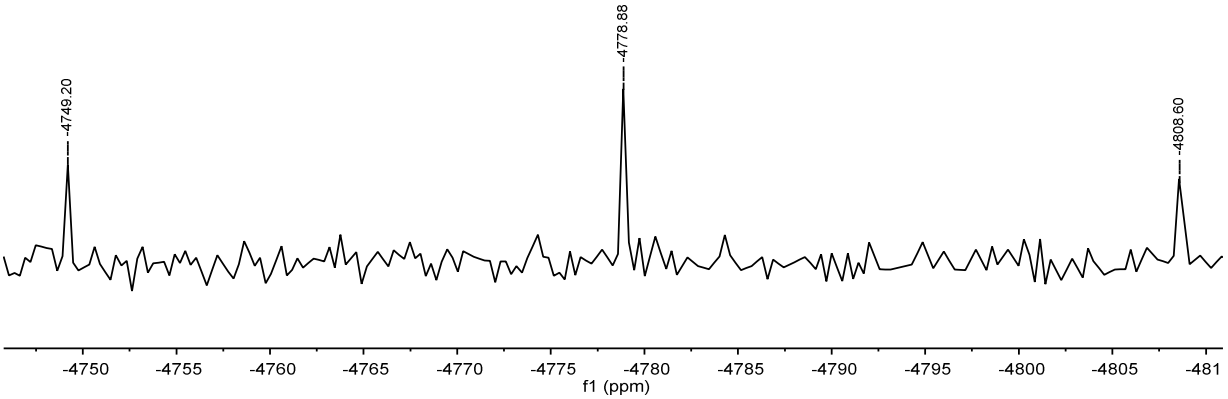


**Figure S8.** $^{195}$Pt{$^{1}$H} NMR spectrum of **2-Pt-6I** in $C_6D_6$.

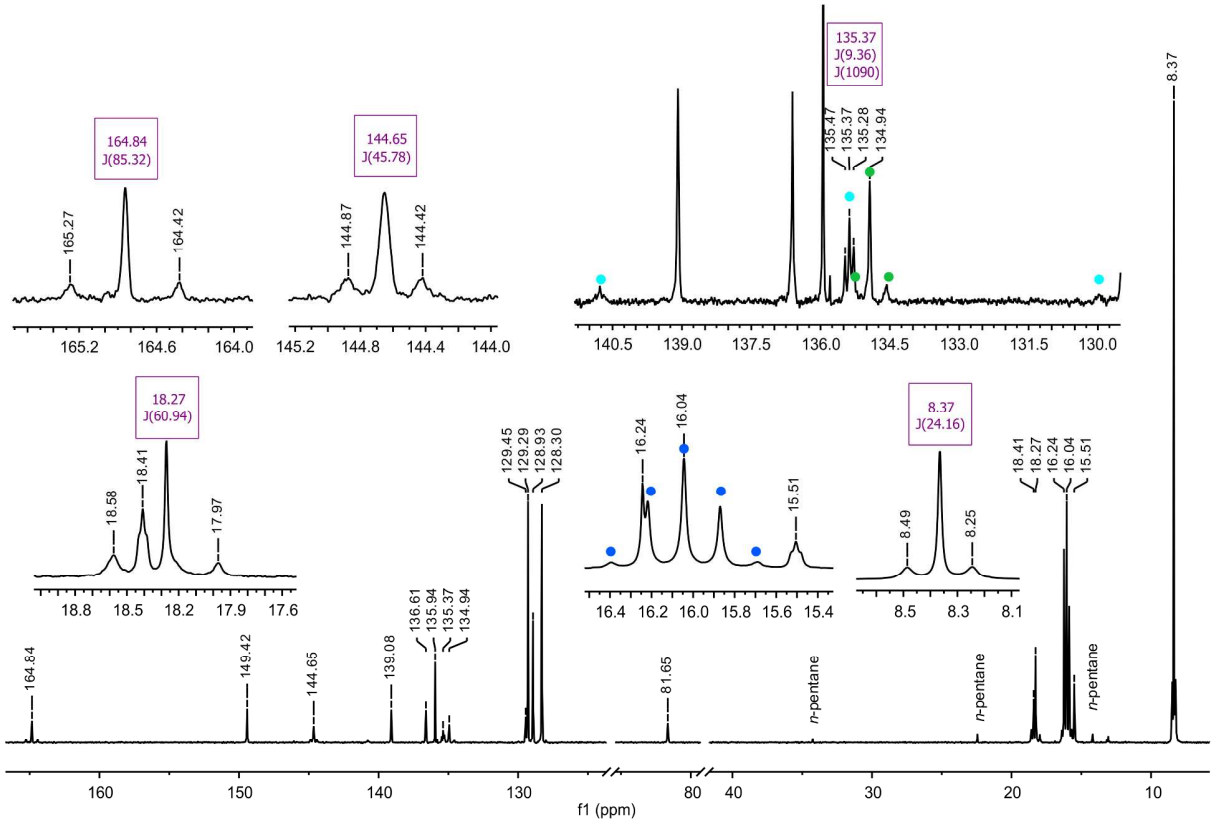


**Figure S9.** $^{13}C\{^{1}H\}$ NMR spectrum of **2-Pt-6I** in $CDCl_3$.

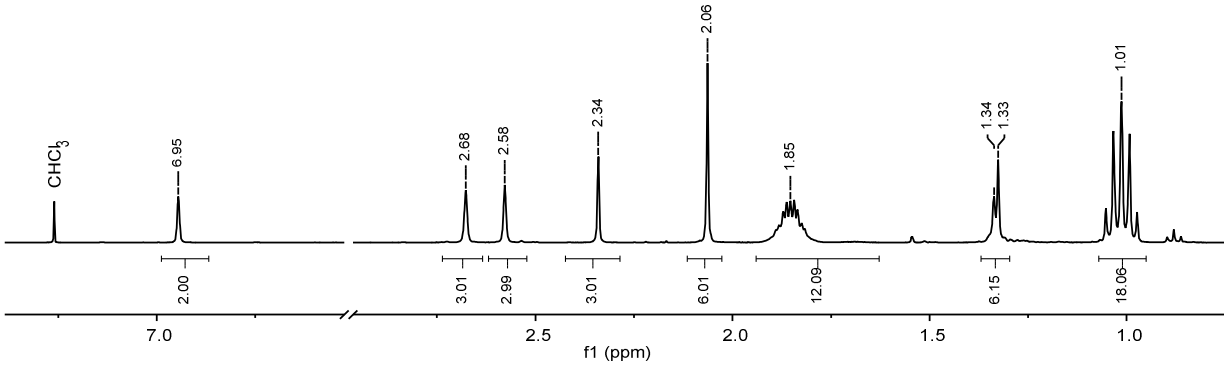


**Figure S10.** $^{1}H$ NMR spectrum of **2-Pt-Mes-6I** in $CDCl_3$.

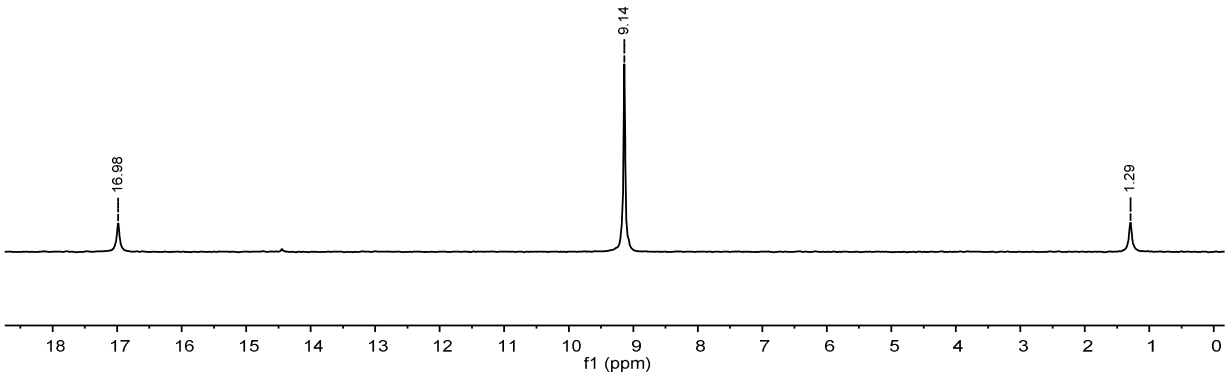


**Figure S11.** $^{31}P\{^{1}H\}$ NMR spectrum of **2-Pt-Mes-6I** in $CDCl_3$.

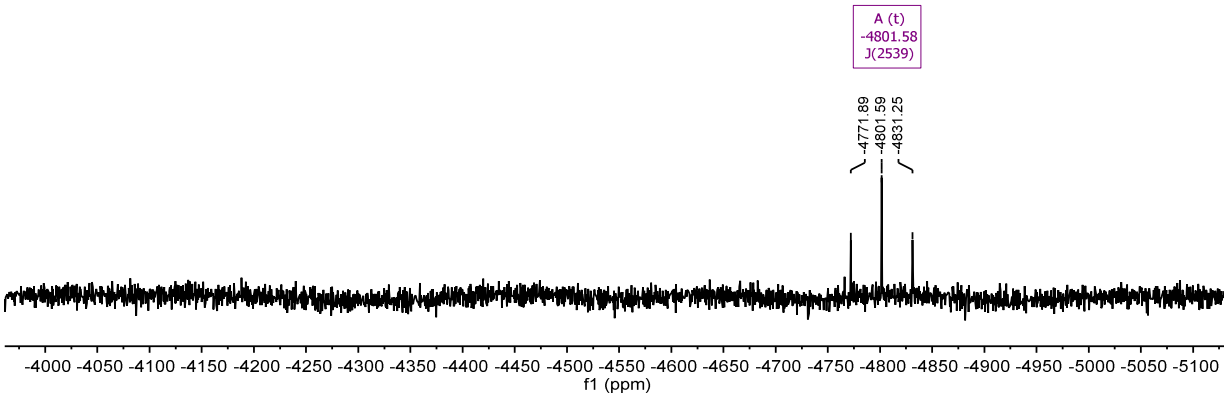


**Figure S12.** $^{195}Pt\{^{1}H\}$ NMR spectrum of **2-Pt-Mes-6I** in $CDCl_3$.

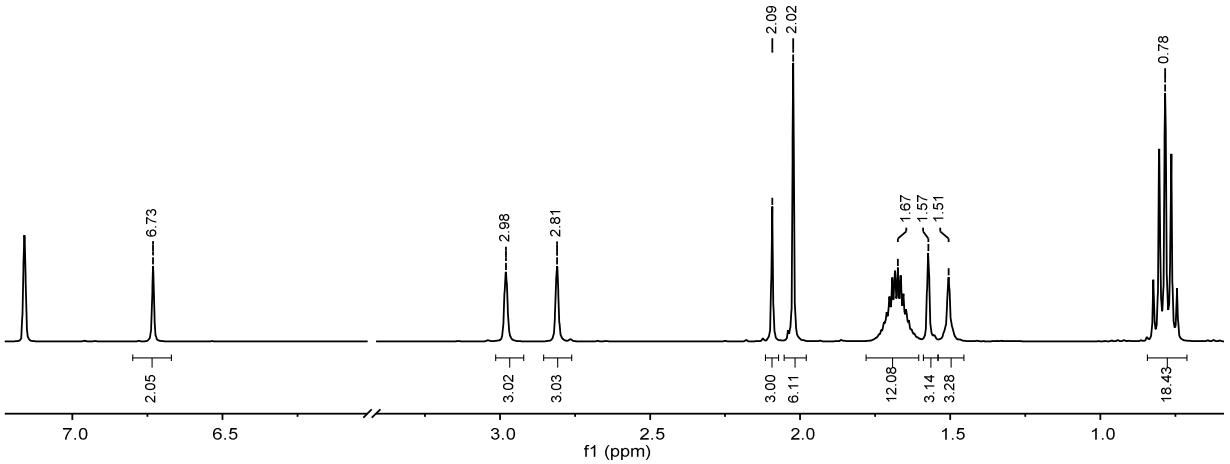


**Figure S13.** $^{1}H$ NMR spectrum of **2-Pt-Mes-6I** in $C_6D_6$.

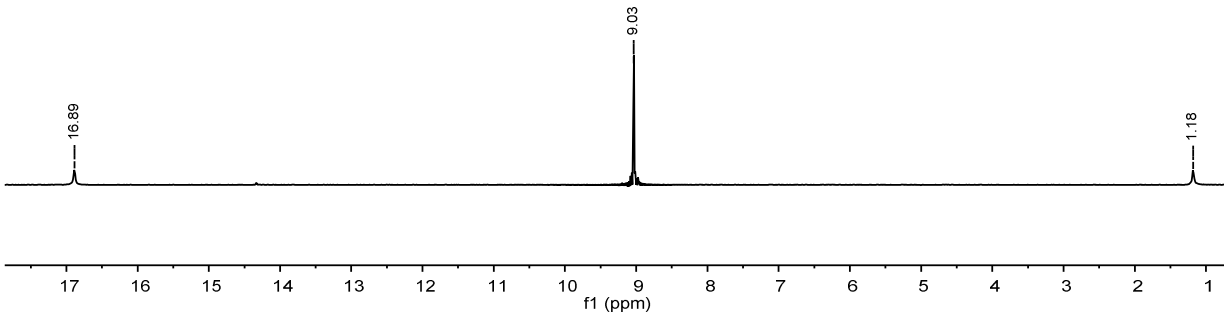


**Figure S14.** $^{31}P\{^{1}H\}$ NMR spectrum of **2-Pt-Mes-6I** in $C_6D_6$.

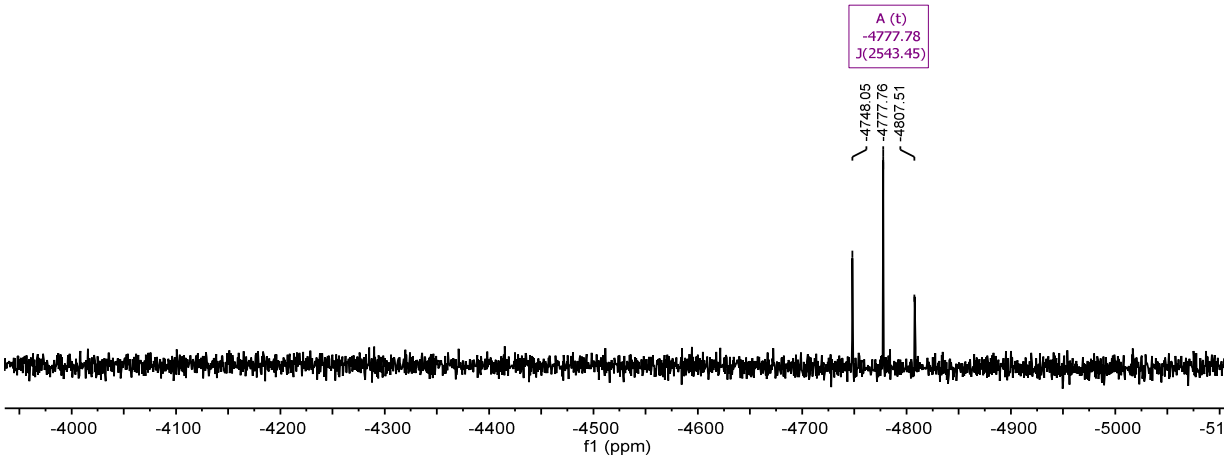


**Figure S15.** $^{195}Pt\{^{1}H\}$ NMR spectrum of **2-Pt-Mes-6I** in $C_6D_6$.

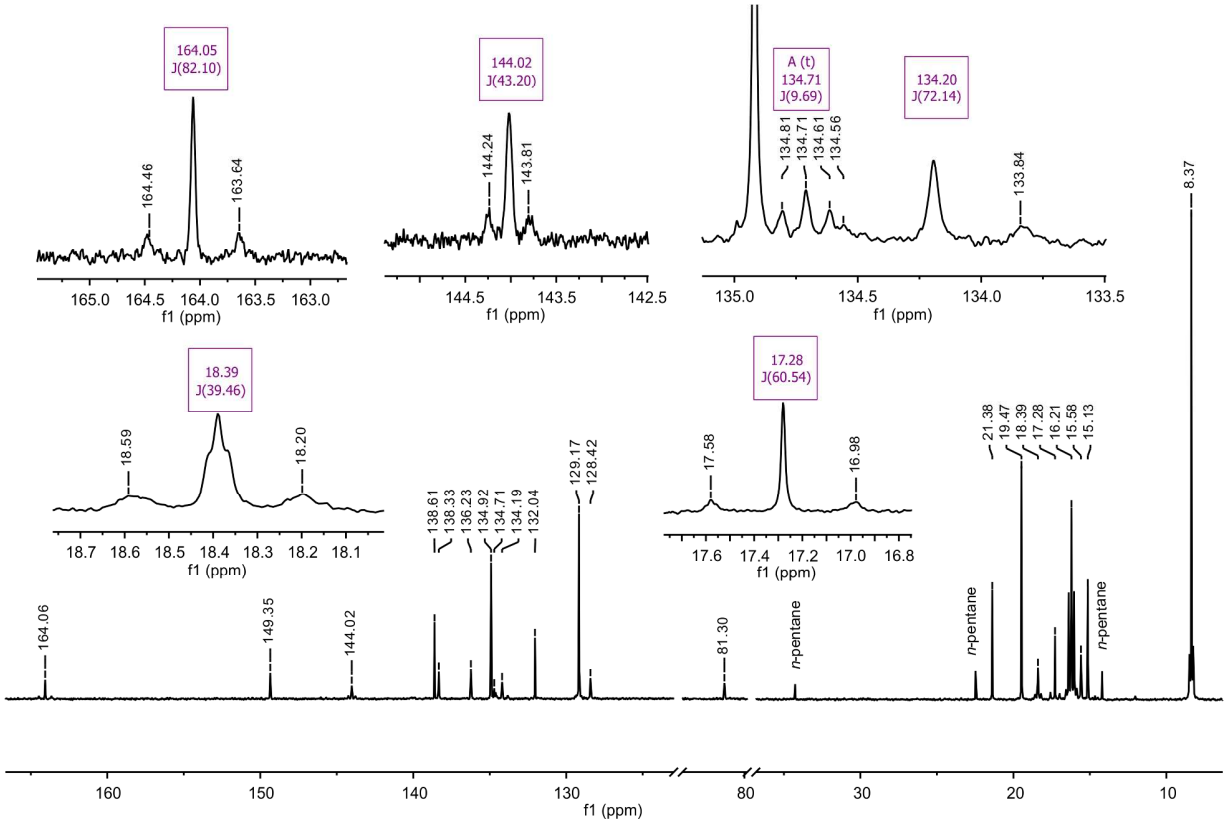


**Figure S16.** $^{13}C\{^{1}H\}$ NMR spectrum of **2-Pt-Mes-6I** in $CDCl_3$.

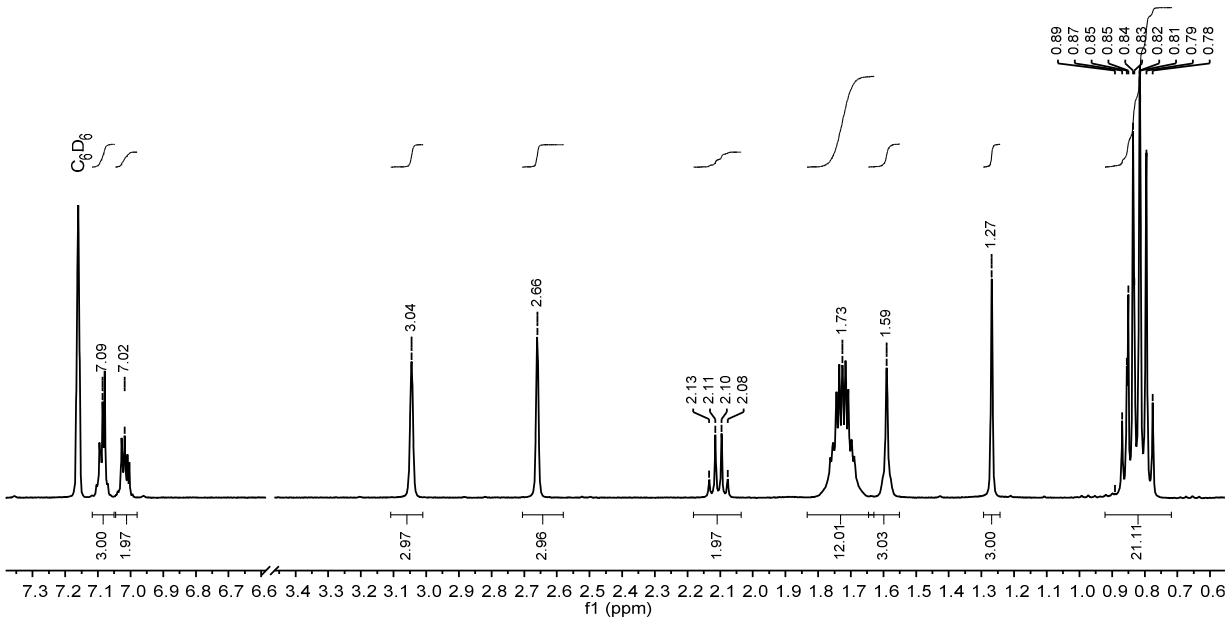


**Figure S17.** $^{1}H$ NMR spectrum of **2-Pt-6Et** in $C_6D_6$.

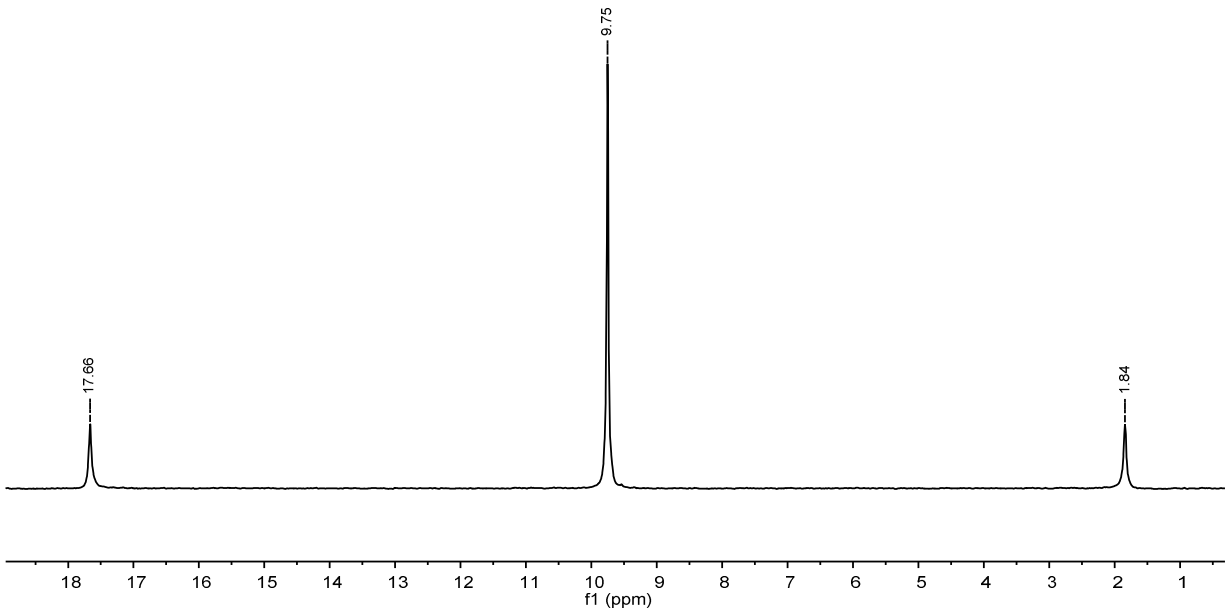


**Figure S18.** $^{31}P\{^{1}H\}$ NMR spectrum of **2-Pt-6Et** in $C_6D_6$.

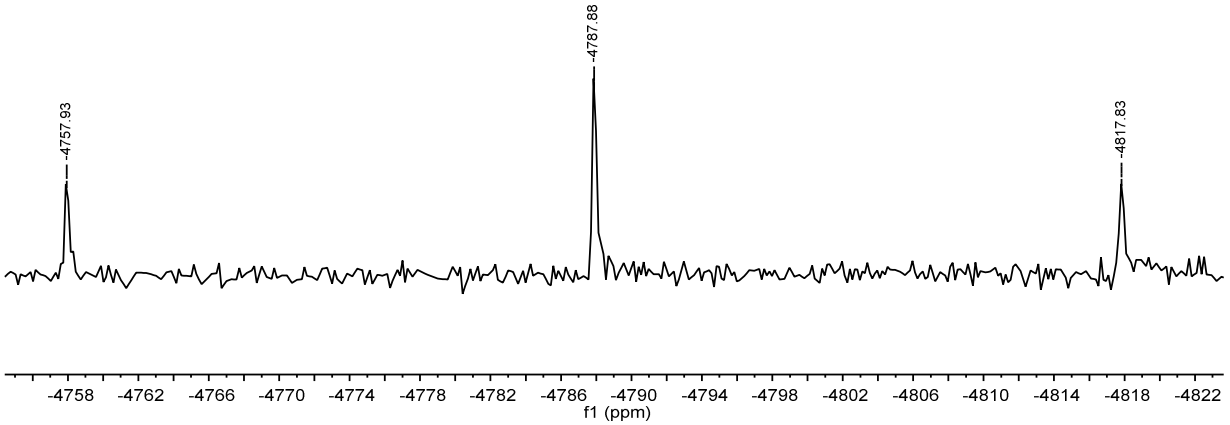


**Figure S19.** $^{195}Pt\{^{1}H\}$ NMR spectrum of **2-Pt-6Et** in $C_6D_6$.

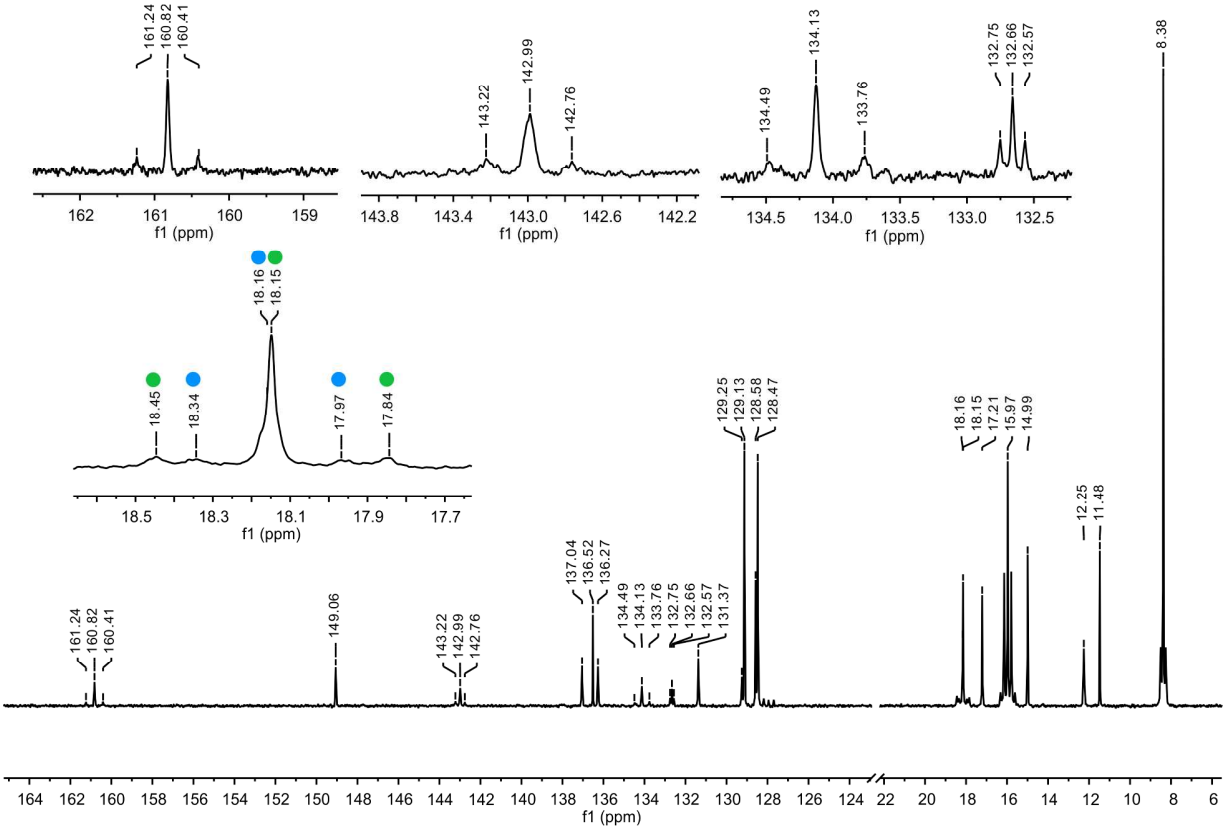


**Figure S20.** $^{13}C\{^{1}H\}$ NMR spectrum of **2-Pt-6Et** in $CDCl_3$.

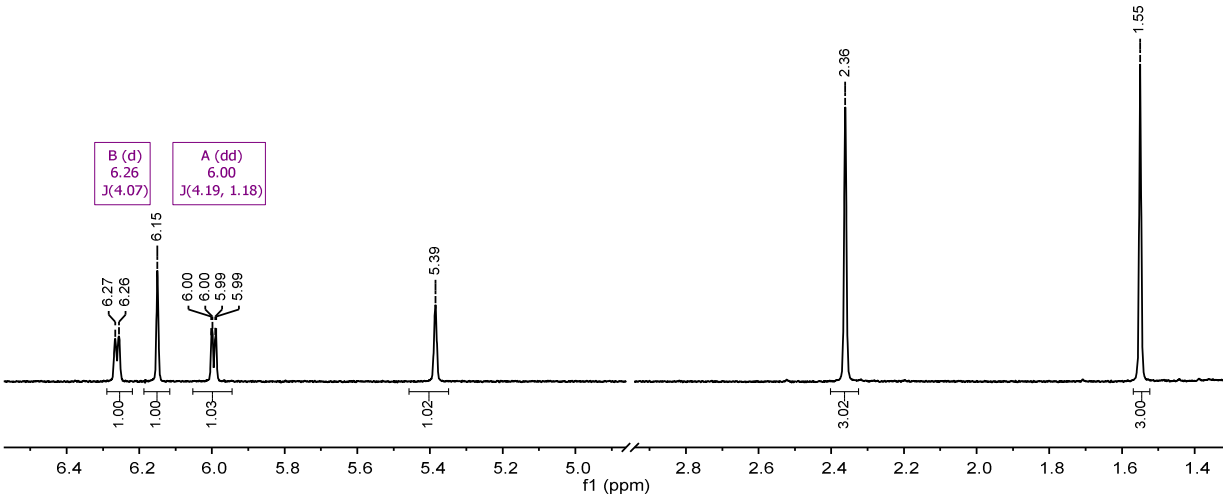


**Figure S21.** $^{1}H$ NMR spectrum of **3-Cl-Bodipy** in $C_6D_6$.

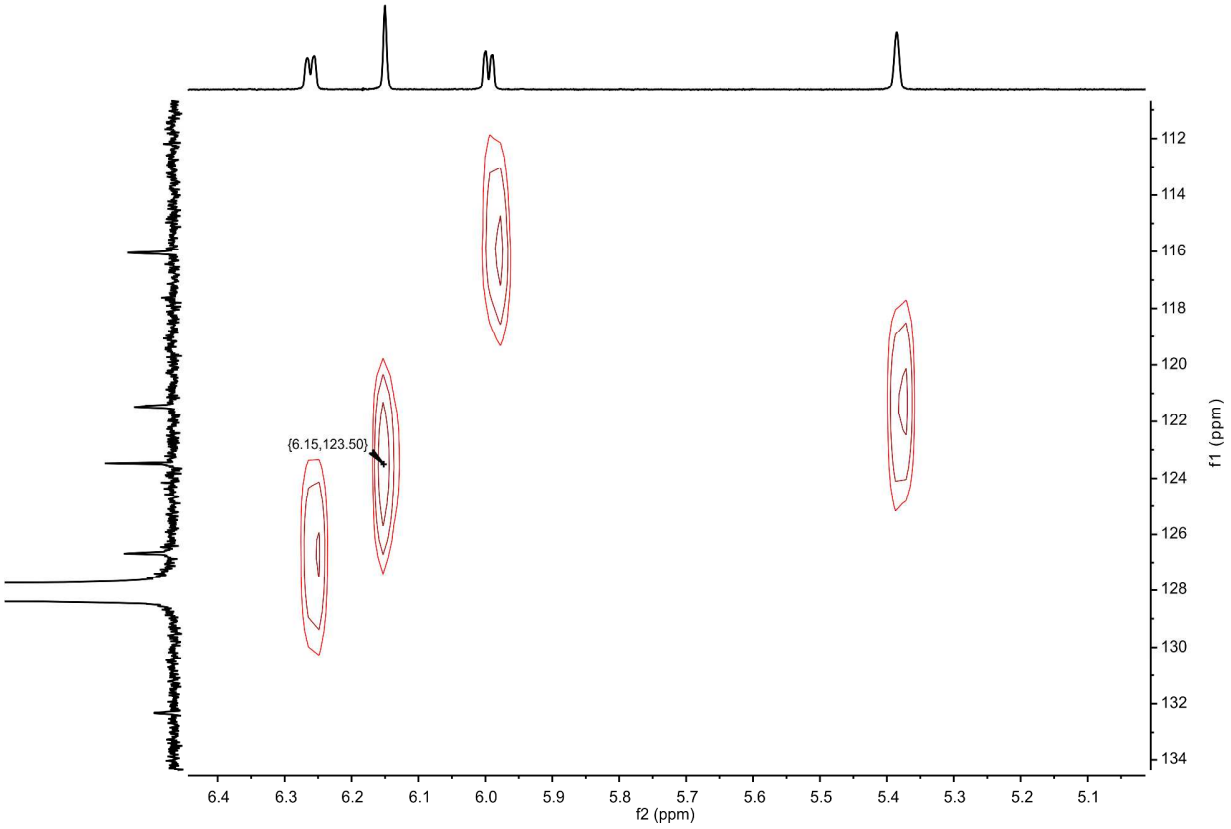


**Figure S22.** HSQC of **3-Cl-bodipy** in $C_6D_6$.

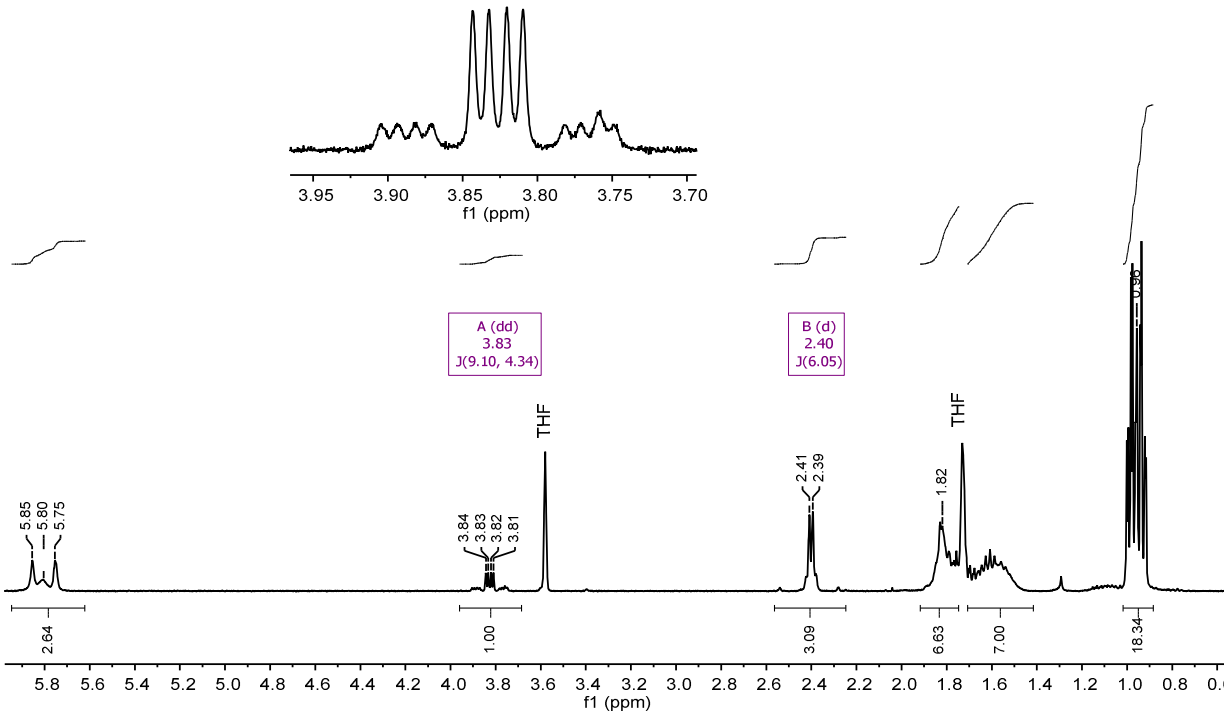


**Figure S23.** $^1$H NMR spectrum of **8,9-Pt** in THF-*d8*.

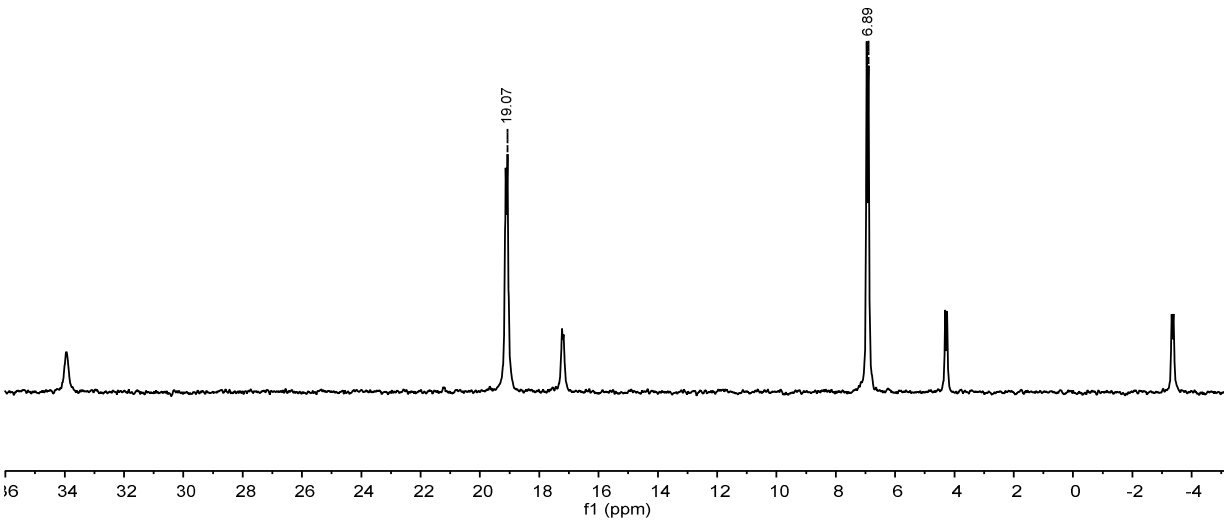


**Figure S24.** $^{31}P\{^{1}H\}$ NMR spectrum of **8,9-Pt** in THF-*d8*.

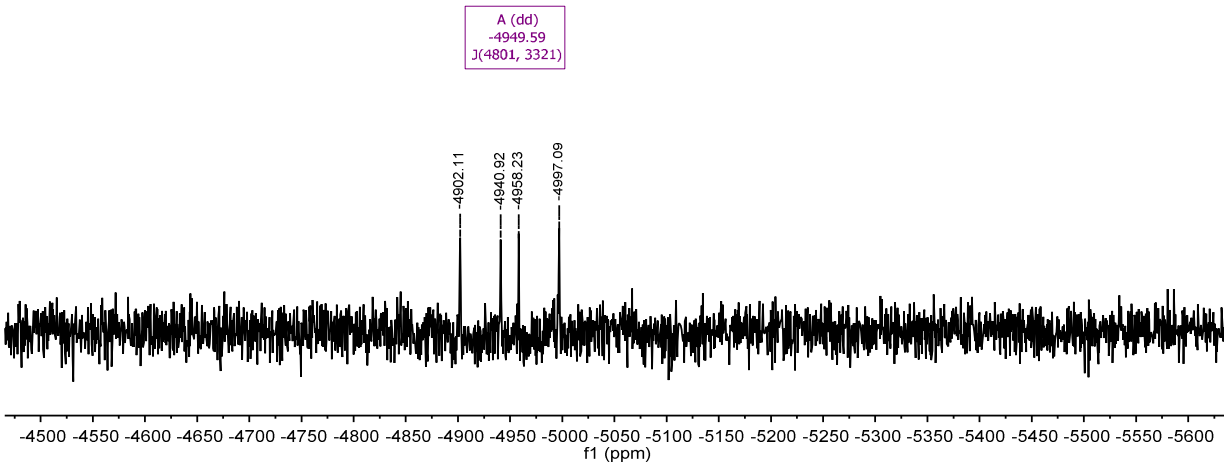


**Figure S25.** $^{195}Pt\{^{1}H\}$ NMR spectrum of **8,9-Pt** in THF-*d8*.

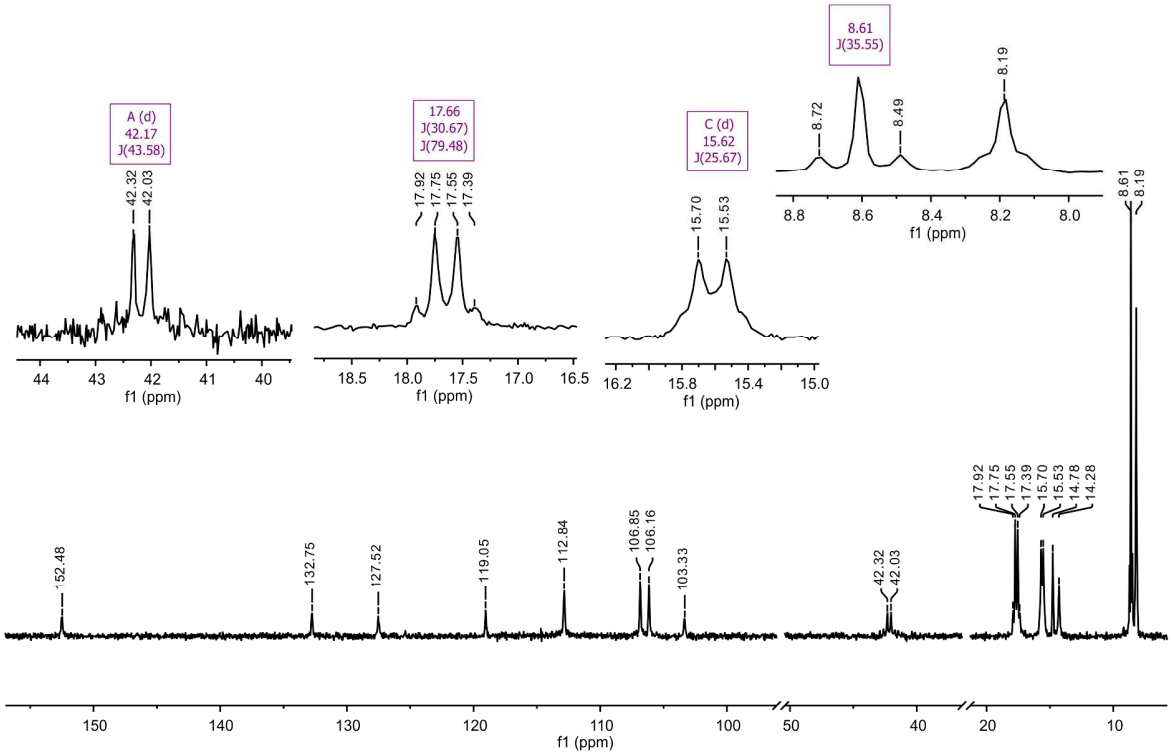


**Figure S26.** $^{13}C\{^{1}H\}$ NMR spectrum of **8,9-Pt** in THF-*d8*.

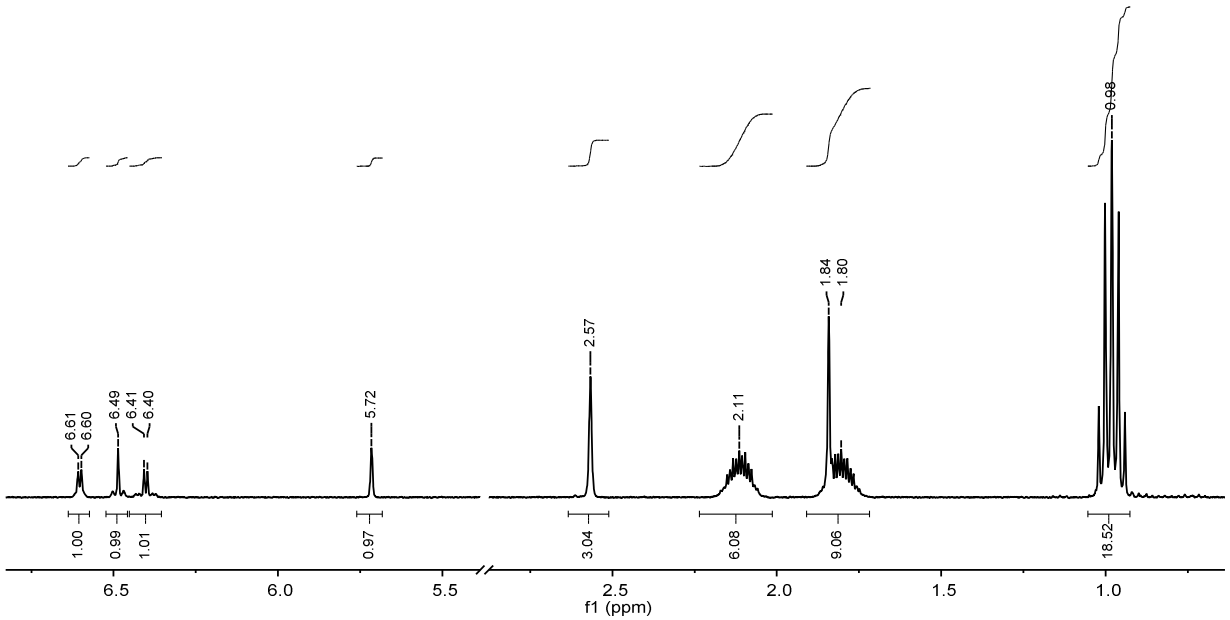


**Figure S27.** $^{1}H$ NMR spectrum of **3-Pt** in $C_6D_6$.

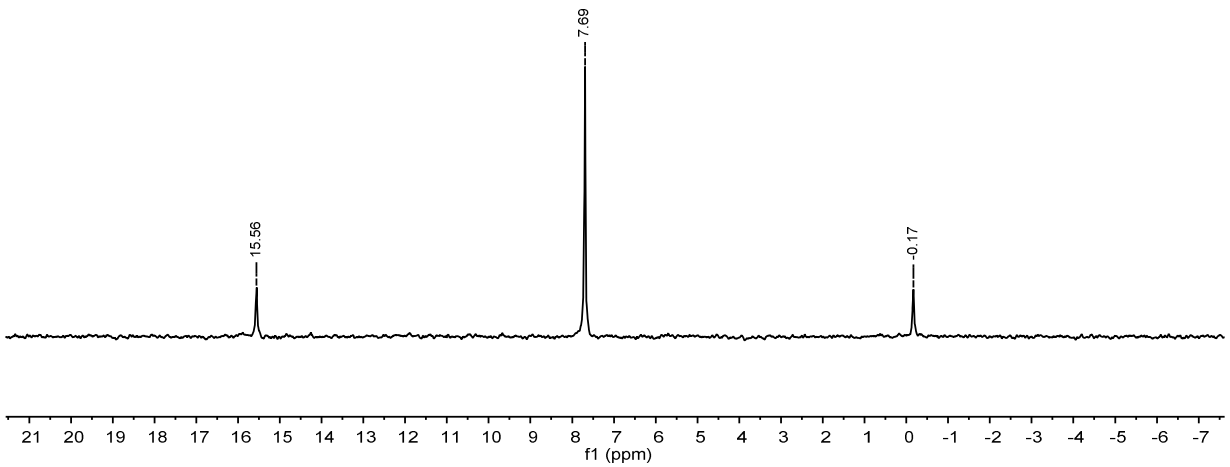


**Figure S28.** $^{31}P\{^{1}H\}$ NMR spectrum of **3-Pt** in $C_6D_6$.

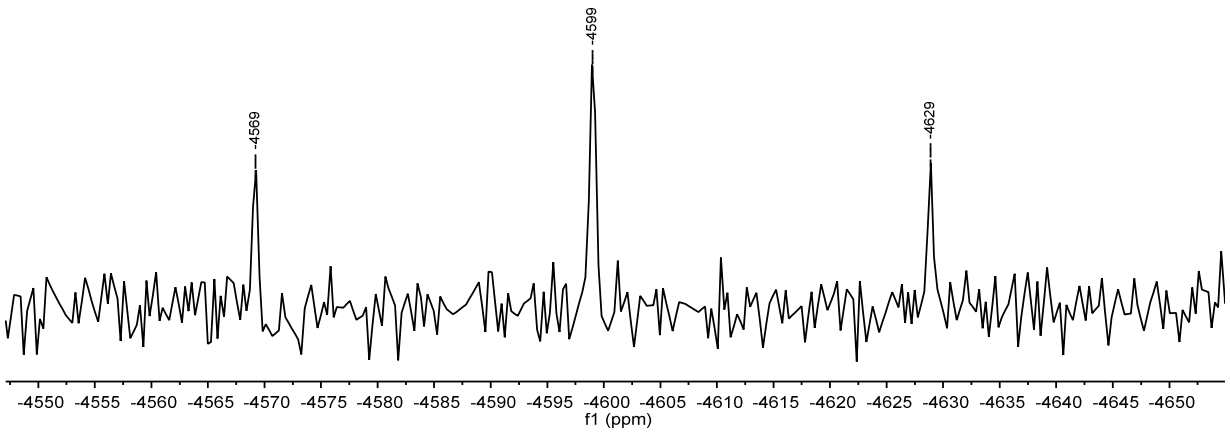


**Figure S29.** $^{195}Pt\{^{1}H\}$ NMR spectrum of **3-Pt** in $C_6D_6$.

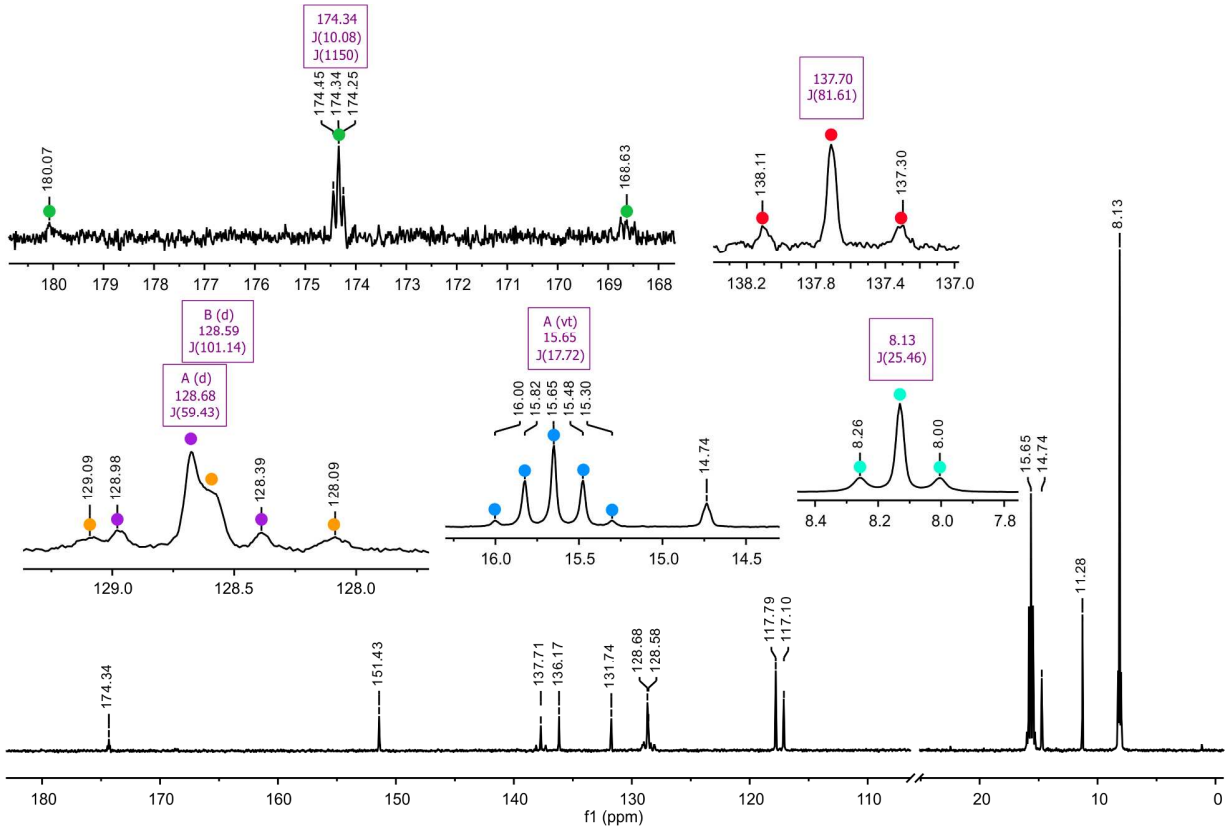


**Figure S30.** $^{13}C\{^{1}H\}$ NMR spectrum of **3-Pt** in $CDCl_3$.

## Single Crystal X-Ray Diffraction

**Table S1.** Crystal and refinement data of **2-Pt-6H**, **2-Pt-6I**, **2-Pt-Mes-6I**, **2-Pt-6Et**, **8,9-Pt** and **3-Pt**.

| Compound | **2-Pt-6H** | **2-Pt-6I** | **2-Pt-Mes-6I** | **2-Pt-6Et** | **8,9-Pt** | **3-Pt** |
|---|---|---|---|---|---|---|
| Emp. formula / f. wt. (g/mol) | $C_{68}H_{102}B_2F_4I_2N_4P_4Pt_2$/ 1841.01 | $C_{27}H_{53}BF_2I_2N_2P_2Pt$ / 1085.45 | $C_{34}H_{53}BF_2I_2N_2P_2Pt$ / 1049.47 | $C_{34}H_{54}BCl_2F_2IN_2P_2Pt$ / 994.43 | $C_{23}H_{40}BClF_2N_2P_2Pt$ / 685.86 | $C_{23}H_{40}BF_2IN_2P_2Pt$/ 777.31 |
| Temperature (K) | 100(2) | 100(2) | 100(2) | 100(2) | 100(2) | 100(2) |
| Wavelength (Å) | 0.71073 | 0.71073 | 0.71073 | 0.71073 | 0.71073 | 0.71073 |
| Crystal system | Triclinic | Monoclinic | Orthorhombic | Triclinic | Triclinic | Monoclinic |
| Space group | *P*-1 | *C*2/*c* | $P2_12_12_1$ | *P*-1 | *P*-1 | $P\,2_1/n$ |
| *a*, *b*, *c* (Å) | 14.5456(7), 15.5233(8), 17.0814(9) | 18.6509(9), 18.0742(6), 24.9049(12) | 12.8144(19), 14.8823(15), 23.511(2) | 14.9291(11), 15.0847(11), 19.0842(14) | 8.6774(18), 8.6655(16), 18.312(4) | 13.4963(10), 14.4061(8), 14.2044(11) |
| $\alpha, \beta, \gamma$ (°) | 79.469(4), 79.473(4), 83.149(4) | 90, 103.919(4), 90 | 90, 90, 90 | 99.706(6), 103.276(6), 99.075(6) | 91.976(16), 100.361(17), 93.085(16) | 90, 90.143(6), 90 |
| $V$ (Å$^3$) | 3713.4(3) | 8148.9(6) | 4483.8(9) | 4035.7(5) | 1351.2(5) | 2761.7(3) |
| $Z$ | 2 | 8 | 4 | 4 | 2 | 4 |
| $D_{calcd}$ (Mg/m$^3$) | 1.647 | 1.769 | 1.5545 | 1.637 | 1.686 | 1.869 |
| Absorption coefficient (mm$^{-1}$) | 4.731 | 5.074 | 4.607 | 4.488 | 5.438 | 6.342 |
| θ range of data collection | 2.378 to 29.437° | 1.670 to 26.857° | 3.24 to 51.9° | 1.785 to 26.877° | 2.263 to 26.921° | 2.013 to 26.880° |
| Limiting Indices | $-19 \le h \le 20$, $-21 \le k \le 21$, $-23 \le l \le 23$ | $-23 \le h \le 23$, $-22 \le k \le 22$, $-31 \le l \le 31$ | $-15 \le h \le 15$, $-18 \le k \le 18$, $-28 \le l \le 28$ | $-18 \le h \le 18$, $-19 \le k \le 19$, $-24 \le l \le 24$ | $-11 \le h \le 11$, $-10 \le k \le 10$, $-23 \le l \le 23$ | $-17 \le h \le 17$, $-18 \le k \le 18$, $-17 \le l \le 17$ |
| Reflections collected / unique (> 2σ(I)) | 69011 / 20225 [R(int) = 0.0947] | 59033 / 8661 [R(int) = 0.0761] | 61413 / 8745 [R(int)= 0.2093] | 59011 / 17141 [R(int) = 0.1246] | 19804 / 5744 [R(int) = 0.1453] | 39125 / 5861 [R(int) = 0.0894] |
| Data / Restraints / Parameter | 20225 / 0 / 795 | 8661 / 0 / 434 | 8745 / 0 / 411 | 17141 / 0 / 833 | 5744 / 0 / 297 | 5861 / 0 / 298 |
| R (I>2σ(I)) | $R_1 = 0.0411$, $\omega R_2 = 0.0847$ | $R_1 = 0.0282$, $\omega R_2 = 0.0556$ | $R_1 = 0.0588$, $\omega R_2 = 0.1360$ | $R_1 = 0.0504$, $\omega R_2 = 0.0866$ | $R_1 = 0.0582$, $\omega R_2 = 0.1138$ | $R_1 = 0.0369$, $\omega R_2 = 0.0815$ |
| $R_W$ (all data) | $R_1 = 0.0691$, $\omega R_2 = 0.0914$ | $R_1 = 0.0406$, $\omega R_2 = 0.0582$ | $R_1 = 0.0717$, $\omega R_2 = 0.1450$ | $R_1 = 0.1003$, $\omega R_2 = 0.0977$ | $R_1 = 0.0876$, $\omega R_2 = 0.1233$ | $R_1 = 0.0432$, $\omega R_2 = 0.0834$ |
| GooF (all data) | 0.881 | 0.983 | 0.940 | 0.900 | 1.068 | 1.025 |
| Max. and min. res. dens. (eA$^{-3}$) | 1.946 and -2.655 | 1.080 and -1.821 | 2.5681 and -3.0695 | 2.091 and -1.995 | 2.128 and -1.623 | 2.186 and -2.014 |

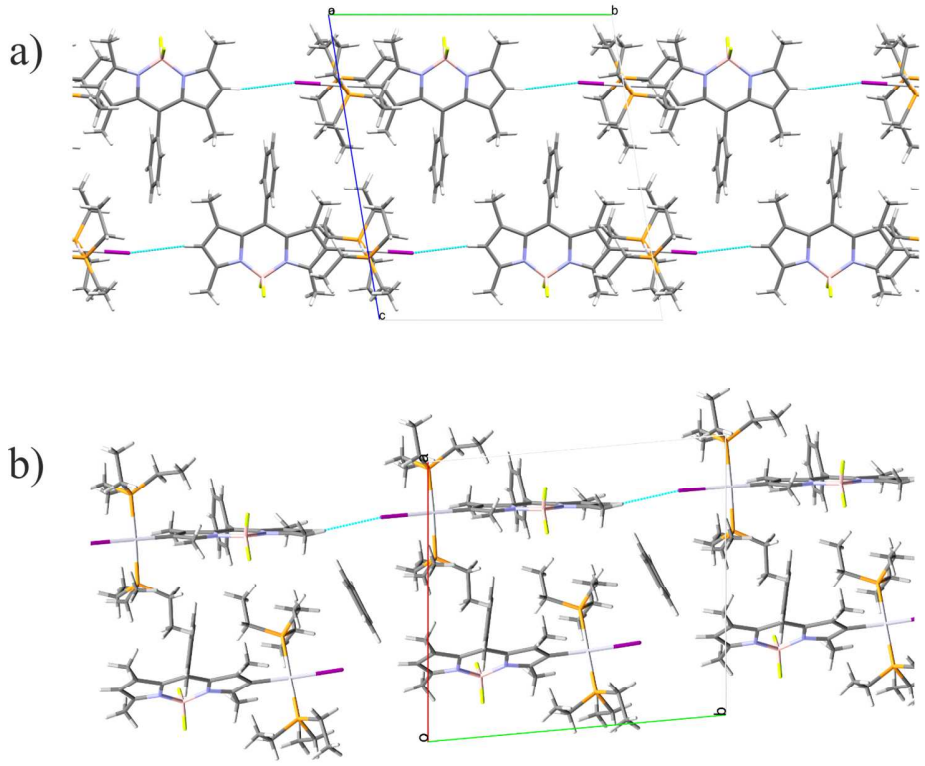


**Figure S31.** View along the crystallographic (a) *a*- and (b) *c*-axis displaying chains of **2-Pt-6H** molecules formed by I···H contacts of 3.178 Å.

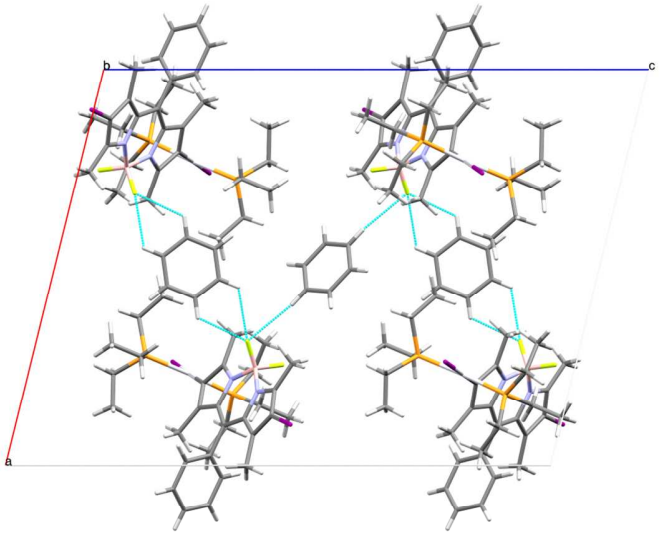

**Figure S32.** View along the crystallographic *a*-axis of the benzene monosolvate of **2-Pt-6I** displaying short H···F contacts of 2.537, 2.571 and 2.658 Å.

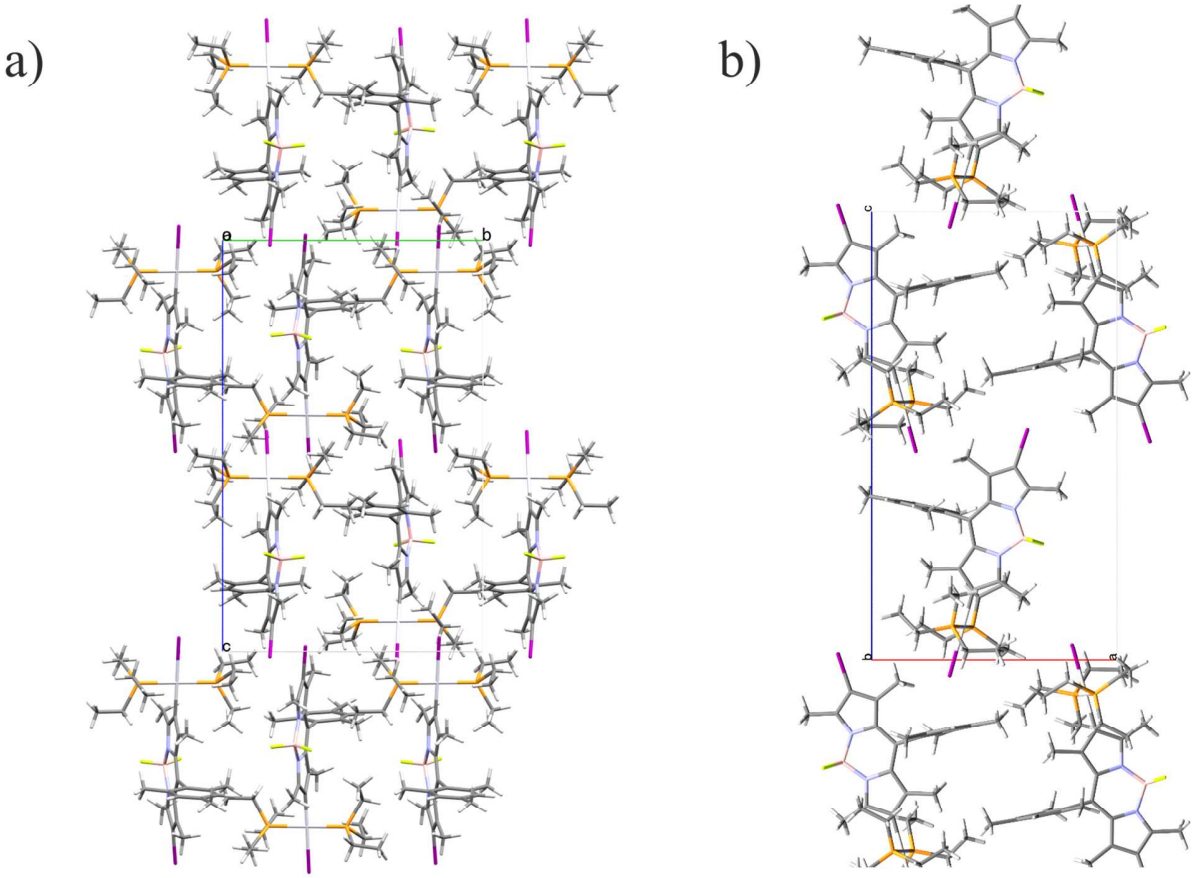


**Figure S33.** Packing of **2-Pt-Mes-6I** along the crystallographic (a) *a*- and (b) *b*-axis.

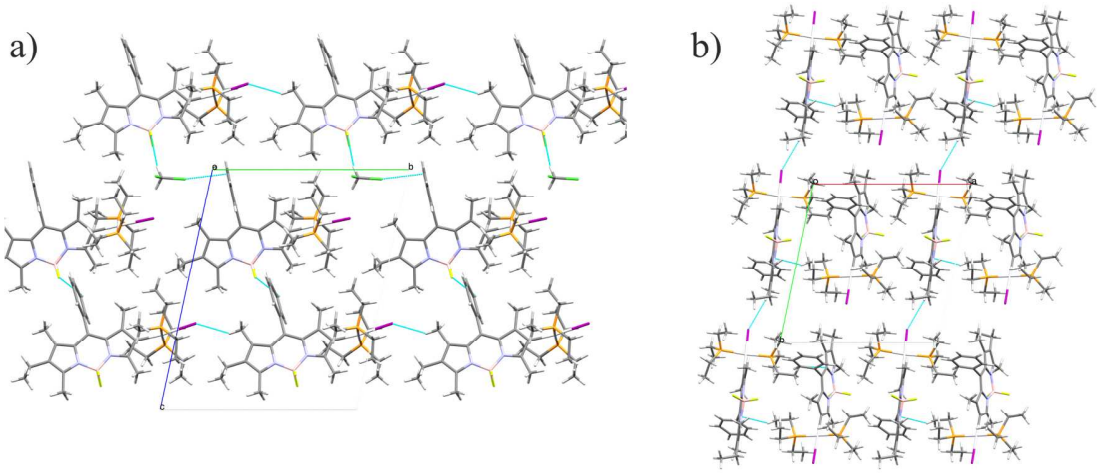


**Figure S34.** View along the crystallographic (a) *a*- and (b) *c*-axis revealing attractive interactions between molecules of **2-Pt-6Et** and cocrystallized $CH_2Cl_2$ solvent. Short contact H···I (3.171 Å), H···F (2.480 Å), H···Cl (3.356 Å) and H···N (2.677 Å).

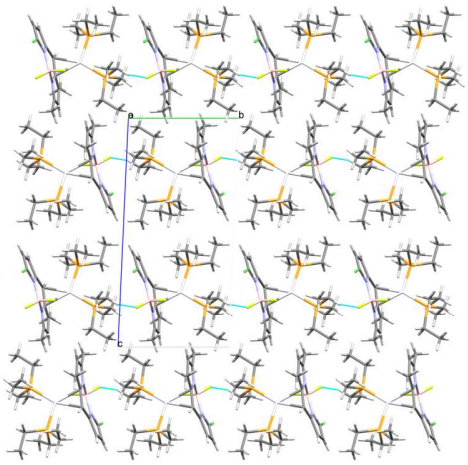

**Figure S35.** Packing of **8,9-Pt** displayed along the crystallographic *c*-axis with short H···F contacts of 2.573 Å.

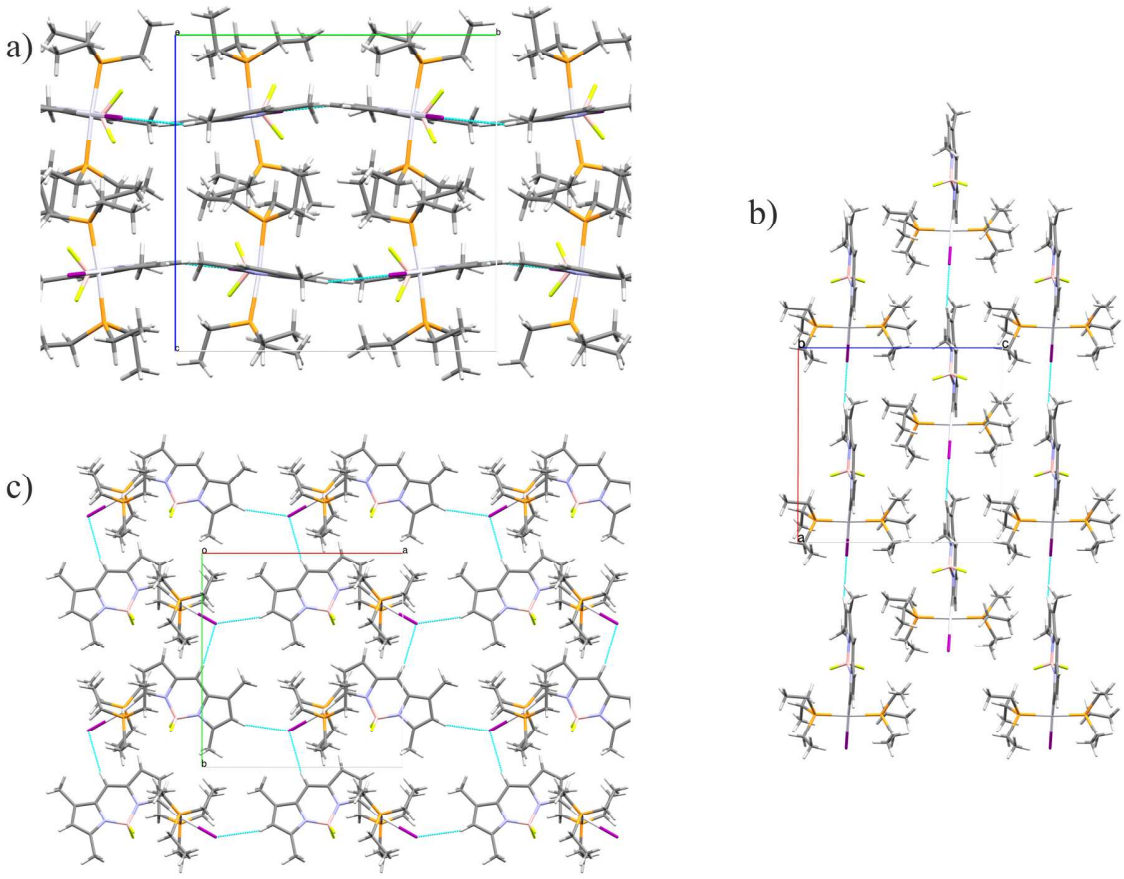


**Figure S36.** Projections on the crystallographic (a) a-, (b) b- and (c) c-axis of **3-Pt** displaying H···I contacts (3.005 and 3.048 Å).

## Electronic Absorption Spectroscopy

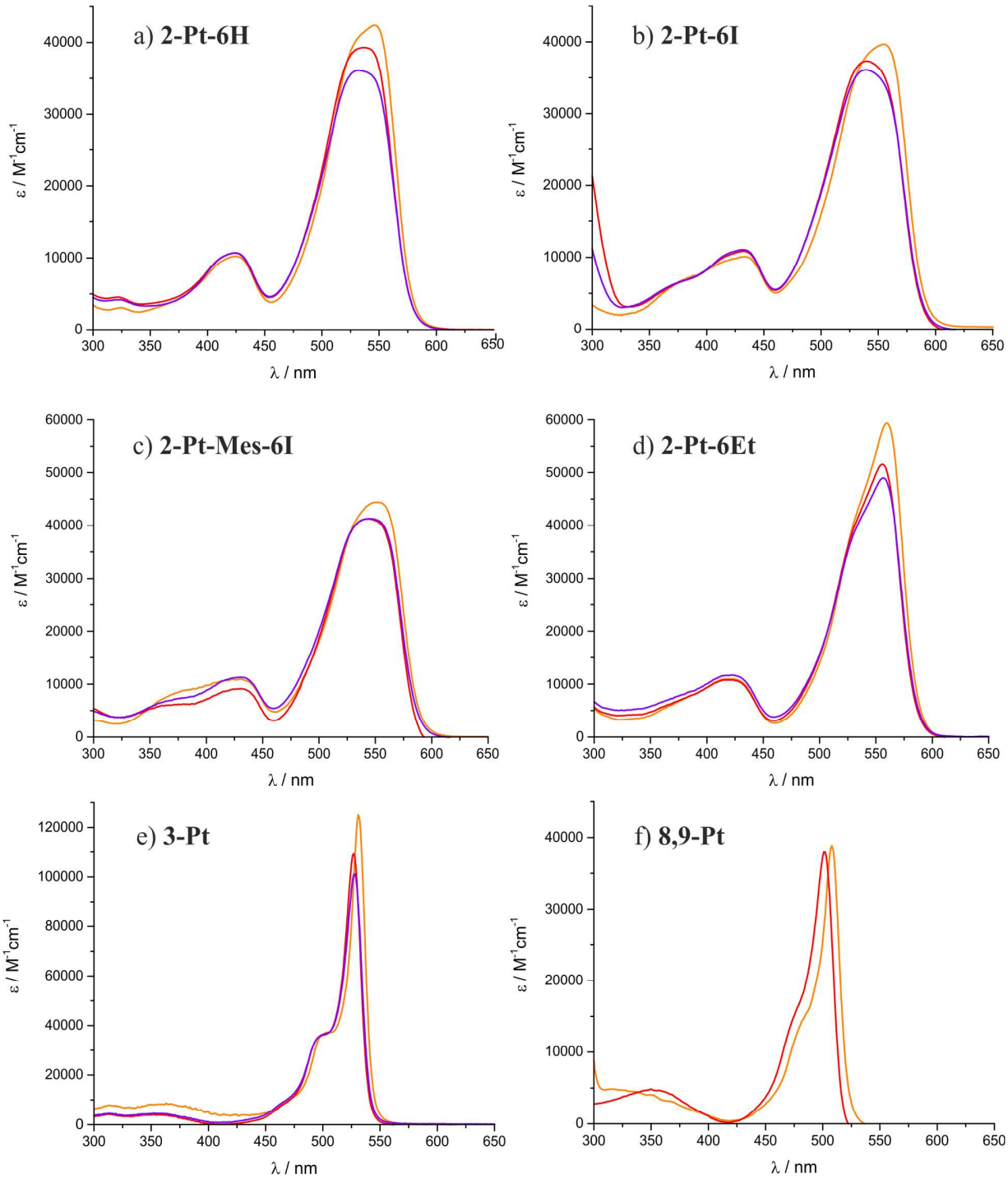


**Figure S37.** Electronic Absorption Spectra of (a) **2-Pt-6H**, (b) **2-Pt-6I**, (c) **2-Pt-Mes-6I**, (d) **2-Pt-6Et**, (e) **3-Pt** and (f) **8,9-Pt** in $CH_2Cl_2$ (*violet*), toluene (*orange*) and THF (*red*) at concentrations of ca. $10^{-5}$ M.

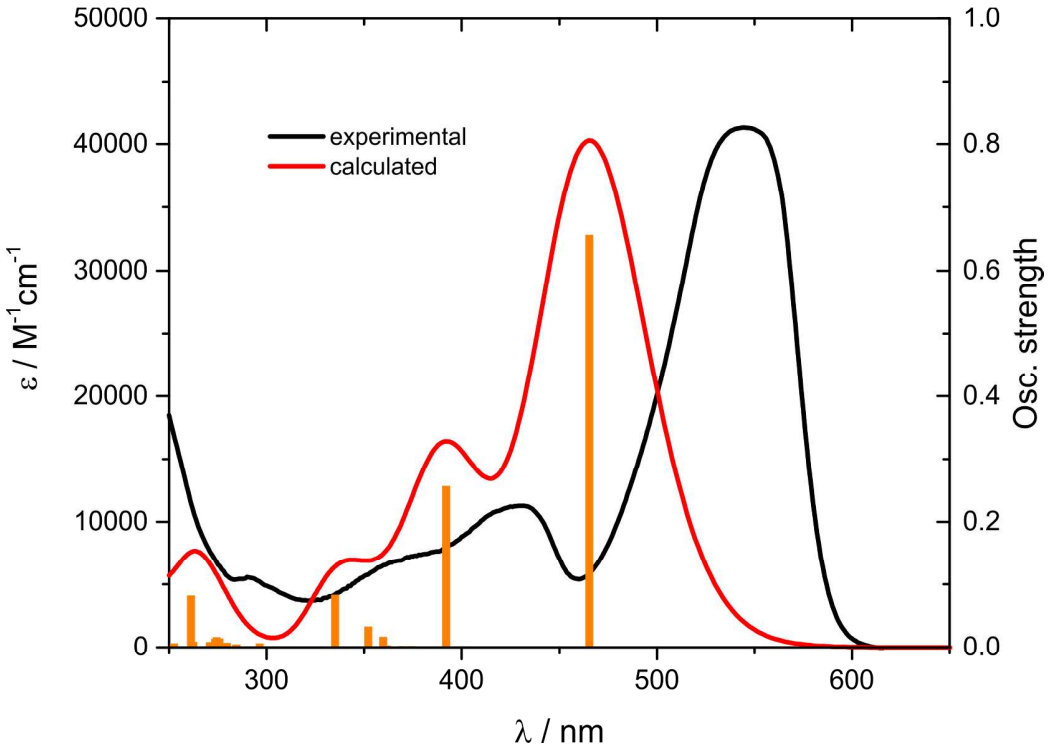


**Figure S38.** Comparison of calculated (*red*, *orange*) and experimental (*black*) absorption data of **2-Pt-Mes-6I** in $CH_2Cl_2$.

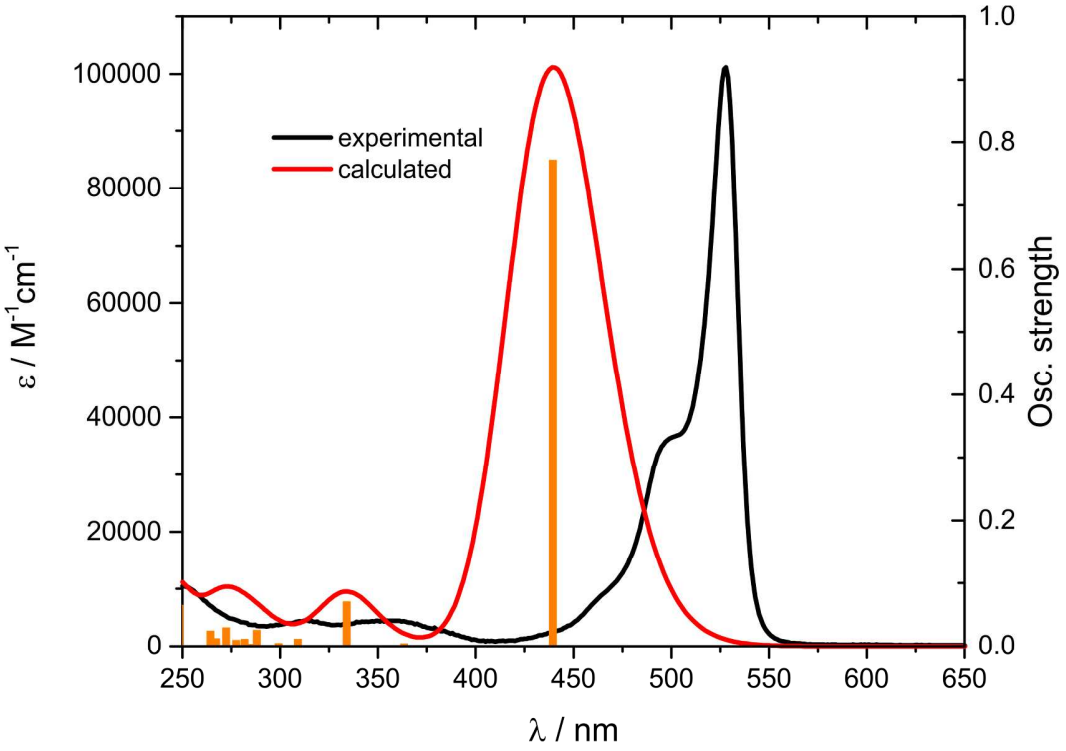


**Figure S39.** Comparison of calculated (*red*, *orange*) and experimental (*black*) absorption data of **3-Pt** in $CH_2Cl_2$.

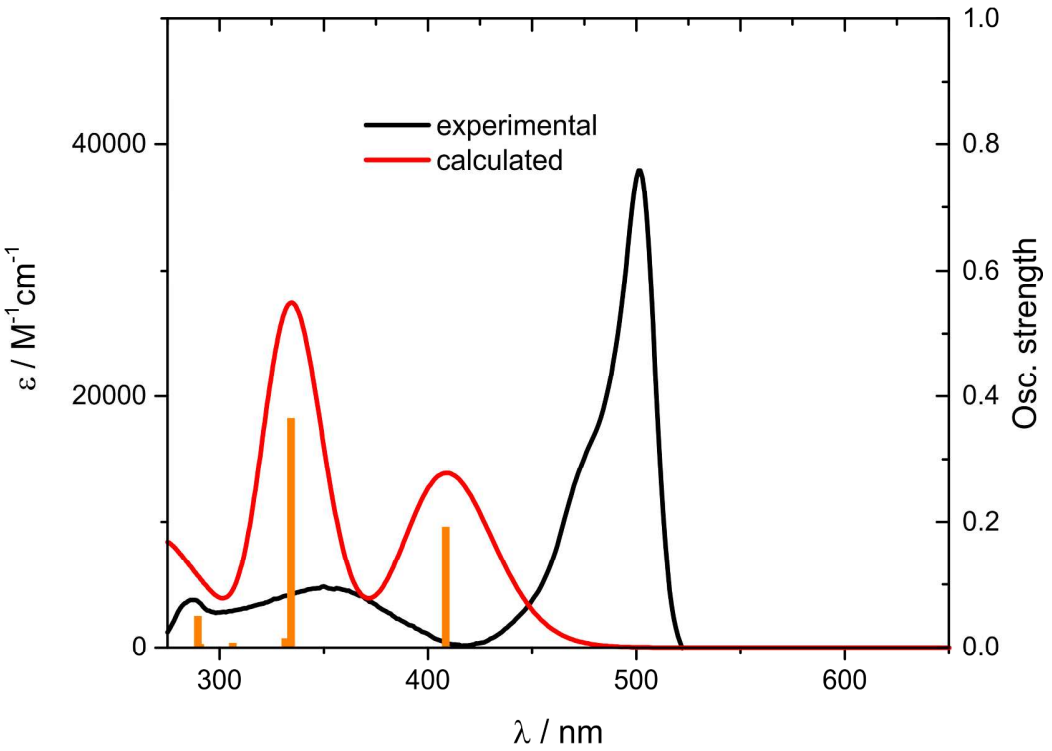


**Figure S40.** Comparison of calculated (*red*, *orange*, $CH_2Cl_2$) and experimental (*black*, THF) absorption data of **8,9-Pt**.

## Quantum Chemical Calculations on the Neutral Complexes

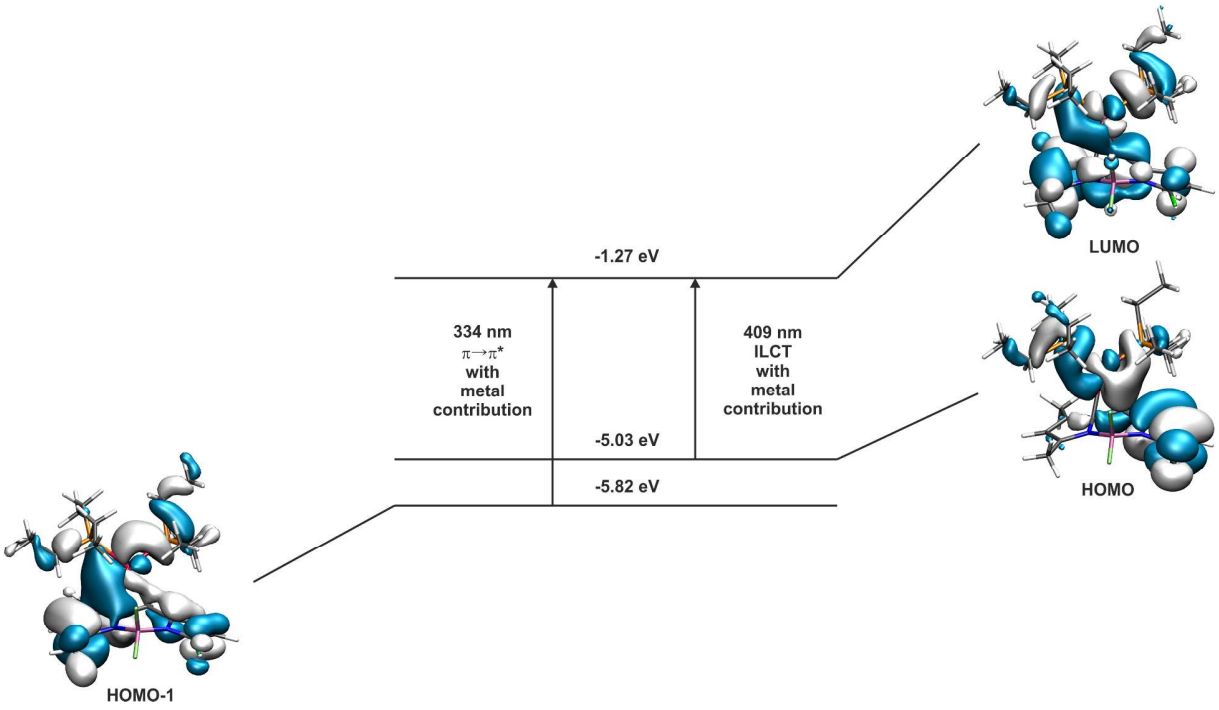


**Figure S41.** Graphical representation of the relevant MOs and TD-DFT energies of **8,9-Pt** in the neutral form. Solid arrows symbolize the main contributor to the respective transition.

**Table S2.** Calculated Mulliken parameters of **8,9-Pt** in the neutral form. Contributions of the given fragments are given in percent.

| | Pt | bodipy | $PEt_3$ |
|---|---|---|---|
| LUMO | 19 | 63 | 18 |
| HOMO | 10 | 75 | 16 |
| HOMO-1 | 19 | 60 | 21 |

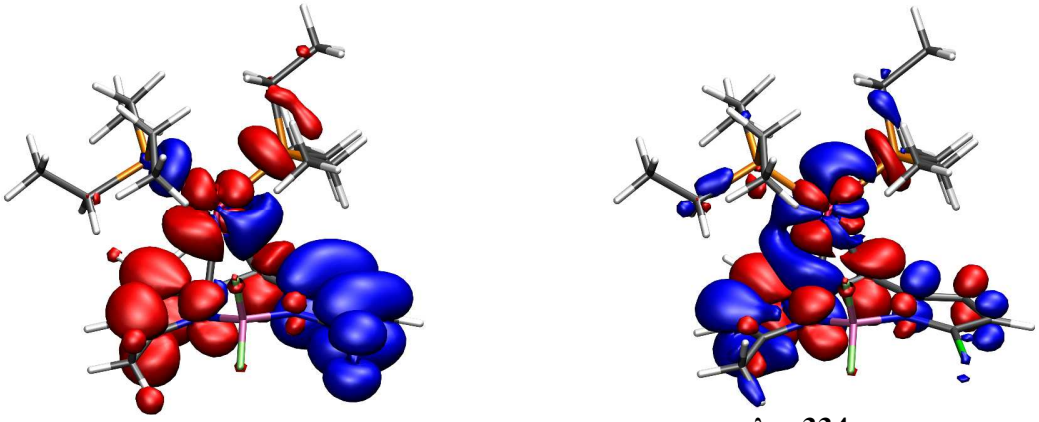


**Figure S42.** Electron Density Difference Maps (EDDMs) for the calculated transitions (blue = electron density loss, red = electron density gain) in the neutral form of **8,9-Pt** calculated on the PBE1PBE/6-31G(d) level.

**Table S3.** Calculated Mulliken parameters of **2-Pt-Mes-6I** in the neutral form. Contributions of the given fragments are given in percent.

| | Pt | bodipy | $PEt_3$ | I |
|---|---|---|---|---|
| LUMO | 1 | 98 | 1 | 0 |
| HOMO | 5 | 92 | 3 | 1 |
| HOMO-1 | 14 | 36 | 3 | 47 |
| HOMO-3 | 1 | 50 | 19 | 30 |
| HOMO-5 | 1 | 95 | 3 | 1 |
| HOMO-7 | 0 | 100 | 0 | 0 |
| HOMO-13 | 12 | 51 | 29 | 8 |

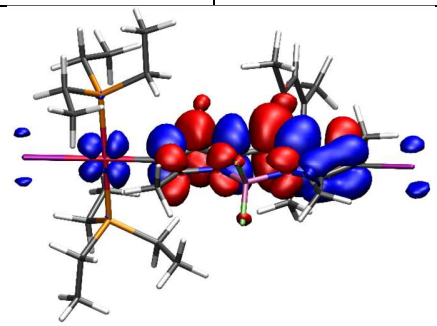

**λ = 465 nm**

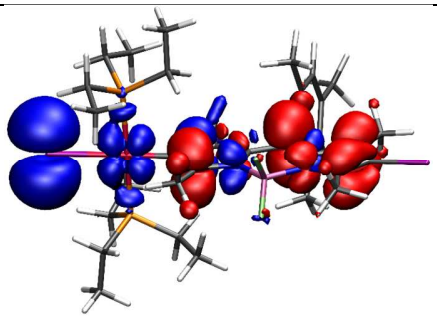

**λ = 392 nm**

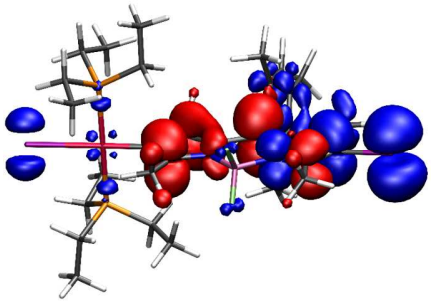

**λ = 352 nm**

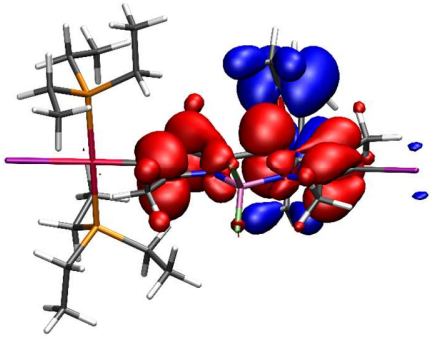

**λ = 335 nm**

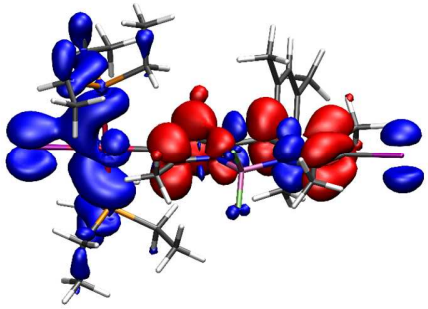

**λ = 261 nm**

**Figure S43.** Electron Density Difference Maps (EDDMs) for the calculated transitions (*blue* = electron density loss, *red* = electron density gain) in the neutral form of **2-Pt-Mes-6I** calculated on the PBE1PBE/6-31G(d) level.

**Table S4.** Calculated Mulliken parameters of **3-Pt** in the neutral form. Contributions of the given fragments are given in percent.

| | Pt | bodipy | $PEt_3$ | I |
|---|---|---|---|---|
| LUMO | 2 | 97 | 1 | 0 |
| HOMO | 5 | 91 | 3 | 1 |
| HOMO-4 | 0 | 100 | 0 | 0 |
| HOMO-10 | 26 | 39 | 26 | 9 |

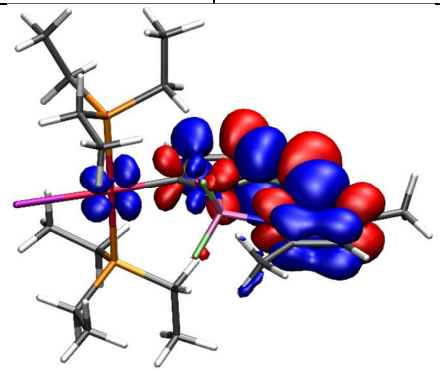

**λ = 439 nm**

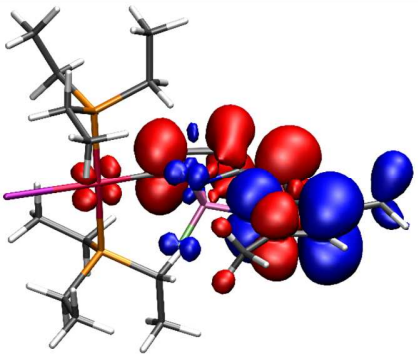

**λ = 334 nm**

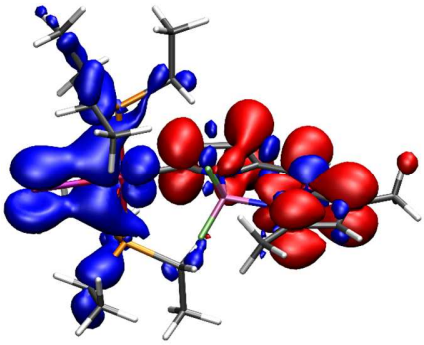

**λ = 248 nm**

**Figure S44.** EDDMs for the calculated transitions (blue = electron density loss, red = electron density gain) in the neutral form of **3-Pt** calculated on the PBE1PBE/6-31G(d) level of theory.

## Luminescence Spectroscopy

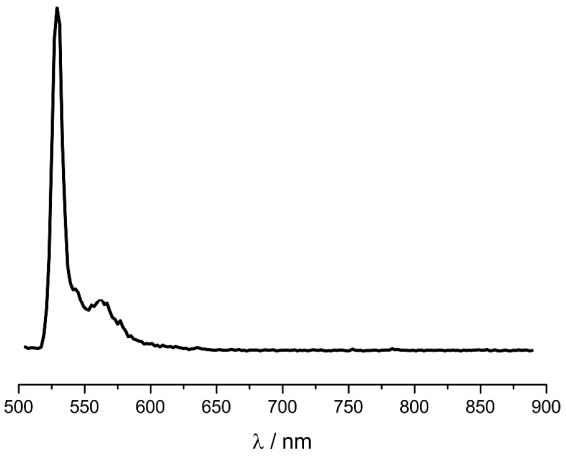


**Figure S45.** Luminescence spectrum of **3-Pt** in 2-MeTHF at 77K.

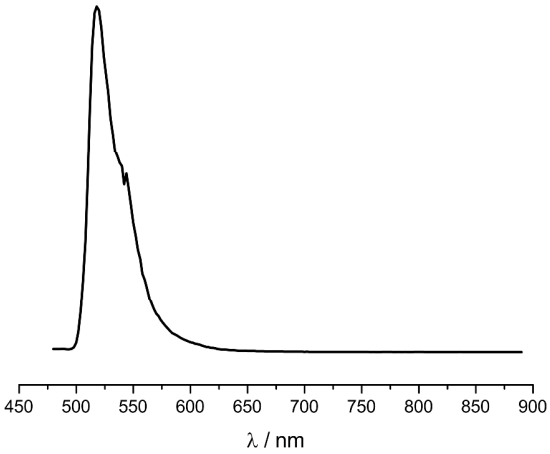


**Figure S46.** Luminescence spectrum of **8,9-Pt** in toluene at 77K.

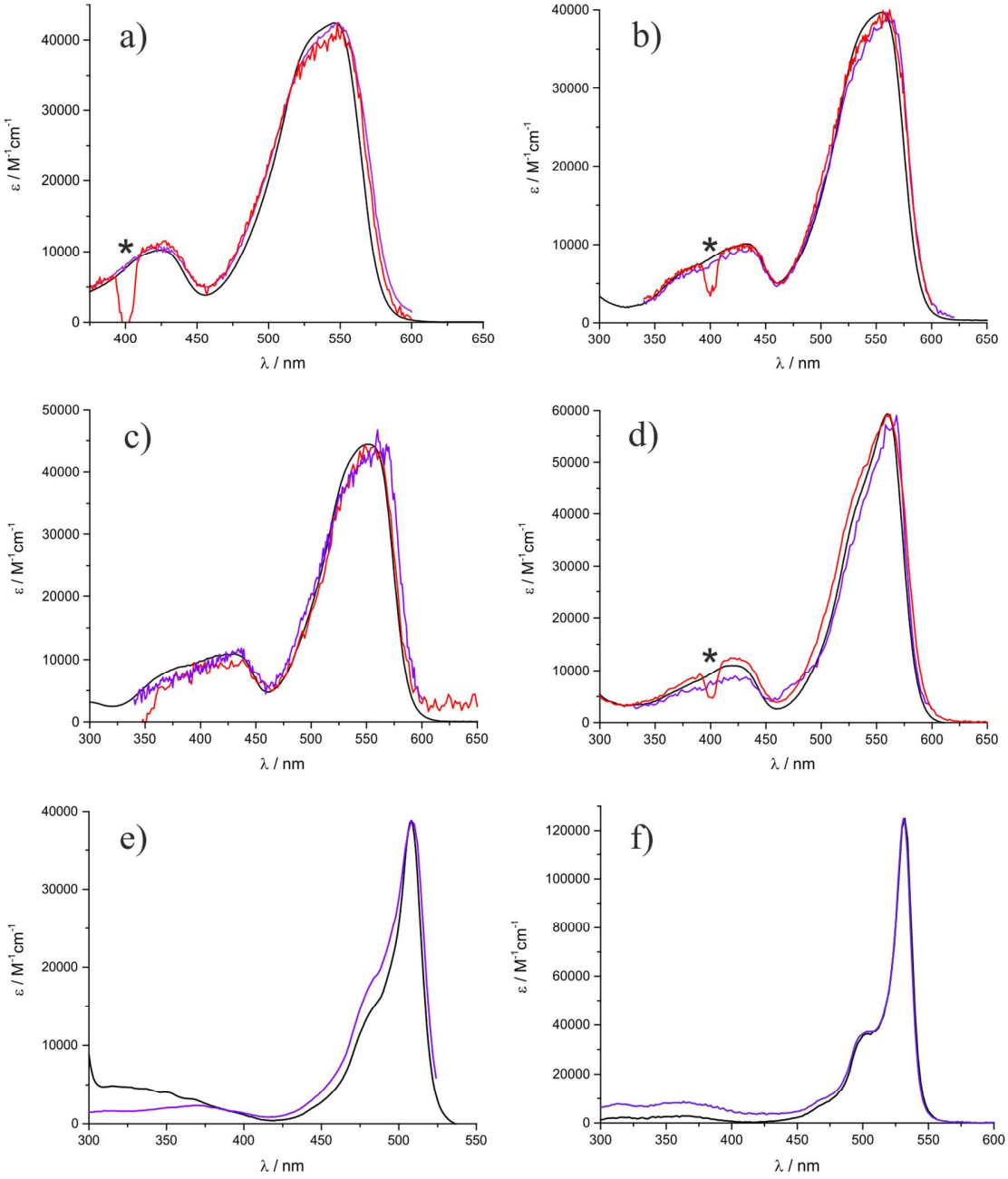


**Figure S47.** Comparison of excitation spectra (*purple* is detected at the fluorescence and *red* at the phosphorescence emission) with the absorption spectrum (*black*) for (a) **2-Pt-6H**, (b) **2-Pt-6I**, (c) **2-Pt-Mes-6I**, (d) **2-Pt-6Et**, (e) **8,9-Pt** and (f) **3-Pt**. * marks an artefact due to the 2nd order of the detection wavelength.

**Table S5.** Spin density contribution of the respective fragment to the spin density surfaces in the triplet states of **2-Pt-Mes-6I**, **3-Pt** and **8-Pt.**[1]

| Compound | **2-Pt-Mes-6I** | **3-Pt** | **8-Pt** |
|---|---|---|---|
| Pt | 0.021 | 0.028 | 0.009 |
| $PEt_3$ | 0.017 | 0.028 | 0.019 |
| I | -0.001 | -0.004 | -0.006 |
| BODIPY | 1.960 | 1.950 | 1.978 |

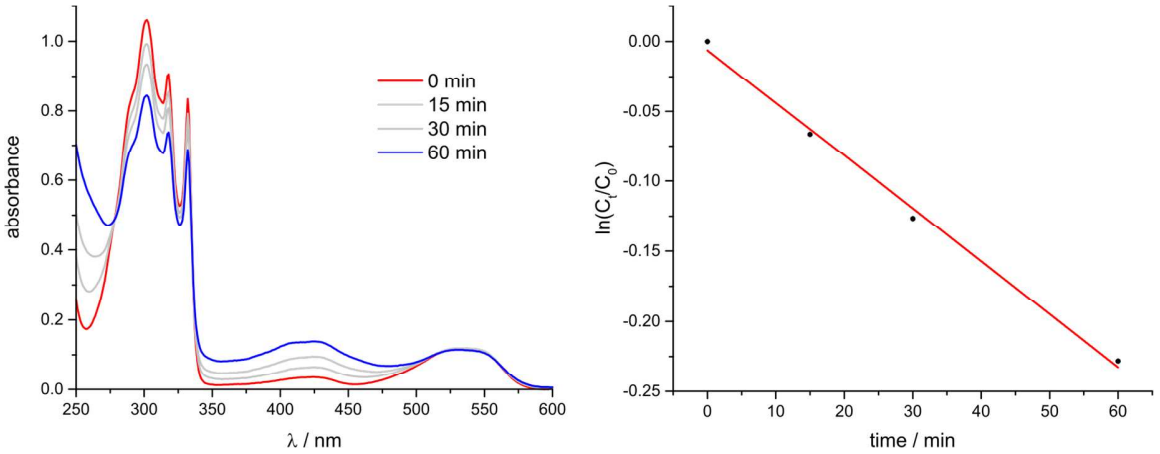


**Figure S48.** Spectral change upon irradiation of a DHN solution containing **2-Pt-6H** as a sensitizer (left) and plot of $\ln(C_t/C_0)$ vs. irradiation time (right hand side).

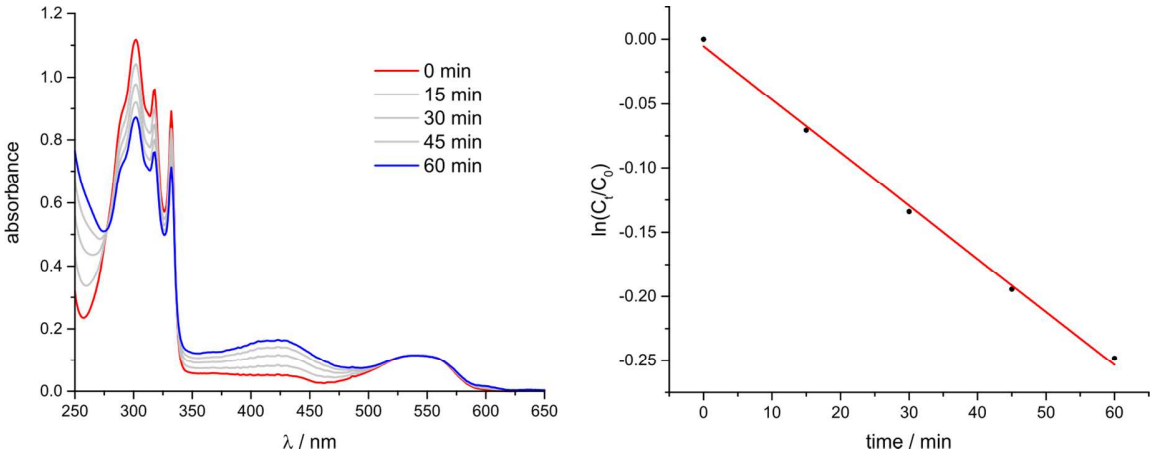


**Figure S49.** Spectral change upon irradiation of a DHN solution containing **2-Pt-6I** as a sensitizer (left) and plot of $\ln(C_t/C_0)$ vs. irradiation time (right hand side).

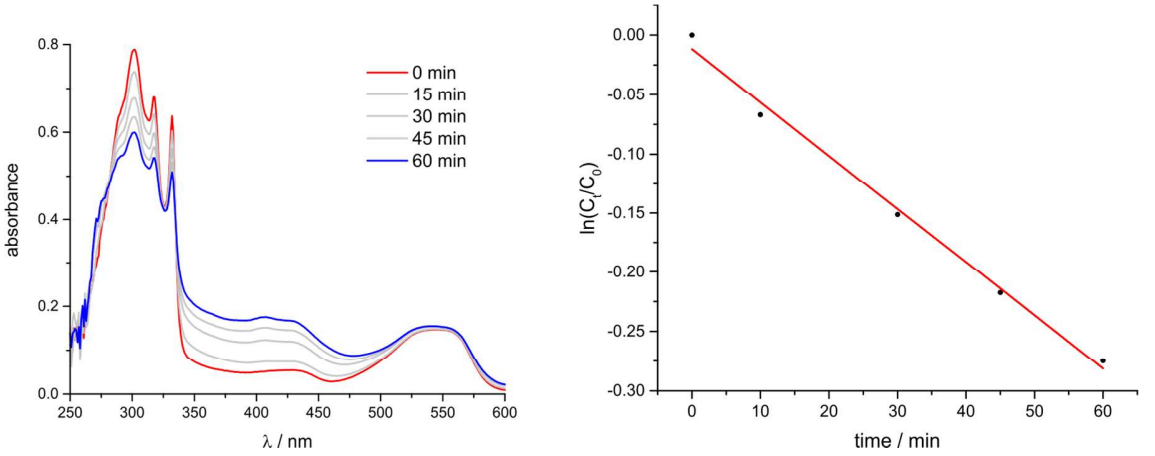


**Figure S50.** Spectral change upon irradiation of a DHN solution containing **2-Pt-Mes-6I** as a sensitizer (left) and plot of $\ln(C_t/C_0)$ vs. irradiation time (right hand side).

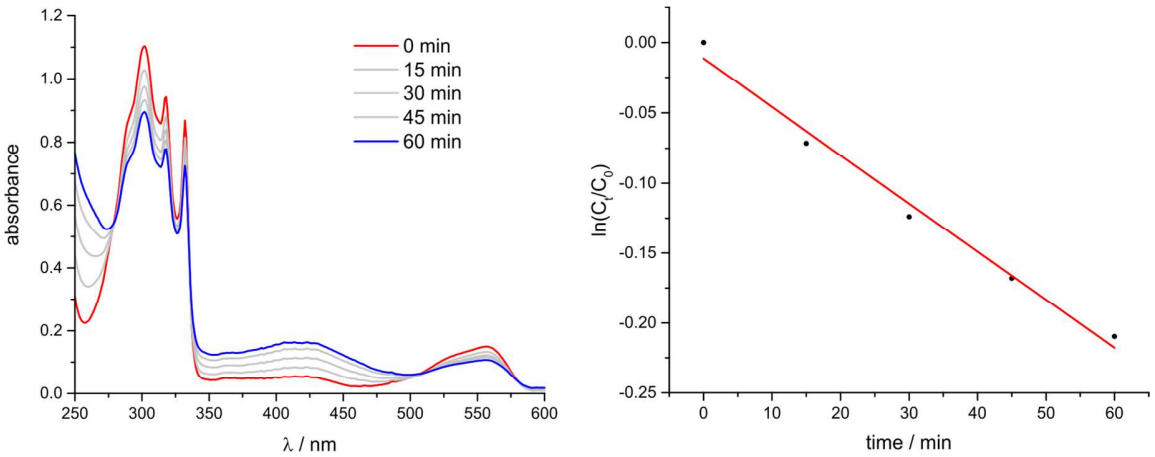


**Figure S51.** Spectral change upon irradiation of a DHN solution containing **2-Pt-6Et** as a sensitizer (left) and plot of $\ln(C_t/C_0)$ vs. irradiation time (right hand side).

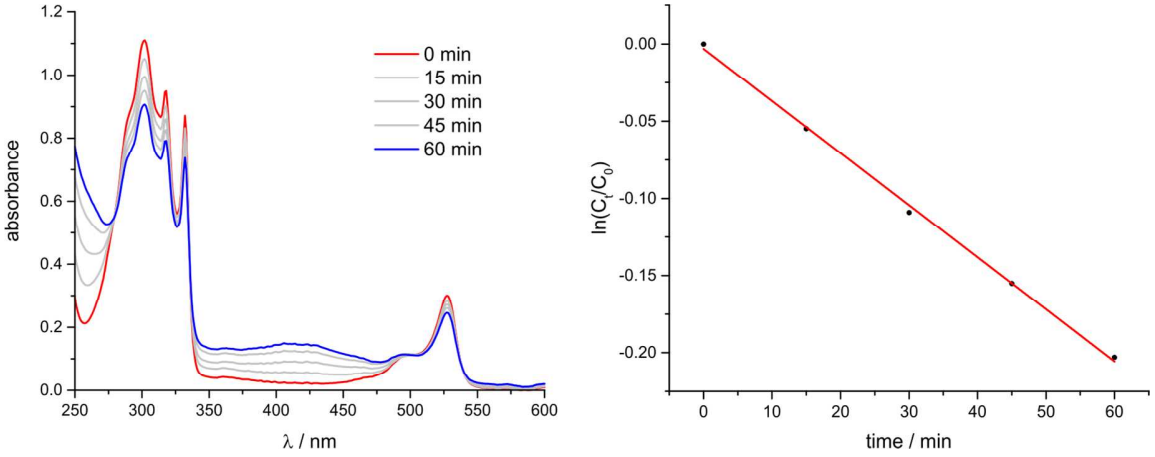


**Figure S52.** Spectral change upon irradiation of a DHN solution containing **3-Pt** as a sensitizer (left) and plot of $\ln(C_t/C_0)$ vs. irradiation time (right hand side).

## Stern-Volmer quenching experiments

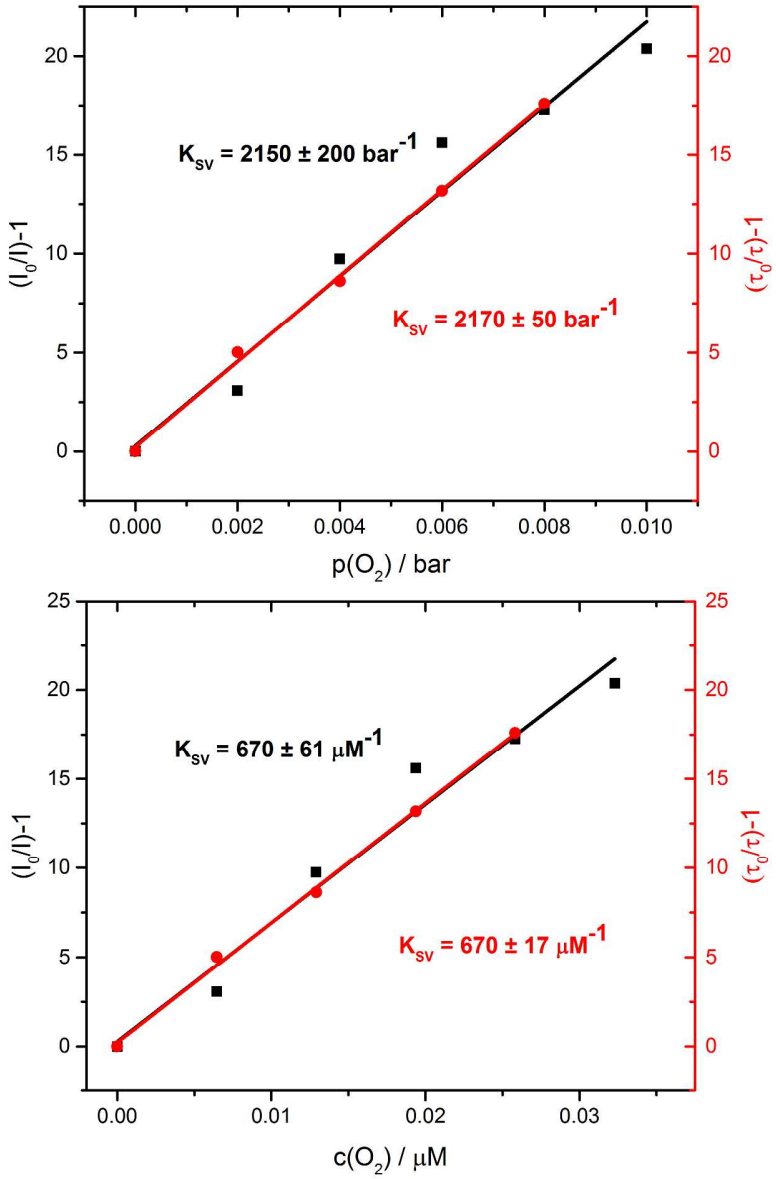


**Figure S53.** Stern-Volmer plot of **2-Pt-Mes-6I** using $O_2$ as a quencher.

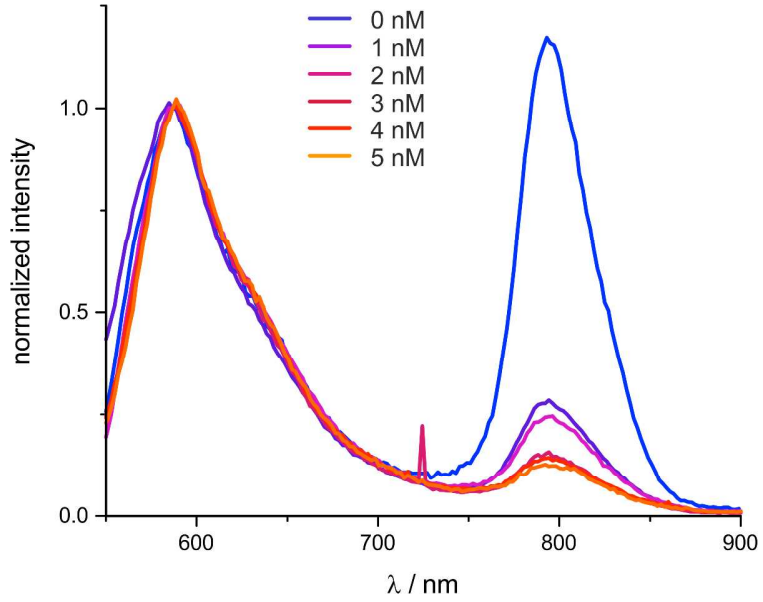


**Figure S54.** Stacked luminescence spectra of **2-Pt-Mes-6I** at different oxygen concentrations.

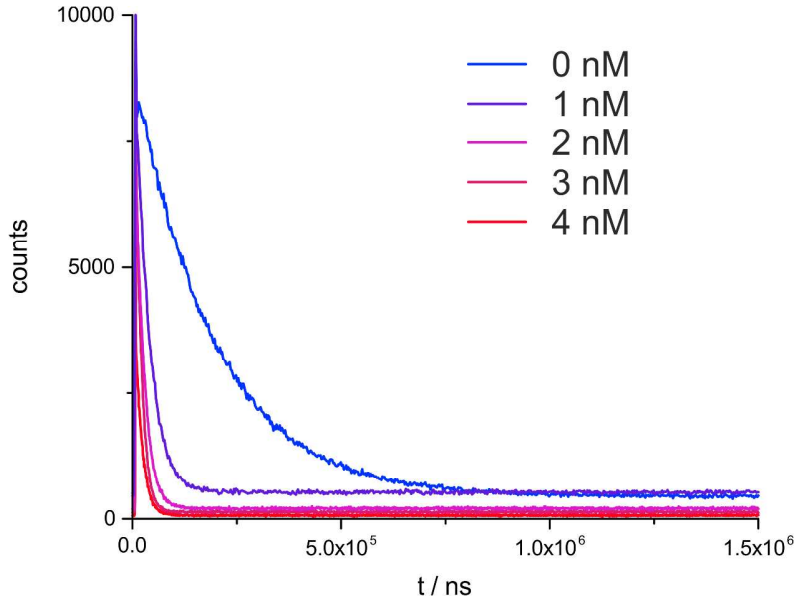


**Figure S55.** Stacked luminescence decays of **2-Pt-Mes-6I** monitored at 800 nm for different oxygen concentrations.

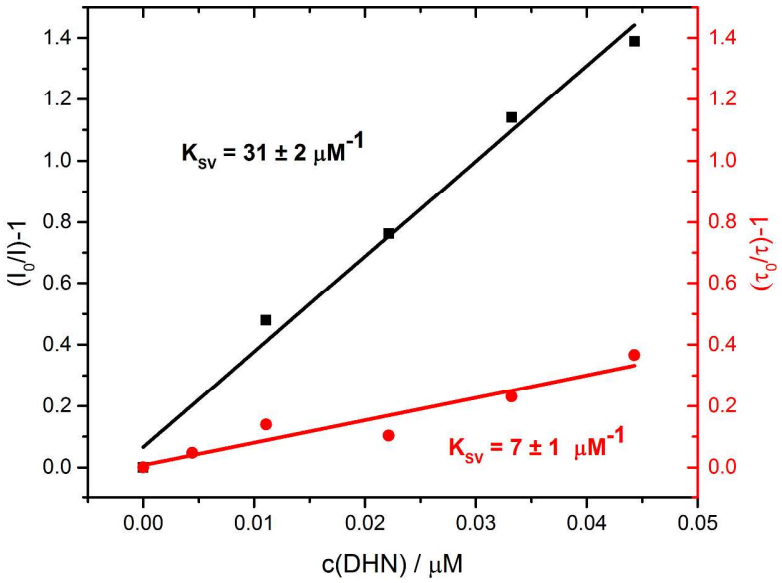


**Figure S56.** Stern-Volmer plot of **2-Pt-Mes-6I** using 1,5-dihydroxynaphthalene (DHN) as a quencher.

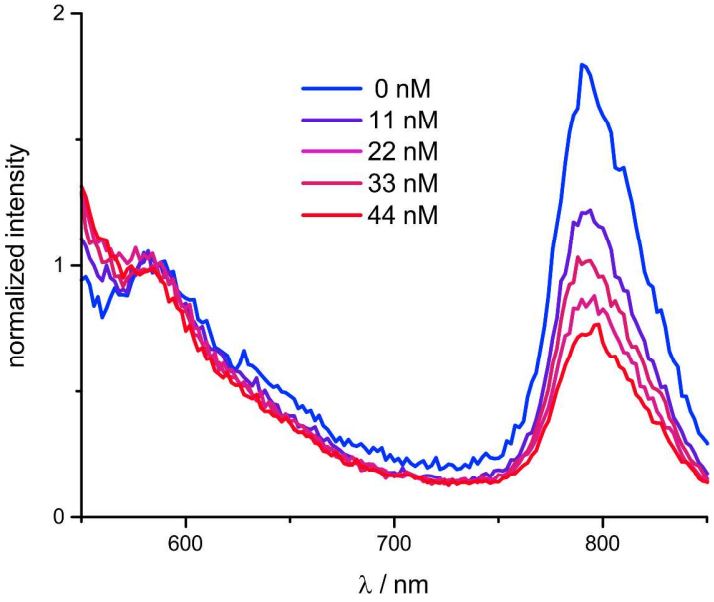


**Figure S57.** Stacked luminescence spectra of **2-Pt-Mes-6I** at different DHN concentrations.

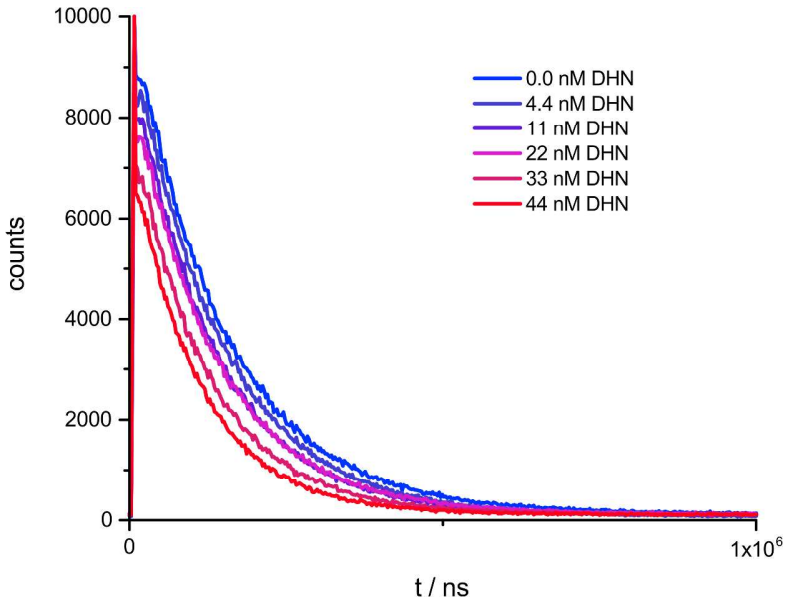


**Figure S58.** Stacked luminescence decays of **2-Pt-Mes-6I** monitored at 797 nm for different DHN concentrations.

**Table S6.** Relevant electrochemical data for the oxidation of 1,5-dihydroxynaphthalene in the ground and excited state.

| | $\lambda_{max,Ph}$ / nm | $E^*(T_1S_0)$ / eV | $E_{1/2}$(reduction) / V | $E^*$(reduction)[a] / V | $\Delta G_{ET}$[b] / eV |
|---|---|---|---|---|---|
| **8-Pt** | 641 | 1.93 | -1.77 | 0.16 | 0.55 |
| **2-Pt-6H** | 804 | 1.54 | -1.92 | -0.38 | 1.09 |
| **2-Pt-6I** | 804 | 1.54 | -1.81 | -0.27 | 0.98 |
| **2-Pt-Mes-6I** | 797 | 1.56 | -1.86 | -0.30 | 1.01 |
| **2-Pt-6Et** | 815 | 1.52 | -1.96 | -0.44 | 1.15 |

[a]Excited state redox potential was derived from $E^* = E_{1/2}+E^*(T_1S_0)$. [b]Estimated from the Rehm-Weller equation. $\Delta G_{ET} = E_{1/2}(\text{reduction})-E_{1/2}(\text{DHN})-e_0^2/(4\pi\varepsilon_0\varepsilon(CH_2Cl_2)r)-E^*(T_1S_0)$ with $E_{1/2}$ (DHN) = 0.705 V. As the Coulomb term is small for polar solvents, it is neglected for this estimation.

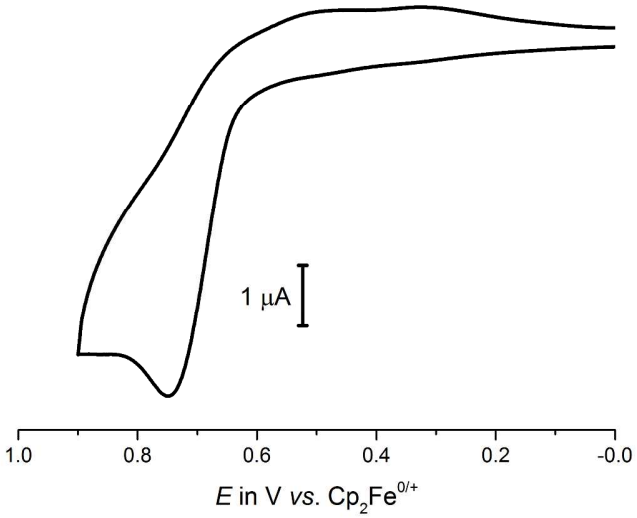


**Figure S59.** Cyclic voltammogram of 1,5-dihydroxynaphthalene (DHN) in $CH_2Cl_2$ at T = 293 K with $NBu_4PF_6$ as supporting electrolyte ($\nu$ = 100 mV/s).

## Electrochemistry

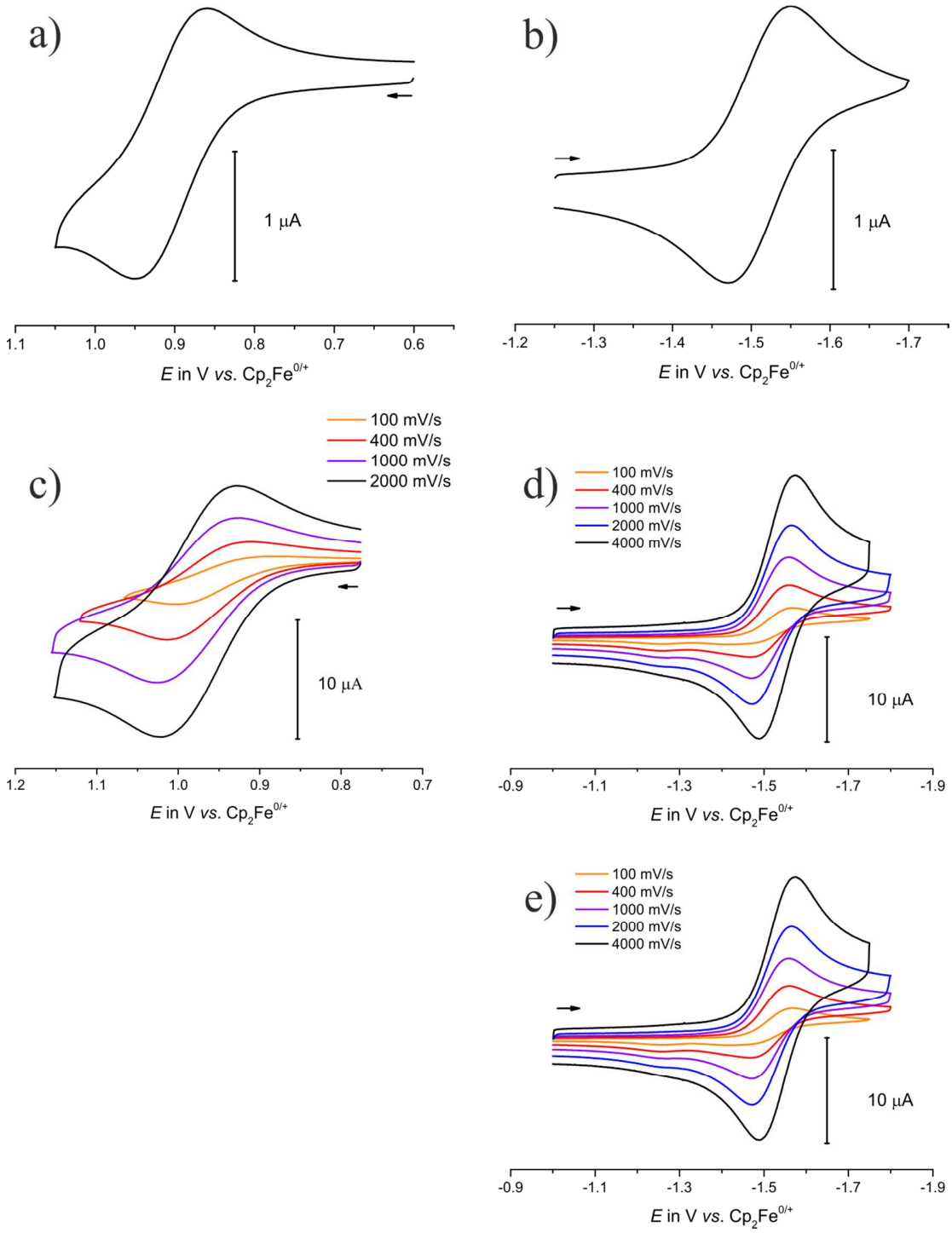


**Figure S60.** Cyclic voltammograms for the anodic (left) and cathodic (right) sweeps of (a,b) 8-mesityl-2,6-diiodo-bodipy ($v$ = 100 mV/s), (c,d) 3-Cl-5,7-$Et_2$-bodipy and (e) 8-Br-bodipy in $CH_2Cl_2$ at T = 293 K with $NBu_4PF_6$ as supporting electrolyte.

## UV/Vis/NIR Spectroelectrochemistry

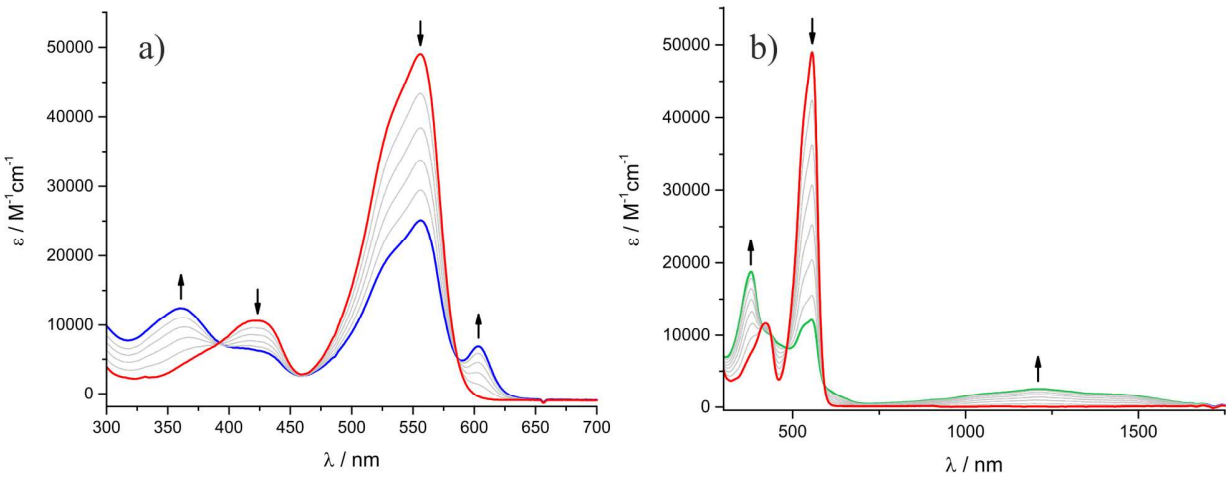


**Figure S61.** Changes of the UV/Vis/NIR spectrum (1,2-$C_2H_4Cl_2$, $NBu_4PF_6$, T= 293 K) of **2-Pt-6Et** during the (a) reduction (red to blue) and (b) oxidation (red to green).

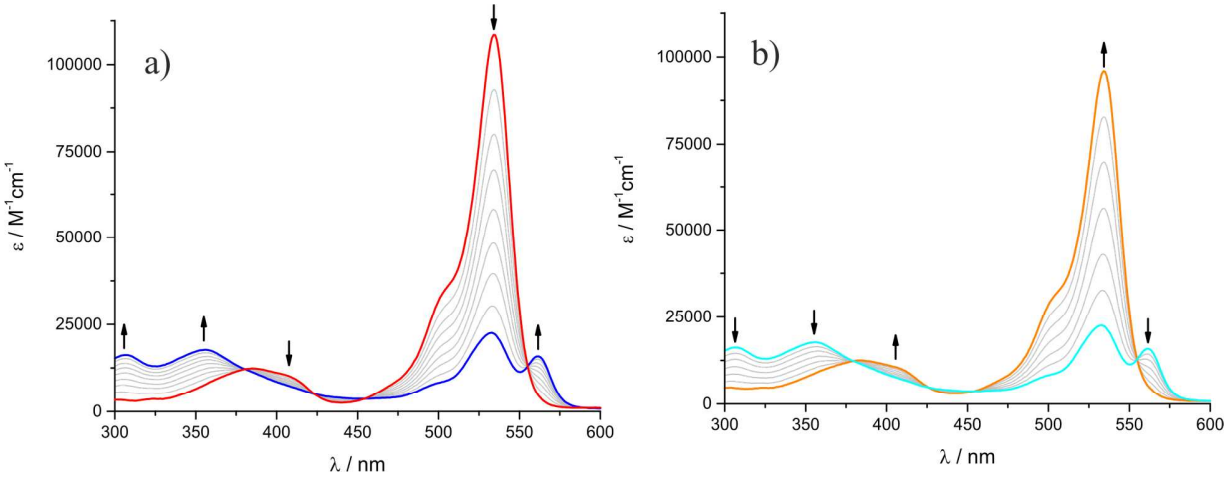


**Figure S62.** Changes of the UV/Vis/NIR spectrum (1,2-$C_2H_4Cl_2$, $NBu_4PF_6$, T= 293 K) of 8-mesityl-2,6-diiodo-bodipy during the (a) reduction (red to blue) and (b) re-oxidation (cyan to orange).

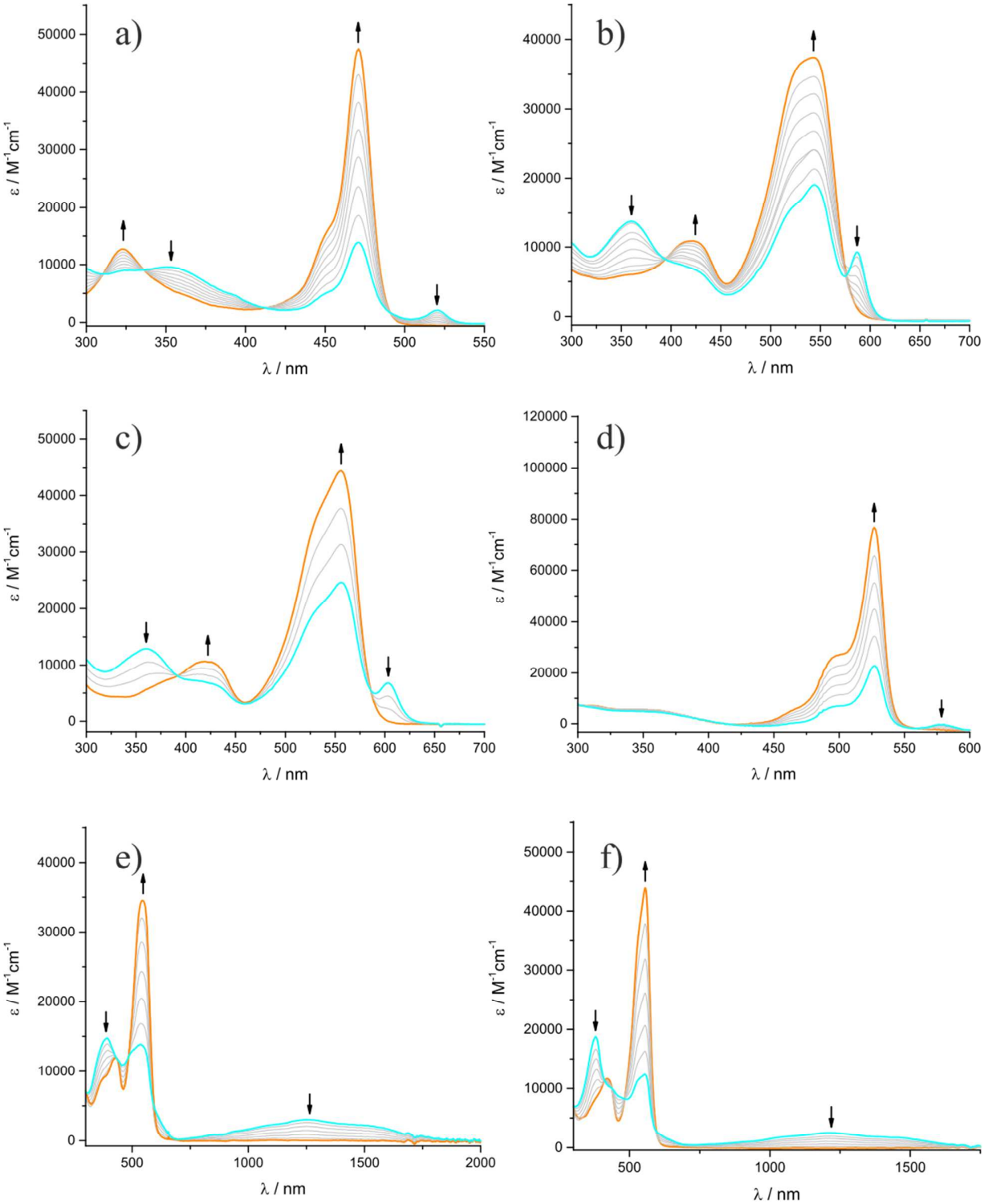


**Figure S63.** Changes of the UV/Vis/NIR spectra (1,2-$C_2H_4Cl_2$, $NBu_4PF_6$, T= 293 K) upon re-oxidation (a-d) or re-reduction (e,f) of (a) **8-Pt**, (b) **2-Pt-Mes-6I**, (c) **2-Pt-6Et**, (d) **3-Pt**, (e) **2-Pt-Mes-6I** and (f) **2-Pt-6Et.**

## Quantum Chemical Calculations on the Oxidized and Reduced Complexes

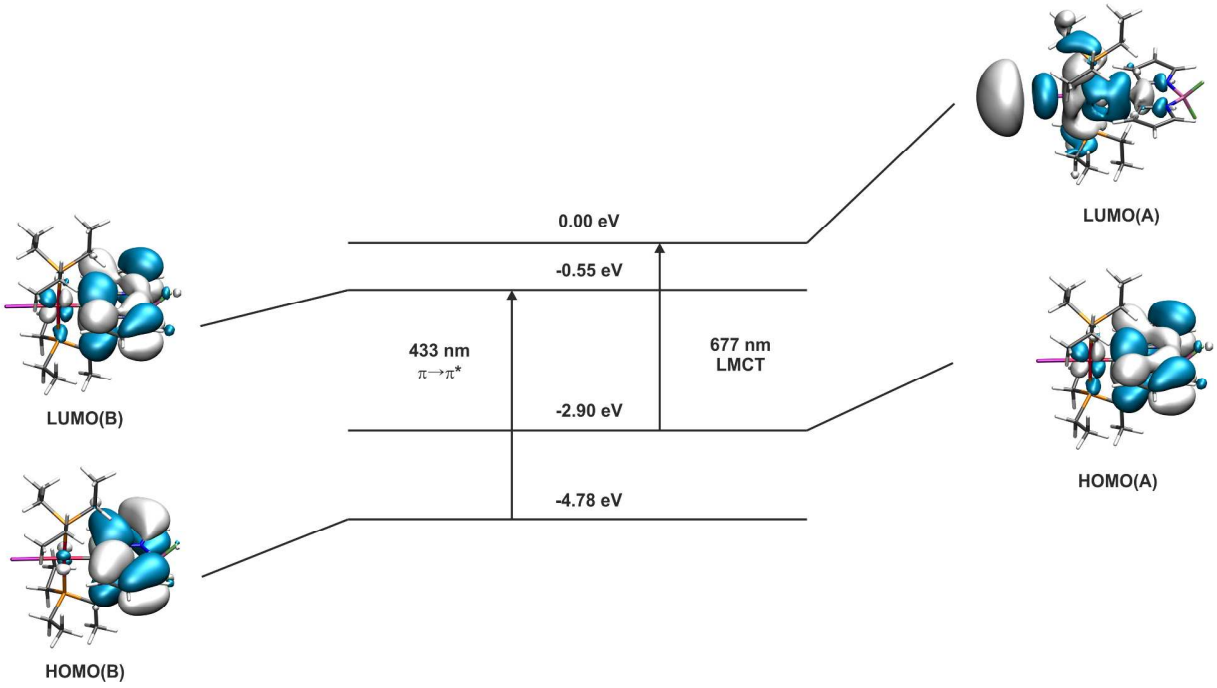


**Figure S64.** Graphical representation of the relevant MOs and TD-DFT energies of the one-electron reduced form of complex **8-Pt**. Solid arrows symbolize the main contributor to the respective transition.

**Table S7.** Calculated Mulliken parameters of **8-Pt** in the one-electron reduced form. Contributions of the given fragments are given in percent.

| | Pt | bodipy | $PEt_3$ | I |
|---|---|---|---|---|
| LUMO(A) | 48 | 13 | 22 | 17 |
| LUMO(B) | 4 | 93 | 3 | 0 |
| HOMO(A) | 3 | 94 | 2 | 0 |
| HOMO(B) | 4 | 97 | 3 | 0 |

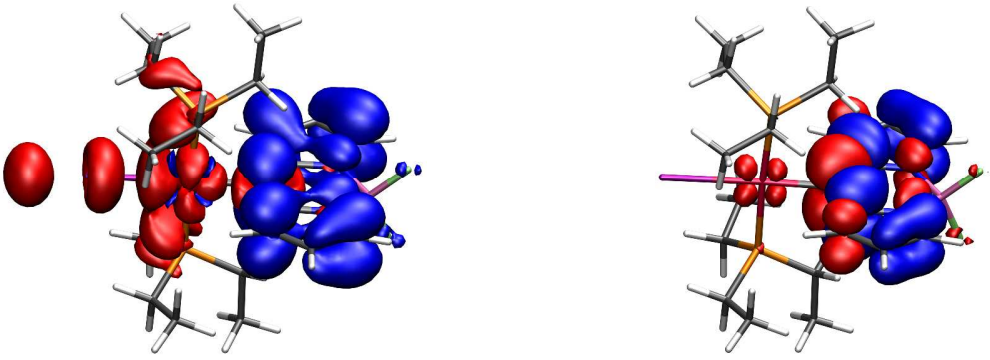

**677 nm** **433 nm**

**Figure S65.** EDDMs for the calculated transitions (blue = electron density loss, red = electron density gain) for the reduced, monoanionic form of **8-Pt** calculated on the PBE1PBE/6-31G(d) level of theory.

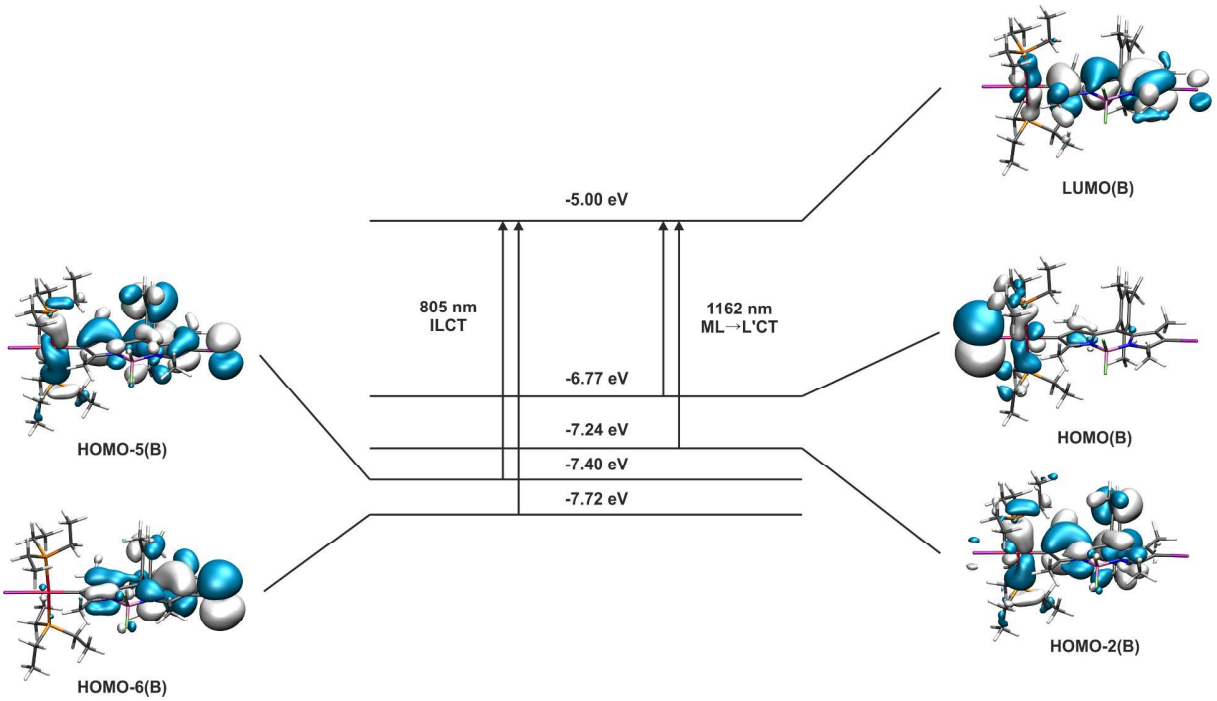


**Figure S66.** Graphical representation of the relevant MOs and TD-DFT energies for the oxidized form of complex **2-Pt-Mes-6I**. Solid arrows symbolize the main contributor to the respective transition.

**Table S8.** Calculated Mulliken parameters of **2-Pt-Mes-6I** in the oxidized form. Contributions of the given fragments are given in percent.

| | Pt | bodipy | $PEt_3$ | I |
|---|---|---|---|---|
| LUMO(B) | 5 | 91 | 3 | 1 |
| HOMO(B) | 7 | 4 | 10 | 79 |
| HOMO-2(B) | 5 | 80 | 14 | 1 |
| HOMO-5(B) | 6 | 84 | 6 | 0 |
| HOMO-6(B) | 0 | 98 | 1 | 0 |

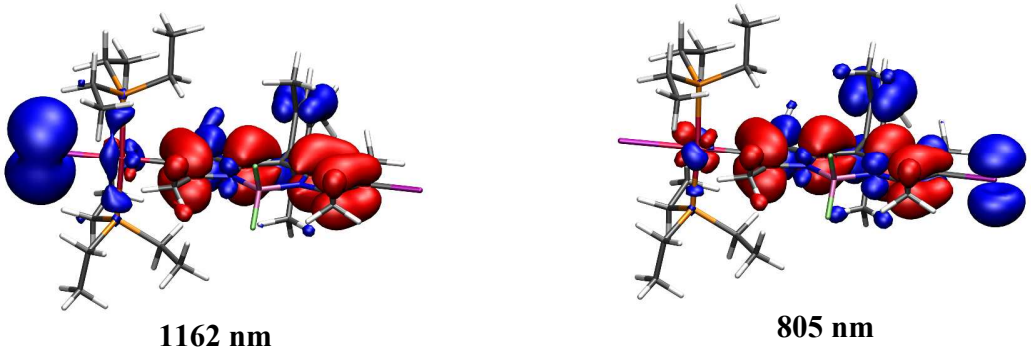


**Figure S67.** EDDMs for the calculated transitions (blue = electron density loss, red = electron density gain) of the cationic form of **2-Pt-Mes-6I** calculated on the PBE1PBE/6-31G(d) level of theory.

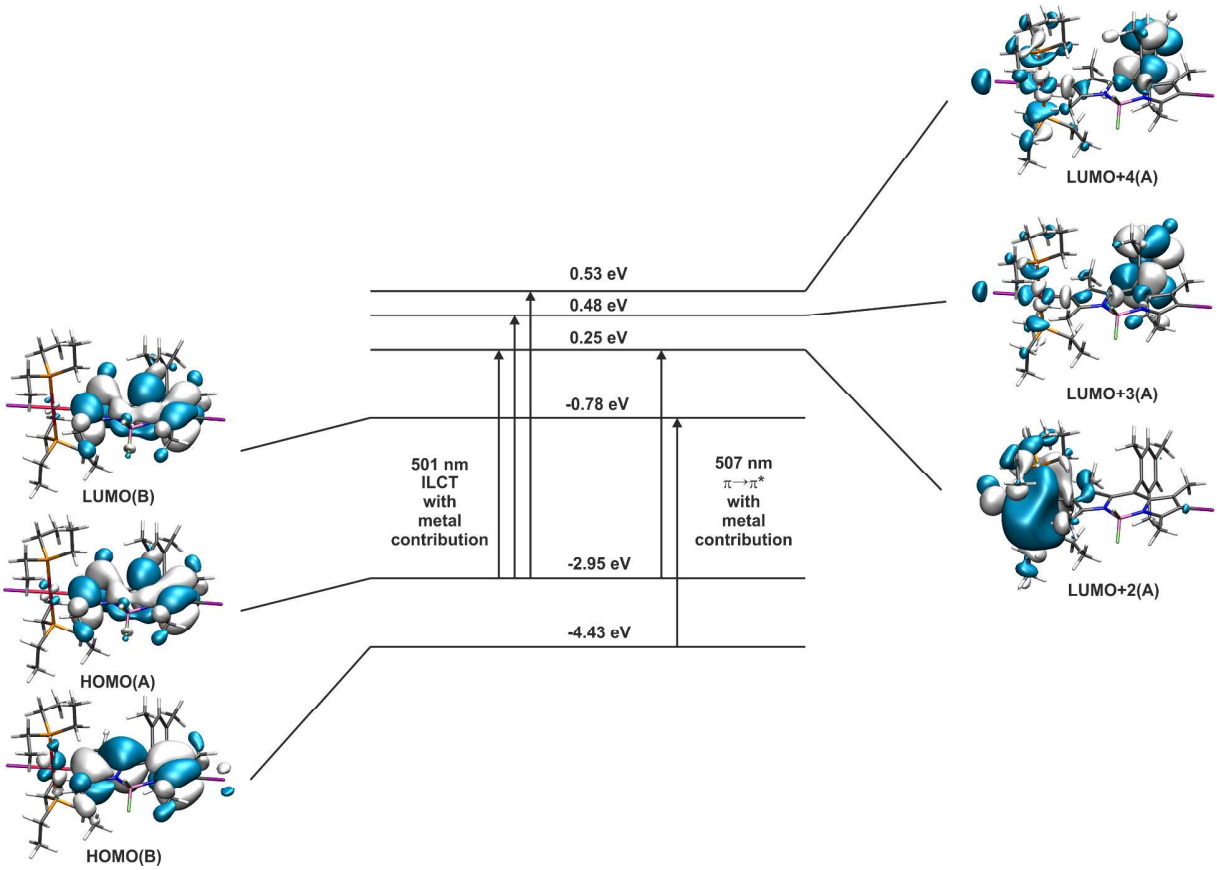


**Figure S68.** Graphical representation of the relevant MOs and TD-DFT energies of the reduced form of complex **2-Pt-Mes-6I**. Solid arrows symbolize the main contributor to the respective transition.

**Table S9.** Calculated Mulliken parameters of **2-Pt-Mes-6I** in the reduced form. Contributions of the given fragments are given in percent.

| | Pt | bodipy | $PEt_3$ | I |
|---|---|---|---|---|
| LUMO+4(A) | 51 | 42 | 6 | 1 |
| LUMO+3(A) | 33 | 64 | 2 | 1 |
| LUMO+2(A) | 56 | 7 | 38 | 0 |
| LUMO(B) | 0 | 98 | 1 | 0 |
| HOMO(A) | 1 | 99 | 1 | 0 |
| HOMO(B) | 2 | 96 | 2 | 0 |

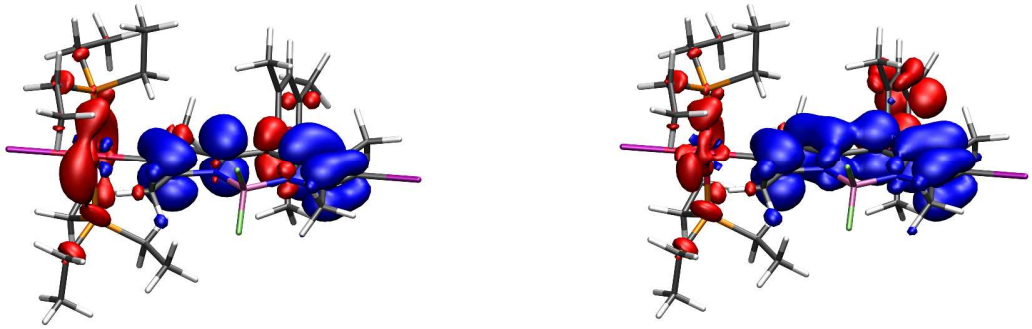

**507 nm** **501 nm**

**Figure S69.** EDDMs for the calculated transitions (blue = electron density loss, red = electron density gain) for the reduced, monoanionic form of **2-Pt-Mes-6I** calculated on the PBE1PBE/6-31G(d) level of theory.

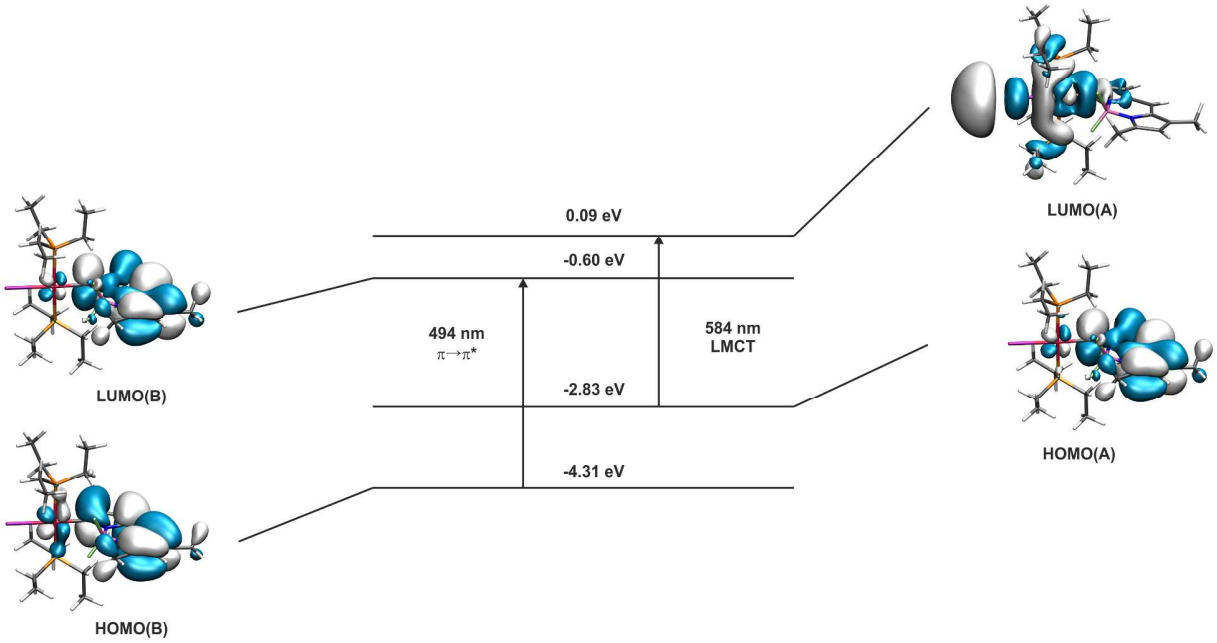


**Figure S70.** Graphical representation of the relevant MOs and TD-DFT energies of the reduced form of complex **3-Pt**. Solid arrows symbolize the main contributor to the respective transition.

**Table S10.** Calculated Mulliken parameters of **3-Pt** in the reduced form. Contributions of the given fragments are given in percent.

| | Pt | bodipy | $PEt_3$ | I |
|---|---|---|---|---|
| LUMO(A) | 49 | 11 | 22 | 18 |
| LUMO(B) | 1 | 97 | 1 | 1 |
| HOMO(A) | 2 | 97 | 1 | 0 |
| HOMO(B) | 4 | 94 | 2 | 0 |

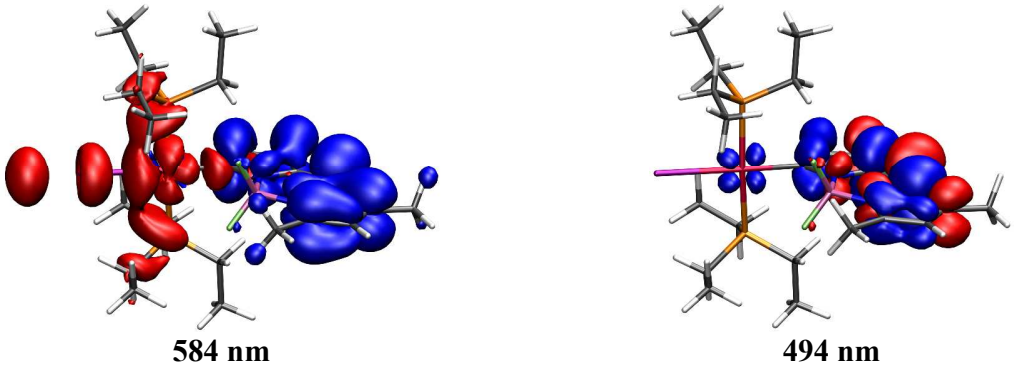


**Figure S71.** EDDMs for the calculated transitions (blue = electron density loss, red = electron density gain) in the anionic form of **3-Pt** calculated on the PBE1PBE/6-31G(d) level of theory.

## EPR Spectroscopy

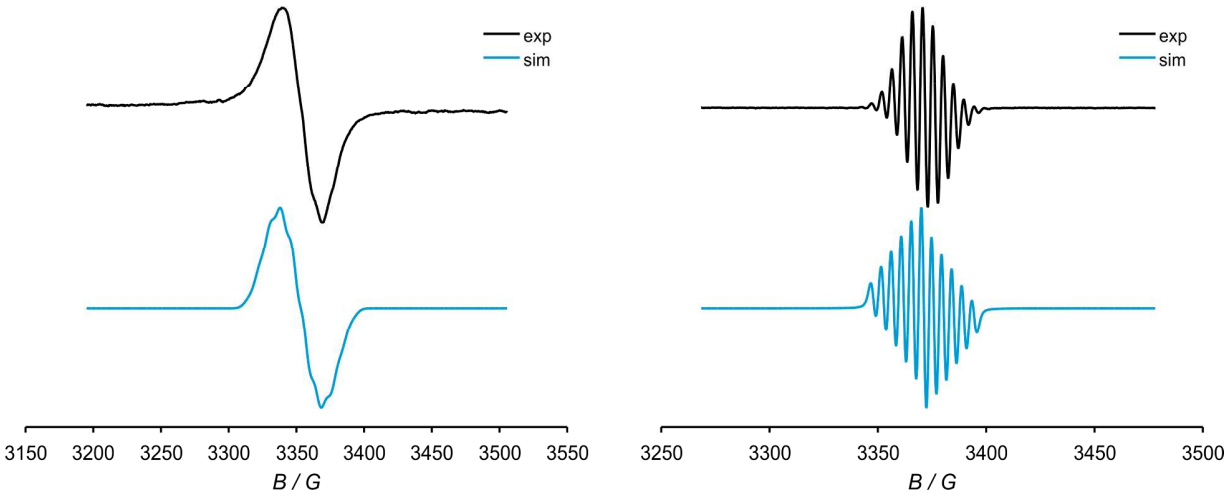


**Figure S72.** Experimental (top curve) and simulated (bottom curve) EPR spectra of the radical cation (left) and radical anion (right) of **8-Mes-2,6-$I_2$-bodipy** in $CH_2Cl_2/NBu_4^+$ $PF_6^-$ solution at 273 K.

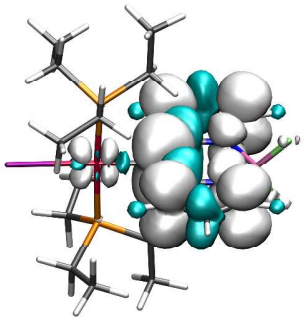

**Figure S73.** Calculated spin density of the radical anion of **8-Pt** (PBE1PBE/6-31G(d) PCM ($CH_2Cl_2$)).

**Table S51.** Spin density contribution of the respective fragment to the spin density surfaces of the radical cation or anion of **2-Pt-Mes-6I**, **3-Pt** and **8-Pt.**

| Compound<br>Ox. State | **2-Pt-Mes-6I**<br>anion | **2-Pt-Mes-6I**<br>cation | **3-Pt**<br>anion | **3-Pt**<br>cation | **8-Pt**<br>anion |
|---|---|---|---|---|---|
| Pt | 0.003 | 0.042 | -0.002 | 0.054 | -0.006 |
| $PEt_3$ | 0.004 | 0.026 | 0.012 | 0.026 | 0.017 |
| I | 0.000 | 0.003 | -0.003 | 0.007 | -0.008 |
| BODIPY | 0.992 | 0.929 | 0.993 | 0.913 | 0.996 |

## References

1. Irmler, P.; Winter, R. F., *Dalton Trans.* **2016,** *45*, 10420-34.

## 5.4 Four Different Emissions from a Pt(Bodipy)($PEt_3$)$_2$(S-Pyrene) Dyad

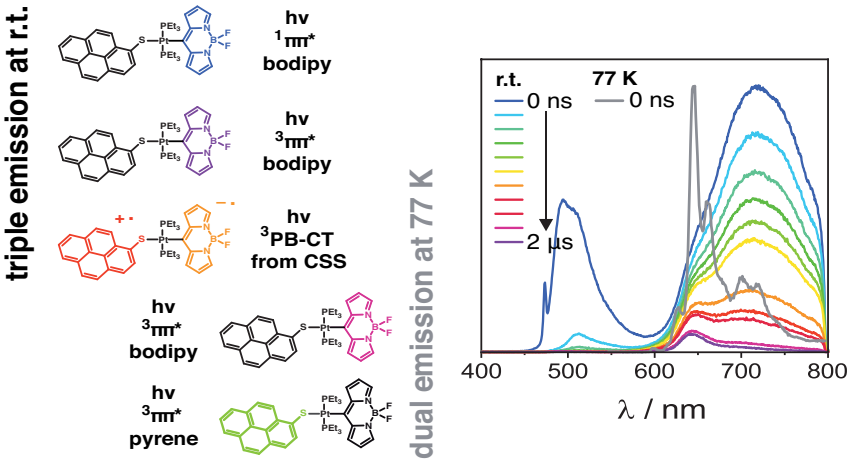


Reprinted from *Dalton Transactions* **2019**, *48*, 1171-1174 (DOI: 10.1039/c8dt04823a) with permission from The Royal Society of Chemistry.

Dalton Transactions

COMMUNICATION

View Article Online
View Journal | View Issue





Cite this: *Dalton Trans.*, 2019, **48**, 1171

Received 6th December 2018,
Accepted 7th December 2018

DOI: 10.1039/c8dt04823a

rsc.li/dalton

# Four different emissions from a Pt(Bodipy)$(PEt_3)_2$(S-Pyrene) dyad†

Peter Irmler,[a] Franciska S. Gogesch,[a] Christopher B. Larsen,[b] Oliver S. Wenger [b] and Rainer F. Winter *[a]

**The Pt(bodipy)-(mercaptopyrene) dyad BPtSPyr shows four different emissions: intense near-infrared phosphorescence ($\Phi_{ph}$ up to 15%) from a charge-transfer state $pyrS^{\bullet+}$-Pt-$BDP^{\bullet-}$, additional fluorescence and phosphorescence emissions from the $^1\pi\pi^*$ and $^3\pi\pi^*$ states of the bodipy ligand at r.t., and phosphorescence from the pyrene $^3\pi\pi^*$ and the bodipy $^3\pi\pi^*$ states in a glassy matrix at 77 K.**

In accordance with Kasha's rule, the vast majority of compounds emits solely from their lowest excited electronic state.[1] Dual fluorescence and phosphorescence emissions may, however, be observed if intersystem crossing (ISC) occurs at a competitive timescale to fluorescence and if the rate constant for phosphorescence emission is increased by a proximal heavy atom with a large spin–orbit coupling constant.[2–5] By capitalizing on this remote heavy-atom effect we and others have recently observed dual fluorescence and phosphorescence emissions at r.t. from metal complexes with a σ-bonded[6–11] or remotely attached bodipy (BDP) ligand.[12,13] Multiple emissions from a single compound can also result from inefficient Förster resonance energy transfer in dyads with two electronically decoupled, orthogonally aligned chromophores.[14] Intriguing examples are multiply emissive $Ir(ppy)_2(Q)$ complexes with two cyclometalated phenylpyridine (ppy) and a 2-hydroxyquinoline ligand Q, which show ligand-localized fluorescence from $^1n\pi^*$ and phosphorescence from $^3$MLCT (MLCT = metal–ligand charge-transfer) states of the different ligands.[15] We report here on the new *meso*-Pt bodipy complex **BPtSPyr** (Scheme 1), which combines the above principles and presents four different emissions owing to the coexistence of energetically close-lying ligand-localized and charge-separated excited states.

**BPtSPyr** was synthesized from *trans*-Pt(bodipy)I$(PEt_3)_2$ (**BPtI**)[7] by halogenide abstraction with AgOTf and subsequent addition to a solution of deprotonated 1-mercaptopyrene (pyrS). The same protocol was also used to prepare the complex **MesPtSPyr**, where the BDP chromophore is replaced by mesityl (Mes, Mes = 2,4,6-trimethylphenyl) from newly synthesized *trans*-PtBr(Mes)$(PEt_3)_2$ (for synthetic details and NMR spectroscopic characterization see ESI and Fig. S1–S18† therein).

The electronic absorption spectrum of **MesPtSPyr** is dominated by the ππ* band of the mercaptopyrene ligand at 431 nm (Fig. 1). Upon excitation into this band, **MesPtSPyr** exhibits dual fluorescence and phosphorescence emissions, at r.t. and at 77 K. Both emissions emanate from the mercaptopyrene ligand as follows from the typical shapes of the emissions and their lifetimes (Fig. S19–S25, ESI† and Table 1).[5,16,17] ISC in **MesPtSPyr** is obviously triggered by the heavy-metal effect of the attached Pt ion, similar to what has been observed in Pt complexes with a σ-bonded pyrenyl ligand.[5,16,17]

**BPtSPyr** reveals a three-band absorption pattern comprising of the structured pyrS-based ππ* band at 350–425 nm, the bodipy (BDP) ππ* absorption at 470 nm, and a partially overlapping, weaker pyrS-to-BDP charge-transfer (PB-CT) band at *ca.*

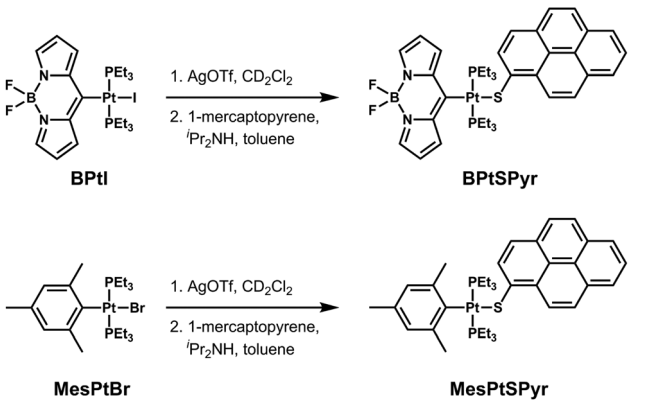


**Scheme 1** Synthesis of **BPtSPyr** and **MesPtSPyr**.

[a]*Fachbereich Chemie, Universität Konstanz, Universitätsstraße 10, D-78457 Konstanz, Germany. E-mail: rainer.winter@uni-konstanz.de*
[b]*Department of Chemistry, University of Basel, St.-Johanns-Ring 19, CH-4056 Basel, Switzerland*

†Electronic supplementary information (ESI) available. See DOI: 10.1039/c8dt04823a

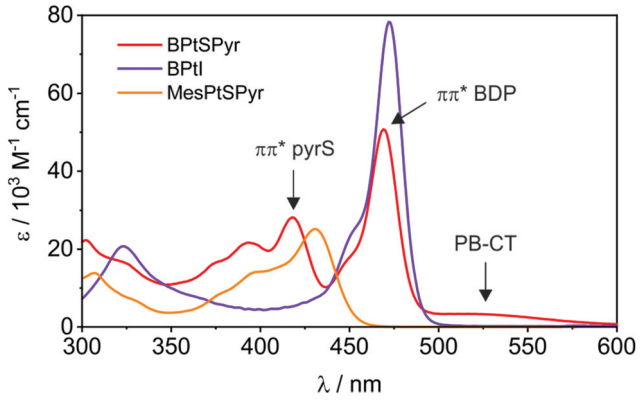


Fig. 1 UV/Vis spectra of **BPtSPyr**, **MesPtSPyr** and **BPtI** in toluene.

Table 1 Emission data of **MesPtSPyr** and **BPtSPyr**

| Solvent | $\lambda_{exc}$ [a] | $\lambda_{fl}$ [b] | $\lambda_{ph}$ [b] (assignment) | $\Phi_{ph}$ [c] | $\tau_{ph}$ [d] |
|---|---|---|---|---|---|
| **MesPtSPyr** | | | | | |
| Toluene | 430 | 460[e] | 664 ($^3$pyrS) | <0.01 | 448 ± 6 μs |
| Me-THF[f] | 430 | 450 | 658 ($^3$pyrS) | n.d. | 1.04 ± 0.06 ms |
| **BPtSPyr** | | | | | |
| Toluene | 520 | | 724 ($^3$PB-CT) | 0.08 | 6.7 ± 0.4 μs |
| | 470 | 484 | 724 ($^3$PB-CT) | 0.15 | 6.7 ± 0.5 μs |
| | 420 | | 724 ($^3$PB-CT) | 0.15 | 6.4 ± 0.3 μs |
| THF | 520 | | 784 ($^3$PB-CT) | n.d. | n.d. |
| | 470 | 484[g] | 635 ($^3$BDP) | n.d. | 78.0 ± 0.4 μs, |
| | | | 784 ($^3$PB-CT) | | 51.4 ± 0.8 ns |
| | 420 | | 784 ($^3$PB-CT) | n.d. | 50.4 ± 0.3 ns |
| Acetone | 520 | | 861 ($^3$PB-CT) | n.d. | n.d. |
| | 470 | 484 | 635 ($^3$BDP) | n.d. | 49.9 ± 0.3 μs |
| | | | 861 ($^3$PB-CT) | | 2.44 ± 0.02 ns |
| Me-THF[f] | 530 | n.o. | 635 ($^3$BDP) | n.d. | 279 ± 1 μs |
| | 450 | | 649 ($^3$pyrS) | | 1.12 ± 0.02 ms |
| | 415 | | | | |

[a] Excitation wavelength in nm. [b] Wavelength of the fluorescence (fl) or phophorescence (ph) emissions in nm. [c] Phosphorescence quantum yield. [d] Lifetime of the phosphorescence emissions. [e] $\tau_{fl}$ = 1.113 ± 0.005 ns, $\Phi_{ph}$ = 0.24. [f] Measured in a 2-MeTHF glass at 77 K. [g] $\tau_{fl}$ = 3.70 ± 0.2 ns.

500 nm. The latter has no equivalent in the precursors **BPtI** and **MesPtSPyr** (Fig. 1, Table S1, ESI†). The above band assignments are supported by time-dependent density functional theory (TD-DFT) calculations (Fig. S26, ESI†). According to our calculations all transitions are ligand-based with only minor Pt contributions to the corresponding donor and acceptor orbitals (Table S2†). In line with a CT character, the PB-CT excitation is solvatochromic while the pyrS and BDP ππ* absorptions are only modestly influenced by solvent polarity (Fig. S27, ESI†).

Importantly, and in contrast to **MesPtSPyr**, **BPtSPyr** exhibits four different emissions depending on excitation wavelength, solvent polarity and temperature (Fig. 2). As shown in Fig. 2a, excitation into the PB-CT absorption band at 520 nm leads to broad and unstructured NIR emission with a quantum yield of 8% in toluene. The emission shifts red with increasing solvent polarity, from 724 nm in toluene to 784 nm in THF and to 816 nm in acetone (Table 1). Its strong solvatochromism and the lifetime of

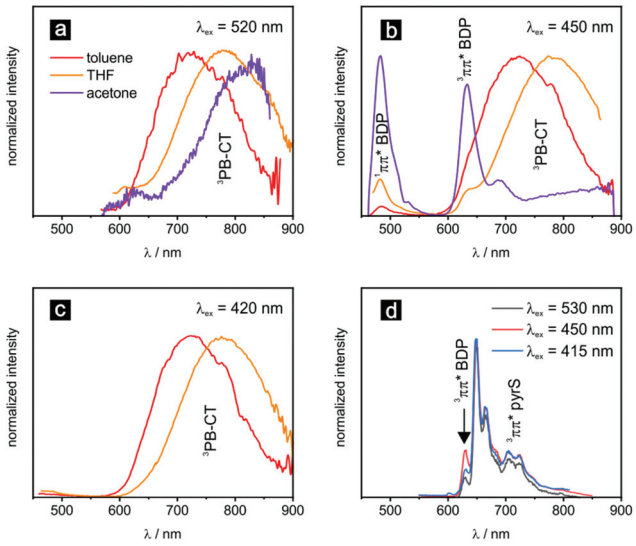


Fig. 2 Emission spectra of **BPtSPyr** in *ca.* 1 μM solutions of acetone, THF or toluene at r.t. on excitation at (a) 520 nm, (b) 450 nm and (c) 405 nm. (d) Emission spectra recorded in 2-MeTHF at 77 K at different excitation wavelengths.

6.7 μs in toluene (for lifetime decays see Fig. S28–S30, ESI†) indicate that this emission emanates from the $^3$PB-CT state. We note that heavy atom-free donor-substituted BDPs were also shown to undergo efficient ISC to the $T_1$ state *via* an excited CT state; the latter systems are, however, non-phosphorescent.[18–20]

Excitation into the BDP ππ* absorption band at 470 nm (Fig. 2b and S31, ESI†) opens two further radiative pathways: BDP-based fluorescence at 484 nm and phosphorescence at 635 nm are observed in addition to the $^3$PB-CT emission. Changing the solvent from toluene to THF or acetone increases the energy separation between the BDP $^3$ππ* and the $^3$PB-CT states and allows for tuning of the emission colour from red in toluene (CIE coordinates 0.6052/0.3211 in toluene) to almost white in THF (CIE coordinates: 0.2209/0.3206) or acetone (CIE coordinates 0.3357/0.2901). Concomitantly with its red-shift, the lifetime of the $^3$PB-CT emission decreases from 6.7 μs in toluene solution to only 2.4 ns in acetone (Fig. S30a, ESI†). This in turn increases the intensity ratio of the $^1$ππ*/$^3$ππ* to the $^3$PB-CT emissions (Fig. 2b). We note that the BDP-based emissions of **BPtSPyr** are not due to contamination with the **BPtI** precursor (Fig. S32, ESI†). Triple emission upon excitation into the BDP ππ* band at 470 nm indicates that ISC from the $^1$ππ* to the $^3$ππ* state of the BDP ligand as well as formation of the $^1$PB-CT state and subsequent ISC to the $^3$PB-CT state occur at similar rates as fluorescence from the BDP $^1$ππ* state. When the sample is excited into the pyrS ππ* band at 415 nm, again solely $^3$PB-CT emission is observed, but with an even increased quantum yield of 15% ($\lambda_{exc}$ = 420 nm) as compared to 8% for $\lambda_{exc}$ = 520 nm (Fig. 2a and c), rendering **BPtSPyr** a powerful NIR emitter. All the above conclusions are fully supported by excitation *vs.* emission maps and excitation spectra (Fig. S33 and S34, ESI†).

Emission spectra recorded in a glassy Me-THF matrix at 77 K show only two features, irrespective of the excitation wave-

 

length: the $^3\pi\pi^*$ BDP emission with a maximum at 635 nm and a typical lifetime of 279 μs (Fig. S35, ESI†) as well as a structured emission enveloping the region in from 649 to 750 nm (Fig. 2d). This latter feature and its lifetime of 1.12 ms (Fig. S35, ESI†) are typical of a pyrene-based $^3\pi\pi^*$ emission.[5,16,17] The $^3\pi\pi^*$ excited states of the BDP and pyrS ligands are hence both accessible from excitation into any band in the rigid matrix. This indicates that, at 77 K, population of the close-lying BDP and pyrS $^3\pi\pi^*$ from the $^1$PB-CT state of **BPtSPyr** is more rapid than direct intersystem crossing to the $^3$PB-CT state and that deactivation to the $^3$PB-CT state is blocked under these conditions. One possible explanation is that the $^1$PB-CT and $^3$PB-CT states possess very similar nuclear coordinates and the BDP and pyrS $^3\pi\pi^*$ potential wells have more easily accessible intersections with the $^1$PB-CT potential well. Previous studies have similarly demonstrated direct singlet-to-triplet electron-transfer by spin–orbit coupling.[21–23]

The Jablonski diagram of Scheme 2 summarizes the processes following the different excitations of **BPtSPyr**. Electronic decoupling of the pyrS- and the BDP-localized $^1\pi\pi^*$ states, as indicated by the confinement of the HOMO to the pyrS and of the LUMO to the BDP ligand (Fig. S26, ESI†), explains the absence of pyrS to BDP energy transfer from the pyrene-based $^1\pi\pi^*$ state $S_3$ and of any BDP emission after excitation into the pyrS ππ* band at 415 nm. The BDP-based $^1\pi\pi^*$ and $^3\pi\pi^*$ states $S_2$ and $T_3$ are thus exclusively populated by excitation into the BDP $^1\pi\pi^*$ band. In contrast, the $^3$PB-CT state, which constitutes the energetically lowest excited triplet state $T_1$, is accessible from all three excited singlet states, either *via* IC to the $^1$PB-CT and subsequent ISC, or *via* ISC and subsequent electron transfer from the higher-lying pyrS-based $T_2$ and BDP-based $T_3$ states (note that **MesPtSPyr** also undergoes ISC from the pyrene-based $^1\pi\pi^*$ state). At 77 K, direct singlet to triplet electron-transfer from the $^1$PB-CT state allows population of the pyrS- and BDP-based triplet states $T_2$ and $T_3$ (blue arrows in Scheme 2) and renders the pyrS-based phosphorescence emission observable, which, at r.t., is quenched by rapid decay into the lower-lying $^3$PB-CT state.

The proposed excited state cascade is further supported by transient absorption (TA) spectroscopy in THF. TA spectra recorded over the first 200 ns after excitation are very similar to each other, irrespective of whether the sample is excited at 410

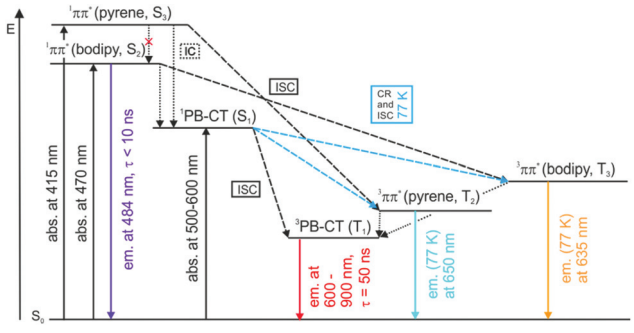


**Scheme 2** Qualitative Jablonski diagram.

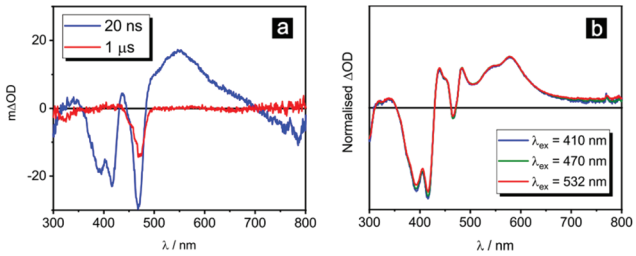


**Fig. 3** Transient absorption spectra of **BPtSPyr** at r.t. (a) in deaerated 20 μM THF solution at different time delays after excitation at 470 nm; and (b) in a 20 μM toluene solution directly after laser excitation at the given wavelength. All spectra are time-integrated over 200 ns.

(pyrS), 470 (BDP), or 532 nm (PB-CT absorption) (Fig. 3 and Fig. S36, ESI†). Three main features are observed: the bleached pyrS and BDP ground state absorption signals at *ca.* 400 nm or 470 nm, and an excited state absorption (ESA) signal at 550 nm, which we assign to the $pyrS^{\bullet+}$ radical cation (*vide infra*). Identical monoexponential kinetics with a common time constant of 50 ns were found for all three transients when excited at 532 nm (for single point kinetics for each TA feature see Fig. S37 and S38, ESI†). When excited into the BDP absorption at 470 nm the features at 415 nm and 550 nm still have a time constant of 50 ns, but the bleach recovery at 475 nm has much longer kinetics of 16.5 μs in THF. This is in accordance with the long-lived BDP $^3\pi\pi^*$ excited state in that solvent (red trace in Fig. S37a, ESI†). Transient absorption bleach recoveries and decays match the luminescence lifetimes in all cases. This corroborates that none of the observable emissions originate from impurities but represent inherent photoluminescence from **BPtSPyr**.

The common CT state after excitation should exhibit spectroscopic features similar to the oxidized and reduced forms of **BPtSPyr**. Cyclic voltammograms show a reversible oxidation at +0.18 V and a reduction at −1.97 V against the ferrocene/ferrocenium couple (Fig. S39 and Table S3, ESI†). This allowed us to experimentally probe the UV/Vis/NIR features of the oxidized and reduced forms of **BPtSPyr** by means of spectroelectrochemistry. Upon oxidation, the pyrS-based ππ* absorption band bleaches while the BDP ππ* band exhibits an only minor red-shift of 316 $cm^{-1}$ (Fig. 4). Based on literature data[24,25] and the results of our TD-DFT calculations (Fig. S40 and Table S4, ESI†), the new absorption bands at *ca.* 520, 550, 750, and 1000 nm can be assigned to ππ* transitions of the $pyrS^{\bullet+}$ radical cation. When **BPtSPyr** is reduced, the BDP ππ* and the PB-CT absorption bands bleach while the pyrS-based ππ* band experiences a moderate red-shift. The weak new band at 518 nm constitutes mainly a ππ* transition of the reduced BDP ligand (Fig. S41 and S42, Table S5, ESI†); it is essentially identical in shape and energy to that observed for $\mathbf{BPtI}^{\bullet-}$.[9] Calculated spin densities for the **BPtSPyr** radical cation and anion also agree with a pyrS-based oxidation and a BDP-based reduction (Fig. 5 and Table S6, ESI†). The results of our spectroelectrochemical experiments and our calculations thus confirm our assignment of the ESA signal to the $pyrS^{\bullet+}$ constituent as well as the character of the HOMO and LUMO of **BPtSPyr**.

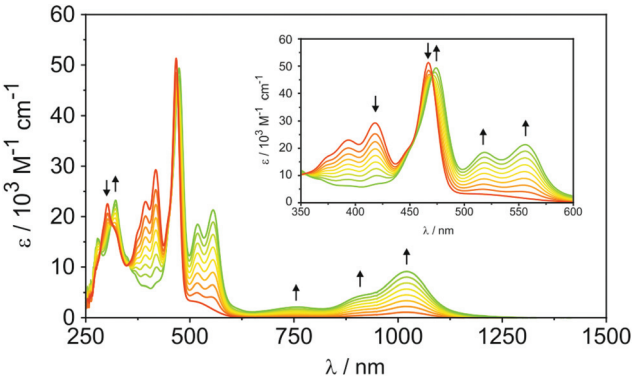


**Fig. 4** Changes of UV/Vis/NIR spectra of **BPtSPyr** on oxidation (THF, $NBu_4PF_6$, 293 K).

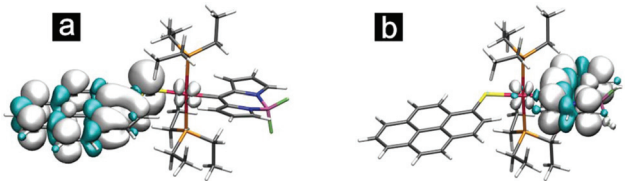


**Fig. 5** Calculated spin densities of (a) the radical cation and (b) the radical anion of **BPtSPyr**.

In summary, the **BPtSPyr** dyad combines several remarkable features. It constitutes an extremely rare case of a compound showing emissions from four different excited states and acts as a powerful NIR emitter. Its emission profiles and colour can be tuned by the excitation wavelength and solvent polarity from deep red to almost white. The crucial role of the $pyrS^{\bullet+}$–Pt-$BDP^{\bullet-}$ charge-transfer state within the excited state cascade was identified by TA spectroscopy, spectroelectrochemical methods and TD-DFT calculations.

## Conflicts of interest

The authors declare no competing financial interests.

## Acknowledgements

This work was supported by Deutsche Forschungsgemeinschaft (grant Wi1262/10-2) and the Swiss National Science Foundation (grant number 200021_176780).

## Notes and references

1 M. Kasha, *Discuss. Faraday Soc.*, 1950, **9**, 14–19.
2 C.-W. Hsu, C.-C. Lin, M.-W. Chung, Y. Chi, G.-H. Lee, P.-T. Chou, C.-H. Chang and P.-Y. Chen, *J. Am. Chem. Soc.*, 2011, **133**, 12085–12099.
3 C.-C. Hsu, C.-C. Lin, P.-T. Chou, C.-H. Lai, C.-W. Hsu, C.-H. Lin and Y. Chi, *J. Am. Chem. Soc.*, 2012, **134**, 7715–7724.
4 Y.-C. Chang, K.-C. Tang, H.-A. Pan, S.-H. Liu, I. O. Koshevoy, A. J. Karttunen, W.-Y. Hung, M.-H. Cheng and P.-T. Chou, *J. Phys. Chem. C*, 2013, **117**, 9623–9632.
5 W. Y. Heng, J. Hu and J. H. K. Yip, *Organometallics*, 2007, **26**, 6760–6768.
6 F. Geist, A. Jackel and R. F. Winter, *Inorg. Chem.*, 2015, **54**, 10946–10957.
7 P. Irmler and R. F. Winter, *Dalton Trans.*, 2016, **45**, 10420–10434.
8 F. Geist, A. Jackel, P. Irmler, M. Linseis, S. Malzkuhn, M. Kuss-Petermann, O. S. Wenger and R. F. Winter, *Inorg. Chem.*, 2017, **56**, 914–930.
9 P. Irmler and R. F. Winter, *Organometallics*, 2018, **37**, 235–253.
10 W. Wu, J. Zhao, H. Guo, J. Sun, S. Ji and Z. Wang, *Chem. – Eur. J.*, 2012, **18**, 1961–1968.
11 F. Zhong, A. Karatay, L. Zhao, J. Zhao, C. He, C. Zhang, H. G. Yaglioglu, A. Elmali, B. Küçüköz and M. Hayvali, *Inorg. Chem.*, 2015, **54**, 7803–7817.
12 J. Sun, F. Zhong, X. Yi and J. Zhao, *Inorg. Chem.*, 2013, **52**, 6299–6310.
13 W. Wu, J. Sun, X. Cui and J. Zhao, *J. Mater. Chem. C*, 2013, **1**, 4577–4589.
14 B. Ma, P. I. Djurovich, M. Yousufuddin, R. Bau and M. E. Thompson, *J. Phys. Chem. C*, 2008, **112**, 8022–8031.
15 T. Tsuboi, D.-F. Huang, T. J. Chow and W. Huang, *Opt. Mater.*, 2014, **36**, 1734–1738.
16 J. Hu, J. H. K. Yip, D.-L. Ma, K.-Y. Wong and W.-H. Chung, *Organometallics*, 2009, **28**, 51–59.
17 W. Wu, W. Wu, S. Ji, H. Guo and J. Zhao, *Eur. J. Inorg. Chem.*, 2010, **2010**, 4470–4482.
18 M. A. Filatov, S. Karuthedath, P. M. Polestshuk, S. Callaghan, K. J. Flanagan, M. Telitchko, T. Wiesner, F. Laquai and M. O. Senge, *Phys. Chem. Chem. Phys.*, 2018, **20**, 8016–8031.
19 X.-F. Zhang and N. Feng, *Chem. – Asian J.*, 2017, **12**, 2447–2456.
20 S. Ji, J. Ge, D. Escudero, Z. Wang, J. Zhao and D. Jacquemin, *J. Org. Chem.*, 2015, **80**, 5958–5963.
21 M. R. Wasielewski, D. G. Johnson, W. A. Svec, K. M. Kersey and D. W. Minsek, *J. Am. Chem. Soc.*, 1988, **110**, 7219–7221.
22 S.-H. Lee, A. G. Larsen, K. Ohkubo, Z.-L. Cai, J. R. Reimers, S. Fukuzumi and M. J. Crossley, *Chem. Sci.*, 2012, **3**, 257–269.
23 T. Higashino, T. Yamada, M. Yamamoto, A. Furube, N. V. Tkachenko, T. Miura, Y. Kobori, R. Jono, K. Yamashita and H. Imahori, *Angew. Chem., Int. Ed.*, 2016, **55**, 629–633.
24 T. Shida and S. Iwata, *J. Am. Chem. Soc.*, 1973, **95**, 3473–3483.
25 J. Maurer, M. Linseis, B. Sarkar, B. Schwederski, M. Niemeyer, W. Kaim, S. Záliš, C. Anson, M. Zabel and R. F. Winter, *J. Am. Chem. Soc.*, 2008, **130**, 259–268.

 

# Four Different Emissions from a Pt(Bodipy)(PEt$_3$)$_2$(S-Pyrene) Dyad

Peter Irmler,[†] Franciska S. Gogesch,[†] Christopher B. Larsen,[‡] Olvier S. Wenger,[‡] Rainer F. Winter*,[†]

[†]Fachbereich Chemie, Universität Konstanz, Universitätsstraße 10, D-78457 Konstanz, Germany

[‡]Department of Chemistry, University of Basel, St.-Johanns-Ring 19, CH-4056 Basel, Switzerland

**ABSTRACT:** The Pt(bodipy)–(mercaptopyrene) dyad **BPtSPyr** shows four different emissions: Intense near-infrared phosphorescence ($\Phi_{ph}$ up to 15%) from a charge-transfer state pyrS$^{\bullet+}$–Pt–BDP$^{\bullet-}$, additional fluorescence and phosphorescence emissions from the $^1\pi\pi^*$ and $^3\pi\pi^*$ states of the bodipy ligand at r.t., and phosphorescence from the pyrene $^3\pi\pi^*$ and the bodipy $^3\pi\pi^*$ states in a glassy matrix at 77 K.

# Content

## Experimental Procedures

**Methods.** Oxidative addition reactions and ligand manipulations were performed under a $N_2$ atmosphere using standard Schlenk techniques or inside a glove box. $C_6D_6$, $CD_2Cl_2$, $CDCl_3$ and THF-*d8* were supplied from Eurisotop. All other solvents were used as received. Complex *trans*-Pt(bodipy)I($PEt_3$)$_2$ (**BPtI**) was synthesized according to the literature protocol.[1]

NMR experiments were carried out on a Varian Unity Inova 400, a Bruker Avance III DRX 400 or a Bruker Avance DRX 600 spectrometer. $^1$H and $^{13}$C spectra were referenced to the solvent signal, while $^{31}$P and $^{195}$Pt spectra were referenced to external standards (85% $H_3PO_4$ or saturated $K_2[PtCl_6]$ in $D_2O$, respectively). NMR data are given as follows: chemical shift (δ in ppm), multiplicity (br, broad; d, doublet; dd, doublet of doublets; m, multiplet; s, singlet; t, triplet, vt virtual triplet), integration, coupling constant (Hz). Unequivocal signal assignments were achieved by 2D NMR experiments. The numbering of the nuclei follows that of the chemical structures displayed at the synthesis protocol.

Combustion analysis was conducted with an Elementar vario MICRO cube CHN-analyzer from Heraeus. Luminescence spectra and lifetimes as well as quantum yields were measured in acetone, $CH_2Cl_2$, 2-MeTHF, THF, or toluene solutions of the complex on a PicoQuant FluoTime 300 spectrometer. Unless stated otherwise, absolute quantum yields were determined with an integrating sphere within the FluoTime 300 spectrometer. Emission spectroscopy under inert gas atmosphere was conducted in a quartz cuvette modified with an angle valve from Normag. The emission data of **BPtSPyr** in acetone with excitation at 405 nm is not reported due to sample decomposition upon laser excitation.

UV/Vis/NIR spectra were recorded on a TIDAS fiber optic diode array spectrometer (combined MCS UV/NIR and PGS NIR instrumentation) from J&M in HELLMA quartz cuvettes with 0.1 cm optical path lengths.

Transient absorption spectroscopy was performed using an LP920-KS instrument from Edinburgh Instruments. 410 nm and 470 nm excitation were obtained from pulsed third-harmonic radiation from a Quantel Brilliant b Nd:YAG laser equipped with a Rainbow optical parameter oscillator (OPO). 532 nm excitation was obtained from pulsed second-harmonic generation from a Quantel Brilliant b Nd:YAG laser. The laser pulse duration was ~10 ns and the pulse frequency 10 Hz with a typical pulse energy of 7 mJ. Detection of transient absorption spectra occurred on an iCCD camera from Andor. Single-wavelength kinetics were recorded using a photomultiplier tube. All optical spectroscopic experiments were performed under deaerated conditions using quartz cuvettes in which oxygen can be removed by the freeze-pump-

thaw technique. Solutions were typically 20 μM in the compound and deaerated through three cycles of freeze-pump-thaw.

All electrochemical experiments were executed in a home-built cylindrical vacuum-tight one-compartment cell. A spiral shaped Pt wire and an Ag wire as the counter and pseudoreference electrodes are sealed into glass capillaries and fixed by quickfit screws via standard joints. A platinum electrode is introduced as the working electrode through the top port via a Teflon screw cap with a suitable fitting. It is polished with first 1 μm and then 0.25 μm diamond paste before measurements. The cell may be attached to a conventional Schlenk line via a side arm equipped with a Teflon screw valve, allowing experiments to be performed under an argon atmosphere with approximately 5-7 mL of analyte solution. $NBu_4PF_6$ (0.1 mM) was used as the supporting electrolyte. Referencing was done with addition of an appropriate amount of decamethylferrocene ($Cp^*_2Fe$) as an internal standard to the analyte solution after all data of interest had been acquired. Representative sets of scans were repeated with the added standard. Electrochemical data were acquired with a computer-controlled BASi CV50 potentiostat. The optically transparent thin-layer electrochemical (OTTLE) cell was home-built and followed the design of Hartl et al.[2] It comprised a Pt working and counter electrode and a thin silver wire as a pseudoreference electrode sandwiched between two $CaF_2$ windows of a conventional liquid IR cell with the working electrode positioned in the center of the spectrometer beam.

**Computational Details.** The ground-state electronic structures were calculated by density functional theory (DFT) methods using the Gaussian 09[3] program package. Quantum-chemical studies were performed without any symmetry constraints. Open-shell systems were calculated by the unrestricted Kohn−Sham approach.[4] Geometry optimizations followed by vibrational analysis were performed either in a vacuum or in solvent media. The quasi-relativistic Wood−Boring small-core pseudopotentials (MWB),[5,6] the corresponding optimized set of basis functions[7] for platinum and the halogen atoms, and the 6-31G(d)-polarized double-ζ basis set[8] for the remaining atoms were employed together with the Perdew−Burke−Ernzerhof exchange and correlation functional (PBE0).[9,10] Solvent effects were accounted for by the polarizable conductor continuum model (PCM)[11-14] with standard parameters for dichloromethane. Absorption spectra and orbital energies were calculated using time-dependent DFT (TD-DFT)[15] with the same functional/basis set combinations as those mentioned above. For an easier comparison with the experiment, the obtained absorption and emission energies were converted into wavelengths and broadened by a Gaussian distribution (full width at half-maximum = 3000 $cm^{-1}$) using the program GaussSum.[16] Atomic coordinates of the calculated structures are provided in Tables Table S8 and Table S9.

## Preparation of Compounds

### 1-Mercaptopyrene

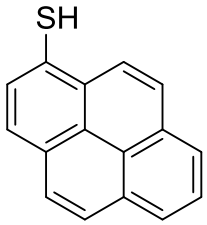


Original synthesis: In a Schlenk flask 503 mg (1.79 mmol) 1-bromopyrene were suspended in 20 ml of $Et_2O$ and cooled to -78 °C. 1.1 ml (1.8 mmol, 1.6 M) of an *n*-buthyllithium solution in hexane were added dropwise. The solution was stirred at -78 °C for 1 h before the suspension was transferred into a cooled (-60 °C) dropping funnel. The solution of the lithiated pyrene was added dropwise to a solution of 248 mg (17.9 mmol) of $SO_2Cl_2$ in 20 ml of $Et_2O$, which was precooled to -78 °C. The solution was slowly warmed to r.t. overnight and the solvent was evaporated. A yellow powder was obtained.

The pyrene sulfonic acid chloride was dissolved in abs. toluene, filtered and added to a solution of 1.4 g (5.37 mmol) of $PPh_3$ in 20 ml of toluene. After stirring the yellow solution, containing some colorless solid, for 20 min at r.t. 10 ml of water were added and the solution was stirred for additional 10 min. The aqueous phase was discarded and the toluene phase was extracted with 10 x 20 ml of 1 M NaOH. The aqueous phase was washed with 2 x 10 ml of toluene, acidified with diluted HCl and extracted with 4 x 20 ml of $CH_2Cl_2$. The combined organic phases were dried over $MgSO_4$ and evaporated to dryness. Yield: 20 % (84 mg).

Alternative, improved synthesis: 275 mg (0.8 mmol) of 1-bromopyrene and 240 mg (3.42 mmol) of sodium methanethiolate were dissolved in DMF under nitrogen and heated to reflux for 2 h. 50 ml of 0.1 N HCl were added and the mixture was extracted with diethyl ether (3 x 50 ml). After washing the organic phase with water (2 x 50 ml), drying over $MgSO_4$ and removing all volatiles, the crude product was purified by column chromatography (petroleum ether / ethyl acetate, 5:1) to give the title compound as a yellow solid in 73 % yield (137 mg). $^1$H NMR ($CDCl_3$, 399.79 MHz, 300 K): δ 8.37 (d, $^3J_{HH}$ = 9.2 Hz, 1H, $H_{Aryl}$), 8.18 (m, 2H, $H_{Aryl}$), 8.14 (d, $^3J_{HH}$ = 9.2 Hz, 1H, $H_{Aryl}$), 8.02 (m, 5H, $H_{Aryl}$), 3.85 (s, 1H, -S*H*). $^{13}$C {$^1$H} NMR (150.93 MHz, DMSO-$d_6$, 300 K): δ 131.6, 131.1, 130.1, 129.6, 129.3, 128.0, 127.4, 127.2, 126.4, 125.7, 125.5, 125.4, 125.3, 125.0, 124.5, 124.4. Anal. Calcd for $C_{16}H_{10}S$: C, 82.02; H, 4.30; S, 13.68. Found: C, 81.94; H, 4.39; S, 12.65.

***trans*-Pt(bodipy)(PEt$_3$)$_2$(*S*-1-thiopyrene) (BPtSPyr)**

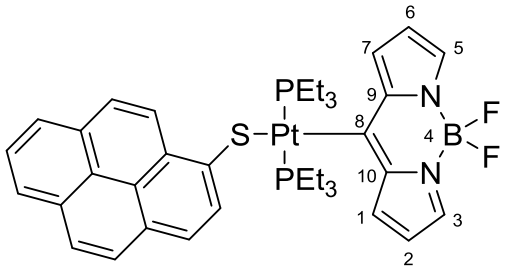


134 mg (172 µmol) of *trans*-Pt(bodipy)I(PEt$_3$)$_2$ (**BPtI**) and 49 mg (189 µmol) of AgOTf were dissolved in 0.5 ml of $CD_2Cl_2$ and heated to reflux for 10 min. After reaction control by $^{31}$P NMR spectroscopy, all volatiles were removed and the solids were taken up in toluene and filtered. The filtered solution was poured into a toluene solution of 49 mg (207 µmol) of 1-mercaptopyrene and 38 µl (275 µmol) of $^{i}Pr_2NH$ and the mixture was stirred at r.t. for 1.5 h. All volatiles were removed, the crude solids were dissolved in benzene and the solution was filtered over Celite. After recrystallization from *n*-pentane / benzene 6:1, the product was obtained as a red crystalline solid. Yield: 60 % (88 mg). $^1$H NMR (600.33 MHz, THF-*d8*, 298 K): δ 8.99 (d, $^3J_{HH}$ = 9.2 Hz, 1H, $H_{Pyr}$), 8.76 (d, $^3J_{HH}$ = 7.9 Hz, 1H, $H_{Pyr}$), 8.07 (d, $^3J_{HH}$ = 7.5 Hz, 1H, $H_{Pyr}$), 8.03 (m, 3H, $H_{Pyr}$), 7.92 (d, $^3J_{HH}$ = 8.8 Hz, 1H, $H_{Pyr}$), 7.89 (vt, $^3J_{HH}$ = 7.5 Hz, 1H, $H_{Pyr}$), 7.85 (d, $^3J_{HH}$ = 8.8 Hz, 1H, $H_{Pyr}$), 7.69 (br s, 2H, H3, H5), 7.65 (d, $^3J_{HH}$ = 3.9 Hz, 2H, H1, H7), 6.52 (dd, $^3J_{HH}$ = 3.9 Hz, $^3J_{HH}$ = 2.0 Hz, 2H, H2, H6), 1.78 (m, 12H, PC*H*$_2$CH$_3$), 1.01 (m, 18H, PCH$_2$C*H*$_3$). $^{13}$C {$^1$H} NMR (150.97 MHz, THF-*d8*, 298 K): δ 188.0 (t, $^2J_{PC}$ = 8.3 Hz, with satellites $J_{PtC}$ = 848 Hz, C8), 146.4 (s, with shoulders, $C_{Pyr}$), 144.4 (s with satellites, $^2J_{PtC}$ = 38.2 Hz, C9, C10), 138.0 (s, C3, C5), 133.6 (s with satellites, $^3J_{PtC}$ = 45.2 Hz, C1, C7), 133.2 (s, $C_{Pyr}$), 132.9 (s, $C_{Pyr}$), 132.4 (s, $C_{Pyr}$), 132.0 (s with satellites, $J_{PtC}$ = 34.7 Hz, $C_{Pyr}$), 128.5 (s, $C_{Pyr}$), 128.1 (s, $C_{Pyr}$), 127.3 (s, $C_{Pyr}$), 126.9 (s, $C_{Pyr}$), 126.7 (s, $C_{Pyr}$), 126.6 (s, $C_{Pyr}$), 126.1 (s, $C_{Pyr}$), 126.0 (s, $C_{Pyr}$), 124.8 (s, $C_{Pyr}$), 124.7 (s, $C_{Pyr}$), 124.3 (s, $C_{Pyr}$), 116.6 (s, C2, C6), 14.8 (t, $J_{PC}$ = 17.4 Hz, with satellites, $^2J_{PtC}$ = 23.6 Hz, P*C*H$_2$CH$_3$), 8.3 (s with shoulders, PCH$_2$*C*H$_3$). $^{31}$P {$^1$H NMR (161.83 MHz, THF-*d8*, 300 K): δ 6.84 (s with satellites, $J_{PtP}$ = 2484 Hz). $^{195}$Pt {$^1$H} NMR (85.55 MHz, THF-*d8*, 300 K): δ -4378 (t, $J_{PtP}$ = 2484 Hz). Anal. Calcd for $C_{37}H_{45}BF_2N_2P_2PtS$: C, 51.94; H, 5.30; N, 3.22; S, 3.75. Found: C, 51.96; H, 5.19; N, 3.59; S, 2.69.

***cis*/*trans*-PtBr(mesityl)($PEt_3$) (*cis*/*trans*-MesPtBr)**

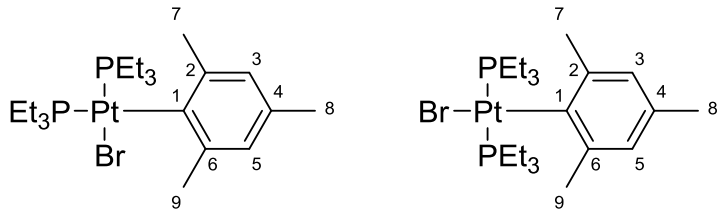

In a Young-tube 98 mg (200 µmol) of $Pt(Et)_2(PEt_3)_2$ were dissolved in 0.5 ml of $C_6D_6$ and placed under vacuum before heating to 115°C for 45 min. The progress of the reaction was controlled by $^{31}P$ NMR spectroscopy. After conversion to $Pt(PEt_3)_2(\eta^2\text{-}C_2H_4)$ was complete, 34 µl (220 µmol) of degassed mesityl bromide in 0.5 ml of $C_6D_6$ were added. The mixture was placed under vacuum again and then heated to 110 °C for 7 h. On addition of 4 ml of *n*-pentane 10 mg of pure ***cis*-MesPtBr** crystallized from the solution. From the remaining solution all volatiles were removed and the remaining solid was washed with 2 x 1 ml of *n*-pentane. This fraction contained slightly impure ***trans*-MesPtBr** with about 3 % of the *cis*-isomer. Overall yield: 51 % (64 mg). ***cis*-MesPtBr**: $^1H$ NMR (399.79 MHz, $CDCl_3$, 300 K): δ 6.63 (s, 2H, H3, H5), 2.46 (s, 6H, H7, H9), 2.18 (s, 3H, H8), 2.06 (m, 6H, PC*H*$_2$CH$_3$), 1.64 (m, 6H, PC*H*$_2$CH$_3$), 1.17 (m, 9H, PCH$_2$C*H*$_3$), 1.03 (m, 9H, PCH$_2$C*H*$_3$). $^{13}C$ {$^1H$} NMR (100.54 MHz, $CDCl_3$, 300 K): δ 150.6 (dd, $^2J_{PC}$ = 110 Hz, $^2J_{PC}$ = 7.4 Hz, C1), 141.4 (vt, $^3J_{PC}$ = 1.6 Hz, C2, C6), 132.3 (s, C4), 127.6 (d, with shoulders, $^4J_{PC}$ = 7.1 Hz, C3, C5), 26.3 (d, with satellites, $^4J_{PC}$ = 3.0 Hz, $^3J_{PtC}$ = 53.1 Hz, C7, C9), 21.0 (s, C8), 18.3 (dd, with satellites, $J_{PC}$ = 37.4 Hz, $^3J_{PC}$ = 3.0 Hz, $^2J_{PtC}$ = 57.4 Hz, P*C*H$_2$CH$_3$), 15.5 (d, with satellites, $J_{PC}$ = 26.5 Hz, $^2J_{PtC}$ = 18 Hz, P*C*H$_2$CH$_3$), 8.6 (d, with satellites, $^2J_{PC}$ = 3.0 Hz, $^3J_{PtC}$ = 32.0 Hz, PCH$_2$*C*H$_3$), 8.4 (s, with satellites, $^3J_{PtC}$ = 14.0 Hz, PCH$_2$*C*H$_3$). $^{31}P$ {$^1H$ NMR} (161.84 MHz, $CDCl_3$, 300 K): δ 8.19 (d, with satellites, $^2J_{PP}$ = 16.6 Hz, $J_{PtP}$ = 1615 Hz), 0.7 (d, with satellites, $^2J_{PP}$ = 16.6 Hz, $J_{PtP}$ = 4272 Hz). $^{195}Pt$ {$^1H$} NMR (85.56 MHz, $CDCl_3$, 300 K): δ -4488 (dd, $J_{PtP}$ = 4272 Hz, 1615 Hz). ***trans*-MesPtBr**: $^1H$ NMR (399.79 MHz, $CDCl_3$, 300 K): δ 6.58 (s, with satellites, $^4J_{PtH}$ = 14.6 Hz, 2H, H3, H5), 2.47 (s, with shoulders, 6H, H7, H9), 2.16 (s, 3H, H8), 1.67 (m, 12H, PC*H*$_2$CH$_3$), 1.04 (m, 18H, PCH$_2$C*H*$_3$). $^{13}C$ {$^1H$} NMR (100.54 MHz, $CDCl_3$, 300 K): δ 140.2 (vt, $^3J_{PC}$ = 2.2 Hz, C2, C6), 135.7 (s, C1), 132.0 (br s, C4), 126.7 (s, with satellites, $^3J_{PtC}$ = 50.5 Hz, C3, C5), 27.3 (s, with satellites, $^3J_{PtC}$ = 88.8 Hz, C7, C9), 20.7 (s, C8), 15.4 (m, P*C*H$_2$CH$_3$), 8.4 (s, with satellites, $^3J_{PtC}$ = 24.4 Hz, PCH$_2$*C*H$_3$). $^{31}P$ {$^1H$} NMR (161.84 MHz, $CDCl_3$, 300 K): δ 9.32 (s, with satellites, $J_{PtP}$ = 2791 Hz). $^{195}Pt$ {$^1H$} NMR (85.56 MHz, $CDCl_3$, 300 K): δ -4409 (t, $J_{PtP}$ = 2791 Hz). Anal. Calcd for $C_{21}H_{41}BrP_2Pt$: C, 40.01; H, 6.55. Found: C, 40.35; H, 6.51.

***trans*-Pt(mesityl)($PEt_3$)$_2$(*S*-1-thiopyrene) (MesPtSPyr)**

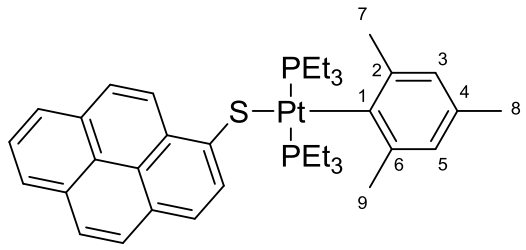


Under an atmosphere of nitrogen 104 mg (73 µmol) of **MesPtBr** and 18 mg (70 µmol) of AgOTf were dissolved in 0.5 ml $CD_2Cl_2$ and heated to reflux for 20 min. After reaction control by $^{31}P$ NMR spectroscopy indicated complete conversion to the triflato complex the solvent was removed. The solid residue was re-dissolved in 5 ml of toluene and filtered. This solution was added to a mixture containing 18 mg (76 µmol) of 1-mercaptopyrene and 20 µl (126 µmol) of $^{i}Pr_2NH$ in 5 ml of toluene. After 10 min of stirring at r.t. all volatiles were removed and the solid was purified by column chromatography (silica, petrol ether/$NEt_3$ 30:1, $R_f$ = 0.35). The product was obtained as a bright yellow solid in 76 % (37 mg) yield. $^1H$ NMR (399.79 MHz, $CDCl_3$, 300 K): δ 9.02 (d, $^3J_{HH}$ = 9.2 Hz, 1H, $H_{pyr}$), 8.74 (d, with shoulders, $^3J_{HH}$ = 8.0 Hz, 1H, $H_{pyr}$), 8.00 (dd, $^3J_{HH}$ = 7.6 Hz, $^4J_{HH}$ = 1.6 Hz, 1H, $H_{pyr}$), 7.95 (m, 2H, $H_{pyr}$), 7.83 (m, 3H, $H_{pyr}$), 7.76 (d, $^3J_{HH}$ = 8.9 Hz, 1H, $H_{pyr}$), 6.67 (s, with satellites, $^4J_{PtH}$ = 10.9 Hz, 1H, H3, H5), 2.66 (s, with shoulders, 6H, H7, H9), 2.17 (s, 3H, H8), 1.66 (m, 12H, $PCH_2CH_3$), 0.97 (m, 18H, $PCH_2CH_3$). $^{13}C$ {$^1H$} NMR (150.97 MHz, THF-*d8*, 298 K): δ 149.2 (s, with satellites, $^3J_{PtC}$ = 13.7 Hz, $C_{pyr}$), 144.8 (t, $^2J_{PC}$ = 9.0 Hz, with satellites, $J_{PtC}$ = 864 Hz, C1), 141.9 (t, $^3J_{PC}$ = 1.8 Hz, with shoulders, C2, C6), 133.4 (s, $C_{pyr}$), 133.1 (s, $C_{pyr}$), 132.6 (s, C4), 132.4 (s, $C_{pyr}$), 132.0 (s, with satellites, $^4J_{PtC}$ = 35.2 Hz, $C_{pyr}$), 128.6 (s, $C_{pyr}$), 128.1 (s, with satellites, $^3J_{PtC}$ = 39.8 Hz, C3, C5), 128.0 (s, $C_{pyr}$), 127.3 (s, $C_{pyr}$), 126.5 (s, $C_{pyr}$), 126.4 (s, $C_{pyr}$), 126.3 (s, $C_{pyr}$), 126.1 (s, $C_{pyr}$), 124.7 (s, $C_{pyr}$), 124.2 (s, $C_{pyr}$), 124.1 (s, $C_{pyr}$), 124.0 (s, $C_{pyr}$), 28.0 (s, with satellites, $^3J_{PtC}$ = 78.7 Hz, C7, C9), 21.1 (s, C8), 15.8 (t, $J_{PC}$ = 16.9 Hz, with satellites, $^2J_{PtC}$ = 34.9 Hz, $PCH_2CH_3$), 8.3 (s, with satellites, $^3J_{PtC}$ = 19.9 Hz, $PCH_2CH_3$). $^{31}P$ {$^1H$} NMR (161.84 MHz, THF-*d8*, 300 K): δ 6.96 (s, with satellites, $J_{PtP}$ = 2734 Hz). $^{195}Pt$ {$^1H$} NMR (85.56 MHz, $CDCl_3$, 300 K): δ -4494 (t, $J_{PtP}$ = 2734 Hz). Anal. Calcd for $C_{37}H_{50}P_2PtS$: C, 56.69; H, 6.43; S, 4.09. Found: C, 55.70; H, 6.66; S, 3.08.

## NMR Spectroscopy

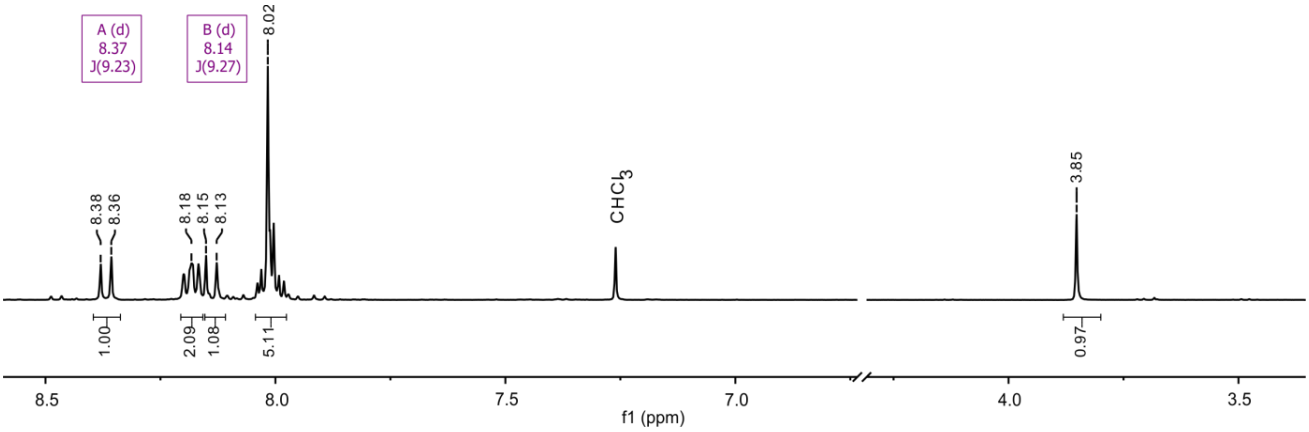


Figure S1. $^{1}H$ NMR spectrum of 1-mercaptopyrene in CDCl3.

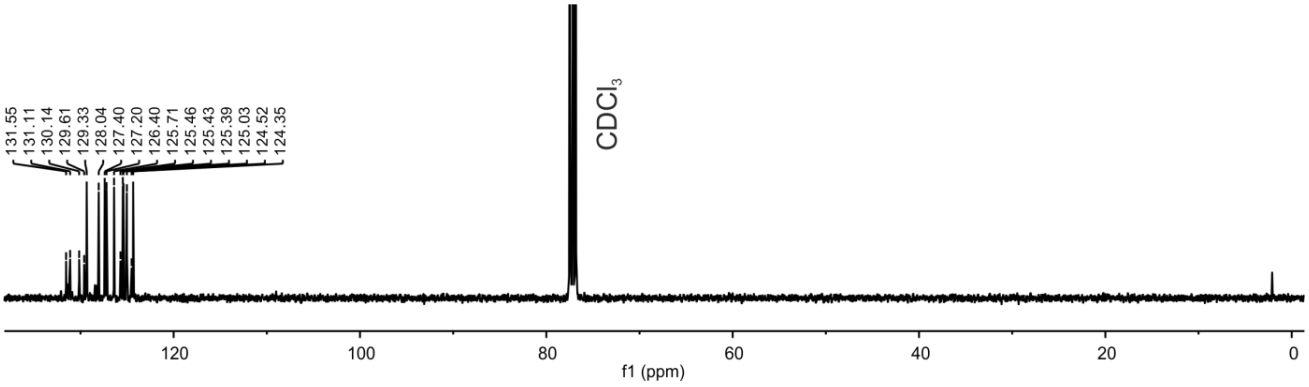


Figure S2. $^{13}C$ NMR spectrum of 1-mercaptopyrene in $CDCl_3$.

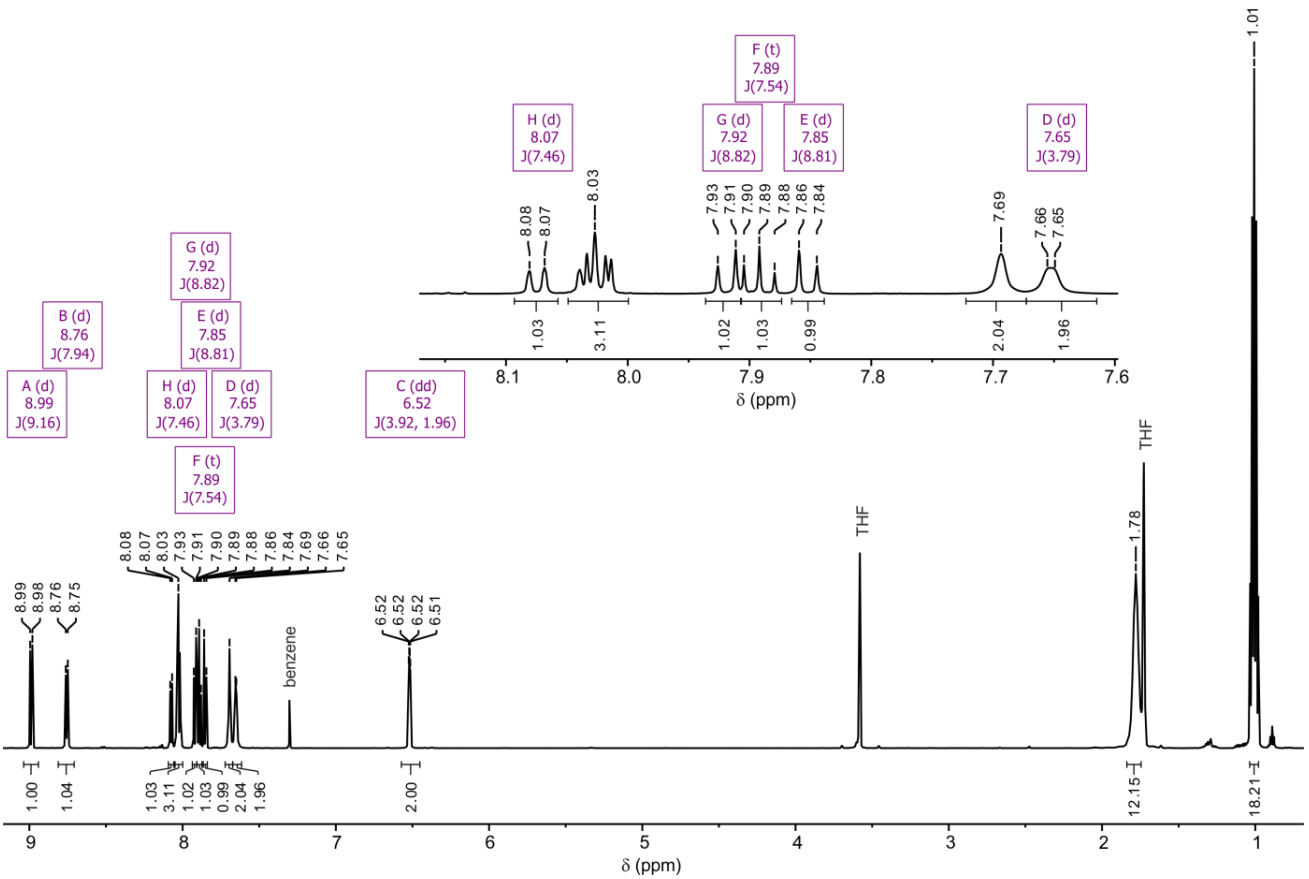


Figure S3. $^{1}$H NMR spectrum of **BPtSPyr** in THF-*d8*.

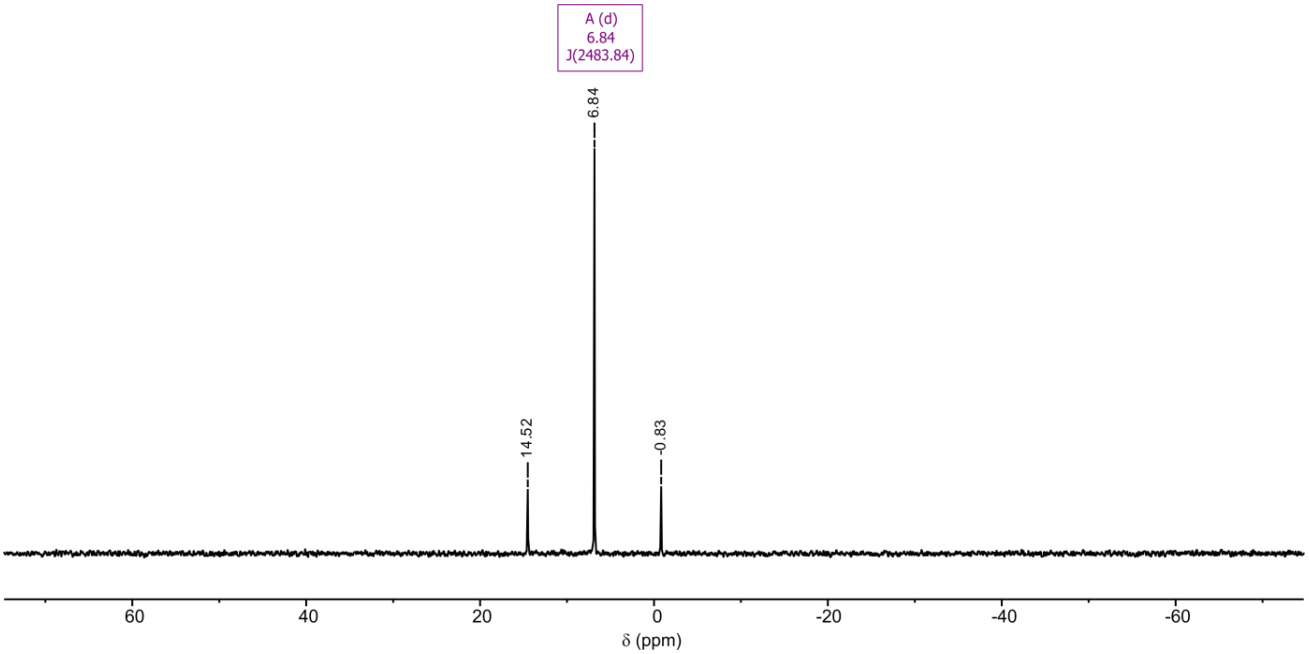


Figure S4. $^{31}$P{$^{1}$H} NMR spectrum of **BPtSPyr** in THF-*d8*.

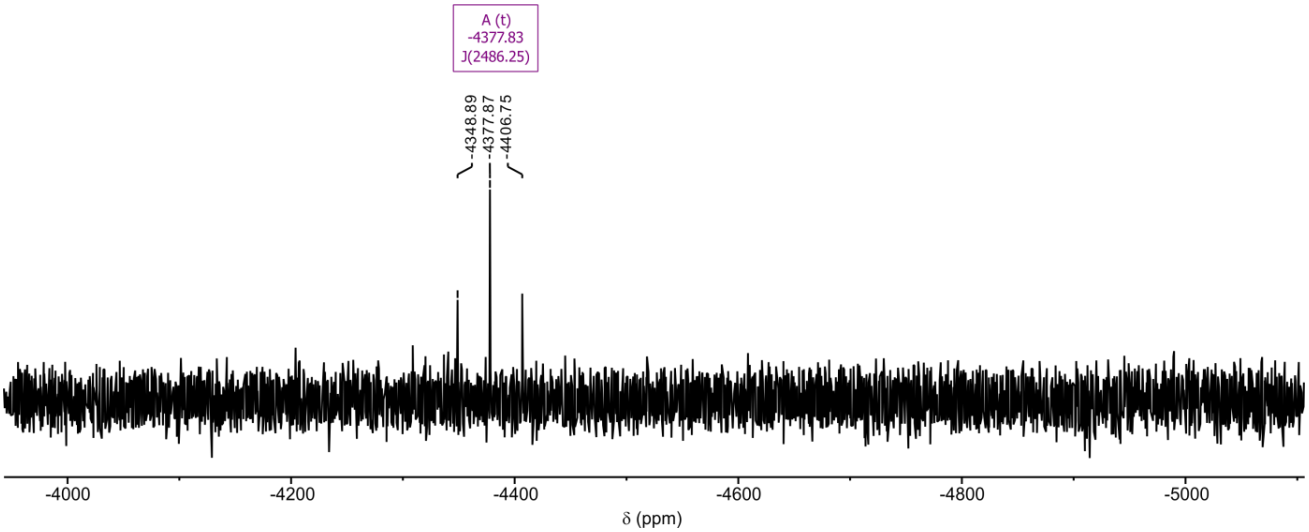


Figure S5. $^{195}Pt\{^{1}H\}$ NMR spectrum of **BPtSPyr** in THF-*d8*.

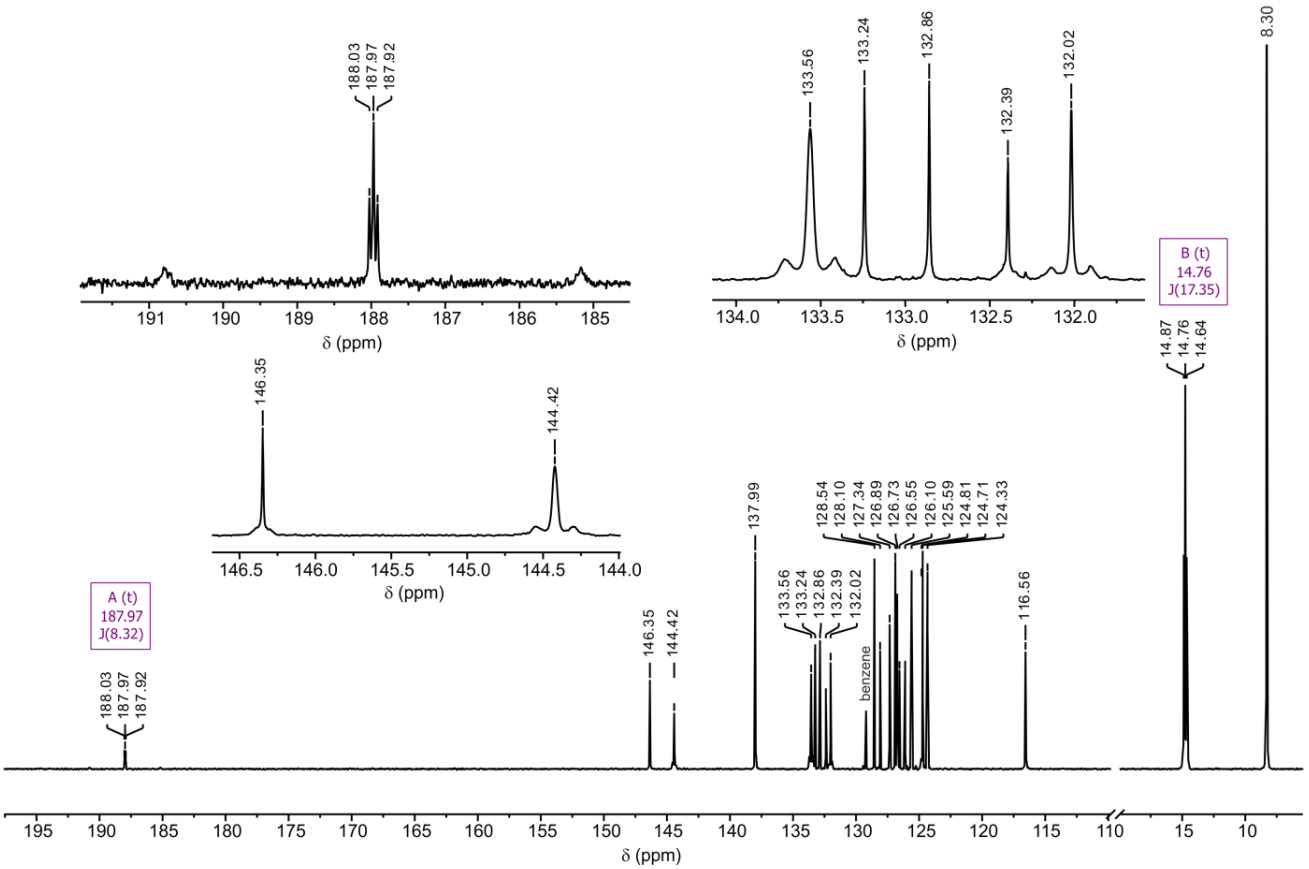


Figure S6. $^{13}C\{^{1}H\}$ NMR spectrum of **BPtSPyr** in THF-*d8*.

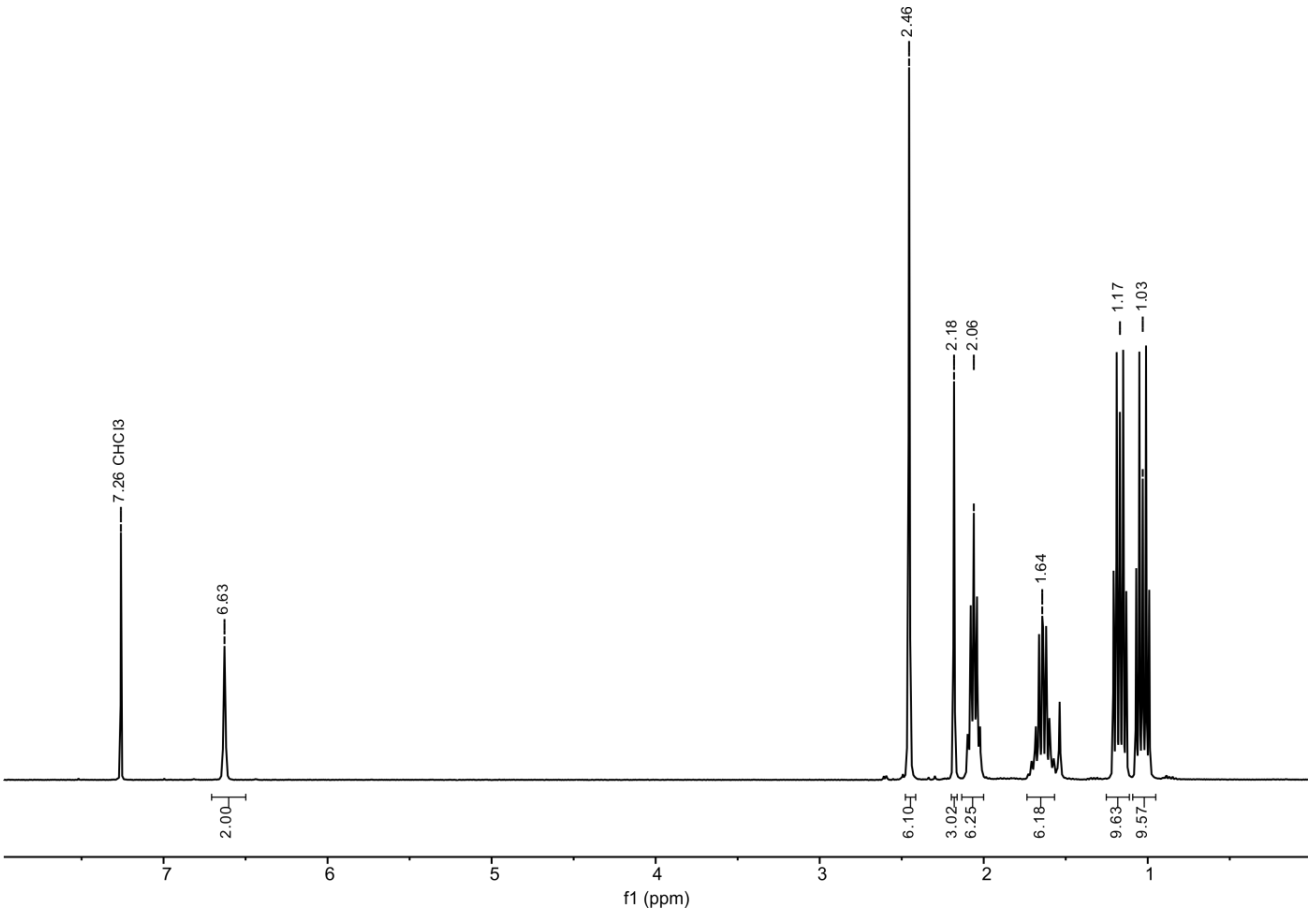


Figure S7. $^{1}H$ NMR spectrum of ***cis*-MesPtBr** in $CDCl_3$.

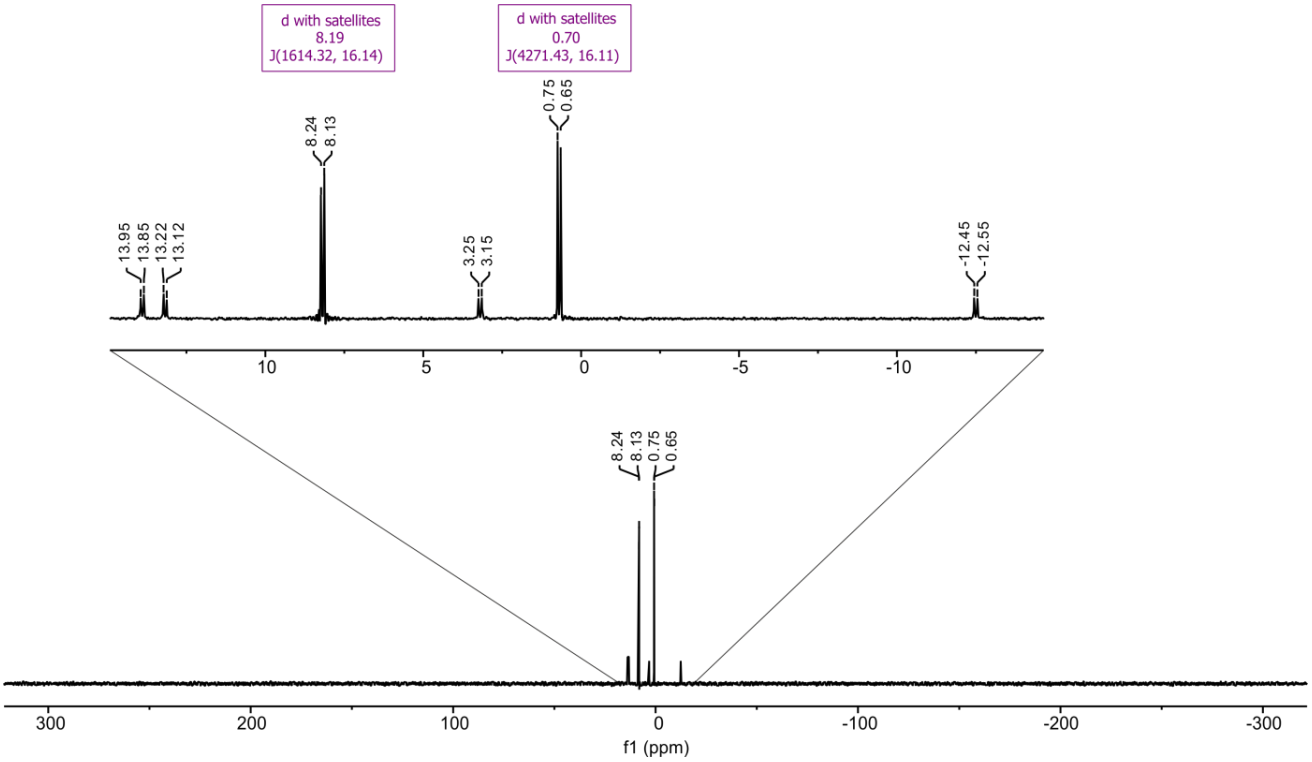


Figure S8. $^{31}$P NMR spectrum of ***cis*-MesPtBr** in $CDCl_3$.

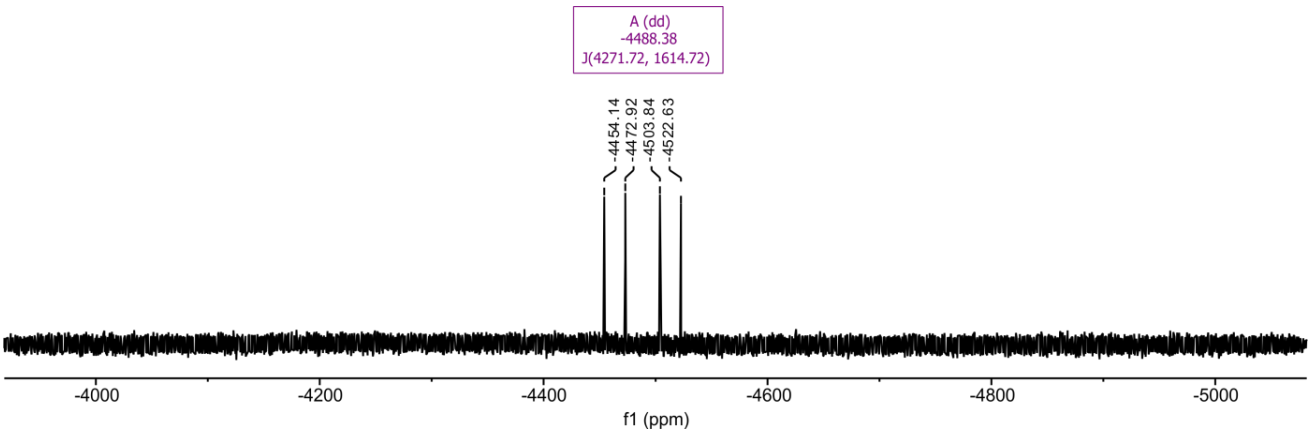


Figure S9. $^{195}$Pt NMR spectrum of ***cis*-MesPtBr** in $CDCl_3$.

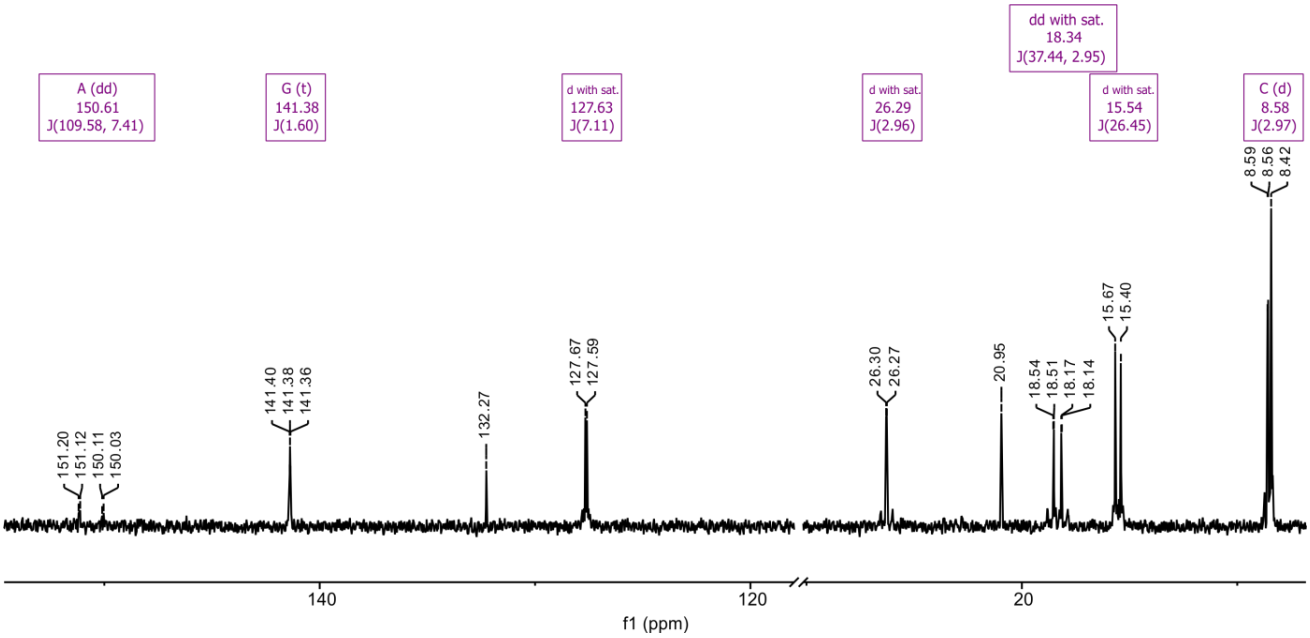


Figure S10. $^{13}C$ NMR spectrum of ***cis*-MesPtBr** in $CDCl_3$.

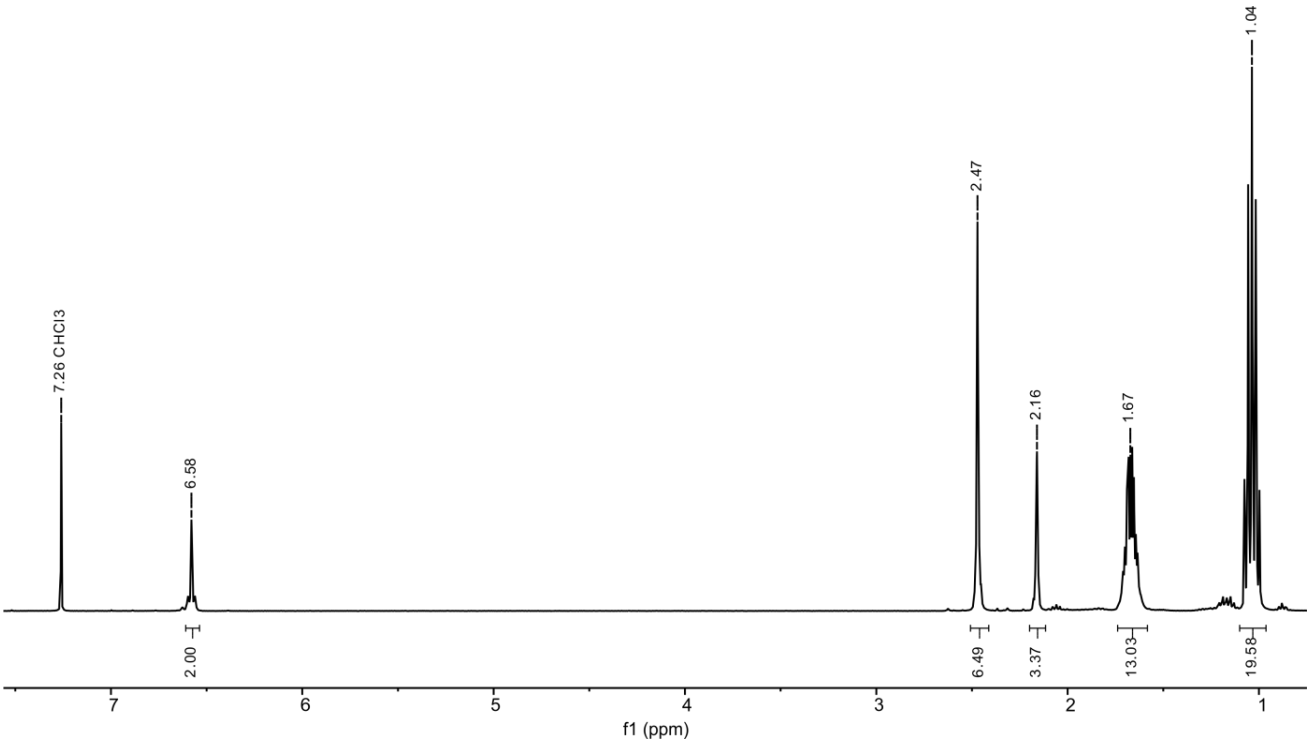


Figure S11. $^{1}H$ NMR spectrum of ***trans*-MesPtBr** in $CDCl_3$.

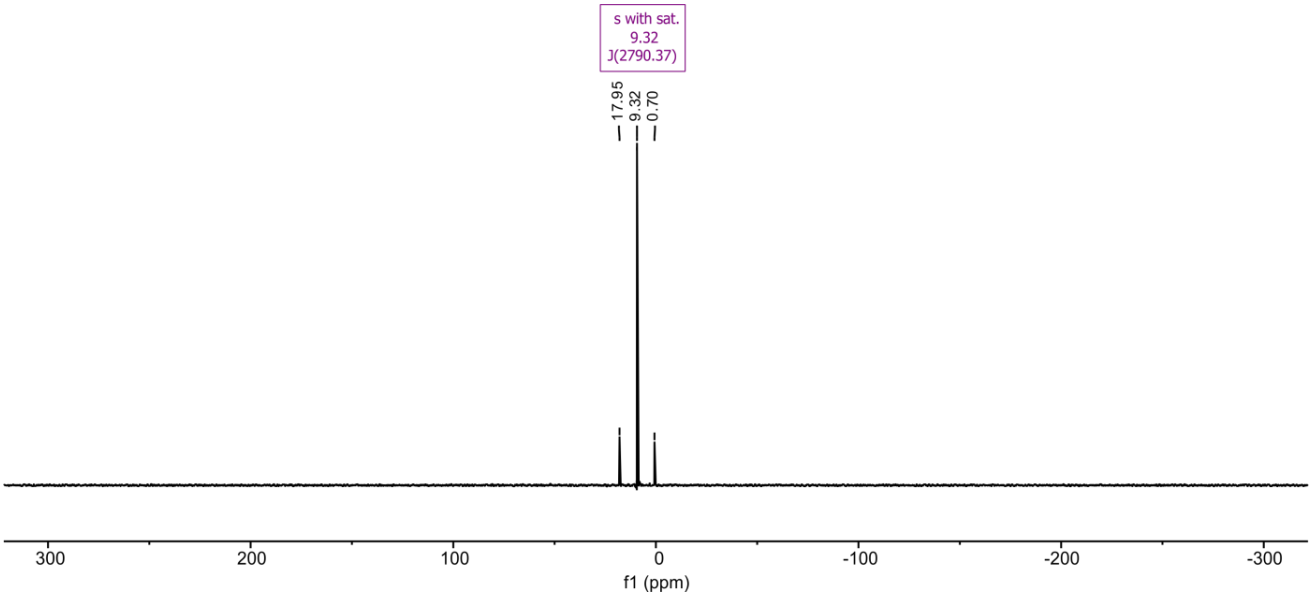


Figure S12. $^{31}$P NMR spectrum of ***trans*-MesPtBr** in $CDCl_3$.

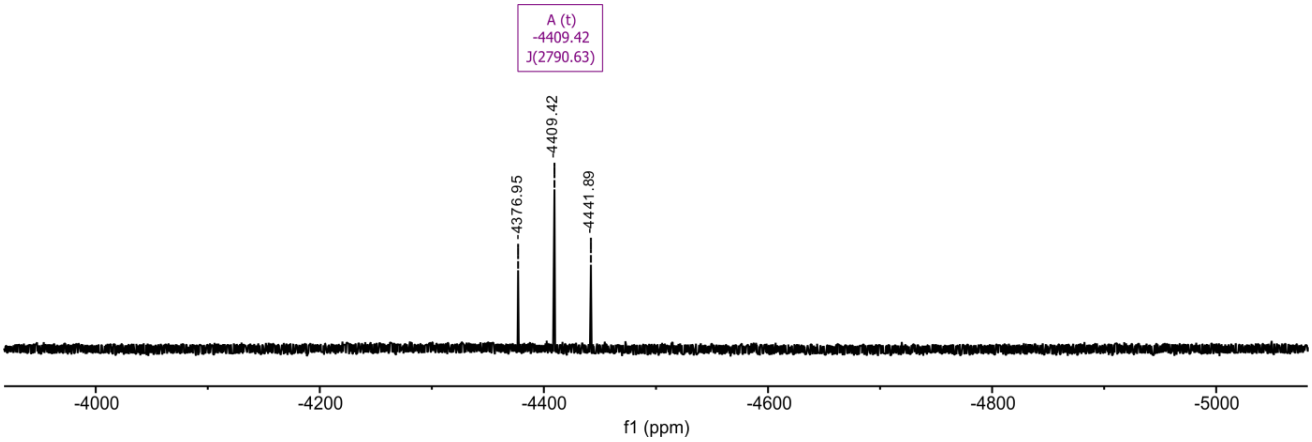


Figure S13. $^{195}$Pt NMR spectrum of ***cis*-MesPtBr** in $CDCl_3$.

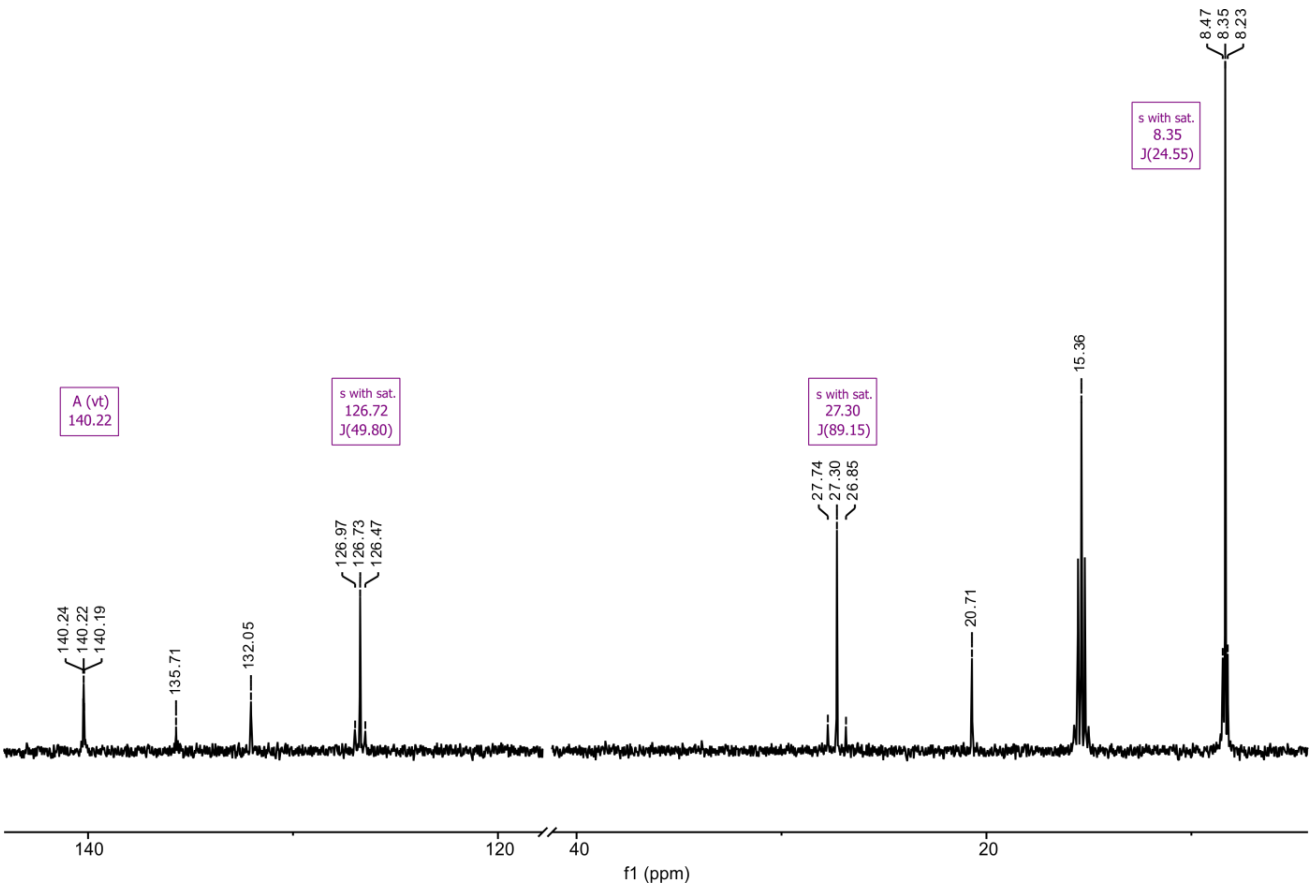


Figure S14. $^{13}$C NMR spectrum of ***trans*-MesPtBr** in $CDCl_3$.

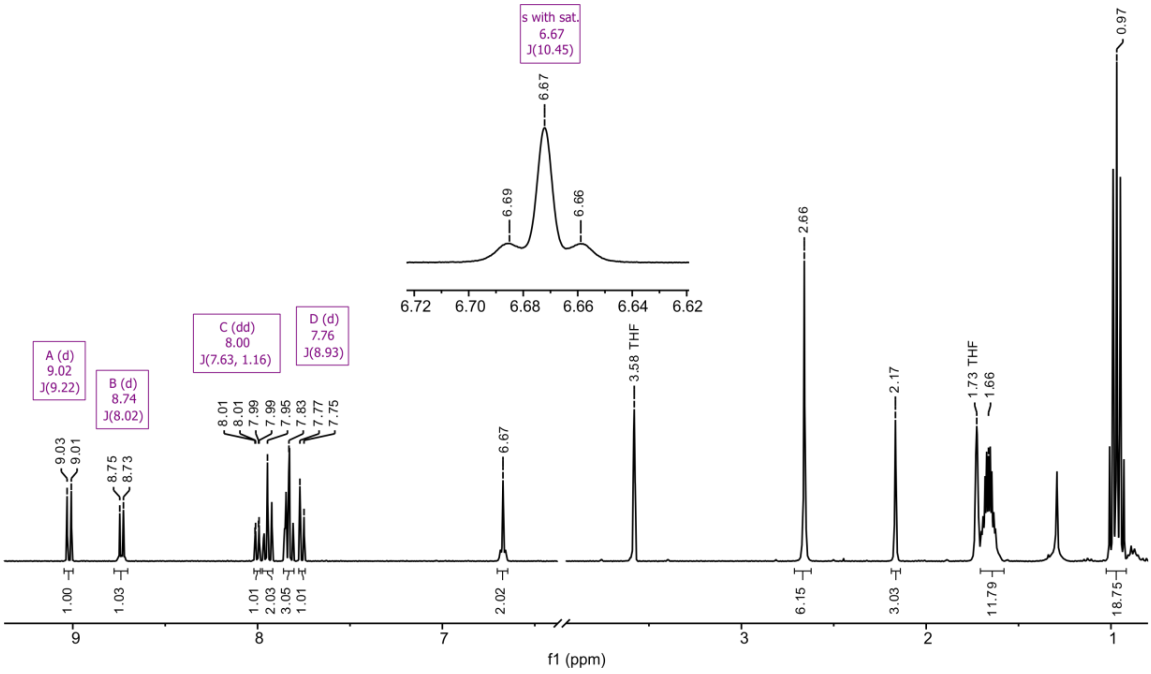


Figure S15. $^{1}$H NMR spectrum of **MesPtSPyr** in THF-*d8*.

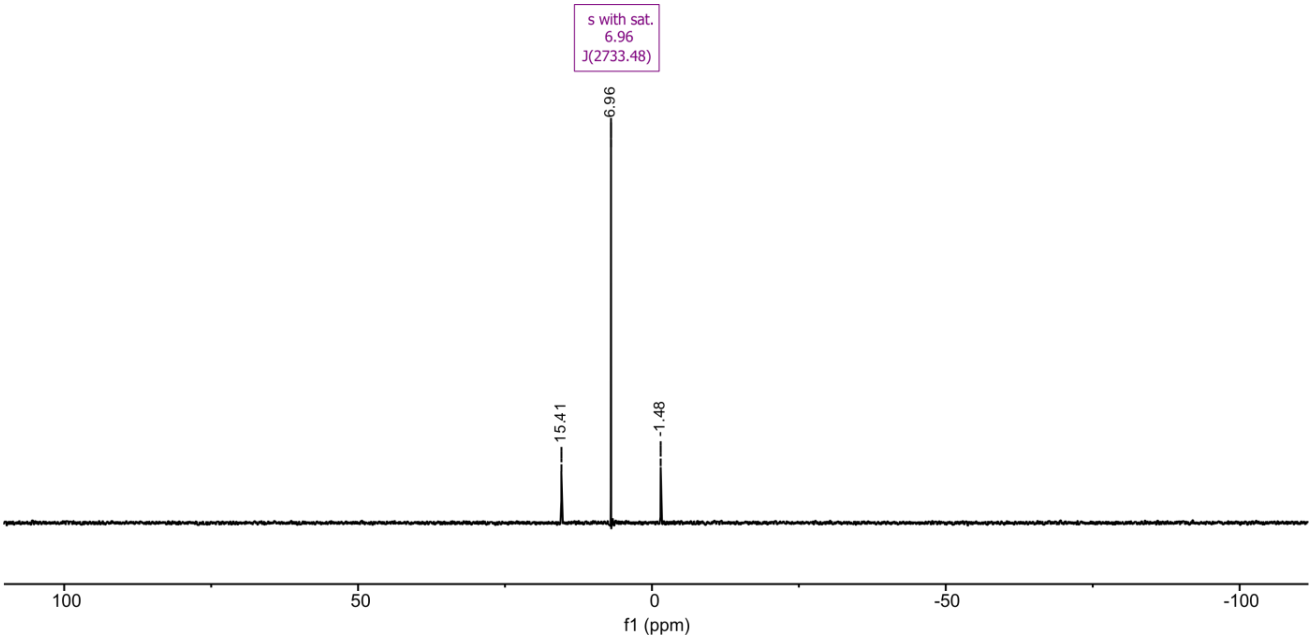


Figure S16. $^{31}$P NMR spectrum of **MesPtSPyr** in THF-*d8*.

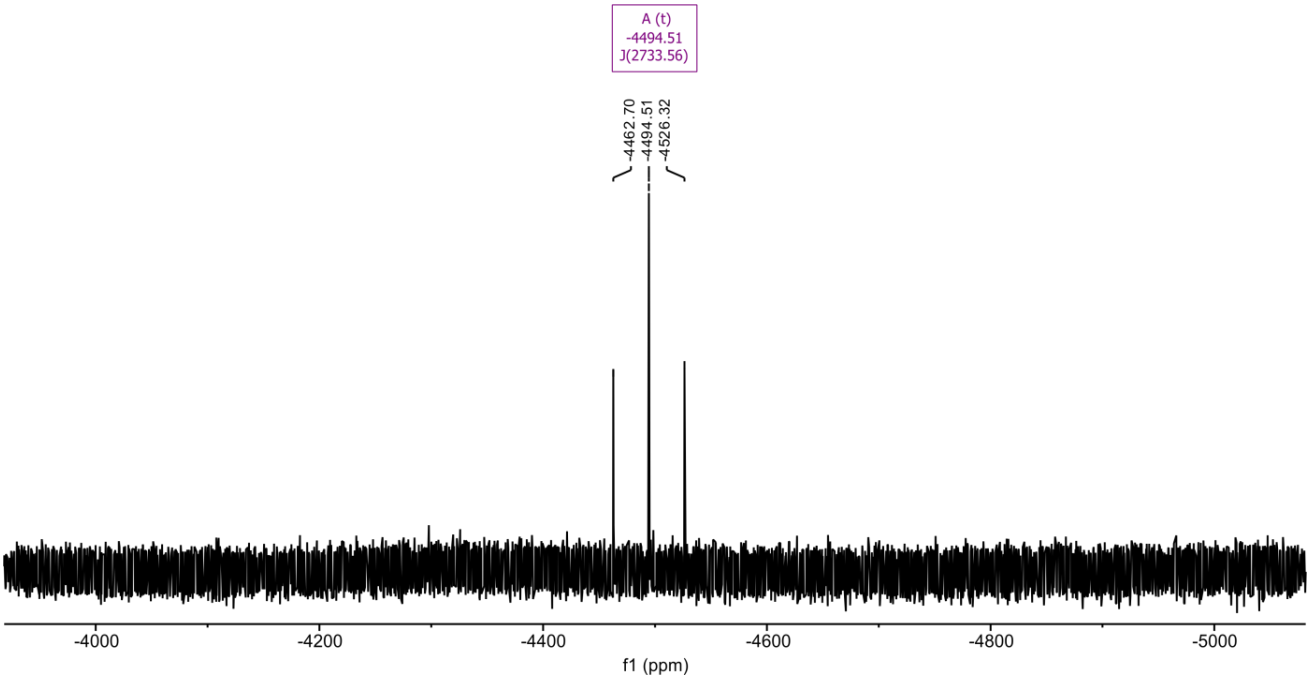


Figure S17. $^{195}$Pt NMR spectrum of **MesPtSPyr** in THF-*d8*.

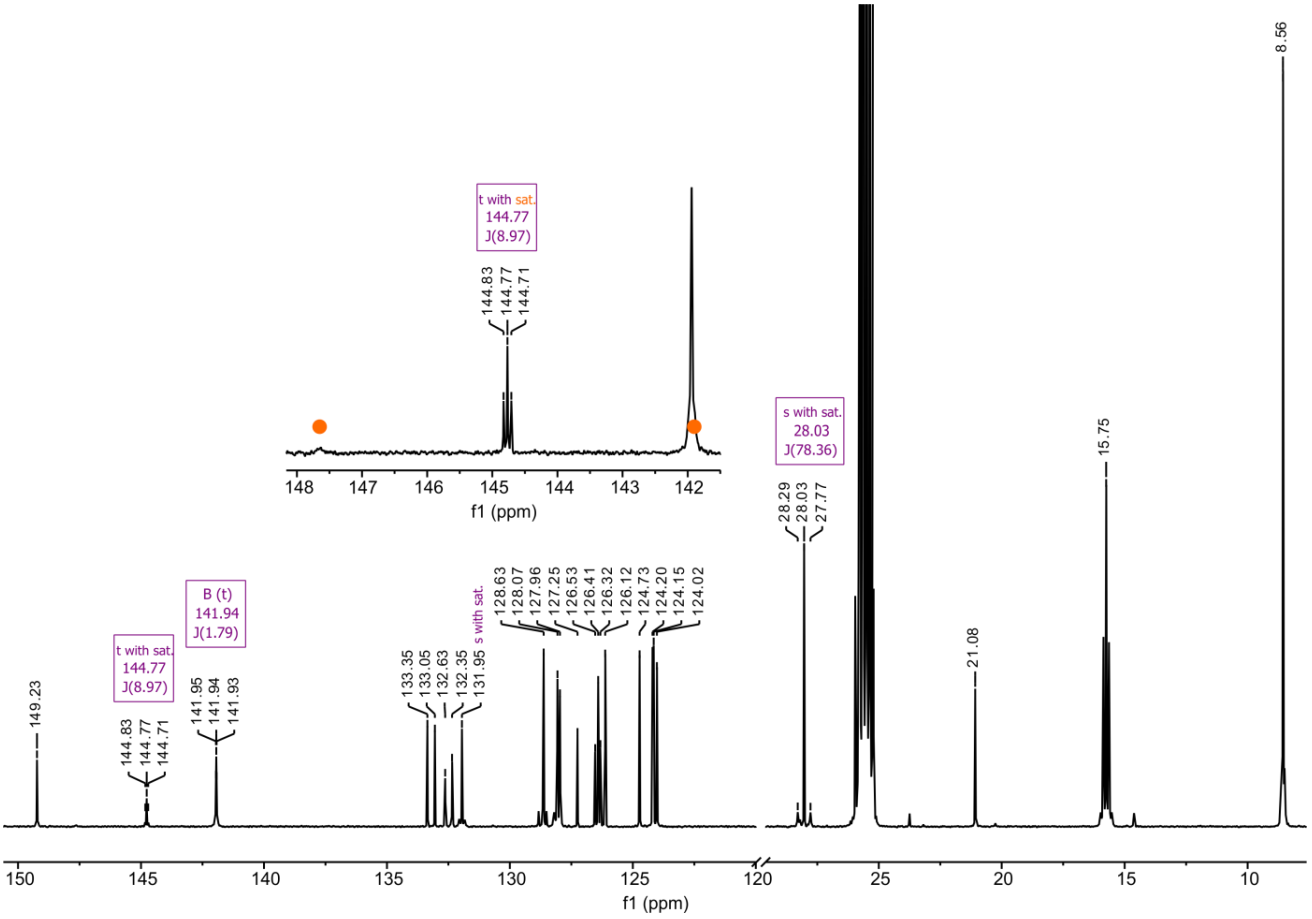


Figure S18. $^{13}$C NMR spectrum of **MesPtSPyr** in THF-*d8*.

## Emission Spectroscopy of MesPtSPyr

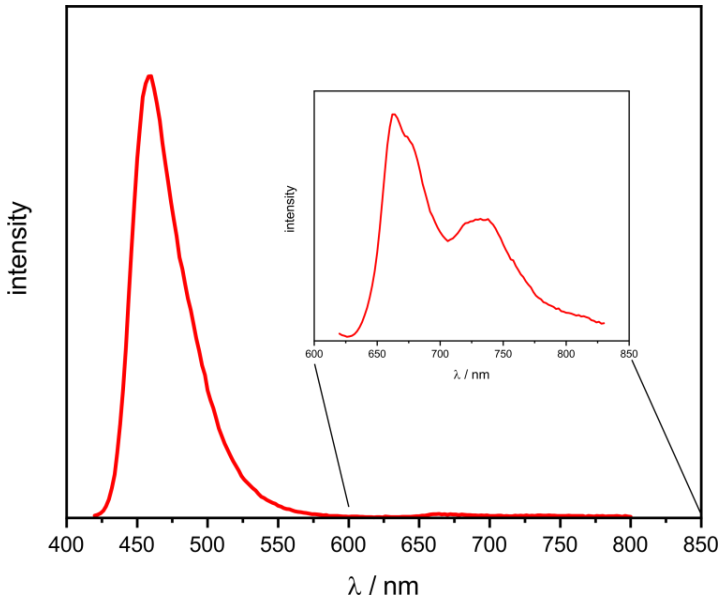


Figure S19. Emission of **MesPtSPyr** in a ca 1 μM degassed toluene solution at r.t.

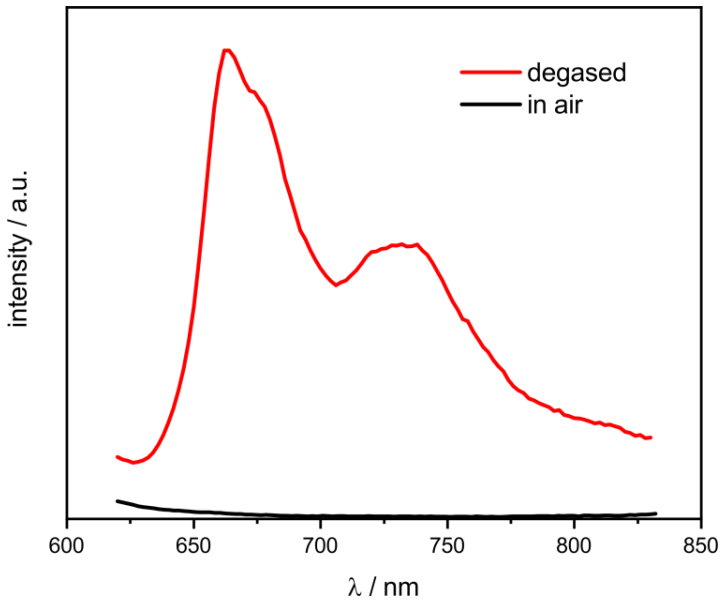


Figure S20. Phosphorescence emission of **MesPtSPyr** in a ca 1 μM toluene solution at r.t.

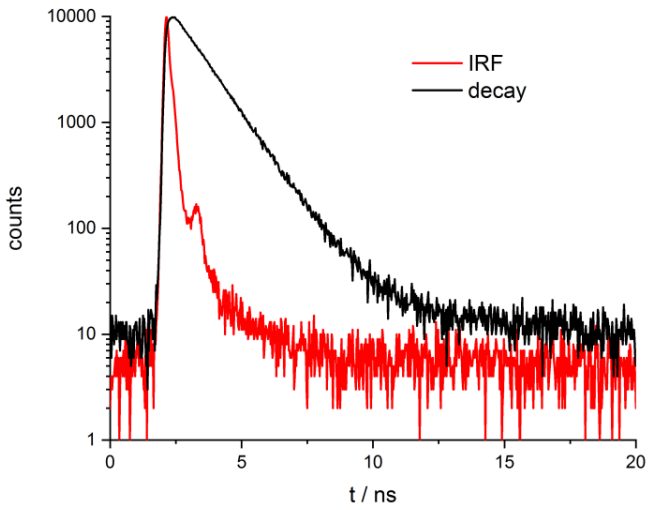


Figure S21. Fluorescence decay traces of **MesPtSPyr** in a deaerated and nitrogen-saturated 1 μM toluene solution at r.t. Decay can be fitted as a monoexponential decay with a lifetime of 1.113 ± 0.005 ns.

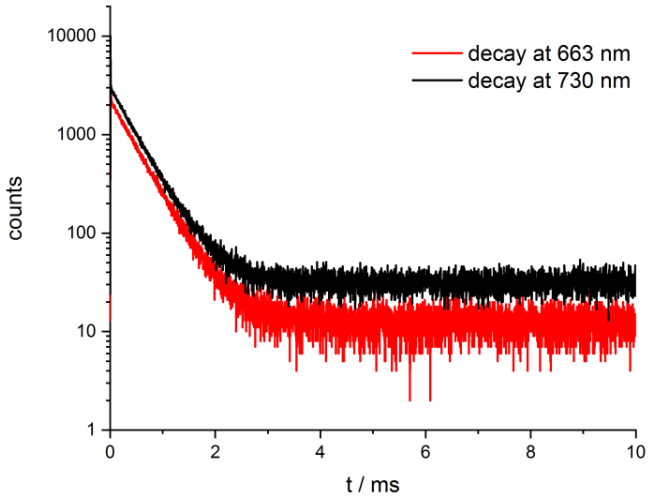


Figure S22. Phosphorescence decay traces of **MesPtSPyr** in a deaerated and nitrogen-saturated 1 μM toluene solution at r.t. Decay can be fitted as a monoexponential decay with a lifetime of 448 ± 6 μs.

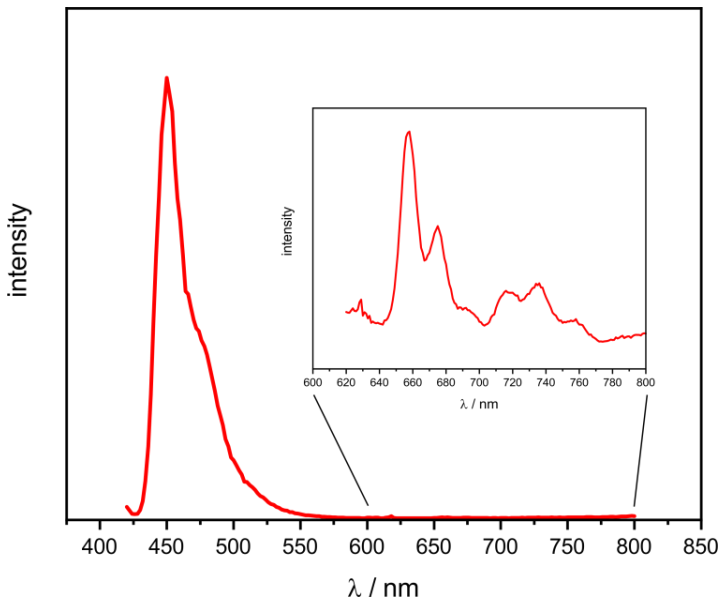


Figure S23. Emission of **MesPtSPyr** in a 2-MeTHF matrix at 77K.

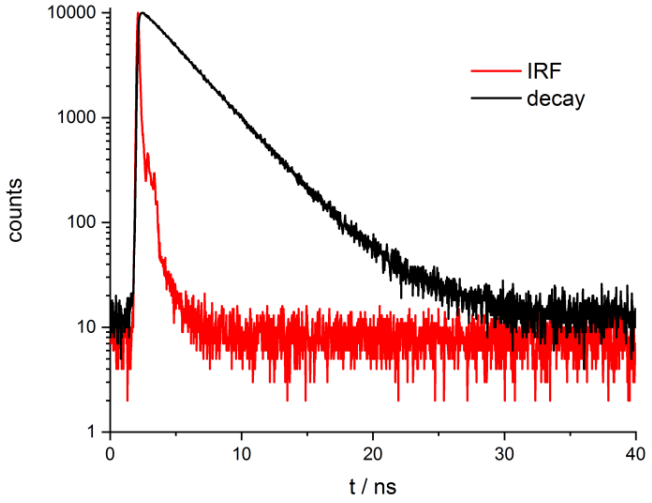


Figure S24. Fluorescence decay traces of **MesPtSPyr** in a 2-MeTHF matrix at 77 K. Decay can be fitted with a monoexponential decay with a lifetime of 3.19 ± 0.03 ns.

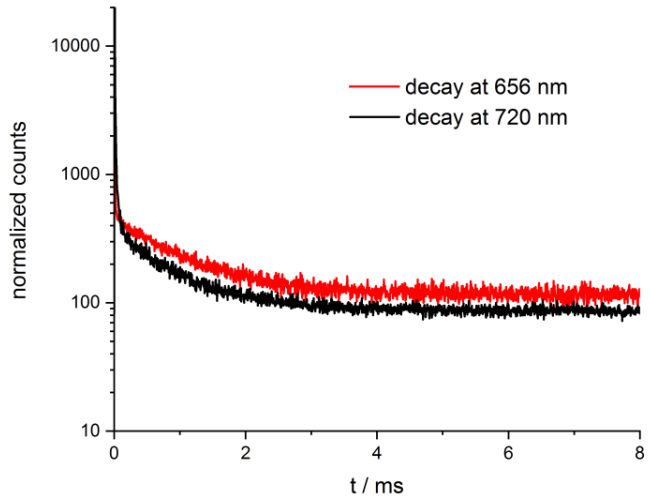


Figure S25. Phosphorescence decay traces of **MesPtSPyr** in a 2-MeTHF matrix at 77 K. Decay can be fitted with a monoexponential decay and a lifetime of 1.04 ± 0.06 ms.

# UV/Vis and Quantum Chemical Calculations

**Table S1. Absorption data for BPtSPyr and MesPtSPyr as well as TD-DFT-calculated band energies and assignments**

| absorption data | | TD-DFT calculations[a] | | | |
|---|---|---|---|---|---|
| solvent | $\lambda_{max}$[b] ($\varepsilon$[c]) | $\lambda$[b] | $f$[d] | m.c.[e] | assignment |
| | | **MesPtSPyr** | | | |
| toluene | 307 (14), 431 (25) | n.d. | n.d. | n.d. | n.d. |
| THF | 306 (12), 431 (22) | | | | |
| acetone | 430 (23) | | | | |
| | | **BPtSPyr** | | | |
| toluene | 418 (28), 469 (51), 499 (4) | 392 | 0.37 | H→L | $\pi\pi^*$ BDP |
| THF | 419 (29), 467 (51), 493 (4) | 402 | 0.66 | H→L+1 | $\pi\pi^*$ pyrS |
| acetone | 416 (29), 465 (50), 483 (4) | 567 | 0.05 | H-1→L | PB-CT |

[a]DFT calculations on the pbe1pbe/6-31G(d) level of therory; PCM model for $CH_2Cl_2$. [b]$\lambda$ in nm. [c]$\varepsilon$ / $10^3$ $M^{-1}$ $cm^{-1}$. [d]$f$ = oscillator strength. [e]m.c. = major contribution. H refers to HOMO and L to LUMO.

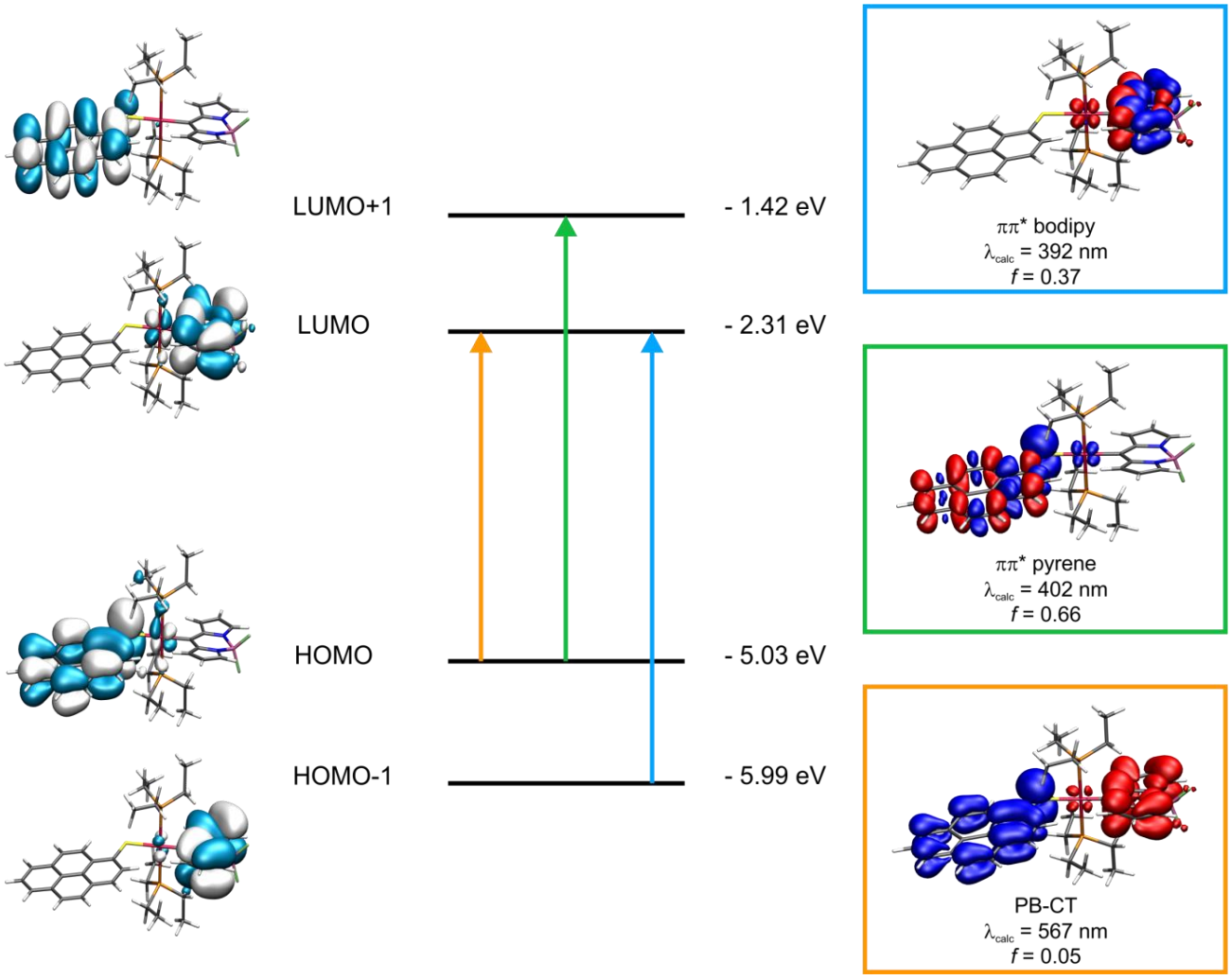


Figure S26. Graphical representation of the relevant MOs and TD-DFT energies of **BPtSPyr** in the neutral form as well as electron density difference maps (*blue* = electron density loss, *red* = electron density gain).

**Table S2. Calculated Mulliken parameters of BPtSPyr in the neutral form. Fragment contributions are given in percent.**

| Orbital | Pt | $PEt_3$ | bodipy | mercaptopyrene |
|---|---|---|---|---|
| LUMO+1 | 1 | 0 | 0 | 99 |
| LUMO | 4 | 2 | 94 | 0 |
| HOMO | 3 | 2 | 1 | 94 |
| HOMO-1 | 1 | 1 | 98 | 0 |

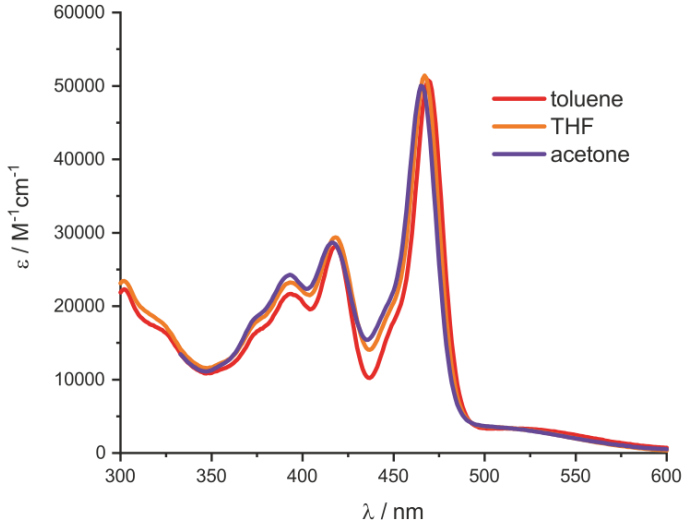


Figure S27. UV-Vis spectra of **BPtSPyr** in three different solvents.

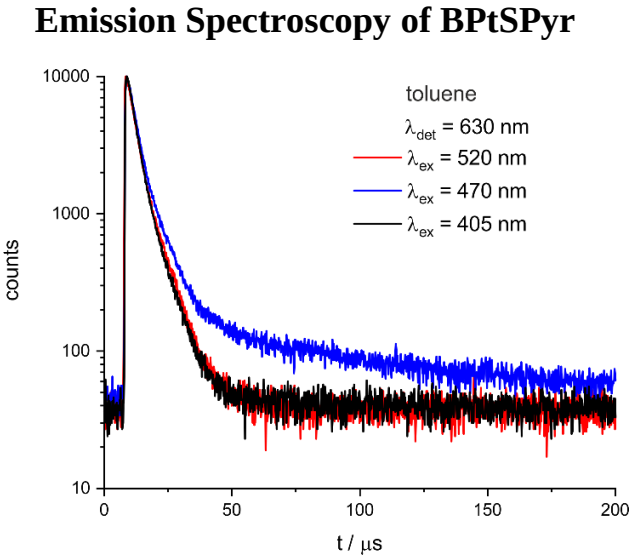


Figure S28. Emission decay traces of **BPtSPyr** detected at 630 nm in a deaerated and nitrogen-saturated 1 μM toluene solution at r.t. The blue curve has two components for the overlapping emission from the $^{3}$BDP and the $^{3}$PB-CT states.

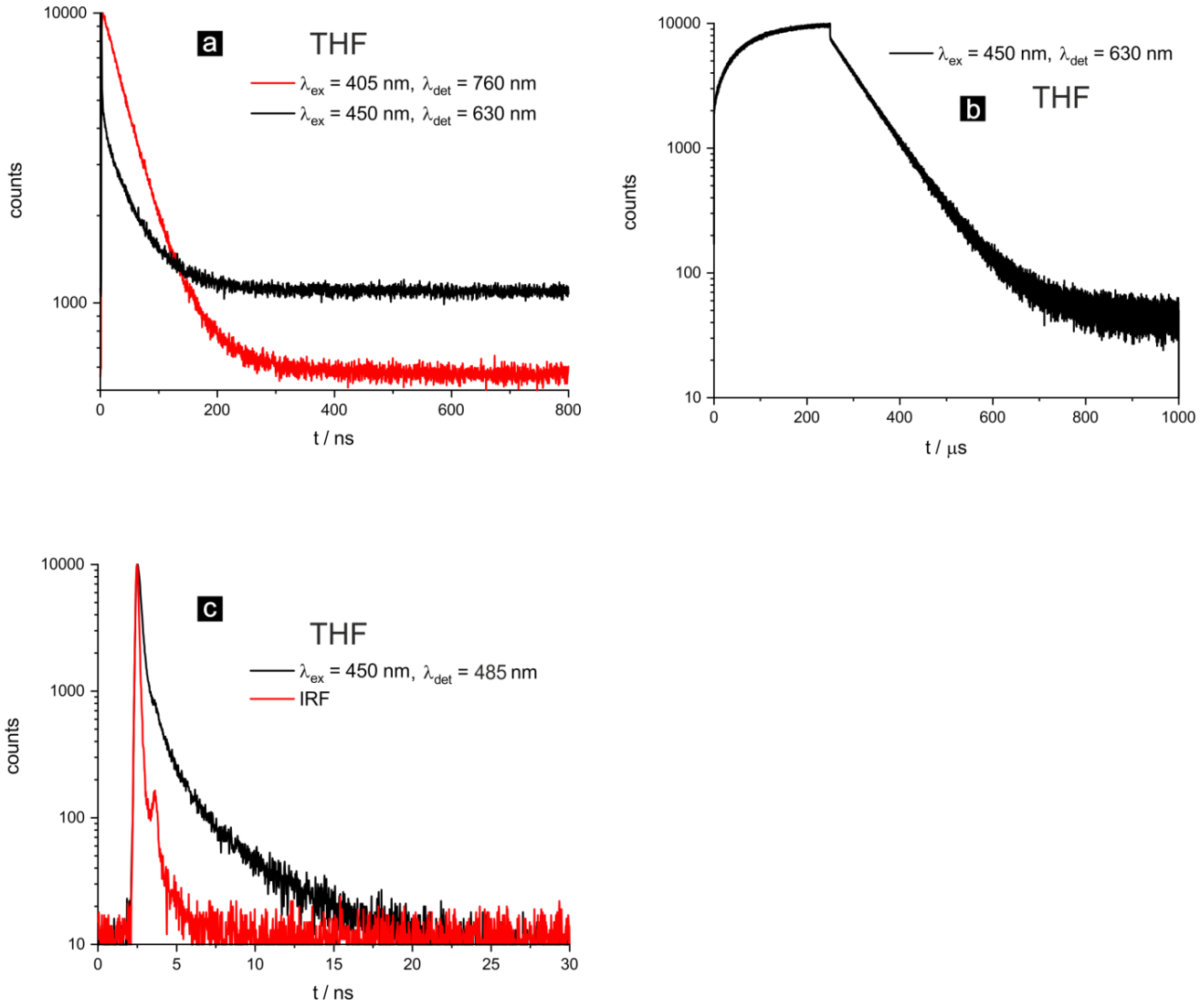


Figure S29. Emission decay traces of **BPtSPyr** in a deaerated and nitrogen-saturated 1 µM THF solution at r.t. In a) the 50 ns component is depicted; b) depicts the 78 µs component; c) shows the fluorescence lifetime decay. The rise time of 300 µs in Figure S29b is due to prior excited state saturation in the "burst mode".

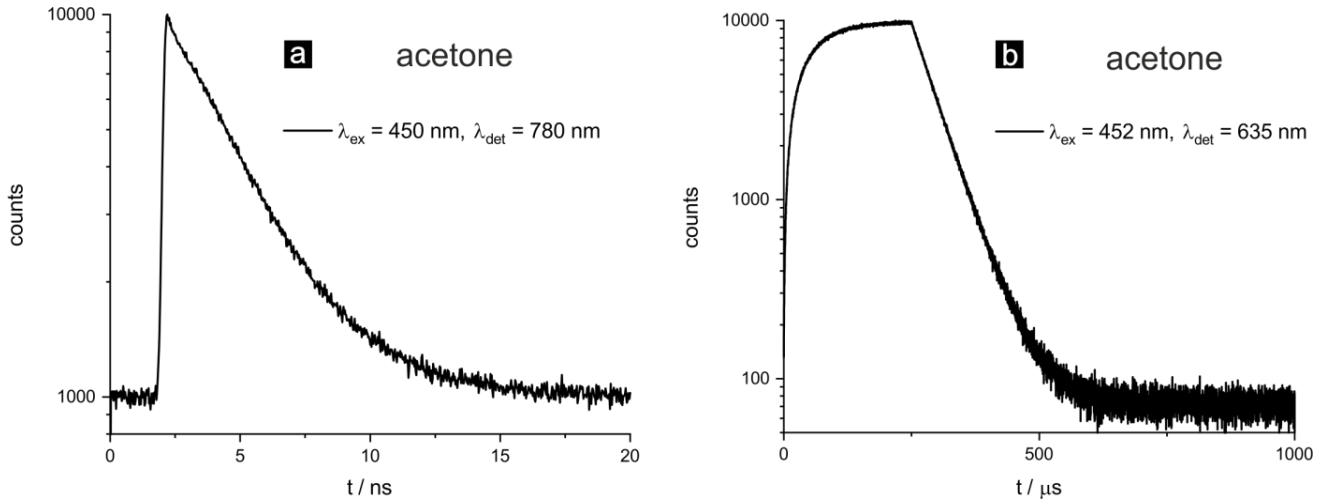


Figure S30. Emission decay traces of **BPtSPyr** in a deaerated and nitrogen-saturated 1 µM acetone solution at r.t. with a) depicting the 2.4 ns component and b) the 279 µs component. The rise time of 300 µs in Figure S30b is due to prior excited state saturation in the "burst mode".

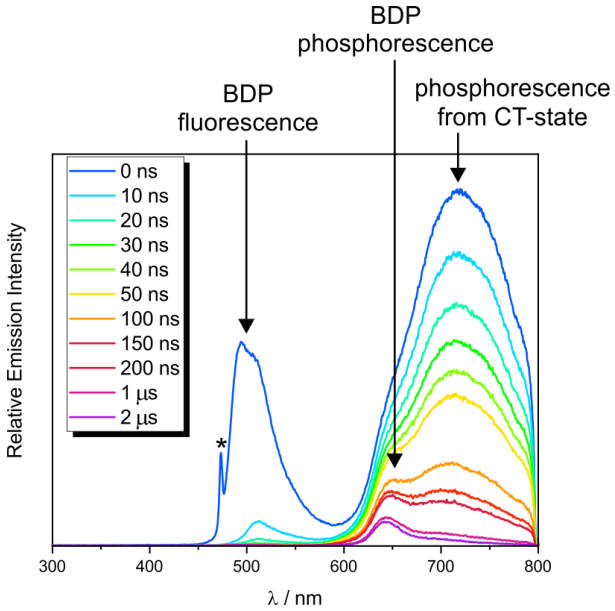


Figure S31. Transient emission spectra recorded after indicated delay times after laser excitation at 470 nm in a ca. 20 µM THF solution and time-integrated over 200 ns. *Residual excitation light. The shift of the NIR emission maximum in THF with respect to that in Figure 2 arises from its proximity to the low-energy limit of the detector.

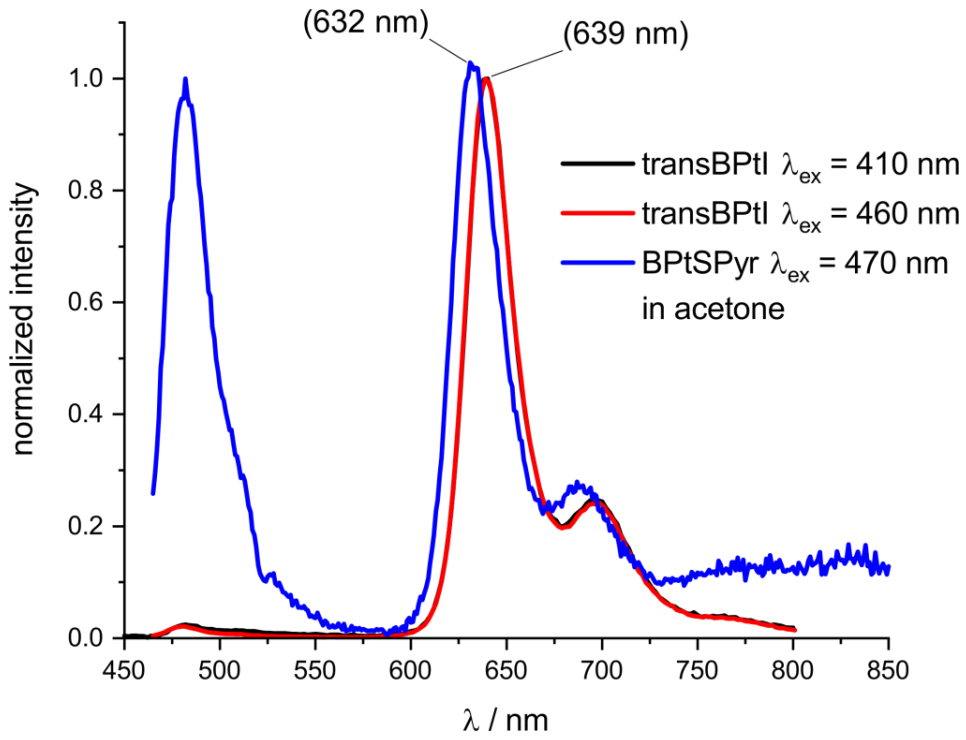


Figure S32. Comparison of the emission spectra of **BPtSPyr** (blue curve) and of **BPtI** at $\lambda_{exc}$ = 410 nm (black curve) or $\lambda_{exc}$ = 460 nm (red curve) in deaerated and nitrogen-saturated 1 µM acetone solutions at r.t. The different emission energies and intensity ratios of the fluorescence and phosphorescence emissions under identical conditions prove that the BDP-based emissions are also inherent features of **BPtSPyr** and are not due to contamination with the **BPtI** precursor.

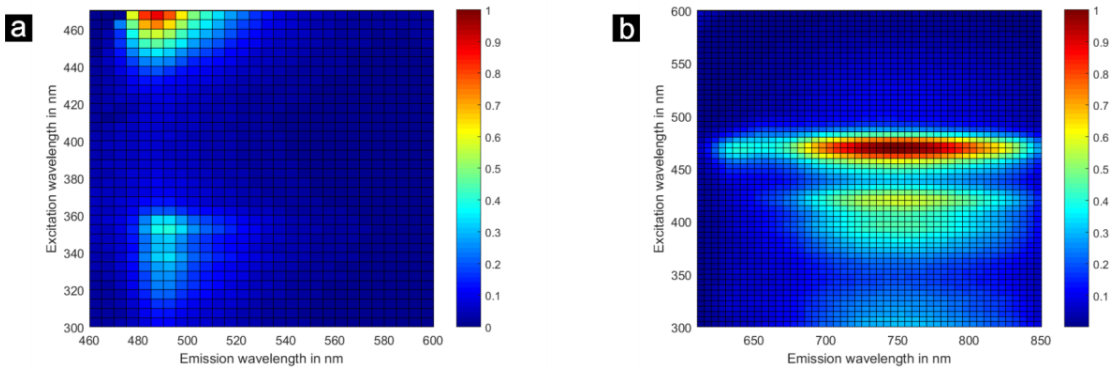


Figure S33. Emission vs. excitation maps recorded on a ca. 1 µM THF solution of **BPtSPyr** at r.t. for a) the fluorescence emission and b) the phosphorescence emission.

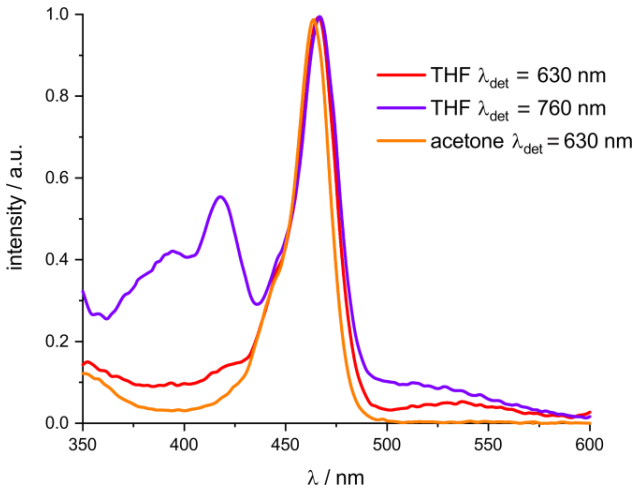


Figure S34. Excitation spectra of **BPtSPyr** recorded in ca. 1 µM THF or acetone solutions at r.t. with different detection wavelengths.

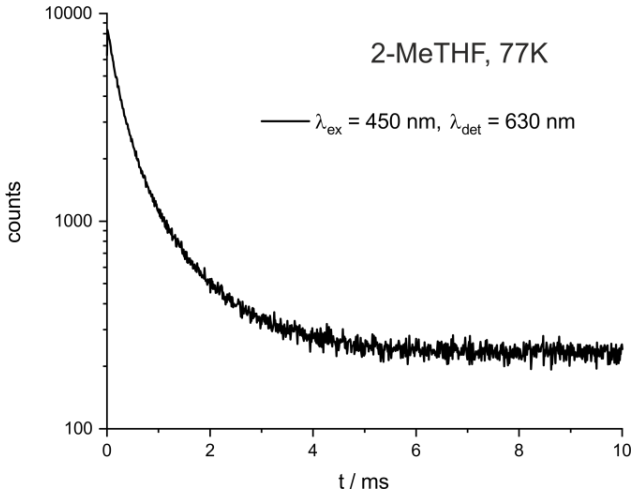


Figure S35. Emission decay trace of BPtSPyr in a 1 µM 2-MeTHF matrix at 77 K. The decay can be fitted with a biexponential model with decay times of 279 µs and 1.12 ms, which is due to the close energetic proximity of the two emissions.

## Transient Absorption Spectroscopy

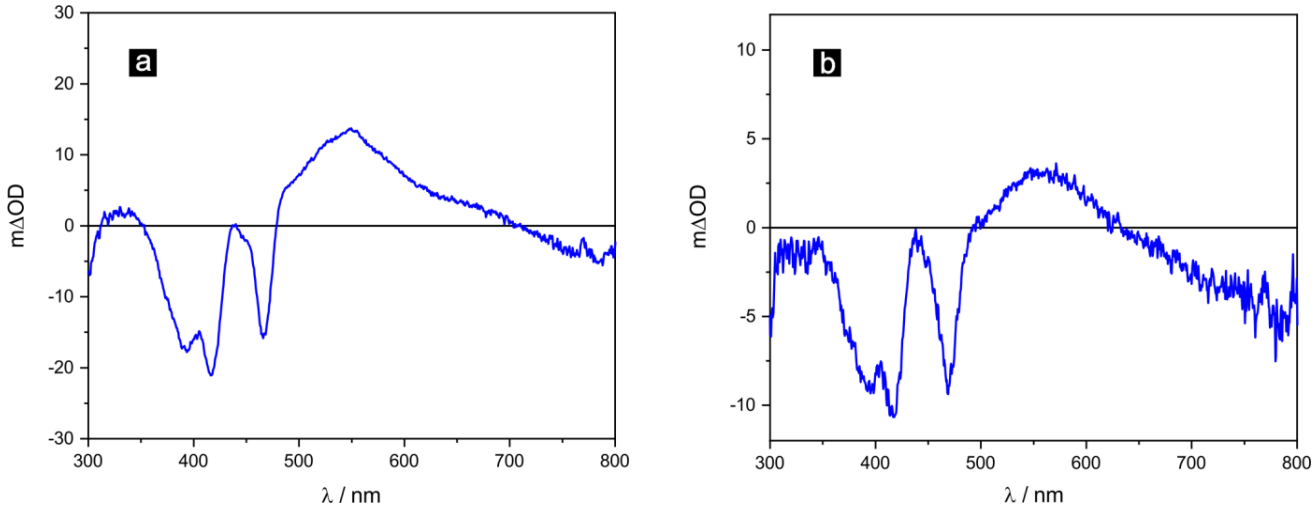


Figure S36. Transient absorption spectra of **BPtSPyr** recorded in a 20 μM THF solution at r.t. with laser excitation adjusted to a) 532 nm, or b) 410 nm time-integrated over 200 ns.

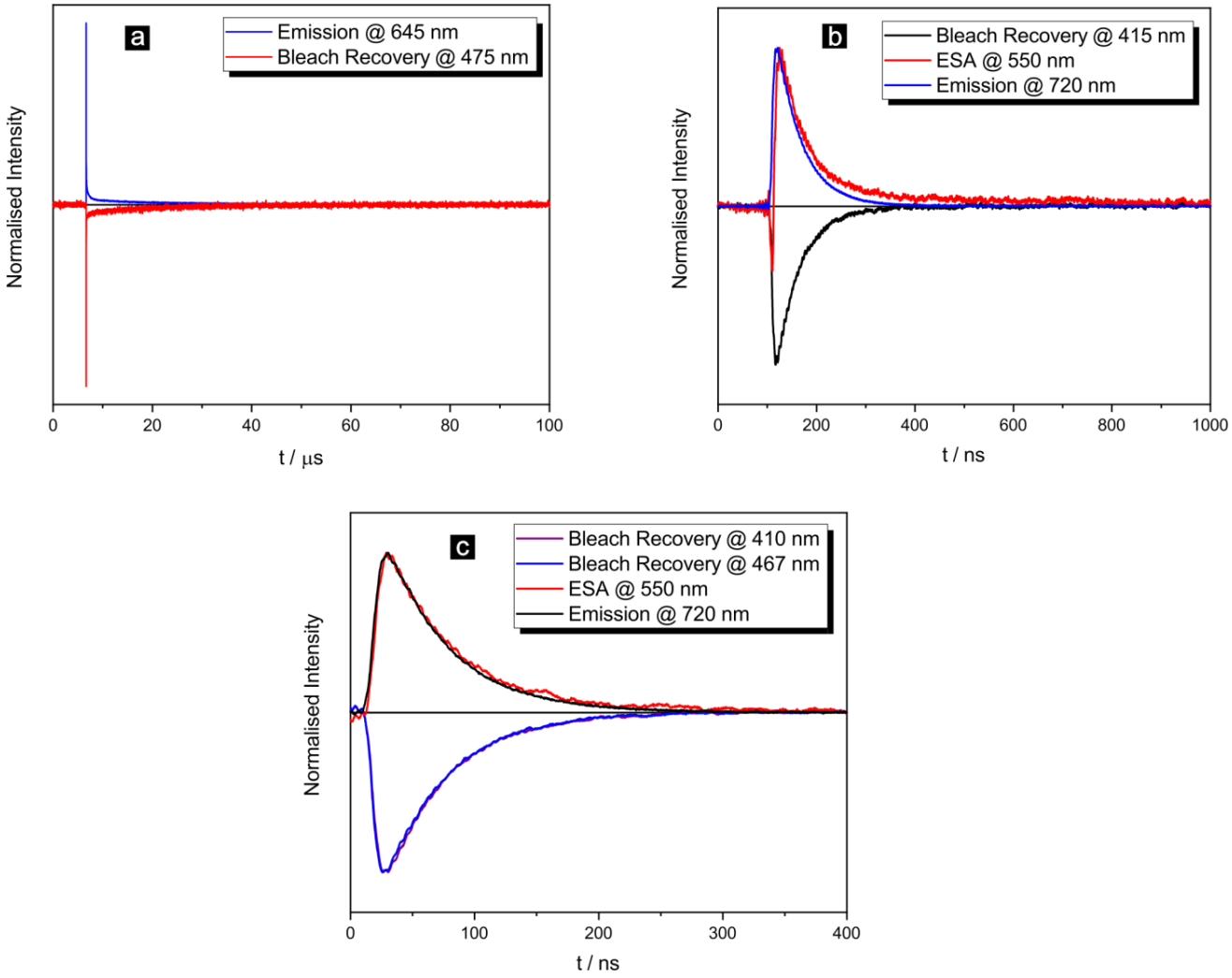


Figure S37. Single point kinetics of **BPtSPyr** recorded in 20 µM THF solution at r.t. after laser excitation at a,b) 470 nm, or c) 532 nm for the different features of the transient absorption spectrum. The exponential decays can be fitted with a lifetime of 16.5 µs for a) and 50 ns for b) and c).

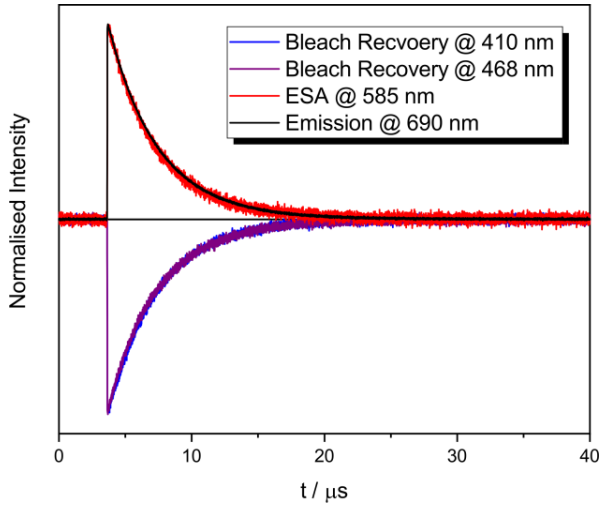


Figure S38. Single point kinetics of **BPtSPyr** recorded in 20 µM toluene solution at r.t. after laser excitation at 532 nm for the different features of the transient absorption spectm. The mono exponential decays can be fitted with a lifetime of 3.6 µs.

## Electrochemistry

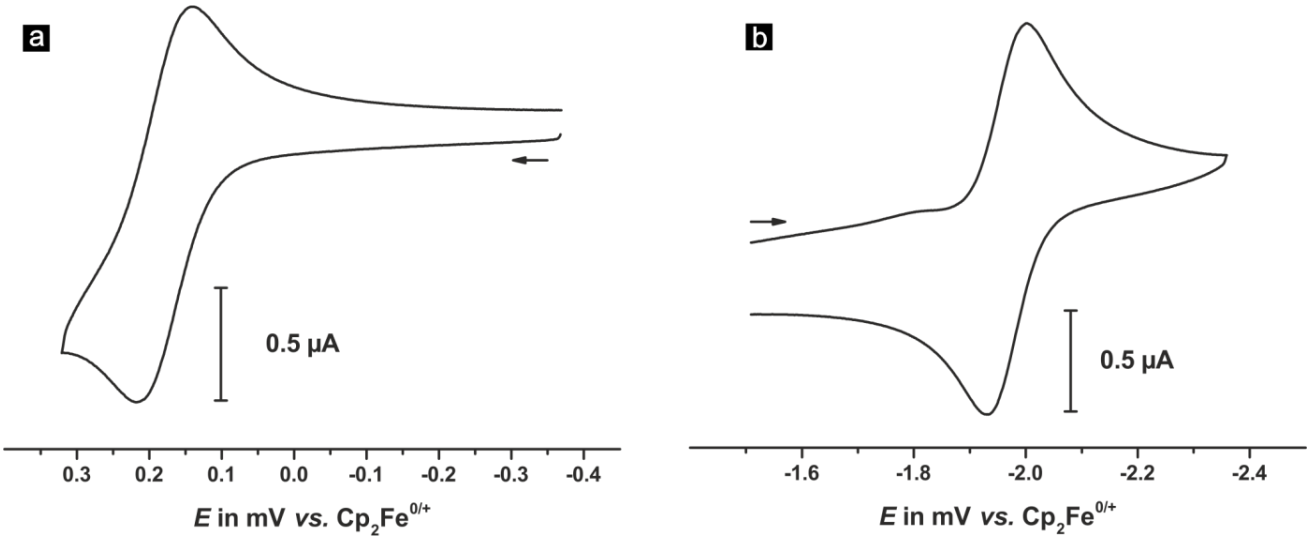


Figure S39. Cyclic voltammograms (ν = 100 mV/s) of a) the anodic and b) the cathodic sweep of **BPtSPyr** in THF at r.t. with $NBu_4PF_6$ (0.1 M) as the supporting electrolyte referenced to the $Cp_2Fe^{0/+}$ couple ($E_{1/2}$ =0.000 V).

**Table S3. Electrochemical Data for BPtI and BPtSPyr**[a]

| complex | $E_{1/2}$ / mV (anodic sweep) | $E_{1/2}$ / mV (cathodic sweep) |
|---|---|---|
| **BPtI** | | -1770 |
| **BPtSPyr** | 180 | -1970 |

[a]All potentials are referenced to the $Cp_2Fe^{0/+}$ couple ($E_{1/2}$ =0.000 V) and were measured in $CH_2Cl_2$ at 293 K with $NBu_4PF_6$ as the supporting electrolyte.

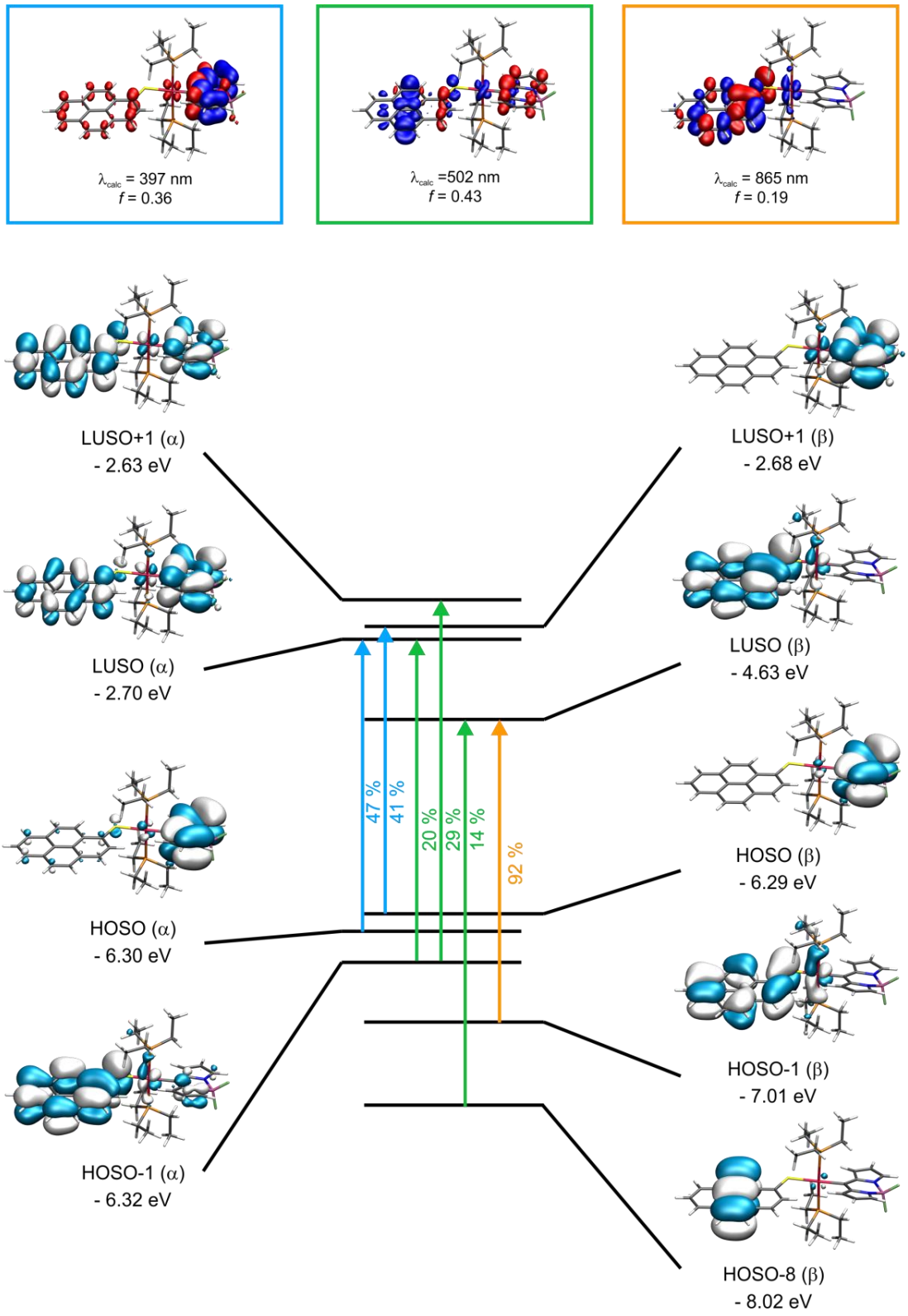


Figure S40. Graphical representations of the relevant spin orbitals and TD-DFT energies of **BPtSPyr** in the cationic form as well as electron density difference maps (*blue* = electron density loss, *red* = electron density gain).

**Table S4. Calculated Mulliken parameters of BPtSPyr in the cationic form. Fragment contributions are given in percent.**

| Orbital | Pt | $PEt_3$ | bodipy | mercaptopyrene |
|---|---|---|---|---|
| LUSO+1(β) | 3 | 2 | 93 | 2 |
| LUSO+1(α) | 2 | 1 | 31 | 66 |
| LUSO(β) | 2 | 2 | 1 | 95 |
| LUSO(α) | 1 | 2 | 63 | 34 |
| HOSO(α) | 1 | 1 | 93 | 5 |
| HOSO(β) | 1 | 1 | 98 | 0 |
| HOSO-1(α) | 2 | 2 | 5 | 90 |
| HOSO-1(β) | 6 | 6 | 1 | 87 |
| HOSO-8(β) | 1 | 0 | 0 | 99 |

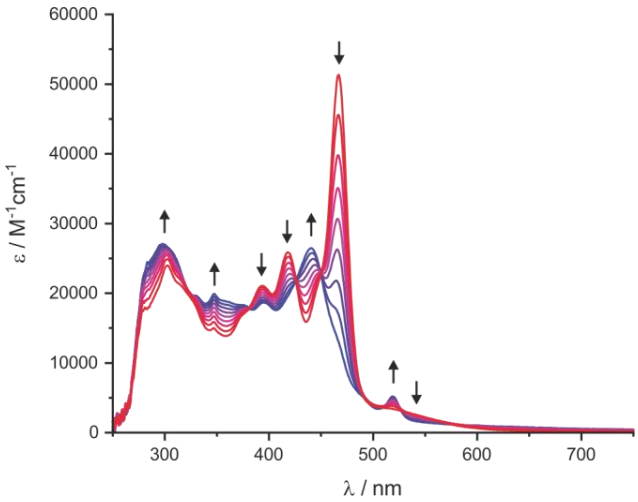


Figure S41. Changes of UV/Vis/NIR spectra of **BPtSPyr** on reductions (THF, $NBu_4PF_6$, 293 K).

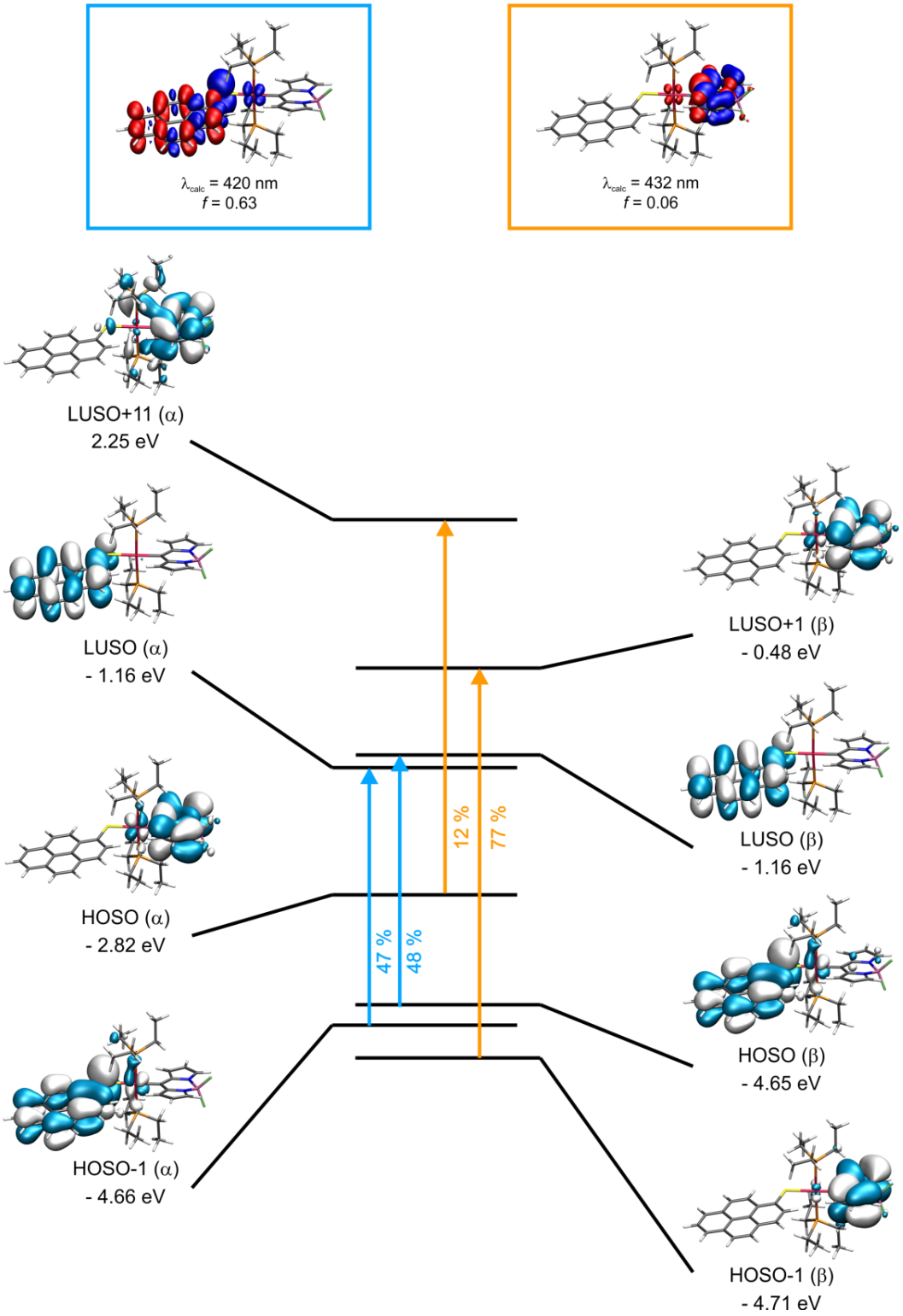


Figure S42. Graphical representations of the relevant spin orbitals and TD-DFT energies of **BPtSPyr** in the anionic form as well as electron density difference maps (*blue* = electron density loss, *red* = electron density gain).

**Table S5. Calculated Mulliken parameters of BPtSPyr in the anionic form. Fragment contributions are given in percent.**

| Orbital | Pt | $PEt_3$ | bodipy | mercaptopyrene |
|---|---|---|---|---|
| LUSO+11(α) | 9 | 14 | 77 | 0 |
| LUSO+1(β) | 4 | 3 | 92 | 1 |
| LUSO(β) | 1 | 0 | 0 | 99 |
| LUSO(α) | 1 | 0 | 0 | 99 |
| HOSO(α) | 3 | 2 | 94 | 0 |
| HOSO(β) | 4 | 3 | 2 | 91 |
| HOSO-1(α) | 4 | 3 | 1 | 92 |
| HOSO-1(β) | 1 | 1 | 96 | 1 |

**Table S6. Calculated spin density contributions of the respective fragments to the spin density surfaces of the radical cation and anion of BPtSPyr.**

| Oxidation State | cation | anion |
|---|---|---|
| Pt | -0.004 | -0.002 |
| $PEt_3$ | 0.023 | 0.017 |
| bodipy | -0.004 | 0.990 |
| mercaptopyrene | 0.984 | -0.006 |

# Molecular Structures Obtained by Quantum Chemical Calculations

**Table S7. Atomic coordinates of the optimized ground state geometry of BPtSPyr in the neutral form**

| Atom | x | y | z |
|---|---|---|---|
| Pt | 0.85753 | 0.29072 | -0.35315 |
| B | 5.49065 | -1.06605 | 1.10122 |
| F | 5.73372 | -2.41268 | 0.83786 |
| F | 6.59998 | -0.48414 | 1.69619 |
| N | 5.12667 | -0.33054 | -0.21147 |
| N | 4.24586 | -0.92401 | 2.01058 |
| P | 0.64512 | -1.8441 | -1.32242 |
| P | 1.10724 | 2.49799 | 0.43654 |
| C | 2.72634 | -0.13259 | 0.25332 |
| C | 3.8367 | 0.0043 | -0.6064 |
| C | 3.91647 | 0.52447 | -1.91704 |
| H | 3.0707 | 0.88711 | -2.48778 |
| C | 5.25475 | 0.50063 | -2.2975 |
| H | 5.68257 | 0.83554 | -3.2329 |
| C | 5.96476 | -0.03869 | -1.21555 |
| H | 7.02642 | -0.22797 | -1.12073 |
| C | 2.97273 | -0.57741 | 1.57222 |
| C | 2.09945 | -0.6984 | 2.67565 |
| H | 1.03894 | -0.48145 | 2.65069 |
| C | 2.8552 | -1.11431 | 3.76786 |
| H | 2.51279 | -1.29731 | 4.77746 |
| C | 4.17318 | -1.24381 | 3.31031 |
| H | 5.05809 | -1.55068 | 3.85316 |
| C | 2.2037 | -2.82444 | -1.42058 |
| H | 2.91932 | -2.21815 | -1.98708 |
| H | 2.60775 | -2.88129 | -0.40283 |
| C | 2.08085 | -4.21782 | -2.03 |
| H | 3.06198 | -4.70458 | -2.03211 |
| H | 1.73071 | -4.18363 | -3.06668 |
| H | 1.39815 | -4.85897 | -1.46297 |
| C | 0.03115 | -1.76713 | -3.0547 |
| H | -0.01609 | -2.79357 | -3.43789 |
| H | -0.9961 | -1.39247 | -2.99162 |
| C | 0.86207 | -0.87704 | -3.97111 |
| H | 0.45322 | -0.89522 | -4.987 |
| H | 1.90625 | -1.20351 | -4.02761 |
| H | 0.84904 | 0.16073 | -3.62076 |
| C | -0.56388 | -2.96631 | -0.5074 |
| H | -1.5025 | -2.40646 | -0.43722 |

| | | | |
|---|---|---|---|
| H | -0.74263 | -3.81278 | -1.18226 |
| C | -0.1275 | -3.45479 | 0.86965 |
| H | -0.93015 | -4.0377 | 1.33335 |
| H | 0.11025 | -2.61938 | 1.53608 |
| H | 0.75857 | -4.09591 | 0.81308 |
| C | 2.86399 | 3.05635 | 0.53283 |
| H | 3.33791 | 2.43275 | 1.30069 |
| H | 3.34057 | 2.7755 | -0.41209 |
| C | 3.09348 | 4.53634 | 0.82394 |
| H | 4.16878 | 4.73017 | 0.9007 |
| H | 2.63807 | 4.85459 | 1.76692 |
| H | 2.70161 | 5.17542 | 0.02622 |
| C | 0.47862 | 2.81214 | 2.14154 |
| H | 0.9235 | 2.04019 | 2.78087 |
| H | 0.89536 | 3.77173 | 2.4699 |
| C | -1.03926 | 2.82706 | 2.28272 |
| H | -1.31141 | 2.96299 | 3.33501 |
| H | -1.49128 | 1.8942 | 1.93462 |
| H | -1.48741 | 3.65041 | 1.71747 |
| C | 0.27747 | 3.7567 | -0.61301 |
| H | -0.78814 | 3.50686 | -0.61358 |
| H | 0.39201 | 4.73408 | -0.12836 |
| C | 0.80779 | 3.78039 | -2.04259 |
| H | 0.6677 | 2.80706 | -2.52599 |
| H | 1.87449 | 4.02708 | -2.08195 |
| H | 0.27072 | 4.52968 | -2.63357 |
| S | -1.3789 | 0.80589 | -1.14951 |
| C | -2.58324 | 0.14241 | -0.05091 |
| C | -3.96532 | 0.22373 | -0.37986 |
| C | -2.2237 | -0.45556 | 1.16858 |
| C | -4.93729 | -0.28863 | 0.53007 |
| C | -4.43124 | 0.80883 | -1.60268 |
| C | -3.16909 | -0.96172 | 2.0471 |
| H | -1.16697 | -0.519 | 1.41726 |
| C | -6.32756 | -0.20365 | 0.21758 |
| C | -4.53682 | -0.88957 | 1.7583 |
| C | -5.75565 | 0.88943 | -1.90146 |
| H | -3.69558 | 1.19395 | -2.30179 |
| H | -2.84538 | -1.41862 | 2.97997 |
| C | -6.75324 | 0.39045 | -1.00468 |
| C | -7.3009 | -0.71237 | 1.1282 |
| C | -5.53443 | -1.39388 | 2.65212 |
| H | -6.07933 | 1.33887 | -2.83745 |
| C | -8.12358 | 0.46687 | -1.2926 |
| C | -8.65993 | -0.61414 | 0.79935 |

| | | | |
|---|---|---|---|
| C | -6.85825 | -1.30999 | 2.35413 |
| H | -5.20713 | -1.84886 | 3.58434 |
| C | -9.06402 | -0.0306 | -0.39761 |
| H | -8.44306 | 0.9217 | -2.22721 |
| H | -9.40035 | -1.00201 | 1.49498 |
| H | -7.60661 | -1.69579 | 3.04215 |
| H | -10.1226 | 0.03619 | -0.63421 |

**Table S8. Atomic coordinates of the optimized ground state geometry of BPtSPyr in the cationic form**

| | | | |
|---|---|---|---|
| Pt | 0.83696 | 0.27223 | -0.31157 |
| B | 5.51449 | -0.98943 | 0.9736 |
| F | 5.6453 | -2.34494 | 0.67998 |
| F | 6.68656 | -0.48383 | 1.50539 |
| N | 5.11361 | -0.21852 | -0.31014 |
| N | 4.33164 | -0.7855 | 1.95413 |
| P | 0.73877 | -1.90917 | -1.23363 |
| P | 1.05924 | 2.50569 | 0.44941 |
| C | 2.73826 | -0.06591 | 0.2449 |
| C | 3.80463 | 0.09039 | -0.66048 |
| C | 3.82742 | 0.60914 | -1.97577 |
| H | 2.95776 | 0.95785 | -2.51915 |
| C | 5.15065 | 0.61074 | -2.4008 |
| H | 5.5398 | 0.95489 | -3.34942 |
| C | 5.90897 | 0.08491 | -1.34291 |
| H | 6.97614 | -0.08761 | -1.28691 |
| C | 3.03581 | -0.47061 | 1.56236 |
| C | 2.21304 | -0.56099 | 2.70868 |
| H | 1.15034 | -0.3534 | 2.72734 |
| C | 3.02323 | -0.92482 | 3.77825 |
| H | 2.73088 | -1.07054 | 4.80925 |
| C | 4.32195 | -1.05836 | 3.26487 |
| H | 5.23374 | -1.33855 | 3.77654 |
| C | 2.3577 | -2.76633 | -1.4214 |
| H | 2.97961 | -2.12583 | -2.05599 |
| H | 2.84213 | -2.76624 | -0.4382 |
| C | 2.29072 | -4.18142 | -1.98917 |
| H | 3.30465 | -4.58781 | -2.06342 |
| H | 1.85542 | -4.20387 | -2.9932 |
| H | 1.71284 | -4.85765 | -1.35132 |
| C | 0.00305 | -1.90002 | -2.92083 |
| H | 0.01511 | -2.93235 | -3.28995 |
| H | -1.0502 | -1.62081 | -2.80127 |
| C | 0.6956 | -0.96218 | -3.90317 |
| H | 0.21393 | -1.02593 | -4.88424 |
| H | 1.7525 | -1.21608 | -4.03562 |

| | | | |
|---|---|---|---|
| H | 0.63642 | 0.07883 | -3.56669 |
| C | -0.32896 | -3.09993 | -0.32421 |
| H | -1.32136 | -2.64228 | -0.24657 |
| H | -0.44267 | -3.98724 | -0.95921 |
| C | 0.19895 | -3.48517 | 1.05333 |
| H | -0.51302 | -4.14787 | 1.55551 |
| H | 0.35171 | -2.60695 | 1.68875 |
| H | 1.15549 | -4.01364 | 0.98789 |
| C | 2.79708 | 3.11759 | 0.46502 |
| H | 3.33185 | 2.4999 | 1.19612 |
| H | 3.23138 | 2.87121 | -0.50927 |
| C | 2.98591 | 4.6001 | 0.7741 |
| H | 4.05572 | 4.83347 | 0.77331 |
| H | 2.5938 | 4.87596 | 1.75754 |
| H | 2.51126 | 5.24124 | 0.02471 |
| C | 0.47302 | 2.83634 | 2.16289 |
| H | 1.07351 | 2.20156 | 2.8251 |
| H | 0.74043 | 3.87498 | 2.39094 |
| C | -1.01548 | 2.61619 | 2.40175 |
| H | -1.26139 | 2.85839 | 3.44082 |
| H | -1.30647 | 1.57739 | 2.22422 |
| H | -1.63078 | 3.25534 | 1.76031 |
| C | 0.1492 | 3.70735 | -0.60387 |
| H | -0.91301 | 3.44469 | -0.55493 |
| H | 0.25462 | 4.69872 | -0.14689 |
| C | 0.62725 | 3.71611 | -2.05227 |
| H | 0.52509 | 2.7263 | -2.51145 |
| H | 1.67739 | 4.01609 | -2.13302 |
| H | 0.03315 | 4.42245 | -2.64077 |
| S | -1.39703 | 0.70367 | -1.07735 |
| C | -2.5965 | 0.05314 | -0.0481 |
| C | -3.99171 | 0.1981 | -0.3932 |
| C | -2.25641 | -0.61983 | 1.15559 |
| C | -4.97615 | -0.33007 | 0.48953 |
| C | -4.42356 | 0.8457 | -1.57929 |
| C | -3.21583 | -1.12508 | 1.99253 |
| H | -1.20368 | -0.72565 | 1.40176 |
| C | -6.35559 | -0.19804 | 0.17754 |
| C | -4.59575 | -0.99491 | 1.69041 |
| C | -5.75528 | 0.97205 | -1.87941 |
| H | -3.68291 | 1.2479 | -2.26219 |
| H | -2.92334 | -1.63389 | 2.90716 |
| C | -6.7586 | 0.4582 | -1.01538 |
| C | -7.34233 | -0.7229 | 1.05893 |
| C | -5.59243 | -1.51073 | 2.5527 |

| | | | |
|---|---|---|---|
| H | -6.05792 | 1.47352 | -2.79452 |
| C | -8.13224 | 0.57948 | -1.30685 |
| C | -8.70247 | -0.579 | 0.72918 |
| C | -6.92459 | -1.37952 | 2.24952 |
| H | -5.28561 | -2.01552 | 3.46424 |
| C | -9.08991 | 0.06588 | -0.4419 |
| H | -8.43475 | 1.08248 | -2.22135 |
| H | -9.45336 | -0.9806 | 1.40427 |
| H | -7.67999 | -1.77931 | 2.92026 |
| H | -10.14415 | 0.16695 | -0.67953 |

**Table S9. Atomic coordinates of the optimized ground state geometry of BPtSPyr in the anionic form**

| | | | |
|---|---|---|---|
| Pt | 0.83493 | 0.29354 | -0.38434 |
| B | 5.4689 | -1.01715 | 1.13749 |
| F | 5.76969 | -2.38336 | 0.93466 |
| F | 6.59285 | -0.4184 | 1.73252 |
| N | 5.1307 | -0.33815 | -0.1926 |
| N | 4.2349 | -0.86746 | 2.03286 |
| P | 0.67126 | -1.84617 | -1.31051 |
| P | 1.15253 | 2.46551 | 0.4174 |
| C | 2.72479 | -0.13498 | 0.24066 |
| C | 3.85025 | -0.01057 | -0.61961 |
| C | 3.95692 | 0.45797 | -1.9435 |
| H | 3.12341 | 0.80333 | -2.54351 |
| C | 5.32207 | 0.40649 | -2.30463 |
| H | 5.76096 | 0.70412 | -3.24981 |
| C | 6.00856 | -0.08766 | -1.20871 |
| H | 7.06605 | -0.27875 | -1.0782 |
| C | 2.96121 | -0.53718 | 1.58665 |
| C | 2.09075 | -0.64881 | 2.68912 |
| H | 1.02668 | -0.44559 | 2.65855 |
| C | 2.86175 | -1.0493 | 3.80325 |
| H | 2.51145 | -1.21956 | 4.81452 |
| C | 4.16786 | -1.17421 | 3.36218 |
| H | 5.06012 | -1.46283 | 3.90298 |
| C | 2.23961 | -2.80871 | -1.4053 |
| H | 2.95358 | -2.17919 | -1.94835 |
| H | 2.62994 | -2.86347 | -0.38262 |
| C | 2.14184 | -4.19632 | -2.03105 |
| H | 3.124 | -4.68151 | -2.01068 |
| H | 1.82055 | -4.15451 | -3.07748 |
| H | 1.44482 | -4.84674 | -1.49132 |
| C | 0.02783 | -1.83323 | -3.03705 |
| H | -0.01248 | -2.86949 | -3.39421 |
| H | -1.00334 | -1.46935 | -2.96749 |

| | | | |
|---|---|---|---|
| C | 0.83136 | -0.95588 | -3.98924 |
| H | 0.40633 | -0.99744 | -4.99842 |
| H | 1.87818 | -1.27245 | -4.05311 |
| H | 0.8173 | 0.08721 | -3.65542 |
| C | -0.51551 | -2.98164 | -0.47185 |
| H | -1.45975 | -2.43115 | -0.39635 |
| H | -0.69413 | -3.8417 | -1.12992 |
| C | -0.05674 | -3.44322 | 0.90747 |
| H | -0.85469 | -4.00509 | 1.40545 |
| H | 0.21488 | -2.59559 | 1.54599 |
| H | 0.81973 | -4.09721 | 0.84331 |
| C | 2.91642 | 2.99996 | 0.5131 |
| H | 3.37247 | 2.37315 | 1.28803 |
| H | 3.39174 | 2.68974 | -0.42367 |
| C | 3.16924 | 4.47892 | 0.78857 |
| H | 4.24696 | 4.65794 | 0.87296 |
| H | 2.71077 | 4.81686 | 1.72396 |
| H | 2.79443 | 5.11706 | -0.01881 |
| C | 0.5423 | 2.79897 | 2.12762 |
| H | 1.00642 | 2.03556 | 2.76359 |
| H | 0.94895 | 3.7683 | 2.44104 |
| C | -0.97336 | 2.79115 | 2.28828 |
| H | -1.23958 | 2.93022 | 3.34222 |
| H | -1.41124 | 1.84743 | 1.95055 |
| H | -1.44362 | 3.60069 | 1.72021 |
| C | 0.33702 | 3.76051 | -0.60657 |
| H | -0.73188 | 3.52226 | -0.60961 |
| H | 0.46329 | 4.73099 | -0.11021 |
| C | 0.86154 | 3.79927 | -2.03807 |
| H | 0.70799 | 2.83357 | -2.53262 |
| H | 1.9324 | 4.02821 | -2.0763 |
| H | 0.33533 | 4.56443 | -2.61945 |
| S | -1.42784 | 0.8212 | -1.17968 |
| C | -2.62754 | 0.15398 | -0.08713 |
| C | -4.0171 | 0.24004 | -0.39149 |
| C | -2.25401 | -0.46264 | 1.12195 |
| C | -4.97732 | -0.28226 | 0.52529 |
| C | -4.50024 | 0.83999 | -1.59934 |
| C | -3.18759 | -0.97615 | 2.00713 |
| H | -1.19255 | -0.53235 | 1.35 |
| C | -6.37223 | -0.19246 | 0.23363 |
| C | -4.56069 | -0.89863 | 1.74037 |
| C | -5.82877 | 0.92608 | -1.87976 |
| H | -3.77098 | 1.23161 | -2.30171 |
| H | -2.85149 | -1.4455 | 2.92972 |

| | | | |
|---|---|---|---|
| C | -6.81464 | 0.41699 | -0.97564 |
| C | -7.33374 | -0.71194 | 1.15177 |
| C | -5.54562 | -1.41236 | 2.64118 |
| H | -6.16498 | 1.38727 | -2.80577 |
| C | -8.18917 | 0.49747 | -1.24341 |
| C | -8.69748 | -0.60891 | 0.84258 |
| C | -6.87439 | -1.32454 | 2.36378 |
| H | -5.20519 | -1.87908 | 3.56311 |
| C | -9.11741 | -0.01058 | -0.3415 |
| H | -8.52112 | 0.96381 | -2.16809 |
| H | -9.42851 | -1.00495 | 1.54373 |
| H | -7.61315 | -1.71839 | 3.0578 |
| H | -10.17929 | 0.05962 | -0.56272 |

## References


(1) Irmler, P.; Winter, R. F. *Dalton Trans.* **2016**, *45*, 10420.
(2) Krejčik, M.; Daněk, M.; Hartl, F. *J. Electroanal. Chem. Interfacial Electrochem.* **1991**, *317*, 179.
(3) Frisch, M. J.; Trucks, G. W.; Schlegel, H. B.; Scuseria, G. E.; Robb, M. A.; Cheeseman, J. R.; Scalmani, G.; Barone, V.; Mennucci, B.; Petersson, G. A.; Nakatsuji, H.; Caricato, M.; Li, X.; Hratchian, H. P.; Izmaylov, A. F.; Bloino, J.; Zheng, G.; Sonnenberg, J. L.; Hada, M.; Ehara, M.; Toyota, K.; Fukuda, R.; Hasegawa, J.; Ishida, M.; Nakajima, T.; Honda, Y.; Kitao, O.; Nakai, H.; Vreven, T.; Montgomery Jr., J. A.; Peralta, J. E.; Ogliaro, F.; Bearpark, M. J.; Heyd, J.; Brothers, E. N.; Kudin, K. N.; Staroverov, V. N.; Kobayashi, R.; Normand, J.; Raghavachari, K.; Rendell, A. P.; Burant, J. C.; Iyengar, S. S.; Tomasi, J.; Cossi, M.; Rega, N.; Millam, N. J.; Klene, M.; Knox, J. E.; Cross, J. B.; Bakken, V.; Adamo, C.; Jaramillo, J.; Gomperts, R.; Stratmann, R. E.; Yazyev, O.; Austin, A. J.; Cammi, R.; Pomelli, C.; Ochterski, J. W.; Martin, R. L.; Morokuma, K.; Zakrzewski, V. G.; Voth, G. A.; Salvador, P.; Dannenberg, J. J.; Dapprich, S.; Daniels, A. D.; Farkas, O. d. o. n.; Foresman, J. B.; Ortiz, J. V.; Cioslowski, J.; Fox, D. J.; Gaussian, Inc.: Wallingford, CT, USA, 2009.
(4) Gunnarsson, O.; Lundqvist, B. I. *Phys. Rev. B* **1976**, *13*, 4274.
(5) Küchle, W.; Dolg, M.; Stoll, H.; Preuss, H. *J. Chem. Phys.* **1994**, *100*, 7535.
(6) Dolg, M.; Stoll, H.; Preuss, H. *J. Chem. Phys.* **1989**, *90*, 1730.
(7) Andrae, D.; Häußermann, U.; Dolg, M.; Stoll, H.; Preuß, H. *Theor. Chim. Acta* **1990**, *77*, 123.
(8) Hariharan, P. C.; Pople, J. A. *Theor. Chim. Acta* **1973**, *28*, 213.
(9) Perdew, J. P.; Burke, K.; Ernzerhof, M. *Phys. Rev. Lett.* **1996**, *77*, 3865.
(10) Adamo, C.; Barone, V. *J. Chem. Phys.* **1999**, *110*, 6158.
(11) Cancés, E.; Mennucci, B.; Tomasi, J. *J. Chem. Phys.* **1997**, *107*, 3032.
(12) Mennucci, B.; Tomasi, J. *J. Chem. Phys.* **1997**, *106*, 5151.
(13) Cossi, M.; Rega, N.; Scalmani, G.; Barone, V. *J. Comput. Chem.* **2003**, *24*, 669.
(14) Scalmani, G.; Frisch, M. J. *J. Chem. Phys.* **2010**, *132*, 114110.
(15) Runge, E.; Gross, E. K. U. *Phys. Rev. Lett.* **1984**, *52*, 997.
(16) O'Boyle, N. M.; Tenderholt, A. L.; Langner, K. M. *J. Comput. Chem.* **2008**, *29*, 839.

## 5.5 Directing Energy Transfer in Pt(Bodipy)(Mercaptopyrene) Dyads

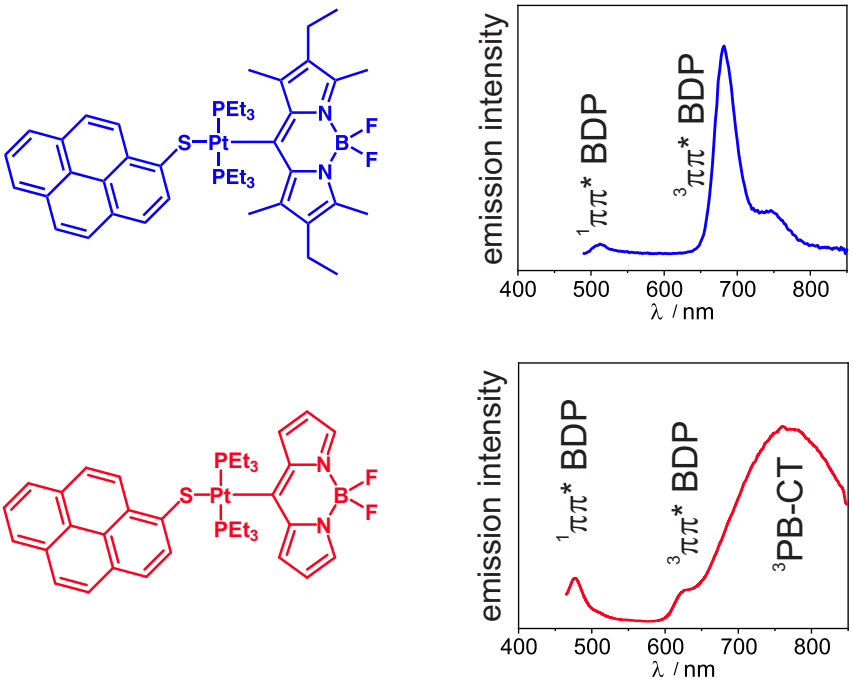


Reprinted from *Dalton Transactions* **2019**, *48*, 11690-11705 DOI: 10.1039/c9dt01737b with permission from The Royal Society of Chemistry.

Dalton Transactions

PAPER

View Article Online
View Journal | View Issue





Cite this: *Dalton Trans.*, 2019, **48**, 11690

# Directing energy transfer in Pt(bodipy)(mercaptopyrene) dyads†

Peter Irmler,[a] Franciska S. Gogesch,[a] André Mang,[a] Michael Bodensteiner,[b] Christopher B. Larsen,[c] Oliver S. Wenger [c] and Rainer F. Winter *[a]

Received 25th April 2019,
Accepted 16th June 2019

DOI: 10.1039/c9dt01737b

rsc.li/dalton

We report on the photophysical properties of three dyads that combine a 4,4-difluoro-4-bora-3a,4a-diaza-*s*-indacene (bodipy, BDP) and a mercaptopyrene (SPyr) dye ligand at a $Pt(PEt_3)_2$ fragment. σ-Bonding of the dyes to the Pt ion promotes intersystem crossing (ISC) *via* the external heavy atom effect. The coupling of efficient ISC with charge-transfer from the electron-rich mercaptopyrene to the electron-accepting BDP ligand (PB-CT) gives rise to a multitude of (potentially) emissive states. This culminates in the presence of four different emissions for the mono- and dinuclear complexes **BPtSPyr** and **BPtSPyrSPtB** with an unsubstituted BDP ligand and either a terminal 1-mercaptopyrene or a bridging pyrene-1,6-dithiolate ligand. Thus, in fluid solution, near IR emission at 724 nm from the $^3$PB-CT state is observed with a quantum yield of up to 15%. Excitation into the BDP-based $^1\pi\pi^*$ or the pyrene-based $^1\pi\pi^*$ band additionally trigger fluorescence and phosphorescence emissions from the BDP-centred $^1\pi\pi^*$ and $^3\pi\pi^*$ states. In frozen solution, at 77 K, phosphorescence from the pyrene ligand becomes the prominent emission channel, while PB-CT emission is absent. Alkylation of the BDP ligand in **KBPtSPyr** funnels all excitation energy into fluorescence and phosphorescence emissions from the KBDP ligand. The assignments of the various excited states and the deactivation cascades were probed by absorption and emission spectroscopy, transient absorption spectroscopy, electrochemical and UV/Vis/NIR spectroelectrochemical measurements, and by quantum chemical calculations. Our conclusions are further corroborated with the aid of suitable reference compounds comprising of just one chromophore. All dyads are triplet sensitizers and are able to generate singlet oxygen.

## Introduction

Luminescent molecules capable of displaying multiple emissions are of great interest, *e.g.* as one-component white-light emitters,[1–4] and, in the case of dual fluorescence and phosphorescence emitters, as one-component sensors for triplet molecules. The latter quench selectively the longer-lived phosphorescence emission, while leaving the fluorescence unperturbed.[5–9] An observation of multiple emissions from the same compound obviously necessitates the presence and competitive population of two or more emissive states. One possible strategy to achieve dual fluorescence and phosphorescence emissions is to match the intersystem crossing (ISC) rate constant $k_{ISC}$ to the fluorescence time constant $k_f$. According to El-Sayed's rule,[10,11] this can be achieved by capitalizing on the large spin orbit coupling constant of a proximal heavy atom[12–15] or by admixing sufficient charge-transfer character to the underlying absorption. Both effects are capable of changing the angular momentum of the excited electron.[11,16–18] Alternatively, multiple emissions are also known for dyads with different electronically decoupled or weakly coupled chromophores.[19,20] Examples of such a multi-chromophore approach with an ensuing competition between dye-based fluorescence and MLCT- or spin–orbit coupling-(SOC-) triggered phosphorescence emissions come from iridium, ruthenium, rhenium or platinum complexes that

[a]*Fachbereich Chemie, Universität Konstanz, Universitätsstraße 10, D-78457 Konstanz, Germany. E-mail: rainer.winter@uni-konstanz.de*
[b]*Fakultät für Chemie und Pharmazie, Universität Regensburg, Universitätsstraße 31, D-93053 Regensburg, Germany*
[c]*Department of Chemistry, University of Basel, St.-Johanns-Ring 19, CH-4056 Basel, Switzerland*

†Electronic supplementary information (ESI) available: $^1$H, $^{13}C\{^1H\}$, and, if applicable, $^{31}P\{^1H\}$, $^{195}Pt\{^1H\}$ NMR spectra of all compounds; data pertaining to the structure solution and refinement as well as packing diagrams; UV/Vis spectra in different solvents, MO diagrams, TD-DFT computed transitions and electron density difference maps for individual transitions; cyclic voltammograms and electrochemistry data; luminescence spectra in different solvents and at different excitation wavelengths as well as time decay traces, computed energies of the frontier MOs; absorption data, MO calculations of relevant MOs, spin densities and MO compositions of the oxidized and reduced forms of the complexes; decay traces for transient spectra of the individual complexes; atomic coordinates of geometry-optimized structures. CCDC 1898598 and 1908870. For ESI and crystallographic data in CIF or other electronic format see DOI: 10.1039/c9dt01737b

 

contain dye-modified cyclometalating,[21,22] 2,2′-bipyridine or phenanthroline,[23–25] or alkynyl ligands.[18,26–28] Phosphorescence quantum yields of such dyads are, however, usually lower than 10%.[24] Particularly impressive are Ir(ppy)$_2$(Q) complexes with a 2-hydroxyquinoline ligand Q and two mutually orthogonally aligned, cyclometalated phenylpyridine (ppy) ligands, which show quadruple emissions comprising of ligand-localized fluorescence from the $^1$n$\pi^*$ and phosphorescence from $^3$MLCT (MLCT = metal–ligand charge-transfer) states of the different ligands as a consequence of inefficient Förster resonance energy transfer.[29]

Platination of a dye, *i.e.* metal attachment *via* a direct Pt–carbon σ-bond, has been shown to be a viable means of accelerating ISC *via* the remote heavy atom effect,[15,30,31] in particular when using compact thioxanthone[32] or 4,4-difluoro-4-bora-3a,4a-diaza-*s*-indacene (BDP) dyes[8,9,33] (note that the remote heavy atom effect scales with $r^{-6}$, where $r$ denotes the distance between the heavy atom and the centre of gravity of the dye).[12] In this manner, quantum yields of up to 41% for dye-based phosphorescence emission in fluid solution at r.t. could be achieved. Complexes *trans*-X(PR$_3$)$_2$Pt(BDP) (R = Ph, Et) were also found to be efficient sensors for the detection of triplet molecules and efficient photosensitizers for the production of singlet oxygen.[8,9,33,34] An example of a panchromatically absorbing dyad of such a complex with an ethynylnaphthalimide (NI) dye as the anionic ligand X was also reported. The latter shows complete energy transfer from the locally excited $^1$NI or $^1$NI → BDP charge-transfer states to the lower-lying excited states of the BDP ligand.[34] One drawback of this system, however, was its only limited stability under laser irradiation due to the mutual *trans*-arrangement of two carbyl ligands, which both exert a strong σ-*trans* influence.[9] We therefore sought to improve on this general architecture by attaching the second dye *via* a more robust Pt–thiolate bond. In doing so, we have chosen mercaptopyrenes as the second dye.

Pyrenes usually absorb in a spectral region where BDP dyes are almost transparent. Most pyrenes are highly fluorescent and show rather inefficient intersystem crossing with negligible phosphorescence quantum yields.[13,35] The latter is a result of their long triplet-state lifetimes, which increases the probability of excited state decay by radiationless deactivation channels.[13] Pyrenes were already introduced into the coordination sphere of platinum ions, either by direct platination, or as ethynylpyrene ligands. In both cases, phosphorescence from the pyrene ligand could be obtained due to the proximity of the pyrene dye to the platinum ion, however with only modest quantum yields, even in frozen, glassy matrices.[15,18,21,31,36]

We note in this vein that pyrene-BDP dyads with a direct connection between the two different dyes have been known for more than ten years.[37,38] More recently it was observed that these compounds, due to a near orthogonal arrangement of the pyrene donor and the BDP acceptor, are capable of forming a charge-separated (CS) excited state, which promotes efficient ISC to the corresponding $^3$CS state. Such dyads are characterized by a strong dependence of their absorption and emission properties and their associated emission quantum yields on solvent polarity. They are capable of photogenerating singlet oxygen, sometimes with high quantum yields $\Phi_\Delta$, particularly in polar solvents. These $^3$CS states are usually non-emissive though.[39–41]

Very recently we communicated our results on the complex **BPtSPyr**, which combines a *meso*-platinated BDP acceptor and a mercaptopyrene donor ligand at a common *trans*-Pt(PEt$_3$)$_2$ entity.[42] The most remarkable features of **BPtSPyr** are its multiple emissions and the dependence of its emission profile on the excitation wavelength, the solvent polarity, and the temperature. This behaviour indicates the presence of several competing pathways for the decay of the individual excited states to the ground state. Most prominent is the long-lived emission from the $^3$CS state in the near infrared (NIR), which becomes observable due to an SOC-accelerated ISC rate for radiative decay from the corresponding charge-separated triplet state $T_{CS}$ to the $S_0$ state. We have now further elaborated on this complex by selectively manipulating the relative energies of the $^3$CS and the $^3$BDP excited states. This was done through either alkylation of the BDP ligand or through interlinking two *trans*-Pt(PEt$_3$)$_2$(BDP) fragments with a bridging pyrene-1,6-dithiolate ligand. These alterations have the effect of (re)directing the deactivation cascade to either BDP-localized or CS excited states. Suitable reference compounds, which contain only one of these two chromophores, were also included to aid in the understanding of their complex emissive behaviour. The results of this study are described herein.

## Results and discussion

### Synthesis

The general synthesis route is depicted in Scheme 1 (for detailed syntheses and NMR characterization and a brief discussion of the NMR spectroscopic trends see the ESI and Fig. S1–S21 as well as Table S1† therein). The *meso*-Pt-BDP complexes were synthesized according to our previously reported protocol by oxidative addition of the corresponding 8-chloro-BDP dye to the Pt$^0$(ethene)(PEt$_3$)$_2$ precursor.[8] The latter is generated *in situ* by thermally induced reductive elimination of ethane from the corresponding bis(ethyl) complex.[43] In the case of the peralkylated 8-chloro-krypto-BDP ligand KBDP, an elevated temperature and longer reaction time were required in order for the oxidative addition to proceed, most probably as the result of a larger steric hindrance. Subsequent abstraction of the chlorido ligand with AgOTf followed by addition of the resulting triflato complex to a solution of deprotonated 1-mercaptopyrene, or respectively, pyrene-1,6-dithiole, provided the target dyads in good to moderate yields.

The general pattern of resonance signals and, in particular, the observation of Pt-satellites for the appropriate proton and carbon resonances in the NMR spectra[44] confirm the constitution of the complexes and the presence of the Pt–C and the Pt–S bonds to the BDP and mercaptopyrene ligands. Single crystals of **KBPtSPyr** and its precursor **KBPtI** for molecular structure determination by X-ray diffraction analysis were obtained by slow diffusion of *n*-pentane into saturated solu-

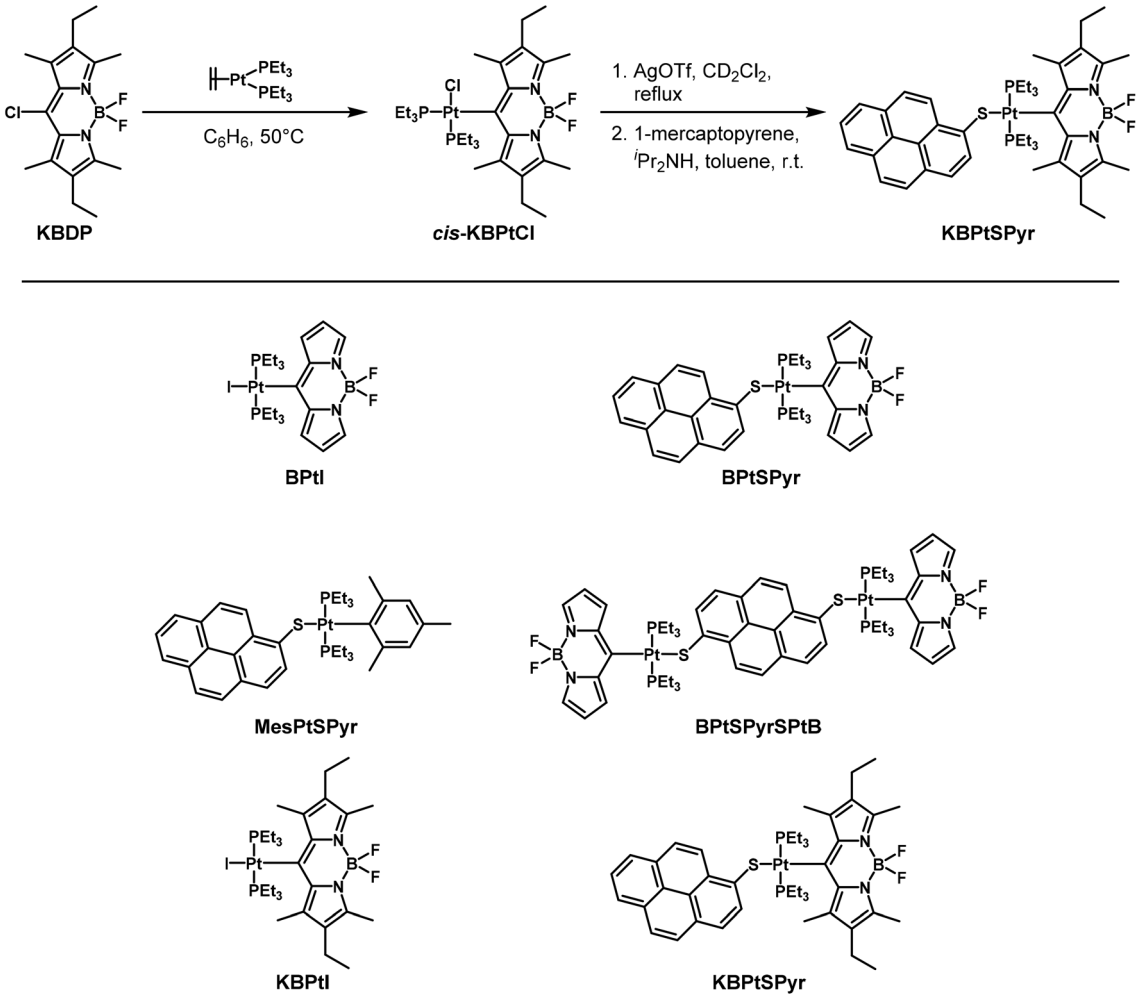


**Scheme 1** Exemplary synthesis of **KBPtSPyr** and the structures of all relevant compounds.

tions of the complexes in $CH_2Cl_2$. Relevant crystal and refinement data are collected in Table S2 of the ESI.† Fig. 1 depicts their molecular structures (only one of the two independent molecules in the unit cell of **KBPtSPyr** is shown), while Table S3 of the ESI† summarizes the most relevant bond parameters together with those of **BPtI**.[9]

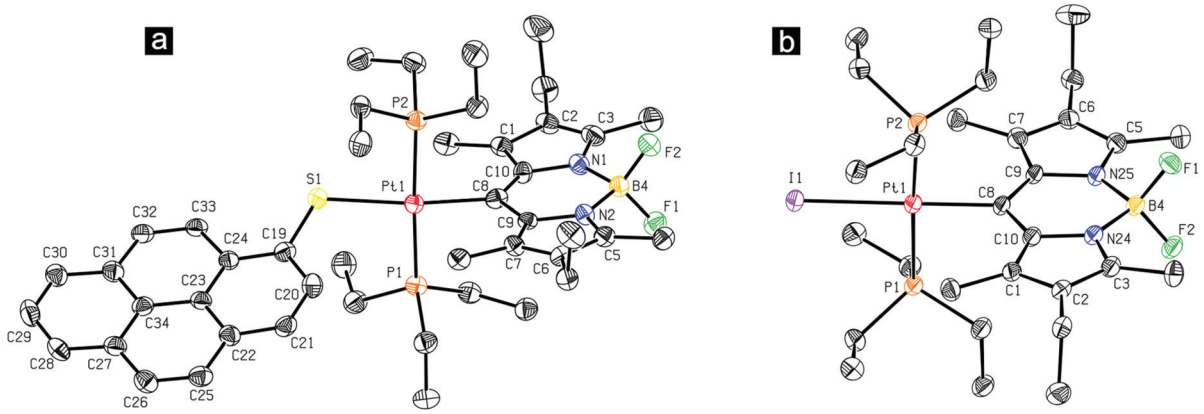


**Fig. 1** ORTEPs of (a) **KBPtSPyr** (only one of the two independent molecules of the units cell is shown) and of (b) **KBPtI**. Ellipsoids are drawn on a 40% probability level. Solvent molecules and protons are omitted for reasons of clarity.

 

In all complexes, the Pt(II) ion adopts the expected square planar coordination geometry with all *cis*-bond angles close to 90° and the *trans*-P–Pt–P and I–Pt–C angles close to 180°, whereas the C8–Pt1–S1 angle of 172.7(3)° or 167.9(3)° in **KBPtSPyr** shows larger deviations from ideality. Substitution of the simple BDP ligand of **BPtI** by peralkylated KBDP in **KBPtI** lengthens the Pt–$C_{bodipy}$ and the Pt–I bonds by *ca.* 0.02 Å, the former probably as the result of increased steric interactions between the alkyl substituents of the $PEt_3$ and the KBDP ligands, and the latter as the result of the increased σ-*trans*-influence of the KBDP ligand.[9] Substitution of the iodo by the 1-mercaptopyrene ligand lengthens the Pt1–C8 bond further by 0.03 Å, which is expected on the basis of the π-accepting character of an S donor ligand and the associated, larger σ-*trans*-influence. The BDP chromophore is aligned orthogonally to the Pt coordination plane with an interplanar angle of 87.0° to 90°. In contrast, the pyrenyl substituent of **KBPtSPyr** forms an interplanar angle of 70.0° or 73.2° with the Pt coordination plane, such that the interplanar angle between the two chromophores is 19.7° or 18.2° for the two independent molecules of the unit cell. The centroids of the pyrene and BDP dye ligands are 9.96 or 9.80 Å apart. Several intermolecular contacts are found in the crystal packing of **KBPtSPyr**. Details are provided in the ESI.†

## Photophysical properties

A common feature of all BDP-Pt-SPyr dyads of this study is that their HOMO is centred on the mercapto-substituted pyrene ligand while their LUMO is essentially BDP-based. DFT-computed contour diagrams of the relevant MOs of complexes **BPtSPyr**, **BPtSPyrSPtB** and **KBPtSPyr** and the spin densities for their oxidized and reduced forms are displayed as Fig. S23–S28 of the ESI;† the respective contributions and spin densities of the individual fragments according to Mulliken analysis are collected in Tables S4–S11.† According to these calculations, both frontier MOs (HOMO, LUMO) of the dyads receive only minor contributions (3%–7%) from the $Pt(PEt_3)_2$ fragment(s), such that its (their) influence is of a primarily inductive nature. Substitution of the BDP by the more electron donating, peralkylated KBDP and of the terminal mercaptopyrene by the pyrene-1,6-dithiolate ligand induce sizable energy shifts of the LUMO or the HOMO, respectively, as revealed by our electrochemical measurements. Representative voltammograms can be found as Fig. S29–S33 of the ESI,† while all pertinent data are collected in Table S12† therein. In brief, substitution of the BDP by the KBDP ligand shifts the half-wave potential for the BDP-centred reduction negative (cathodically) by 340 mV, while causing an only minor cathodic shift of 50 mV of the pyrene-based oxidation. *Vice versa*, comparing **BPtSPyr** with **BPtSPyrSPtB** reveals a 190 mV cathodic shift of the oxidation potential, resulting from the attachment of a second $^{-}$S-Pt$(PEt_3)_2$BDP-type donor, while leaving the potential of the BDP-based reduction essentially unaltered.

Fig. 2 depicts the UV/Vis spectra of all dyad molecules along with those of suitable reference compounds, which contain only the Pt-BDP or the mercatopyrene moiety. Tabulated data and the corresponding TD-DFT-derived band assignments can be found in Table 1.

Complexes **BPtSPyr**, **BPtSPyrSPtB** and **BPtI** with the unsubstituted BDP dye as a σ-bonded ligand exhibit the characteristic BDP-based $^1$ππ* absorption band at 470 nm to 490 nm with an extinction coefficient $\varepsilon$ of *ca.* $50 \times 10^3$ $M^{-1}$ $cm^{-1}$ for the mononuclear, and of $90 \times 10^3$ $M^{-1}$ $cm^{-1}$ for the dinuclear complex with twice the number of BDP chromophores. The electron-donating $Pt(PEt_3)_2$-BDP moieties shift the pyrene-based ππ* absorption bands bathochromically to 375–450 nm with a main peak at 418 nm for **BPtSPyr**. They are even more red-shifted in **BPtSPyrSPtB**, where they overlap partly with the BDP absorption. The even lower energy of the main mercaptopyrene ππ* absorption at $\lambda_{max}$ = 431 nm in the mesityl complex is consistent with this trend and relates to the larger donor capacity of the mesityl ligand. The spectra of **BPtSPyr** and **BPtSPyrSPtB** also feature a broad, solvatochromic (see Fig. S34 of the ESI†) SPyr-to-BDP charge transfer (PB-CT) band, which is located at *ca.* 500 nm in toluene solution for **BPtSPyr**.[42] Attachment of a dinegatively charged bridging dithiolate donor and doubling the number of the BDP acceptors has the effect of shifting the PB-CT band further red to 550 nm and increasing its extinction coefficient (Table 1). The presence of

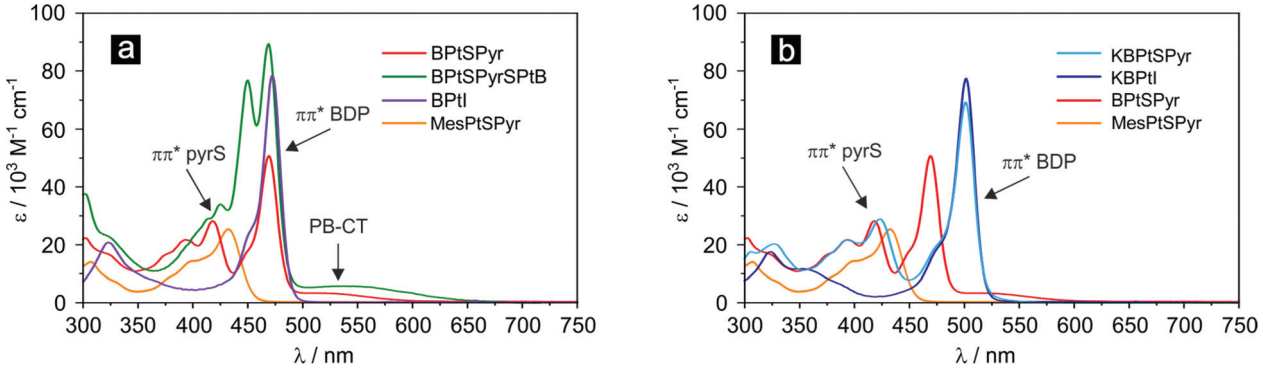


Fig. 2 UV/Vis spectra of (a) **BPtSPyr**, **BPtSPyrSPtB**, **BPtI** and **MesPtSPyr**, and (b) of **KBPtSPyr**, **KBPtI**, **BPtSPyr** and **MesPtSPyr** in toluene.

**Table 1** Absorption data for **BPtI**, **KBPtI**, **MesPtSPyr**, **BPtSPyr**, **BPtSPyrSPtB**, and **KBPtSPyr** as well as TD-DFT-calculated band energies and assignments

| Absorption data | | TD-DFT calculations[a] | | | |
|---|---|---|---|---|---|
| Solvent | $\lambda_{max}$ [b] ($\varepsilon$[c]) | $\lambda$[b] | $f$[d] | m.c.[e] | Assignment |
| **BPtI** from ref. 9 | | | | | |
| $CH_2Cl_2$ | 322 (12.5), 352 (4.3), 471 (52.6) | 295 | 0.17 | H−6 → L (90%) | ππ* BDP |
| | | 309 | 0.07 | H−5 → L (81%) | $Pt(PEt_3)_2$ to BDP CT |
| | | 392 | 0.39 | H → L (97%) | ππ* BDP |
| **KBPtI** | | | | | |
| Toluene | 353 (12), 502 (80) | n.d. | n.d. | n.d. | n.d. |
| THF | 351 (9), 500 (74) | | | | |
| Acetone | 347 (10), 498 (72) | | | | |
| **MesPtSPyr** from ref. 42 | | | | | |
| Toluene | 307 (14), 431 (25) | n.d. | n.d. | n.d. | n.d. |
| THF | 306 (12), 431 (22) | | | | |
| Acetone | 430 (23) | | | | |
| **BPtSPyr** from ref. 42 | | | | | |
| Toluene | 418 (28), 469 (51), 499 (4) | 392 | 0.37 | H−1 → L (97%) | ππ* BDP |
| THF | 419 (29), 467 (51), 493 (4) | 402 | 0.66 | H → L + 1 (95%) | ππ* SPyr |
| Acetone | 416 (29), 465 (50), 483 (4) | 567 | 0.05 | H → L (99%) | PB-CT |
| **BPtSPyrSPtB** | | | | | |
| Toluene | 425 (34), 450 (77), 469 (90), 540 (6) | 391 | 0.71 | H−3 → L+1 (48%), H−2 → L (49%) | ππ* BDP |
| THF | 425 (41), 449 (84), 467 (91), 515 (8) | 426 | 0.52 | H−1 → L+1 (41%), H → L+2 (55%) | ππ* SPyr & PB-CT |
| Acetone | 424 (38), 448 (76), 465 (88), 475 (8) | 433 | 0.68 | H−1 → L+1 (53%), H → L+2 (41%) | ππ* SPyr & PB-CT |
| | | 618 | 0.08 | H → L (97%) | PB-CT |
| **KBPtSPyr** | | | | | |
| Toluene | 423 (30), 501 (72) | 406 | 0.68 | H → L+1 (95%) | ππ* SPyr |
| THF | 423 (31), 499 (69) | 423 | 0.47 | H−1 → L (97%) | ππ* BDP |
| Acetone | 421 (24), 498 (58) | 494 | 0.03 | H → L (98%) | PB-CT |

[a] DFT calculations on the pbe1pbe/6-31G(d) level of therory; PCM model for $CH_2Cl_2$. [b] $\lambda$ in nm. [c] $\varepsilon \times 10^3$ $M^{-1}$ $cm^{-1}$. [d] $f$ = oscillator strength. [e] m.c. = major contribution. H refers to HOMO and L to LUMO.

the solvatochromic PB-CT band provides first evidence for optical charge transfer on excitation to generate a charge-separated excited state.

In the complexes **KBPtSPyr** and **KBPtI** with the peralkylated KBDP ligand, the BDP $^1$ππ* absorption band is red-shifted to 500 nm, and its extinction coefficient is increased to 70 × $10^3$ $M^{-1}$ $cm^{-1}$. In agreement with the better electron donating properties of the more electron-rich KBDP ligand, the SPyr-based absorption in **KBPtSPyr** is red-shifted by 5 nm (283 $cm^{-1}$) with respect to **BPtSPyr**, but still blue of that in **MesPtSPyr**. More importantly however, **KBPtSPyr** completely lacks the PB-CT absorption. TD-DFT calculations suggest that such a transition should also be present in **KBPtSPyr**, but is associated with a small oscillator strength and blue shifted by 73 nm (2600 $cm^{-1}$) compared to **BPtSPyr** (see Fig. S25 of the ESI†), such that it overlaps with the much more intense KBDP $^1$ππ* absorption. The blue-shift and the lower oscillator strength of the PB-CT band are immediate consequences of the inferior acceptor properties of the peralkylated BDP ligand. The latter notion is also supported by our electrochemistry data (*vide supra*). Neither of the two major absorption bands of **KBPtSPyr** shows a significant dependence on solvent polarity as is evident from Fig. S35 of the ESI.† Importantly, the clear separation of the SPyr and the BDP $^1$ππ* transitions in the present dyad systems suggests that the two chromophores are electronically decoupled from each other in the ground state.

Let us now turn to the emission properties of the dyads. In order to aid in the interpretation of their complex, multiple emission features, we will first discuss the corresponding reference compounds with only one type of chromophore. Upon excitation into the SPyr-based $^1$ππ* band, **MesPtSPyr** exhibits dual fluorescence and phosphorescence emissions, both at r.t. and at 77 K. Both emissions emanate from the mercaptopyrene ligand as follows from the typical shapes of the emission bands and their associated lifetimes of 1.11 ns and 448 μs to 1 ms (see Fig. S36–S42 of the ESI†).[42] The observation of phosphorescence indicates that the heavy-metal effect of the attached Pt ion is operative in promoting ISC, similar to Pt complexes with a σ-bonded pyrenyl ligand.[15,21,31]

**BPtI**[9] and **KBPtI** are also dual fluorescence and phosphorescence emitters (see Table 2 and Fig. S43 of the ESI†). While both exhibit much larger phosphorescence quantum yields than **MesPtSPyr**, there are major differences between them. Thus, **KBPtI** is associated with significantly larger fluorescence and lower phosphorescence quantum yields, which attests to less efficient ISC. This is also evident from the increased fluorescence lifetime of 0.96 ns as compared to 0.48 ns for **BPtI** and the derived rate constants $k_{ISC}$ of 2.1 × $10^9$ for **BPtI** and of 9.4 × $10^8$ $s^{-1}$ for **KBPtI**. When considering that the two complexes share a common site of platinum attachment to the BDP chromophore and show only small differences in their Pt–C8(bodipy) bond lengths, a reduced external heavy atom effect seems a rather unlikely explanation for the decreased

 

Table 2 Emission data of **BPtSPyr**, **KBPtSPyr** and **BPtSPyrSPtB**

| Solvent | $\lambda_{exc}$ [a] | $\lambda_{fl}$ [b] (assignment) | $\Phi_{fl}$ [c] | $\tau_{fl}$ [d] | $\lambda_{ph}$ [b] (assignment) | $\Phi_{ph}$ [c] | $\tau_{ph}$ [d] |
|---|---|---|---|---|---|---|---|
| **BPtI** from ref. 9 | | | | | | | |
| $CH_2Cl_2$ | 467 | 481 ($^1$BDP) | 0.002 | 0.48 ± 0.02 ns | 641 | 0.364 | 297 ± 2 μs |
| **KBPtI** | | | | | | | |
| Toluene | 485 | 512 | 0.10 | 0.959 ± 0.007 ns | 684 | 0.04 | 239 ± 2 μs |
| Me-THF[e] | 485 | 506 | n.d. | 1.171 ± 0.007 ns | 673 | n.d. | 436 ± 2 μs |
| **MesPtSPyr** from ref. 42 | | | | | | | |
| Toluene | 430 | 460 ($^1$ SPyr) | 0.24 | 1.113 ± 0.005 ns | 664 ($^3$pyrS) | <0.01 | 448 ± 6 μs |
| Me-THF[e] | 430 | 450 ($^1$ SPyr) | | | 658 ($^3$pyrS) | n.d. | 1.04 ± 0.06 ms |
| **BPtSPyr** | | | | | | | |
| Toluene | 520 | | | | 724 ($^3$PB-CT) | 0.08 | 6.7 ± 0.4 μs |
| | 470 | 484 ($^1$BDP) | n.d. | n.d. | 724 ($^3$PB-CT) | 0.15 | 6.7 ± 0.5 μs |
| | 420 | | | | 724 ($^3$PB-CT) | 0.15 | 6.4 ± 0.3 μs |
| Me-THF[e] | 530 | n.o. | | | | | |
| | 450 or 415 | | | | 635 ($^3$BDP) and 649 ($^3$SPyr) | n.d. | 78 ± 0.4 μs<br>1.12 ± 0.02 ms |
| **KBPtSPyr** from ref. 42 | | | | | | | |
| Toluene | 485 | 512 ($^1$BDP) | <0.01 | 4.42 ± 0.07 ns | 682 ($^3$BDP) | 0.03 | 204 ± 1 μs |
| | 405 | n.o. | | | 682 ($^3$BDP) | 0.05 | 203.7 ± 0.9 μs |
| Me-THF[e] | 485 | 510 ($^1$BDP) | n.d. | 2.34 ± 0.05 ns | 674 ($^3$BDP) | n.d. | 423 ± 2 μs |
| | 405 | 510 ($^1$BDP) | n.d. | n.d. | 674 ($^3$BDP) | n.d. | n.d. |
| **BPtSPyrSPtB** | | | | | | | |
| Toluene | 550 | | | | 770 ($^3$PB-CT) | <0.01 | 32 ± 5 μs |
| | 460 | 482 ($^1$BDP) | <0.01 | | 635 ($^3$BDP) | 0.01 | 178 ± 1 μs |
| | | | | | 760 ($^3$PB-CT) | | 31 ± 2 μs |
| | 420 | 482 ($^1$BDP) | <0.01 | 5.0 ± 0.2 ns | 653 ($^3$BDP) | <0.01 | 164 ± 12 μs |
| | | | | | 760 ($^3$PB-CT) | | 31 ± 1 μs |
| Me-THF[e] | 550 | | | | 696 ($^3$SPyrS) | n.d. | 369 ± 6 μs |
| | 460 | 480 ($^1$BDP) | n.d. | n.d. | 626 ($^3$BDP) | n.d. | 499 ± 6 μs |
| | | | | | 696 ($^3$SPyrS) | | 369 ± 3 μs |
| | 420 | 480 ($^1$BDP) | n.d. | 4.1 ± 0.1 ns | 626 ($^3$BDP) | n.d. | 479 ± 12 μs |
| | | | | | 696($^3$SPyrS) | | 348 ± 2 μs |

[a] Excitation wavelength in nm. [b] Wavelength of the fluorescence (fl) or phosphorescence (ph) emissions in nm. [c] Fluorescence (fl) or phosphorescence (ph) quantum yield. [d] Lifetime of the fluorescence (fl) or phosphorescence (ph) emissions. [e] Measured in a 2-MeTHF glass at 77 K.

$k_{ISC}$. We are therefore drawn to the hypothesis that these differences may be due to the more locked, orthogonal conformation of the complexes with the KBDP ligand due to strongly hindered rotation around the Pt–C8(bodipy) bond.

Importantly, and in contrast to **MesPtSPyr** and **BPtI**, dyad **BPtSPyr** exhibits three different emissions in fluid solution at r.t., depending on the excitation wavelength and solvent polarity. Excitation into the PB-CT absorption band at 520 nm gives rise to a broad and unstructured NIR emission (see Fig. S44a of the ESI†) with a quantum yield of 8% in toluene. On increasing the solvent polarity, the emission peak shifts red with a concomitant, drastic decrease of its associated lifetime (see Table S13 of the ESI†). When excited into the BDP $^1\pi\pi^*$ absorption band at 470 nm, fluorescence and phosphorescence emissions from the BDP-based $^1\pi\pi^*$ and $^3\pi\pi^*$ excited states add to the emission profile. The latter emissions are hardly influenced by solvent polarity and hence become the dominant features in polar solvents, where the $^3$PB-CT emission is very weak (Fig. 3a). On excitation into the SPyr-based $^1\pi\pi^*$ transition, again solely the $^3$PB-CT emission can be observed, but with an increased quantum yield of up to 15% at r.t. in toluene solution (Fig. S44c of the ESI†). This renders **BPtSPyr** an unusually powerful NIR emitter. In a glassy Me-THF matrix at 77 K, only $^3\pi\pi^*$ BDP and pyrene-based $^3\pi\pi^*$ [18,36] emissions are observed, irrespective of the excitation wavelength (Fig. 3b).

Dinuclear **BPtSPyrSPtB** has very similar properties to **BPtSPyr**, but shows also subtle differences. As **BPtSPyr**, it emits solely from the $^3$PB-CT state, when excited into the PB-CT band at 550 nm. In toluene solution, the associated emission wavelength is 770 nm with an associated lifetime of 32 μs (see Fig. 3c and S45 of the ESI†). Mirroring the trends in the absorption spectra and cyclic voltammetry, the higher electron richness (and hence the higher HOMO energy, *vide supra*) of the bridging pyrene-1,6-dithiolate ligand lowers the energy of the corresponding CT-state with respect to mononuclear **BPtSPyr**. As a consequence, the $^3$PB-CT emission is red-shifted by 825 $cm^{-1}$ with a concomitant decrease of the quantum yield from 8% to a value of *ca.* 1%. While one may be drawn to ascribe this decrease in quantum yield to the smaller energy gap to the ground state, in line with the predications of the energy gap law,[45–47] the strongly decreased rate constant for radiationless decay of $k_{nr} = 3.1 \times 10^3$ $s^{-1}$ as compared to $k_{nr} = 1 \times 10^5$ $s^{-1}$ for **BPtSPyr** does not support this view and points to less efficient ISC from the $^3$PB-CT to the ground state as the underlying reason. No emission from the $^3$PB-CT state was observed down to 1270 nm in solvents of higher polarity like THF, *o*-difluorobenzene or acetone.

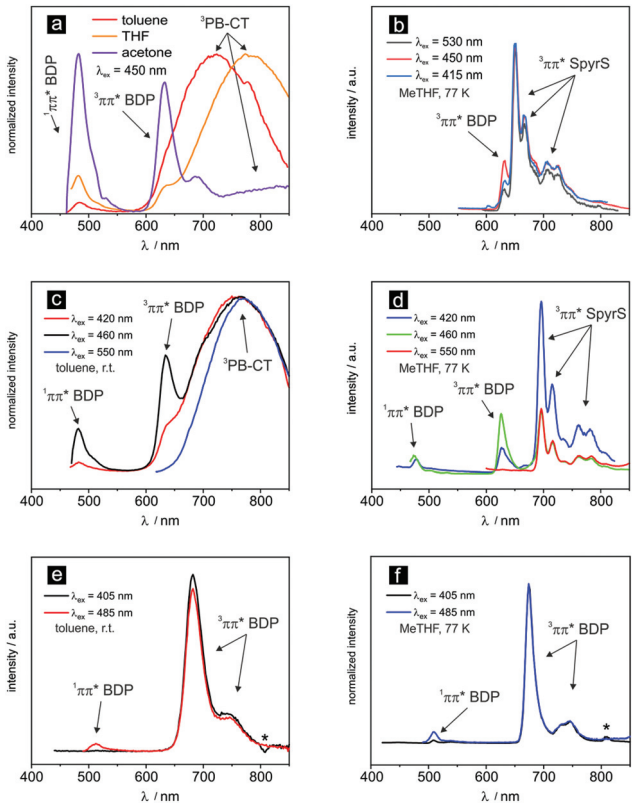


**Fig. 3** Emission spectra of **BPtSPyr** (a) in toluene, THF and acetone at r.t., and (b) at 77 K in 2-MeTHF. Emission spectra of **BPtSPyrSPtB** (c) at r.t. in toluene, and (d) at 77 K in 2-MeTHF. Emission spectra of **KBPtSPyr** (e) at r.t. in toluene, and (f) at 77 K in 2-MeTHF.

As in **BPtSPyr**, the $^3$PB-CT emission is complemented by fluorescence and phosphorescence emissions from the BDP-localized $^1\pi\pi^*$ and $^3\pi\pi^*$ excited states, when irradiated into the BDP $^1\pi\pi^*$ band at 460 nm in toluene solution; these are the only emissions in more polar solvents. Associated lifetimes are 5.0 ns and 178 μs, respectively (see Fig. S46† for emission spectra and lifetime decay traces in *o*-$C_6F_2H_4$). At odds with **BPtSPyr**, excitation into the SPyr $^1\pi\pi^*$ band at 420 nm also gives rise to all three emissions. This indicates subtle differences in excited state decay pathways between the two compounds (*vide infra*).

As in fluid solution, emission spectra of **BPtSPyrSPtB** in frozen, glassy matrices at 77 K strongly depend on the excitation wavelength (Fig. 3d). Selective irradiation into the $^3$PB-CT band ($\lambda_{exc}$ = 550 nm) gives rise to a richly structured emission with a main peak at 696 nm and several vibrational subbands with an associated lifetime of 396 μs. This feature is again identified as phosphorescence from the pyrene-based $^3\pi\pi^*$ state.[15,21,31] Mirroring its influence on the energy of the pyrene-localized excited singlet state, the stronger donor substitution of the bridging pyrene-1,6-dithiolate ligand reduces the energy of the $^3\pi\pi^*$ state of the pyrene constituent by 1040 $cm^{-1}$ compared to **BPtSPyr**. As in the fluid solution spectra, excitation into the BDP-based or, to a lesser degree, into the pyrene-based $^1\pi\pi^*$ absorption bands at 460 or 420 nm adds the $^1\pi\pi^*$ and $^3\pi\pi^*$ BDP emissions to the emission profile of **BPtSPyrSPtB** with associated lifetimes of 4.1 ns and 490 μs, respectively (for emission decay traces see Fig. S47 of the ESI†). All these observations match with the 77 K excitation spectra. Thus, when detecting at the BDP phosphorescence emission at 626 nm, the PB-CT band is absent and the intensity of the $^1\pi\pi^*$ pyrene band is strongly reduced, while all three excitations contribute to the emission from the $^3\pi\pi^*$ state of the pyrene (see Fig. S48 of the ESI†).

At odds with **BPtSPyr** and **BPtSPyrSPtB**, **KBPtSPyr** shows only the same two emissions as the iodo complexes **BPtI** and **KBPtI**, independent of the excitation wavelength and temperature (compare Fig. 3e and f with Fig. S43 of the ESI† and see Table 2; for emission decay traces see Fig. S49–S51 of the ESI†). In particular, neither the $^3$PB-CT nor the $^3\pi\pi^*$ pyrene emissions are observed. This striking dichotomy is due to the different energies of the corresponding excited states that are involved in the deactivation cascade and energy differences between them. The inductive effect of the alkyl substituents on the KBDP ligand decreases its electron-accepting capability and the energies of the BDP-localized excited singlet and triplet states, which is reflected by their respective red shifts of 1260 $cm^{-1}$ or 980 $cm^{-1}$. On the other hand, the energy of the $^3\pi\pi^*$ state of the mercaptopyrene ligand is much less affected by substitution of the BDP ligand, such that it remains at an only marginally lower energy than in **BPtSPyr** (Table 2). In this case, the mercaptopyrene ligand acts as an efficient antenna for populating the BPD-localized $\pi\pi^*$ state. Concomitantly, the phosphorescence quantum yield increases to 5% as compared to 3% on direct excitation into the BDP $\pi\pi^*$ band. The absence of any fluorescence emission from the mercaptopyrene and the BDP ligands on excitation at 420 nm likewise attest to efficient ISC from the higher-lying $^1\pi\pi^*$ SPyr to the $^3\pi\pi^*$ KBDP state and the absence of detectable energy transfer from the $^1\pi\pi^*$ SPyr to the $^1\pi\pi^*$ KBDP excited state. Other examples of a direct singlet-to-triplet electron transfer by spin–orbit coupling were already reported in the literature.[48–50] The above conclusions are fully supported by the excitation spectra (see Fig. S52 of the ESI†). The same overall behaviour also prevails at 77 K.

Our results thus clearly show that the energy levels of the excited singlet and triplet states of either the BDP or the mercaptopyrene ligands as well as those of the PB-CT excited states of both manifolds can be selectively manipulated. This has drastic consequences for the energy cascade underlying the interconversion between the different excited states and their deactivation into the ground state.

An intriguing feature of Pt-BDP complexes is their ability to generate singlet oxygen, sometimes with exceptionally high quantum yields.[9,33,34] The amount of singlet oxygen formed in aerated solutions of the complexes was quantified by comparing the intensity of the $^1O_2$ emission at 1275 nm to that in the presence of tetraphenylporphyrin (TPP) in air-saturated $C_6H_6$ at r.t. Fig. 4 compares the results of this study while Table S14 of the ESI† lists the quantum yields $\Phi_\Delta$. Quite intriguingly, all

 

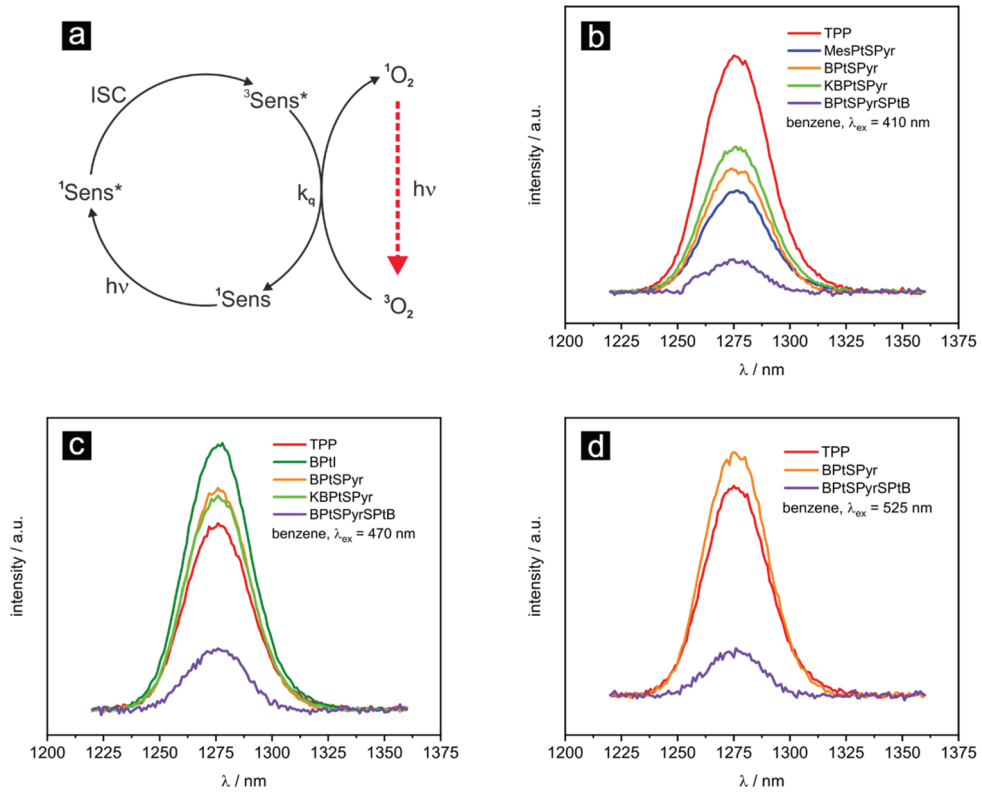


**Fig. 4** (a) Scheme for the generation of singlet oxygen with a triplet sensitizer. (b–d) Singlet oxygen emission upon excitation of the given sensitizers at the stated excitation wavelength at an absorbance of the sensitizer of 0.05 at $\lambda_{exc}$.

complexes of this study produce singlet oxygen. This is particularly true for the simple iodo complex **BPtI**, which, upon excitation into the principal BDP absorption band, achieves a quantum yield of 94%. In **KBPtI**, the value of $\Phi_\Delta$ is reduced to 65%, most probably due to a lower ISC rate constant (*vide supra*). Mononuclear dyads **BPtSPyr** and **KBPtSPyr** also perform well when excited in either the PB-CT or the BDP ππ* absorption bands, and their quantum yields of 74% are also superior to that of TPP. In contrast to our observation of enhanced quantum yields for $^3$PB-CT emission, excitation into the ππ* band of the mercaptopyrene chromophore reduces $\Phi_\Delta$ to 33–40%. **MesPtSPyr**, which lacks a bodipy chromophore, has an even lower quantum yield of 28%. **BPtSPyrSPtB** has the smallest value of $\Phi_\Delta$ (7–18%, depending on the excitation wavelength). Reasons are the lower ISC rate and a rapid degradation under continuous irradiation of this complex in aerated solutions.

The chemical reversibility of the oxidations and reductions allowed us to determine the spectroscopic characteristics of the oxidized mercaptopyrene and reduced bodipy ligands, which are both present in the charge-separated states, and to further substantiate our above conclusions. For doing so we resorted to *in situ* UV/Vis/NIR spectroelectrochemistry inside an optically transparent thin-layer electrolysis cell.[52] Fig. 5 displays the results of such measurements for the complexes **BPtSPyr**, **BPtSPyrSPtB** and **KBPtSPyr**, while the corresponding data are summarized in Table S15 of the ESI.† Multiple isosbestic points attest to clean interconversions between the different redox forms.

Oxidation of these complexes is accompanied by the bleach of the SPyr-based ππ* absorption features while the BDP ππ* band experiences an only minor red-shift. Based on literature data[53,54] and the results of our TD-DFT calculations on **BPtSPyr**$^{\bullet+}$ (Fig. S53 of the ESI†), the new absorption bands at *ca.* 520, 550, 750, and 1000 nm of **BPtSPyr**$^{\bullet+}$ are safely assigned to ππ* transitions of the oxidized mercatopyrene ligand. The results for **KBPtSPyr**$^{\bullet+}$ are very similar with only minor shifts between these two complexes. The new bands appearing during oxidation of **BPtSPyrSPtB** have the same general appearance but are shifted further red due to the presence of two auxochromic thiolate donors. Reduction of **BPtSPyr** and **KBPtSPyr** in turn bleaches the BDP ππ* band and shifts the SPyr ππ* transition slightly red (Fig. 5b and d; for a TD-DFT assignment of the bands see Fig. S54 of the ESI†). Spectral changes upon reduction of **BPtSPyrSPtB** are similar but less characteristic as the BDP and the SPyrS ππ* bands overlap (Fig. 5f).

Knowledge of the characteristic absorption features of the Pt-bonded SPyr$^{\bullet+}$ and BDP$^{\bullet-}$ chromophores allows us to identify them in the transient absorption (TA) spectra of the dyads. Fig. 6 compares the TA spectra of **BPtI**, **MesPtSPyr**, **BPtSPyr** and **KBPtSPyr** in THF. Associated kinetic traces can be found in Fig. S55–S59 of the ESI.† **BPtI** shows two TA features when excited at 470 nm (Fig. 6a): the bleached BDP signal at 470 nm

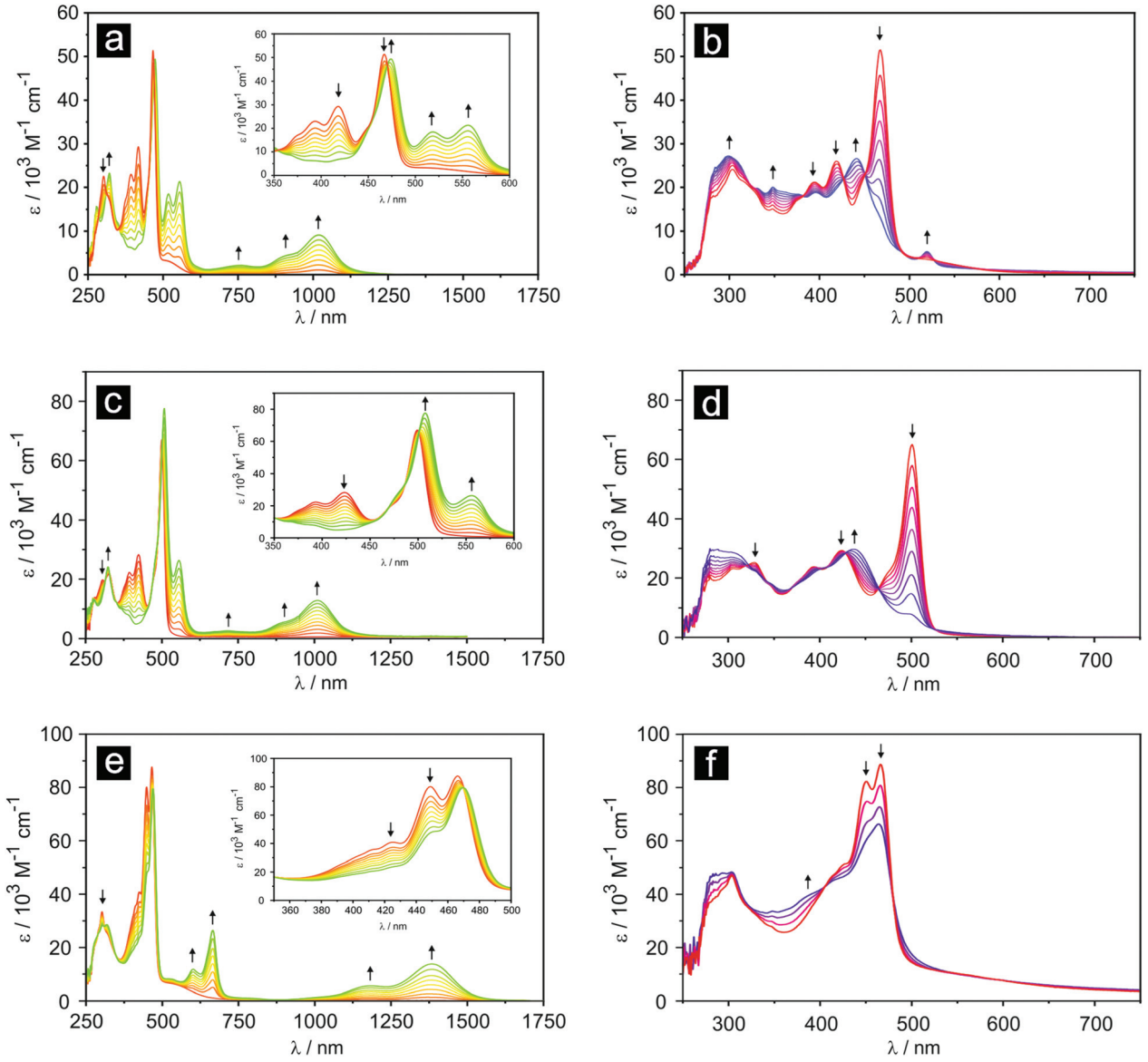


**Fig. 5** Changes of UV/Vis/NIR spectra of **BPtSPyr** (a) on oxidation and (b) on reduction; of **KBPtSPyr** (c) on oxidation and (d) on reduction; as well as that of **BPtSPyrSPtB** (e) on oxidation and (f) on reduction in THF/0.1 M $NBu_4PF_6$ or, in the case of (5e) $CH_2Cl_2$/0.1 M $NBu_4PF_6$ as the supporting electrolyte at $T$ = 293 K.

and, at *ca.* 400 nm, an excited state absorption (ESA) signal, which we assign to the triplet state of the BDP chromophore.[55–57] The bleach and the ESA features share the same kinetics with two time constants. The longer one of about 149 μs microseconds fits with the corresponding emission data (Table 2 and Fig. S55†). The shorter lifetime of about 30 μs is most likely due to triplet–triplet annihilation of two molecules of **BPtI** because of the high optical densities required in the TA measurements. On exciting **MesPtSPyr** into its SPyr band at 430 nm, the ground state bleach of the SPyr band and a distinct ESA signal with peaks at 520, 600 and 760 nm are observed. The latter are assigned to the $^3\pi\pi^*$ states of the SPyr chromophore and closely resemble those reported by Pomestchenko *et al.*[36] and Wu *et al.*[58] Again, the kinetics of ground-state bleach recovery and ESA decay match with the phosphorescence lifetime (Fig. S56 of the ESI†).

TA spectra of **BPtSPyr** show three common features, irrespective of the excitation wavelength. These features are the bleaches of the SPyr and BDP ground state absorption signals at *ca.* 400 nm or 470 nm, and an ESA signal at 550 nm, which we assign to the $SPyr^{\bullet+}$ radical cation (see Fig. 5a for comparison). All these features show identical monoexponential decay kinetics with a common time constant of 50 ns when excited at 532 nm (for single wavelength kinetics for each TA feature see Fig. S57 and S58 of the ESI†). Excitation into the BDP absorption band at 470 nm leaves the time constants for the features at 415 nm and 550 nm of the SPyr chromophore unchanged, but alters the time constant for recovery of the

 

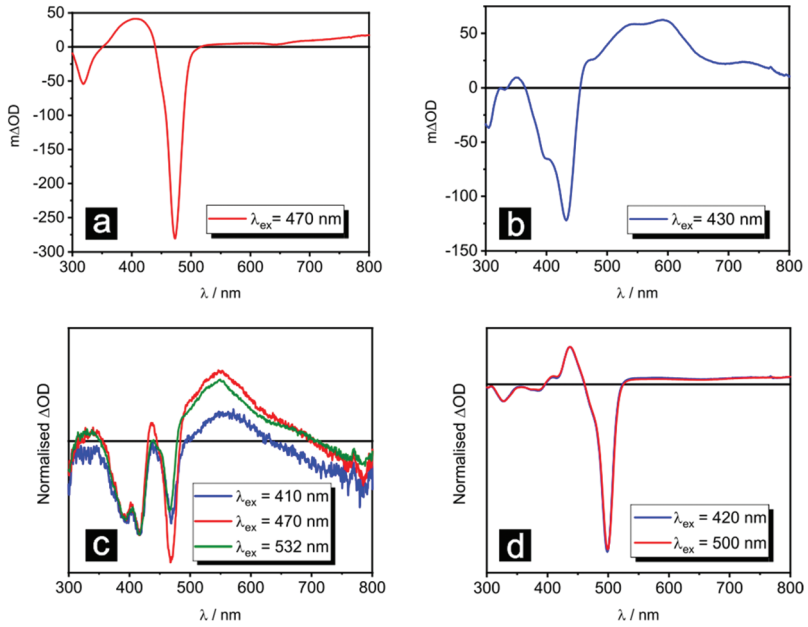


**Fig. 6** Transient absorption spectra of (a) **BPtI**, (b) **MesPtSPyr**, (c) **BPtSPyr** and (d) **KBPtSPyr** in *ca.* 20 μM THF solutions at r.t. directly after laser excitation at the given wavelength. All spectra are time-integrated over 200 ns.

ground state bleach of the BDP $^1\pi\pi^*$ band at 475 nm to 16.5 μs, in accordance with the long-lived BDP $^3\pi\pi^*$ excited state in that solvent (red trace in Fig. S57a of the ESI†). **BPtSPyrSPtB** was unfortunately not sufficiently photostable to allow for the recording of TA spectra.

The TA spectrum of **KBPtSPyr**, which solely emits from excited BDP ππ* states, differs strongly from that of **BPtSPyr** (compare Fig. 6c and d), but shows close resemblance to that of the parent complex **BPtI**. Following excitations at either 420 nm or 500 nm, an ESA signal at 425 nm is observed in addition to the ground state bleach at 500 nm. The TA spectra of **KBPtSPyr** are thus completely devoid of the ESA signatures of an excited PB-CT or $^3\pi\pi^*$ state of the mercaptopyrene ligand. Again, single wavelength kinetics for all TA features agree with the time constant of the phosphorescence emission (see Fig. S59 of the ESI†).

The differences in the TA spectra of complexes **BPtSPyr** and **KBPtSPyr** thus match with those of their absorption and emission properties. The underlying reason for this dichotomy are the different energies of the various excited states and the concomitant changes of their energy transfer cascades. This is best illustrated with the aid of a schematic Jablonski diagram for **BPtSPyr** in Fig. 7. Given the close energetic proximity of three excited states within the singlet and triplet manifolds each and the different degrees of structural reorganization from the initial Franck–Condon states, there is no guarantee that the energy ordering of the structurally relaxed excited states follows that of the corresponding transitions in their absorption or emission spectra. Indeed, test calculations place the BDP-centered $^1\pi\pi^*$ state energetically below the $^1$PB-CT state, although the absorption spectra suggest a different energy ordering. A thorough analysis of this issue, including the identification of the crossing points between the different potential wells, is, however, beyond our present capabilities.

We start our discussion with the emissive properties of **BPtSPyr** at 77 K. Excitation into any absorption band triggers dual phosphorescence emission from the $^3\pi\pi^*$ states of the SPyr and the BDP ligands. This signals that the $^3$PB-CT state is not directly populated from any of the excited singlet states and that all excited states of the singlet manifold relax into these two emissive triplet states. One possible explanation for this odd behaviour is that the $^1$PB-CT and $^3$PB-CT states possess very similar nuclear coordinates and the BDP and SPyr $^3\pi\pi^*$ potential wells have more easily accessible intersections with the $^1$PB-CT potential well. Similar accounts of a direct singlet-to-triplet electron-transfer by spin–orbit coupling have been published on previous occasions.[48–50]

The observed room-temperature emission from the $^3$PB-CT state is therefore likely due to thermal equilibration of that state with the longer lived BDP- and SPyr-based $^3\pi\pi^*$ states (*cf.* the short lifetime of the CT-phosphorescence emission of less than 7 μs). The presence of a competitive deactivation channel for the BDP $^3\pi\pi^*$ state of **BPtSPyr** is also indicated by the significant decrease of its associated lifetime to 78 μs as compared to 279 μs in **BPtI** and 204 μs in **KBPtSPyr**. The latter scenario also explains the further boosting of the quantum yield of the $^3$PB-CT emission on excitation into the $^1\pi\pi^*$ band of the SPyr ligand and the complete quenching of the associated pyrene-based phosphorescence at r.t. All these observations strongly suggest that the $^3$PB-CT state does not constitute the energetically lowest state of the triplet manifold.

The overall behaviour of **BPtSPyrSPtB** is very similar with the exception that the ratio of the time constants for internal conversion from the pyrene-based $^1\pi\pi^*$ state to the $^1\pi\pi^*$ BDP

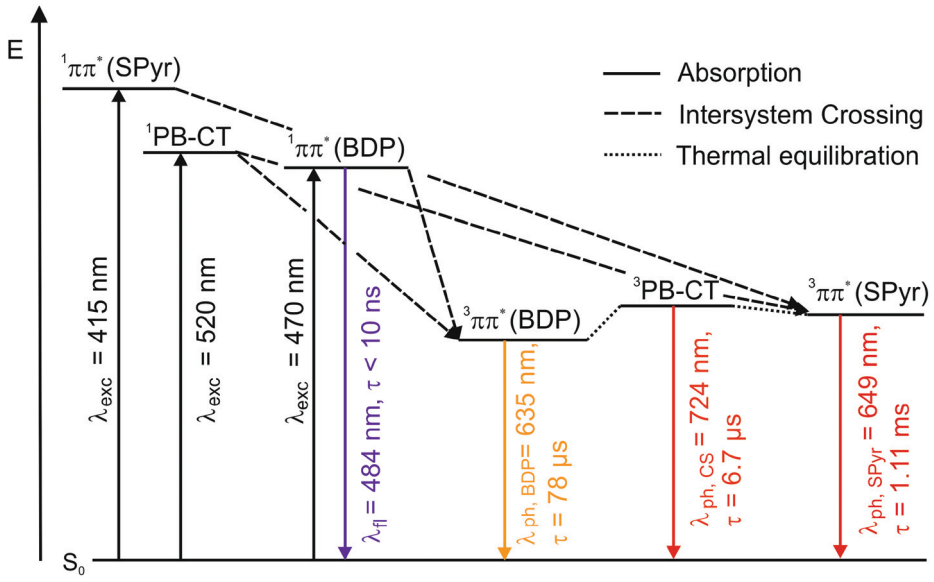


**Fig. 7** Schematic Jablonski diagrams for **BPtSPyr**.

state to that of the ISC to the $^3\pi\pi^*$ state of the pyrenedithiolate ligand is somewhat increased. This allows the BDP-based fluorescence and phosphorescence bands to be observed on irradiation at 420 nm.

Compared to the rather complex characteristics of **BPtSPyr**, that of its peralkylated counterpart **KBPtSPyr** is much simpler. Here, the $^3\pi\pi^*$ BDP state is so much lowered in energy that it is populated from all excited triplet states and no thermal equilibration with the $^3$PB-CT state occurs.

## Summary

We present three dyads of the type *trans*-Pt(σ-BDP)$(PEt_3)_2$(SPyr), where σ-BDP denotes a *meso*-bonded 4,4-difluoro-4-bora-3a,4a-diaza-*s*-indacene (BDP) dye and SPyr is a mercaptopyrene ligand. Variations over this basic motif are made by exchanging the unsubstituted BDP ligand of **BPtSPyr** by its peralkylated krypto-BDP derivative in **KBPtSPyr**, or by employing either a terminal 1-mercaptopyrene ligand in the mononuclear complexes or a bridging pyrene-1,6-dithiolate ligand in dinuclear **BPtSPyrSPtB**. Our results show that BDP peralkylation has drastic consequences for the energy ordering of the different excited states involved in the deactivation cascades and hence the emissive properties. Thus, **BPtSPyr** and **BPtSPyrSPtB** emit *via* four different radiative channels, featuring the charge-separated $^3$PB-CT state and the singlet and triplet BDP-centred ππ* states at r.t., or the BDP and SPyr-centred $^3\pi\pi^*$ states in a frozen matrix at 77 K. The multitude of potentially emissive states and their various interconnections render the emission profiles of these complexes sensitive to the excitation wavelength, the polarity of the solvent, and the temperature. Peralkylation of the BDP ligand in **KBPtSPyr** renders the BDP ligand a less strong acceptor. This makes pyrene-to-BDP charge transfer much less exergonic. As a consequence, **KBPtSPyr** is a dual fluorescence and phosphorescence emitter from the BDP-based $^1\pi\pi^*$ and $^3\pi\pi^*$ states. In this constellation, the SPyr ligand acts as an antenna for the BDP-based excited states. The interrelations between the various deactivation channels were further probed by transient absorption spectroscopy. UV/Vis/NIR spectroelectrochemistry and comparison to reference compounds with either only the BDP or the SPyr chromophore aid in the assignment of excited state absorption signals.

All complexes act as panchromatic sensitizers for singlet oxygen generation. The mononuclear complexes **BPtI**, **KBPtSPyr** and **BPtSPyr** outperform the tetraphenylporphyrin standard in this respect.

## Experimental section

### Methods

Oxidative addition reactions and ligand manipulations were performed under a $N_2$ atmosphere using standard Schlenk techniques or inside a glove box. $C_6D_6$, $CD_2Cl_2$, $CDCl_3$ and THF-*d*8 were supplied from Eurisotop and stored under $N_2$-atomosphere over molecular sieves. All other solvents were used as received. Complex *trans*-Pt(bodipy)I$(PEt_3)_2$ (**BPtI**), *trans*-Pt(bodipy)$(PEt_3)_2$(*S*-1-thiopyrene) (**BPtSPyr**) and *trans*-Pt(mesityl)$(PEt_3)_2$(*S*-1-thiopyrene) (**MesPtSPyr**) were synthesized according to the literature protocols.[9,42]

NMR experiments were carried out on a Varian Unity Inova 400, a Bruker Avance III DRX 400 or a Bruker Avance DRX 600 spectrometer. $^1$H and $^{13}$C spectra were referenced to the solvent signal, while $^{31}$P and $^{195}$Pt spectra were referenced to external standards (85% $H_3PO_4$ or saturated $K_2[PtCl_6]$ in $D_2O$, respectively). NMR data are given as follows: chemical shift

 

($\delta$ in ppm), multiplicity (br, broad; d, doublet; dd, doublet of doublets; m, multiplet; s, singlet; t, triplet, vt virtual triplet), integration, coupling constant (Hz). Unequivocal signal assignments were achieved by 2D NMR experiments. The numbering of the nuclei follows that of the chemical structures displayed at the synthesis protocols.

Combustion analysis was conducted with an Elementar vario MICRO cube CHN-analyzer from Heraeus.

Luminescence spectra and lifetimes as well as quantum yields were measured in acetone, $CH_2Cl_2$, 2-MeTHF, THF, or toluene solutions of the complex on a PicoQuant FluoTime 300 spectrometer. Unless stated otherwise, absolute quantum yields were determined with an integrating sphere within the FluoTime 300 spectrometer. Emission spectroscopy under inert gas atmosphere was conducted in a quartz cuvette modified with an angle valve from Normag. The emission data of **BPtSPyr** in acetone with excitation at 405 nm are not reported due to sample decomposition upon laser excitation. The singlet oxygen generation quantum yields $\Phi_\Delta$ were determined by detecting the luminescence signal of singlet oxygen at 1275 nm in air-saturated benzene solution containing the corresponding sensitizer at a concentration to render its absorbance as 0.05 at $\lambda_{ex}$. The integrated intensity of the phosphorescence signal of $^1O_2$ was compared to that obtained for a solution containing the reference sensitizer tetraphenylporphyrin ($\Phi_\Delta$(TPP) = 0.66),[51] with an absorbance of 0.05 at $\lambda_{ex}$.

UV/Vis/NIR spectra were recorded on a TIDAS fiber optic diode array spectrometer (combined MCS UV/NIR and PGS NIR instrumentation) from J&M in HELLMA quartz cuvettes with 0.1 cm optical path lengths.

Transient absorption spectroscopy was performed using an LP920-KS instrument from Edinburgh Instruments. 410 nm and 470 nm excitations were obtained from pulsed third-harmonic radiation from a Quantel Brilliant b Nd:YAG laser equipped with a Rainbow optical parameter oscillator (OPO). 532 nm excitation was obtained from pulsed second-harmonic generation from a Quantel Brilliant b Nd:YAG laser. The laser pulse duration was ~10 ns and the pulse frequency 10 Hz with a typical pulse energy of 7 mJ. Detection of transient absorption spectra was performed with an iCCD camera from Andor. Single-wavelength kinetics were recorded using a photomultiplier tube. All optical spectroscopic experiments were performed under deaerated conditions using quartz cuvettes. Oxygen was removed by the freeze–pump–thaw technique. Solutions were typically 20 μM in the compound and deaerated through three cycles of freeze–pump–thaw.

All electrochemical experiments were executed in a home-built cylindrical vacuum-tight one-compartment cell. A spiral shaped Pt wire and an Ag wire as the counter and pseudoreference electrodes are sealed into glass capillaries and fixed by Quickfit screws *via* standard joints. A platinum electrode is introduced as the working electrode through the top port *via* a Teflon screw cap with a suitable fitting. It is polished with first 1 μm and then 0.25 μm diamond paste before measurements. The cell may be attached to a conventional Schlenk line *via* a side arm equipped with a Teflon screw valve, allowing experiments to be performed under an argon atmosphere with approximately 5–7 mL of analyte solution. $NBu_4PF_6$ (0.1 mM) was used as the supporting electrolyte. Referencing was done with addition of an appropriate amount of decamethylferrocene ($Cp^*_2Fe$) as an internal standard to the analyte solution after all data of interest had been acquired. Representative sets of scans were repeated with the added standard. Electrochemical data were acquired with a computer-controlled BASi CV50 potentiostat. The optically transparent thin-layer electrochemical (OTTLE) cell was home-built and followed the design of Hartl *et al.*[52] It comprised of a Pt working and counter electrode and a thin silver wire as a pseudoreference electrode sandwiched between two $CaF_2$ windows of a conventional liquid IR cell with the working electrode positioned in the centre of the spectrometer beam.

### Computational details

The ground-state electronic structures were calculated by density functional theory (DFT) methods using the Gaussian 09[59] program package. Quantum-chemical studies were performed without any symmetry constraints. Open-shell systems were calculated by the unrestricted Kohn–Sham approach.[60] Geometry optimizations followed by vibrational analysis were performed either in a vacuum or in solvent media. The quasi-relativistic Wood–Boring small-core pseudopotentials (MWB),[61,62] the corresponding optimized set of basis functions[63] for platinum and the halogen atoms, and the 6-31G(d)-polarized double-ζ basis set[64] for the remaining atoms were employed together with the Perdew–Burke–Ernzerhof exchange and correlation functional (PBE0).[65,66] Solvent effects were accounted for by the polarizable conductor continuum model (PCM)[67–70] with standard parameters for dichloromethane. Absorption spectra and orbital energies were calculated using time-dependent DFT (TD-DFT)[71] with the same functional/basis set combinations as those mentioned above. For an easier comparison with the experiment, the obtained absorption and emission energies were converted into wavelengths and broadened by a Gaussian distribution (full width at half-maximum = 3000 $cm^{-1}$) using the program GaussSum.[72] Atomic coordinates of the calculated structures are provided in Tables S16–S21.†

**X-ray diffraction analysis** of single crystals was performed at 100 K on a STOE IPDS-II diffractometer equipped with a graphite-monochromated radiation source ($\lambda$ = 0.71073 Å) and an image plate detection system. A crystal mounted on a fine glass fiber with silicon grease was employed. If not indicated otherwise, the selection, integration, and averaging procedure of the measured reflection intensities, the determination of the unit cell dimensions and a least-squares fit of the $2\theta$ values as well as data reduction, LP-correction and space group determination were performed using the X-Area software package delivered with the diffractometer. A semiempirical absorption correction was performed.[73] All structures were solved by the heavy-atom methods (SHELXS-97,[74] SHELXS-2013,[75] SHELXS-2014,[76] or OLEX2[77]). Structure solutions were completed with difference Fourier syntheses and

full-matrix last-squares refinements using SHELXL-97,[74] SHELXS-2013,[75] SHELXS-2014,[76] or OLEX2[77] minimizing $\omega(F_o^2 - F_c^2)^2$. The weighted $R$ factor ($wR^2$) and the goodness of the fit GOF are based on $F^2$. All non-hydrogen atoms were refined with anisotropic displacement parameters, while hydrogen atoms were treated in a riding model. Molecular structures in this work are plotted with PLATON[78] or Mercury.[79] CIF files of the complexes have been deposited at the Cambridge Structure Data Base as CCDC 1908870 (**KBPtI**), and 1898598 (**KBPtSPyr**).

**Bis-(4-ethyl-3,5-dimethyl-pyrrol-2-yl)-ketone**[80]

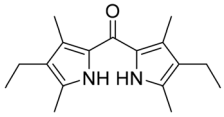

2 ml (14.8 mmol) of 2,4-dimethyl-3-ethyl-pyrrole were dissolved in 40 ml abs. $Et_2O$ and 5.1 ml (15.4 mmol) of a 3 M EtMgBr solution in $Et_2O$ were slowly added at r.t. before heating to reflux for 3 h. After cooling to r.t., 3.9 ml (7.4 mmol) of a 20% phosgene solution in toluene were added dropwise within 1 h. A pale precipitate was observed during addition. The solution was stirred for 72 h at r.t., cooled to 0 °C and 60 ml of water were added. Phases were separated and the aqueous phase was extracted with $CH_2Cl_2$. Combined organic phases were dried over $MgSO_4$ and all volatiles were removed. Recrystallization from 2-propanol and washing with $Et_2O$ gave the product as colorless solid. Yield: 1.00 g, 50%. $^1$H NMR (399.79 MHz, $CDCl_3$, 300 K): $\delta$ 8.68 (s, 2H, N*H*), 2.42 (q, 4H, $^3J_{HH}$ = 7.5 Hz, C$H_2$CH$_3$), 2.25 (s, 6H, C$H_3$), 2.17 (s, 6H, C$H_3$), 1.09 (t, 6H, $^3J_{HH}$ = 7.5 Hz, CH$_2$C$H_3$). $^{13}$C NMR (100.54 MHz, $CDCl_3$, 300 K): $\delta$ 175.4, 129.8, 127.4, 125.4, 124.4, 17.5, 15.3, 11.5, 10.8.

**8-Cloro-2,6-diethyl-1,3,5,7-tetramethyl-bodipy (KBDP)**

1.0 g (3.7 mmol) of **1** were dissolved in 50 ml of abs. $C_2H_4Cl_2$ and 0.67 ml (7.3 mmol) of $POCl_3$ were added. The mixture was heated to reflux for 2 h, then cooled to 0 °C, 5 ml (36.7 mmol) of $NEt_3$ were added and the solution was stirred for 5 min before adding 5 ml (40.4 mmol) of $BF_3{\cdot}Et_2O$ dropwise. The solution was slowly warmed to r.t. and stirred overnight. All volatiles were removed and water was added. The dark mixture was extracted with 4 × 100 ml of $Et_2O$, the organic phases were dried over $MgSO_4$ and the solvent was removed. Column chromatography (silica, petrol ether/$CH_2Cl_2$ 2 : 1, $R_f$ = 0.25) yielded the product as a red solid. Yield: 0.53 g, 43%. $^1$H NMR (399.79 MHz, $CDCl_3$, 300 K): $\delta$ 2.50 (s, 6H, C$H_3$), 2.40 (q, 4H, $^3J_{HH}$ = 7.5 Hz, C$H_2$CH$_3$), 2.39 (s, 6H, C$H_3$), 1.05 (t, 6H, $^3J_{HH}$ = 7.5 Hz, CH$_2$C$H_3$). $^{13}$C NMR (100.54 MHz, $CDCl_3$, 300 K): $\delta$ 153.8, 138.2, 135.3, 133.3, 129.3, 17.2, 14.9, 13.9, 12.6. Anal. Calcd for $C_{17}H_{22}BClF_2N_2$: C, 60.30; H, 6.55; N, 8.27. Found: C, 60.31; H, 6.44; N, 9.42.

***cis*-Pt(krypto-bodipy)Cl(PEt$_3$)$_2$ (*cis*-KBPtCl)**

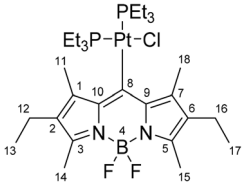

In a flame-dried Schlenk flask 255 µmol Pt(Et)$_2$(PEt$_3$)$_2$ were dissolved in 2 ml of dry degassed benzene. The solution was frozen, evacuated and sealed. Heating of the closed vessel for 2 h to 110 °C results in a brown solution. A solution of 278 µmol Cl-bodipy (**2**) in 2 ml of benzene was added at r.t. The solution was kept at 50 °C overnight. Filtration of the solid and washing with *n*-pentane affords the product as a brown solid. Yield: 136 mg, 70%. $^1$H NMR (399.79 MHz, $CDCl_3$, 300 K): $\delta$ 2.90 (s, 6H, H11, H18), 2.41 (s, 6H, H14, H15), 2.36 (q, $^3J_{HH}$ = 7.5 Hz, 4H, H12, H16), 2.06 (m, 6H, P$_{cis}$-C$H_2$CH$_3$), 1.71 (m, 6H, P$_{trans}$-C$H_2$CH$_3$), 1.17 (m, 9H, P$_{trans}$-CH$_2$C$H_3$), 1.01 (t, $^3J_{HH}$ = 7.5 Hz, 6H, H13, H17), 0.93 (m, 9H, P$_{cis}$-CH$_2$C$H_3$). $^{13}$C {$^1$H} NMR (100.53 MHz, $CDCl_3$, 300 K): $\delta$ 147.9 (s, C3, C5), 139.7 (s, C9, C19), 138.1 (s, C1, C7), 130.3 (s, C2, C6), 17.7 (s, C12, C16), 17.4 (dd, $J_{PC}$ = 38.0 Hz, $^4J_{PC}$ = 2.0 Hz, PCH$_2$CH$_3$), 16.8 (s, C11, C18), 15.3 (d, $J_{PC}$ = 28.5 Hz, PCH$_2$CH$_3$), 15.0 (s, C13, C17), 12.4 (d, $J$ = 4.5 Hz, C14, C15), 7.9 (d, $^2J_{PC}$ = 3.9 Hz, PCH$_2$C$H_3$), 7.8 (d, $^2J_{PC}$ = 2.6 Hz, PCH$_2$C$H_3$); the signal for C8 is missing due to low signal to noise ratio. $^{31}$P {$^1$H} NMR (161.84 MHz, $CDCl_3$, 300 K): $\delta$ 3.73 (d, $^2J_{PP}$ = 17.7 Hz, with satellites $J_{PtP}$ = 1810 Hz), −4.36 (d, $^2J_{PP}$ = 17.7 Hz, with satellites $J_{PtP}$ = 3954 Hz). $^{195}$Pt {$^1$H} NMR (85.56 MHz, $CDCl_3$, 300 K): $\delta$ −4241 (dd, $J_{PtP}$ = 3954 Hz, 1810 Hz).

***trans*-Pt(krypto-bodipy)I(PEt$_3$)$_2$ (KBPtI)**

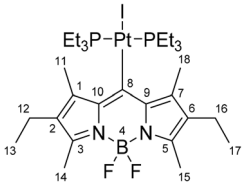

65 µmol of **KBPtCl** and 84 µmol of AgOTf were dissolved in 1 ml of $CH_2Cl_2$ and heated to reflux for 1 h. The filtered solution was added to a methanolic solution of 130 µmol of NaI and stirred for 30 min at r.t. All volatiles were removed and the product was purified by column chromatography (silica, petrol ether/$CH_2Cl_2$ 1 : 1, $R_f$ = 0.1). Crystals suitable for X-ray structure analysis were obtained by slow diffusion of pentane into a saturated $CH_2Cl_2$ solution of the compound at r.t. Yield: 25 mg, 45%. $^1$H NMR (399.79 MHz, $CDCl_3$, 300 K): $\delta$ 2.93 (s, 6H, H11, H18), 2.41 (s, 6H, H14, H15), 2.39 (q, $^3J_{HH}$ = 7.5 Hz, 4H, H12, H16), 1.82 (m, 12H, P-C$H_2$CH$_3$), 1.02 (m, 24H, H13, H17, PCH$_2$C$H_3$). $^{13}$C {$^1$H} NMR (100.53 MHz, $CDCl_3$, 300 K): $\delta$ 161.7 (t, $^2J_{PC}$ = 8.5 Hz, C8), 147.9 (s, C3, C5), 138.4 (s with satellites, $^2J_{PtC}$ = 32.2 Hz, C9, C10), 137.5 (s with satellites, $^3J_{PtC}$ = 23.9 Hz, C1, C7), 131.1 (s, C2, C6), 17.9 (s, C12, C16), 16.0 (vquint, $J_{PC}$ = $^3J_{PC}$ = 17.2 Hz, with satellites $^2J_{PtC}$ = 34.2 Hz, P-CH$_2$CH$_3$), 15.3 (s, C11, C18), 14.7 (s, C13, C17), 12.3 (br s, C14, C15), 8.2 (s with satellites, $^3J_{PtC}$ = 15.7 Hz, P-CH$_2$C$H_3$). $^{31}$P {$^1$H}

 

NMR (161.84 MHz, $CDCl_3$, 300 K): $\delta$ −4.90 (s with satellites, $J_{PtP}$ = 2583 Hz). $^{195}$Pt $\{^1H\}$ NMR (85.56 MHz, $CDCl_3$, 300 K): $\delta$ −4432 (t, $J_{PtP}$ = 2583 Hz). Anal. Calcd for $C_{29}H_{52}BF_2IN_2P_2Pt$: C, 40.43; H, 6.08; N, 3.25. Found: C, 40.25; H, 5.90; N, 4.57.

***trans*-Pt(krypto-bodipy)(PEt$_3$)$_2$(*S*-1-mercaptopyrene) (KBPtSPyr)**

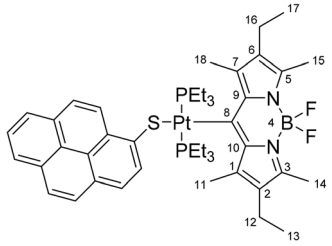

57 μmol of **KBPtCl** and 62 μmol of AgOTf were dissolved in 0.4 ml of dry degassed $CD_2Cl_2$ in a Young-tube and heated to 40 °C for 10 min. $^{31}$P NMR spectroscopy indicated full conversion. All volatiles were removed and the remaining solids were dissolved in toluene. 68 μmol pyrene-1-thiol and 91 μmol of diisopropylamine were dissolved in 5 ml dry toluene. The solution containing the Pt complex was filtered and added to the pyrene solution. After stirring for 0.5 h at r.t. the solvent was evaporated. The residue washed with 2 × 10 ml *n*-pentane and recrystallized twice from a benzene/hexane (1 : 10) at −25 °C. Crystals suitable for X-ray structure analysis were obtained by slow diffusion of pentane into a saturated $CH_2Cl_2$ solution of the compound at −25 °C. Yield: 8.3 mg, 15%. $^1$H NMR (399.78 MHz, THF-*d*8, 300 K): $\delta$ 9.07 (d, $^3J_{HH}$ = 9.2 Hz, 1H, $H_{Pyr}$), 8.42 (d, $^3J_{HH}$ = 8.0 Hz, 1H, $H_{Pyr}$), 8.06 (d, $^3J_{HH}$ = 7.5 Hz, 1H, $H_{Pyr}$), 8.01 (m, 2H, $H_{Pyr}$), 7.88 (m, 3H, $H_{Pyr}$), 7.83 (d, $^3J_{HH}$ = 8.8 Hz, 1H, $H_{Pyr}$), 3.29 (s, 6H, H11, H18), 2.49 (q, $^3J_{HH}$ = 7.6 Hz, 4H, H12, H16), 2.39 (s, 6H, H14, H15), 1.75 (m, 12H, PC$H_2$CH$_3$), 1.10 (t, $^3J_{HH}$ = 7.6 Hz, 4H, H13, H17), 0.92 (m, 18H, PCH$_2$C$H_3$). $^{13}$C $\{^1H\}$ NMR (100.53 MHz, THF-*d*8, 300 K): $\delta$ 169.0 (t, $^2J_{PC}$ = 9.0 Hz, C8), 148.0 (s, C3, C5), 145.8 (s, $C_{Pyr}$), 141.0 (s, C9, C10), 137.9 (s, C1, C7), 133.3 (s, $C_{Pyr}$), 133.0 (s, $C_{Pyr}$), 132.9 (s, $C_{Pyr}$), 132.3 (s, $C_{Pyr}$), 131.4 (s, C3, C6), 128.5 (s, $C_{Pyr}$), 128.0 (s, $C_{Pyr}$), 127.7 (s, $C_{Pyr}$), 126.8 (s, $C_{Pyr}$), 126.64 (s, $C_{Pyr}$), 126.62 (s, $C_{Pyr}$), 126.2 (s, $C_{Pyr}$), 125.5 (s, $C_{Pyr}$), 124.7 (s, $C_{Pyr}$), 124.6 (s, $C_{Pyr}$), 124.4 (s, $C_{Pyr}$), 18.6 (s, C12, C16), 17.0 (s, C11, C18), 15.8 (t, $J_{PC}$ = 16.9 Hz, PC$H_2$CH$_3$), 15.2 (s, C13, C17), 12.4 (s, C14, C15), 8.2 (s, PCH$_2$C$H_3$). $^{31}$P $\{^1H\}$ NMR (161.83 MHz, $C_6D_6$, 300 K): $\delta$ −2.63 (s with satellites, $J_{PtP}$ = 2611 Hz). $^{195}$Pt $\{^1H\}$ NMR (85.55 MHz, $C_6D_6$, 300 K): $\delta$ −4249 (t, $J_{PtP}$ = 2611 Hz). HR ESI-MS Calcd for $[(C_{45}H_{61}BF_2N_2P_2PtS)^+]$: *m*/*z* 967.3732. Found: *m*/*z* 967.3549.

***trans*-Pt$_2$(bodipy)$_2$(PEt$_3$)$_4$(*S*,*S*′-1,6-dimercaptopyrene) (BPtSPyrSPtB)**

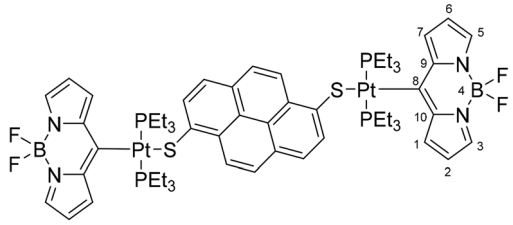

Under an atmosphere of nitrogen 119 mg (169 μmol) of **BPtBr** and 65 mg (254 μmol) of AgOTf were dissolved in 0.6 ml $CD_2Cl_2$ and heated to reflux for 20 min. After reaction control by $^{31}$P NMR spectroscopy the solvent was removed, the residue re-dissolved in 5 ml of benzene and filtered. This solution was added to a mixture containing 23 mg (85 μmol) of 1,6-dimercaptopyrene and 24 μl (170 μmol) of $^i$Pr$_2$NH in 5 ml of toluene. After 90 min all volatiles were removed and the product was washed with 1 × 5 ml benzene, 2 × 5 ml MeOH, 2 × 5 ml $Et_2O$ and 2 × 5 ml *n*-pentane. The product was obtained as a brown solid. Yield: 57 mg, 45%. $^1$H NMR (399.78 MHz, THF-*d*8, 300 K): $\delta$ 8.80 (d, $^3J_{HH}$ = 9.2 Hz, 1H, $H_{pyr}$), 8.68 (d, $^3J_{HH}$ = 7.9 Hz, 1H, $H_{pyr}$), 7.92 (d, $^3J_{HH}$ = 7.9 Hz, 1H, $H_{pyr}$), 7.88 (d, $^3J_{HH}$ = 9.2 Hz, 1H, $H_{pyr}$), 7.68 (br s, 4H, H3, H5), 7.65 (br s, 4H, H1, H7), 6.51 (br s, 4H, H2, H6), 1.78 (m, 24 H, PC$H_2$CH$_3$), 1.01 (m, 36 H, PCH$_2$C$H_3$). $^{13}$C $\{^1H\}$ NMR (150.97 MHz, THF-*d*8, 298 K): $\delta$ 188.3 (s, C8), 144.5 (s, C7/10, S-$C_{pyr}$), 137.9 (s, C3, C5), 133.6 (s, with shoulders, C1, C7), 133.2 (s, $C_{pyr}$), 132.1 (s, $C_{pyr}$), 128.7 (s, $C_{pyr}$), 127.2 (s, $C_{pyr}$), 126.8 (s, $C_{pyr}$), 124.8 (s, $C_{pyr}$), 123.2 (s, $C_{pyr}$), 116.5 (s, C2, C6), 14.8 (t, $J_{PC}$ = 17.2 Hz, PC$H_2$CH$_3$), 8.3 (s, PCH$_2$C$H_3$). $^{31}$P $\{^1H\}$ NMR (161.83 MHz, THF-*d*8, 300 K): $\delta$ 6.46 (s, with satellites, $J_{PtP}$ = 2493 Hz). $^{195}$Pt $\{^1H\}$ NMR (85.56 MHz, $CDCl_3$, 300 K): $\delta$ −4344 (t, $J_{PtP}$ = 2491 Hz). Anal. Calcd for $C_{58}H_{80}B_2F_4N_4P_4Pt_2S_2$: C, 46.16; H, 5.34; N, 3.71; Found: C, 44.70; H, 5.32; N, 4.60.

## Conflicts of interest

The authors declare no competing financial interest.

## Acknowledgements

We gratefully acknowledge financial support of this work by the Deutsche Forschungsgemeinschaft (DFG, grant number Wi1262/10-2) and the Swiss national Science Foundation (grant number 200021_176780). We also wish to thank the reviewers for their insightful comments.

## References

1 M. Bachmann, O. Blacque and K. Venkatesan, *Chem. – Eur. J.*, 2017, **23**, 9451–9456.
2 Y. Yang, M. Lowry, C. M. Schowalter, S. O. Fakayode, J. O. Escobedo, X. Xu, H. Zhang, T. J. Jensen, F. R. Fronczek, I. M. Warner and R. M. Strongin, *J. Am. Chem. Soc.*, 2006, **128**, 14081–14092.
3 S. Park, J. E. Kwon, S. H. Kim, J. Seo, K. Chung, S. Y. Park, D. J. Jang, B. Milian Medina, J. Gierschner and S. Y. Park, *J. Am. Chem. Soc.*, 2009, **131**, 14043–14049.
4 Y. Liu, M. Nishiura, Y. Wang and Z. Hou, *J. Am. Chem. Soc.*, 2006, **128**, 5592–5593.
5 Y. Liu, H. Guo and J. Zhao, *Chem. Commun.*, 2011, **47**, 11471–11473.
6 H. Xiang, L. Zhou, Y. Feng, J. Cheng, D. Wu and X. Zhou, *Inorg. Chem.*, 2012, **51**, 5208–5212.

7 H. Hochreiner, I. Sanchez-Barragan, J. M. Costa-Fernandez and A. Sanz-Medel, *Talanta*, 2005, **66**, 611–618.
8 F. Geist, A. Jackel and R. F. Winter, *Inorg. Chem.*, 2015, **54**, 10946–10957.
9 P. Irmler and R. F. Winter, *Dalton Trans.*, 2016, **45**, 10420–10434.
10 M. A. El-Sayed, *J. Chem. Phys.*, 1963, **38**, 2834–2838.
11 E. Y.-T. Li, T. Y. Jiang, Y. Chi and P. T. Chou, *Phys. Chem. Chem. Phys.*, 2014, **16**, 26184–26192.
12 P.-T. Chou, Y. Chi, M.-W. Chung and C.-C. Lin, *Coord. Chem. Rev.*, 2011, **255**, 2653–2665.
13 M. Montalti, A. Credi, L. Prodi and M. Teresa Gandolfi, *Handbook of Photochemistry*, CRC Press, Boca Raton, 3rd edn, 2006.
14 S. P. McGlynn, T. Azumi and M. Kinoshita, *Molecular Spectroscopy of the Triplet State*, Prentice-Hall, Englewood Cliffs, N.J, 1969.
15 W. Y. Heng, J. Hu and J. H. K. Yip, *Organometallics*, 2007, **26**, 6760–6768.
16 C. C. Hsu, C. C. Lin, P. T. Chou, C. H. Lai, C. W. Hsu, C. H. Lin and Y. Chi, *J. Am. Chem. Soc.*, 2012, **134**, 7715–7724.
17 C.-W. Hsu, C.-C. Lin, M.-W. Chung, Y. Chi, G.-H. Lee, P.-T. Chou, C.-H. Chang and P.-Y. Chen, *J. Am. Chem. Soc.*, 2011, **133**, 12085–12099.
18 E. O. Danilov, I. E. Pomestchenko, S. Kinayyigit, P. L. Gentili, M. Hissler, R. Ziessel and F. N. Castellano, *J. Phys. Chem. A*, 2005, **109**, 2465–2471.
19 B. Ma, P. I. Djurovich, M. Yousufuddin, R. Bau and M. E. Thompson, *J. Phys. Chem. C*, 2008, **112**, 8022–8031.
20 W. Yang, A. Karatay, J. Zhao, J. Song, L. Zhao, Y. Xing, C. Zhang, C. He, H. G. Yaglioglu, M. Hayvali, A. Elmali and B. Kucukoz, *Inorg. Chem.*, 2015, **54**, 7492–7505.
21 W. Wu, W. Wu, S. Ji, H. Guo and J. Zhao, *Eur. J. Inorg. Chem.*, 2010, **2010**, 4470–4482.
22 A. J. Hallett, N. White, W. Wu, X. Cui, P. N. Horton, S. J. Coles, J. Zhao and S. J. Pope, *Chem. Commun.*, 2012, **48**, 10838–10840.
23 A. F. Morales, G. Accorsi, N. Armaroli, F. Barigelletti, S. J. A. Pope and M. D. Ward, *Inorg. Chem.*, 2002, **41**, 6711–6719.
24 N. D. McClenaghan, Y. Leydet, B. Maubert, M. T. Indelli and S. Campagna, *Coord. Chem. Rev.*, 2005, **249**, 1336–1350.
25 K. Oppelt, D. A. M. Egbe, U. Monkowius, M. List, M. Zabel, N. S. Sariciftci and G. Knör, *J. Organomet. Chem.*, 2011, **696**, 2252–2258.
26 R. Liu, N. Dandu, Y. Li, S. Kilina and W. Sun, *Dalton Trans.*, 2013, **42**, 4398–4409.
27 A. J. Howarth, M. B. Majewski and M. O. Wolf, *Coord. Chem. Rev.*, 2015, **282–283**, 139–149.
28 I. E. Pomestchenko and F. N. Castellano, *J. Phys. Chem. A*, 2004, **108**, 3485–3492.
29 T. Tsuboi, D.-F. Huang, T. J. Chow and W. Huang, *Opt. Mater.*, 2014, **36**, 1734–1738.
30 J. Brooks, Y. Babayan, S. Lamansky, P. I. Djurovich, I. Tsyba, R. Bau and M. E. Thompson, *Inorg. Chem.*, 2002, **41**, 3055–3066.
31 J. Hu, J. H. K. Yip, D.-L. Ma, K.-Y. Wong and W.-H. Chung, *Organometallics*, 2009, **28**, 51–59.
32 F. Geist, A. Jackel and R. F. Winter, *Dalton Trans.*, 2015, **44**, 3974–3987.
33 P. Irmler and R. F. Winter, *Organometallics*, 2018, **37**, 235–253.
34 F. Geist, A. Jackel, P. Irmler, M. Linseis, S. Malzkuhn, M. Kuss-Petermann, O. S. Wenger and R. F. Winter, *Inorg. Chem.*, 2017, **56**, 914–930.
35 N. Kanamaru, H. R. Bhattacharjee and E. C. Lim, *Chem. Phys. Lett.*, 1974, **26**, 174–179.
36 I. E. Pomestchenko, C. R. Luman, M. Hissler, R. Ziessel and F. N. Castellano, *Inorg. Chem.*, 2003, **42**, 1394–1396.
37 J. P. Rostron, G. Ulrich, P. Retailleau, A. Harriman and R. Ziessel, *New J. Chem.*, 2005, **29**, 1241.
38 R. Ziessel, C. Goze, G. Ulrich, M. Cesario, P. Retailleau, A. Harriman and J. P. Rostron, *Chem. – Eur. J.*, 2005, **11**, 7366–7378.
39 X. F. Zhang and N. Feng, *Chem. – Asian J.*, 2017, **12**, 2447–2456.
40 M. A. Filatov, S. Karuthedath, P. M. Polestshuk, H. Savoie, K. J. Flanagan, C. Sy, E. Sitte, M. Telitchko, F. Laquai, R. W. Boyle and M. O. Senge, *J. Am. Chem. Soc.*, 2017, **139**, 6282–6285.
41 M. A. Filatov, S. Karuthedath, P. M. Polestshuk, S. Callaghan, K. J. Flanagan, M. Telitchko, T. Wiesner, F. Laquai and M. O. Senge, *Phys. Chem. Chem. Phys.*, 2018, **20**, 8016–8031.
42 P. Irmler, F. S. Gogesch, C. B. Larsen, O. S. Wenger and R. F. Winter, *Dalton Trans.*, 2019, **48**, 1171–1174.
43 T. J. McCarthy, R. G. Nuzzo and G. M. Whitesides, *J. Am. Chem. Soc.*, 1981, **103**, 3396–3403.
44 M. A. Cairns, K. R. Dixon and G. A. Rivett, *J. Organomet. Chem.*, 1979, **171**, 373–385.
45 J. S. Wilson, N. Chawdhury, M. R. A. Al-Mandhary, M. Younus, M. S. Khan, P. R. Raithby, A. Köhler and R. H. Friend, *J. Am. Chem. Soc.*, 2001, **123**, 9412–9417.
46 C. E. Whittle, J. A. Weinstein, M. W. George and K. S. Schanze, *Inorg. Chem.*, 2001, **40**, 4053–4062.
47 E. M. Kober, J. V. Caspar, R. S. Lumpkin and T. J. Meyer, *J. Phys. Chem.*, 1986, **90**, 3722–3734.
48 M. R. Wasielewski, D. G. Johnson, W. A. Svec, K. M. Kersey and D. W. Minsek, *J. Am. Chem. Soc.*, 1988, **110**, 7219–7221.
49 S.-H. Lee, A. G. Larsen, K. Ohkubo, Z.-L. Cai, J. R. Reimers, S. Fukuzumi and M. J. Crossley, *Chem. Sci.*, 2012, **3**, 257–269.
50 T. Higashino, T. Yamada, M. Yamamoto, A. Furube, N. V. Tkachenko, T. Miura, Y. Kobori, R. Jono, K. Yamashita and H. Imahori, *Angew. Chem., Int. Ed.*, 2016, **55**, 629–633.
51 F. Wilkinson, W. P. Helman and A. B. Ross, *J. Phys. Chem. Ref. Data*, 1993, **22**, 113–262.

 

52 M. Krejčik, M. Daněk and F. Hartl, *J. Electroanal. Chem.*, 1991, **317**, 179–187.
53 T. Shida and S. Iwata, *J. Am. Chem. Soc.*, 1973, **95**, 3473–3483.
54 J. Maurer, M. Linseis, B. Sarkar, B. Schwederski, M. Niemeyer, W. Kaim, S. Zalis, C. Anson, M. Zabel and R. F. Winter, *J. Am. Chem. Soc.*, 2008, **130**, 259–268.
55 R. P. Sabatini, T. M. McCormick, T. Lazarides, K. C. Wilson, R. Eisenberg and D. W. McCamant, *J. Phys. Chem. Lett.*, 2011, **2**, 223–227.
56 X. F. Zhang and X. Yang, *J. Phys. Chem. B*, 2013, **117**, 5533–5539.
57 Z. Wang and J. Zhao, *Org. Lett.*, 2017, **19**, 4492–4495.
58 W. Wu, J. Sun, S. Ji, W. Wu, J. Zhao and H. Guo, *Dalton Trans.*, 2011, **40**, 11550–11561.
59 M. J. Frisch, G. W. Trucks, H. B. Schlegel, G. E. Scuseria, M. A. Robb, J. R. Cheeseman, G. Scalmani, V. Barone, B. Mennucci, G. A. Petersson, H. Nakatsuji, M. Caricato, X. Li, H. P. Hratchian, A. F. Izmaylov, J. Bloino, G. Zheng, J. L. Sonnenberg, M. Hada, M. Ehara, K. Toyota, R. Fukuda, J. Hasegawa, M. Ishida, T. Nakajima, Y. Honda, O. Kitao, H. Nakai, T. Vreven, J. A. Montgomery Jr., J. E. Peralta, F. Ogliaro, M. J. Bearpark, J. Heyd, E. N. Brothers, K. N. Kudin, V. N. Staroverov, R. Kobayashi, J. Normand, K. Raghavachari, A. P. Rendell, J. C. Burant, S. S. Iyengar, J. Tomasi, M. Cossi, N. Rega, N. J. Millam, M. Klene, J. E. Knox, J. B. Cross, V. Bakken, C. Adamo, J. Jaramillo, R. Gomperts, R. E. Stratmann, O. Yazyev, A. J. Austin, R. Cammi, C. Pomelli, J. W. Ochterski, R. L. Martin, K. Morokuma, V. G. Zakrzewski, G. A. Voth, P. Salvador, J. J. Dannenberg, S. Dapprich, A. D. Daniels, Ö. Farkas, J. B. Foresman, J. V. Ortiz, J. Cioslowski and D. J. Fox, *Gaussian 09, Revision C.01*, Gaussian Inc., Wallingford, CT, USA, 2009.
60 O. Gunnarsson and B. I. Lundqvist, *Phys. Rev. B: Solid State*, 1976, **13**, 4274–4298.
61 W. Küchle, M. Dolg, H. Stoll and H. Preuss, *J. Chem. Phys.*, 1994, **100**, 7535–7542.
62 M. Dolg, H. Stoll and H. Preuss, *J. Chem. Phys.*, 1989, **90**, 1730.
63 D. Andrae, U. Häußermann, M. Dolg, H. Stoll and H. Preuss, *Theor. Chim. Acta*, 1990, **77**, 123–141.
64 P. C. Hariharan and J. A. Pople, *Theor. Chim. Acta*, 1973, **28**, 213–222.
65 J. P. Perdew, K. Burke and M. Ernzerhof, *Phys. Rev. Lett.*, 1996, **77**, 3865–3868.
66 C. Adamo and V. Barone, *J. Chem. Phys.*, 1999, **110**, 6158–6170.
67 E. Cancés, B. Mennucci and J. Tomasi, *J. Chem. Phys.*, 1997, **107**, 3032–3041.
68 B. Mennucci and J. Tomasi, *J. Chem. Phys.*, 1997, **106**, 5151–5158.
69 M. Cossi, N. Rega, G. Scalmani and V. Barone, *J. Comput. Chem.*, 2003, **24**, 669–681.
70 G. Scalmani and M. J. Frisch, *J. Chem. Phys.*, 2010, **132**, 114110.
71 E. Runge and E. K. U. Gross, *Phys. Rev. Lett.*, 1984, **52**, 997–1000.
72 N. M. O'Boyle, A. L. Tenderholt and K. M. Langner, *J. Comput. Chem.*, 2008, **29**, 839–845.
73 W. Herrendorf and W. Bärnighausen, *X-Area, Version 1.06*, Stoe, Darmstadt, 1999.
74 G. M. Sheldrick, *Program for Crystal Structure Solution and Refinement*, University of Göttingen, Germany, 1997.
75 G. M. Sheldrick, *Acta Crystallogr., Sect. A: Found. Crystallogr.*, 2008, **64**, 112–122.
76 G. M. Sheldrick, *Acta Crystallogr., Sect. A: Found. Crystallogr.*, 2008, **64**, 112–122.
77 O. V. Dolomanov, L. J. Bourhis, R. J. Gildea, J. A. K. Howard and H. Puschmann, *J. Appl. Crystallogr.*, 2009, **42**, 339–341.
78 A. L. Spek, *Acta Crystallogr., Sect. D: Biol. Crystallogr.*, 2009, **65**, 148–155.
79 C. F. Macrae, I. J. Bruno, J. A. Chisholm, P. R. Edgington, P. McCabe, E. Pidcock, L. Rodriguez-Monge, R. Taylor, J. van de Streek and P. A. Wood, *J. Appl. Crystallogr.*, 2008, **41**, 466–470.
80 H. Fischer and H. Orth, *Ann. Chem.*, 1933, **502**, 237–264.

# Supporting Information

## Directing Energy Transfer in Pt(bodipy)(mercaptopyrene) Dyads

*Peter Irmler,[†] Franciska S. Gogesch,[†] André Mang,[†] Michael Bodensteiner,[‡] Christopher B. Larsen,[§] Oliver S. Wenger,[§] and Rainer F. Winter*[,†]*

[†]Fachbereich Chemie, Universität Konstanz, Universitätsstraße 10, D-78457 Konstanz, Germany

[‡]Fakultät für Chemie und Pharmazie, Universität Regensburg, Universitätsstraße 31, D-93053 Regensburg, Germany

[§]Department of Chemistry, University of Basel, St.-Johanns-Ring 19, CH-4056 Basel, Switzerland.

# Table of Contents

## NMR-Spectra

### Brief Discussion of the Spectroscopic trends

The (pyrS)Pt($PEt_3$)$_2$ moiety of the dyad molecules acts as a net electron donor towards the respective BDP ligand. The $^{31}$P and $^{195}$Pt NMR data of Table 1 indicate that the coupling constant $J_{PtP}$ increases with an increasing electron-richness of the Pt-fragment, which is due to stronger back-bonding to the $PEt_3$ coligands. Such observations have been pivotal in elucidating the *cis*-effect of ligands in Pt(II) chemistry.[1] This sequence is, however, not reflected by the chemical shifts, which follow an inverse ordering for $^{195}$Pt and $^{31}$P NMR data with extreme positions for the mesityl (mesityl = 2,4,6-tripmethylphenyl) and krypto-BDP (KBDP) complexes. For **BPtSPyr** and **BPtSPyrSPtB**, the chemical shifts and coupling constants are very similar, which indicates that the pyrene-1,6-dithiolate ligand does not differ appreciably from mercaptopyrene in terms of net electron-donation to every individual Pt ion.

**Table S1.** $^{195}$Pt, $^{31}$P and $^{13}$C NMR Spectroscopic Data for the complexes

| | $\delta(^{195}Pt)$ / ppm | $\delta(^{31}P)$ / ppm | $J_{PtP}$ / Hz | $\delta(^{13}C)^a$ / ppm | $J_{PtC}$ / Hz |
|---|---|---|---|---|---|
| **MesPtSPyr**[b] | -4494 | 9.32 | 2734 | 144.8 | 864 |
| **KBPtSPyr** | -4249[c] | -4.90[c] | 2611[c] | 169.0[d] | n.o. |
| **BPtSPyrSPtB** | -4344[b] | 6.46[d] | 2491[b] / 2493[d] | 188.3[d] | n.o. |
| **BPtSPyr**[d] | -4378 | 6.84 | 2486 | 188.0 | 848 |
| **KBPtI**[b] | -4432 | -4.90 | 2583 | 161.7 | n.o. |
| **BPtI**[c] | -4503 | 4.02 | 2450 | 181.1 | n.o. |

[a]Chemical shift of the carbon atom attached to the platinum via a direct Pt-C σ-bond. Measured in [b]$CDCl_3$, [c]$C_6D_6$, or [d]THF-*d8* solution.

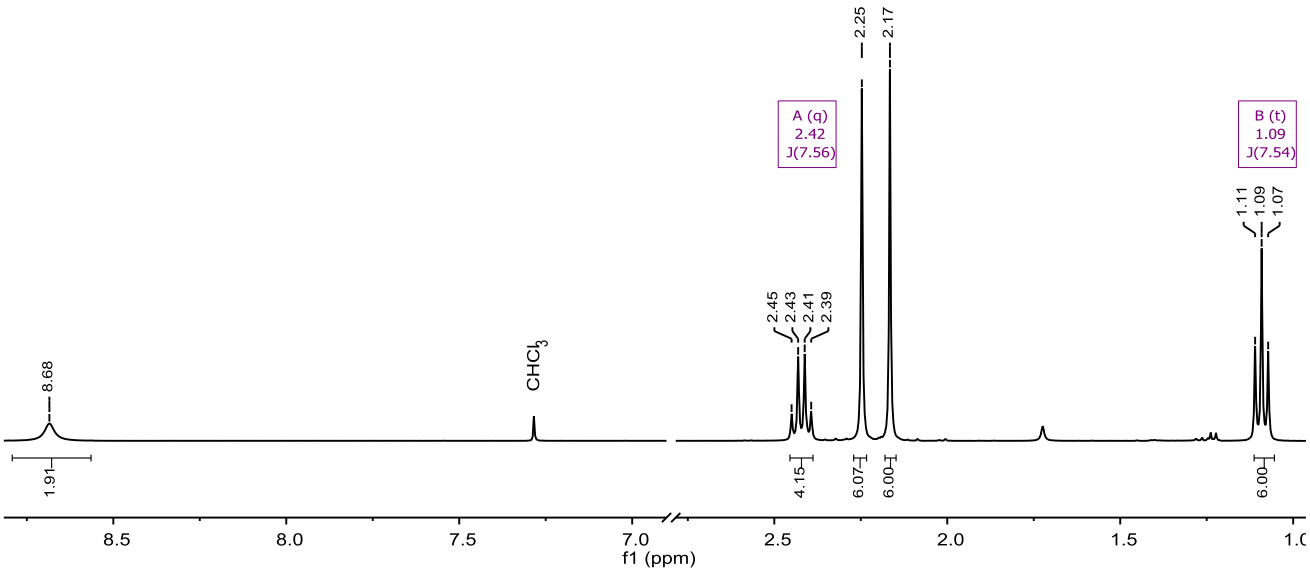


**Figure S1.** $^{1}$H NMR spectrum of bis-(4-ethyl-3,5-dimethyl-pyrrol-2-yl)-ketone in $CDCl_3$.

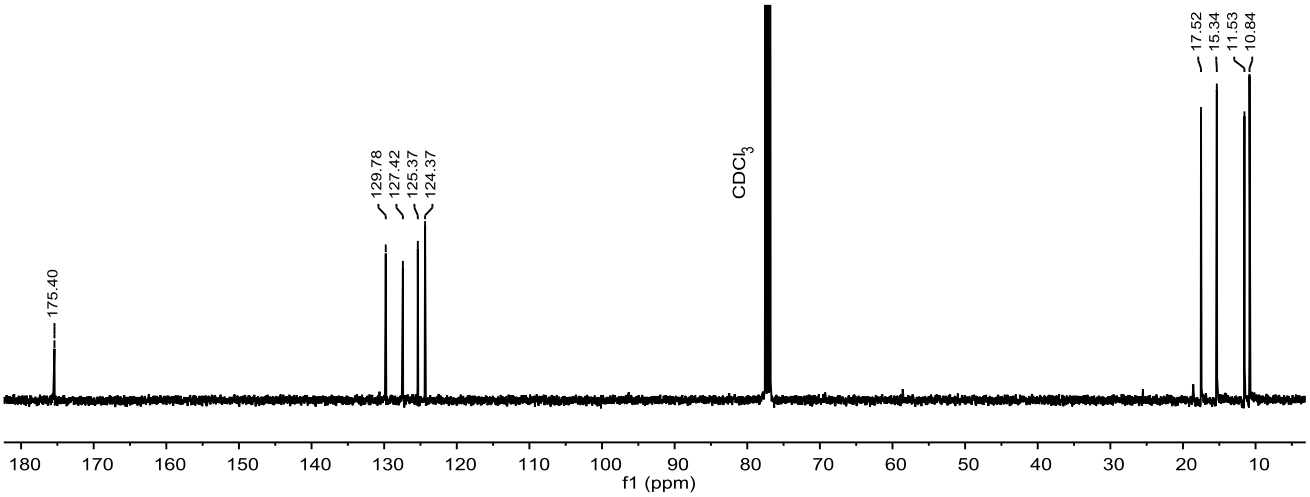


**Figure S2.** $^{13}$C {$^{1}$H} NMR spectrum of bis-(4-ethyl-3,5-dimethyl-pyrrol-2-yl)-ketone in $CDCl_3$.

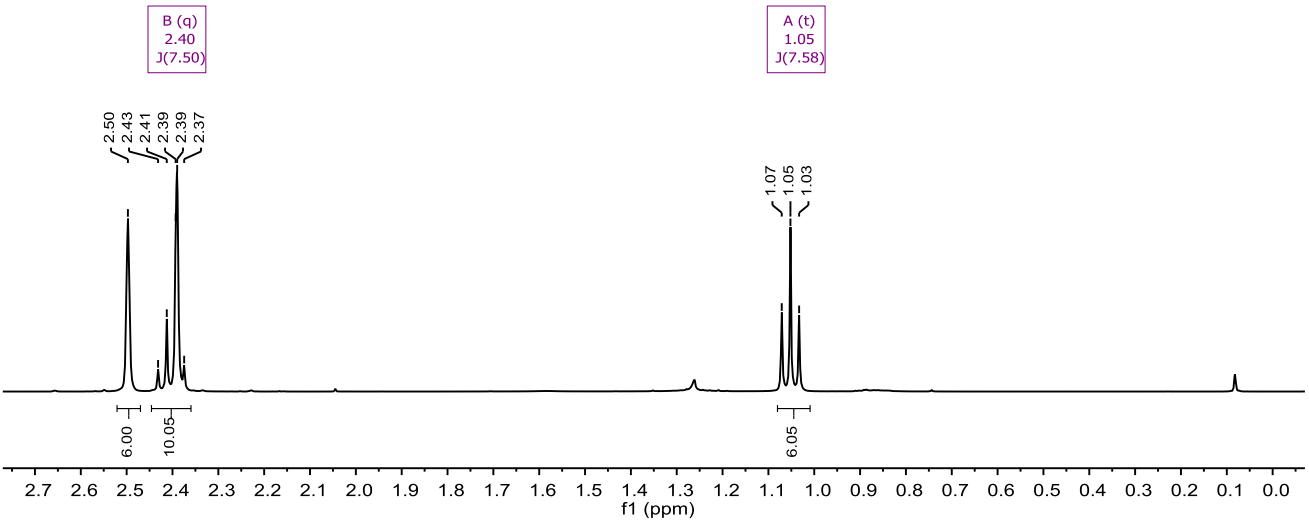


**Figure S3.** $^{1}$H NMR spectrum of 8-cloro-2,6-diethyl-1,3,5,7-tetramethyl-bodipy in $CDCl_3$.

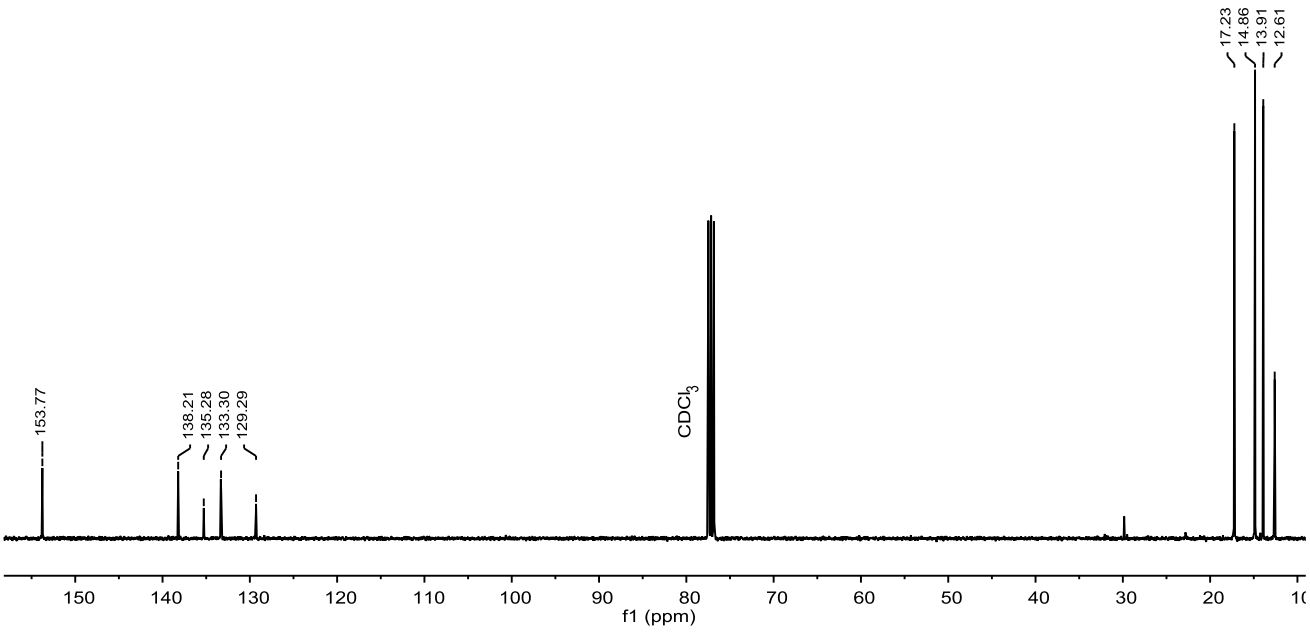


**Figure S4.** $^{13}$C {$^{1}$H} NMR spectrum of 8-cloro-2,6-diethyl-1,3,5,7-tetramethyl-bodipy in $CDCl_3$.

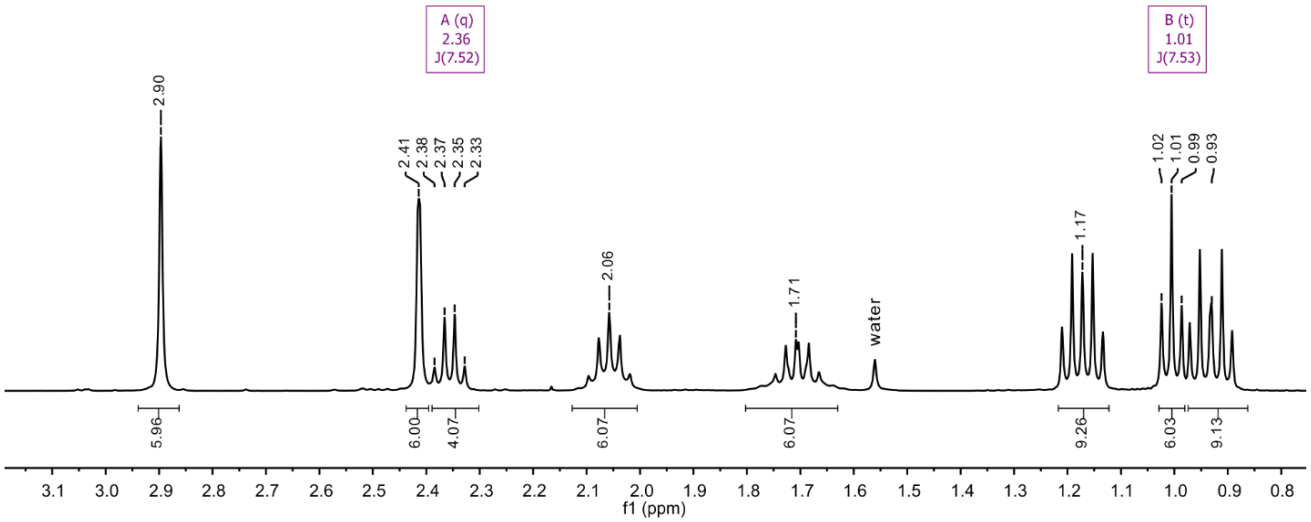


**Figure S5.** $^{1}$H NMR spectrum of ***cis*-KBPtCl** in $CDCl_3$.

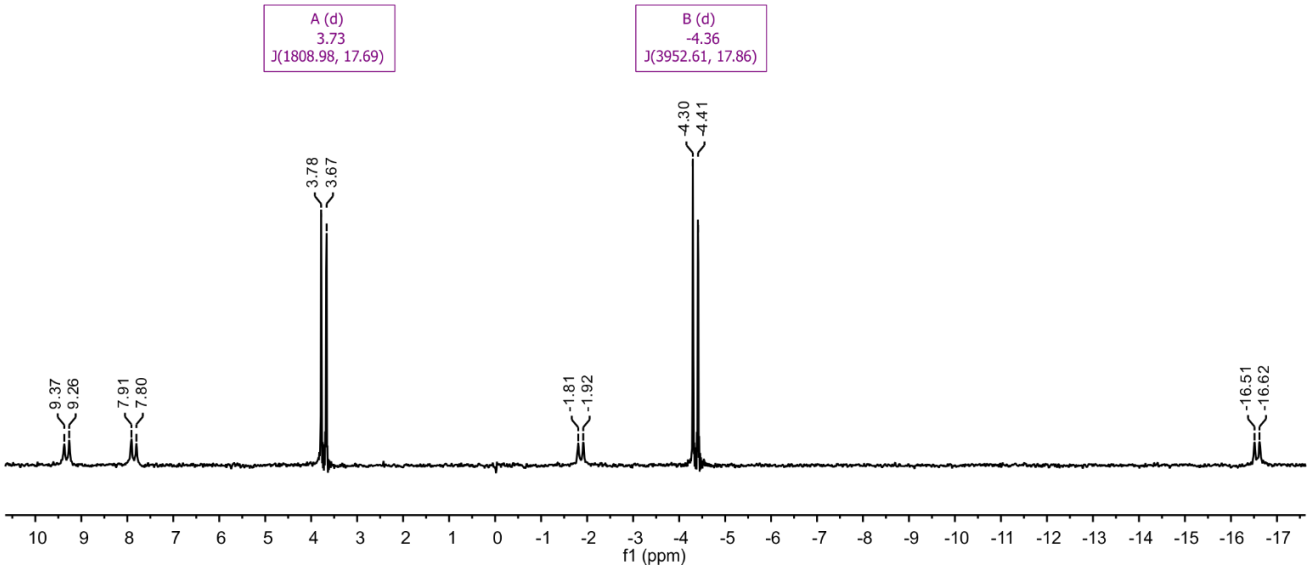


**Figure S6.** $^{31}P\{^{1}H\}$ NMR spectrum of ***cis*-KBPtCl** in $CDCl_3$.

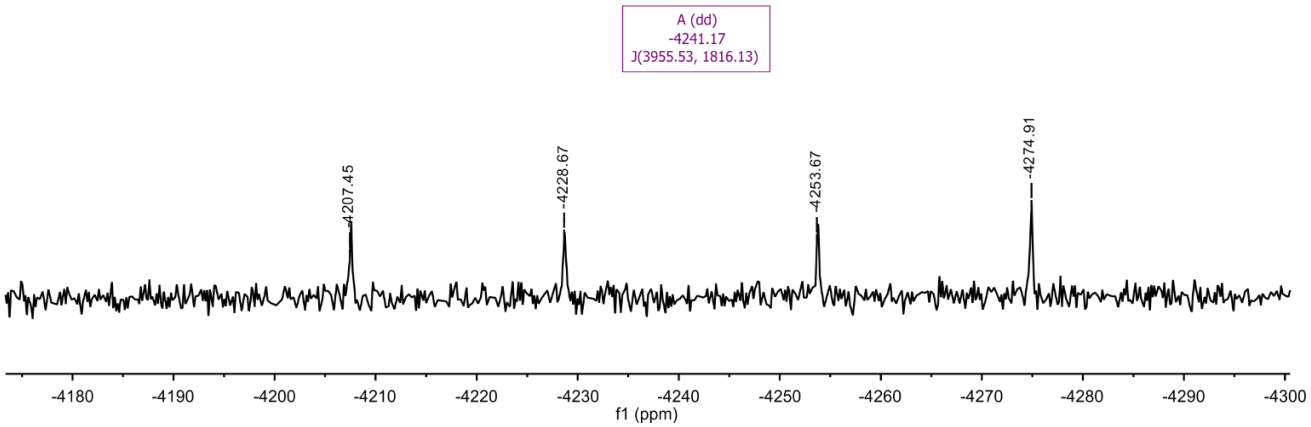


**Figure S7.** $^{195}Pt\{^{1}H\}$ NMR spectrum of ***cis*-KBPtCl** in $CDCl_3$.

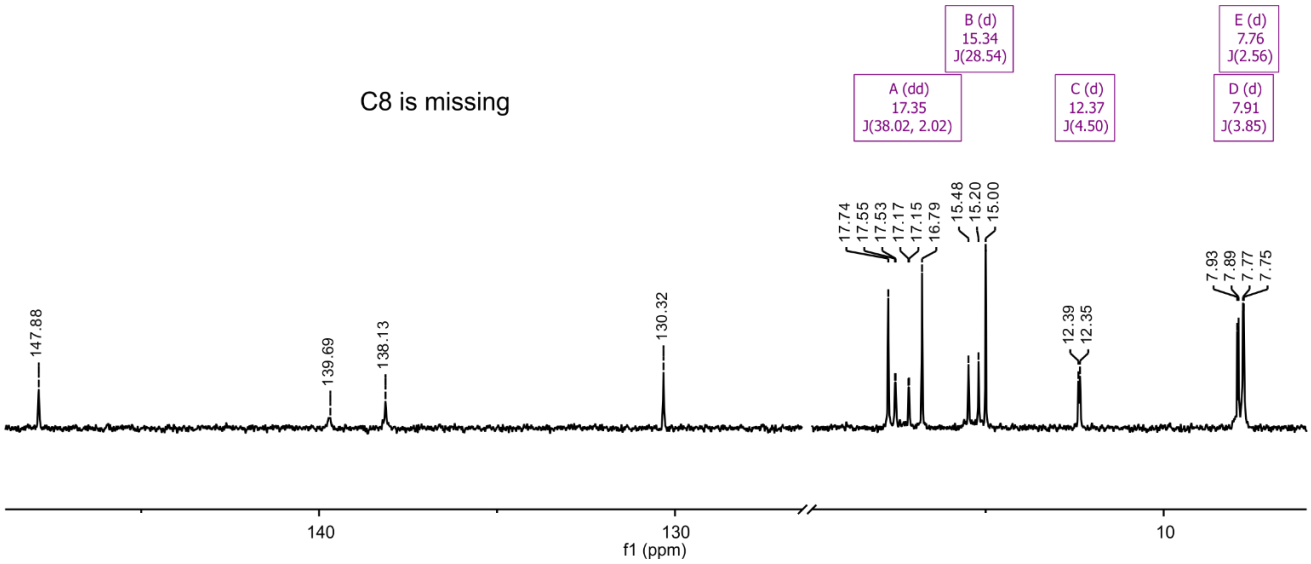


**Figure S8.** $^{13}C\{^{1}H\}$ NMR spectrum of ***cis*-KBPtCl** in $CDCl_3$.

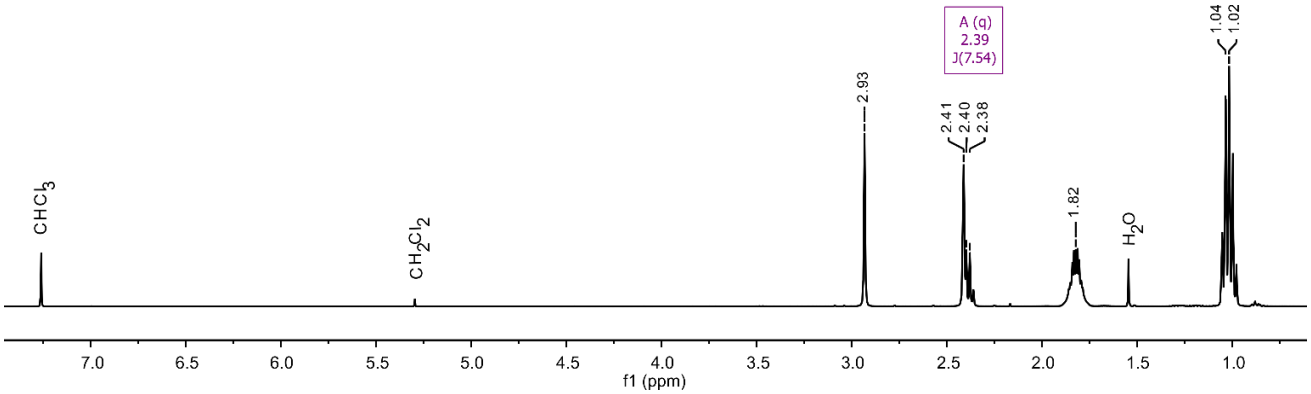


**Figure S9.** $^{1}$H NMR spectrum of **KBPtI** in $CDCl_3$.

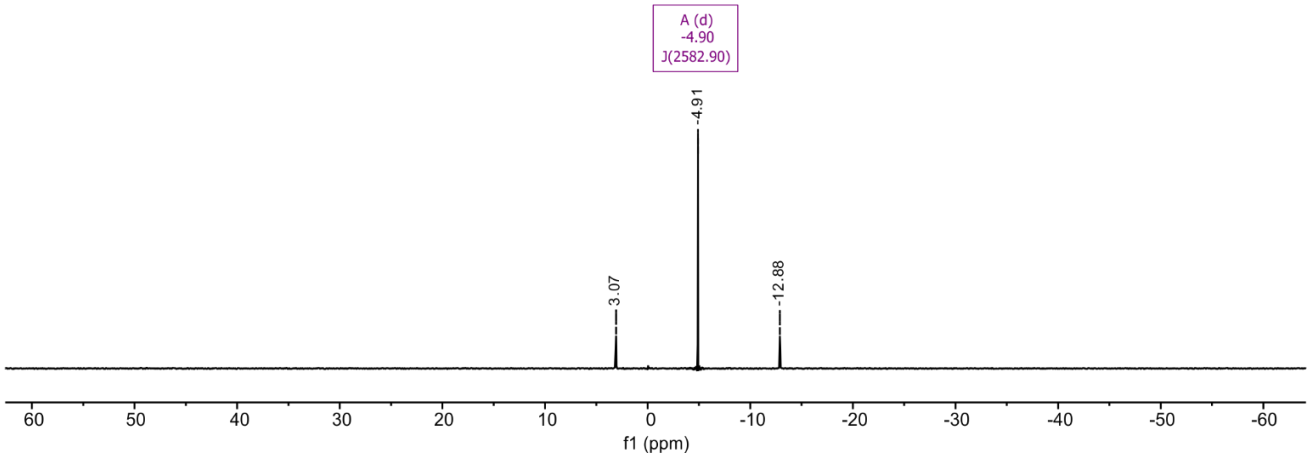


**Figure S10.** $^{31}P\{^{1}H\}$ NMR spectrum of **KBPtI** in $CDCl_3$.

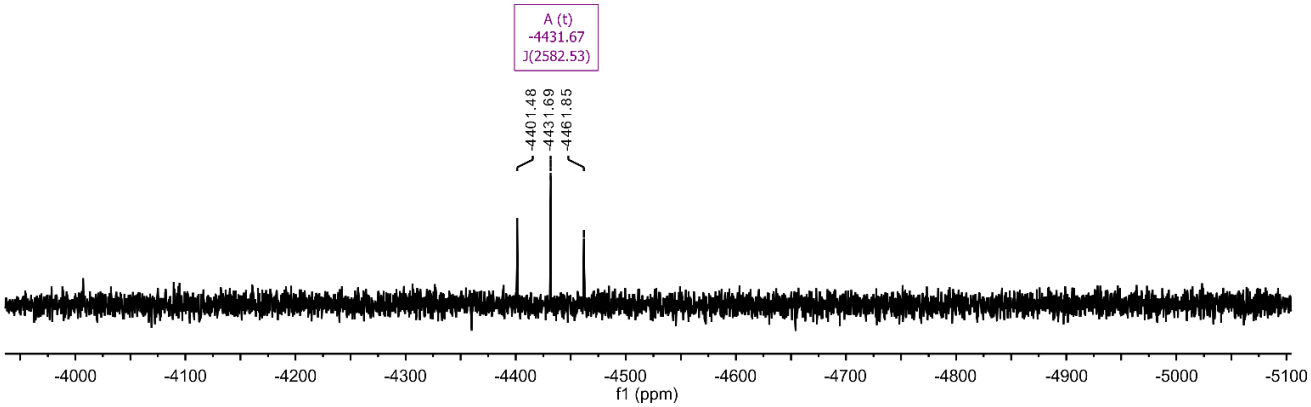


**Figure S11.** $^{195}Pt\{^{1}H\}$ NMR spectrum of **KBPtI** in $CDCl_3$.

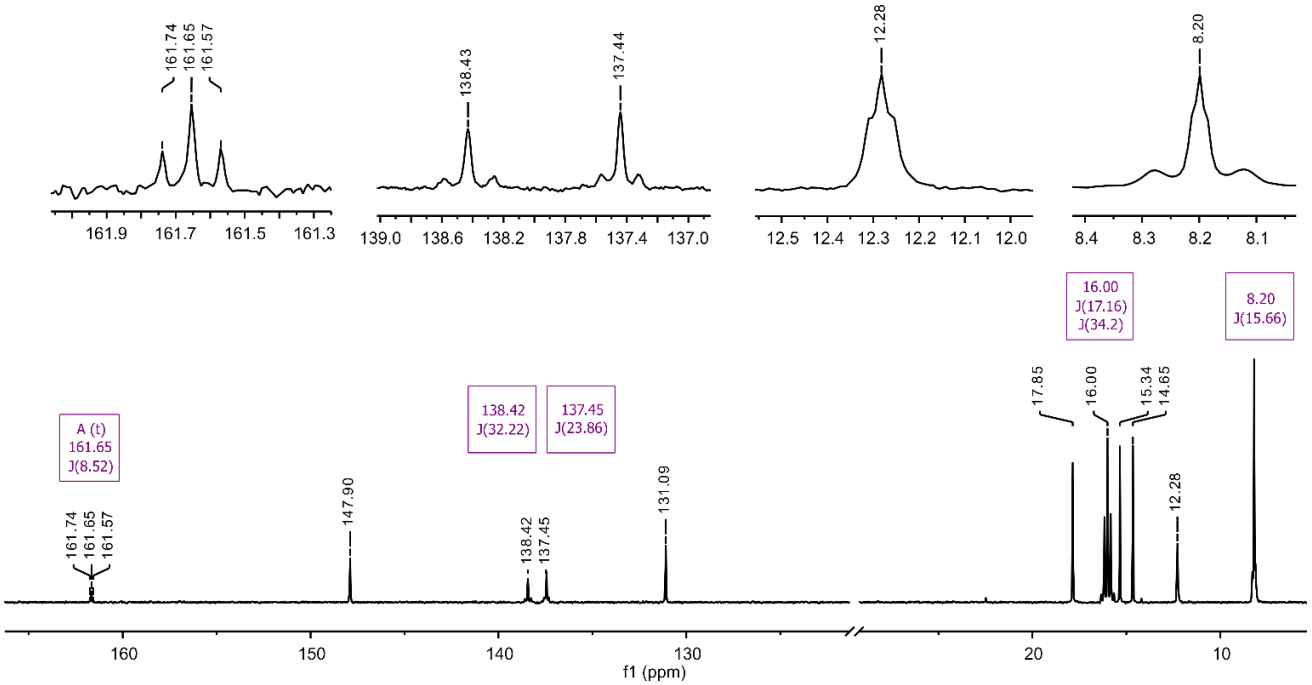


**Figure S12.** $^{13}C\{^{1}H\}$ NMR spectrum of **KBPtI** in $CDCl_3$.

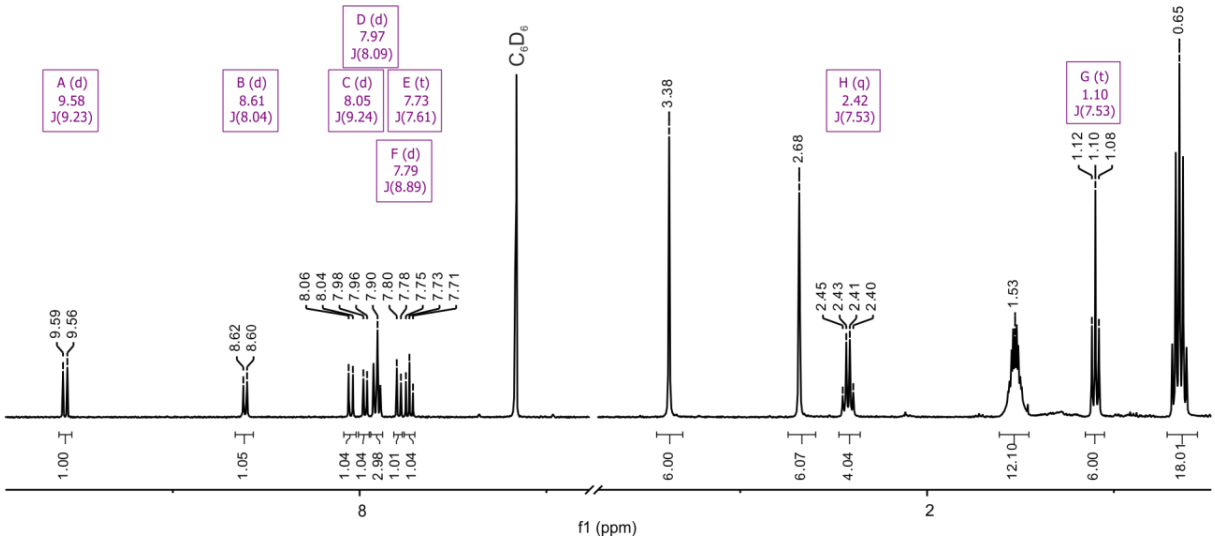


**Figure S13.** $^{1}H$ NMR spectrum of **KBPtSPyr** in $C_6D_6$.

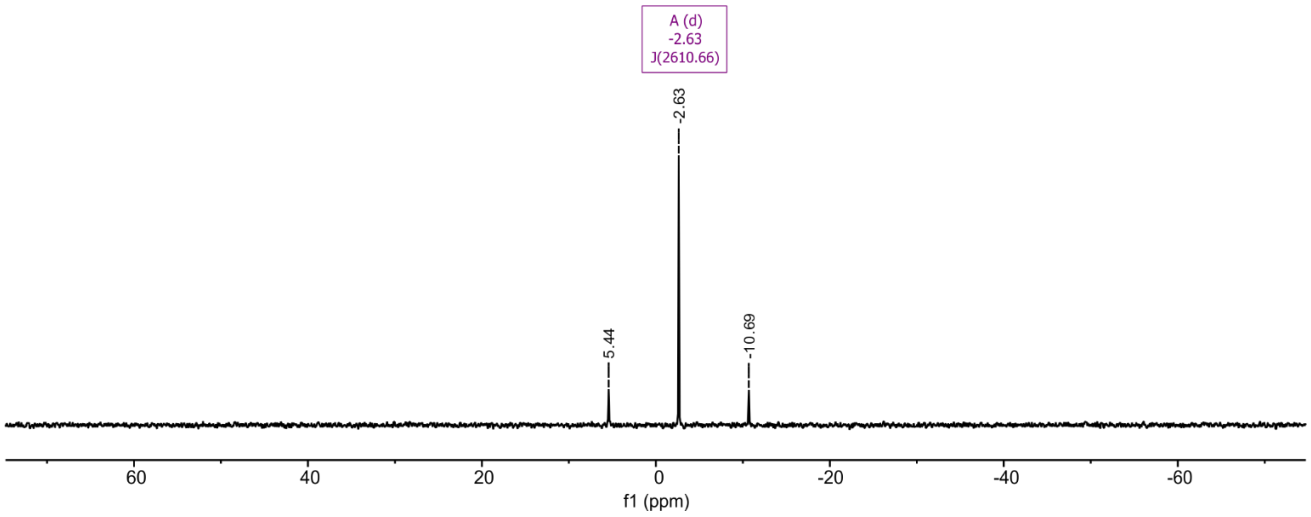


**Figure S14.** $^{31}P\{^{1}H\}$ NMR spectrum of **KBPtSPyr** in $C_6D_6$.

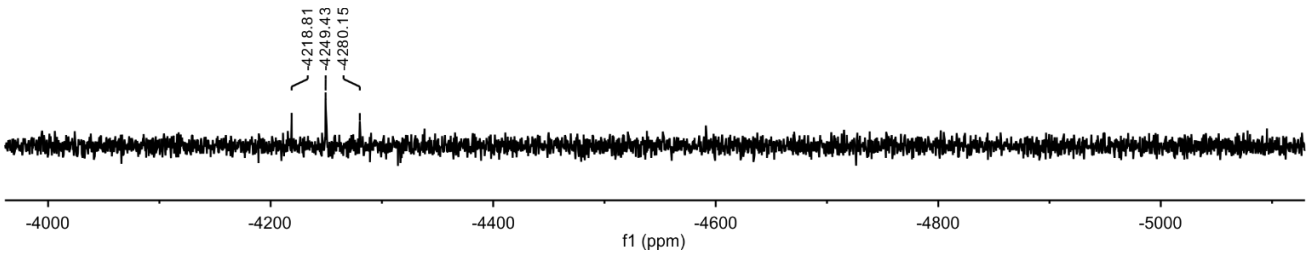


**Figure S15.** $^{195}Pt\{^{1}H\}$ NMR spectrum of **KBPtSPyr** in $C_6D_6$.

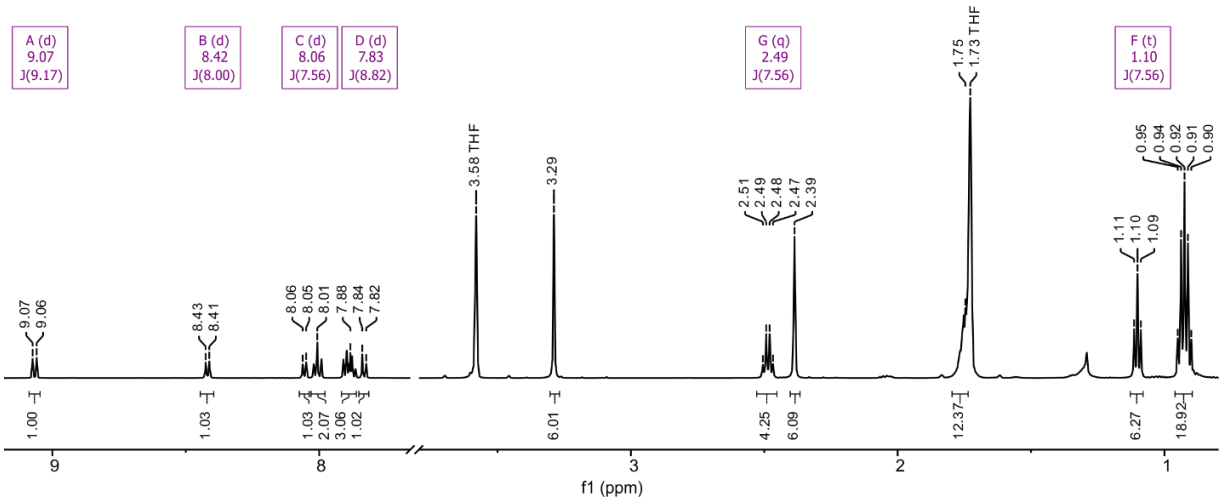


**Figure S16.** $^{1}H$ NMR spectrum of **KBPtSPyr** in THF-*d8*.

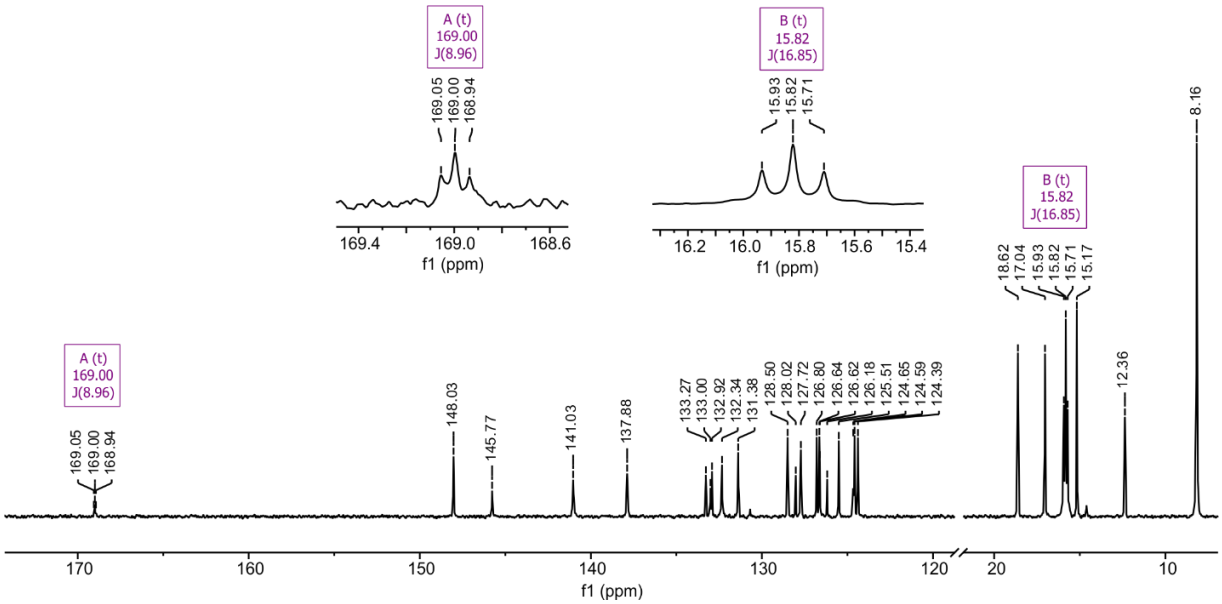


**Figure S17.** $^{13}C\{^{1}H\}$ NMR spectrum of **KBPtSPyr** in THF-*d8*.

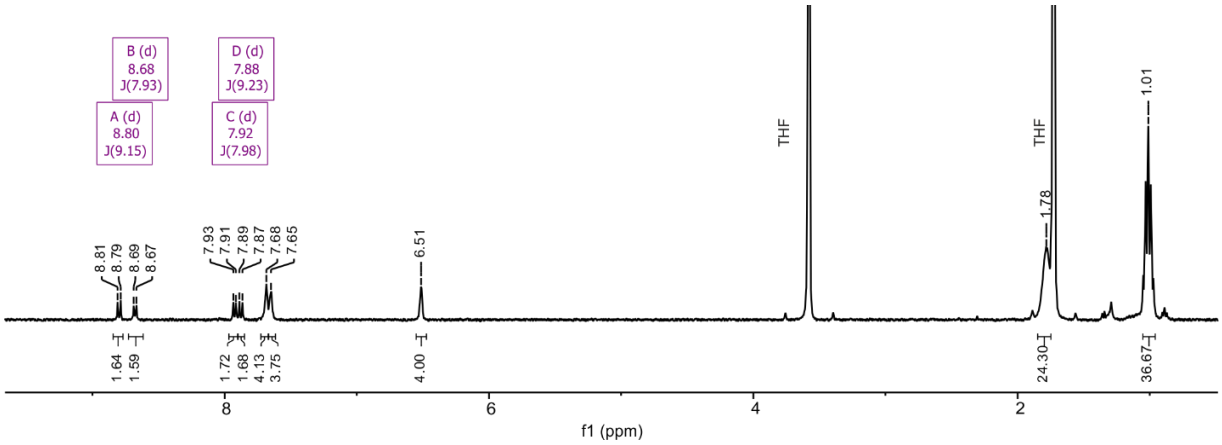


**Figure S18.** $^{1}H$ NMR spectrum of **BPtSPyrSPtB** in THF-*d8*.

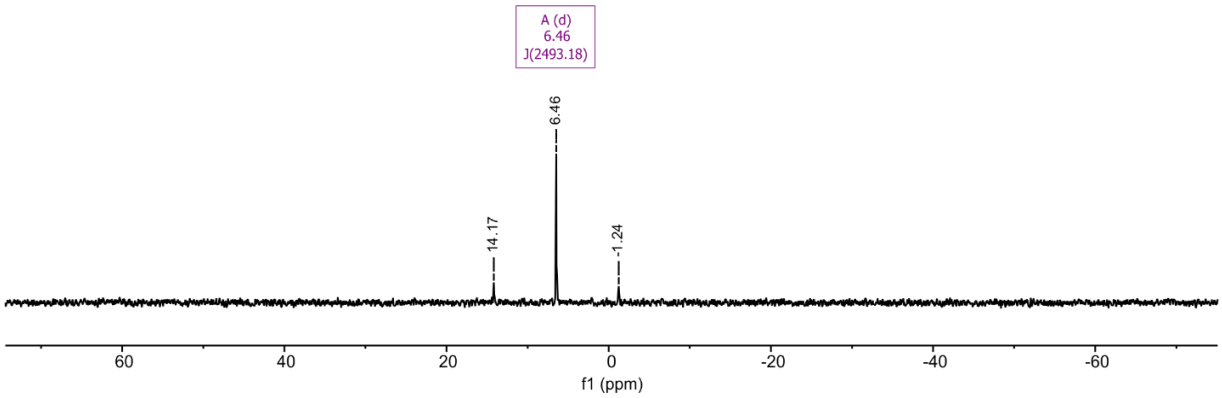


**Figure S19.** $^{31}P\{^{1}H\}$ NMR spectrum of **BPtSPyrSPyr** in THF-*d8*.

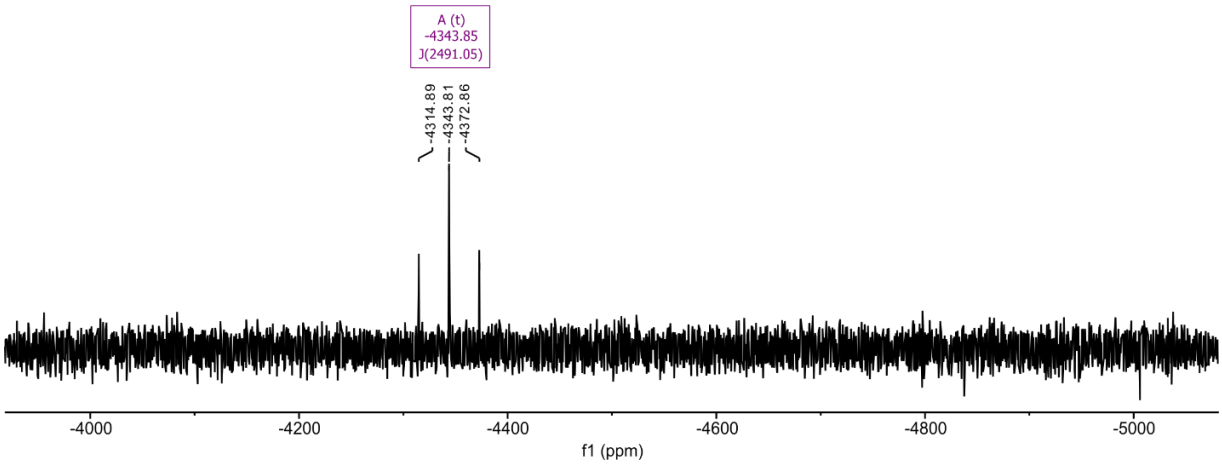


**Figure S20.** $^{195}Pt\{^{1}H\}$ NMR spectrum of **BPtSPyrSPyr** in THF-*d8*.

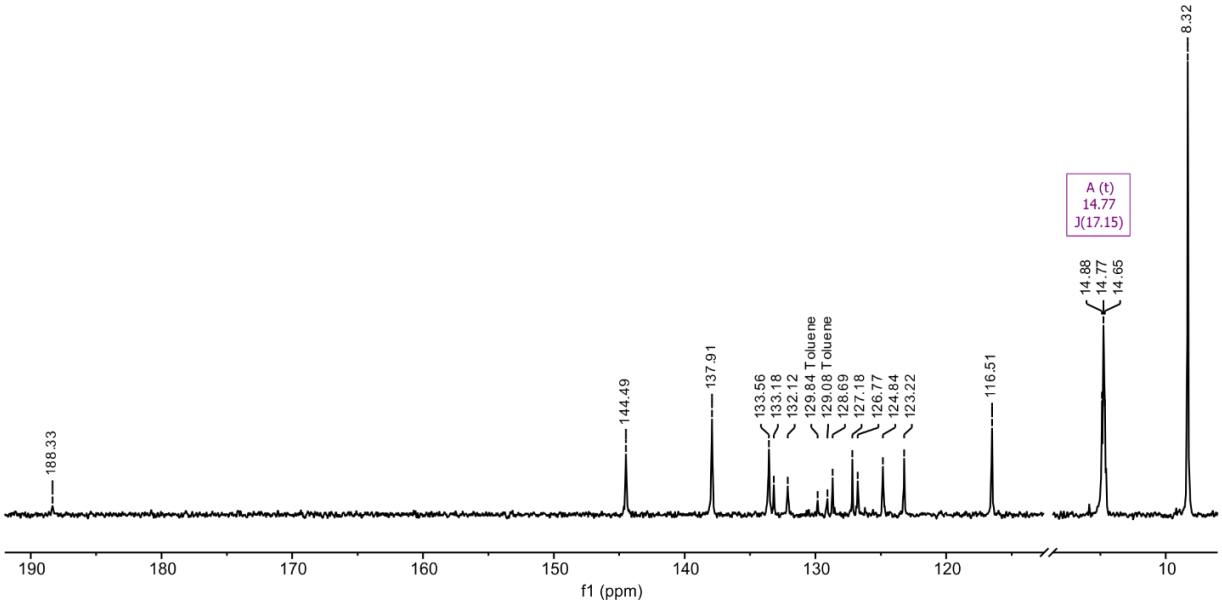


**Figure S21.** $^{13}C\{^{1}H\}$ NMR spectrum of **BPtSPyrSPyr** in THF-*d8*.

## Single Crystal X-Ray Diffraction

**Table S2.** Crystal and refinement data of **KBPtI** and **KBPtSPyr**.

| **Compound** | **KBPtI** | **KBPtSPyr** |
|---|---|---|
| Emp. formula / f. wt. (g/mol) | $C_{29}H_{52}BF_2IN_2P_2Pt$ / 861.46 | $C_{98.60}H_{142}B_2Cl_{3.20}F_4N_4P_4Pt_2S_2$ / 2172.59 |
| Temperature (K) | 100(2) | 100(2) |
| Wavelength (Å) | 0.71073 | 0.71073 |
| Crystal system | monoclinic | triclinic |
| Space group | $P\,2_1/n$ | $P\bar{1}$ |
| $a, b, c$ (Å) | 9.3246(5), 34.723(2), 10.3829(5) | 14.1734(9), 16.7856(12), 22.6728(15) |
| $\alpha, \beta, \gamma$ (°) | 90, 92.701(4), 90 | 78.562(5), 88.157(5), 74.328(5) |
| $V$ (Å$^3$) | 3358.0(3) | 5089.1(6) |
| $Z$ | 4 | 2 |
| $D_{calcd}$ (Mg/m$^3$) | 1.704 | 1.418 |
| Absorption coefficient (mm$^{-1}$) | 5.225 | 2.987 |
| θ range of data collection | 2.049 to 27.200° | 1.73 to 27.98° |
| Limiting Indices | $-11 \le h \le 11$, $-44 \le k \le 44$, $-13 \le l \le 13$ | $-15 \le h \le 17$, $-19 \le k \le 20$, $-27 \le l \le 27$ |
| Reflections collected / unique (> 2σ(I)) | 52908 / 7480 [R(int) = 0.1765] | 19048 / 13599 [R(int) = 0.0889] |
| Data / Restraints / Parameter | 7480 / 0 / 355 | 19048 / 668 / 1296 |
| R (I>2σ(I)) | $R_1$ = 0.0448, $\omega R_2$ = 0.1126 | $R_1$ = 0.0576, $\omega R_2$ = 0.1401 |
| $R_W$ (all data) | $R_1$ = 0.0496, $\omega R_2$ = 0.1153 | $R_1$ = 0.0870, $\omega R_2$ = 0.1505 |
| GooF (all data) | 1.005 | 1.052 |
| Max. and min. res. dens. (eA$^{-3}$) | 2.574 and -2.783 | 1.640 and -1.747 |

**Table S3.** Selected Bond Lengths [Å] and Angles [deg] for Complexes **KBPtI**, **KBPtSPyr**, and **BPtI**.

| bond parameters | **KBPtI** | **KBPtSPyr**[a] | **BPtI** |
|---|---|---|---|
| Pt1-C8 | 2.019(4) | 2.046(8) / 2.057(8) | 1.994(10) |
| Pt1-P1 | 2.3281(12) | 2.332(2) / 2.308(2) | 2.3206(15) |
| Pt1-P2 | 2.3300(12) | 2.333(2) / 2.344(2) | 2.3206(15) |
| Pt1-I1 / Pt1-S1 | 2.6914(4) | 2.389(2) / 2.385(2) | 2.6689(9) |
| C8-Pt1-P1 | 89.40(13) | 90.5(3) / 91.7(3) | 91.37(7) |
| C8-Pt1-P2 | 87.79(13) | 86.8(3) / 87.8(3) | 91.37(7)[b] |
| P1-Pt1-I1/S1 | 90.86(3) | 93.23(8) / | 88.71(7) |
| P2-Pt1-I1/S1 | 91.98(3) | 89.23(8) / | 88.71(7)[b] |
| P1-Pt1-P2 | 176.94(4) | 176.91(8) / | 176.8(3) |
| C8-Pt1-I1/S1 | 179.66(14) | 172.7(3)/167.9(3) | 176.03(8) |
| [Pyr]-[BDP][b] | n. a. | 19.7 / 18.2 | n. a. |
| [Pt]-[BDP][b] | 87.0 | 88.8 / 88.8 | 90.0 |
| [Pt]-[Pyr][b] | n. a. | 70.0 / 73.2 | n. a. |

[a]Bond parameters for the two independent molecules in the unit cell. [b]Interplanar angle between planes defined by the central six-membered ring of the BDP unit and the carbon atoms C19-C24 of the pyrene ring, or the coordination plane of the platinum ion, respectively.

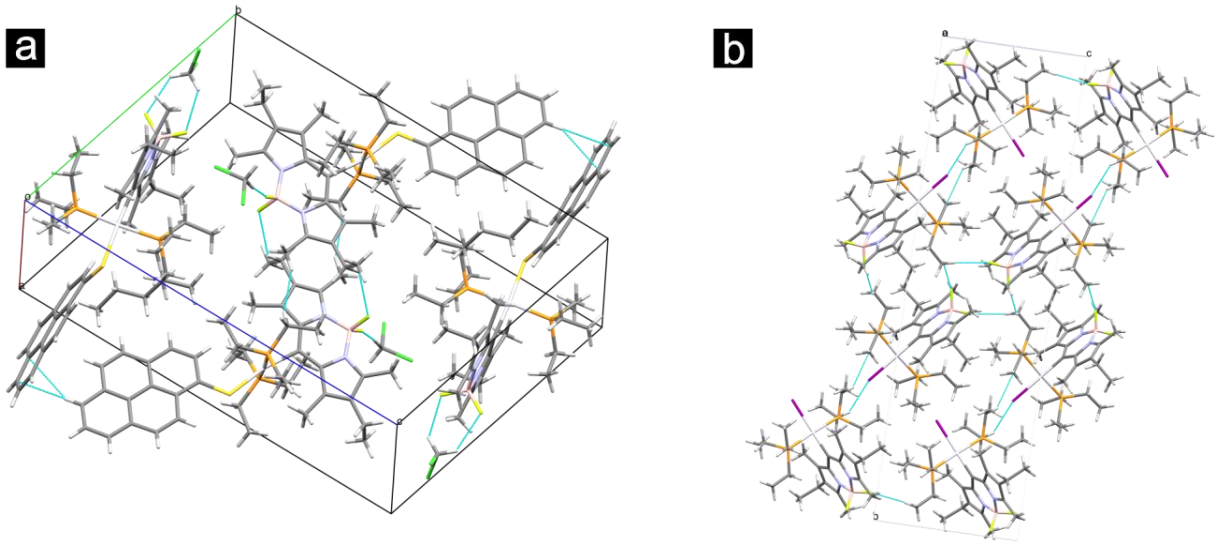


**Figure S22.** Packing in the crystal lattice of a) **KBPtSPyr** and b) **KBPtI**.

In the crystal lattice of complex **KBPtSPyr**, pairs of the crystallographically unique molecules pack in a centrosymmetric fashion. Molecules of type 1 form two strong hydrogen bonds of 2.423 Å and 2.431 Å with the two hydrogen atoms of a $CH_2Cl_2$ solvent molecule, while molecules of type 2 engage in an even stronger hydrogen bond of 2.223 Å to one H atom of another $CH_2Cl_2$ solvent molecule and a weaker contact of 2.618 Å to an ethyl proton of the KBDP ligand of its immediate neighbour (see Figure S22 of the Supporting Information). Molecules 1 and 2 are interconnected by CH···π hydrogen bonds between atoms C27/C28 and H77 of their pyrene substituents, which are disposed at an interplanar angle of 62.7°, as well as CH···π contacts of 2.729 and 2.770 Å to a methylene or a methyl proton of the $PEt_3$ ligands.

## Quantum Chemical Calculations

**Table S4. Calculated Mulliken parameters of BPtSPyr. Fragment contributions are given in percent.**

| Orbital | Pt | $PEt_3$ | bodipy | mercaptopyrene |
|---|---|---|---|---|
| LUMO+1 | 1 | 0 | 0 | 99 |
| LUMO | 4 | 2 | 94 | 0 |
| HOMO | 3 | 2 | 1 | 94 |
| HOMO-1 | 1 | 1 | 98 | 0 |

**Table S5. Calculated Mulliken parameters of BPtSPyrSPtB. Fragment contributions are given in percent.**

| Orbital | bodipy(1) | Pt(1) | $PEt_3$(1) | SpyrS | $PEt_3$(2) | Pt(2) | bodipy(2) |
|---|---|---|---|---|---|---|---|
| LUMO+2 | 0 | 1 | 0 | 96 | 0 | 1 | 0 |
| LUMO+1 | 47 | 2 | 1 | 0 | 1 | 2 | 47 |
| LUMO | 47 | 2 | 1 | 1 | 1 | 2 | 47 |
| HOMO | 0 | 2 | 1 | 94 | 1 | 2 | 0 |
| HOMO-1 | 1 | 3 | 3 | 87 | 3 | 3 | 1 |
| HOMO-2 | 50 | 1 | 1 | 0 | 1 | 1 | 48 |
| HOMO-3 | 48 | 1 | 1 | 0 | 1 | 1 | 50 |

**Table S6. Calculated Mulliken parameters of KBPtSPyr. Fragment contributions are given in percent.**

| Orbital | Pt | $PEt_3$ | bodipy | mercaptopyrene |
|---|---|---|---|---|
| LUMO+1 | 1 | 0 | 0 | 98 |
| LUMO | 3 | 2 | 95 | 0 |
| HOMO | 4 | 2 | 1 | 94 |
| HOMO-1 | 0 | 0 | 0 | 99 |

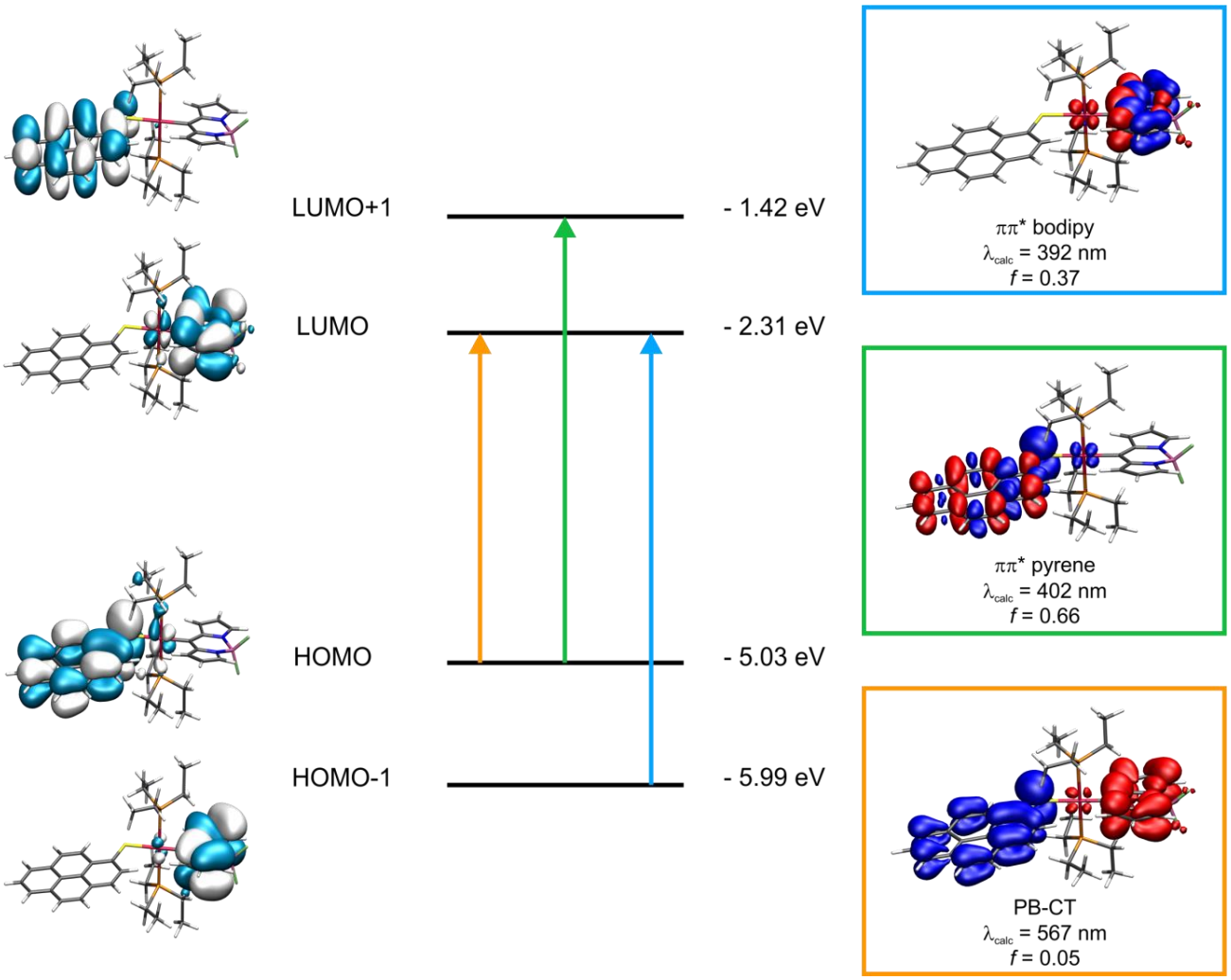


**Figure S23**. Graphical representation of the relevant MOs and TD-DFT energies of **BPtSPyr** as well as electron density difference maps (*blue* = electron density loss, *red* = electron density gain).

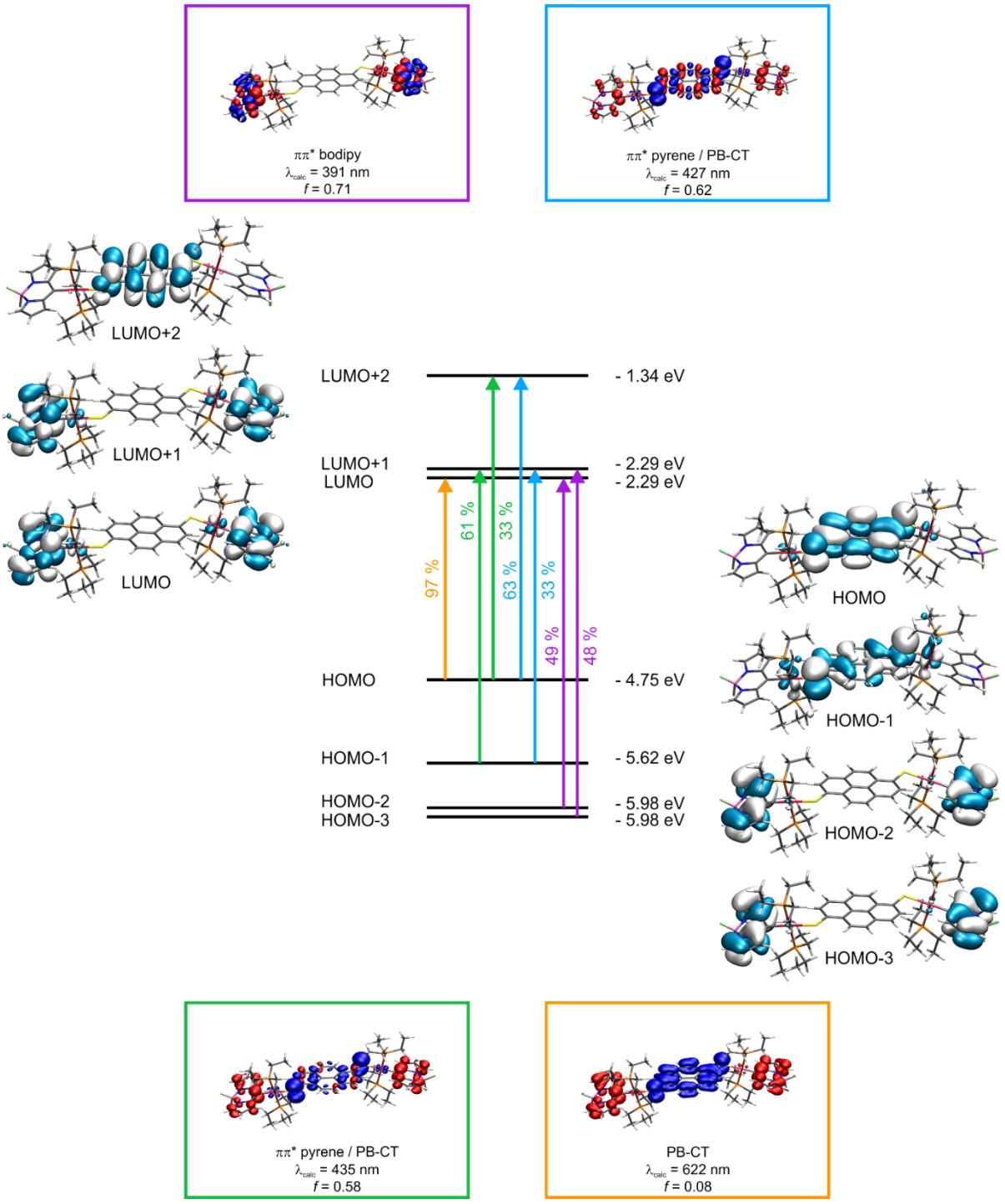


**Figure S24**. Graphical representation of the relevant MOs and TD-DFT energies of **BPtSPyrSPtB** as well as electron density difference maps (*blue* = electron density loss, *red* = electron density gain).

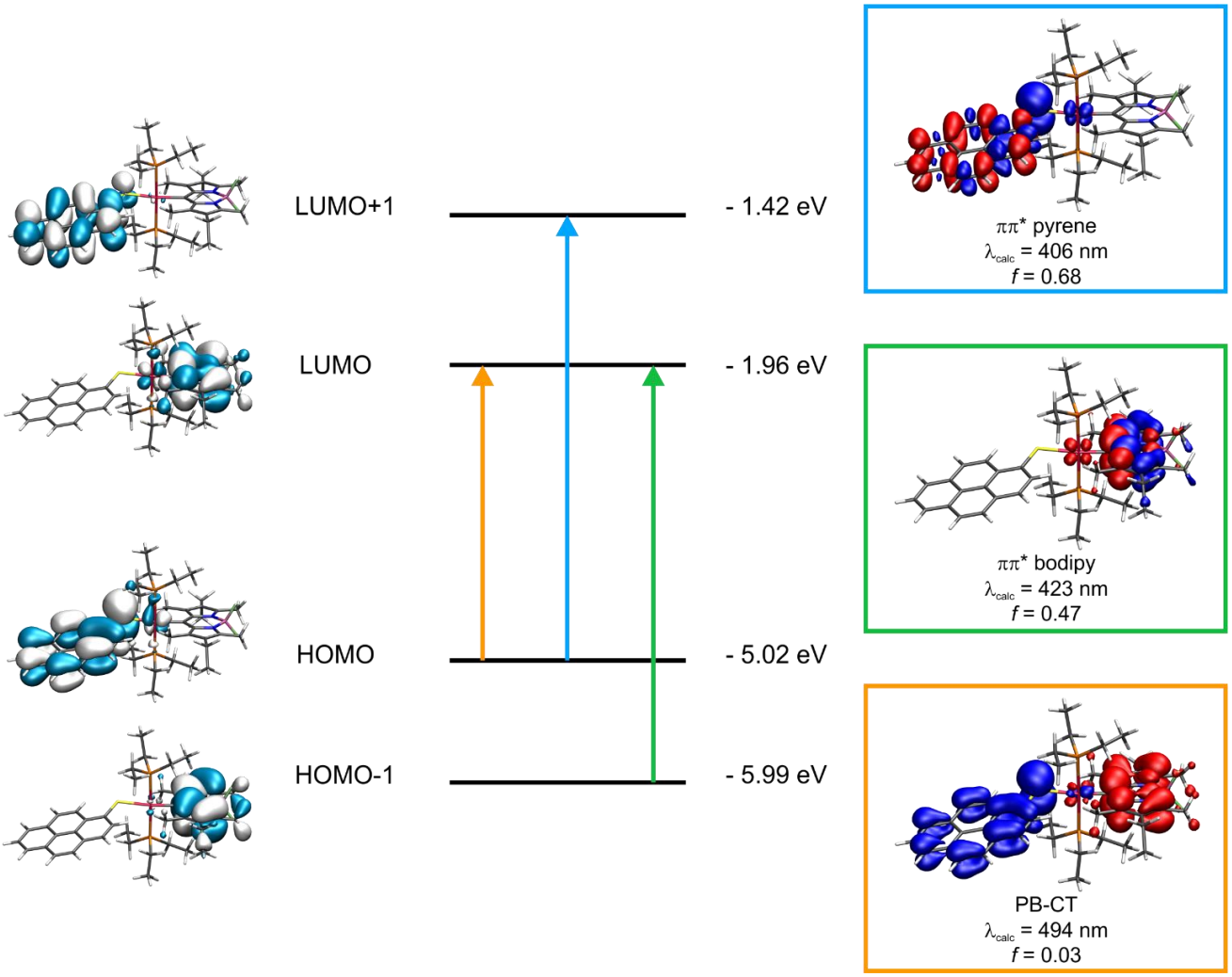


**Figure S25.** Graphical representation of the relevant MOs and TD-DFT energies of **KBPtSPyr** as well as electron density difference maps (blue = electron density loss, red = electron density gain).

**Table S7. Calculated Mulliken parameters of the BPtSPyr radical cation. Fragment contributions are given in percent.**

| Orbital | Pt | $PEt_3$ | bodipy | mercaptopyrene |
|---|---|---|---|---|
| LUSO+1(β) | 3 | 2 | 93 | 2 |
| LUSO+1(α) | 2 | 1 | 31 | 66 |
| LUSO(β) | 2 | 2 | 1 | 95 |
| LUSO(α) | 1 | 2 | 63 | 34 |
| HOSO(α) | 1 | 1 | 93 | 5 |
| HOSO(β) | 1 | 1 | 98 | 0 |
| HOSO-1(α) | 2 | 2 | 5 | 90 |
| HOSO-1(β) | 6 | 6 | 1 | 87 |
| HOSO-8(β) | 1 | 0 | 0 | 99 |

**Table S8. Calculated Mulliken parameters of BPtSPyr radical anion. Fragment contributions are given in percent.**

| Orbital | Pt | $PEt_3$ | bodipy | mercaptopyrene |
|---|---|---|---|---|
| LUSO+11(α) | 9 | 14 | 77 | 0 |
| LUSO+1(β) | 4 | 3 | 92 | 1 |
| LUSO(β) | 1 | 0 | 0 | 99 |
| LUSO(α) | 1 | 0 | 0 | 99 |
| HOSO(α) | 3 | 2 | 94 | 0 |
| HOSO(β) | 4 | 3 | 2 | 91 |
| HOSO-1(α) | 4 | 3 | 1 | 92 |
| HOSO-1(β) | 1 | 1 | 96 | 1 |

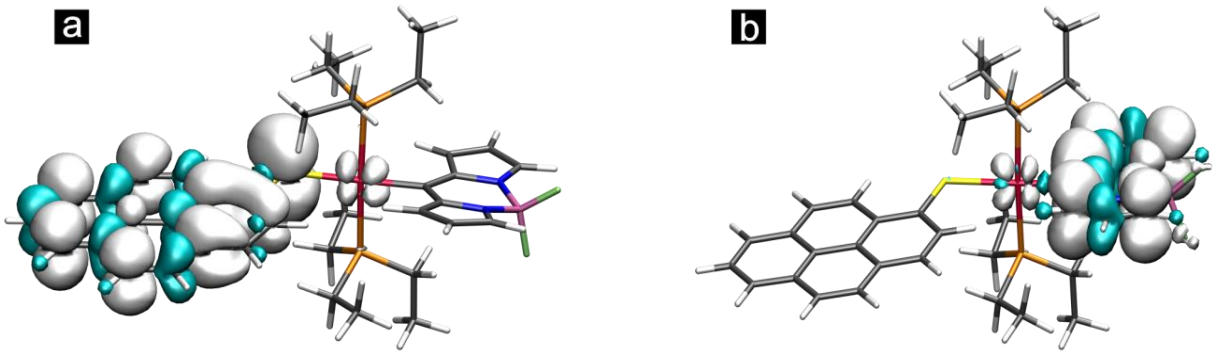


**Figure S26.** Calculated spin densities of the a) radical cation and b) the radical anion of **BPtSPyr**.

**Table S9. Calculated spin density contributions of the respective fragments to the spin density surfaces of the radical cation and anion of BPtSPyr.**

| Oxidation State | cation | anion |
|---|---|---|
| Pt | -0.004 | -0.002 |
| $PEt_3$ | 0.023 | 0.017 |
| bodipy | -0.004 | 0.990 |
| mercaptopyrene | 0.984 | -0.006 |

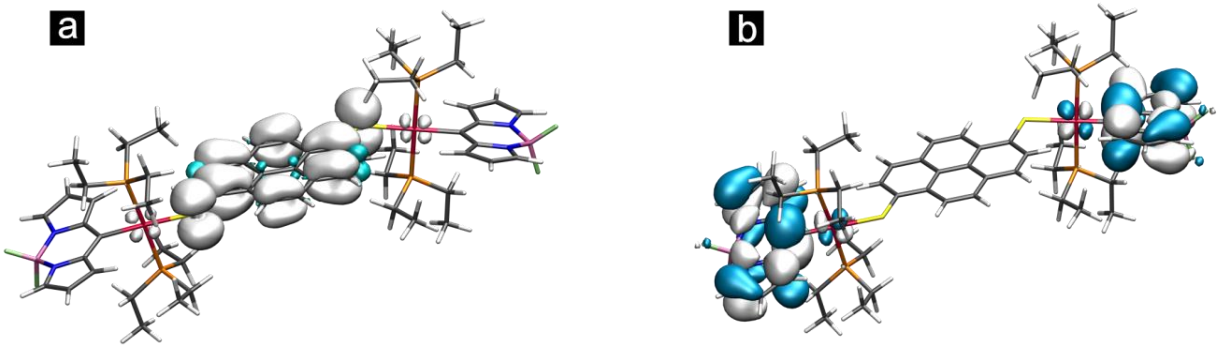


**Figure S27.** a) Calculated spin density of the radical cation and b) the HOMO of the two electron reduced form (open shell singlet) of **BPtSPyrSPtB**.

**Table S10. Calculated spin density contributions of the respective fragments to the spin density surfaces of the radical cation of BPtSPyrSPtB.**

| Oxidation state | bodipy(1) | Pt(1) | $PEt_3$(1) | mercaptopyrene | $PEt_3$(2) | Pt(2) | bodipy(2) |
|---|---|---|---|---|---|---|---|
| cation | -0.001 | -0.001 | 0.001 | 0.983 | 0.001 | -0.001 | -0.001 |

**Table S11. Calculated spin density contributions of the respective fragments to the spin density surfaces of the radical cation and anion of KBPtSPyr.**

| Oxidation state | bodipy | Pt | $PEt_3$ | mercaptopyrene |
|---|---|---|---|---|
| cation | -0.002 | -0.009 | 0.020 | 0.973 |
| anion | 1.000 | -0.010 | 0.012 | -0.005 |

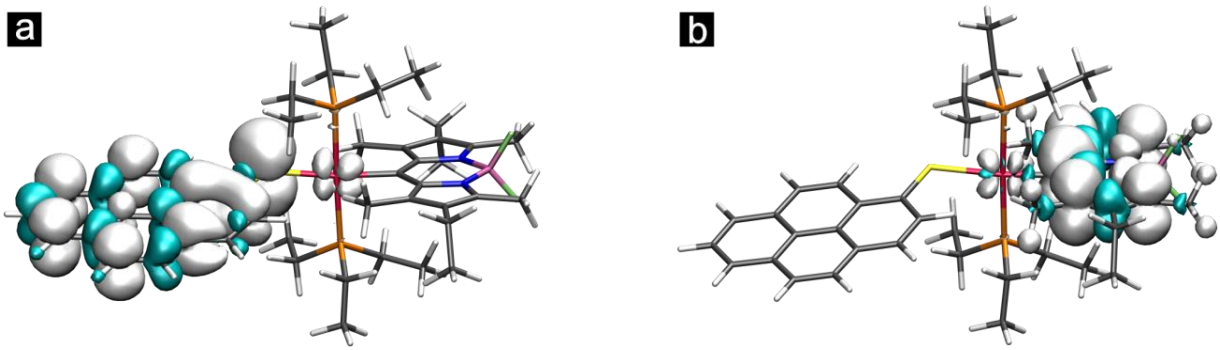


**Figure S28**. Calculated spin densities of a) the radical cation and b) the radical anion of **KBPtSPyr**.

## Electrochemistry

Cyclic voltammograms of all complexes were recorded in the THF /0.1 M $NBu_4PF_6$ supporting electrolyte. Under these conditions, all BDP or KBDP containing complexes display a chemically (partially) reversible oxidation, while all complexes with a terminal mercaptopyrene or a bridging pyrene-1,6-dithiolate ligand offer a reversible oxidation. Owing to the lack of a mercaptopyrene donor ligand and the placement of the platinum complex entity outside the π-conjugated cyanine core of the bodipy ligand (note that the HOMO of a bodipy has a nodal plane at the meso position), iodo precursors **BPtI** and **KBPtI** do not exhibit any voltammetric oxidation wave within the accessible potential window of the THF/$NBu_4PF_6$ supporting electrolyte. BDP peralkylation has, however, the expected effect on the reduction potential as demonstrated by the cathodic shift of 370 mV between **BPtI** and **KBPtI** (see Table 4). Replacement of the iodo by the mercaptopyrene ligand leaves the potential for the BDP-centred reduction nearly unaltered (Table 4), but adds the reversible oxidation wave of the pyrS ligand to the voltammograms. The half-wave potential of this wave follows the electron richness of the (σ-aryl)$Pt(PEt_3)_2$ entity and decreases in the order **BPtSPyr** > **KBPtSPyr** > **MesPtSPyr** > **BPtSPyrSPtB** in excellent match with the positioning of the pyrene-based $^1\pi\pi^*$ absorption band. Representative voltammograms of all complexes are compiled in Figures S50 to S54 of the Supporting Information. Worthy of note and reassuring our above assignment is that the peak current of the reductive wave in the dinuclear complex **BPtSPyrSPtB** is twice that of the anodic oxidation. The computed HOMO of the corresponding dianion is consequently localized on the two bodipy ligands without any contributions of the bridging pyrene-1,6-dithiolate ligand.

As a consequence of the only minor, inductive influence of BDP peralkylation on the half-wave potential of the oxidation and a considerably larger effect on that for the BDP-centred reduction,

the half-wave potential difference $\Delta E_{1/2}$ for these processes increases by almost 300 mV (Table 4). This explains the large blue-shift of the CT absorption band and renders formation of the charge separated, excited state for **KBPtSPyr** energetically less favorable.

**Table S12.** Electrochemical Data for **BPtI**, **KBPtI**, **MesPtSPyr**, **BPtSPyr**, **KBPtSPyr**, and **BPtSPyrSPtB**[a]

| complex | $E_{1/2}$ / mV (anodic sweep) | $E_{1/2}$ / mV (cathodic sweep) | $\Delta E_{1/2}$ / mV |
|---|---|---|---|
| **BPtI** | - | -1930 | |
| **KBPtI** | - | -2300 | |
| **MesPtSPyr** | 30 | | |
| **BPtSPy**[b] | 180 | -1970 | 2150 |
| **KBPtSPyr** | 130 | -2310 | 2440 |
| **BPtSPyrSPtB** | -60 | -1980 | 1920 |

[a]All potentials are referenced to the $Cp_2Fe^{0/+}$ couple ($E_{1/2}$ =0.000 V) and were measured in THF at 293 K with $NBu_4PF_6$ as the supporting electrolyte. [b]Data from ref. 2.

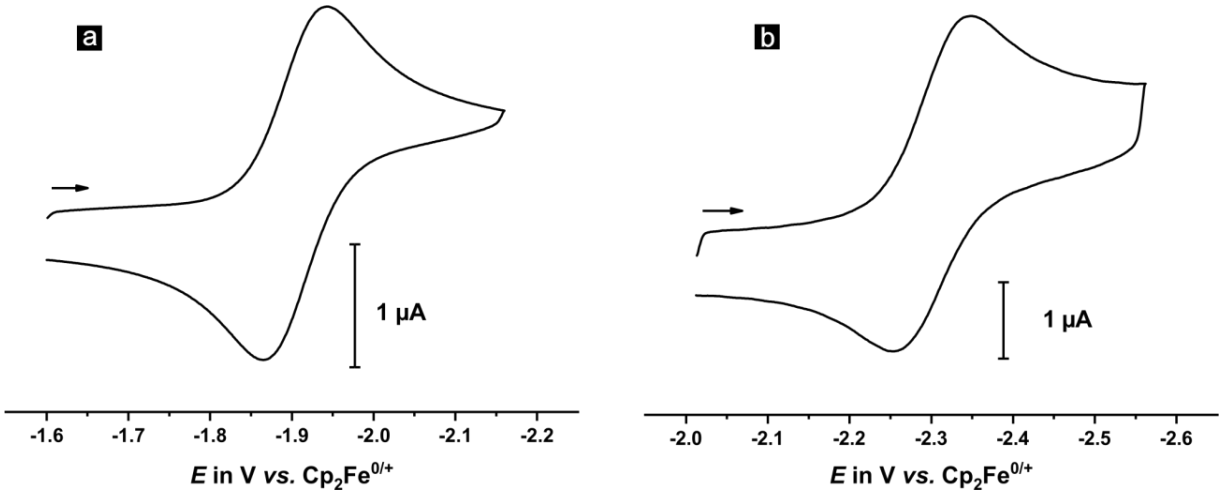


**Figure S29.** Cyclic voltammograms of the cathodic sweep of a) **BPtI** (ν = 200 mV/s) and b) **KBPtI** (ν = 2000 mV/s) in THF at r.t. with $NBu_4PF_6$ (0.1 M) as the supporting electrolyte referenced to the $Cp_2Fe^{0/+}$ couple ($E_{1/2}$ = 0.000 V).

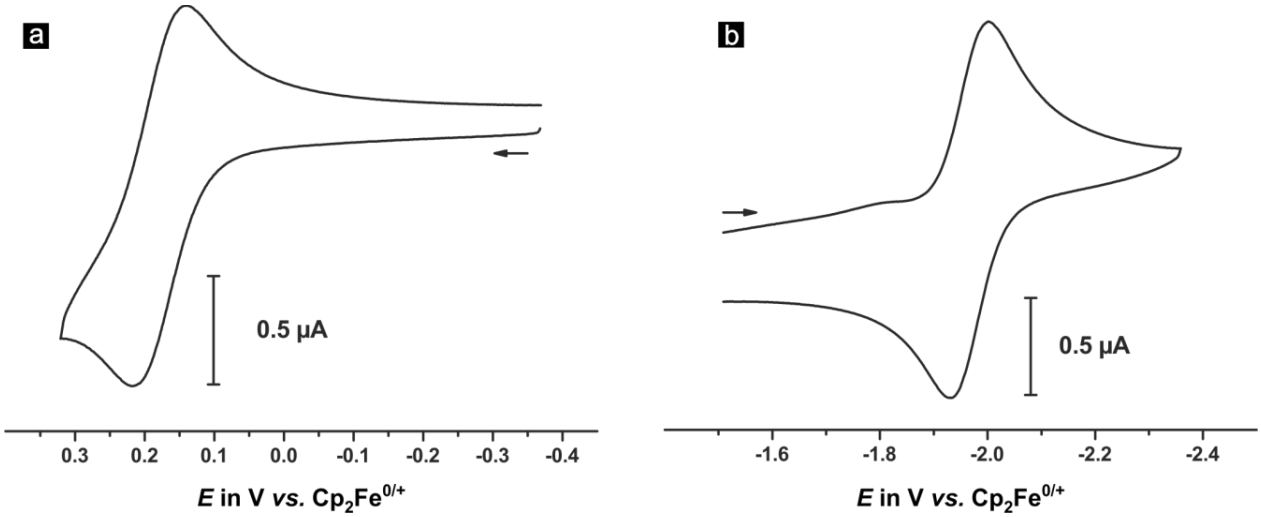


**Figure S30.** Cyclic voltammograms (ν = 100 mV/s) of a) the anodic and b) the cathodic sweep of **BPtSPyr** in THF at r.t. with $NBu_4PF_6$ (0.1 M) as the supporting electrolyte referenced to the $Cp_2Fe^{0/+}$ couple ($E_{1/2}$ =0.000 V).

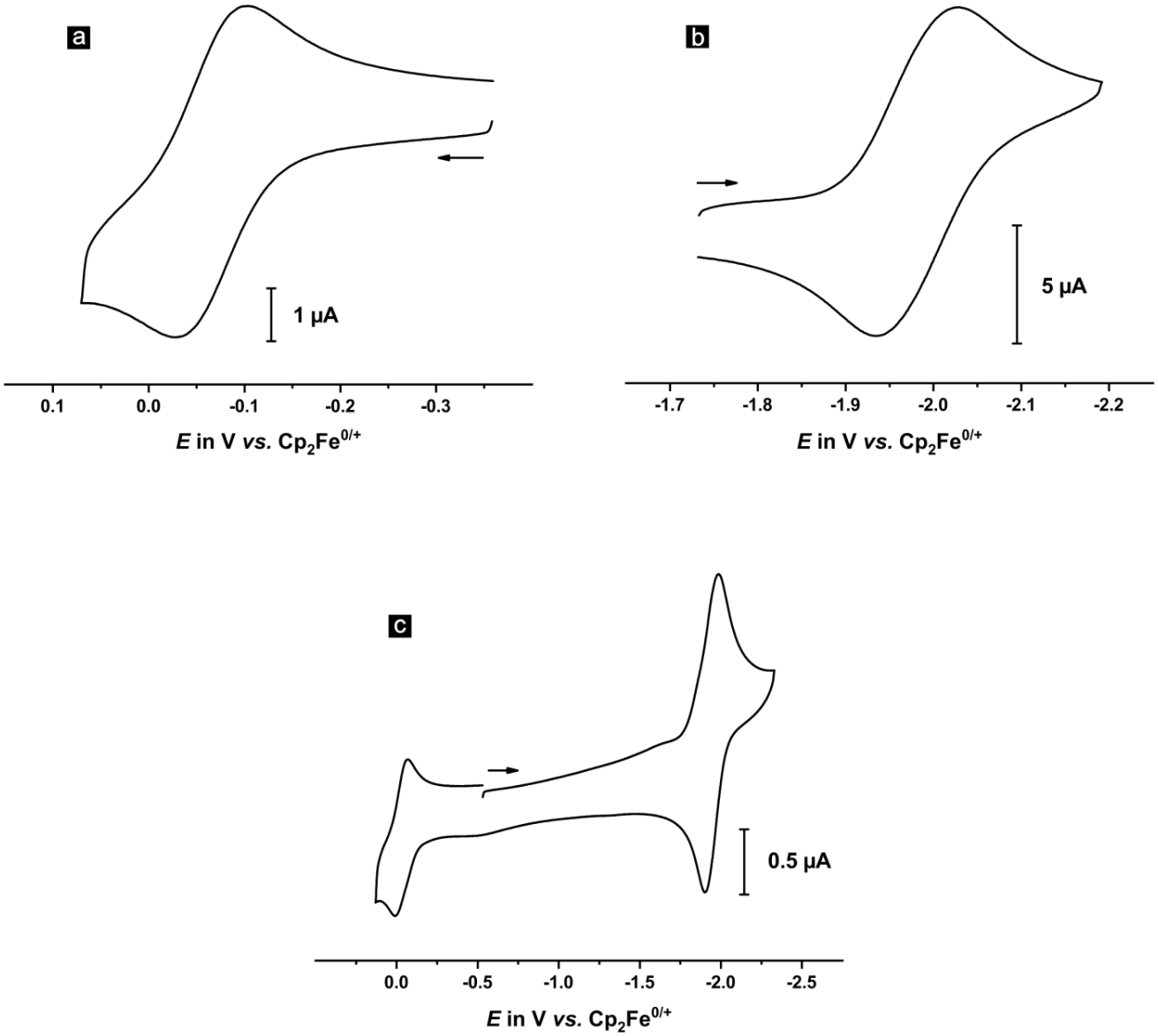


**Figure S31.** Cyclic voltammograms (ν = 100 mV/s) of a) the anodic and b) the cathodic sweep of **BPtSPyrSPtB** in THF at r.t. with $NBu_4PF_6$ (0.1 M) as the supporting electrolyte referenced to the $Cp_2Fe^{0/+}$ couple ($E_{1/2}$ =0.000 V) as well as c) the full sweep in the anodic and cathodic directions.

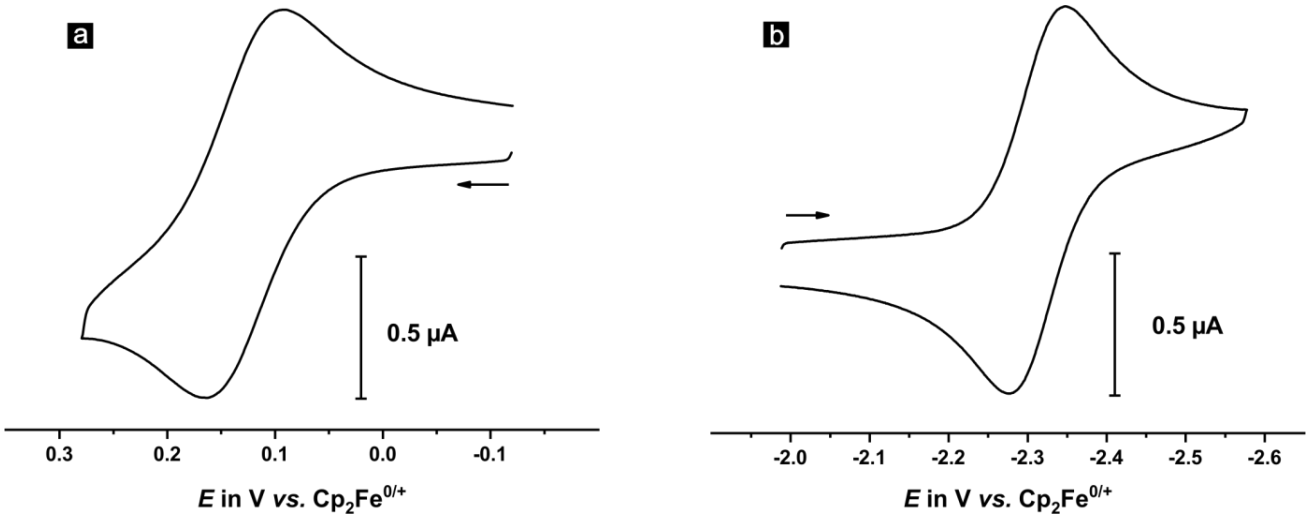


**Figure S32.** Cyclic voltammograms (ν = 100 mV/s) of a) the anodic and b) the cathodic sweep of **KBPtSPyr** in THF at r.t. with $NBu_4PF_6$ (0.1 M) as the supporting electrolyte referenced to the $Cp_2Fe^{0/+}$ couple ($E_{1/2}$ =0.000 V).

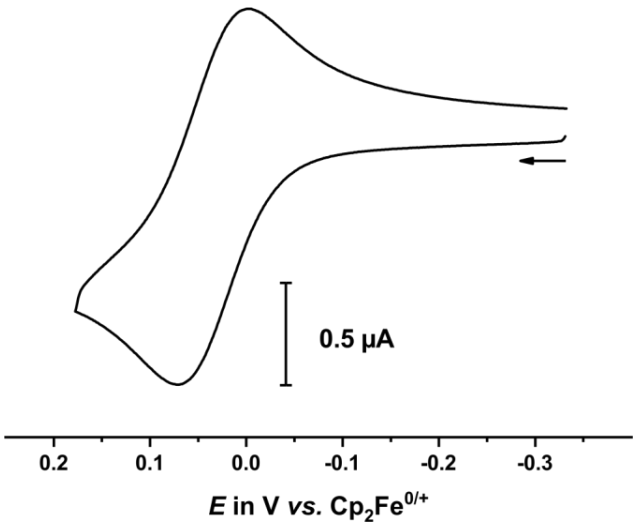


**Figure S33.** Cyclic voltammogram (ν = 2000 mV/s) of the anodic sweep of **MesPtSPyr** in THF at r.t. with $NBu_4PF_6$ (0.1 M) as the supporting electrolyte referenced to the $Cp_2Fe^{0/+}$ couple ($E_{1/2}$ = 0.000 V).

## Electronic Absorption Spectroscopy

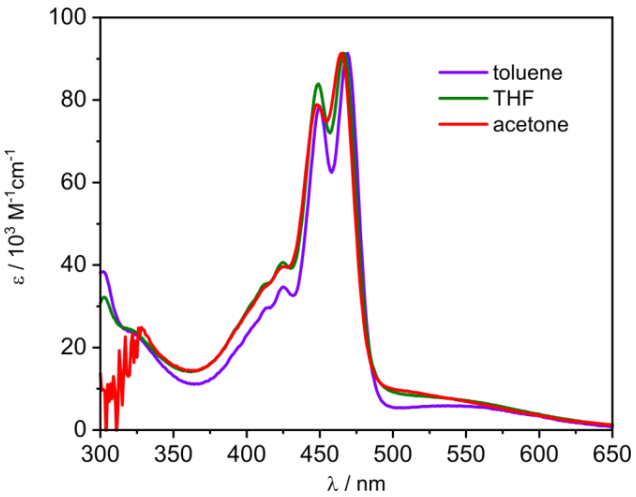


**Figure S34.** Electronic absorption spectra of **BPtSPyrSPyr** in different solvents. Due to the low solubility of the compound in acetone and toluene the respective spectra were normalized to that in THF.

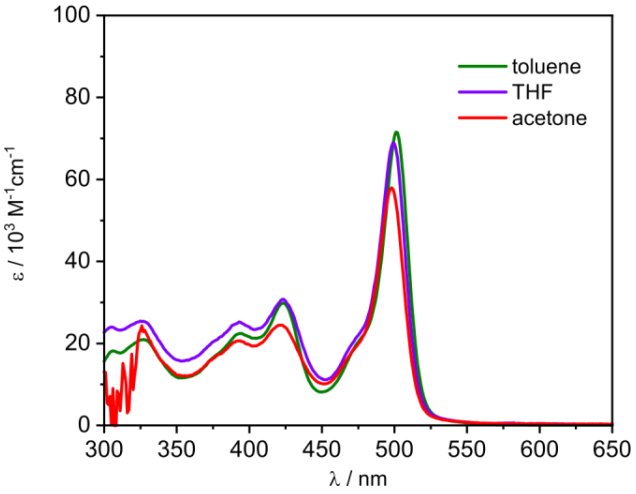


**Figure S35.** Electronic absorption spectra of **KBPtSPyr** in different solvents.

## Luminescence Spectroscopy

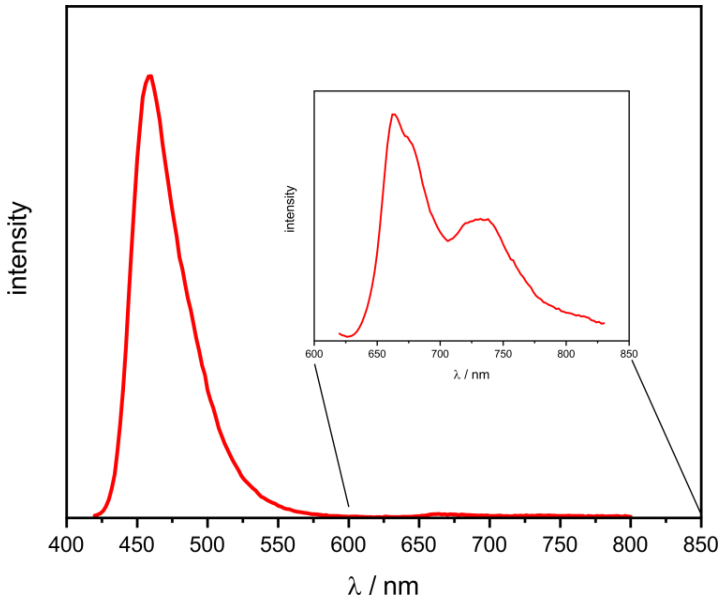


**Figure S36.** Emission of **MesPtSPyr** in a ca 1 μM degassed toluene solution at r.t.

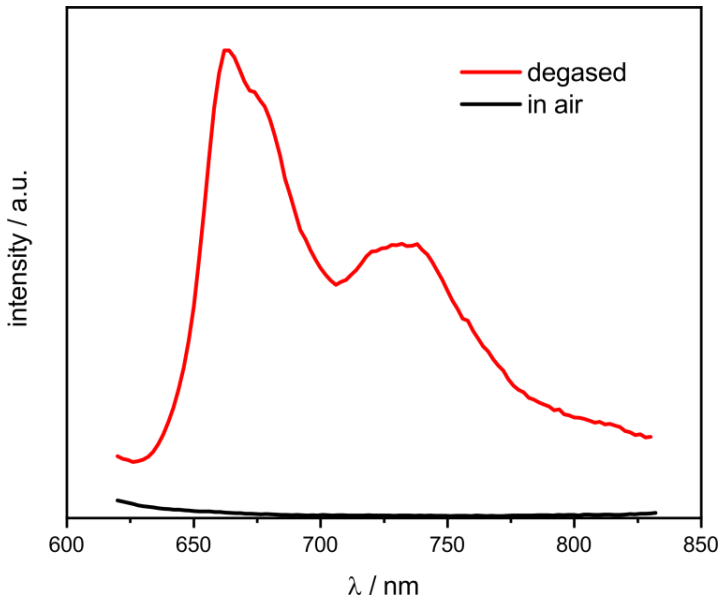


**Figure S37.** Phosphorescence emission of **MesPtSPyr** in a ca 1 μM toluene solution at r.t.

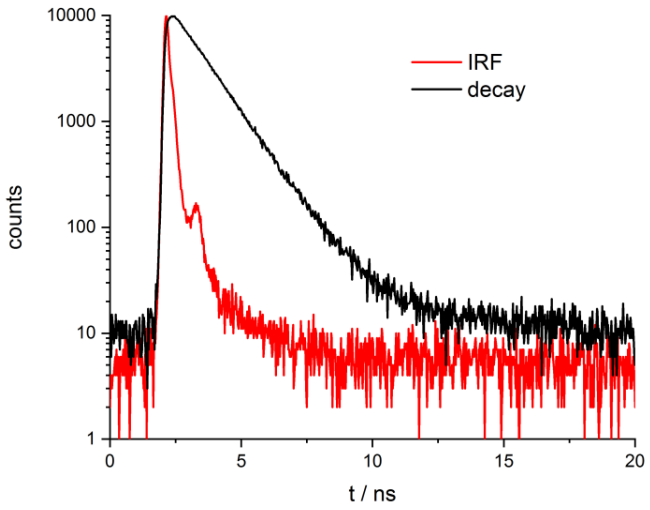


**Figure S38.** Fluorescence decay traces of **MesPtSPyr** in a deaerated and nitrogen-saturated 1 µM toluene solution at r.t. Decay can be fitted as a monoexponential decay with a lifetime of 1.113 ± 0.005 ns.

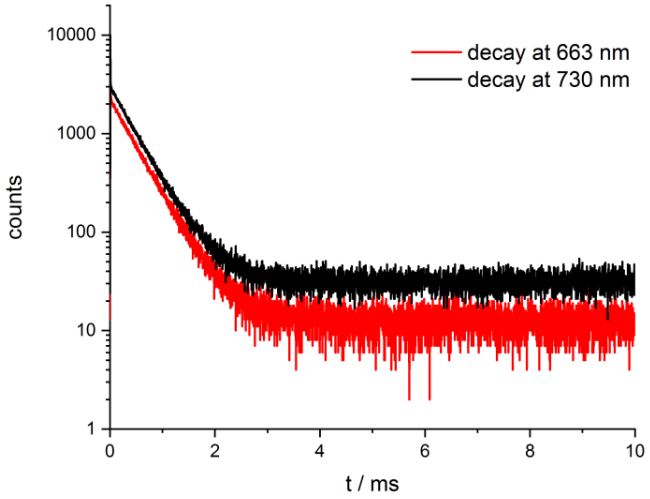


**Figure S39.** Phosphorescence decay traces of **MesPtSPyr** in a deaerated and nitrogen-saturated 1 µM toluene solution at r.t. Decay can be fitted as a monoexponential decay with a lifetime of 448 ± 6 µs.

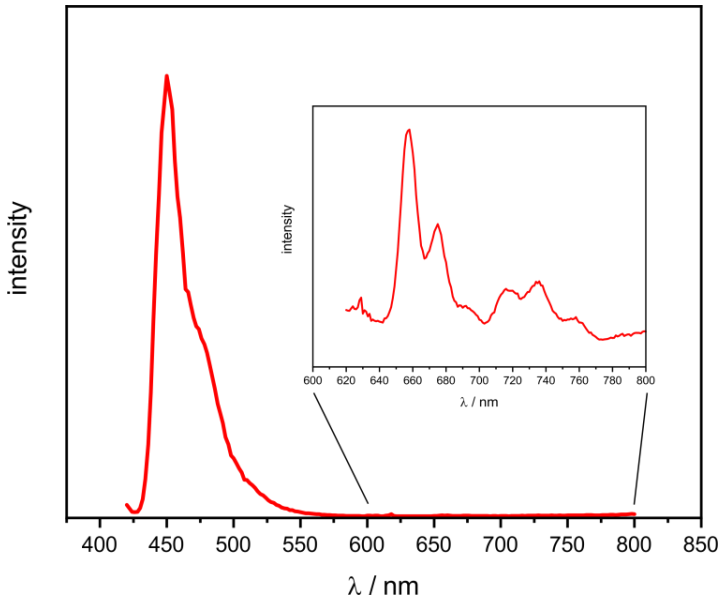


**Figure S40.** Emission of **MesPtSPyr** in a 2-MeTHF matrix at 77K.

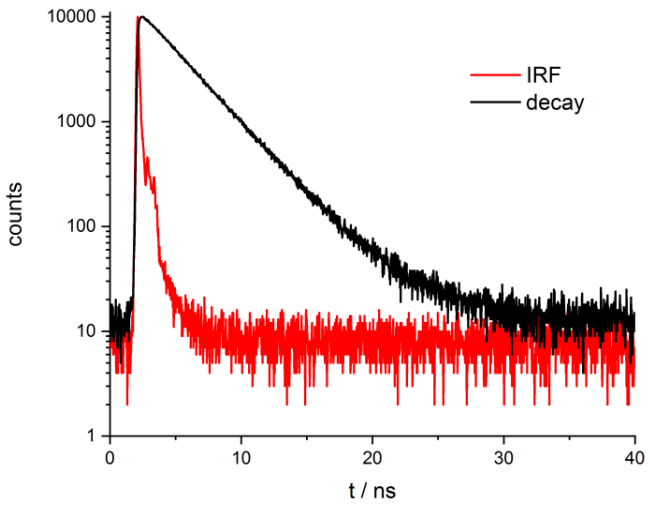


**Figure S41.** Fluorescence decay traces of **MesPtSPyr** in a 2-MeTHF matrix at 77 K. Decay can be fitted with a monoexponential decay with a lifetime of 3.19 ± 0.03 ns.

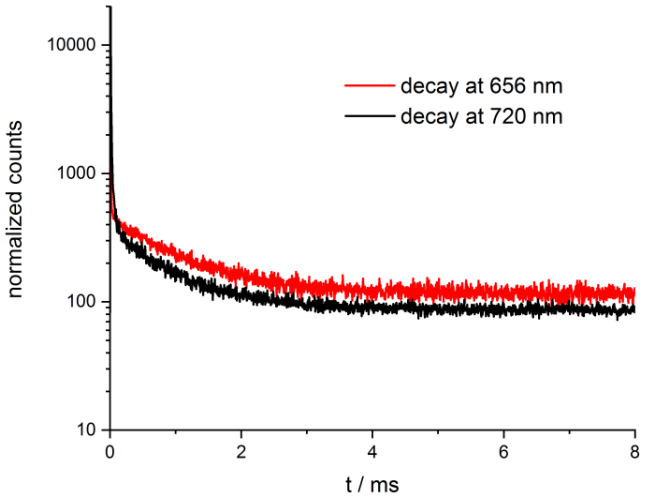


**Figure S42.** Phosphorescence decay traces of **MesPtSPyr** in a 2-MeTHF matrix at 77 K. Decay can be fitted with a monoexponential decay and a lifetime of 1.04 ± 0.06 ms.

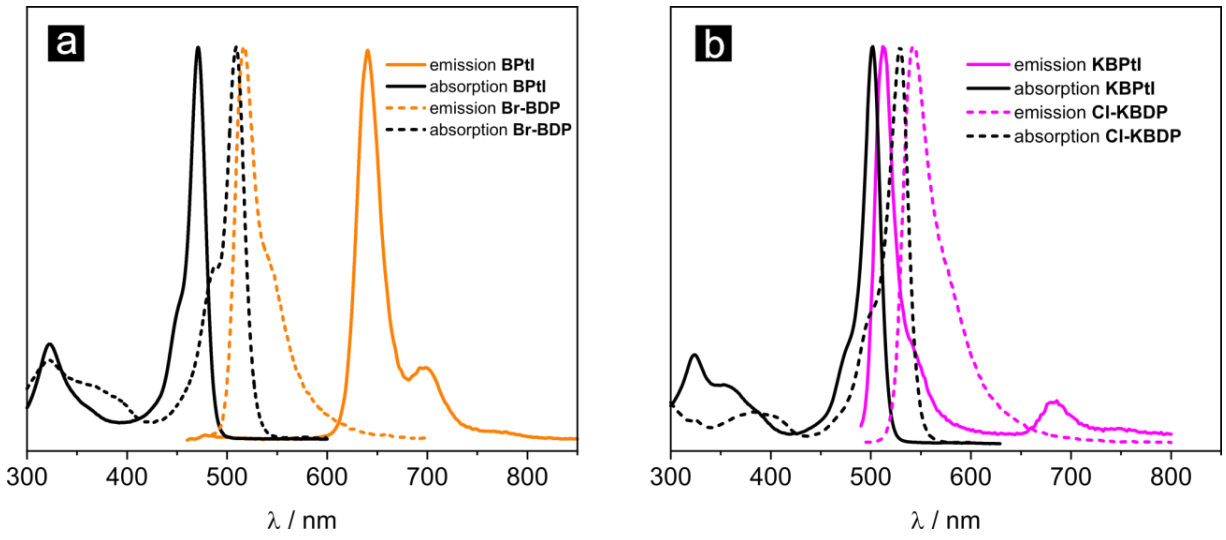


**Figure S43.** Absorption and emission spectra of a) **Br-BDP** and **BPtI** in $CH_2Cl_2$ solution at r.t. as well as b) of **Cl-KBDP** and **KBPtI** in toluene solution at r.t.

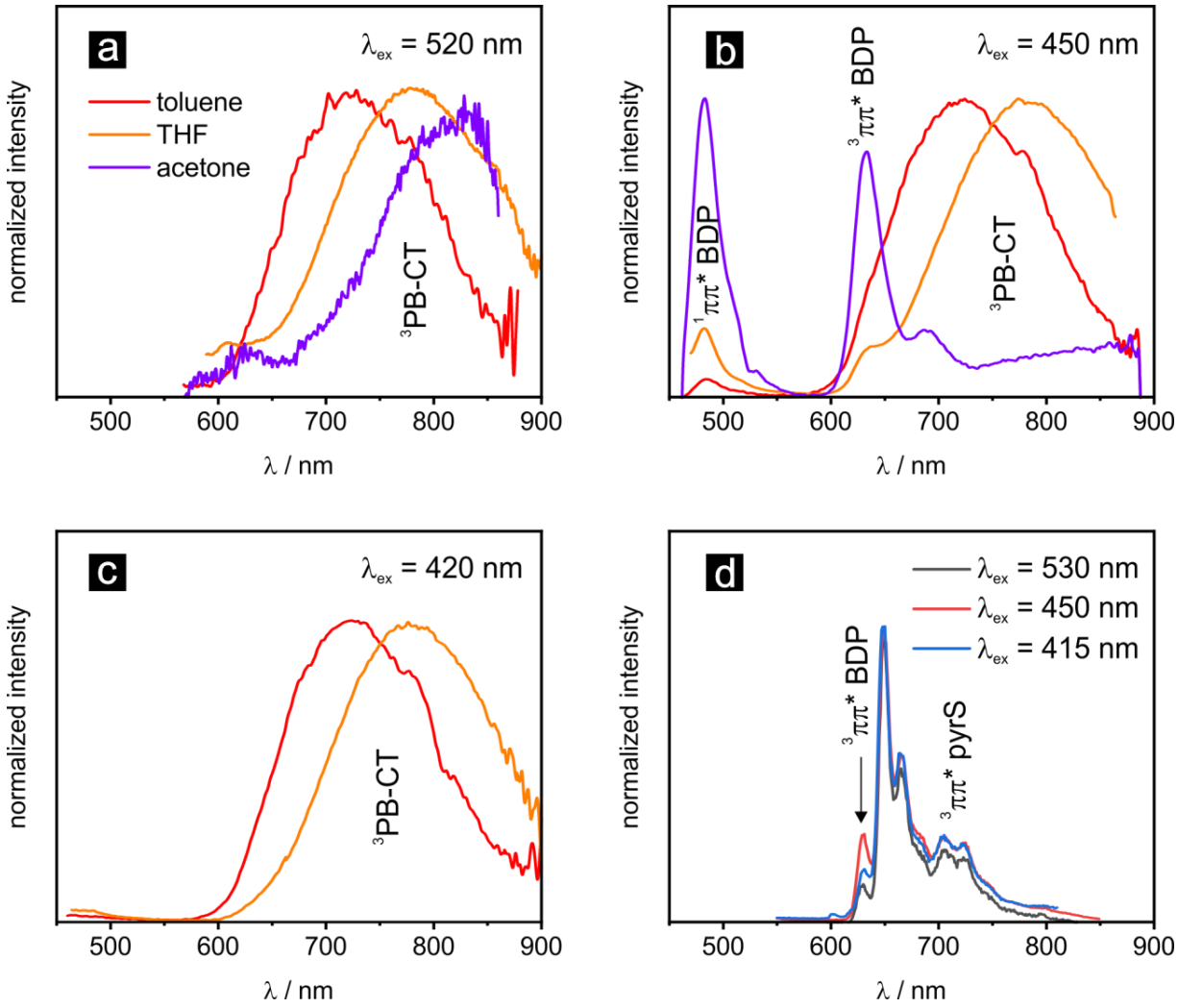


**Figure S44.** Emission spectra of **BPtSPyr** in *ca.* 1 μM solutions of acetone, THF or toluene at r.t. on excitation at a) 520 nm, b) 450 nm and c) 420 nm. d) Emission spectra recorded in 2-MeTHF at 77 K at different excitation wavelengths.

**Table S13. Emission data of BPtI, KBPtI, MesPtSPyr, BPtSPyr, KBPtSPyr and BPtSPyrSPtB**

| solvent | $\lambda_{exc}$[a] | $\lambda_{fl}$[b] (assignment) | $\Phi_{fl}$[c] | $\tau_{fl}$[d] | $\lambda_{ph}$[b] (assignment) | $\Phi_{ph}$[c] | $\tau_{ph}$[d] |
|---|---|---|---|---|---|---|---|
| | | | | **BPtI** *from ref.* 3 | | | |
| $CH_2Cl_2$ | 467 | 481 ($^1$BDP) | 0.002 | 0.48 ± 0.02 ns | 641 | 0.364 | 297 ± 2 µs |
| | | | | **KBPtI** | | | |
| toluene | 485 | 512 | 0.10 | 0.959 ± 0.007 ns | 684 | 0.04 | 239 ± 2 µs |
| Me-THF[e] | 485 | 506 | n.d. | 1.171 ± 0.007 ns | 673 | n.d. | 436 ± 2 µs |
| | | | | **MesPtSPyr** *from ref.* 4 | | | |
| toluene | 430 | 460 ($^1$ pyrS ) | 0.24 | 1.113 ± 0.005 ns | 664 ($^3$pyrS) | <0.01 | 448 ± 6 µs |
| Me-THF[e] | 430 | 450 ($^1$ pyrS ) | | | 658 ($^3$pyrS) | n.d. | 1.04 ± 0.06 ms |
| | | | | **BPtSPyr** *from ref.* 4 | | | |
| toluene | 520 | | | | 724 ($^3$PB-CT) | 0.08 | 6.7 ± 0.4 µs |
| | 470 | 484 ($^1$BDP) | | | 724 ($^3$PB-CT) | 0.15 | 6.7 ± 0.5 µs |
| | 420 | | | | 724 ($^3$PB-CT) | 0.15 | 6.4 ± 0.3 µs |
| THF | 520 | | | | 784 ($^3$PB-CT) | n.d. | n.d. |
| | 470 | 484 ($^1$BDP) | | 3.70 ± 0.2 ns | 635 ($^3$BDP)<br>784 ($^3$PB-CT) | n.d. | 78.0 ± 0.4 µs,<br>51.4 ± 0.8 ns |
| | 420 | | | | 784 ($^3$PB-CT) | n.d. | 50.4 ± 0.3 ns |
| acetone | 520 | | | | 816 ($^3$PB-CT) | n.d. | n.d. |
| | 470 | 484 ($^1$BDP) | | | 635 ($^3$BDP)<br>816 ($^3$PB-CT) | n.d. | 49.9 ± 0.3 µs<br>2.44 ± 0.02 ns |
| Me-THF[e] | 530<br>450<br>415 | n.o. | | | 635 ($^3$BDP)<br>649 ($^3$pyrS) | n.d. | 279 ± 1 µs<br>1.12 ± 0.02 ms |
| | | | | **KBPtSPyr** | | | |
| toluene | 485 | 512 ($^1$BDP) | <0.01 | 4.42 ± 0.07 ns | 682 ($^3$BDP) | 0.03 | 204 ± 1 µs |
| | 405 | n.o. | | | 682 ($^3$BDP) | 0.05 | 203.7 ± 0.9 µs |
| THF | 485 | 510 ($^1$BDP) | n.d. | 2.14 ± 0.07 ns | 682 ($^3$BDP) | n.d. | 273 ± 1 µs |
| Me-THF[e] | 485 | 510 ($^1$BDP) | n.d. | 2.34 ± 0.05 ns | 674 ($^3$BDP) | n.d. | 423 ± 2 µs |
| | | | | **BPtSPyrSPtB** | | | |
| toluene | 550 | | | | 770 ($^3$PB-CT) | <0.01 | 32 ± 5 µs |
| | 460 | 482 ($^1$BDP) | <0.01 | | 635 ($^3$BDP)<br>760 ($^3$PB-CT) | 0.01 | 178 ± 1 µs<br>31 ± 2 µs |
| | 420 | 482 ($^1$BDP) | <0.01 | 5.0 ± 0.2 ns | 653 ($^3$BDP)<br>760 ($^3$PB-CT) | <0.01 | 164 ± 12 µs<br>31 ± 1 µs |
| *o*-$C_6F_2H_4$ | 530 | no emission observed | | | no emission observed | | |
| | 450 | 480 ($^1$BDP) | n.d. | n.d. | 634 ($^3$BDP) | n.d. | 82 ± 6 µs |
| Me-THF[e] | 550 | | | | 696 ($^3$pyrS) | n.d. | 369 ± 6 µs |
| | 460 | 480 ($^1$BDP) | n.d. | n.d. | 626 ($^3$BDP)<br>696 ($^3$pyrS) | n.d. | 499 ± 6 µs<br>369 ± 3 µs |
| | 420 | 480 ($^1$BDP) | n.d. | 4.1 ± 0.1 ns | 626 ($^3$BDP)<br>696($^3$pyrS) | n.d. | 479 ± 12 µs<br>348 ± 2 µs |

[a]Excitation wavelength in nm. [b]Wavelength of the fluorescence (fl) or phosphorescence (ph) emissions in nm. [c]Fluorescence (fl) or phosphorescence (ph) quantum yield. [d]Lifetime of the fluorescence (fl) or phosphorescence (ph) emissions. [e]Measured in a 2-MeTHF glass at 77 K.

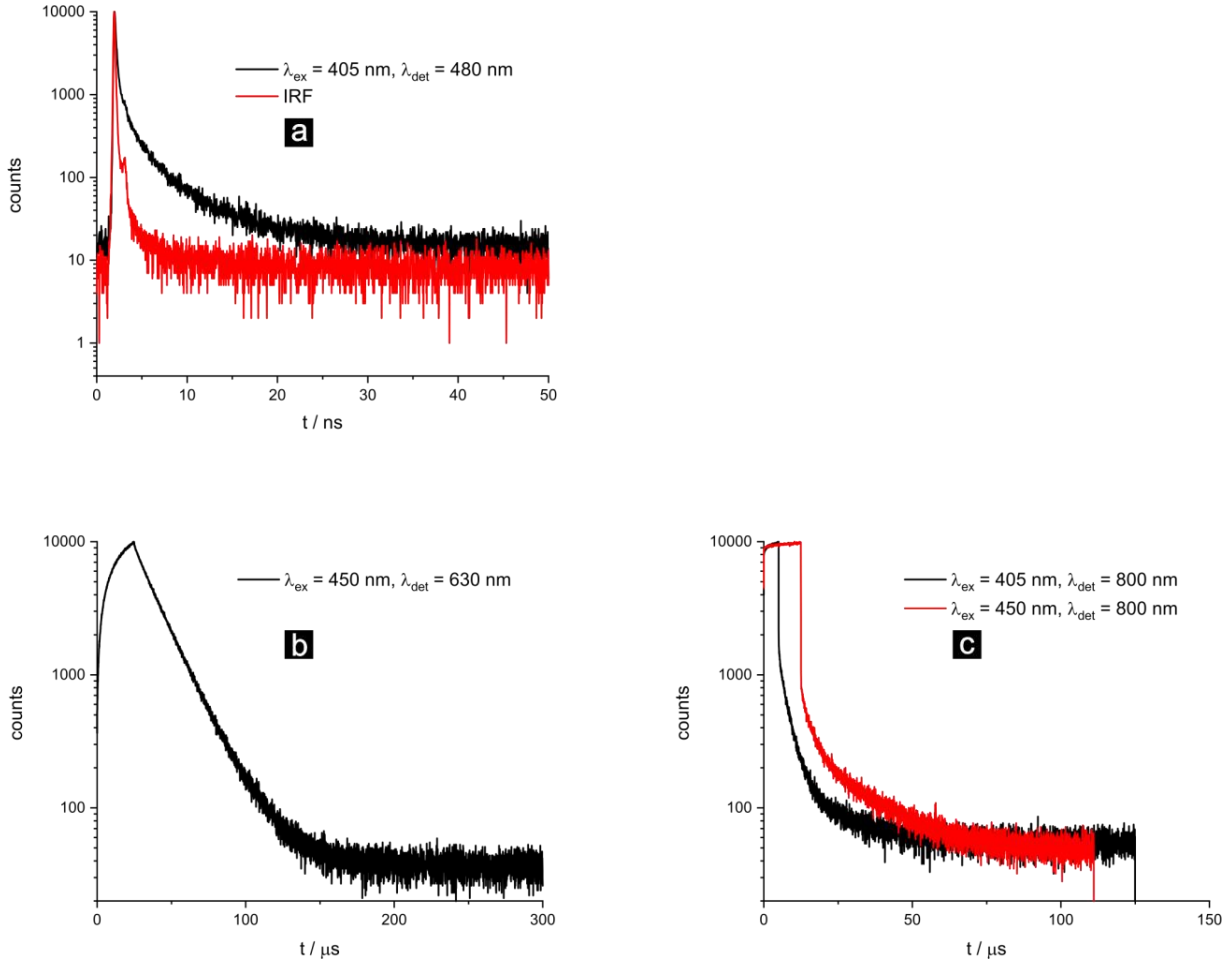


**Figure S45.** Emission decay traces of **BPtSPyrSPtB** in a deaerated and nitrogen-saturated 1 µM toluene solution at r.t.; a) shows the fluorescence lifetime decay with 5.0 ns; b) depicts the 178 µs component; c) depicts the 32 µs component. The rise times of 49 µs in Figure S45b and 10 or 30 µs in c) are due to foregoing excited state saturation in the "burst mode".

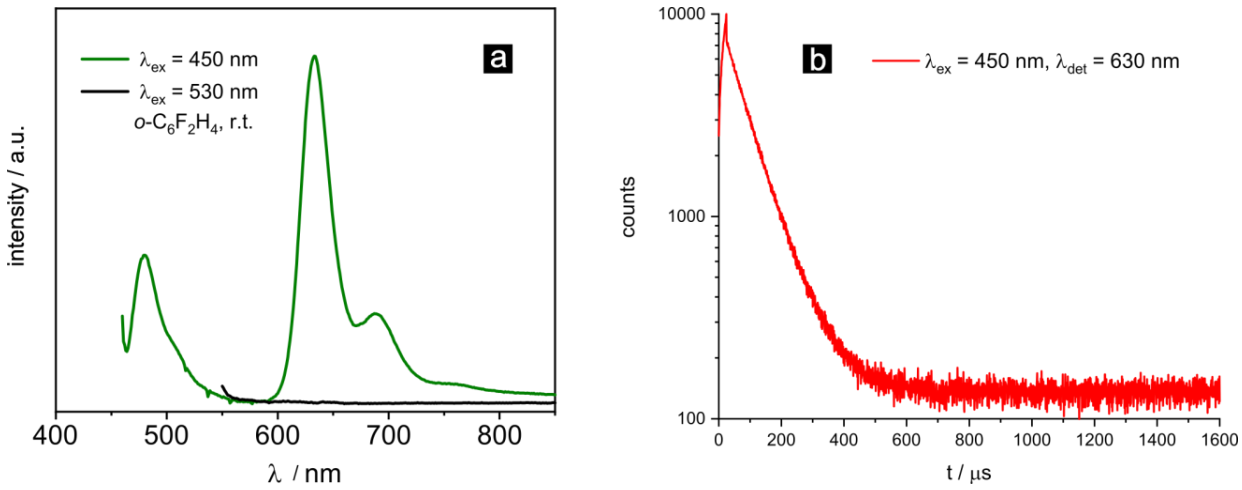


**Figure S46.** a) Emission spectra and b) emission decay trace of **BPtSPyrSPtB** in a ca. 1 µM o-difluorobenzene solution at r.t. (82 µs).

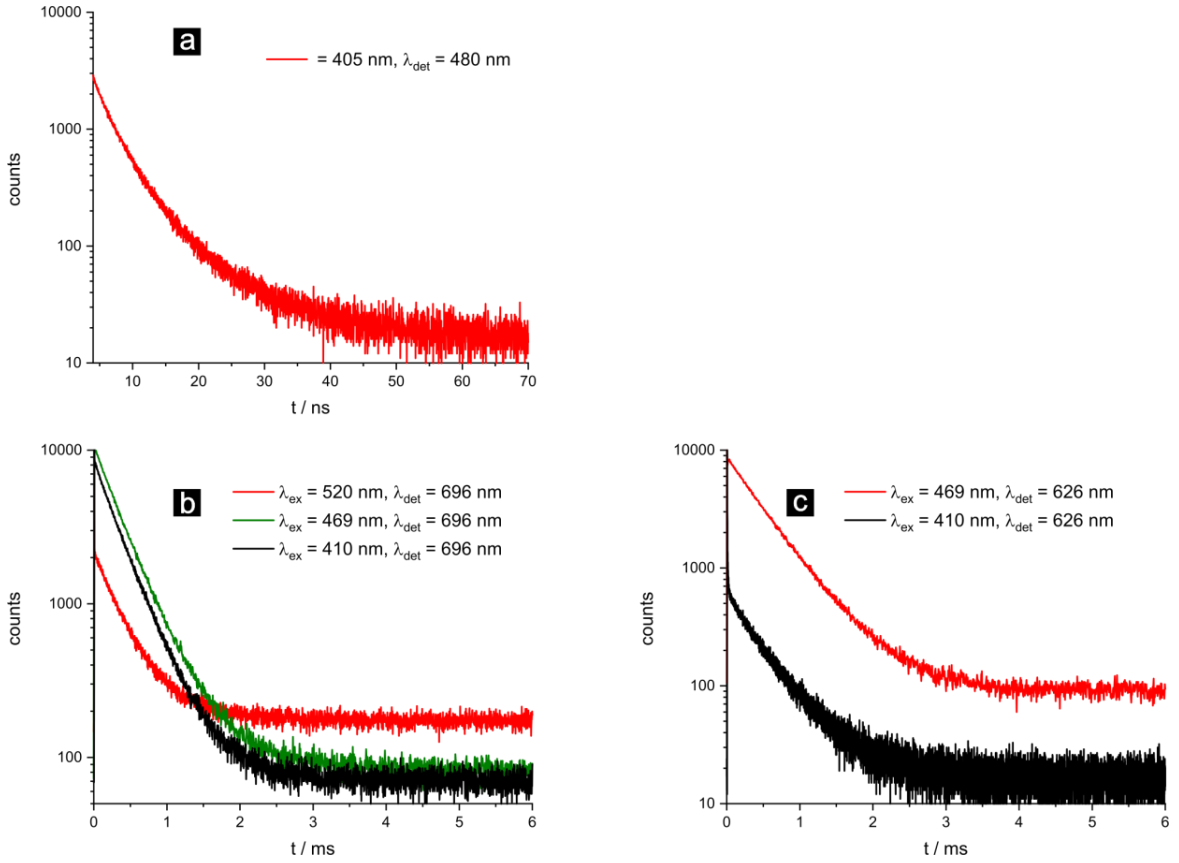


**Figure S47.** Emission decay traces of **BPtSPyrSPtB** in a 1 µM 2-MeTHF matrix at 77 K a) depicting the 4.1 ns component, b) depicting the 369 µs component and c) showing the 499 µs component.

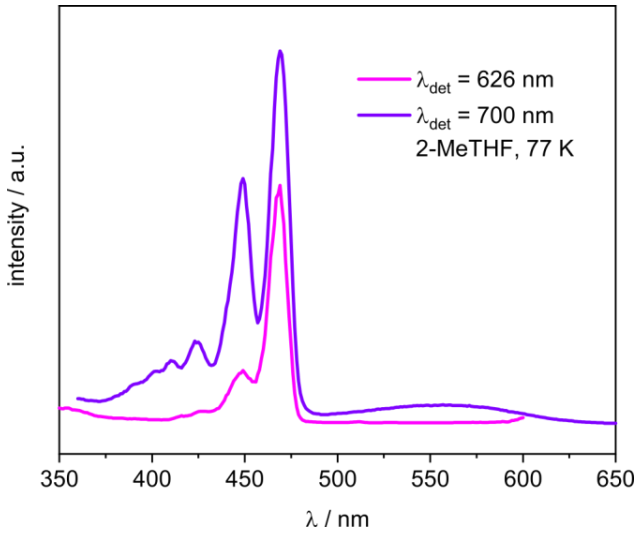


**Figure S48.** Excitation spectra of **BPtSPyrSPtB** recorded on a 1 mM 2-MeTHF matrix at 77 K.

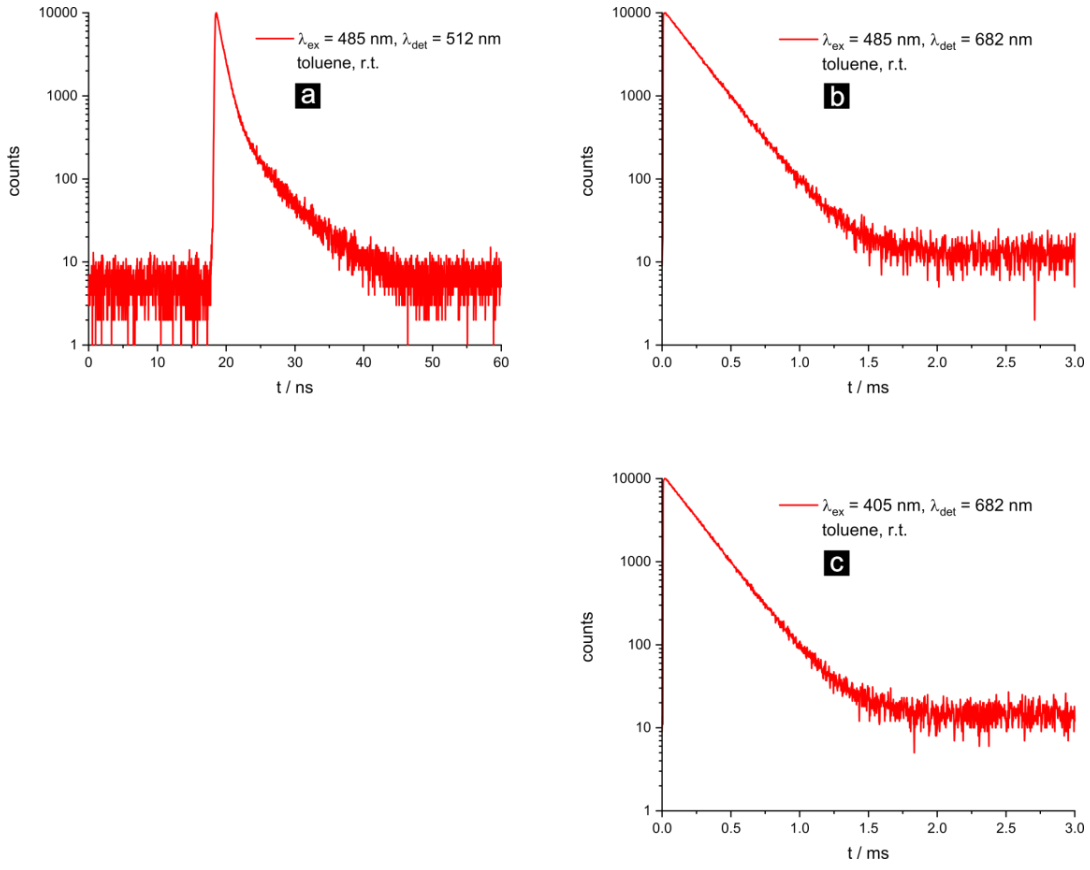


**Figure S49.** Emission decay traces of **KBPtSPyr** in a deaerated and nitrogen-saturated 1 µM toluene solution at r.t. a) depicting the 4.4 ns component, b) depicting the 204 µs component and c) showing the 204 µs component.

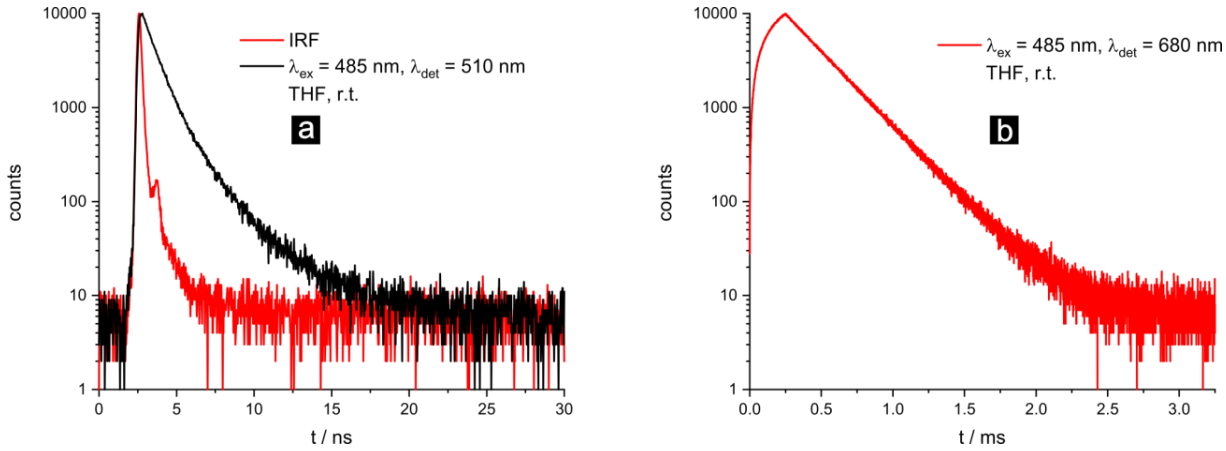


**Figure S50.** Emission decay traces of **KBPtSPyr** in a deaerated and nitrogen-saturated 1 µM THF solution at r.t. The rise time of 500 µs in Figure S50b is due to prior excited state saturation in the "burst mode". a) depicts the 2.1 ns component and b) shows the 273 µs component.

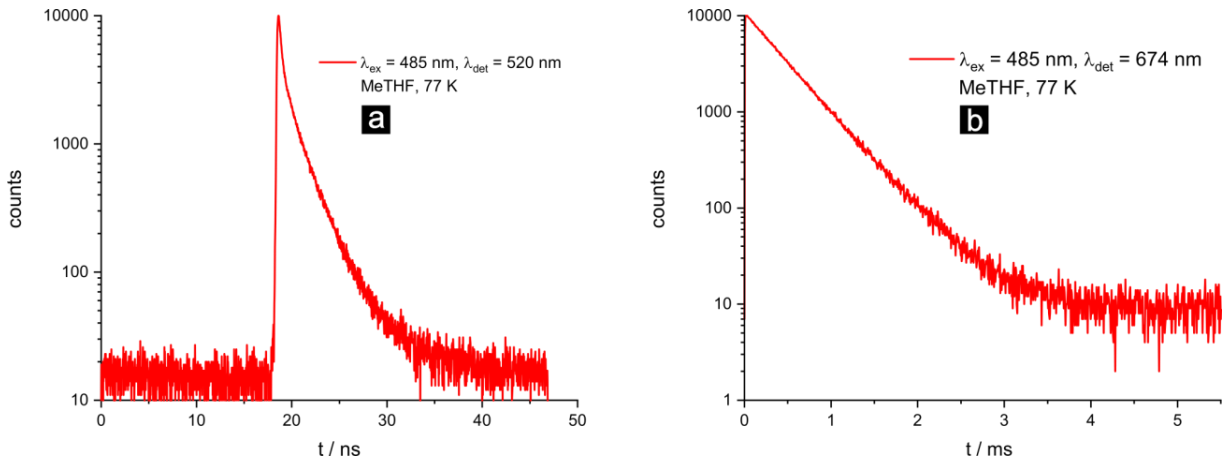


**Figure S51.** Emission decay traces of **KBPtSPyr** in a 1 µM 2-MeTHF matrix at 77 K a) depicting the 2.3 ns component and b) showing the 423 µs component.

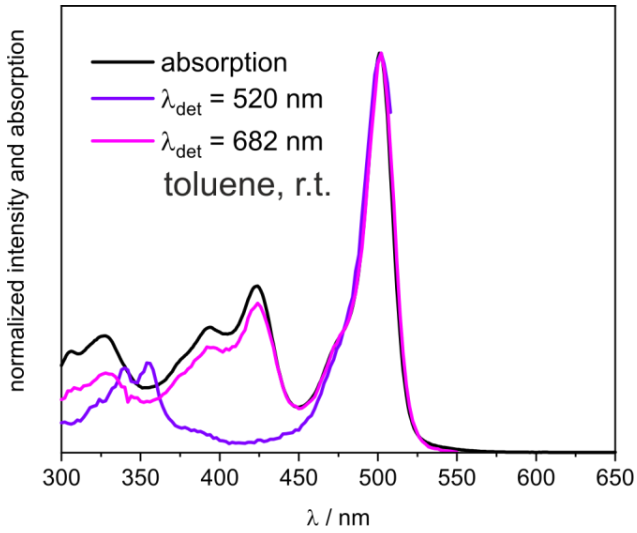


**Figure S52.** Comparison of the excitation spectra of **KBPtSPyr** recorded at 682 nm and 520 nm with the UV/Vis spectrum for a 1 μM toluene solution at r.t.

**Table S14.** Singlet Oxygen Generation Quantum Yield $\Phi_\Delta$ Compared to Tetraphenylporphyrin (**TPP**) as Reference Sensitizer

| sensitizer | $\lambda_{ex}$ / nm | $\Phi_\Delta$[b] |
|---|---|---|
| **TPP**[a] | 525 | 0.66 ± 0.08 |
| | 470 | 0.66 ± 0.08 |
| | 410 | 0.66 ± 0.08 |
| **BPtI** | 470 | 0.94 ± 0.11 |
| **KBPtI** | 470 | 0.65 ± 0.08 |
| **MesPtSPyr** | 410 | 0.28 ± 0.03 |
| **BPtSPyr** | 525 | 0.74 ± 0.09 |
| | 470 | 0.75 ± 0.09 |
| | 410 | 0.33 ± 0.04 |
| **KBPtSPyr** | 470 | 0.74 ± 0.09 |
| | 410 | 0.40 ± 0.05 |
| **BPtSPyrSPtB** | 525 | 0.11 ± 0.01 |
| | 470 | 0.18 ± 0.02 |
| | 410 | 0.07 ± 0.01 |

[a]Value from reference [5]. [b]Standard deviations were calculated by error propagation.

## Electronic Absorption Spectroscopy and Quantum Chemical Calculations on the Oxidized and Reduced Forms

### Table S15. Absorption Data for the Oxidized and Reduced Forms of BPtSPyr, KBPtSPyr, and BPtSPyrSPtB as well as TD-DFT-Calculated Band Energies and Assignments

| absorption data | | TD-DFT calculations[a] | | | |
|---|---|---|---|---|---|
| solvent | $\lambda_{max}$[b] ($\varepsilon$[c]) | $\lambda$[b] | $f$[d] | m.c.[e] | assignment |
| **radical cation of BPtSPyr** | | | | | |
| THF[f] | 322 (23), 474 (49), 518 (18), 556 (21), 755 (2), 920 (5), 1020 (9) | 397 | 0.36 | H($\alpha$) → L($\alpha$) (41%), H($\beta$) → L+1($\beta$) (47%) | $\pi\pi$* BDP with some BP-CT contribution |
| | | 502 | 0.43 | H-1($\alpha$) → L($\alpha$) (20%), H-1($\alpha$) → L+1($\alpha$) (29%), H-8($\beta$) → L($\beta$) (14%) | $\pi\pi$* pyrS and $\pi\pi$* BDP with some PB-CT contribution |
| | | 865 | 0.19 | H-1($\beta$) → L($\beta$) (92%) | $\pi\pi$* pyrS |
| **radical anion of BPtSPyr** | | | | | |
| THF[f] | 347 (20), 395 (19), 441 (26), 519 (5) | 420 | 0.63 | H($\alpha$) → L+11($\alpha$) (12%) H-1($\beta$) → L+1($\beta$) (77%) | $\pi\pi$* pyrS |
| | | 432 | 0.06 | H-1($\alpha$) → L ($\alpha$) (47%), H($\beta$) → L($\beta$) (48%) | $\pi\pi$* BDP |
| **radical cation of KBPtSPyr** | | | | | |
| THF[f] | 323 (24), 507 (77), 555 (26), 717 (3), 898 (6), 1008 (13) | n.d. | n.d. | n.d. | n.d. |
| **radical anion of KBPtSPyr** | | | | | |
| $CH_2Cl_2$[f] | 401 (23), 437 (30), 498 (7) | n.d. | n.d. | n.d. | n.d. |
| **radical cation of BPtSPyrSPtB** | | | | | |
| THF[f] | 319 (29), 452 (48), 470 (79), 527 (8), 600 (12), 666 (26), 1181 (6), 1383 (14) | n.d. | n.d. | n.d. | n.d. |
| **radical anion of BPtSPyrSPtB** | | | | | |
| $CH_2Cl_2$[f] | 394 (41), 421 (46), 464 (66) | n.d. | n.d. | n.d. | n.d. |

[a]DFT calculations on the pbe1pbe/6-31G(d) level of therory; PCM model for $CH_2Cl_2$. [b]$\lambda$ in nm. [c]$\varepsilon \cdot 10^3$ $M^{-1}$ $cm^{-1}$. [d]$f$ = oscillator strength. [e]m.c. = major contribution. H refers to HOSO and L to LUSO. [f]With 0.1 M $NBu_4PF_6$ as the supporting electrolyte.

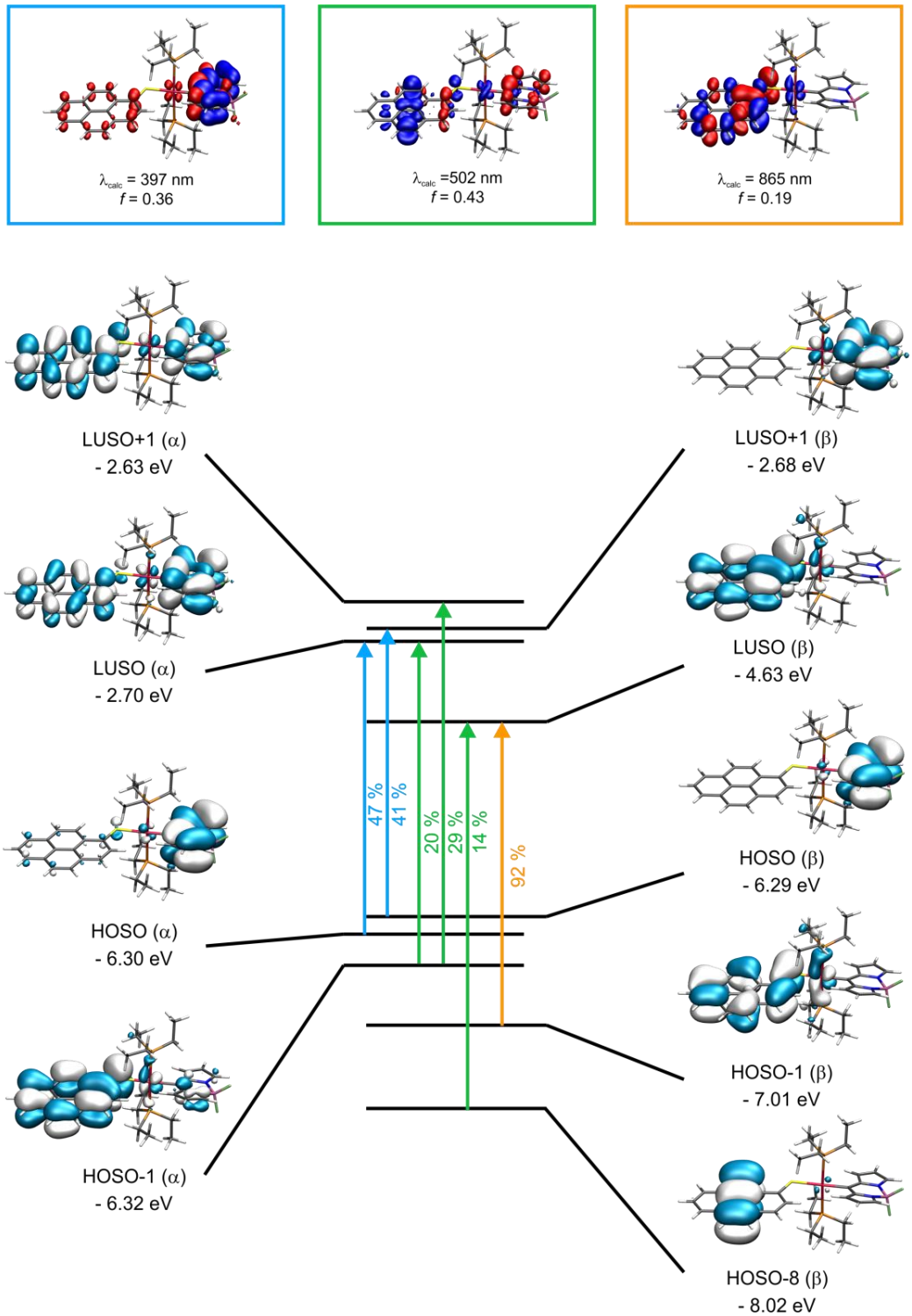


**Figure S53.** Graphical representations of the relevant spin orbitals and TD-DFT energies of **BPtSPyr** in the cationic form as well as electron density difference maps (*blue* = electron density loss, *red* = electron density gain).

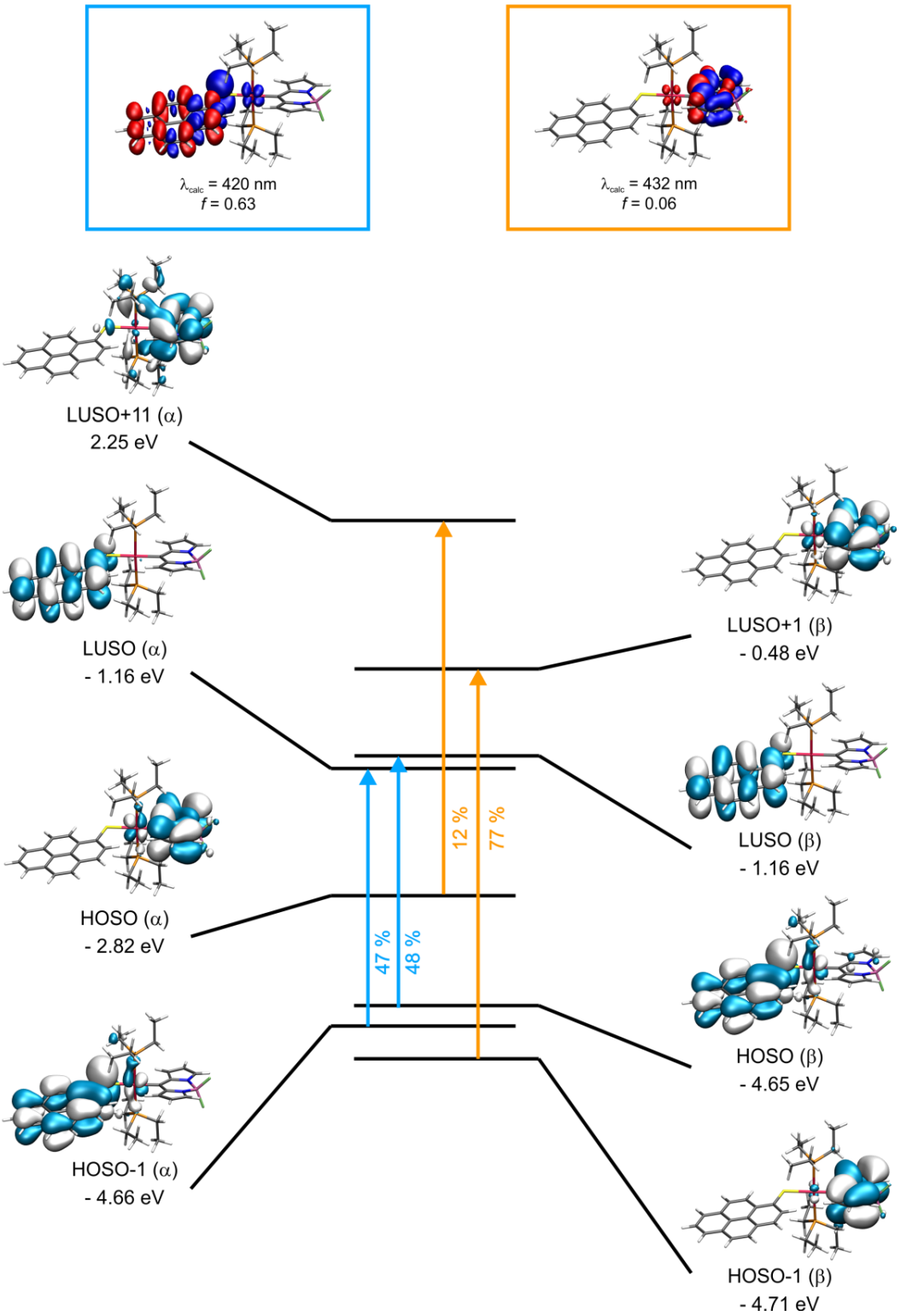


**Figure S54.** Graphical representations of the relevant spin orbitals and TD-DFT energies of **BPtSPyr** in the anionic form as well as electron density difference maps (*blue* = electron density loss, *red* = electron density gain).

## Transient Absorption Spectroscopy

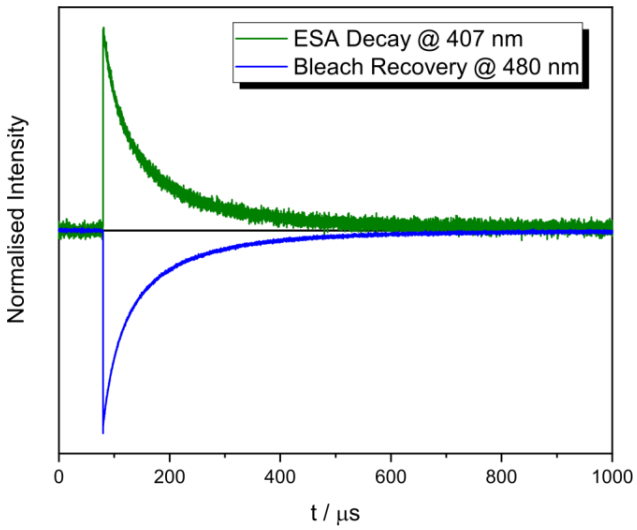


**Figure S55.** Single wavelength kinetics of **BPtI** recorded in 20 µM THF solution at r.t. after laser excitation at 470 nm for the different features of the transient absorption spectrum. Exponential decays can be fitted with a biexponential model with time constants of $\tau_1$ = 30.2 µs and $\tau_2$ = 149 µs.

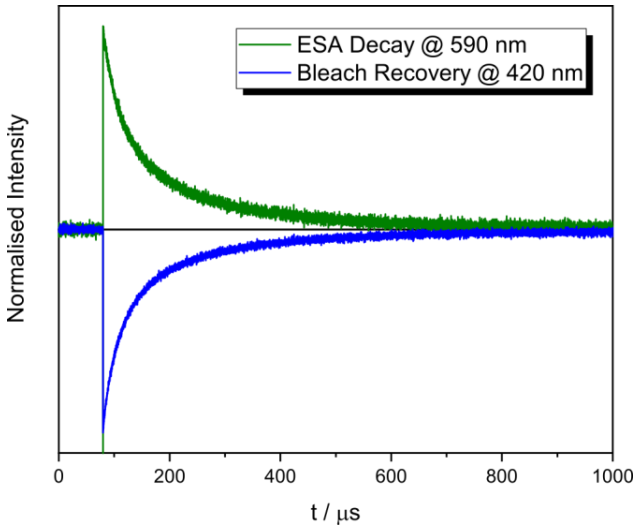


**Figure S56.** Single wavelength kinetics of **MesPtSPyr** recorded in 20 µM THF solution at r.t. after laser excitation at 430 nm for the different features of the transient absorption spectrum. Exponential decays can be fitted with a biexponential model with time constants of $\tau_1$ = 34.7 µs and $\tau_2$ = 174 µs.

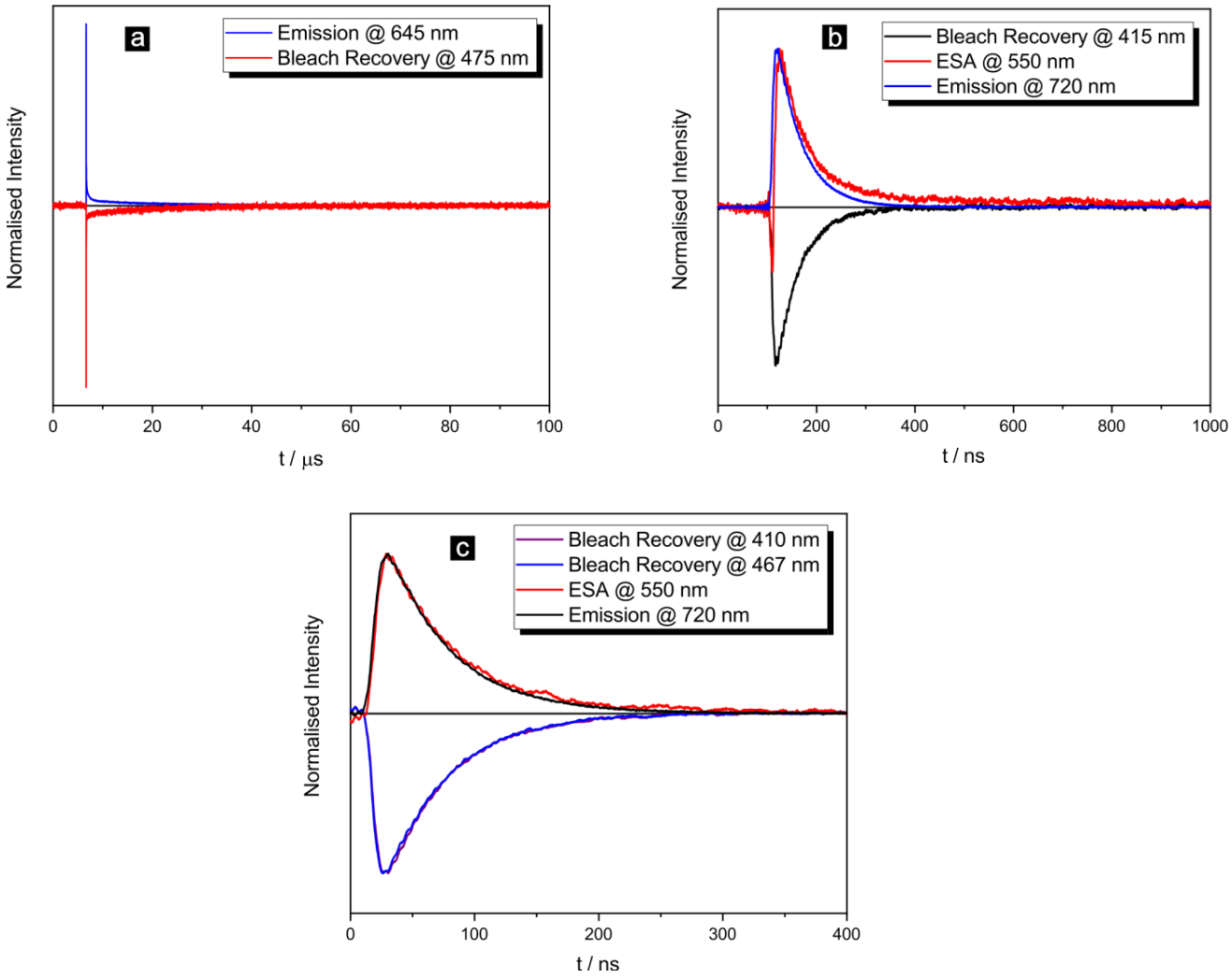


**Figure S57**. Single wavelength kinetics of **BPtSPyr** recorded in 20 µM THF solution at r.t. after laser excitation at a) 410 nm, b) 470 nm, or c) 532 nm for the different features of the transient absorption spectrum. The exponential decays can be fitted with a lifetime of 16.5 µs for a) and 50 ns for b) and c).

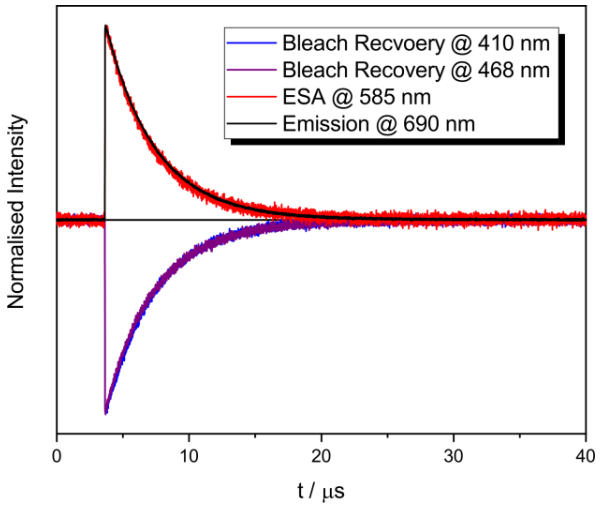


**Figure S58.** Single wavelength kinetics of **BPtSPyr** recorded in 20 µM toluene solution at r.t. after laser excitation at 532 nm for the different features of the transient absorption spectrum. The mono exponential decays can be fitted with a lifetime of 3.6 µs.

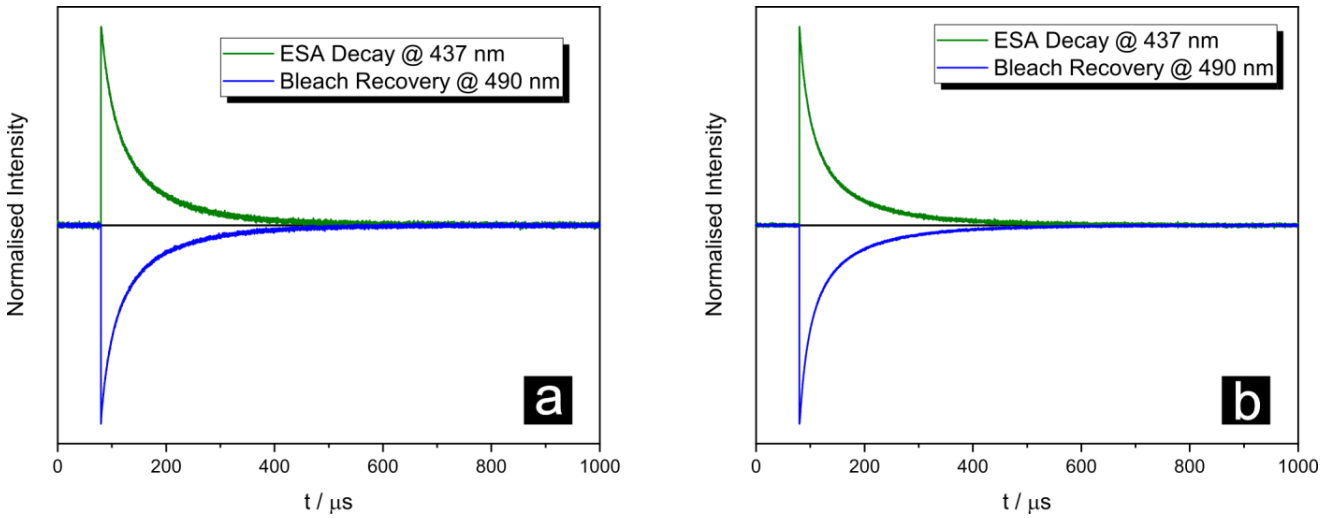


**Figure S59.** Single wavelength kinetics of **KBPtSPyr** recorded in 20 µM THF solution at r.t. after laser excitation at a) 420 nm and b) 500 nm for the different features of the transient absorption spectrum. Exponential decays can be fitted with a biexponential model with time constants of $\tau_1$ = 25.0 µs and $\tau_2$ = 104.6 µs for a) as well as $\tau_1$ = 23.8 µs and $\tau_2$ = 109.4 µs for b).

# Molecular Structures Obtained by Quantum Chemical Calculations

## Table S16. Atomic coordinates of the optimized ground state geometry of BPtSPyrSPtB in the neutral form

| Atom | x | y | z |
|---|---|---|---|
| Pt | 6.49556 | 0.14968 | -0.49673 |
| Pt | -6.49558 | 0.14969 | 0.49674 |
| B | 10.88273 | -1.17254 | 1.63173 |
| F | 10.98538 | -2.53431 | 1.90718 |
| F | 12.03966 | -0.5154 | 2.02584 |
| N | 10.62253 | -0.95724 | 0.12131 |
| N | 9.6482 | -0.57878 | 2.35255 |
| P | 5.93046 | -2.13228 | -0.59855 |
| P | 7.0656 | 2.43209 | -0.56242 |
| P | -5.93069 | -2.1323 | 0.59886 |
| P | -7.06539 | 2.43218 | 0.56219 |
| C | 8.27118 | -0.28686 | 0.34098 |
| C | 9.39499 | -0.6276 | -0.44204 |
| C | 9.55189 | -0.65526 | -1.84481 |
| H | 8.76529 | -0.43201 | -2.55379 |
| C | 10.87366 | -0.99745 | -2.1137 |
| H | 11.3466 | -1.10161 | -3.081 |
| C | 11.49631 | -1.17749 | -0.87076 |
| H | 12.51988 | -1.45476 | -0.65299 |
| C | 8.44168 | -0.25171 | 1.74342 |
| C | 7.54873 | 0.14467 | 2.76301 |
| H | 6.52899 | 0.46844 | 2.59841 |
| C | 8.2257 | 0.05502 | 3.97553 |
| H | 7.84946 | 0.29019 | 4.96204 |
| C | 9.51691 | -0.39776 | 3.67435 |
| H | 10.34378 | -0.59871 | 4.34361 |
| C | 7.28212 | -3.30345 | -0.1529 |
| H | 8.12582 | -3.07622 | -0.81391 |
| H | 7.61448 | -3.02726 | 0.85491 |
| C | 6.93268 | -4.78698 | -0.21778 |
| H | 7.80133 | -5.3826 | 0.08277 |
| H | 6.6566 | -5.09939 | -1.22988 |
| H | 6.10812 | -5.04761 | 0.45378 |
| C | 5.39938 | -2.63352 | -2.28781 |
| H | 5.17618 | -3.7071 | -2.2682 |
| H | 4.4574 | -2.10465 | -2.46919 |
| C | 6.40668 | -2.29985 | -3.38124 |
| H | 6.03778 | -2.6443 | -4.35328 |
| H | 7.37842 | -2.77438 | -3.20666 |
| H | 6.56354 | -1.21745 | -3.44356 |
| C | 4.50314 | -2.64332 | 0.44484 |
| H | 3.68883 | -1.94993 | 0.20874 |
| H | 4.18689 | -3.63995 | 0.11217 |
| C | 4.78836 | -2.6396 | 1.94265 |
| H | 3.87649 | -2.88251 | 2.49811 |
| H | 5.13566 | -1.65887 | 2.28196 |
| H | 5.55056 | -3.37712 | 2.21559 |
| C | 8.87192 | 2.76253 | -0.36974 |
| H | 9.13005 | 2.44437 | 0.64804 |
| H | 9.39579 | 2.07091 | -1.03825 |
| C | 9.3344 | 4.1944 | -0.62199 |
| H | 10.40778 | 4.27244 | -0.41837 |
| H | 8.82823 | 4.9208 | 0.02208 |
| H | 9.17573 | 4.49737 | -1.66201 |
| C | 6.30422 | 3.46499 | 0.76636 |
| H | 6.4002 | 2.88753 | 1.69321 |
| H | 6.93084 | 4.35674 | 0.88618 |
| C | 4.85388 | 3.87517 | 0.53335 |
| H | 4.48561 | 4.43087 | 1.40256 |
| H | 4.20308 | 3.00926 | 0.38549 |
| H | 4.75727 | 4.52763 | -0.34012 |
| C | 6.60975 | 3.25186 | -2.14198 |
| H | 5.52117 | 3.17775 | -2.22647 |
| H | 6.86514 | 4.31565 | -2.06484 |
| C | 7.27241 | 2.60853 | -3.35546 |
| H | 6.98418 | 1.55492 | -3.44063 |
| H | 8.36568 | 2.65667 | -3.30356 |
| H | 6.9596 | 3.1185 | -4.27266 |
| S | 4.3742 | 0.63959 | -1.57842 |
| C | 3.08496 | 0.58787 | -0.37513 |
| C | 1.72366 | 0.57844 | -0.78702 |
| C | 3.36853 | 0.58407 | 1.00031 |
| C | 0.68764 | 0.57635 | 0.19796 |
| C | 1.34537 | 0.56919 | -2.16893 |
| C | 2.36565 | 0.57064 | 1.95571 |
| H | 4.41076 | 0.58734 | 1.31016 |
| C | -0.68763 | 0.57626 | -0.19796 |
| C | 1.01548 | 0.57177 | 1.58407 |
| C | 0.03905 | 0.56525 | -2.5473 |
| H | 2.12942 | 0.56249 | -2.91935 |
| H | 2.62664 | 0.56474 | 3.01192 |
| C | -1.01547 | 0.57144 | -1.58407 |
| C | -1.72365 | 0.57843 | 0.78702 |
| C | -0.03904 | 0.56566 | 2.5473 |
| H | -0.22592 | 0.55626 | -3.60238 |
| C | -2.36564 | 0.57013 | -1.95571 |
| C | -3.08495 | 0.58769 | 0.37513 |
| C | -1.34536 | 0.56944 | 2.16893 |
| H | 0.22594 | 0.55687 | 3.60239 |
| C | -3.36852 | 0.58365 | -1.00031 |
| H | -2.62663 | 0.56405 | -3.01191 |
| H | -2.12941 | 0.5628 | 2.91936 |
| H | -4.41075 | 0.58678 | -1.31017 |
| S | -4.37419 | 0.63953 | 1.57841 |
| C | -8.2712 | -0.28679 | -0.34101 |
| C | -7.28246 | -3.30339 | 0.15332 |
| C | -5.3997 | -2.63339 | 2.28818 |
| C | -4.50339 | -2.6436 | -0.44445 |
| C | -8.87168 | 2.76279 | 0.36955 |
| C | -6.30394 | 3.46484 | -0.76673 |
| C | -6.60939 | 3.25208 | 2.14164 |
| C | -9.3951 | -0.62728 | 0.44199 |
| C | -8.44158 | -0.25193 | -1.74347 |
| H | -8.12615 | -3.07599 | 0.81429 |
| H | -7.61477 | -3.02728 | -0.85453 |
| C | -6.93319 | -4.78695 | 0.21838 |
| H | -5.17663 | -3.70701 | 2.26869 |
| H | -4.45764 | -2.10463 | 2.46951 |
| C | -6.40696 | -2.29948 | 3.38156 |
| H | -3.68901 | -1.95029 | -0.20837 |
| H | -4.18728 | -3.64025 | -0.11168 |
| C | -4.78856 | -2.63995 | -1.94226 |
| H | -9.1299 | 2.44452 | -0.64817 |
| H | -9.39559 | 2.07131 | 1.03819 |
| C | -9.33399 | 4.19474 | 0.62163 |
| H | -6.40001 | 2.88728 | -1.69351 |
| H | -6.93047 | 4.35664 | -0.88664 |
| C | -4.85355 | 3.87489 | -0.5338 |
| H | -5.52082 | 3.17783 | 2.22611 |
| H | -6.86465 | 4.31589 | 2.06438 |
| C | -7.2721 | 2.60897 | 3.35521 |
| N | -10.62262 | -0.95693 | -0.12139 |

| | | | | | | | |
|---|---|---|---|---|---|---|---|
| C | -9.5521 | -0.65468 | 1.84475 | H | -6.98401 | 1.55533 | 3.44049 |
| N | -9.64808 | -0.579 | -2.35263 | H | -8.36537 | 2.65727 | 3.30335 |
| C | -7.54849 | 0.1441 | -2.76308 | H | -6.95918 | 3.11901 | 4.27234 |
| H | -7.8019 | -5.38251 | -0.0821 | B | -10.88273 | -1.1725 | -1.63178 |
| H | -6.65713 | -5.09927 | 1.23051 | C | -11.4965 | -1.17689 | 0.87066 |
| H | -6.10867 | -5.04775 | -0.45317 | H | -8.76553 | -0.43138 | 2.55375 |
| H | -6.03812 | -2.64389 | 4.35364 | C | -10.87393 | -0.99667 | 2.11361 |
| H | -7.37876 | -2.77389 | 3.20702 | C | -9.51667 | -0.39828 | -3.67446 |
| H | -6.56367 | -1.21705 | 3.44378 | H | -6.52872 | 0.46776 | -2.59846 |
| H | -3.87671 | -2.88304 | -2.49767 | C | -8.22539 | 0.0543 | -3.97563 |
| H | -5.13569 | -1.65919 | -2.28166 | F | -10.9855 | -2.53431 | -1.90697 |
| H | -5.55087 | -3.37737 | -2.21518 | F | -12.03956 | -0.51532 | -2.02611 |
| H | -10.40738 | 4.27287 | 0.41807 | H | -12.52008 | -1.4541 | 0.65286 |
| H | -8.82778 | 4.921 | -0.02258 | H | -11.34695 | -1.10059 | 3.08089 |
| H | -9.17523 | 4.49784 | 1.6616 | H | -10.34351 | -0.59927 | -4.34374 |
| H | -4.48524 | 4.43044 | -1.40308 | H | -7.84904 | 0.28923 | -4.96216 |
| H | -4.20284 | 3.00893 | -0.38583 | | | | |
| H | -4.75687 | 4.52746 | 0.33959 | | | | |

**Table S17. Atomic coordinates of the optimized ground state geometry of BPtSPyrSPtB in the mono cationic form**

| Atom | x | y | z |
|---|---|---|---|
| Pt | -6.51214 | 0.14825 | 0.46749 |
| Pt | 6.51213 | 0.14801 | -0.46746 |
| B | -10.98114 | -1.08606 | -1.50195 |
| F | -11.07643 | -2.45733 | -1.72205 |
| F | -12.14898 | -0.44944 | -1.88894 |
| N | -10.68055 | -0.81448 | -0.00653 |
| N | -9.76615 | -0.51332 | -2.27512 |
| P | -6.08167 | -2.17409 | 0.60274 |
| P | -7.0156 | 2.45621 | 0.46323 |
| P | 6.08206 | -2.17441 | -0.6026 |
| P | 7.01513 | 2.45607 | -0.46342 |
| C | -8.32259 | -0.23006 | -0.31779 |
| C | -9.42688 | -0.5103 | 0.51043 |
| C | -9.54087 | -0.48939 | 1.91871 |
| H | -8.72715 | -0.26743 | 2.59777 |
| C | -10.86366 | -0.77736 | 2.2357 |
| H | -11.31137 | -0.83378 | 3.21868 |
| C | -11.52966 | -0.97466 | 1.01653 |
| H | -12.56785 | -1.22401 | 0.83812 |
| C | -8.53012 | -0.21359 | -1.71323 |
| C | -7.66279 | 0.14745 | -2.76889 |
| H | -6.62989 | 0.44783 | -2.64719 |
| C | -8.38529 | 0.0649 | -3.95406 |
| H | -8.0395 | 0.28124 | -4.95578 |
| C | -9.67742 | -0.34999 | -3.60168 |
| H | -10.53248 | -0.53621 | -4.23884 |
| C | -7.53174 | -3.26609 | 0.29481 |
| H | -8.29307 | -2.99019 | 1.03275 |
| H | -7.94579 | -2.97683 | -0.67812 |
| C | -7.25589 | -4.76569 | 0.3402 |
| H | -8.18404 | -5.31187 | 0.14217 |
| H | -6.88996 | -5.08801 | 1.32013 |
| H | -6.52618 | -5.0751 | -0.41486 |
| C | -5.45109 | -2.66442 | 2.26184 |
| H | -5.29652 | -3.75005 | 2.25326 |
| H | -4.46315 | -2.20088 | 2.36177 |
| C | -6.3482 | -2.24935 | 3.42209 |
| H | -5.91482 | -2.58526 | 4.36991 |
| H | -7.35064 | -2.6835 | 3.34402 |
| H | -6.45229 | -1.1598 | 3.46744 |
| C | -4.7679 | -2.78981 | -0.529 |
| H | -3.87897 | -2.17904 | -0.33666 |
| H | -4.52138 | -3.81326 | -0.22005 |
| C | -5.13841 | -2.747 | -2.00722 |
| H | -4.2904 | -3.07882 | -2.61503 |
| H | -5.40635 | -1.73514 | -2.32598 |
| H | -5.98591 | -3.40187 | -2.23457 |
| C | -8.81804 | 2.83115 | 0.35702 |
| H | -9.14579 | 2.47206 | -0.62617 |
| H | -9.32213 | 2.19295 | 1.09048 |
| C | -9.21745 | 4.28955 | 0.56144 |
| H | -10.29911 | 4.3904 | 0.42392 |
| H | -8.73503 | 4.9641 | -0.15307 |
| H | -8.98182 | 4.64078 | 1.57115 |
| C | -6.29003 | 3.40757 | -0.94207 |
| H | -6.45925 | 2.80503 | -1.84183 |
| H | -6.8862 | 4.31992 | -1.05835 |
| C | -4.81479 | 3.76484 | -0.79681 |
| H | -4.4667 | 4.26638 | -1.70585 |
| H | -4.19173 | 2.87943 | -0.64421 |
| H | -4.64705 | 4.4479 | 0.04152 |
| C | -6.44722 | 3.31452 | 1.98537 |
| H | -5.35861 | 3.20432 | 2.02576 |
| H | -6.66183 | 4.38448 | 1.87507 |
| C | -7.08089 | 2.753 | 3.25429 |
| H | -6.85219 | 1.68769 | 3.37034 |
| H | -8.17036 | 2.86471 | 3.25279 |
| H | -6.69358 | 3.27811 | 4.13338 |
| S | -4.36736 | 0.54635 | 1.51411 |
| C | -3.09626 | 0.45586 | 0.35468 |
| C | -1.72083 | 0.45244 | 0.78203 |
| C | -3.3715 | 0.41164 | -1.03488 |
| C | -0.68356 | 0.44415 | -0.19953 |
| C | -1.35539 | 0.44441 | 2.14881 |
| C | -2.36769 | 0.40166 | -1.97024 |
| H | -4.41229 | 0.39859 | -1.34705 |
| C | 0.68346 | 0.44396 | 0.1995 |
| C | -1.00494 | 0.42878 | -1.58411 |
| C | -0.03681 | 0.4304 | 2.53605 |
| H | -2.13555 | 0.44007 | 2.90279 |
| H | -2.61367 | 0.37907 | -3.02885 |
| C | 1.00483 | 0.42836 | 1.58408 |
| C | 1.72073 | 0.45214 | -0.78205 |
| C | 0.0367 | 0.43072 | -2.53608 |
| H | 0.21744 | 0.41659 | 3.59244 |
| C | 2.36758 | 0.40089 | 1.9702 |
| C | 3.09616 | 0.45521 | -0.3547 |
| C | 1.35529 | 0.44437 | -2.14884 |
| H | -0.21755 | 0.4171 | -3.59247 |
| C | 3.37139 | 0.41076 | 1.03485 |
| H | 2.61356 | 0.37812 | 3.02881 |
| H | 2.13545 | 0.43995 | -2.90281 |
| H | 4.41216 | 0.39739 | 1.34704 |
| S | 4.36728 | 0.54563 | -1.51413 |
| C | 8.32266 | -0.22988 | 0.31783 |
| C | 7.53231 | -3.26615 | -0.29465 |
| C | 5.45151 | -2.66493 | -2.26166 |
| C | 4.76843 | -2.79033 | 0.52918 |
| C | 8.81749 | 2.83142 | -0.35721 |
| C | 6.28929 | 3.4074 | 0.94177 |
| C | 6.44659 | 3.31408 | -1.98566 |
| C | 9.42701 | -0.50992 | -0.51038 |
| C | 8.5302 | -0.21325 | 1.71326 |
| H | 8.29357 | -2.99019 | -1.03264 |
| H | 7.94635 | -2.97674 | 0.67824 |
| C | 7.2567 | -4.7658 | -0.33988 |
| H | 5.2972 | -3.7506 | -2.25303 |
| H | 4.46345 | -2.20164 | -2.36155 |
| C | 6.34846 | -2.24969 | -3.42198 |
| H | 3.8794 | -2.17969 | 0.33686 |
| H | 4.52207 | -3.81382 | 0.22026 |
| C | 5.13898 | -2.74745 | 2.00739 |
| H | 9.14526 | 2.4726 | 0.62608 |
| H | 9.32175 | 2.19318 | -1.09051 |
| C | 9.21658 | 4.28986 | -0.56192 |
| H | 6.4587 | 2.80502 | 1.84161 |
| H | 6.88518 | 4.31994 | 1.05793 |
| C | 4.81393 | 3.76418 | 0.79648 |
| H | 5.358 | 3.20369 | -2.02603 |
| H | 6.66103 | 4.38409 | -1.87551 |
| C | 7.08035 | 2.75248 | -3.2545 |
| N | 10.68076 | -0.81373 | 0.00659 |
| C | 9.54099 | -0.48911 | -1.91866 |
| N | 9.76631 | -0.51261 | 2.27517 |
| C | 7.66279 | 0.14766 | 2.76889 |

| | | | | | | | |
|---|---|---|---|---|---|---|---|
| H | 8.18496 | -5.31181 | -0.14185 | H | 8.1698 | 2.86443 | -3.25305 |
| H | 6.89076 | -5.08828 | -1.31976 | H | 6.69289 | 3.27733 | -4.13367 |
| H | 6.52709 | -5.07524 | 0.41525 | B | 10.98147 | -1.08506 | 1.50204 |
| H | 5.91515 | -2.58583 | -4.36975 | C | 11.5299 | -0.97381 | -1.01646 |
| H | 7.35104 | -2.68351 | -3.3439 | H | 8.7272 | -0.26742 | -2.59774 |
| H | 6.4522 | -1.16011 | -3.46743 | C | 10.86384 | -0.7768 | -2.23564 |
| H | 4.29104 | -3.07941 | 2.61523 | C | 9.67754 | -0.34923 | 3.60172 |
| H | 5.40674 | -1.73555 | 2.32613 | H | 6.62982 | 0.44778 | 2.64717 |
| H | 5.9866 | -3.40217 | 2.23472 | C | 8.3853 | 0.06536 | 3.95408 |
| H | 10.29818 | 4.39101 | -0.42424 | F | 11.07719 | -2.45627 | 1.72228 |
| H | 8.73388 | 4.96448 | 0.15232 | F | 12.14911 | -0.44803 | 1.88894 |
| H | 8.98102 | 4.64078 | -1.57177 | H | 12.56815 | -1.2229 | -0.83804 |
| H | 4.46571 | 4.26578 | 1.70544 | H | 11.31154 | -0.83321 | -3.21862 |
| H | 4.19114 | 2.87857 | 0.64403 | H | 10.53264 | -0.5352 | 4.23889 |
| H | 4.64596 | 4.44705 | -0.04197 | H | 8.03946 | 0.28166 | 4.95578 |
| H | 6.85188 | 1.68709 | -3.37035 | | | | |

**Table S18. Atomic coordinates of the optimized ground state geometry of BPtSPyrSPtB in the dianionic form (open shell singlet).**

| Atom | x | y | z |
|---|---|---|---|
| Pt | -6.53504 | -0.102 | -0.53716 |
| Pt | 6.53501 | -0.10209 | 0.53714 |
| B | -10.96606 | 0.77625 | 1.70658 |
| F | -11.10188 | 2.11383 | 2.14663 |
| F | -12.14399 | 0.0926 | 2.05495 |
| N | -10.73246 | 0.73155 | 0.19453 |
| N | -9.74409 | 0.12153 | 2.35551 |
| P | -6.15803 | 2.20358 | -0.42564 |
| P | -7.06593 | -2.36339 | -0.77764 |
| P | 6.15791 | 2.20354 | 0.4254 |
| P | 7.06597 | -2.3634 | 0.7777 |
| C | -8.35209 | 0.16067 | 0.33672 |
| C | -9.49555 | 0.53089 | -0.41178 |
| C | -9.67585 | 0.72681 | -1.79918 |
| H | -8.89244 | 0.6277 | -2.54108 |
| C | -11.03372 | 1.04553 | -2.01142 |
| H | -11.51882 | 1.24568 | -2.95972 |
| C | -11.64808 | 1.04218 | -0.76898 |
| H | -12.67823 | 1.24173 | -0.50261 |
| C | -8.51805 | -0.07335 | 1.7251 |
| C | -7.61897 | -0.54946 | 2.70627 |
| H | -6.58259 | -0.80645 | 2.52155 |
| C | -8.32319 | -0.63516 | 3.92538 |
| H | -7.93902 | -0.97328 | 4.88063 |
| C | -9.61885 | -0.21343 | 3.67275 |
| H | -10.46534 | -0.12775 | 4.34202 |
| C | -7.61079 | 3.23483 | 0.04595 |
| H | -8.4038 | 2.98893 | -0.66909 |
| H | -7.96403 | 2.8456 | 1.00765 |
| C | -7.37509 | 4.73976 | 0.11506 |
| H | -8.29968 | 5.2468 | 0.41302 |
| H | -7.07242 | 5.15497 | -0.85243 |
| H | -6.60636 | 5.00417 | 0.84946 |
| C | -5.57771 | 2.90833 | -2.02597 |
| H | -5.43577 | 3.98839 | -1.89642 |
| H | -4.59131 | 2.46454 | -2.20232 |
| C | -6.5011 | 2.61261 | -3.20149 |
| H | -6.10521 | 3.0586 | -4.12089 |
| H | -7.50899 | 3.01114 | -3.0418 |
| H | -6.58967 | 1.53181 | -3.35588 |
| C | -4.82479 | 2.73695 | 0.73005 |
| H | -3.94209 | 2.14316 | 0.46875 |
| H | -4.58369 | 3.78638 | 0.51748 |
| C | -5.17521 | 2.55095 | 2.20261 |
| H | -4.30482 | 2.76953 | 2.83111 |
| H | -5.49744 | 1.52514 | 2.41179 |
| H | -5.98609 | 3.21909 | 2.51286 |
| C | -8.87298 | -2.72818 | -0.71623 |
| H | -9.18432 | -2.50021 | 0.31008 |
| H | -9.36264 | -1.97173 | -1.33962 |
| C | -9.30418 | -4.13354 | -1.12259 |
| H | -10.3861 | -4.24111 | -0.98585 |
| H | -8.8224 | -4.91245 | -0.52167 |
| H | -9.08607 | -4.33971 | -2.17591 |
| C | -6.3771 | -3.50238 | 0.50397 |
| H | -6.66037 | -3.06717 | 1.47011 |
| H | -6.9064 | -4.45981 | 0.41856 |
| C | -4.87085 | -3.7289 | 0.43094 |
| H | -4.54526 | -4.35483 | 1.26952 |
| H | -4.31638 | -2.78695 | 0.47528 |
| H | -4.58567 | -4.2421 | -0.49348 |
| C | -6.50807 | -3.09255 | -2.37405 |
| H | -5.41766 | -2.99834 | -2.39543 |
| H | -6.7495 | -4.16303 | -2.3727 |
| C | -7.11191 | -2.39115 | -3.58632 |
| H | -6.84459 | -1.32845 | -3.58977 |
| H | -8.20551 | -2.4607 | -3.59855 |
| H | -6.73806 | -2.83774 | -4.51434 |
| S | -4.3624 | -0.41164 | -1.6306 |
| C | -3.08413 | -0.3804 | -0.4207 |
| C | -1.71408 | -0.37701 | -0.81054 |
| C | -3.38484 | -0.38008 | 0.95303 |
| C | -0.6909 | -0.37722 | 0.18818 |
| C | -1.31558 | -0.37105 | -2.18613 |
| C | -2.3947 | -0.3734 | 1.92153 |
| H | -4.43316 | -0.3765 | 1.24538 |
| C | 0.6909 | -0.37726 | -0.18827 |
| C | -1.03802 | -0.37456 | 1.57017 |
| C | -0.00329 | -0.3703 | -2.54682 |
| H | -2.09074 | -0.36564 | -2.94592 |
| H | -2.6702 | -0.36884 | 2.97452 |
| C | 1.03803 | -0.37476 | -1.57026 |
| C | 1.71408 | -0.37698 | 0.81045 |
| C | 0.00329 | -0.36998 | 2.54673 |
| H | 0.27648 | -0.36485 | -3.59854 |
| C | 2.39471 | -0.37365 | -1.92162 |
| C | 3.08413 | -0.38049 | 0.42062 |
| C | 1.31559 | -0.37081 | 2.18604 |
| H | -0.27648 | -0.36436 | 3.59844 |
| C | 3.38484 | -0.38027 | -0.95312 |
| H | 2.67021 | -0.3692 | -2.97461 |
| H | 2.09075 | -0.36531 | 2.94582 |
| H | 4.43316 | -0.37674 | -1.24547 |
| S | 4.36238 | -0.41179 | 1.63055 |
| C | 8.35208 | 0.16071 | -0.33667 |
| C | 7.61072 | 3.23484 | -0.04591 |
| C | 5.57721 | 2.90834 | 2.02559 |
| C | 4.82486 | 2.73678 | -0.73058 |
| C | 8.87303 | -2.72809 | 0.71616 |
| C | 6.37709 | -3.50242 | -0.50386 |
| C | 6.50829 | -3.09267 | 2.37412 |
| C | 9.49545 | 0.53105 | 0.41194 |
| C | 8.5182 | -0.07333 | -1.72502 |
| H | 8.40358 | 2.98905 | 0.66933 |
| H | 7.96422 | 2.84558 | -1.0075 |
| C | 7.37495 | 4.73976 | -0.11517 |
| H | 5.43515 | 3.98837 | 1.8959 |
| H | 4.59086 | 2.46442 | 2.20183 |
| C | 6.50045 | 2.61285 | 3.20128 |
| H | 3.94214 | 2.14297 | -0.46939 |
| H | 4.58369 | 3.78621 | -0.51814 |
| C | 5.17554 | 2.55065 | -2.20306 |
| H | 9.18425 | -2.50006 | -0.31018 |
| H | 9.36269 | -1.97162 | 1.33952 |
| C | 9.3044 | -4.13341 | 1.12244 |
| H | 6.66028 | -3.06718 | -1.47001 |
| H | 6.90643 | -4.45983 | -0.4185 |
| C | 4.87086 | -3.72905 | -0.43073 |
| H | 5.41784 | -2.99896 | 2.39546 |
| H | 6.75016 | -4.16305 | 2.37277 |
| C | 7.11181 | -2.39103 | 3.58639 |
| N | 10.73241 | 0.73176 | -0.19423 |
| C | 9.67556 | 0.72708 | 1.79935 |
| N | 9.74429 | 0.12165 | -2.3553 |
| C | 7.61926 | -0.5495 | -2.70628 |

| | | | | | | | |
|---|---|---|---|---|---|---|---|
| H | 8.29956 | 5.24682 | -0.41301 | H | 8.20546 | -2.45998 | 3.59854 |
| H | 7.07211 | 5.15502 | 0.85226 | H | 6.73828 | -2.83789 | 4.51441 |
| H | 6.60633 | 5.00409 | -0.8497 | B | 10.96624 | 0.77628 | -1.70625 |
| H | 6.10432 | 3.05881 | 4.12058 | C | 11.64788 | 1.04256 | 0.76937 |
| H | 7.5083 | 3.01154 | 3.04176 | H | 8.89204 | 0.62797 | 2.54114 |
| H | 6.58916 | 1.53206 | 3.35575 | C | 11.03336 | 1.04596 | 2.01173 |
| H | 4.30528 | 2.7693 | -2.83173 | C | 9.61922 | -0.21331 | -3.67255 |
| H | 5.49767 | 1.52479 | -2.41212 | H | 6.58288 | -0.80656 | -2.52167 |
| H | 5.98656 | 3.21866 | -2.51321 | C | 8.32361 | -0.63515 | -3.92531 |
| H | 10.38629 | -4.24092 | 0.98545 | F | 11.10232 | 2.1138 | -2.1464 |
| H | 8.82252 | -4.91236 | 0.52165 | F | 12.14414 | 0.09244 | -2.05438 |
| H | 9.08657 | -4.33957 | 2.17582 | H | 12.67804 | 1.24218 | 0.50311 |
| H | 4.54525 | -4.35489 | -1.26938 | H | 11.51834 | 1.2462 | 2.96007 |
| H | 4.3163 | -2.78715 | -0.47486 | H | 10.46577 | -0.12755 | -4.34174 |
| H | 4.58581 | -4.24242 | 0.49363 | H | 7.93957 | -0.97328 | -4.88062 |
| H | 6.84392 | -1.32847 | 3.58993 | | | | |

**Table S19. Atomic coordinates of the optimized ground state geometry of KBPtSPyr in the neutral form.**

| Atom | x | y | z |
|---|---|---|---|
| Pt | -0.2733 | -0.3559 | 0.30649 |
| P | 0.0962 | -0.14906 | -2.01813 |
| P | -0.56161 | -0.5621 | 2.64025 |
| S | 1.95422 | -1.25618 | 0.6719 |
| C | -2.04865 | 0.20239 | 3.43146 |
| H | -1.7952 | 0.36064 | 4.48774 |
| H | -2.16693 | 1.19427 | 2.98067 |
| C | -2.24306 | 0.08702 | 0.0405 |
| F | -5.91295 | 0.96461 | -1.47464 |
| F | -6.10132 | 0.65198 | 0.77971 |
| C | 3.23363 | -0.09127 | 0.34638 |
| C | -2.74169 | 1.41159 | 0.12095 |
| C | -2.98465 | -2.37159 | -0.40169 |
| N | -4.51798 | -0.70371 | -0.43391 |
| C | 0.80832 | 0.11013 | 3.67693 |
| H | 0.61904 | -0.23378 | 4.70104 |
| H | 1.72607 | -0.373 | 3.32665 |
| C | -0.62703 | -2.34828 | 3.09578 |
| H | -1.52241 | -2.74898 | 2.60641 |
| H | 0.23107 | -2.81726 | 2.59959 |
| N | -4.09776 | 1.6929 | -0.0666 |
| C | 4.57609 | -0.53169 | 0.17543 |
| C | -0.66013 | 2.93523 | 0.64208 |
| H | -0.53901 | 3.45277 | 1.6021 |
| H | -0.21174 | 3.57807 | -0.1259 |
| H | -0.08832 | 2.00091 | 0.6835 |
| C | 3.97296 | 2.21576 | 0.04165 |
| H | 3.72415 | 3.274 | -0.00468 |
| C | 2.97204 | 1.28572 | 0.27318 |
| H | 1.9496 | 1.6202 | 0.41335 |
| C | 5.60836 | 0.42762 | -0.05145 |
| C | 7.29 | -1.38227 | -0.14739 |
| C | 4.94388 | -1.91636 | 0.22352 |
| H | 4.15937 | -2.64954 | 0.38266 |
| C | -2.09668 | 2.66214 | 0.36012 |
| C | 6.96105 | 0.00185 | -0.21238 |
| C | -4.29865 | 3.01891 | 0.04375 |
| C | -1.74741 | -3.20162 | -0.31223 |
| H | -1.47886 | -3.62539 | -1.28881 |
| H | -1.89494 | -4.05038 | 0.36779 |
| H | -0.88705 | -2.62352 | 0.04439 |
| C | -3.15749 | -0.96222 | -0.24321 |
| C | 5.30508 | 1.81769 | -0.12264 |
| C | -5.16077 | -1.85683 | -0.69515 |
| C | -4.2414 | -2.91882 | -0.68478 |
| C | 6.36001 | 2.75695 | -0.35256 |
| H | 6.10622 | 3.81347 | -0.40268 |
| C | 7.64837 | 2.34994 | -0.50363 |
| H | 8.44154 | 3.07335 | -0.67652 |
| C | 7.99371 | 0.96 | -0.43846 |
| C | -3.07619 | 3.65877 | 0.31098 |
| C | 6.23311 | -2.3225 | 0.07212 |
| H | 6.48204 | -3.38047 | 0.11221 |
| C | 8.62528 | -1.78045 | -0.30495 |
| H | 8.87107 | -2.83852 | -0.25454 |
| C | -0.63199 | -2.67705 | 4.58625 |
| H | -0.79519 | -3.75103 | 4.72671 |
| H | -1.42658 | -2.14934 | 5.12453 |
| H | 0.32159 | -2.42602 | 5.05997 |
| C | 9.31463 | 0.5165 | -0.59066 |
| H | 10.10018 | 1.24841 | -0.76299 |
| C | 0.96106 | 1.62664 | 3.66269 |
| H | 0.04297 | 2.13654 | 3.97407 |
| H | 1.23571 | 1.99439 | 2.67112 |
| H | 1.75454 | 1.92246 | 4.3573 |
| C | 9.62433 | -0.83839 | -0.52369 |
| H | 10.65468 | -1.16238 | -0.64384 |
| B | -5.21021 | 0.66167 | -0.30468 |
| C | -2.85978 | 5.13244 | 0.47085 |
| H | -3.72731 | 5.58721 | 0.96604 |
| H | -2.00773 | 5.30366 | 1.14077 |
| C | -5.6442 | 3.6381 | -0.11538 |
| H | -5.96972 | 3.60555 | -1.16132 |
| H | -5.62844 | 4.68216 | 0.2069 |
| H | -6.39281 | 3.09696 | 0.47054 |
| C | -2.60703 | 5.85236 | -0.85717 |
| H | -3.46109 | 5.7363 | -1.53388 |
| H | -1.72514 | 5.44337 | -1.36319 |
| H | -2.44141 | 6.92434 | -0.70016 |
| C | -6.62682 | -1.91135 | -0.95443 |
| H | -7.17698 | -1.35138 | -0.19255 |
| H | -6.97988 | -2.94543 | -0.95836 |
| H | -6.87041 | -1.45998 | -1.92277 |
| C | 1.48269 | -1.15568 | -2.69613 |
| H | 1.62092 | -0.84586 | -3.73902 |
| H | 2.38719 | -0.87883 | -2.14481 |
| C | -1.28995 | -0.61525 | -3.15676 |
| H | -0.82492 | -0.90249 | -4.10882 |
| H | -1.75088 | -1.51867 | -2.74343 |
| C | -4.54562 | -4.35708 | -0.97336 |
| H | -5.54892 | -4.60858 | -0.60664 |
| H | -3.85216 | -4.99655 | -0.41281 |
| C | 0.51019 | 1.58671 | -2.48723 |
| H | -0.37846 | 2.17743 | -2.23526 |
| H | 1.30299 | 1.91451 | -1.80689 |
| C | -3.35431 | -0.57947 | 3.32062 |
| H | -3.29209 | -1.54964 | 3.82413 |
| H | -3.64009 | -0.75394 | 2.2811 |
| H | -4.16096 | -0.01215 | 3.79717 |
| C | 1.25579 | -2.66165 | -2.62019 |
| H | 0.36884 | -2.97098 | -3.18385 |
| H | 1.14203 | -2.98659 | -1.58216 |
| H | 2.11674 | -3.1882 | -3.04634 |
| C | 0.93151 | 1.81887 | -3.93609 |
| H | 0.20581 | 1.42101 | -4.65294 |
| H | 1.90255 | 1.36283 | -4.15108 |
| H | 1.02569 | 2.89382 | -4.12479 |
| C | -2.36338 | 0.44141 | -3.40362 |
| H | -3.12997 | 0.02932 | -4.06891 |
| H | -1.95647 | 1.33515 | -3.8867 |
| H | -2.85808 | 0.75009 | -2.48045 |
| C | -4.45496 | -4.70443 | -2.46238 |
| H | -4.66993 | -5.76526 | -2.63442 |
| H | -3.45324 | -4.49385 | -2.854 |
| H | -5.17019 | -4.11389 | -3.04588 |

**Table S20. Atomic coordinates of the optimized ground state geometry of KBPtSPyr in the mono cationic form.**

| Atom | x | y | z |
|---|---|---|---|
| Pt | -0.24062 | -0.34303 | 0.1185 |
| P | -0.20528 | 0.04748 | -2.22592 |
| P | -0.36163 | -0.68054 | 2.46928 |
| S | 1.9887 | -1.2131 | 0.17979 |
| C | -1.6726 | 0.21137 | 3.41957 |
| H | -1.28617 | 0.31359 | 4.44177 |
| H | -1.73816 | 1.22165 | 3.00119 |
| C | -2.23089 | 0.06151 | 0.10259 |
| F | -6.01189 | 0.93337 | -1.00543 |
| F | -6.00404 | 0.55516 | 1.24852 |
| C | 3.26734 | -0.09106 | 0.01511 |
| C | -2.72154 | 1.37312 | 0.29885 |
| C | -2.97499 | -2.39255 | -0.36418 |
| N | -4.52452 | -0.75158 | -0.13637 |
| C | 1.16793 | -0.21649 | 3.38882 |
| H | 1.0125 | -0.52507 | 4.42953 |
| H | 1.98823 | -0.82482 | 2.99167 |
| C | -0.58999 | -2.47069 | 2.83657 |
| H | -1.56663 | -2.74288 | 2.4191 |
| H | 0.15766 | -3.0065 | 2.23941 |
| N | -4.09126 | 1.64189 | 0.26455 |
| C | 4.63463 | -0.55689 | 0.02915 |
| C | -0.61042 | 2.90054 | 0.69849 |
| H | -0.39718 | 3.29987 | 1.69842 |
| H | -0.25842 | 3.64666 | -0.02414 |
| H | -0.01578 | 1.98821 | 0.56924 |
| C | 4.04134 | 2.2018 | -0.26358 |
| H | 3.81923 | 3.25988 | -0.37307 |
| C | 3.02033 | 1.29789 | -0.1345 |
| H | 1.98943 | 1.63407 | -0.13433 |
| C | 5.68486 | 0.39539 | -0.10423 |
| C | 7.35211 | -1.41037 | 0.05251 |
| C | 4.97696 | -1.92697 | 0.16986 |
| H | 4.18518 | -2.6616 | 0.26958 |
| C | -2.06463 | 2.62062 | 0.53198 |
| C | 7.0394 | -0.0327 | -0.09142 |
| C | -4.29132 | 2.95866 | 0.45133 |
| C | -1.72227 | -3.19704 | -0.4744 |
| H | -1.57261 | -3.56428 | -1.49807 |
| H | -1.76493 | -4.08139 | 0.1733 |
| H | -0.83275 | -2.61911 | -0.19823 |
| C | -3.14863 | -0.99368 | -0.11998 |
| C | 5.39569 | 1.7826 | -0.25184 |
| C | -5.17701 | -1.90378 | -0.37159 |
| C | -4.24757 | -2.94951 | -0.51886 |
| C | 6.45735 | 2.71056 | -0.38209 |
| H | 6.21972 | 3.76452 | -0.4941 |
| C | 7.76423 | 2.2941 | -0.3678 |
| H | 8.56986 | 3.01621 | -0.46856 |
| C | 8.09168 | 0.91687 | -0.22257 |
| C | -3.05248 | 3.60359 | 0.62462 |
| C | 6.28403 | -2.33853 | 0.18139 |
| H | 6.51738 | -3.394 | 0.29109 |
| C | 8.70167 | -1.81509 | 0.06334 |
| H | 8.9344 | -2.87084 | 0.17345 |
| C | -0.48969 | -2.87638 | 4.30509 |
| H | -0.75277 | -3.93399 | 4.41117 |
| H | -1.16943 | -2.30189 | 4.94256 |
| H | 0.52574 | -2.74977 | 4.69151 |
| C | 9.42472 | 0.46931 | -0.20524 |
| H | 10.22564 | 1.19697 | -0.3041 |
| C | 1.52101 | 1.26486 | 3.3305 |
| H | 0.72448 | 1.8907 | 3.74616 |
| H | 1.71098 | 1.59243 | 2.30473 |
| H | 2.4277 | 1.45276 | 3.9147 |
| C | 9.7234 | -0.88287 | -0.0638 |
| H | 10.75858 | -1.20924 | -0.05299 |
| B | -5.21473 | 0.60499 | 0.09231 |
| C | -2.83713 | 5.07146 | 0.83169 |
| H | -3.65139 | 5.48618 | 1.4393 |
| H | -1.91988 | 5.22626 | 1.41333 |
| C | -5.65038 | 3.56695 | 0.44853 |
| H | -6.06683 | 3.58578 | -0.56508 |
| H | -5.61525 | 4.5923 | 0.82422 |
| H | -6.33803 | 2.98407 | 1.0676 |
| C | -2.74123 | 5.85631 | -0.48009 |
| H | -3.66079 | 5.7519 | -1.0665 |
| H | -1.91131 | 5.49193 | -1.09638 |
| H | -2.57924 | 6.92314 | -0.28948 |
| C | -6.66161 | -1.97494 | -0.46207 |
| H | -7.12672 | -1.45405 | 0.37971 |
| H | -6.99927 | -3.01391 | -0.46887 |
| H | -7.01907 | -1.48897 | -1.37688 |
| C | 1.15458 | -0.81422 | -3.12368 |
| H | 1.14449 | -0.43812 | -4.15357 |
| H | 2.10354 | -0.49876 | -2.67589 |
| C | -1.68984 | -0.45764 | -3.21043 |
| H | -1.31769 | -0.67174 | -4.22066 |
| H | -2.04474 | -1.40713 | -2.79704 |
| C | -4.56896 | -4.3784 | -0.83316 |
| H | -5.50287 | -4.66883 | -0.3357 |
| H | -3.79094 | -5.02843 | -0.41415 |
| C | 0.03598 | 1.83483 | -2.60727 |
| H | -0.84545 | 2.34716 | -2.20311 |
| H | 0.88812 | 2.17767 | -2.01158 |
| C | -3.05745 | -0.42935 | 3.45002 |
| H | -3.03965 | -1.42251 | 3.90913 |
| H | -3.49345 | -0.52166 | 2.45369 |
| H | -3.72769 | 0.19706 | 4.04788 |
| C | 1.03683 | -2.33515 | -3.12458 |
| H | 0.12088 | -2.66939 | -3.62269 |
| H | 1.041 | -2.74228 | -2.10873 |
| H | 1.88387 | -2.7719 | -3.66351 |
| C | 0.25459 | 2.19015 | -4.07649 |
| H | -0.53774 | 1.80377 | -4.72509 |
| H | 1.21106 | 1.80939 | -4.44658 |
| H | 0.26937 | 3.27935 | -4.18869 |
| C | -2.84471 | 0.53763 | -3.28543 |
| H | -3.6427 | 0.11035 | -3.9018 |
| H | -2.54476 | 1.48295 | -3.74732 |
| H | -3.26845 | 0.7578 | -2.30404 |
| C | -4.69605 | -4.6495 | -2.33525 |
| H | -4.92192 | -5.70448 | -2.52681 |
| H | -3.76634 | -4.40118 | -2.85978 |
| H | -5.49735 | -4.04556 | -2.77547 |

**Table S21. Atomic coordinates of the optimized ground state geometry of KBPtSPyr in the mono anionic form.**

| Atom | x | y | z |
|---|---|---|---|
| Pt | -0.24696 | -0.38864 | 0.26415 |
| P | -4.9E-4 | -0.12303 | -2.05273 |
| P | -0.56574 | -0.59201 | 2.5762 |
| S | 2.0053 | -1.31351 | 0.5796 |
| C | -2.01668 | 0.24421 | 3.36215 |
| H | -1.75418 | 0.41674 | 4.41456 |
| H | -2.09789 | 1.22436 | 2.87832 |
| C | -2.23336 | 0.0855 | 0.03248 |
| F | -5.9498 | 1.02268 | -1.3643 |
| F | -6.08176 | 0.67499 | 0.88672 |
| C | 3.28241 | -0.14902 | 0.27935 |
| C | -2.72006 | 1.42647 | 0.14888 |
| C | -3.03295 | -2.36312 | -0.41913 |
| N | -4.53263 | -0.67609 | -0.38893 |
| C | 0.83184 | 2.8E-4 | 3.62859 |
| H | 0.62597 | -0.32208 | 4.65677 |
| H | 1.72099 | -0.53559 | 3.27921 |
| C | -0.71226 | -2.37395 | 3.04152 |
| H | -1.61281 | -2.74186 | 2.53577 |
| H | 0.13459 | -2.87805 | 2.55944 |
| N | -4.0798 | 1.70994 | 0.00401 |
| C | 4.64077 | -0.56473 | 0.16238 |
| C | -0.62632 | 2.93228 | 0.6427 |
| H | -0.45988 | 3.42181 | 1.6135 |
| H | -0.17594 | 3.58719 | -0.11819 |
| H | -0.06371 | 1.98925 | 0.64792 |
| C | 3.99266 | 2.16524 | -0.05933 |
| H | 3.72668 | 3.21754 | -0.1405 |
| C | 3.00155 | 1.22398 | 0.16236 |
| H | 1.96708 | 1.53816 | 0.25952 |
| C | 5.66253 | 0.40674 | -0.05829 |
| C | 7.3784 | -1.37437 | -0.06095 |
| C | 5.03204 | -1.93949 | 0.25791 |
| H | 4.25452 | -2.68068 | 0.41546 |
| C | -2.0726 | 2.66583 | 0.38965 |
| C | 7.0272 | 0.00206 | -0.16946 |
| C | -4.28584 | 3.05772 | 0.14558 |
| C | -1.80347 | -3.21271 | -0.37784 |
| H | -1.51272 | -3.58671 | -1.37154 |
| H | -1.94761 | -4.10108 | 0.25457 |
| H | -0.9425 | -2.65586 | 0.01614 |
| C | -3.17328 | -0.96091 | -0.24536 |
| C | 5.33763 | 1.78918 | -0.17297 |
| C | -5.22191 | -1.83385 | -0.6385 |
| C | -4.32746 | -2.89341 | -0.66594 |
| C | 6.38193 | 2.74054 | -0.39485 |
| H | 6.11121 | 3.79093 | -0.47888 |
| C | 7.68214 | 2.35443 | -0.499 |
| H | 8.46703 | 3.08807 | -0.66709 |
| C | 8.0497 | 0.97323 | -0.38993 |
| C | -3.06804 | 3.67742 | 0.38476 |
| C | 6.33205 | -2.32732 | 0.15362 |
| H | 6.59791 | -3.37934 | 0.22945 |
| C | 8.72482 | -1.75192 | -0.17119 |
| H | 8.98742 | -2.80396 | -0.08761 |
| C | -0.75331 | -2.7031 | 4.53132 |
| H | -0.95947 | -3.77007 | 4.67252 |
| H | -1.53533 | -2.14411 | 5.05646 |
| H | 0.20089 | -2.48692 | 5.02147 |
| C | 9.38228 | 0.54974 | -0.49386 |
| H | 10.15964 | 1.29159 | -0.66176 |
| C | 1.07407 | 1.50479 | 3.59551 |
| H | 0.1956 | 2.06932 | 3.92746 |
| H | 1.33319 | 1.84522 | 2.58982 |
| H | 1.90474 | 1.76391 | 4.26163 |
| C | 9.7131 | -0.79744 | -0.38515 |
| H | 10.75208 | -1.10572 | -0.46848 |
| B | -5.1874 | 0.68881 | -0.21732 |
| C | -2.82405 | 5.14568 | 0.56466 |
| H | -3.7128 | 5.62738 | 0.99428 |
| H | -2.01856 | 5.29832 | 1.29709 |
| C | -5.64552 | 3.6639 | 0.04524 |
| H | -6.0726 | 3.54274 | -0.95774 |
| H | -5.60603 | 4.73358 | 0.27358 |
| H | -6.34726 | 3.18692 | 0.73984 |
| C | -2.4516 | 5.86958 | -0.7333 |
| H | -3.25615 | 5.7778 | -1.47208 |
| H | -1.54657 | 5.43882 | -1.17743 |
| H | -2.26769 | 6.93765 | -0.56112 |
| C | -6.7029 | -1.84421 | -0.81984 |
| H | -7.21051 | -1.39285 | 0.04101 |
| H | -7.06915 | -2.86835 | -0.94109 |
| H | -7.00952 | -1.26324 | -1.69786 |
| C | 1.38316 | -1.07699 | -2.81627 |
| H | 1.49241 | -0.73695 | -3.85328 |
| H | 2.29634 | -0.80407 | -2.27625 |
| C | -1.41992 | -0.58878 | -3.15061 |
| H | -0.98685 | -0.88809 | -4.11458 |
| H | -1.87388 | -1.47975 | -2.70456 |
| C | -4.64781 | -4.33128 | -0.94451 |
| H | -5.68856 | -4.54547 | -0.66734 |
| H | -4.03024 | -4.97989 | -0.30675 |
| C | 0.36393 | 1.63095 | -2.50259 |
| H | -0.52912 | 2.19481 | -2.20805 |
| H | 1.16722 | 1.96482 | -1.83771 |
| C | -3.35304 | -0.48479 | 3.26277 |
| H | -3.33002 | -1.45385 | 3.77292 |
| H | -3.64048 | -0.64847 | 2.22213 |
| H | -4.13551 | 0.11872 | 3.73655 |
| C | 1.18108 | -2.58794 | -2.77575 |
| H | 0.28854 | -2.89432 | -3.33245 |
| H | 1.08182 | -2.93715 | -1.74413 |
| H | 2.04208 | -3.09574 | -3.22524 |
| C | 0.73913 | 1.90608 | -3.95653 |
| H | 0.00473 | 1.50309 | -4.66195 |
| H | 1.71487 | 1.47904 | -4.2085 |
| H | 0.80088 | 2.98684 | -4.12741 |
| C | -2.4972 | 0.47054 | -3.3671 |
| H | -3.29007 | 0.0568 | -4.00087 |
| H | -2.1057 | 1.36019 | -3.87118 |
| H | -2.95031 | 0.78083 | -2.42338 |
| C | -4.43407 | -4.73578 | -2.40661 |
| H | -4.66585 | -5.79588 | -2.56974 |
| H | -3.39488 | -4.56712 | -2.71243 |
| H | -5.07347 | -4.14151 | -3.06966 |

## References


1. M. A. Cairns, K. R. Dixon and G. A. Rivett, *J. Organomet. Chem.*, 1979, **171**, 373-385.
2. P. Irmler, F. S. Gogesch, C. B. Larsen, O. S. Wenger and R. F. Winter, *Dalton Trans.*, 2019, **48**, 1171-1174.
3. P. Irmler and R. F. Winter, *Dalton Trans.*, 2016, **45**, 10420-10434.
4. P. Irmler, F. S. Gogesch, C. B. Larsen, O. S. Wenger and R. F. Winter, *Dalton Trans.*, 2019, **48**, 1171-1174.
5. F. Wilkinson, W. P. Helman and A. B. Ross, *J. Phys. Chem. Ref. Data*, 1993, **22**, 113-262.

# 6 Summary

Within this dissertation the family of platinated BDP dyes was expanded by a number of efficient triplet sensitizers. The first project focused on the influence of the ligand X in the *trans*-position to the BDP chromophore. Our hope was that the $\sigma$-*trans*-influence of the respective ligand X would empower the target complexes with an increased phosphorescence and triplet state quantum yield, respectively. In this project, we have reported on the synthesis and the spectroscopic and photophysical properties of five new complexes *trans*-Pt(BDP)X($PEt_3$)$_2$ (**Pt–X**, $X^-$ = $Cl^-$, $I^-$, $NO_2^-$, $NCS^-$, $CH_3^-$, see Fig. 29). All complexes are dual fluorescence and phosphorescence emitters from BDP-centered $^{1/3}\pi\pi^*$ states. The phosphorescence quantum yields increased parallel to a lengthening of the Pt–$C_{BDP}$ bond lengths in the order **Pt–NO$_2$** < **Pt–NCS** < **Pt–Cl** < **Pt–I** in parallel with the $\sigma$-*trans*-influence of the ligand $X^-$. For **Pt-I** an exceptionally high phosphorescence quantum yield of 40% in solution at r.t. was observed. Although the alterations of the Pt-C8 bond length are rather small, they have a measurable effect on $k_{isc}$. An other important finding was that the ratio of phosphorescence to fluorescence intensities of each complex depends on the excitation wavelength. As highlighted in the introduction, the larger the MLCT character of either the corresponding singlet or triplet state, the stronger is the spin-orbit coupling integral. This can be referred to as the expansion of El-Sayed's rule to metalorganic complexes. In addition the similar orbital characters of the $S_1$ and the $T_1$ state leads to a negligible SOC and hence a low $k_{isc}$ via the internal heavy-atom effect. In our case both concepts are mingled: excitation into a higher excited state than the BDP-based $\pi \rightarrow \pi^*$ state with appreciable Pt($PEt_3$)$_2$ $\rightarrow$ BDP (ML $\rightarrow$ L') charge transfer character results in a larger rate constant $k_{isc}$. Thus, a considerable admixture

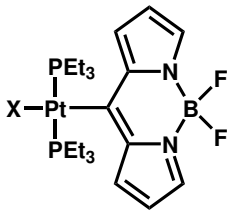


**Pt-Cl**: X = Cl
**Pt-I** / **8-Pt** / **BPtI**: X = I
**Pt-NO$_2$**: X = $NO_2$
**Pt-NCS**: X = NCS,
**Pt-CH$_3$**: X = $CH_3$

Figure 29: Overview of the synthesized and characterized complexes included in publication one.

of MLCT into the higher-energy absorption offers a more direct pathway for Pt-triggered ISC than just the external heavy atom effect. Additional studies into phosphorescence quenching by $^3O_2$ have yielded exceptionally large Stern-Volmer quenching constants of ca. 2000 $bar^{-1}$ and demonstrated that these complexes are excellent one-component sensors for triplet molecules. Moreover, this set of complexes constitute highly efficient sensitizers for photocatalytic reactions involving $^1O_2$ as the reactant, combining exceptionally high quantum efficiencies near unity for $^1O_2$ generation with good photostabilities, even in the presence of a large excess of molecular oxygen. This renders the **Pt-X** complexes of this series highly potent candidates for the application in photocatalysis and more specifically in photodynamic therapy for cancer treatment.

The second project dealt with the influence of the attachment site of the platinum fragment at the BDP dye. In the introduction to this dissertation we discussed how crucial the position of the binding of the heavy-atom to the chromophore in terms of the 'internal' vs. 'external heavy-atom effect' is. In the resulting publication, five new platinum BDP complexes, where a *trans*-$Pt(PEt_3)_2I$ moiety attaches to the pyrrolic carbon atom C2 or C3 of the BDP dye via a direct Pt-BDP $\sigma$-bond, have been reported (see Fig. 30). During the synthesis of **3-Pt** a higher activation barrier for the oxidative addition of the $Pt(PEt_3)_2$ fragment to a $C_{aryl}$-Cl bond as compared to a $C_{aryl}$-I or $C_{aryl}$-Br bond has also allowed us to isolate **8,9-Pt** as an intermediate of the oxidative addition. In this complex, the BDP ligand $\eta^2$-coordinates to the zerovalent platinum atom (similar to **Pt-4a** discussed in the Introduction). **8,9-Pt** was thermally converted to **3-Cl-Pt**. As a main difference to **8-Pt**, platinum attachment to either position C2 or C3 puts the $Pt(PEt_3)_2I$ entity within the conjugated $\pi$-system and thus induces a sizable red-shift of the characteristic BDP absorption band along with a broadening of the $\pi\pi^*$ absorption band for the 2-isomers. Nevertheless, the dominant absorption and emission features are BDP $\pi\pi^*$

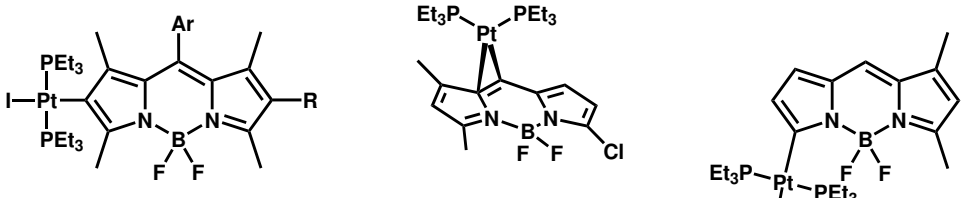


**2-Pt-6H**: Ar = Ph, R = H
**2-Pt-6I**: Ar = Ph, R = I
**2-Pt-6Et**: Ar = Ph, R = Et
**2-Pt-Mes-6I**: Ar = Mes, R = I

**8,9-Pt**

**3-Pt**

Figure 30: Complexes discussed in the second publication.

transitions. The complexes show rich electrochemical behavior, which we probed for by cyclic voltammetry, UV/Vis-NIR-spectroelectrochemistry and by EPR spectroscopy on their one-electron oxidized and reduced forms. In parallel to **8-Pt**, all complexes where the Pt ion is bonded to carbon atom C2 dually emit through fluorescence and phosphorescence with phosphorescence emissions well in the NIR, between 797 and 815 nm. However, quantum yields for the phosphorescence are very modest with values of 0.14% or lower. Nevertheless, all complexes are active sensitizers for photochemical $^1O_2$ generation and therefore may be considered as candidates for photodynamic therapy. Our results show that the attachment of a Pt(II) ion to either the 2- or 3-position is no viable route to Pt-BDP dyes with intense NIR phosphorescence emission. The reduced triplet state quantum yield is most likely the consequence of an interplay between a reduced 'external heavy-atom effect' due to the larger distance between the chromophore and the Pt ion compared to **8-Pt**, and an increased 'internal heavy-atom effect' (due to a larger number of CT states) that, however, cannot compensate for the former.

In addition, the low energy of the $^3\pi\pi^*$ excited state makes the energy-gap law an important player in terms of promoting radiationless decay. It is also very likely that for Pt-BDP complexes with attachment to C8, the *meso*-position of the BDP, the $Pt(PEt_3)_2I$ entity acts, in addition to the 'external heavy-atom effect', as an electron donor. In parallel to the dimethylaniline-BDP compound discussed in the introduction, this would promote the ISC.

The third project within this dissertation, which resulted in publications 3 and 4, dealt with dyads comprising of a BDP and a mercaptopyrene dye within the coordination sphere of a platinum ion. This project complements the studies of Filatov *et al.*, Zhang *et al.* and others, which have been discussed in the last part of the introduction. Their *meso*-linked BDP dyads did not exhibit an emission from the triplet excited states. We presented three dyads of the type *trans*-Pt($\sigma$-BDP)$(PEt_3)_2$(SPyr) and related model compounds that contain only one of the chromophore ligands as depicted in Fig. 31. Our working hypothesis - that has proven true - was that the design of our dyads would increase the spin-orbit coupling and in consequence would lead to a fast rate constant for the $T_n \rightarrow S_0$ transition. Thus, this should open a radiative transition for the charge-separated triplet state. We employed some variations over the basic dyad motif in order to be able to study the complex deactivation cascades of our dyads. While the peralkylated **KBPtSPyr** emits solely from the BDP $\pi\pi^*$ singlet and triplet states, the dyads **BPtSPyr** and **BPtSPyrSPtB** emit via four different radiative channels, including the charge-separated $^3$PB-CT state and the BDP-based $^1\pi\pi^*$ and $^3\pi\pi^*$ state at r.t., as well as the BDP- and SPyr-based

$^3\pi\pi^*$ excited states at 77 K. Transient absorption spectroscopy studies and the related band assignments of the excited CT states via UV/Vis-NIR-spectroelectrochemistry have provided a comprehensive picture of the interrelations between the various deactivation channels. For **BPtSPyr** TA spectroscopy has revealed the presence of a $SPyr^{+\bullet}$ radical cation as a substantial part of the PB-CT excited state. Also a bleach of the SPyr and BDP ground state absorption signals were observed. **KBPtSPyr**, which shows only emission from the $^{1/3}\pi\pi^*$ states, exhibits similar TA features as **BPtI** and corresponding BDP dyes and lacks any ESA signature of an excited PB-CT or $^3\pi\pi^*$ state of the mercaptopyrene ligand. This proves a fast energy transfer from the SPyr-centered excited states to energetically lower BDP-centered excited states. **KBPtSPyr** and **BPtSPyr** act as panchromatic sensitizers for the generation of singlet oxygen. This project showed, how a platinum ion can open a variety of deactivation channels, including phosphorescence emission from a triplet charge-separated state with an exceptionally high quantum yield of 15% in the NIR. The donor-acceptor dyad design with orthogonal arrangement opens the opportunity for a heavy-atom free ISC, but for a phosphorescence from the respective triplet excited states, the coordination to a platinum ion seems to be crucial in order to accelerate the backward $T_n \rightarrow S_0$ ISC rate.

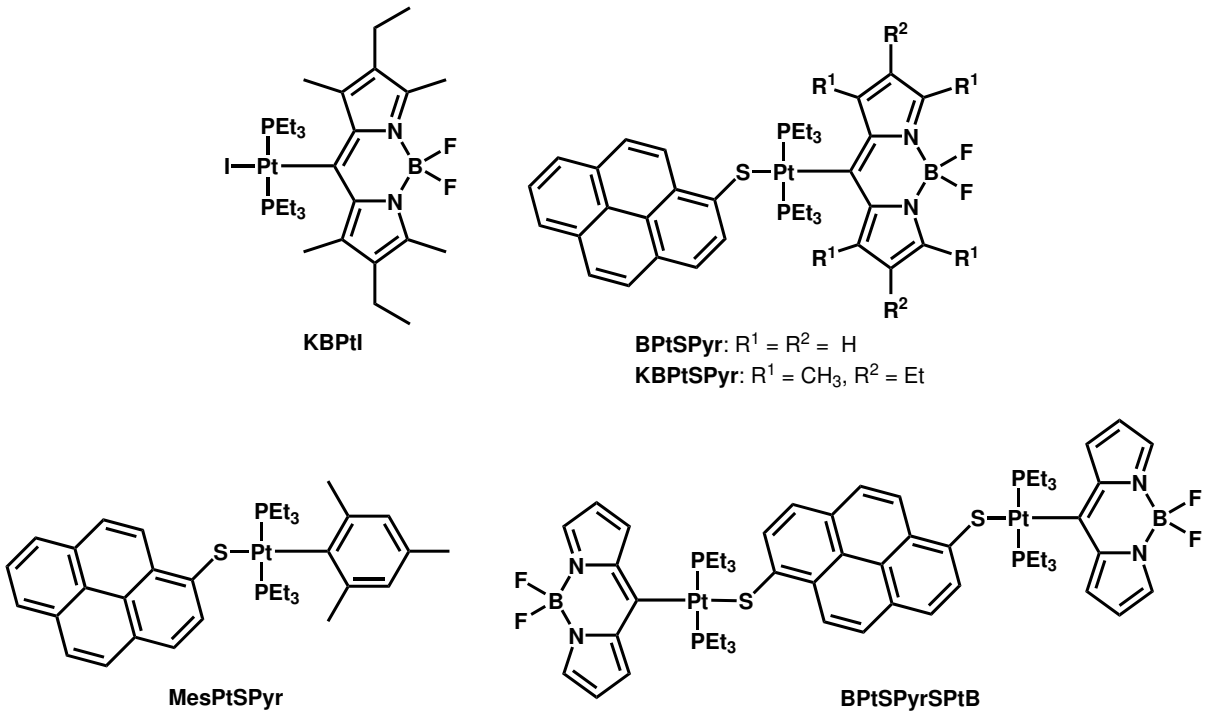


Figure 31: $Pt(BDP)(PEt_3)_2$(S-Pyrene) dyads and corresponding control compounds reported in publications 3 and 4.

# 7 Zusammenfassung

Im Rahmen dieser Dissertation wurde die wichtige Familie der BDP-Farbstoffe um eine Reihe effizienter Triplett-Sensibilisatoren auf Basis von Platinkomplexen mit BDP-Liganden erweitert. Das erste Projekt konzentrierte sich auf den Einfluss des Liganden in der *trans*-Position des BDP-Chromophors. Die Arbeitshypothese war, dass der $\sigma$-*trans*-Einfluss des jeweiligen Liganden X die Phosphoreszenz- bzw. Triplett-Quantenausbeute unserer Zielkomplexe beeinflusst. In der aus diesem Projekt hervorgegangenen Publikation berichteten wir über die Synthese und die spektroskopischen und photophysikalischen Eigenschaften von fünf neuen Komplexen des Typs *trans*-Pt(BDP)X$(PEt_3)_2$ (**Pt-X**, $X^- = Cl^-$, $I^-$, $NO_2^-$, $NCS^-$, $CH_3^-$, siehe Abb. 32). Die duale Fluoreszenz und Phosphoreszenz aller Komplexe entspringt dem Singulett bzw. Triplett $\pi\pi^*$ Zustand des BDP-Chromophors. Der Komplex **Pt-CH$_3$** erwies sich als derart photolabil, dass keine Aussagen zu dessen photophysikalischen Eigenschaften möglich sind. Die Phosphoreszenzquantenausbeuten stiegen mit zunehmender Pt-$C_{BDP}$-Bindungslänge in der Reihenfolge **Pt-NO$_2$** < **Pt-NCS** < **Pt-Cl** < **Pt-I**, parallel zu steigendem $\sigma$-*trans*-Einfluss des Liganden $X^-$. Für **Pt-I** wurde eine außergewöhnlich hohe Phosphoreszenzquantenausbeute von 40% in Lösung bei Raumtemperatur beobachtet. Obwohl der Pt-C8 Abstand in der beschriebenen Reihung nur kleineren Änderungen unterliegt, hat dies einen merklichen Einfluss auf $k_{isc}$. Ein weiteres wichtiges Ergebnis war, dass das Verhältnis der Intensitäten der Phosphoreszenz- und der Fluoreszenzemission eines jeden Komplexes von der Anregungswellenlänge abhängt. Wie in der Einleitung hervorgehoben wurde, gilt: Je größer der MLCT-Charakter entweder des Singulett- oder des Triplett-Zustandes ist, desto größer ist das Spin-Bahn-Kopplungsintegral. Dies kann als die Erweiterung

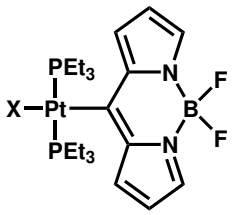


**Pt-Cl**: X = Cl
**Pt-I** / **8-Pt** / **BPtI**: X = I
**Pt-NO$_2$**: X = $NO_2$
**Pt-NCS**: X = NCS,
**Pt-CH$_3$**: X = $CH_3$

Abbildung 32: Überblick über die synthetisierten und charakterisierten Komplexe, welche in Publikation eins enthalten sind.

der Regel von El-Sayed auf metallorganische Komplexe bezeichnet werden. Zusätzlich führen die gleichen Orbitalcharaktere des $S_1$- und des $T_1$-Zustands zu einer vernachlässigbar kleinen Spin-Bahn-Kopplung und damit zu einer kleineren Ratenkonstante $k_{\mathrm{isc}}$. In unserem Fall werden beide Konzepte kombiniert: Anregung in einen höher angeregten Zustand als der BDP-basierte $\pi \rightarrow \pi^*$ Zustand mit nennenswertem $Pt(PEt_3)_2 \rightarrow$ BDP (ML $\rightarrow$ L') Ladungstransfer-Charakter führt zu einer größeren Geschwindigkeitskonstante $k_{\mathrm{isc}}$. Somit bietet eine beträchtliche Beimischung von MLCT Zuständen in der Absorption bei höherer Energie einen direkteren Weg für Pt-getriggertes ISC als lediglich der 'externe Schweratomeffekt'. Dieses Konzept wurde in der Einleitung unter dem Stichwort 'interner Schweratomeffekt' eingeführt. Zusätzliche Studien zur Phosphoreszenz-Löschung mittels $^3O_2$ haben außergewöhnlich große Stern-Volmer Löschkonstanten von ca. 2000 $bar^{-1}$ ergeben und gezeigt, dass diese Komplexe ausgezeichnete Einkomponentensensoren für Triplettmoleküle sind. Darüber hinaus bilden sie hocheffiziente Sensibilisatoren für photokatalytische Reaktionen mit $^1O_2$ als Reaktionspartner. Außergewöhnlich hohe Quantenausbeuten von nahe 100% für die Generierung von $^1O_2$ und gute Photostabilitäten wurden beobachtet. Damit sind die **Pt-X**-Komplexe dieser Serie hochaktive Kandidaten für den Einsatz in der Photokatalyse und, potenziell, in der photodynamischen Therapie zur Krebsbehandlung.

Das zweite Projekt beschäftigte sich mit dem Einfluss der Position der Anbindung der Platineinheit an den BDP-Farbstoff. In der Einleitung zu dieser Dissertation wird diskutiert, wie entscheidend die Position der Anbindung des Schweratoms an den Chromophor im Hinblick auf das Zusammenspiel zwischen 'internem' und 'externem' Schweratomeffekt ist. In der aus diesem Projekt resultierenden Publikation wurden fünf neue Platin-BDP-Komplexe vorgestellt, in denen eine *trans*-$Pt(PEt_3)_2I$-Einheit an das pyrrolische Kohlenstoffatom C2 oder C3 eines BDP-Farbstoffs über eine direkte Pt-BDP $\sigma$-Bindung bindet

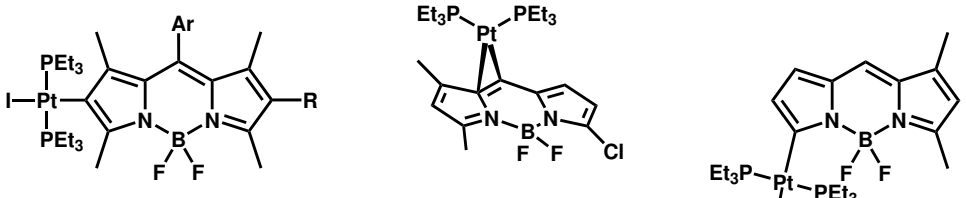


**2-Pt-6H**: Ar = Ph, R = H
**2-Pt-6I**: Ar = Ph, R = I
**2-Pt-6Et**: Ar = Ph, R = Et
**2-Pt-Mes-6I**: Ar = Mes, R = I

**8,9-Pt**

**3-Pt**

Abbildung 33: Komplexe, die in der zweiten Veröffentlichung diskutiert wurden.

(siehe Abb. 33). Während der Synthese von **3-Pt** hat uns eine höhere Aktivierungsbarriere für die oxidative Addition des $Pt(PEt_3)_2$-Fragments an eine $C_{aryl}$-Cl-Bindung im Vergleich zu einer $C_{aryl}$-I- oder $C_{aryl}$-Br-Bindung zusätzlich erlaubt den Komplex **8,9-Pt** als Zwischenprodukt der oxidativen Addition zu isolieren. In diesem Komplex koordiniert der BDP-Ligand $\eta^2$ an das Platin in der Oxidationsstufe 0 (in gleicher Weise wie dies für Verbindung **Pt-4a** in der Einleitung diskutiert wurde). **8,9-Pt** lässt sich thermisch in **3-Cl-Pt** umwandeln. Der Hauptunterschied zu **8-Pt** ist, dass die $Pt(PEt_3)_2I$-Einheiten in den Positionen C2 oder C3 in das konjugierte $\pi$-System des BDP-Liganden integriert sind und so eine beträchtliche Rotverschiebung der charakteristischen BDP-Absorptionsbande sowie deren Verbreiterung für die 2-Isomere bewirken. Dennoch sind die dominanten Absorptions- und Emissionsbanden BDP-lokalisierte $\pi\pi^*$ Übergänge. Die Komplexe lassen sich reversibel oxidieren und reduzieren, was wir mit Hilfe der Zyklovoltammetrie, der UV/Vis-NIR-Spektroelektrochemie und der EPR-Spektroskopie an den zugehörigen Radikalkationen und -anionen untersucht haben. Parallel zu **8-Pt** zeigen alle Komplexe in denen das Pt-Ion an das Kohlenstoffatom C2 gebunden ist, duale Fluoreszenz und Phosphoreszenz mit Phosphoreszenzemissionen im NIR. Die Quantenausbeuten für die Phosphoreszenz sind jedoch mit Werten von 0,14% oder weniger sehr gering. Dennoch sind alle Komplexe aktive Sensibilisatoren für die photochemische $^1O_2$ Erzeugung und können daher als Kandidaten für die photodynamische Therapie angesehen werden. Unsere Ergebnisse zeigen, dass die Bindung eines Pt(II)-Ions an die 2- oder 3-Position des BDP-Farbstoffs kein gangbarer Weg zu Pt-BDP-Farbstoffen mit intensiver NIR-Phosphoreszenzemission ist. Die kleinere Triplett-Quantenausbeute ist höchstwahrscheinlich die Folge eines Zusammenspiels zwischen einem geringeren 'externen Schweratomeffekt' aufgrund des größeren Abstands zwischen dem Zentrum des Chromophors und dem Pt-Ion, verglichen mit dem Komplex **8-Pt** aus dem ersten Projekt, und einem größeren 'internen Schweratomeffekt' (aufgrund einer größeren Anzahl von CT-Zuständen), der allerdings den geringeren externen Effekt nicht kompensieren kann. Zusätzlich macht die geringe Energie des angeregten $^3\pi\pi^*$ Zustandes das Energielücken-Gesetz zu einem wichtigen Mitspieler im Hinblick auf die strahlungslose Desaktivierung. Es ist außerdem sehr wahrscheinlich, dass bei Pt-BDP-Komplexen mit Bindung an C8, der *meso*-Position des BDP, die $Pt(PEt_3)_2I$-Einheit zusätzlich zum 'externen Schweratomeffekt' als Elektronendonor fungiert. Parallel zu dem in der Einleitung diskutierten Dimethylanilin-BDP, würde dies das ISC beschleunigen.

Das dritte Projekt dieser Dissertation, das in die Publikationen 3 und 4 mündete, beschäftigte sich mit der Wechselwirkung zwischen einem BDP-Farbstoff und einem Thiolat-

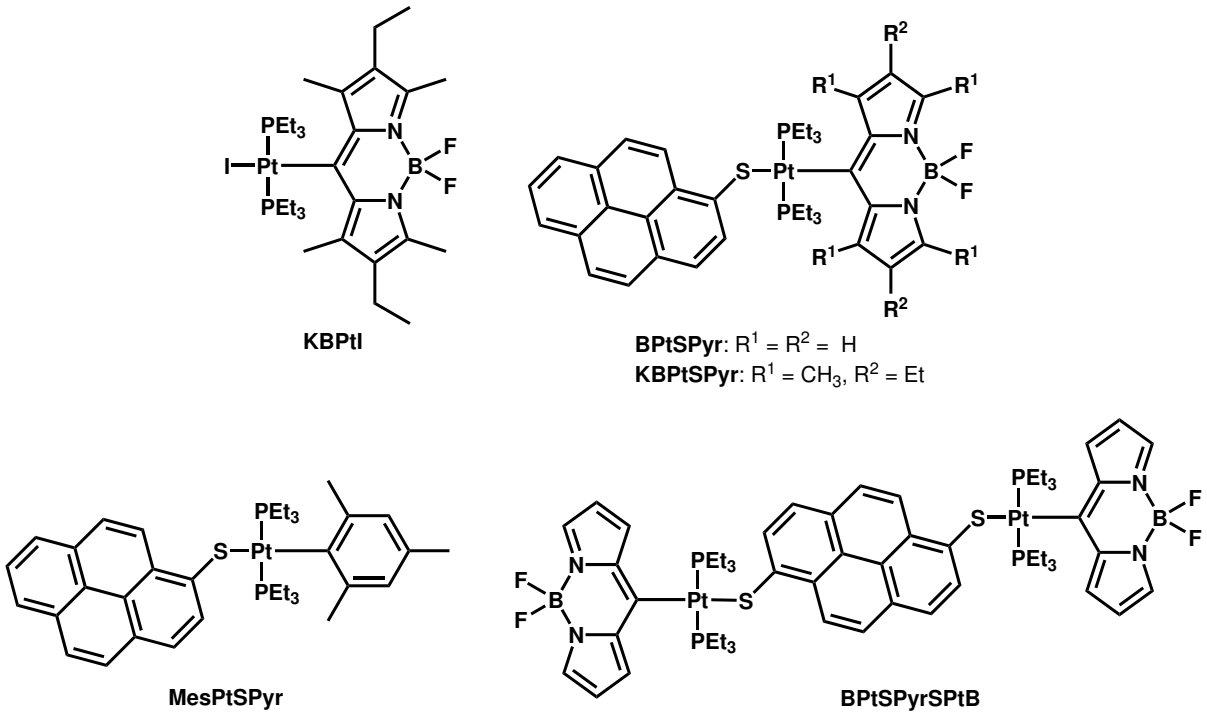


Abbildung 34: Pt(BDP)$(PEt_3)_2$(S-Pyrene) Diaden und zugehörige Kontrollverbindungen über die in den Veröffentlichungen 3 und 4 berichtet wurde.

modifizierten Pyrenfarbstoff innerhalb der Koordinationssphäre eines Platinions. Dieses Projekt ergänzt die Studien von Filatov *et al.*, Zhang *et al.* und anderen, die im letzten Teil der Einleitung dieser Arbeit diskutiert wurden. Die anderen Gruppen, die *meso*-verknüpfte BDP-Diaden untersucht haben, beobachteten keine Emission aus den angeregten Triplett-Zuständen. Wir präsentierten drei Diaden des Typs *trans*-Pt($\sigma$-BDP)-$(PEt_3)_2$(SPyr) und verwandte Kontrollverbindungen, die nur einen der Farbstoff-Liganden aufweisen (siehe Abb. 34). Unsere Arbeitshypothese - die sich als richtig erwiesen hat - war, dass das Design unserer Diaden die Spin-Bahn-Kopplung erhöhen und in dessen Folge zu einer höheren Geschwindigkeitskonstante für den $T_n \rightarrow S_0$ Übergang führen würde und somit einen Pfad für Emission aus dem ladungsgetrennten Triplettzustand eröffnen sollte. Wir haben unterschiedliche Varianten unseres Diadenmotivs verwendet, um die komplexen Deaktivierungskaskaden unserer Diaden untersuchen zu können. Während das peralkylierte **KBPtSPyr** ausschließlich aus dem BDP $\pi\pi^*$ Singulett- und Triplett-Zustand emittiert, emittieren die Verbindungen **BPtSPyr** und **BPtSPyrSPtB** über vier verschiedene Kanäle, einschließlich des ladungsgetrennten $^3$PB-CT-Zustands und des BDP-basierten $^1\pi\pi^*$- und $^3\pi\pi^*$-Zustands bei Raumtemperatur, sowie der BDP- und SPyr-basierten angeregten $^3\pi\pi^*$ Zustände bei 77 K. Studien mittels transienter Absorp-

tionsspektroskopie und der damit verbundenen Bandenzuordungen der angeregten CT-Zustände mittels UV/Vis-NIR-Spektroelektroelektrochemie haben die Zusammenhänge zwischen den verschiedenen Deaktivierungskanälen erhellt. Für **BPtSPyr** wurde mittels TA Spektroskopie die Anwesenheit eines $SPyr^{+\bullet}$ Radikal-Kations nach erfolgter Anregung nachgewiesen. Dies ist ein Nachweis für einen angeregten PB-CT Zustand innerhalb der Desaktivierungskaskade. Außerdem wurden Signale für die Grundzustandsabsorption der SPyr und BDP-Einheit detektiert. Der Komplex **KBPtSPyr**, welcher lediglich aus den $^{1/3}\pi\pi^*$ Zuständen emittiert, zeigt sehr ähnliche TA Signale wie **BPtI** und vergleichbare BDP-Farbstoffe und weist keine ESA Signale eines PB-CT Zustands oder $^{3}\pi\pi^*$ Zustands der SPyr Einheit auf. Das zeigt, dass ein effektiver Energietransfer von den energetisch höher liegenden SPyr-zentrierten Zuständen auf die energetisch tiefer liegenden BDP-zentrierten Zustände erfolgt (Antenneneffekt). **KBPtSPyr** und **BPtSPyr** bewirken als effektive panchromatische Sensibilisatoren die Erzeugung von Singulett-Sauerstoff. Dieses Projekt zeigte, wie die von einem Platinion induzierte Spin-Bahn-Kopplung eine Vielzahl von Deaktivierungskanälen öffnen kann, einschließlich der Emission aus einem ladungsgetrennten Triplett-Zustand mit einer außergewöhnlich hohen Quantenausbeute von 15% im NIR. Das Donor-Akzeptor-Diadendesign mit orthogonaler Anordnung eröffnet die Möglichkeit für ein schweratomfreies ISC. Für Phosphoreszenz aus den jeweiligen Triplett-Zuständen ist die Koordination an ein Platinion dennoch erforderlich.

# References of the Introduction


[1] K. Hübner, *Chemie in unserer Zeit* **2006**, *40*, 274–275, DOI: 10.1002/ciuz.200690054.

[2] H. Zollinger, *Color Chemistry*, 3., rev. ed., VHCA, Verl. Helvetica Chimica Acta, Zürich, **2003**.

[3] A. Jabłoński, *Nature* **1933**, *131*, 839–840, DOI: 10.1038/131839b0.

[4] M. Kasha, *Acta Phys. Pol. A* **1999**, *95*, 15–36, DOI: 10.12693/APhysPolA.95.15.

[5] G. G. Stokes, *Philos. Trans. Royal Soc.* **1852**, *142*, 463–562, DOI: 10.1098/rstl.1852.0022.

[6] G. G. Stokes, *Philos. Trans. Royal Soc.* **1853**, *143*, 385–396, DOI: 10.1098/rstl.1853.0016.

[7] A. Jabłoński, *Z. Phys.* **1935**, *94*, 38–46, DOI: 10.1007/bf01330795.

[8] G. N. Lewis, D. Lipkin, T. T. Magel, *J. Am. Chem. Soc.* **1941**, *63*, 3005–3018, DOI: 10.1021/ja01856a043.

[9] A. Terenin, *Acta Physicochim. URSS (English version)* **1943**, *18*, 210.

[10] G. N. Lewis, M. Kasha, *J. Am. Chem. Soc.* **1944**, *66*, 2100–2116, DOI: 10.1021/ja01240a030.

[11] A. P. Marchetti, D. R. Kearns, *J. Am. Chem. Soc.* **1967**, *89*, 768–777, DOI: 10.1021/ja00980a007.

[12] A. Klein, M. Kalb, M. S. Gudipati, *J. Phys. Chem. A* **1999**, *103*, 3843–3853, DOI: 10.1021/jp984792j.

[13] J. E. Rogers, T. M. Cooper, P. A. Fleitz, D. J. Glass, D. G. McLean, *J. Phys. Chem. A* **2002**, *106*, 10108–10115, DOI: 10.1021/jp021263d.

[14] M. K. S. P. McGlynn, T. Azumi, *Molecular Spectroscopy of the Triplet State*, Prentice-Hall, Englewood Cliffs, N.J, **1969**.

[15] E. Yu-Tzu Li, T. Y. Jiang, Y. Chi, P. T. Chou, *Phys. Chem. Chem. Phys.* **2014**, *16*, 26184–26192,
DOI: 10.1039/c4cp03540b.

[16] M. A. El-Sayed, *J. Chem. Phys.* **1963**, *38*, 2834–2838,
DOI: 10.1063/1.1733610.

[17] M. T. Colvin, A. B. Ricks, A. M. Scott, D. T. Co, M. R. Wasielewski, *J. Phys. Chem. A* **2012**, *116*, 1923–1930,
DOI: 10.1021/jp212546w.

[18] N. Epelde-Elezcano, E. Palao, H. Manzano, A. Prieto-Castaneda, A. R. Agarrabeitia, A. Tabero, A. Villanueva, S. de la Moya, I. Lopez-Arbeloa, V. Martinez-Martinez, M. J. Ortiz, *Chem. - Eur. J.* **2017**, *23*, 4837–4848,
DOI: 10.1002/chem.201605822.

[19] P.-T. Chou, Y. Chi, M.-W. Chung, C.-C. Lin, *Coord. Chem. Rev.* **2011**, *255*, 2653–2665,
DOI: 10.1016/j.ccr.2010.12.013.

[20] Y.-C. Chang, K.-C. Tang, H.-A. Pan, S.-H. Liu, I. O. Koshevoy, A. J. Karttunen, W.-Y. Hung, M.-H. Cheng, P.-T. Chou, *J. Phys. Chem. C* **2013**, *117*, 9623–9632,
DOI: 10.1021/jp402666r.

[21] C.-W. Hsu, C.-C. Lin, M.-W. Chung, Y. Chi, G.-H. Lee, P.-T. Chou, C.-H. Chang, P.-Y. Chen, *J. Am. Chem. Soc.* **2011**, *133*, 12085–12099,
DOI: 10.1021/ja2026568.

[22] C. C. Hsu, C. C. Lin, P. T. Chou, C. H. Lai, C. W. Hsu, C. H. Lin, Y. Chi, *J. Am. Chem. Soc.* **2012**, *134*, 7715–7724,
DOI: 10.1021/ja2107788.

[23] M. Montalti, A. Credi, L. Prodi, M. Teresa Gandolfi, *Handbook of Photochemistry*, 3rd, CRC Press, Boca Raton, **2006**,
DOI: 10.1201/9781420015195.

[24] J. S. Wilson, N. Chawdhury, M. R. A. Al-Mandhary, M. Younus, M. S. Khan, P. R. Raithby, A. Köhler, R. H. Friend, *J. Am. Chem. Soc.* **2001**, *123*, 9412–9417,
DOI: 10.1021/ja010986s.

[25] C. E. Whittle, J. A. Weinstein, M. W. George, K. S. Schanze, *Inorg. Chem.* **2001**, *40*, 4053–4062,
DOI: 10.1021/ic0102182.

[26] H. Yersin in *Transition Metal and Rare Earth Compounds*, Topics in Current Chemistry, Springer Berlin Heidelberg, **2004**, Chapter 1, pp. 1–26, DOI: 10.1007/b96858.

[27] T. Yoshihara, Y. Yamaguchi, M. Hosaka, T. Takeuchi, S. Tobita, *Angew. Chem. Int. Ed.* **2012**, *51*, 4148–51, DOI: 10.1002/anie.201107557.

[28] Y. Liu, H. Guo, J. Zhao, *Chem. Commun.* **2011**, *47*, 11471–11473, DOI: 10.1039/c1cc14582g.

[29] J. A. G. Williams in *Photochemistry and Photophysics of Coordination Compounds II*, (Eds.: V. Balzani, S. Campagna), Topics in Current Chemistry, Springer Berlin Heidelberg, **2007**, Chapter 134, pp. 205–268, DOI: 10.1007/128_2007_134.

[30] V. W. Yam, K. M. Wong, *Chem. Commun.* **2011**, *47*, 11579–11592, DOI: 10.1039/c1cc13767k.

[31] S. Y. Leung, S. Evariste, C. Lescop, M. Hissler, V. W. Yam, *Chem. Sci.* **2017**, *8*, 4264–4273, DOI: 10.1039/c7sc00041c.

[32] M. Klessinger, J. Michl, *Excited States and Photochemistry of Organic Molecules*, VCH, New York ; Weinheim, **1995**.

[33] T. Shigehiro, S. Yagi, T. Maeda, H. Nakazumi, H. Fujiwara, Y. Sakurai, *J. Phys. Chem. C* **2012**, *117*, 532–542, DOI: 10.1021/jp307853t.

[34] J. Brooks, Y. Babayan, S. Lamansky, P. Djurovich, I. Tsyba, R. Bau, M. Thompson, *Inorg. Chem.* **2002**, *41*, 3055–3066, DOI: 10.1021/ic0255508.

[35] W. Wu, W. Wu, S. Ji, H. Guo, J. Zhao, *Dalton Trans.* **2011**, *40*, 5953–5963, DOI: 10.1039/c1dt10344j.

[36] A. Jackel, M. Linseis, C. Häge, R. Winter, *Inorganics* **2015**, *3*, 55–81, DOI: 10.3390/inorganics3020055.

[37] I. E. Pomestchenko, C. R. Luman, M. Hissler, R. Ziessel, F. N. Castellano, *Inorg. Chem.* **2003**, *42*, 1394–1396, DOI: 10.1021/ic0261631.

[38] E. O. Danilov, I. E. Pomestchenko, S. Kinayyigit, P. L. Gentili, M. Hissler, R. Ziessel, F. N. Castellano, *J. Phys. Chem. A* **2005**, *109*, 2465–2471, DOI: 10.1021/jp045269+.

[39] F. Nastasi, F. Puntoriero, S. Campagna, S. Diring, R. Ziessel, *Phys. Chem. Chem. Phys.* **2008**, *10*, 3982–6, DOI: 10.1039/b805972a.

[40] W. Wu, J. Zhao, H. Guo, J. Sun, S. Ji, Z. Wang, *Chem. - Eur. J.* **2012**, *18*, 1961–1968, DOI: 10.1002/chem.201102634.

[41] W. Wu, L. Liu, X. Cui, C. Zhang, J. Zhao, *Dalton Trans.* **2013**, *42*, 14374–9, DOI: 10.1039/c3dt51927a.

[42] M.-H. Nguyen, J. H. K. Yip, *Organometallics* **2010**, *29*, 2422–2429, DOI: 10.1021/om100046h.

[43] W. Y. Heng, J. Hu, J. H. K. Yip, *Organometallics* **2007**, *26*, 6760–6768, DOI: 10.1021/om700716p.

[44] J. Hu, J. H. K. Yip, D.-L. Ma, K.-Y. Wong, W.-H. Chung, *Organometallics* **2009**, *28*, 51–59, DOI: 10.1021/om800410m.

[45] W. Wu, W. Wu, S. Ji, H. Guo, J. Zhao, *Eur. J. Inorg. Chem.* **2010**, *2010*, 4470–4482, DOI: 10.1002/ejic.201000488.

[46] J. W. Facendola, M. Seifrid, J. Siegel, P. I. Djurovich, M. E. Thompson, *Dalton Trans.* **2015**, *44*, 8456–8466, DOI: 10.1039/c4dt03541k.

[47] P. J. Saris, M. E. Thompson, *Org. Lett.* **2016**, *18*, 3960–3963, DOI: 10.1021/acs.orglett.6b01693.

[48] V. Sicilia, S. Fuertes, A. Martín, A. Palacios, *Organometallics* **2013**, *32*, 4092–4102, DOI: 10.1021/om400159g.

[49] S. Lentijo, J. A. Miguel, P. Espinet, *Inorg. Chem.* **2010**, *49*, 9169–9177, DOI: 10.1021/ic1003319.

[50] B.-Y. Wang, A. R. Karikachery, Y. Li, A. Singh, H. B. Lee, W. Sun, P. R. Sharp, *J. Am. Chem. Soc.* **2009**, *131*, 3150–3151, DOI: 10.1021/ja809046p.

[51] R. A. Begum, P. R. Sharp, *Organometallics* **2005**, *24*, 2670–2678, DOI: 10.1021/om050164u.

[52] H. B. Lee, P. R. Sharp, *Organometallics* **2005**, *24*, 4875–4877, DOI: 10.1021/om050464b.

[53] A. Singh, P. R. Sharp, *J. Am. Chem. Soc.* **2006**, *128*, 5998–5999, DOI: 10.1021/ja060159x.

[54] F. Geist, A. Jackel, R. F. Winter, *Dalton Trans.* **2015**, *44*, 3974–3987, DOI: 10.1039/C4DT02410A.

[55] F. Geist, A. Jackel, R. F. Winter, *Inorg. Chem.* **2015**, *54*, 10946–10957, DOI: 10.1021/acs.inorgchem.5b01969.

[56] F. Geist, A. Jackel, P. Irmler, M. Linseis, S. Malzkuhn, M. Kuss-Petermann, O. S. Wenger, R. F. Winter, *Inorg. Chem.* **2017**, *56*, 914–930, DOI: 10.1021/acs.inorgchem.6b02549.

[57] X. Allonas, C. Ley, C. Bibaut, P. Jacques, J. P. Fouassier, *Chem. Phys. Lett.* **2000**, *322*, 483–490, DOI: 10.1016/s0009-2614(00)00462-0.

[58] L. Cokbaglan, N. Arsu, Y. Yagci, S. Jockusch, N. J. Turro, *Macromolecules* **2003**, *36*, 2649–2653, DOI: 10.1021/ma0214613.

[59] M. Aydin, N. Arsu, Y. Yagci, S. Jockusch, N. J. Turro, *Macromolecules* **2005**, *38*, 4133–4138, DOI: 10.1021/ma047560t.

[60] V. Leen, P. Yuan, L. Wang, N. Boens, W. Dehaen, *Org. Lett.* **2012**, *14*, 6150–6153, DOI: 10.1021/ol3028225.

[61] G. Ulrich, R. Ziessel, A. Harriman, *Angew. Chem. Int. Ed.* **2008**, *47*, 1184–1201, DOI: 10.1002/anie.200702070.

[62] N. Boens, B. Verbelen, W. Dehaen, *Eur. J. Org. Chem.* **2015**, 6577–6595, DOI: 10.1002/ejoc.201500682.

[63] A. Loudet, K. Burgess, *Chem. Rev.* **2007**, *107*, 4891–4932, DOI: 10.1021/cr078381n.

[64] T. Yogo, Y. Urano, Y. Ishitsuka, F. Maniwa, T. Nagano, *J. Am. Chem. Soc.* **2005**, *127*, 12162–12163, DOI: 10.1021/ja0528533.

[65] J. Zhao, K. Xu, W. Yang, Z. Wang, F. Zhong, *Chem. Soc. Rev.* **2015**, *44*, 8904–8939, DOI: 10.1039/C5CS00364D.

[66] X. F. Zhang, X. Yang, *J. Phys. Chem. B* **2013**, *117*, 5533–5539, DOI: 10.1021/jp4013812.

[67] M. Kollmannsberger, K. Rurack, U. Resch-Genger, J. Daub, *J. Phys. Chem. A* **1998**, *102*, 10211–10220, DOI: 10.1021/jp982701c.

[68] W. Hu, X.-F. Zhang, X. Lu, S. Lan, D. Tian, T. Li, L. Wang, S. Zhao, M. Feng, J. Zhang, *Dyes and Pigments* **2018**, *149*, 306–314, DOI: 10.1016/j.dyepig.2017.10.018.

[69] J. Bañuelos, I. J. Arroyo-Córdoba, I. Valois-Escamilla, A. Alvarez-Hernández, E. Peña-Cabrera, R. Hu, B. Zhong Tang, I. Esnal, V. Martínez, I. López Arbeloa, *RSC Adv.* **2011**, *1*, 677–684, DOI: 10.1039/c1ra00020a.

[70] S. Duman, Y. Cakmak, S. Kolemen, E. U. Akkaya, Y. Dede, *J. Org. Chem.* **2012**, *77*, 4516–4527, DOI: 10.1021/jo300051v.

[71] Y. Cakmak, S. Kolemen, S. Duman, Y. Dede, Y. Dolen, B. Kilic, Z. Kostereli, L. T. Yildirim, A. L. Dogan, D. Guc, E. U. Akkaya, *Angew. Chem. Int. Ed.* **2011**, *50*, 11937–11941, DOI: 10.1002/anie.201105736.

[72] W. Wu, X. Cui, J. Zhao, *Chem. Commun.* **2013**, *49*, 9009–9011, DOI: 10.1039/c3cc45470c.

[73] X. F. Zhang, X. Yang, *J. Phys. Chem. B* **2013**, *117*, 9050–9055, DOI: 10.1021/jp405102m.

[74] C. Caltagirone, M. Arca, A. M. Falchi, V. Lippolis, V. Meli, M. Monduzzi, T. Nylander, A. Rosa, J. Schmidt, Y. Talmon, S. Murgia, *RSC Adv.* **2015**, *5*, 23443–23449,
DOI: 10.1039/c5ra01025j.

[75] X.-F. Zhang, *Dyes and Pigments* **2017**, *146*, 491–501,
DOI: 10.1016/j.dyepig.2017.07.051.

[76] X. F. Zhang, X. Yang, B. Xu, *Phys. Chem. Chem. Phys.* **2017**, *19*, 24792–24804,
DOI: 10.1039/c7cp02645e.

[77] X. F. Zhang, N. Feng, *Chem. - Asian J.* **2017**, *12*, 2447–2456,
DOI: 10.1002/asia.201700794.

[78] M. A. Filatov, S. Karuthedath, P. M. Polestshuk, H. Savoie, K. J. Flanagan, C. Sy, E. Sitte, M. Telitchko, F. Laquai, R. W. Boyle, M. O. Senge, *J. Am. Chem. Soc.* **2017**, *139*, 6282–6285,
DOI: 10.1021/jacs.7b00551.

[79] M. A. Filatov, S. Karuthedath, P. M. Polestshuk, S. Callaghan, K. J. Flanagan, M. Telitchko, T. Wiesner, F. Laquai, M. O. Senge, *Phys. Chem. Chem. Phys.* **2018**, *20*, 8016–8031,
DOI: 10.1039/c7cp08472b.

# References of Publication 1


[1] A. Treibs, F.-H. Kreuzer, *Liebigs Ann. Chem.* **1968**, *718*, 208–223, DOI: 10.1002/jlac.19687180119.

[2] A. Loudet, K. Burgess, *Chem. Rev.* **2007**, *107*, 4891–4932, DOI: 10.1021/cr078381n.

[3] G. Ulrich, R. Ziessel, A. Harriman, *Angew. Chem. Int. Ed.* **2008**, *47*, 1184–1201, DOI: 10.1002/anie.200702070.

[4] N. Boens, B. Verbelen, W. Dehaen, *Eur. J. Org. Chem.* **2015**, 6577–6595, DOI: 10.1002/ejoc.201500682.

[5] F. Li, S. I. Yang, Y. Ciringh, J. Seth, C. H. Martin, D. L. Singh, D. Kim, R. R. Birge, D. F. Bocian, D. Holten, J. S. Lindsey, *J. Am. Chem. Soc.* **1998**, *120*, 10001–10017, DOI: 10.1021/ja9812047.

[6] J. Chen, A. Burghart, A. Derecskei-Kovacs, K. Burgess, *J. Org. Chem.* **2000**, *65*, 2900–2906, DOI: 10.1021/jo991927o.

[7] F. E. Alemdaroglu, S. C. Alexander, D. Ji, D. K. Prusty, M. Börsch, A. Herrmann, *Macromolecules* **2009**, *42*, 6529–6536, DOI: 10.1021/ma900727k.

[8] M. T. Whited, P. I. Djurovich, S. T. Roberts, A. C. Durrell, C. W. Schlenker, S. E. Bradforth, M. E. Thompson, *J. Am. Chem. Soc.* **2011**, *133*, 88–96, DOI: 10.1021/ja108493b.

[9] R. Ziessel, G. Ulrich, A. Haefele, A. Harriman, *J. Am. Chem. Soc.* **2013**, *135*, 11330–11344, DOI: 10.1021/ja4049306.

[10] T. Lazarides, T. M. McCormick, K. C. Wilson, S. Lee, D. W. McCamant, R. Eisenberg, *J. Am. Chem. Soc.* **2011**, *133*, 350–364, DOI: 10.1021/ja1070366.

[11] M. Cordaro, P. Mineo, F. Nastasi, G. Magazzù, *RSC Adv.* **2014**, *4*, 43931–43933, DOI: 10.1039/c4ra08213c.

[12] N. Boens, V. Leen, W. Dehaen, *Chem. Soc. Rev.* **2012**, *41*, 1130–1172, DOI: 10.1039/c1cs15132k.

[13] T. Yogo, Y. Urano, Y. Ishitsuka, F. Maniwa, T. Nagano, *J. Am. Chem. Soc.* **2005**, *127*, 12162–12163,
DOI: 10.1021/ja0528533.

[14] J. Zhao, K. Xu, W. Yang, Z. Wang, F. Zhong, *Chem. Soc. Rev.* **2015**, *44*, 8904–8939,
DOI: 10.1039/C5CS00364D.

[15] A. Gorman, J. Killoran, C. O'Shea, T. Kenna, W. M. Gallagher, D. F. O'Shea, *J. Am. Chem. Soc.* **2004**, *126*, 10619–10631,
DOI: 10.1021/ja047649e.

[16] X. F. Zhang, X. Yang, *J. Phys. Chem. B* **2013**, *117*, 5533–5539,
DOI: 10.1021/jp4013812.

[17] W. Wu, J. Zhao, J. Sun, L. Huang, X. Yi, *J. Mater. Chem. C* **2013**, *1*, 705–716,
DOI: 10.1039/c2tc00214k.

[18] W. Wu, J. Zhao, H. Guo, J. Sun, S. Ji, Z. Wang, *Chem. - Eur. J.* **2012**, *18*, 1961–1968,
DOI: 10.1002/chem.201102634.

[19] J. Sun, F. Zhong, X. Yi, J. Zhao, *Inorg. Chem.* **2013**, *52*, 6299–6310,
DOI: 10.1021/ic302210b.

[20] F. Geist, A. Jackel, R. F. Winter, *Inorg. Chem.* **2015**, *54*, 10946–10957,
DOI: 10.1021/acs.inorgchem.5b01969.

[21] P. Batat, M. Cantuel, G. Jonusauskas, L. Scarpantonio, A. Palma, D. F. O'Shea, N. D. McClenaghan, *J. Phys. Chem. A* **2011**, *115*, 14034–14039,
DOI: 10.1021/jp2077775.

[22] X.-d. Wang, O. S. Wolfbeis, *Chem. Soc. Rev.* **2014**, *43*, 3666–3761,
DOI: 10.1039/C4CS00039K.

[23] W. Wu, J. Sun, X. Cui, J. Zhao, *J. Mater. Chem. C* **2013**, *1*, 4577–4589,
DOI: 10.1039/c3tc30592a.

[24] S. G. Awuah, Y. You, *RSC Adv.* **2012**, *2*, 11169–11183,
DOI: 10.1039/C2RA21404K.

[25] A. Kamkaew, S. H. Lim, H. B. Lee, L. V. Kiew, L. Y. Chung, K. Burgess, *Chem. Soc. Rev.* **2013**, *42*, 77–88,
DOI: 10.1039/c2cs35216h.

[26] R. Bonnett, *Chem. Soc. Rev.* **1995**, *24*, 19–33,
DOI: 10.1039/cs9952400019.

[27] T. J. Dougherty, C. J. Gomer, B. W. Henderson, G. Jori, D. Kessel, M. Korbelik, J. Moan, Q. Peng, *J. Natl. Cancer Inst.* **1998**, *90*, 889–905,
DOI: 10.1093/jnci/90.12.889.

[28] D. E. J. G. J. Dolmans, D. Fukumura, R. K. Jain, *Nat. Rev. Cancer* **2003**, *3*, 380–387,
DOI: 10.1038/nrc1071.

[29] P. Agostinis, K. Berg, K. A. Cengel, T. H. Foster, A. W. Girotti, S. O. Gollnick, S. M. Hahn, M. R. Hamblin, A. Juzeniene, D. Kessel, M. Korbelik, J. Moan, P. Mroz, D. Nowis, J. Piette, B. C. Wilson, J. Golab, *CA Cancer J. Clin.* **2011**, *61*, 250–281,
DOI: 10.3322/caac.20114.

[30] W. H. Lam, E. S.-H. Lam, V. W.-W. Yam, *J. Am. Chem. Soc.* **2013**, *135*, 15135–15143,
DOI: 10.1021/ja406810a.

[31] J. A. G. Williams in *Photochemistry and Photophysics of Coordination Compounds II*, (Eds.: V. Balzani, S. Campagna), Topics in Current Chemistry, Springer Berlin Heidelberg, **2007**, Chapter 134, pp. 205–268,
DOI: 10.1007/128_2007_134.

[32] V. W. Yam, K. M. Wong, *Chem. Commun.* **2011**, *47*, 11579–11592,
DOI: 10.1039/c1cc13767k.

[33] P.-T. Chou, Y. Chi, M.-W. Chung, C.-C. Lin, *Coord. Chem. Rev.* **2011**, *255*, 2653–2665,
DOI: 10.1016/j.ccr.2010.12.013.

[34] F. Geist, A. Jackel, R. F. Winter, *Dalton Trans.* **2015**, *44*, 3974–3987,
DOI: 10.1039/C4DT02410A.

[35] T. G. Appleton, H. C. Clark, L. E. Manzer, *Coord. Chem. Rev.* **1973**, *10*, 335–422,
DOI: 10.1016/S0010-8545(00)80238-6.

[36] T. J. McCarthy, R. G. Nuzzo, G. M. Whitesides, *J. Am. Chem. Soc.* **1981**, *103*, 3396–3403,
DOI: 10.1021/ja00402a025.

[37] S. Lentijo, J. A. Miguel, P. Espinet, *Inorg. Chem.* **2010**, *49*, 9169–9177, DOI: 10.1021/ic1003319.

[38] P. Nilsson, F. Plamper, O. F. Wendt, *Organometallics* **2003**, *22*, 5235–5242, DOI: 10.1021/om030524i.

[39] R. Bardi, A. M. Piazzesi, *Inorganica Chim. Acta* **1981**, *47*, 249–254, DOI: 10.1016/s0020-1693(00)89337-8.

[40] C. Albrecht, C. Wagner, K. Merzweiler, T. Lis, D. Steinborn, *Appl. Organomet. Chem.* **2005**, *19*, 1155–1163, DOI: 10.1002/aoc.976.

[41] S. J. Anderson, R. J. Goodfellow, *Dalton Trans.* **1977**, 1683–1686, DOI: 10.1039/dt9770001683.

[42] J. L. Burmeister, F. Basolo, *Inorg. Chem.* **1964**, *3*, 1587–1593, DOI: 10.1021/ic50021a025.

[43] E. Hartmann, R. M. Gschwind, *Angew. Chem. Int. Ed.* **2013**, *52*, 2350–2354, DOI: 10.1002/anie.201208021.

[44] C. Hansch, A. Leo, R. W. Taft, *Chem. Rev.* **1991**, *91*, 165–195, DOI: 10.1021/cr00002a004.

[45] C.-W. Hsu, C.-C. Lin, M.-W. Chung, Y. Chi, G.-H. Lee, P.-T. Chou, C.-H. Chang, P.-Y. Chen, *J. Am. Chem. Soc.* **2011**, *133*, 12085–12099, DOI: 10.1021/ja2026568.

[46] C. C. Hsu, C. C. Lin, P. T. Chou, C. H. Lai, C. W. Hsu, C. H. Lin, Y. Chi, *J. Am. Chem. Soc.* **2012**, *134*, 7715–7724, DOI: 10.1021/ja2107788.

[47] Y.-C. Chang, K.-C. Tang, H.-A. Pan, S.-H. Liu, I. O. Koshevoy, A. J. Karttunen, W.-Y. Hung, M.-H. Cheng, P.-T. Chou, *J. Phys. Chem. C* **2013**, *117*, 9623–9632, DOI: 10.1021/jp402666r.

[48] E. Yu-Tzu Li, T. Y. Jiang, Y. Chi, P. T. Chou, *Phys. Chem. Chem. Phys.* **2014**, *16*, 26184–26192, DOI: 10.1039/c4cp03540b.

[49] W. Wu, C. Cheng, W. Wu, H. Guo, S. Ji, P. Song, K. Han, J. Zhao, X. Zhang, Y. Wu, G. Du, *Eur. J. Inorg. Chem.* **2010**, *2010*, 4683–4696, DOI: 10.1002/ejic.201000327.

[50] W. Wu, W. Wu, S. Ji, H. Guo, P. Song, K. Han, L. Chi, J. Shao, J. Zhao, *J. Mater. Chem.* **2010**, *20*, 9775–9786,
DOI: 10.1039/c0jm01794a.

[51] Y. Liu, H. Guo, J. Zhao, *Chem. Commun.* **2011**, *47*, 11471–11473,
DOI: 10.1039/c1cc14582g.

[52] W. Wu, W. Wu, S. Ji, H. Guo, J. Zhao, *Dalton Trans.* **2011**, *40*, 5953–5963,
DOI: 10.1039/c1dt10344j.

[53] H. Sun, H. Guo, W. Wu, X. Liu, J. Zhao, *Dalton Trans.* **2011**, *40*, 7834–7841,
DOI: 10.1039/c1dt10490j.

[54] H. Xiang, L. Zhou, Y. Feng, J. Cheng, D. Wu, X. Zhou, *Inorg. Chem.* **2012**, *51*, 5208–5212,
DOI: 10.1021/ic300040n.

[55] H. Wasserman, R. W. Murray, *Singlet Oxygen*, Acad. Pr., New York, **1979**.

[56] H. H. Wasserman, J. L. Ives, *Tetrahedron* **1981**, *37*, 1825–1852,
DOI: 10.1016/s0040-4020(01)97932-3.

[57] S.-y. Takizawa, R. Aboshi, S. Murata, *Photochem. Photobiol. Sci.* **2011**, *10*, 895–903,
DOI: 10.1039/C0PP00265H.

[58] Y. Usui, *Chem. Lett.* **1973**, *2*, 743–744,
DOI: 10.1246/cl.1973.743.

[59] F. Wilkinson, W. P. Helman, A. B. Ross, *J. Phys. Chem. Ref. Data* **1993**, *22*, 113–262,
DOI: 10.1063/1.555934.

[60] J. N. Chaon, G. R. Jamieson, R. S. Sinclair, *Chem. Phys. Lipids* **1987**, *43*, 81–99,
DOI: 10.1016/0009-3084(87)90028-4.

[61] W. Herrendorf, W. Bärnighausen, HABITUS, program for the optimization of the crystal shape for numerical absorption correction in X-SHAPE, Computer Program, **1999**.

[62] G. M. Sheldrick, *SHELXTL-97 Program for Crystal Structure Analysis*, University of Göttingen, Göttingen, **1997**.

[63] G. M. Sheldrick, *Acta Crystallogr. A* **2008**, *64*, 112–122,
DOI: 10.1107/S0108767307043930.

[64] L. J. Farrugia, *J. Appl. Crystallogr.* **1997**, *30*, 565–565, DOI: 10.1107/s0021889897003117.

[65] L. J. Farrugia, *J. Appl. Crystallogr.* **2012**, *45*, 849–854, DOI: 10.1107/s0021889812029111.

[66] C. F. Macrae, P. R. Edgington, P. McCabe, E. Pidcock, G. P. Shields, R. Taylor, M. Towler, J. van de Streek, *J. Appl. Crystallogr.* **2006**, *39*, 453–457, DOI: 10.1107/s002188980600731x.

[67] M. J. Frisch, G. W. Trucks, H. B. Schlegel, G. E. Scuseria, M. A. Robb, J. R. Cheeseman, G. Scalmani, V. Barone, B. Mennucci, G. A. Petersson, H. Nakatsuji, M. Caricato, X. Li, H. P. Hratchian, A. F. Izmaylov, J. Bloino, G. Zheng, J. L. Sonnenberg, M. Hada, M. Ehara, K. Toyota, R. Fukuda, J. Hasegawa, M. Ishida, T. Nakajima, Y. Honda, O. Kitao, H. Nakai, T. Vreven, J. A. Montgomery Jr., J. E. Peralta, F. Ogliaro, M. J. Bearpark, J. Heyd, E. N. Brothers, K. N. Kudin, V. N. Staroverov, R. Kobayashi, J. Normand, K. Raghavachari, A. P. Rendell, J. C. Burant, S. S. Iyengar, J. Tomasi, M. Cossi, N. Rega, N. J. Millam, M. Klene, J. E. Knox, J. B. Cross, V. Bakken, C. Adamo, J. Jaramillo, R. Gomperts, R. E. Stratmann, O. Yazyev, A. J. Austin, R. Cammi, C. Pomelli, J. W. Ochterski, R. L. Martin, K. Morokuma, V. G. Zakrzewski, G. A. Voth, P. Salvador, J. J. Dannenberg, S. Dapprich, A. D. Daniels, Ö. Farkas, J. B. Foresman, J. V. Ortiz, J. Cioslowski, D. J. Fox, Gaussian 09, Computer Program, **2009**.

[68] O. Gunnarsson, B. I. Lundqvist, *Phys. Rev. B* **1976**, *13*, 4274–4298.

[69] W. Küchle, M. Dolg, H. Stoll, H. Preuss, *J. Chem. Phys.* **1994**, *100*, 7535–7542, DOI: 10.1063/1.466847.

[70] M. Dolg, H. Stoll, H. Preuss, *J. Chem. Phys.* **1989**, *90*, 1730–1734, DOI: 10.1063/1.456066.

[71] D. Andrae, U. Häußermann, M. Dolg, H. Stoll, H. Preuss, *Theor. Chim. Acta* **1990**, *77*, 123–141, DOI: 10.1007/bf01114537.

[72] P. C. Hariharan, J. A. Pople, *Theor. Chim. Acta* **1973**, *28*, 213–222, DOI: 10.1007/BF00533485.

[73] J. P. Perdew, K. Burke, M. Ernzerhof, *Phys. Rev. Lett.* **1996**, *77*, 3865–3868.

[74] J. P. Perdew, K. Burke, M. Ernzerhof, *Phys. Rev. Lett.* **1997**, *78*, 1396–1396, DOI: 10.1103/PhysRevLett.78.1396.

[75] C. Adamo, V. Barone, *J. Chem. Phys.* **1999**, *110*, 6158–6170, DOI: 10.1063/1.478522.

[76] E. Cancès, B. Mennucci, J. Tomasi, *J. Chem. Phys.* **1997**, *107*, 3032–3041, DOI: 10.1063/1.474659.

[77] B. Mennucci, J. Tomasi, *J. Chem. Phys.* **1997**, *106*, 5151–5158, DOI: 10.1063/1.473558.

[78] M. Cossi, N. Rega, G. Scalmani, V. Barone, *J. Comput. Chem.* **2003**, *24*, 669–681, DOI: 10.1002/jcc.10189.

[79] E. Runge, E. K. U. Gross, *Phys. Rev. Lett.* **1984**, *52*, 997–1000.

[80] N. M. O'Boyle, A. L. Tenderholt, K. M. Langner, *J. Comput. Chem.* **2008**, *29*, 839–845, DOI: 10.1002/jcc.20823.

[81] T. Keith, J. Millam, *GaussView, Version 3*, Semichem Inc., Shawnee Mission KS, **2009**.

[82] M. D. Hanwell, D. E. Curtis, D. C. Lonie, T. Vandermeersch, E. Zurek, G. R. Hutchison, *J. Cheminf.* **2012**, *4*, 1–17, DOI: 10.1186/1758-2946-4-17.

[83] N. Adarsh, M. Shanmugasundaram, R. R. Avirah, D. Ramaiah, *Chem. - Eur. J.* **2012**, *18*, 12655–12662, DOI: 10.1002/chem.201202438.

# References of Publication 2


[1] N. Thejo Kalyani, S. J. Dhoble, *Renewable and Sustainable Energy Rev.* **2012**, *16*, 2696–2723,
DOI: 10.1016/j.rser.2012.02.021.

[2] G. Ulrich, R. Ziessel, A. Harriman, *Angew. Chem. Int. Ed.* **2008**, *47*, 1184–1201,
DOI: 10.1002/anie.200702070.

[3] H. Kobayashi, M. Ogawa, R. Alford, P. L. Choyke, Y. Urano, *Chem. Rev.* **2010**, *110*, 2620–2640,
DOI: 10.1021/cr900263j.

[4] M. Sauer, M. Heilemann, *Chem. Rev.* **2017**, *117*, 7478–7509,
DOI: 10.1021/acs.chemrev.6b00667.

[5] B. Pashaei, H. Shahroosvand, M. Graetzel, M. K. Nazeeruddin, *Chem. Rev.* **2016**, *116*, 9485–94564,
DOI: 10.1021/acs.chemrev.5b00621.

[6] A. A. Ghogare, A. Greer, *Chem. Rev.* **2016**, *116*, 9994–10034,
DOI: 10.1021/acs.chemrev.5b00726.

[7] K. L. Skubi, T. R. Blum, T. P. Yoon, *Chem. Rev.* **2016**, *116*, 10035–10074,
DOI: 10.1021/acs.chemrev.6b00018.

[8] B. Zheng, R. P. Sabatini, W. F. Fu, M. S. Eum, W. W. Brennessel, L. Wang, D. W. McCamant, R. Eisenberg, *Proc. Natl. Acad. Sci. U. S. A.* **2015**, *112*, 3987–3996,
DOI: 10.1073/pnas.1509310112.

[9] J. P. Celli, B. Q. Spring, I. Rizvi, C. L. Evans, K. S. Samkoe, S. Verma, B. W. Pogue, T. Hasan, *Chem. Rev.* **2010**, *110*, 2795–2838,
DOI: 10.1021/cr900300p.

[10] A. Kamkaew, S. H. Lim, H. B. Lee, L. V. Kiew, L. Y. Chung, K. Burgess, *Chem. Soc. Rev.* **2013**, *42*, 77–88,
DOI: 10.1039/c2cs35216h.

[11] T. J. Dougherty, C. J. Gomer, B. W. Henderson, G. Jori, D. Kessel, M. Korbelik, J. Moan, Q. Peng, *J. Natl. Cancer Inst.* **1998**, *90*, 889–905,
DOI: 10.1093/jnci/90.12.889.

[12] B. C. Wilson, M. S. Patterson, *Phys. Med. Biol.* **2008**, *53*, 61–109,
DOI: 10.1088/0031-9155/53/9/R01.

[13] J. Zhao, S. Ji, H. Guo, *RSC Adv.* **2011**, *1*, 937, DOI: 10.1039/c1ra00469g.

[14] T. N. Singh-Rachford, F. N. Castellano, *Coord. Chem. Rev.* **2010**, *254*, 2560–2573, DOI: 10.1016/j.ccr.2010.01.003.

[15] N. Boens, B. Verbelen, W. Dehaen, *Eur. J. Org. Chem.* **2015**, 6577–6595, DOI: 10.1002/ejoc.201500682.

[16] G. Ulrich, R. Ziessel, A. Harriman, *Angew. Chem. Int. Ed.* **2008**, *47*, 1184–1201, DOI: 10.1002/anie.200702070.

[17] A. Loudet, K. Burgess, *Chem. Rev.* **2007**, *107*, 4891–4932, DOI: 10.1021/cr078381n.

[18] J. Zhao, K. Xu, W. Yang, Z. Wang, F. Zhong, *Chem. Soc. Rev.* **2015**, *44*, 8904–8939, DOI: 10.1039/C5CS00364D.

[19] A. Harriman, G. Izzet, R. Ziessel, *J. Am. Chem. Soc.* **2006**, *128*, 10868–10875, DOI: 10.1021/ja0631448.

[20] C. Zhang, J. Zhao, S. Wu, Z. Wang, W. Wu, J. Ma, S. Guo, L. Huang, *J. Am. Chem. Soc.* **2013**, *135*, 10566–10578, DOI: 10.1021/ja405170j.

[21] A. Loudet, K. Burgess, *Chem. Rev.* **2007**, *107*, 4891–4932, DOI: 10.1021/cr078381n.

[22] Y. Luo, G. D. Prestwich, *Bioconjugate Chem.* **1999**, *10*, 755–763, DOI: 10.1021/bc9900338.

[23] G. T. Hermanson, *Bioconjugate techniques*, 3., Acad. Press, Amsterdam ; Heidelberg, **2013**.

[24] S. L. Niu, C. Massif, G. Ulrich, P. Y. Renard, A. Romieu, R. Ziessel, *Chem. - Eur. J.* **2012**, *18*, 7229–42, DOI: 10.1002/chem.201103613.

[25] T. Yogo, Y. Urano, Y. Ishitsuka, F. Maniwa, T. Nagano, *J. Am. Chem. Soc.* **2005**, *127*, 12162–12163, DOI: 10.1021/ja0528533.

[26] N. Epelde-Elezcano, E. Palao, H. Manzano, A. Prieto-Castaneda, A. R. Agarrabeitia, A. Tabero, A. Villanueva, S. de la Moya, I. Lopez-Arbeloa, V. Martinez-Martinez, M. J. Ortiz, *Chem. - Eur. J.* **2017**, *23*, 4837–4848, DOI: 10.1002/chem.201605822.

[27] B. Ventura, G. Marconi, M. Bröring, R. Krüger, L. Flamigni, *New J. Chem.* **2009**, *33*, 428–438, DOI: 10.1039/b813638f.

[28] Y. Cakmak, S. Kolemen, S. Duman, Y. Dede, Y. Dolen, B. Kilic, Z. Kostereli, L. T. Yildirim, A. L. Dogan, D. Guc, E. U. Akkaya, *Angew. Chem. Int. Ed.* **2011**, *50*, 11937–11941, DOI: 10.1002/anie.201105736.

[29] S. Duman, Y. Cakmak, S. Kolemen, E. U. Akkaya, Y. Dede, *J. Org. Chem.* **2012**, *77*, 4516–4527, DOI: 10.1021/jo300051v.

[30] W. Wu, X. Cui, J. Zhao, *Chem. Commun.* **2013**, *49*, 9009–9011, DOI: 10.1039/c3cc45470c.

[31] J. Zhao, K. Xu, W. Yang, Z. Wang, F. Zhong, *Chem. Soc. Rev.* **2015**, *44*, 8904–8939, DOI: 10.1039/C5CS00364D.

[32] W. Wu, J. Zhao, J. Sun, L. Huang, X. Yi, *J. Mater. Chem. C* **2013**, *1*, 705–716, DOI: 10.1039/c2tc00214k.

[33] H. Jia, B. Küçüköz, Y. Xing, P. Majumdar, C. Zhang, A. Karatay, G. Yaglioglu, A. Elmali, J. Zhao, M. Hayvali, *J. Mater. Chem. C* **2014**, *2*, 9720–9736, DOI: 10.1039/c4tc01675k.

[34] W. Yang, A. Karatay, J. Zhao, J. Song, L. Zhao, Y. Xing, C. Zhang, C. He, H. G. Yaglioglu, M. Hayvali, A. Elmali, B. Kucukoz, *Inorg. Chem.* **2015**, *54*, 7492–7505, DOI: 10.1021/acs.inorgchem.5b01107.

[35] P. Majumdar, X. Cui, K. Xu, J. Zhao, *Dalton Trans.* **2015**, *44*, 4032–4045, DOI: 10.1039/c4dt03373f.

[36] M. Galletta, S. Campagna, M. Quesada, G. Ulrich, R. Ziessel, *Chem. Commun.* **2005**, 4222–4224, DOI: 10.1039/b507196h.

[37] A. A. Rachford, R. Ziessel, T. Bura, P. Retailleau, F. N. Castellano, *Inorg. Chem.* **2010**, *49*, 3730–3736,
DOI: 10.1021/ic901996u.

[38] W. Wu, J. Sun, X. Cui, J. Zhao, *J. Mater. Chem. C* **2013**, *1*, 4577–4589,
DOI: 10.1039/c3tc30592a.

[39] X. Yi, J. Zhao, J. Sun, S. Guo, H. Zhang, *Dalton Trans.* **2013**, *42*, 2062–2074,
DOI: 10.1039/c2dt32420b.

[40] P. Wang, Y. H. Koo, W. Kim, W. Yang, X. Cui, W. Ji, J. Zhao, D. Kim, *J. Phys. Chem. C* **2017**, *121*, 11117–11128,
DOI: 10.1021/acs.jpcc.7b02188.

[41] F. Zhong, A. Karatay, L. Zhao, J. Zhao, C. He, C. Zhang, H. G. Yaglioglu, A. Elmali, B. Kucukoz, M. Hayvali, *Inorg. Chem.* **2015**, *54*, 7803–7817,
DOI: 10.1021/acs.inorgchem.5b00822.

[42] C.-W. Hsu, C.-C. Lin, M.-W. Chung, Y. Chi, G.-H. Lee, P.-T. Chou, C.-H. Chang, P.-Y. Chen, *J. Am. Chem. Soc.* **2011**, *133*, 12085–12099,
DOI: 10.1021/ja2026568.

[43] E. Yu-Tzu Li, T. Y. Jiang, Y. Chi, P. T. Chou, *Phys. Chem. Chem. Phys.* **2014**, *16*, 26184–26192,
DOI: 10.1039/c4cp03540b.

[44] Y.-C. Chang, K.-C. Tang, H.-A. Pan, S.-H. Liu, I. O. Koshevoy, A. J. Karttunen, W.-Y. Hung, M.-H. Cheng, P.-T. Chou, *J. Phys. Chem. C* **2013**, *117*, 9623–9632,
DOI: 10.1021/jp402666r.

[45] B.-Y. Wang, A. R. Karikachery, Y. Li, A. Singh, H. B. Lee, W. Sun, P. R. Sharp, *J. Am. Chem. Soc.* **2009**, *131*, 3150–3151,
DOI: 10.1021/ja809046p.

[46] S. Lentijo, J. A. Miguel, P. Espinet, *Inorg. Chem.* **2010**, *49*, 9169–9177,
DOI: 10.1021/ic1003319.

[47] H. B. Lee, P. R. Sharp, *Organometallics* **2005**, *24*, 4875–4877,
DOI: 10.1021/om050464b.

[48] H. Choi, C. Kim, K.-M. Park, J. Kim, Y. Kang, J. Ko, *J. Organomet. Chem.* **2009**, *694*, 3529–3532,
DOI: 10.1016/j.jorganchem.2009.07.015.

[49] A. Singh, P. R. Sharp, *J. Am. Chem. Soc.* **2006**, *128*, 5998–5999, DOI: 10.1021/ja060159x.

[50] T. T. Vu, S. Badré, C. Dumas-Verdes, J.-J. Vachon, C. Julien, P. Audebert, E. Y. Senotrusova, E. Y. Schmidt, B. A. Trofimov, R. B. Pansu, G. Clavier, R. Méallet-Renault, *J. Phys. Chem. C* **2009**, *113*, 11844–11855, DOI: 10.1021/jp9019602.

[51] W. Wu, H. Guo, W. Wu, S. Ji, J. Zhao, *J. Org. Chem.* **2011**, *76*, 7056–7064, DOI: 10.1021/jo200990y.

[52] H. Lim, S. Seo, S. Pascal, Q. Bellier, S. Rigaut, C. Park, H. Shin, O. Maury, C. Andraud, E. Kim, *Sci. Rep.* **2016**, *6*, 18867, DOI: 10.1038/srep18867.

[53] A. B. Nepomnyashchii, M. Bröring, J. Ahrens, A. J. Bard, *J. Am. Chem. Soc.* **2011**, *133*, 8633–8645, DOI: 10.1021/ja2010219.

[54] L. Huang, W. Yang, J. Zhao, *J. Org. Chem.* **2014**, *79*, 10240–10255, DOI: 10.1021/jo5019014.

[55] T. Lazarides, T. M. McCormick, K. C. Wilson, S. Lee, D. W. McCamant, R. Eisenberg, *J. Am. Chem. Soc.* **2011**, *133*, 350–364, DOI: 10.1021/ja1070366.

[56] C. Goze, G. Ulrich, L. J. Mallon, B. D. Allen, A. Harriman, R. Ziessel, *J. Am. Chem. Soc.* **2006**, *128*, 10231–10239, DOI: 10.1021/ja062405a.

[57] T. J. McCarthy, R. G. Nuzzo, G. M. Whitesides, *J. Am. Chem. Soc.* **1981**, *103*, 3396–3403, DOI: 10.1021/ja00402a025.

[58] D. Strawser, A. Karton, O. V. Zenkina, M. A. Iron, L. J. Shimon, J. M. Martin, M. E. van der Boom, *J. Am. Chem. Soc.* **2005**, *127*, 9322–3, DOI: 10.1021/ja050613h.

[59] P. Irmler, R. F. Winter, *Dalton Trans.* **2016**, *45*, 10420–10434, DOI: 10.1039/c6dt01623e.

[60] F. Bauer, H. Braunschweig, K. Gruss, T. Kupfer, *Organometallics* **2011**, *30*, 2869–2884, DOI: 10.1021/om200214w.

[61] H. Braunschweig, R. Bertermann, P. Brenner, M. Burzler, R. D. Dewhurst, K. Radacki, F. Seeler, *Chem. - Eur. J.* **2011**, *17*, 11828–37, DOI: 10.1002/chem.201101823.

[62] L. J. Farrugia, *J. Appl. Crystallogr.* **2012**, *45*, 849–854, DOI: 10.1107/s0021889812029111.

[63] F. Geist, A. Jackel, R. F. Winter, *Inorg. Chem.* **2015**, *54*, 10946–10957, DOI: 10.1021/acs.inorgchem.5b01969.

[64] J. Al Anshori, T. Slanina, E. Palao, P. Klan, *Photochem. Photobiol. Sci.* **2016**, *15*, 250–259, DOI: 10.1039/c5pp00366k.

[65] F. Geist, A. Jackel, P. Irmler, M. Linseis, S. Malzkuhn, M. Kuss-Petermann, O. S. Wenger, R. F. Winter, *Inorg. Chem.* **2017**, *56*, 914–930, DOI: 10.1021/acs.inorgchem.6b02549.

[66] M. T. Whited, P. I. Djurovich, S. T. Roberts, A. C. Durrell, C. W. Schlenker, S. E. Bradforth, M. E. Thompson, *J. Am. Chem. Soc.* **2011**, *133*, 88–96, DOI: 10.1021/ja108493b.

[67] W. Wu, J. Zhao, H. Guo, J. Sun, S. Ji, Z. Wang, *Chem. - Eur. J.* **2012**, *18*, 1961–1968, DOI: 10.1002/chem.201102634.

[68] W. Siebrand, D. F. Williams, *J. Chem. Phys.* **1968**, *49*, 1860–1871, DOI: 10.1063/1.1670318.

[69] R. Englman, J. Jortner, *Mol. Phys.* **1970**, *18*, 145–164, DOI: 10.1080/00268977000100171.

[70] D. R. Scott, O. Maltenieks, *J. Phys. Chem.* **1968**, *72*, 3354–3356, DOI: 10.1021/j100855a057.

[71] A. B. Zaitsev, R. Méallet-Renault, E. Y. Schmidt, A. I. Mikhaleva, S. Badré, C. Dumas, A. M. Vasil'tsov, N. V. Zorina, R. B. Pansu, *Tetrahedron* **2005**, *61*, 2683–2688, DOI: 10.1016/j.tet.2005.01.065.

[72] S. Badré, V. Monnier, R. Méallet-Renault, C. Dumas-Verdes, E. Y. Schmidt, A. I. Mikhaleva, G. Laurent, G. Levi, A. Ibanez, B. A. Trofimov, R. B. Pansu, *J. Photochem. Photobiol. A* **2006**, *183*, 238–246, DOI: 10.1016/j.jphotochem.2006.07.002.

[73] P. Irmler, R. F. Winter, *Dalton Trans.* **2016**, *45*, 10420–10434, DOI: 10.1039/c6dt01623e.

[74] P. Yang, J. Zhao, W. Wu, X. Yu, Y. Liu, *J. Org. Chem.* **2012**, *77*, 6166–6178, DOI: 10.1021/jo300943t.

[75] L. Huang, J. Zhao, *RSC Adv.* **2013**, *3*, 23377–23388, DOI: 10.1039/c3ra43299h.

[76] L. Huang, J. Zhao, S. Guo, C. Zhang, J. Ma, *J. Org. Chem.* **2013**, *78*, 5627–5637, DOI: 10.1021/jo400769u.

[77] W. Wu, Y. Geng, W. Fan, Z. Li, L. Zhan, X. Wu, J. Zheng, J. Zhao, M. Wu, *RSC Adv.* **2014**, *4*, 51349–51352, DOI: 10.1039/C4RA08654F.

[78] A. Gorman, J. Killoran, C. O'Shea, T. Kenna, W. M. Gallagher, D. F. O'Shea, *J. Am. Chem. Soc.* **2004**, *126*, 10619–10631, DOI: 10.1021/ja047649e.

[79] S. G. Awuah, Y. You, *RSC Adv.* **2012**, *2*, 11169–11183, DOI: 10.1039/C2RA21404K.

[80] D. Rehm, A. Weller, *Isr. J. Chem.* **1970**, *8*, 259–271, DOI: 10.1002/ijch.197000029.

[81] Y. Usui, *Chem. Lett.* **1973**, *2*, 743–744, DOI: 10.1246/cl.1973.743.

[82] F. Wilkinson, W. P. Helman, A. B. Ross, *J. Phys. Chem. Ref. Data* **1993**, *22*, 113–262, DOI: 10.1063/1.555934.

[83] J. N. Chaon, G. R. Jamieson, R. S. Sinclair, *Chem. Phys. Lipids* **1987**, *43*, 81–99, DOI: 10.1016/0009-3084(87)90028-4.

[84] K. Rurack, M. Kollmannsberger, J. Daub, *Angew. Chem. Int. Ed.* **2001**, *40*, 385–387, DOI: 10.1002/1521-3773(20010119)40:2<385::aid-anie385>3.0.co;2-f.

[85] S. Hattori, K. Ohkubo, Y. Urano, H. Sunahara, T. Nagano, Y. Wada, N. V. Tkachenko, H. Lemmetyinen, S. Fukuzumi, *J. Phys. Chem. B* **2005**, *109*, 15368–15375, DOI: 10.1021/jp050952x.

[86] Y. Teki, H. Tamekuni, K. Haruta, J. Takeuchi, Y. Miura, *J. Mater. Chem.* **2008**, *18*, 381–391,
DOI: 10.1039/b714868b.

[87] G. H. Summers, J. F. Lefebvre, F. A. Black, E. S. Davies, E. A. Gibson, T. Pullerits, C. J. Wood, K. Zidek, *Phys. Chem. Chem. Phys.* **2016**, *18*, 1059–1070,
DOI: 10.1039/c5cp05177k.

[88] S. J. Hendel, A. M. Poe, P. Khomein, Y. Bae, S. Thayumanavan, E. R. Young, *J. Phys. Chem. A* **2016**, *120*, 8794–8803,
DOI: 10.1021/acs.jpca.6b06590.

[89] A. Iagatti, L. Cupellini, G. Biagiotti, S. Caprasecca, S. Fedeli, A. Lapini, E. Ussano, S. Cicchi, P. Foggi, M. Marcaccio, B. Mennucci, M. Di Donato, *J. Phys. Chem. C* **2016**, *120*, 16526–16536,
DOI: 10.1021/acs.jpcc.6b05738.

[90] G. F. Jin, Y. J. Cho, K. R. Wee, S. A. Hong, I. H. Suh, H. J. Son, J. D. Lee, W. S. Han, D. W. Cho, S. O. Kang, *Dalton Trans.* **2015**, *44*, 2780–2787,
DOI: 10.1039/c4dt03123g.

[91] V. J. Richards, A. L. Gower, J. E. Smith, E. S. Davies, D. Lahaye, A. G. Slater nee Phillips, W. Lewis, A. J. Blake, N. R. Champness, D. L. Kays, *Chem. Commun.* **2012**, *48*, 1751–1753,
DOI: 10.1039/c2cc16047a.

[92] S. J. Hendel, A. M. Poe, P. Khomein, Y. Bae, S. Thayumanavan, E. R. Young, *J. Phys. Chem. A* **2016**, *120*, 8794–8803,
DOI: 10.1021/acs.jpca.6b06590.

[93] M. N. Belzile, R. Godin, A. M. Durantini, G. Cosa, *J. Am. Chem. Soc.* **2016**, *138*, 16388–16397,
DOI: 10.1021/jacs.6b09735.

[94] A. Ruff, E. Heyer, T. Roland, S. Haacke, R. Ziessel, S. Ludwigs, *Electrochim. Acta* **2015**, *173*, 847–859,
DOI: 10.1016/j.electacta.2015.05.093.

[95] A. C. Benniston, G. Copley, A. Harriman, D. Howgego, R. W. Harrington, W. Clegg, *J. Org. Chem.* **2010**, *75*, 2018–2027,
DOI: 10.1021/jo1000803.

[96] M. Krejčik, M. Daněk, F. Hartl, *J. Electroanal. Chem. Interfacial Electrochem.* **1991**, *317*, 179–187,
DOI: 10.1016/0022-0728(91)85012-e.

[97] Y. Chen, J. Zhao, H. Guo, L. Xie, *J. Org. Chem.* **2012**, *77*, 2192–206,
DOI: 10.1021/jo202215x.

[98] L. Fu, F. L. Jiang, D. Fortin, P. D. Harvey, Y. Liu, *Chem. Commun.* **2011**, *47*, 5503–5505,
DOI: 10.1039/c1cc10784d.

[99] R. I. Lerrick, T. P. Winstanley, K. Haggerty, C. Wills, W. Clegg, R. W. Harrington, P. Bultinck, W. Herrebout, A. C. Benniston, M. J. Hall, *Chem. Commun.* **2014**, *50*, 4714–4716,
DOI: 10.1039/c4cc00851k.

[100] M. Ghelfi, L. Ulatowski, D. Manor, J. Atkinson, *Bioorg. Med. Chem.* **2016**, *24*, 2754–2761,
DOI: 10.1016/j.bmc.2016.04.044.

[101] X. Zhou, C. Yu, Z. Feng, Y. Yu, J. Wang, E. Hao, Y. Wei, X. Mu, L. Jiao, *Org. Lett.* **2015**, *17*, 4632–4635,
DOI: 10.1021/acs.orglett.5b02383.

[102] W. Herrendorf, W. Bärnighausen, HABITUS, program for the optimization of the crystal shape for numerical absorption correction in X-SHAPE, Computer Program, **1999**.

[103] G. M. Sheldrick, *SHELXTL-97 Program for Crystal Structure Analysis*, University of Göttingen, Göttingen, **1997**.

[104] G. M. Sheldrick, *Acta Crystallogr. A* **2008**, *64*, 112–122,
DOI: 10.1107/S0108767307043930.

[105] G. M. Sheldrick, *Acta Crystallogr. A* **2008**, *64*, 112–122,
DOI: 10.1107/S0108767307043930.

[106] O. V. Dolomanov, L. J. Bourhis, R. J. Gildea, J. A. K. Howard, H. Puschmann, *J. Appl. Crystallogr.* **2009**, *42*, 339–341,
DOI: 10.1107/s0021889808042726.

[107] A. L. Spek, *Acta Cryst. D* **2009**, *65*, 148–155,
DOI: 10.1107/S090744490804362X.

[108] C. F. Macrae, I. J. Bruno, J. A. Chisholm, P. R. Edgington, P. McCabe, E. Pidcock, L. Rodriguez-Monge, R. Taylor, J. van de Streek, P. A. Wood, *J. Appl. Crystallogr.* **2008**, *41*, 466–470, DOI: 10.1107/s0021889807067908.

[109] S. Stoll, A. Schweiger, *J. Magn. Reson.* **2006**, *178*, 42–55, DOI: 10.1016/j.jmr.2005.08.013.

[110] M. J. Frisch, G. W. Trucks, H. B. Schlegel, G. E. Scuseria, M. A. Robb, J. R. Cheeseman, G. Scalmani, V. Barone, B. Mennucci, G. A. Petersson, H. Nakatsuji, M. Caricato, X. Li, H. P. Hratchian, A. F. Izmaylov, J. Bloino, G. Zheng, J. L. Sonnenberg, M. Hada, M. Ehara, K. Toyota, R. Fukuda, J. Hasegawa, M. Ishida, T. Nakajima, Y. Honda, O. Kitao, H. Nakai, T. Vreven, J. A. Montgomery Jr., J. E. Peralta, F. Ogliaro, M. J. Bearpark, J. Heyd, E. N. Brothers, K. N. Kudin, V. N. Staroverov, R. Kobayashi, J. Normand, K. Raghavachari, A. P. Rendell, J. C. Burant, S. S. Iyengar, J. Tomasi, M. Cossi, N. Rega, N. J. Millam, M. Klene, J. E. Knox, J. B. Cross, V. Bakken, C. Adamo, J. Jaramillo, R. Gomperts, R. E. Stratmann, O. Yazyev, A. J. Austin, R. Cammi, C. Pomelli, J. W. Ochterski, R. L. Martin, K. Morokuma, V. G. Zakrzewski, G. A. Voth, P. Salvador, J. J. Dannenberg, S. Dapprich, A. D. Daniels, Ö. Farkas, J. B. Foresman, J. V. Ortiz, J. Cioslowski, D. J. Fox, Gaussian 09, Computer Program, **2009**.

[111] O. Gunnarsson, B. I. Lundqvist, *Phys. Rev. B* **1976**, *13*, 4274–4298.

[112] W. Küchle, M. Dolg, H. Stoll, H. Preuss, *J. Chem. Phys.* **1994**, *100*, 7535–7542, DOI: 10.1063/1.466847.

[113] M. Dolg, H. Stoll, H. Preuss, *J. Chem. Phys.* **1989**, *90*, 1730–1734, DOI: 10.1063/1.456066.

[114] D. Andrae, U. Häußermann, M. Dolg, H. Stoll, H. Preuss, *Theor. Chim. Acta* **1990**, *77*, 123–141, DOI: 10.1007/bf01114537.

[115] P. C. Hariharan, J. A. Pople, *Theor. Chim. Acta* **1973**, *28*, 213–222, DOI: 10.1007/BF00533485.

[116] J. P. Perdew, K. Burke, M. Ernzerhof, *Phys. Rev. Lett.* **1996**, *77*, 3865–3868.

[117] C. Adamo, V. Barone, *J. Chem. Phys.* **1999**, *110*, 6158–6170, DOI: 10.1063/1.478522.

[118] E. Cancès, B. Mennucci, J. Tomasi, *J. Chem. Phys.* **1997**, *107*, 3032–3041, DOI: 10.1063/1.474659.

[119] B. Mennucci, J. Tomasi, *J. Chem. Phys.* **1997**, *106*, 5151–5158, DOI: 10.1063/1.473558.

[120] M. Cossi, N. Rega, G. Scalmani, V. Barone, *J. Comput. Chem.* **2003**, *24*, 669–681, DOI: 10.1002/jcc.10189.

[121] G. Scalmani, M. J. Frisch, *J. Chem. Phys.* **2010**, *132*, 114110, DOI: 10.1063/1.3359469.

[122] E. Runge, E. K. U. Gross, *Phys. Rev. Lett.* **1984**, *52*, 997–1000.

[123] N. M. O'Boyle, A. L. Tenderholt, K. M. Langner, *J. Comput. Chem.* **2008**, *29*, 839–845, DOI: 10.1002/jcc.20823.

[124] S.-y. Takizawa, R. Aboshi, S. Murata, *Photochem. Photobiol. Sci.* **2011**, *10*, 895–903, DOI: 10.1039/C0PP00265H.

[125] N. Adarsh, M. Shanmugasundaram, R. R. Avirah, D. Ramaiah, *Chem. - Eur. J.* **2012**, *18*, 12655–12662, DOI: 10.1002/chem.201202438.

[126] L. R. Field, E. Wilhelm, R. Battino, *J. Chem. Thermodyn.* **1974**, *6*, 237–243, DOI: 10.1016/0021-9614(74)90175-x.

# References of Publication 3


[1] M. Kasha, *Discuss. Faraday Soc.* **1950**, *9*, 14–19, DOI: 10.1039/df9500900014.

[2] C.-W. Hsu, C.-C. Lin, M.-W. Chung, Y. Chi, G.-H. Lee, P.-T. Chou, C.-H. Chang, P.-Y. Chen, *J. Am. Chem. Soc.* **2011**, *133*, 12085–12099, DOI: 10.1021/ja2026568.

[3] C. C. Hsu, C. C. Lin, P. T. Chou, C. H. Lai, C. W. Hsu, C. H. Lin, Y. Chi, *J. Am. Chem. Soc.* **2012**, *134*, 7715–7724, DOI: 10.1021/ja2107788.

[4] Y.-C. Chang, K.-C. Tang, H.-A. Pan, S.-H. Liu, I. O. Koshevoy, A. J. Karttunen, W.-Y. Hung, M.-H. Cheng, P.-T. Chou, *J. Phys. Chem. C* **2013**, *117*, 9623–9632, DOI: 10.1021/jp402666r.

[5] W. Y. Heng, J. Hu, J. H. K. Yip, *Organometallics* **2007**, *26*, 6760–6768, DOI: 10.1021/om700716p.

[6] F. Geist, A. Jackel, R. F. Winter, *Inorg. Chem.* **2015**, *54*, 10946–10957, DOI: 10.1021/acs.inorgchem.5b01969.

[7] P. Irmler, R. F. Winter, *Dalton Trans.* **2016**, *45*, 10420–10434, DOI: 10.1039/c6dt01623e.

[8] F. Geist, A. Jackel, P. Irmler, M. Linseis, S. Malzkuhn, M. Kuss-Petermann, O. S. Wenger, R. F. Winter, *Inorg. Chem.* **2017**, *56*, 914–930, DOI: 10.1021/acs.inorgchem.6b02549.

[9] P. Irmler, R. F. Winter, *Organometallics* **2018**, *37*, 235–253, DOI: 10.1021/acs.organomet.7b00806.

[10] W. Wu, J. Zhao, H. Guo, J. Sun, S. Ji, Z. Wang, *Chem. - Eur. J.* **2012**, *18*, 1961–1968, DOI: 10.1002/chem.201102634.

[11] F. Zhong, A. Karatay, L. Zhao, J. Zhao, C. He, C. Zhang, H. G. Yaglioglu, A. Elmali, B. Kucukoz, M. Hayvali, *Inorg. Chem.* **2015**, *54*, 7803–7817, DOI: 10.1021/acs.inorgchem.5b00822.

[12] J. Sun, F. Zhong, X. Yi, J. Zhao, *Inorg. Chem.* **2013**, *52*, 6299–6310, DOI: 10.1021/ic302210b.

[13] W. Wu, J. Sun, X. Cui, J. Zhao, *J. Mater. Chem. C* **2013**, *1*, 4577–4589, DOI: 10.1039/c3tc30592a.

[14] B. Ma, P. I. Djurovich, M. Yousufuddin, R. Bau, M. E. Thompson, *J. Phys. Chem. C* **2008**, *112*, 8022–8031, DOI: 10.1021/jp800594j.

[15] T. Tsuboi, D.-F. Huang, T. J. Chow, W. Huang, *Opt. Mater.* **2014**, *36*, 1734–1738, DOI: 10.1016/j.optmat.2014.02.031.

[16] J. Hu, J. H. K. Yip, D.-L. Ma, K.-Y. Wong, W.-H. Chung, *Organometallics* **2009**, *28*, 51–59, DOI: 10.1021/om800410m.

[17] W. Wu, W. Wu, S. Ji, H. Guo, J. Zhao, *Eur. J. Inorg. Chem.* **2010**, *2010*, 4470–4482, DOI: 10.1002/ejic.201000488.

[18] M. A. Filatov, S. Karuthedath, P. M. Polestshuk, S. Callaghan, K. J. Flanagan, M. Telitchko, T. Wiesner, F. Laquai, M. O. Senge, *Phys. Chem. Chem. Phys.* **2018**, *20*, 8016–8031, DOI: 10.1039/c7cp08472b.

[19] X. F. Zhang, N. Feng, *Chem. - Asian J.* **2017**, *12*, 2447–2456, DOI: 10.1002/asia.201700794.

[20] S. Ji, J. Ge, D. Escudero, Z. Wang, J. Zhao, D. Jacquemin, *J. Org. Chem.* **2015**, *80*, 5958–5963, DOI: 10.1021/acs.joc.5b00691.

[21] M. R. Wasielewski, D. G. Johnson, W. A. Svec, K. M. Kersey, D. W. Minsek, *J. Am. Chem. Soc.* **1988**, *110*, 7219–7221, DOI: 10.1021/ja00229a050.

[22] S.-H. Lee, A. G. Larsen, K. Ohkubo, Z.-L. Cai, J. R. Reimers, S. Fukuzumi, M. J. Crossley, *Chem. Sci.* **2012**, *3*, 257–269, DOI: 10.1039/c1sc00614b.

[23] T. Higashino, T. Yamada, M. Yamamoto, A. Furube, N. V. Tkachenko, T. Miura, Y. Kobori, R. Jono, K. Yamashita, H. Imahori, *Angew. Chem. Int. Ed.* **2016**, *55*, 629–633, DOI: 10.1002/anie.201509067.

[24] T. Shida, S. Iwata, *J. Am. Chem. Soc.* **1973**, *95*, 3473–3483, DOI: 10.1021/ja00792a005.

[25] J. Maurer, M. Linseis, B. Sarkar, B. Schwederski, M. Niemeyer, W. Kaim, S. Zalis, C. Anson, M. Zabel, R. F. Winter, *J. Am. Chem. Soc.* **2008**, *130*, 259–268, DOI: 10.1021/ja075547t.

# References of Publication 4


[1] M. Bachmann, O. Blacque, K. Venkatesan, *Chem. - Eur. J.* **2017**, *23*, 9451–9456, DOI: 10.1002/chem.201702341.

[2] Y. Yang, M. Lowry, C. M. Schowalter, S. O. Fakayode, J. O. Escobedo, X. Xu, H. Zhang, T. J. Jensen, F. R. Fronczek, I. M. Warner, R. M. Strongin, *J. Am. Chem. Soc.* **2006**, *128*, 14081–14092, DOI: 10.1021/ja0632207.

[3] S. Park, J. E. Kwon, S. H. Kim, J. Seo, K. Chung, S. Y. Park, D. J. Jang, B. Milian Medina, J. Gierschner, S. Y. Park, *J. Am. Chem. Soc.* **2009**, *131*, 14043–14049, DOI: 10.1021/ja902533f.

[4] Y. Liu, M. Nishiura, Y. Wang, Z. Hou, *J. Am. Chem. Soc.* **2006**, *128*, 5592–5593, DOI: 10.1021/ja058188f.

[5] Y. Liu, H. Guo, J. Zhao, *Chem. Commun.* **2011**, *47*, 11471–11473, DOI: 10.1039/c1cc14582g.

[6] H. Xiang, L. Zhou, Y. Feng, J. Cheng, D. Wu, X. Zhou, *Inorg. Chem.* **2012**, *51*, 5208–5212, DOI: 10.1021/ic300040n.

[7] H. Hochreiner, I. Sanchez-Barragan, J. M. Costa-Fernandez, A. Sanz-Medel, *Talanta* **2005**, *66*, 611–618, DOI: 10.1016/j.talanta.2004.12.030.

[8] F. Geist, A. Jackel, R. F. Winter, *Inorg. Chem.* **2015**, *54*, 10946–10957, DOI: 10.1021/acs.inorgchem.5b01969.

[9] P. Irmler, R. F. Winter, *Dalton Trans.* **2016**, *45*, 10420–10434, DOI: 10.1039/c6dt01623e.

[10] M. A. El-Sayed, *J. Chem. Phys.* **1963**, *38*, 2834–2838, DOI: 10.1063/1.1733610.

[11] E. Yu-Tzu Li, T. Y. Jiang, Y. Chi, P. T. Chou, *Phys. Chem. Chem. Phys.* **2014**, *16*, 26184–26192, DOI: 10.1039/c4cp03540b.

[12] P.-T. Chou, Y. Chi, M.-W. Chung, C.-C. Lin, *Coord. Chem. Rev.* **2011**, *255*, 2653–2665, DOI: 10.1016/j.ccr.2010.12.013.

[13] M. Montalti, A. Credi, L. Prodi, M. Teresa Gandolfi, *Handbook of Photochemistry*, 3rd, CRC Press, Boca Raton, **2006**,
DOI: 10.1201/9781420015195.

[14] M. K. S. P. McGlynn, T. Azumi, *Molecular Spectroscopy of the Triplet State*, Prentice-Hall, Englewood Cliffs, N.J, **1969**.

[15] W. Y. Heng, J. Hu, J. H. K. Yip, *Organometallics* **2007**, *26*, 6760–6768,
DOI: 10.1021/om700716p.

[16] C. C. Hsu, C. C. Lin, P. T. Chou, C. H. Lai, C. W. Hsu, C. H. Lin, Y. Chi, *J. Am. Chem. Soc.* **2012**, *134*, 7715–7724,
DOI: 10.1021/ja2107788.

[17] C.-W. Hsu, C.-C. Lin, M.-W. Chung, Y. Chi, G.-H. Lee, P.-T. Chou, C.-H. Chang, P.-Y. Chen, *J. Am. Chem. Soc.* **2011**, *133*, 12085–12099,
DOI: 10.1021/ja2026568.

[18] E. O. Danilov, I. E. Pomestchenko, S. Kinayyigit, P. L. Gentili, M. Hissler, R. Ziessel, F. N. Castellano, *J. Phys. Chem. A* **2005**, *109*, 2465–2471,
DOI: 10.1021/jp045269+.

[19] B. Ma, P. I. Djurovich, M. Yousufuddin, R. Bau, M. E. Thompson, *J. Phys. Chem. C* **2008**, *112*, 8022–8031,
DOI: 10.1021/jp800594j.

[20] W. Yang, A. Karatay, J. Zhao, J. Song, L. Zhao, Y. Xing, C. Zhang, C. He, H. G. Yaglioglu, M. Hayvali, A. Elmali, B. Kucukoz, *Inorg. Chem.* **2015**, *54*, 7492–7505,
DOI: 10.1021/acs.inorgchem.5b01107.

[21] W. Wu, W. Wu, S. Ji, H. Guo, J. Zhao, *Eur. J. Inorg. Chem.* **2010**, *2010*, 4470–4482,
DOI: 10.1002/ejic.201000488.

[22] A. J. Hallett, N. White, W. Wu, X. Cui, P. N. Horton, S. J. Coles, J. Zhao, S. J. Pope, *Chem. Commun.* **2012**, *48*, 10838–10840,
DOI: 10.1039/c2cc35907c.

[23] A. F. Morales, G. Accorsi, N. Armaroli, F. Barigelletti, S. J. A. Pope, M. D. Ward, *Inorg. Chem.* **2002**, *41*, 6711–6719,
DOI: 10.1021/ic025811d.

[24] N. D. McClenaghan, Y. Leydet, B. Maubert, M. T. Indelli, S. Campagna, *Coord. Chem. Rev.* **2005**, *249*, 1336–1350,
DOI: 10.1016/j.ccr.2004.12.017.

[25] K. Oppelt, D. A. M. Egbe, U. Monkowius, M. List, M. Zabel, N. S. Sariciftci, G. Knör, *J. Organomet. Chem.* **2011**, *696*, 2252–2258,
DOI: 10.1016/j.jorganchem.2010.11.008.

[26] R. Liu, N. Dandu, Y. Li, S. Kilina, W. Sun, *Dalton Trans.* **2013**, *42*, 4398–4409,
DOI: 10.1039/c2dt32153j.

[27] A. J. Howarth, M. B. Majewski, M. O. Wolf, *Coord. Chem. Rev.* **2015**, *282-283*, 139–149,
DOI: 10.1016/j.ccr.2014.03.024.

[28] I. E. Pomestchenko, F. N. Castellano, *J. Phys. Chem. A* **2004**, *108*, 3485–3492,
DOI: 10.1021/jp049641x.

[29] T. Tsuboi, D.-F. Huang, T. J. Chow, W. Huang, *Opt. Mater.* **2014**, *36*, 1734–1738,
DOI: 10.1016/j.optmat.2014.02.031.

[30] J. Brooks, Y. Babayan, S. Lamansky, P. Djurovich, I. Tsyba, R. Bau, M. Thompson, *Inorg. Chem.* **2002**, *41*, 3055–3066,
DOI: 10.1021/ic0255508.

[31] J. Hu, J. H. K. Yip, D.-L. Ma, K.-Y. Wong, W.-H. Chung, *Organometallics* **2009**, *28*, 51–59,
DOI: 10.1021/om800410m.

[32] F. Geist, A. Jackel, R. F. Winter, *Dalton Trans.* **2015**, *44*, 3974–3987,
DOI: 10.1039/C4DT02410A.

[33] P. Irmler, R. F. Winter, *Organometallics* **2018**, *37*, 235–253,
DOI: 10.1021/acs.organomet.7b00806.

[34] F. Geist, A. Jackel, P. Irmler, M. Linseis, S. Malzkuhn, M. Kuss-Petermann, O. S. Wenger, R. F. Winter, *Inorg. Chem.* **2017**, *56*, 914–930,
DOI: 10.1021/acs.inorgchem.6b02549.

[35] N. Kanamaru, H. R. Bhattacharjee, E. C. Lim, *Chem. Phys. Lett.* **1974**, *26*, 174–179,
DOI: 10.1016/0009-2614(74)85390-x.

[36] I. E. Pomestchenko, C. R. Luman, M. Hissler, R. Ziessel, F. N. Castellano, *Inorg. Chem.* **2003**, *42*, 1394–1396,
DOI: 10.1021/ic0261631.

[37] J. P. Rostron, G. Ulrich, P. Retailleau, A. Harriman, R. Ziessel, *New J. Chem.* **2005**, *29*, 1241,
DOI: 10.1039/b507585h.

[38] R. Ziessel, C. Goze, G. Ulrich, M. Cesario, P. Retailleau, A. Harriman, J. P. Rostron, *Chem. - Eur. J.* **2005**, *11*, 7366–7378,
DOI: 10.1002/chem.200500373.

[39] X. F. Zhang, N. Feng, *Chem. - Asian J.* **2017**, *12*, 2447–2456,
DOI: 10.1002/asia.201700794.

[40] M. A. Filatov, S. Karuthedath, P. M. Polestshuk, H. Savoie, K. J. Flanagan, C. Sy, E. Sitte, M. Telitchko, F. Laquai, R. W. Boyle, M. O. Senge, *J. Am. Chem. Soc.* **2017**, *139*, 6282–6285,
DOI: 10.1021/jacs.7b00551.

[41] M. A. Filatov, S. Karuthedath, P. M. Polestshuk, S. Callaghan, K. J. Flanagan, M. Telitchko, T. Wiesner, F. Laquai, M. O. Senge, *Phys. Chem. Chem. Phys.* **2018**, *20*, 8016–8031,
DOI: 10.1039/c7cp08472b.

[42] P. Irmler, F. S. Gogesch, C. B. Larsen, O. S. Wenger, R. F. Winter, *Dalton Trans.* **2019**, *48*, 1171–1174,
DOI: 10.1039/c8dt04823a.

[43] T. J. McCarthy, R. G. Nuzzo, G. M. Whitesides, *J. Am. Chem. Soc.* **1981**, *103*, 3396–3403,
DOI: 10.1021/ja00402a025.

[44] M. A. Cairns, K. R. Dixon, G. A. Rivett, *J. Organomet. Chem.* **1979**, *171*, 373–385,
DOI: 10.1016/s0022-328x(00)82662-5.

[45] J. S. Wilson, N. Chawdhury, M. R. A. Al-Mandhary, M. Younus, M. S. Khan, P. R. Raithby, A. Köhler, R. H. Friend, *J. Am. Chem. Soc.* **2001**, *123*, 9412–9417,
DOI: 10.1021/ja010986s.

[46] C. E. Whittle, J. A. Weinstein, M. W. George, K. S. Schanze, *Inorg. Chem.* **2001**, *40*, 4053–4062,
DOI: 10.1021/ic0102182.

[47] E. M. Kober, J. V. Caspar, R. S. Lumpkin, T. J. Meyer, *J. Phys. Chem.* **1986**, *90*, 3722–3734,
DOI: 10.1021/j100407a046.

[48] M. R. Wasielewski, D. G. Johnson, W. A. Svec, K. M. Kersey, D. W. Minsek, *J. Am. Chem. Soc.* **1988**, *110*, 7219–7221,
DOI: 10.1021/ja00229a050.

[49] S.-H. Lee, A. G. Larsen, K. Ohkubo, Z.-L. Cai, J. R. Reimers, S. Fukuzumi, M. J. Crossley, *Chem. Sci.* **2012**, *3*, 257–269,
DOI: 10.1039/c1sc00614b.

[50] T. Higashino, T. Yamada, M. Yamamoto, A. Furube, N. V. Tkachenko, T. Miura, Y. Kobori, R. Jono, K. Yamashita, H. Imahori, *Angew. Chem. Int. Ed.* **2016**, *55*, 629–633,
DOI: 10.1002/anie.201509067.

[51] F. Wilkinson, W. P. Helman, A. B. Ross, *J. Phys. Chem. Ref. Data* **1993**, *22*, 113–262,
DOI: 10.1063/1.555934.

[52] M. Krejčik, M. Daněk, F. Hartl, *J. Electroanal. Chem. Interfacial Electrochem.* **1991**, *317*, 179–187,
DOI: 10.1016/0022-0728(91)85012-e.

[53] T. Shida, S. Iwata, *J. Am. Chem. Soc.* **1973**, *95*, 3473–3483,
DOI: 10.1021/ja00792a005.

[54] J. Maurer, M. Linseis, B. Sarkar, B. Schwederski, M. Niemeyer, W. Kaim, S. Zalis, C. Anson, M. Zabel, R. F. Winter, *J. Am. Chem. Soc.* **2008**, *130*, 259–268,
DOI: 10.1021/ja075547t.

[55] R. P. Sabatini, T. M. McCormick, T. Lazarides, K. C. Wilson, R. Eisenberg, D. W. McCamant, *J. Phys. Chem. Lett.* **2011**, *2*, 223–227,
DOI: 10.1021/jz101697y.

[56] X. F. Zhang, X. Yang, *J. Phys. Chem. B* **2013**, *117*, 5533–5539,
DOI: 10.1021/jp4013812.

[57] Z. Wang, J. Zhao, *Org. Lett.* **2017**, *19*, 4492–4495, DOI: 10.1021/acs.orglett.7b02047.

[58] J. Zhao, S. Ji, H. Guo, *RSC Adv.* **2011**, *1*, 937, DOI: 10.1039/c1ra00469g.

[59] M. J. Frisch, G. W. Trucks, H. B. Schlegel, G. E. Scuseria, M. A. Robb, J. R. Cheeseman, G. Scalmani, V. Barone, B. Mennucci, G. A. Petersson, H. Nakatsuji, M. Caricato, X. Li, H. P. Hratchian, A. F. Izmaylov, J. Bloino, G. Zheng, J. L. Sonnenberg, M. Hada, M. Ehara, K. Toyota, R. Fukuda, J. Hasegawa, M. Ishida, T. Nakajima, Y. Honda, O. Kitao, H. Nakai, T. Vreven, J. A. Montgomery Jr., J. E. Peralta, F. Ogliaro, M. J. Bearpark, J. Heyd, E. N. Brothers, K. N. Kudin, V. N. Staroverov, R. Kobayashi, J. Normand, K. Raghavachari, A. P. Rendell, J. C. Burant, S. S. Iyengar, J. Tomasi, M. Cossi, N. Rega, N. J. Millam, M. Klene, J. E. Knox, J. B. Cross, V. Bakken, C. Adamo, J. Jaramillo, R. Gomperts, R. E. Stratmann, O. Yazyev, A. J. Austin, R. Cammi, C. Pomelli, J. W. Ochterski, R. L. Martin, K. Morokuma, V. G. Zakrzewski, G. A. Voth, P. Salvador, J. J. Dannenberg, S. Dapprich, A. D. Daniels, Ö. Farkas, J. B. Foresman, J. V. Ortiz, J. Cioslowski, D. J. Fox, Gaussian 09, Computer Program, **2009**.

[60] O. Gunnarsson, B. I. Lundqvist, *Phys. Rev. B* **1976**, *13*, 4274–4298.

[61] W. Küchle, M. Dolg, H. Stoll, H. Preuss, *J. Chem. Phys.* **1994**, *100*, 7535–7542, DOI: 10.1063/1.466847.

[62] M. Dolg, H. Stoll, H. Preuss, *J. Chem. Phys.* **1989**, *90*, 1730–1734, DOI: 10.1063/1.456066.

[63] D. Andrae, U. Häußermann, M. Dolg, H. Stoll, H. Preuss, *Theor. Chim. Acta* **1990**, *77*, 123–141, DOI: 10.1007/bf01114537.

[64] P. C. Hariharan, J. A. Pople, *Theor. Chim. Acta* **1973**, *28*, 213–222, DOI: 10.1007/BF00533485.

[65] J. P. Perdew, K. Burke, M. Ernzerhof, *Phys. Rev. Lett.* **1996**, *77*, 3865–3868.

[66] C. Adamo, V. Barone, *J. Chem. Phys.* **1999**, *110*, 6158–6170, DOI: 10.1063/1.478522.

[67] E. Cancès, B. Mennucci, J. Tomasi, *J. Chem. Phys.* **1997**, *107*, 3032–3041, DOI: 10.1063/1.474659.

[68] B. Mennucci, J. Tomasi, *J. Chem. Phys.* **1997**, *106*, 5151–5158, DOI: 10.1063/1.473558.

[69] M. Cossi, N. Rega, G. Scalmani, V. Barone, *J. Comput. Chem.* **2003**, *24*, 669–681, DOI: 10.1002/jcc.10189.

[70] G. Scalmani, M. J. Frisch, *J. Chem. Phys.* **2010**, *132*, 114110, DOI: 10.1063/1.3359469.

[71] E. Runge, E. K. U. Gross, *Phys. Rev. Lett.* **1984**, *52*, 997–1000.

[72] N. M. O'Boyle, A. L. Tenderholt, K. M. Langner, *J. Comput. Chem.* **2008**, *29*, 839–845, DOI: 10.1002/jcc.20823.

[73] W. Herrendorf, W. Bärnighausen, HABITUS, program for the optimization of the crystal shape for numerical absorption correction in X-SHAPE, Computer Program, **1999**.

[74] G. M. Sheldrick, *SHELXTL-97 Program for Crystal Structure Analysis*, University of Göttingen, Göttingen, **1997**.

[75] G. M. Sheldrick, *Acta Crystallogr. A* **2008**, *64*, 112–122, DOI: 10.1107/S0108767307043930.

[76] G. M. Sheldrick, *Acta Crystallogr. A* **2008**, *64*, 112–122, DOI: 10.1107/S0108767307043930.

[77] O. V. Dolomanov, L. J. Bourhis, R. J. Gildea, J. A. K. Howard, H. Puschmann, *J. Appl. Crystallogr.* **2009**, *42*, 339–341, DOI: 10.1107/s0021889808042726.

[78] A. L. Spek, *Acta Cryst. D* **2009**, *65*, 148–155, DOI: 10.1107/S090744490804362X.

[79] C. F. Macrae, I. J. Bruno, J. A. Chisholm, P. R. Edgington, P. McCabe, E. Pidcock, L. Rodriguez-Monge, R. Taylor, J. van de Streek, P. A. Wood, *J. Appl. Crystallogr.* **2008**, *41*, 466–470, DOI: 10.1107/s0021889807067908.

[80] H. Fischer, H. Orth, *Ann. Chem.* **1933**, *502*, 237–264, DOI: 10.1002/jlac.19335020114.